SYNTHESIS, *IN SILICO* ANALYSES, ANTIPLASMODIAL, HEME DETOXIFICATION AND CYTOTOXIC ACTIVITIES OF PYRANO[2,3-*C*]PYRAZOLE-4-AMINOQUINOLINE HYBRIDS AS ANTIMALARIAL AGENTS

LEKKALA RAVINDAR

UNIVERSITI KEBANGSAAN MALAYSIA

SYNTHESIS, *IN SILICO* ANALYSES, ANTIPLASMODIAL, HEME DETOXIFICATION AND CYTOTOXIC ACTIVITIES OF PYRANO[2,3-*C*]PYRAZOLE-4-AMINOQUINOLINE HYBRIDS AS ANTIMALARIAL AGENTS

LEKKALA RAVINDAR

THESIS SUBMITTED IN FULFILMENT FOR THE DEGREE OF DOCTOR OF PHILOSOPHY

FACULTY SCIENCE AND TECHNOLOGY
UNIVERSITI KEBANGSAAN MALAYSIA
BANGI
2025

SINTESIS, ANALISIS *IN SILICO*, ANTIPLASMODIAL, PENYAHTOKSIKAN DAN AKTIVITI SITOTOKSIK HIBRID PIRANO[2,3-*C*]PIRAZOL-4-AMINOKUINOLINA SEBAGAI AGEN ANTIMALARIA

LEKKALA RAVINDAR

TESIS YANG DIKEMUKAKAN UNTUK MEMPEROLEH
IJAZAH DOKTOR FALSAFAH

FAKULTI SAINS DAN TEKNOLOGI
UNIVERSITI KEBANGSAAN MALAYSIA
BANGI
2025

DECLARATION

I hereby declare that the work in this thesis is my own except for quotations and summaries which have been duly acknowledged.

12 January 2025

LEKKALA RAVINDAR
P108591

007737

PERAKUAN TESIS SARJANA / DOKTOR FALSAFAH
(DECLARATION OF MASTER / DOCTOR OF PHILOSOPHY THESIS)

A. MAKLUMAT PELAJAR/*STUDENT DETAILS*

Nama / *Name*	
No. Pendaftaran / *Registration No.*	
Fakulti / *Faculty*	
Tajuk / *Title*	

B. PERAKUAN / *DECLARATION*

The thesis is the property of UKM

	RAHSIA *CONFIDENTIAL*	Mengandungi maklumat yang berdarjah KESELAMATAN RASMI 1972 *Consisting of classified information under the OFFICIAL SECRETS ACT 1972*
	TERHAD *RESTRICTED*	Mengandungi maklumat TERHAD yang telah ditentukan oleh organisasi/badan di mana penyelidikan dijalankan *Consisting of RESTRICTED information which has been determined by the organisation/body where the research was conducted*
	AKSES TERBUKA/ TIDAK TERHAD *OPEN ACCESS / NON-RESTRICTED*	Saya memberikan kebenaran supaya tesis ini diterbitkan secara akses terbuka (untuk penyelidikan sahaja) *I give permission for this thesis to be published through open access, (for*

C. PENGESAHAN FAKULTI/INSTITUT | *VERIFICATION OF FACULTY/INSTITUTE*

PROF. MADYA DR. ABDUL MUNIR AB. MURAD
Timbalan Dekan
Siswazah
Fakulti Sains dan Teknologi
Universiti Kebangsaan Malaysia

ACKNOWLEDGEMENT

Thanksgiving is native to man and gratitude if not expressed turns to be the worst of all vices. With deep sense of honesty, I whole-heartedly wish to venerate the God for giving me the wisdom, strength and enthusiasm to accomplish this work.The text of the acknowledgement should not exceed one page. Dedications are not allowed. The acknowledgement should include:

According to Isaac Newton, “If I have seen further, it is by standing upon the shoulders of giants”. With unalloyed gratitude, I thank my tireless, task-tackling supervisors, Assoc. Prof. Dr. Nurul Izzaty Hassan and Assoc. Prof. Dr. Siti Aishah Hasbullah, who were the academic giants that carried me throughout this work. Their excellent supervision and guidance throughout the course of my Doctoral studies is highly appreciated.

At the same time, I would like to express my deep honor to one and all the professors who were educated me and encouraged me during my course works, and also, I would like to thank one and all the teachers, laboratory assistants and staff members from my school and deportment for their help throughout my Doctoral studies.

I would like to thank Prof. Lau Yee Ling’s research group for their help and guidance during antimalarial examination of hybrid compounds at the Department of Parasitology, Faculty of Medicine, University of Malaya.

I would like to thank Dr. Shevin’s research group for their help and guidance during molecular docking and isothermal titration calorimetry (ITC) examination of hybrid compounds at the Department of Biological Sciences and Biotechnology, Faculty of Science and Technology, Universiti Kebangsaan Malaysia.

I wish to express deep appreciation to my wife and my family members for their support throughout my graduation period. I would like to thank my wonderful friends for their encouragement throughout this work.

I would like to express my deep accolade to UKM-Vice Chancellor scholarship unit for the PhD grant from October 2021 to September 2024 and I am grateful to the Ministry of Higher Education (FRGS/1/2019/STG01/ UKM/02/3) for their financial support.

ABSTRAK

Malaria, sejenis penyakit berjangkit yang merebak secara meluas dan membunuh, masih menjadi masalah kesihatan global. Sememangnya diketahui bahawa *Plasmodium falciparum*a dalah parasit protozoa utama dan berbahaya dalam genus *Plasmodium*. Kajian ini telah menambah senarai penyelesaian yang mungkin dengan menghasilkan kumpulan hybrid pirano[2,3-*c*]pirazol-4-aminokuinolina baharu. Sembilan belas hybrid baharu telah disintesis dengan peratusan hasil antara 10 hingga 49% dengan menghubungkan rangka 4-aminokuinolina dan pirano[2,3-*c*]pirazol secara kovalen melalui penghubung etil dan dicirikan menggunakan spektroskopi inframerah transformasi Fourier (IM) dan spektroskopi resonans magnetik nuklear (RMN). Di antara semua, hasil yang tinggi dapat dilihat untuk hibrid yang mengandungi kumpulan penarik elektron, seperti –CN (**24n**, 49%), –COOH (**24p**, 42%), dan $–NO_2$ (**24j**, 38%) pada kedudukan para bagi gelang fenil yang dicantumkan pada moieti piranopirazola. Kesemua sembilan belas sebatian hibrid telah diuji dalam kajian in siliko sebelum pendokkan molekul, termasuk ramalan fizikokimia dan penyerapan, pengedaran, metabolisme, perkumuhan dan ketoksikan (ADMET), seperti pengikatan plasma protein (PPB), perencatan CYP2C19, sempadan darah-otak (BBB), dan perencatan P-glikoprotein (PgP), untuk saringan awal sifat bak ubat hibrid sebatian. Pendokkan molekul digunakan untuk menguji keupayaan setiap hibrid dan klorokuina (CQ) piawai untuk mengikat kepada enzim laktat dehidrogenase *Plasmodium falciparum* (P*f*LDH), enzim penting dalam laluan glikolitik parasit. Sebatian hybrid mempunyai afiniti pengikatan yang lebih kuat berbanding klorokuina piawai. Selain itu, kajian ini meneroka interaksi antara lima hibrid dan hemin, komponen penting dalam laluan penyaktoksikan heme bagi parasit malaria. Kalorimetri titrasi isoterma (ITC) menunjukkan hybrid mempunyai perbezaan kekuatan dalam mengikat kepada hemin. Ini disebabkan oleh struktur sebatiannya yang berbeza. Hibrid **24a** dan **24g** menunjukkan keafinan yang kuat terhadap hemin dengan nilai Ka $(1.43±0.60)×10^6$ M^{-1} dan $(1.64±0.97)×10^6$ M^{-1}, masing-masing, menunjukkan bahawa mereka mungkin dapat menghentikan proses gangguan. Kajian ini turut menentukan potensi aktiviti antimalarial bagi hybrid pirano[2,3-*c*]pirazol-4-aminokuinolina. Kesemua hybrid ini telah menunjukkan interaksi yang baik dengan P*f*LDH dan hemin serta membuka peluang untuk membangunkan strategi terapeutik baru terhadap malaria. Ujian skizon antimalaria bagi sebatian hybrid pirano[2,3-*c*]pirazol-4-aminokuinolina menunjukkan bahawa kesemua Sembilan belas sebatian hybrid adalah poten dengan julat nilai IC_{50} antara 0.0151 hingga 0.301 μM terhadap strain *P. falciparum* 3D7 yang sensitif terhadap CQ, dan juga didapati aktif terhadap strain *P. falciparum* K1 yang tahan terhadap CQ dengan julat nilai IC_{50} antara 0.01895 hingga 2.746 μM. Kesemua sebatian hibrid yang diuji didapati kurang poten berbanding dadah standard Klorokuina dipaspate (CQDP) terhadap strain 3D7 yang sensitif terhadap CQ. Sebaliknya, Sembilan daripada kesembilan belas hibrid (**24d**, **24g**, **24h**, **24i**, **24l**, **24n**, **24o**, **24r**, dan **24s**) menunjukkan aktiviti antimalaria yang lebih baik daripada CQDP terhadap strain *P. falciparum* K1 yang tahan terhadap CQ. Antara semua hibrid yang diuji, **24c** terhadap strain 3D7 dan **24h** terhadap strain K1 terbukti menjadi agenanti malarial yang berpotensi dengan nilai IC_{50} masing-masing 0.0151 dan 0.01895 μM. Kesimpulannya, sintesis hybrid pirano[2,3-*c*]pirazol-4-aminokuinolina telah berjaya memperkenalkan entity kimia baharu yang berpotensi untuk mempamerkan aktiviti antimalarial yang

poten. Ini boleh menyumbang kepada menangani cabaran berterusan rintangan dadah dalam rawatan malaria.

ABSTRACT

Malaria, an infectious disease that spreads widely and can kill people, is still a problem for global health. It is known that the *Plasmodium falciparum* is the major and dangerous protozoan parasite in the *Plasmodium* genus. This study adds to the list of possible solutions by making a group of new pyrano[2,3-*c*]pyrazole-4-aminoquinoline hybrids. Here, nineteen novel hybrids were synthesized with a percentage yield of 10 to 49% by covalently linking the scaffolds of 4-aminoquinoline and pyrano[2,3-*c*]pyrazoles *via* an ethyl linker and characterized using Fourier transform infrared spectroscopy (FTIR) and nuclear magnetic resonance spectroscopy (NMR). Among all, high yields were observed for hybrids containing electron-withdrawing groups, such as –CN (2**4n,** 49%), –COOH (2**4p,** 42%), and –NO_2 (2**4j,** 38%) at the *para* position of the phenyl ring attached to the pyranopyrazole moiety. All the nineteen hybrid compounds were subjected to *in silico* studies prior to molecular docking, including physicochemical and absorption, distribution, metabolism, excretion, and toxicity (ADMET) predictions, such as protein plasma binding (PPB), inhibition of CYP2C19, blood-brain barrier (BBB), and inhibition of P-glycoprotein (PgP), to pre-screen the drug-like properties of the hybrid compounds. Molecular docking was used to test each hybrid's and standard chloroquine's ability to bind to *Plasmodium falciparum* lactate dehydrogenase enzyme (*Pf*LDH), an important enzyme in the parasite's glycolytic pathway. The hybrid compounds had a stronger binding affinity than the standard chloroquine (CQ). Additionally, the study explored the interaction between five hybrids and hemin, a pivotal component in the heme detoxification pathway of malaria parasites. The isothermal titration calorimetry (ITC) showed that the hybrids had different strengths when binding to hemin. This was because their structures were different. Hybrids **24a** and **24g** showed a strong affinity for hemin with *Ka* values of $(1.43\pm0.60)\times10^6$ M^{-1} and $(1.64\pm0.97)\times10^6$ M^{-1}, respectively, indicating that they might be able to stop the disruption process. This study provides insights into the promising antimalarial properties of pyrano[2,3-*c*]pyrazole-4-aminoquinoline hybrids. It details their interactions with *Pf*LDH and hemin and offers potential avenues for developing novel therapeutic strategies against malaria. The schizontical antimalarial test of pyrano[2,3-*c*]pyrazole-4-aminoquinoline hybrid compound shows that all nineteen hybrid compounds were potent with the IC_{50} values ranging from 0.0151 to 0.301 μM against the CQ-sensitive 3D7 *P. falciparum* strain, and were found to be active against the CQ-resistant K1 *P. falciparum* strain with the IC_{50} values ranging from 0.01895 to 2.746 μM. All the tested hybrid compounds were less potent than the standard drug Chloroquine dipaspate (CQDP) against the CQ-sensitive 3D7 strain. In contrast, nine of the nineteen hybrids (**24d**, **24g**, **24h**, **24i**, **24l**, **24n**, **24o**, **24r** and **24s**) displayed superior antimalarial activity than the CQDP against the CQ-resistant K1 *P. falciparum* strain. Among all the tested hybrids, **24c** against the 3D7 strain and **24h** against the K1 strain were the most promising antimalarial agents with 0.0151 and 0.01895 μM of IC_{50} values, respectively. In conclusion, the synthesis of pyrano[2,3-*c*]pyrazole-4-aminoquinoline hybrids introduces new chemical entities that have the potential to exhibit potent antimalarial activity. This could address the ongoing challenge of drug resistance in malaria treatment.

TABLE OF CONTENTS

LIST OF TABLES

LIST OF ILLUSTRATIONS

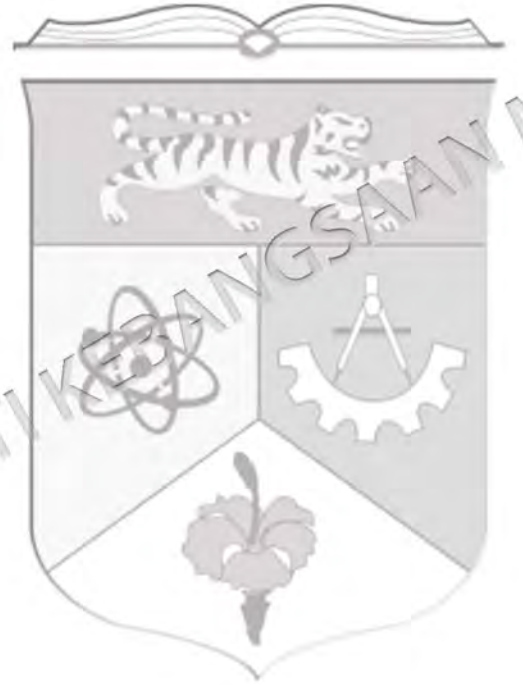

LIST OF ABBREVIATIONS

ADMET	Absorption, Distribution, Metabolism, Excretion, and Toxicity
ATCC	American Type Culture Collection
AQ	Amodiaquine
Å	Angstrom
ART	Artemisinin
ACT	Artemisinin-based Combination Therapy
Ka	Association constant
ABC	ATP-binding Cassette Transporters
BBB	Blood-brain Barrier
^{13}C	13-Carbon
CeiTOS	Cell Traversal Protein for Ookinetes and Sporozoites
CNS	Central Nervous System
δ	Chemical shift
CHO	Chinese Hamster Ovarian
CQ	Chloroquine
CQR	Chloroquine Resistant
CQS	Chloroquine Sensitive
CFX	Ciprofloxacin
CADD	Computer-aided Drug Design
J	Coupling constant
^{o}C	Degree Celcius
DNA	Deoxyribonucleic acid
d	Deuterated
DDT	Dichlorodiphenyltrichloroethane
DMSO	Dimethylsulfoxide
d	doublet
ELISA	Enzyme-linked Immunosorbent Assay

FQ	Ferroquine
FDA	Food and Drug Administration
FTIR	Fourier Transform Infrared
Fsp^3	Fraction sp^3
GEST	Gamete Egress and Sporozoites Traversal Protein
g	gram
GUT	Guanylthiourea
Hz	Hertz
HEPES	4-(2-Hydroxyethyl)-1-piperazineethanesulfonic acid
HIV	Human Immunodeficiency Virus
HBA	Hydrogen Bond Acceptor
HBD	Hydrogen Bond Donor
IMR	Institute for Medical Research
ITC	Isothermal Titration Calorimerty
L	Liter
µ	Micro
mg	milligram
MKCs	Minimum Killing Concentrations
mol	Mole
MW	Molecular Weight
MVD	Molegro Virtual Docker
MCR	Multicomponent Reaction
m	multiplet
NADH	Nicotinamide Adenine Dinucleotide
NRB	Non-rotational Bonding
NMR	Nuclear Magnetic Resonance
PAINS	Pan-assay Interference Compounds
ppm	Parts per million
%	Percentage

PBS	Phosphate Buffer Saline
PL	Phospholipase
π	Pi
*Pf*DHFR-Ts	*Plasmodium falciparum* Dihydrofolate Reductase-Thimidylate synthetase
*Pf*DHODH	*Plasmodium falciparum* Dihydroorotate Dehydrogenase
*Pf*LDH	*Plasmodium falciparum* Lactate Dehydrogenase
PES	Poly Ether Sulfone
PQ	Primaquine
^{1}H	Proton
PDB	Protein Data Bank
PPB	Protein Plasma Binding
q	quartet
QN	Quinine
RI	Resistance Index
RPMI	Roswell Park Memorial Institute
SI	Selectivity Index
s	singlet
SMILES	Simplified Molecular Input Line Entry System
SAR	Structure Activity Relationship
SP	Sulfadoxine-pyrimethamine
SDF	Symyx Spatial Data File
TLC	Thin-layer Chromatograph
TPSA	Total Polar Surface Area
PTA	1,3,5-Triaza-phosphaadamantane
t	triplet
WHO	World Health Organization

CHAPTER I

INTRODUCTION

1.1 MALARIA DISEASE

Malaria is a deadly disease transmitted through mosquito bites (Anopheles). *Plasmodium* protozoa cause the sickness, which can be fatal (Birkholtz et al. 2012). Five species of the *Plasmodium* genus causing the disease are *Plasmodium vivax, Plasmodium malariae, Plasmodium falciparum, Plasmodium ovale* and *Plasmodium knowlesi* (Gildenhard et al. 2019; Manohar & Khan & Rawat 2010). It has been reported that *Plasmodium falciparum* is a significant and dangerous protozoan parasite in the *Plasmodium* genus (Hasan et al. 2015) and is responsible for the majority of deaths and accounts for almost 99% of cases in Africa and 63% in Southeast Asia (Tibon & Ng & Cheong 2020). Malaria symptoms include chills, fever, tiredness, diarrhoea, vomiting, and abdominal discomfort. Sometimes the clinical signs worsen, resulting in kidney failure, convulsions, and contractions, respiratory edoema, and circulatory system shutdown, eventually leading to coma and death. Furthermore, malaria caused by *Plasmodium vivax* and *Plasmodium ovale* causes disease relapses after months to years since these species remain dormant in the human liver as hypnozoites (Kaur et al. 2009).

According to the World Health Organization's (WHO) Malaria Report for 2023, there are over 249 million malaria cases and over 608,000 fatalities in 2022 (World Malaria Report 2023). According to the research, the African region has had a high burden of malaria in recent years and continues to have a high number of cases and deaths. In 2022, the African continent was responsible for more than 90% of malaria infections and deaths. Nigeria (26.8%), the Democratic Republic of the Congo (12.3%), Uganda (5.1%), Mozambique (4.2%), Angola (3.4%), the United Republic of Tanzania (3.2%), Burkina Faso and Mali (3.2% each) accounted for more than half of all malaria

cases globally (Figure 1.1). Children under the age of five accounted for more than 78% of all malaria deaths worldwide. Tropical and subtropical countries counting Malaysia are also affected by this disease.

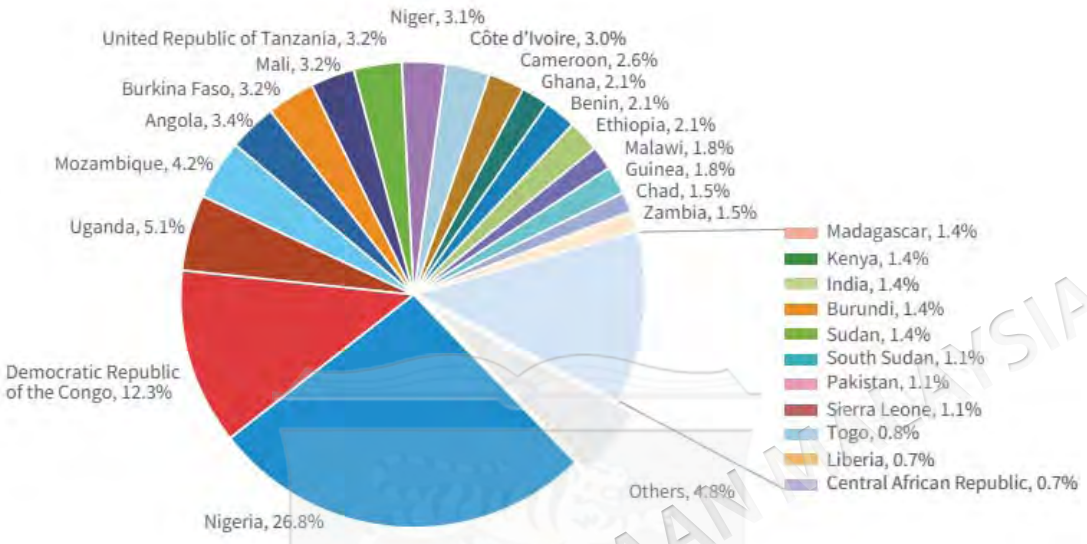

Figure 1.1 Global trends in distribution of malaria cases by country

Source: World Malaria Report 2023

Since the establishment of the Malaria Eradication Program in Malaysian Borneo in 1961 and in Peninsular Malaysia in 1967, Malaysia has observed a significant reduction in the human malaria burden (Ministry of Health Malaysia; 2022). Subsequently, Malaysia transitioned into the control phase (from 1980 to 2010), pre-elimination phase (from 2011 to 2015), and elimination phase (in 2016). Malaria incidence in urban Kuala Lumpur is low and has remained consistent since 2005, according to records from the university hospital in Kuala Lumpur from January 2005 to December 2020 (Dian et al. 2021). With the exception of 2015, cases of malaria were documented in every year. In 2018, the highest prevalence was recorded (10.3%; 3/29) (Figure 1.2). Nationwide, Malaria cases reduced to 3688 in 2021, down from 243,870 in 1961 (Ministry of Health Malaysia; 2022).

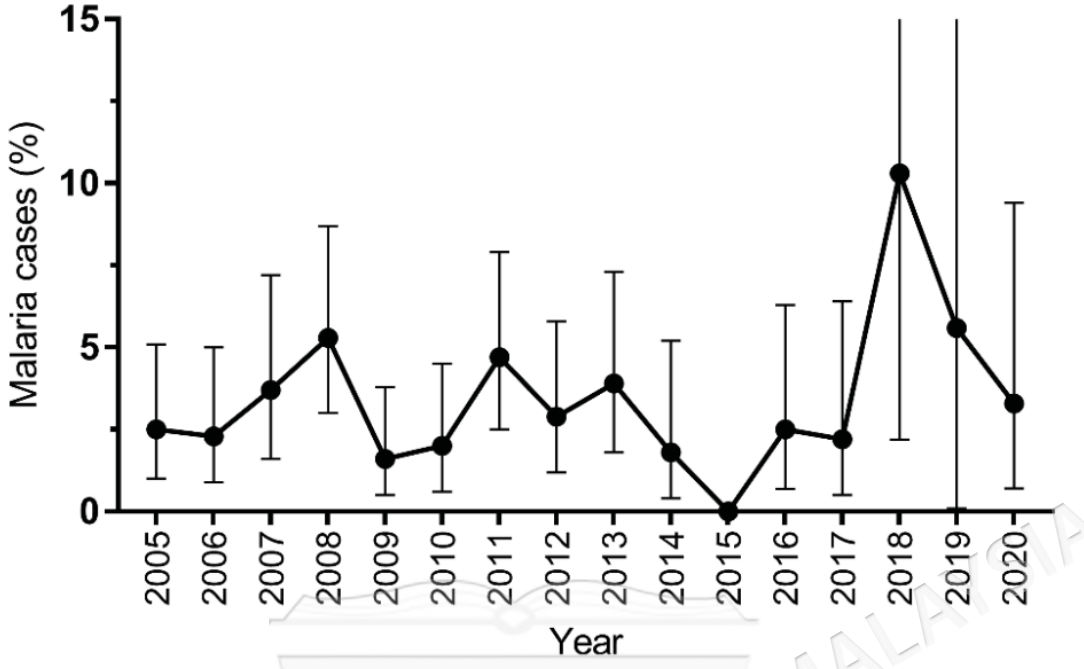

Figure 1.2 Comparative statistics of the number of malaria cases at University Hospital of the National University of Malaysia (UKM) from 2005 to 2020

Source: Dian et al. 2021

Changes in vector habitat are thought to have the ability to alter the transmission of malaria. Changes in the vector habitat, such as temperature, average rainfall, and humidity, can affect the reproduction rate. Mosquito lifespan and blood-sucking rates rose in lockstep with room temperature (Ramasamy & Surendran 2012). Resistance of *P. falciparum* to antimalarial medications such as chloroquine, sulfadoxine, or pyrimethamine exacerbates the condition. Resistance to antimalarial medications refers to the parasite strain's capacity to survive and multiply even after high drug dosages. Many malaria control measures have been implemented, but none have proven effective or cost-efficient. The high cost and difficulty of transporting the drug to the rural areas worsen the problem.

Almost all European countries and the United States succeeded in eliminating malaria through vector management in the early twentieth century by eradicating or eliminating the mosquito from its habitat. Following the discovery of the insecticide Dichlorodiphenyltrichloroethane (DDT), a global malaria eradication program was carried out in the 1950s and 1960s. The Soviet Union, Sri Lanka, and India all contributed to the success of the malaria eradication program. However, global

eradication was not achieved due to the program's high cost, objections from local communities who refused to spray their homes regularly, and the evolution of pesticide resistance. Furthermore, the failure of this programme to eliminate malaria in Western countries resulted in a 25-year loss of global focus on malaria (1970-1996). The drug resistance of *P. falciparum* causes an increase in the fatality rate and the number of malaria cases. A disease becomes more sophisticated when it successfully combats human body's immune system.

Vaccines remain the first defence against malaria without effective chemotherapy (Malaria vaccine 2016). For children in sub-Saharan Africa and other areas with moderate to high *P. falciparum* malaria transmission, the World Health Organisation (WHO) recommends the widespread use of the RTS,S/AS01 (RTS,S) malaria vaccine. The recommendation is based on results from an ongoing pilot programme in Ghana, Kenya and Malawi that has reached more than 900,000 children since 2019 (World Malaria Report 2021). However, reports of chloroquine-resistant *plasmodium* strains hampered this initial line of defence (Narasimhan 2003; Nuwaha 2001; Wellems & Plowe 2001). As a result, artemisinin and its derivatives have become an important component in malaria treatment (Gamo et al. 2010; Wells & Hooft van Huijsduijnen & Van Voorhis 2015; Yeung et al. 2004). This class of drugs was thought to be the only one capable of treating multi-drug-resistant clones of malaria. Given the recent reports of resistance on 21st-century antimalarial "stars" artemisinin and its derivative, the current state of antimalarial therapy is extremely concerning (Agarwal et al. 2015; Miotto et al. 2013; Sahu & Walker & Tekwani 2014; Talundzic et al. 2015; Teixeira et al. 2014; Whit 2010).

The main reasons for the failure of existing therapy can be summarised as follows (Figure 1.3): (i) Traditional medications result from haphazard discovery rather than rationally designed molecular target-based research methodologies. For example, Fidock et al. (2004) discovered the antimalarial potential of natural products such as artemisinin and quinine; (ii) a lack of structural diversity among currently used antimalarial drugs is a major contributor to the development of cross-resistance and multi-drug resistance; and (iii) increasing evidence of tolerance and reduced efficacy to artemisinin-based combination therapies (ACTs) has been consistently reported in some

countries (Teixeira et al. 2014). These considerations necessitate the prompt identification and development of a new class of antimalarial drugs with unique mechanisms of action for treating resistant parasite strains and lowering morbidity and mortality.

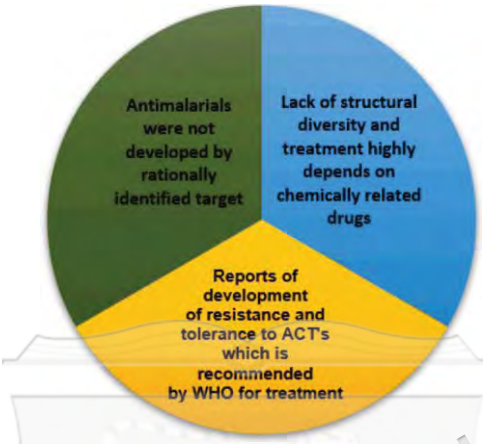

Figure 1.3 Why is there a need to develop a new class of antimalarials?

Source: Rathod et al. 2022

In terms of public health, a cure for malarial diseases aims to reduce the spread of infection to others by reducing the infectious population and spreading resistance to antimalarial medicines. With the aim of progress in the control of malaria, a range of drugs has been utilised, such as 4-aminoquinolines (chloroquine, hydroxy chloroquine, piperaquine, and amodiaquine), 8-aminoquinolines (pamaquine, tafenoquine, aablaquine, and primaquine), 4-amino alcohols (quinine, quinidine, mefloquine, halofantrine, and lumefantrine), endoperoxides (artemisinin, dihydroartemisinin, artesunate, and artemether), antibiotics (doxycycline), antifolates (pyrimethamine, proguanil, and chloroproguanil), napthoquinones (atovaquone), sulfonamides (sulfadoxine and dapsone), and other antimalarial drugs (Figure 1.4) (Okombo & Chibale 2018; Vangapandu et al. 2007). These conventional first-line antimalarial drugs are extremely effective against susceptible malaria parasites. However, their potency is steadily fading as parasites gain resistance to all currently used antimalarial drugs (Figure 1.5).

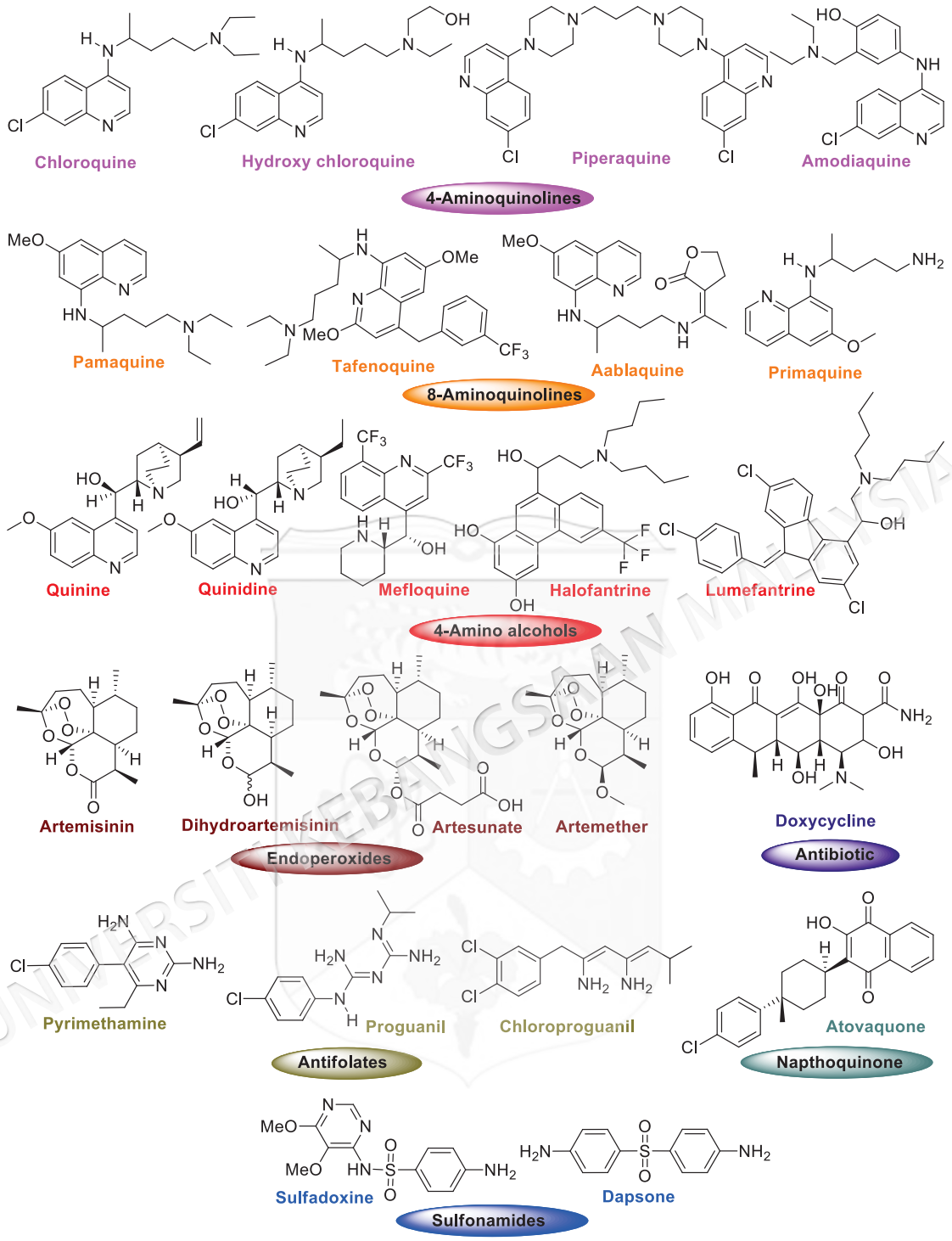

Figure 1.4 Various chemical classes of the clinically used antimalarial drugs

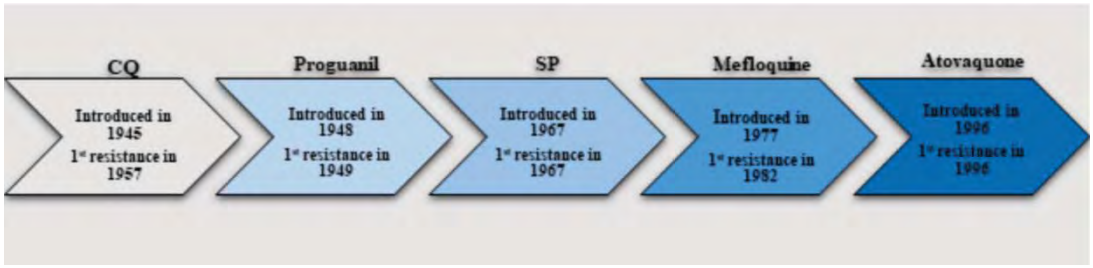

Figure 1.5 Timeline showing the interval between the discovery and development of resistance to the existing antimalarial drugs

Source: Rathod et al. 2022

Despite these drugs, the development of resistance (Singh et al. 2019), particularly to front-line treatments such as artemisinin-based combination therapy (ACT), is concerning, as there are no other options for more effectively treating malaria (Poonam et al. 2018). As a result, it is essential to develop novel, inexpensive, and promising antimalarials with exceptional potency against drug-resistant and drug-sensitive *Plasmodium*, as well as antimalarials that can act on dual-stage and multistage parasite life cycles (Alonso & Tanner 2013; Alven & Aderibigbe 2019; Ashley & Phyo & Woodrow 2018; Kumar et al. 2018). Morphy and Rankovic (2005) and Meunier (2008) proposed the concept of hybrid drugs and hypothesised that they could overcome drug resistance issues.

1.1.1 4-Aminoquinolines as Antimalarial Agents

Out of a wide variety of *N*-heterocyclic compounds used for antimalarial treatment (Faheem et al. 2022; Kalaria & Karad & Raval 2018), a quinoline bycyclic is an efficient moiety in the 21st century (Marinho et al. 2021; Roy et al. 2021; Uddin et al. 2021). Because of its simple chemistry, ease of synthesis, and wide variety of biological applications in both natural and synthetic derivatives, this scaffold is regarded as a biologically relevant active source with several therapeutic potentials including antimalarial (Fan et al. 2018; Firestone et al. 2021; Kucharski & Jaszczak & Boratyński 2022), antiparasitic (Kaur et al. 2010), antioxidant (Abdi et al. 2021), antituberculosis (Shruthi et al. 2019), antiprotozoal (Dorababu 2021), anticonvulsant (Pawar et al. 2017), anticancer (Kamath et al. 2016), antimicrobial (Adeleke et al. 2021), anti-inflammatory (Bekhit et al. 2022), antileishmanial (Costa et al. 2020), anti-analgesic (Bekhit et al. 2022), and antiviral (Kaur & Kumar 2021). Despite reports of resistance to quinoline-

based drugs that act on heme, they are still being used as lead compounds for the development of novel antimalarial drugs (Sashidhara et al. 2012; Vandekerckhove & D'Hooghe 2015), because resistance to this class of drugs is compound specific rather than target-oriented (Payne 1987). Some of the marketed drugs related to quinoline moiety are shown in Figure 1.6.

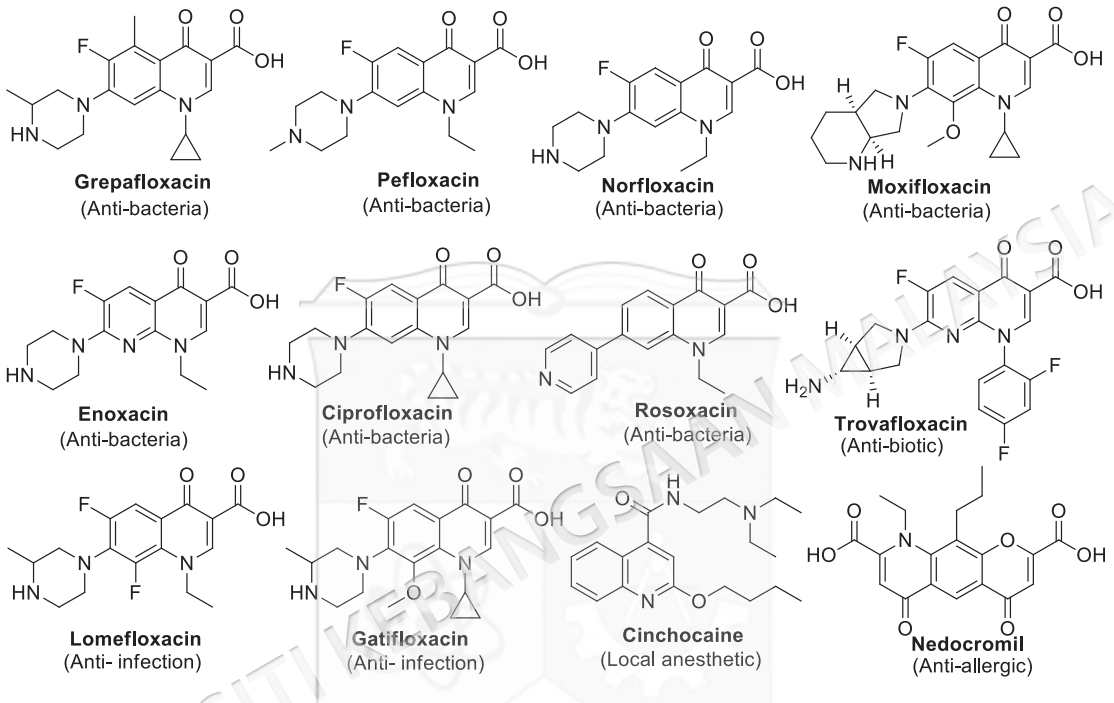

Figure 1.6 Marketed drugs based on quinoline moiety

For decades, aminoquinoline has been utilised as a quinoline scaffold in malaria drug research (Coban 2020; Lawrenson et al. 2018; Zhou et al. 2020). Quinine (QN), derived from Cinchona bark, was first used to treat malaria, followed by other quinoline synthetic derivatives such as primaquine (PQ) and chloroquine (CQ). Pamaquine, the first synthetic 8-aminoquinoline-based antimalarial drug, was developed in 1925 and had greater efficacy than QN. However, due to toxicity concerns, it was eventually discontinued and replaced by 8-aminoquinoline medicines such as aablaquine, bulaquine, pentaquine, quinocide, tefnoquine, and PQ (Crockett & Kain 2007; Fernando & Rodrigo & Rajapakse 2011). CQ, a 4-aminoquinoline, was first chemically synthesised in 1934 as a substitute for QN and has been the mainstay of malaria chemotherapy for about five decades, with advantages such as low cost, fewer side effects than QN, limited toxicity, and excellent clinical profile (Loeb et al. 1946). Amodiaquine (AQ) was found as an alternative to CQ in 1948; however, it was

eventually removed from the market due to adverse effects and host toxicity concerns (Gil 2008). Furthermore, using CQ and AQ as lead compounds, many novel 4-aminoquinoline medicines with increased antimalarial potency and lower toxicity were created, including piperaquine, isoquine, amopyroquine, tebuquine, and hydroxychloroquine. Both 8-aminoquinoline (Leven et al. 2019; Mahmud & Shallangwa & Uzairu 2020) and 4-aminoquinoline (Nqoro & Aderibigbe 2020) chemicals are crucial and often used to treat malaria because of their low cost, ease of synthesis, ease of use, and low toxicity. The United States Food and Drug Administration (FDA) have approved using 4-aminoquinoline to treat malaria (World Malaria Report 2020). The history of the quinoline antimalarial drugs is shown in Figure 1.7.

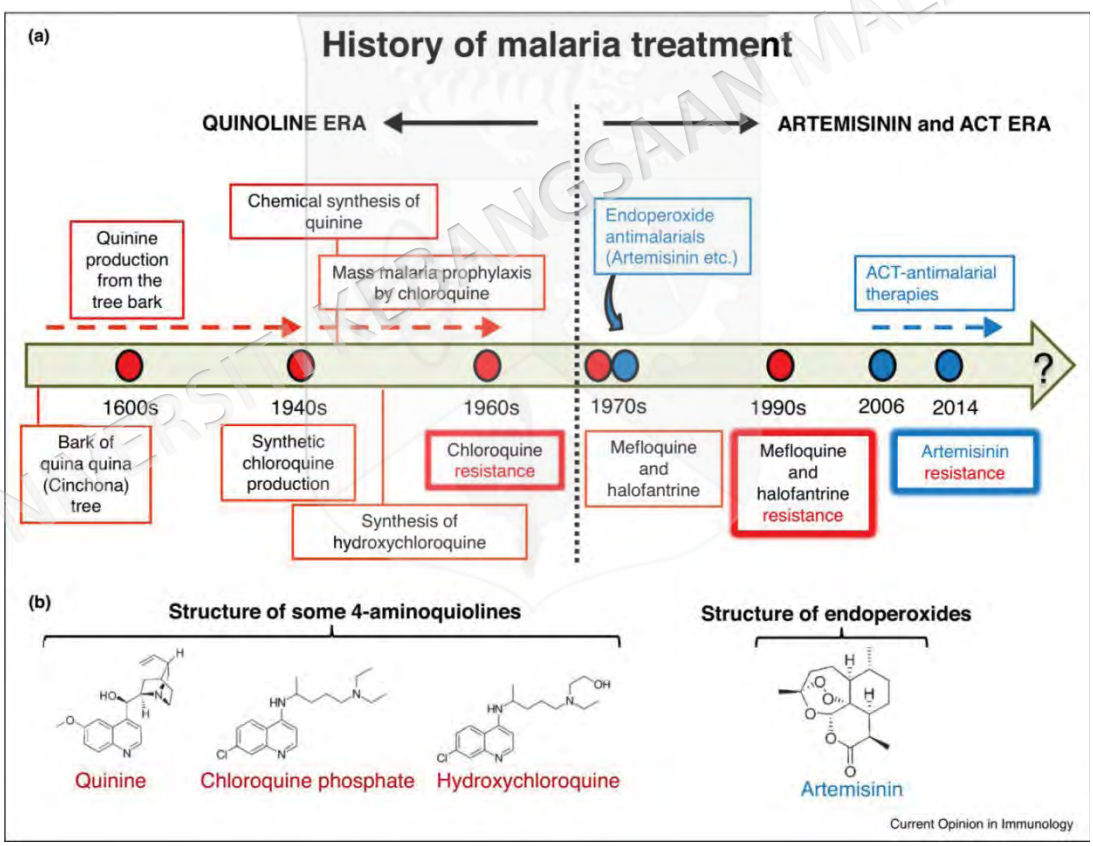

Figure 1.7 History of Malaria Treatment

Source: Coban 2020

According to structure-activity relationship (SAR) results on 4-aminoquinoline moiety, the 7-chloro and 4-amino groups in quinolines are crucial for high-affinity binding to hematin and act by interfering with the parasite feeding process. This is why

the 4-aminoquinoline derivatives are still valuable for malaria drug discovery. The 4-aminoquinoline compound is critical and often employed to treat malaria because of its easy synthesis, easy utilization, and low cost (Manohar et al. 2012). SAR studies on 4-aminoquinoline derivatives suggest that 4-amino and 7-chloro groups are essential for haemozoin inhibition and aid drug accumulation in the parasite's acidic food vacuole (Pandey et al. 2001). The antimalarial activity is diminished when the 4-amino group is replaced with S or O, and the 7-chloro group is replaced with Br, $-OCH_3$, $-CH_3$, or $-CF_3$. The tertiary nitrogen on the side chain and the ring nitrogen of 4-aminopyridine are important for activity because they allow the drug to accumulate in the parasite cell after protonation. Furthermore, the optimal carbon chain length ranges between 2 and 3, allowing the compounds to preserve antimalarial efficacy against CQ-resistant *P. falciparum* (De et al. 1998). Figure 1.8 depicts a compilation of major SAR observations of 4-aminoquinolines (Manohar et al. 2014) based on activity versus CQ-resistant.

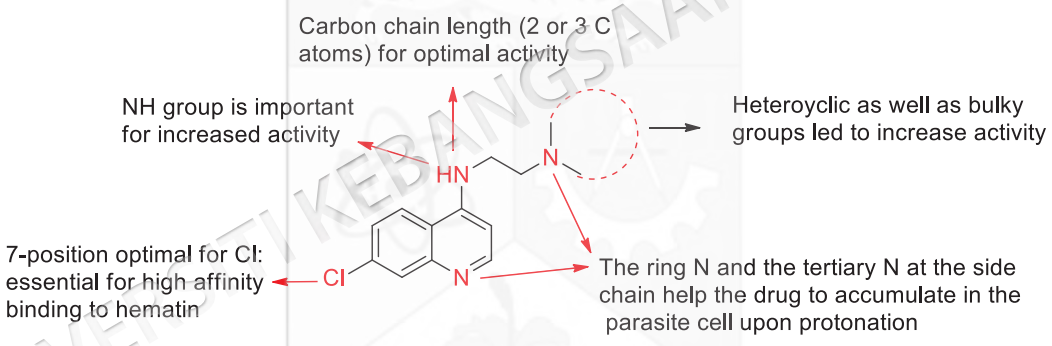

Figure 1.8 Summary of significant SAR observation of 4-aminoquinoline derivatives

Source: Manohar et al. 2014

1.1.2 Pyrano[2,3-*c*]pyrazoles as an Important Class of Heterocycles

On the other hand, pyrano[2,3-*c*]pyrazoles are broadly studied and highly explored and play an important role in pharmaceuticals. It displays diverse appealing biological activities including antimalarial (Witschel et al. 2015; Shamsuddin et al. 2020; García-Cañaveras et al. 2021; Biswas & Das 2022), anti-inflammatory (Mandha et al. 2012), antimicrobial (Mistry et al. 2012), anti-fungicidal (Ramiz et al. 2012), anticancer (Wang et al. 2009), inhibitors of human Chkl kinase (Foloppe et al. 2006), vasodilator (Ahluwalia & Dahiya & Garg 1997), analgesic (Kuo & Huang & Nakamura 1984) as well as biodegradable agrochemical (Kiyani et al. 2013) (Figure 1.9). Because of

potential biological activities and extensive synthetic utilities, functionalised pyrano[2,3-*c*]pyrazole derivatives have gained significant attention as an important class of heterocycles in organic synthesis and the pharmaceutical industry (Guo et al. 2013). It has attracted researchers to explore this moiety by making modifications at various possible positions.

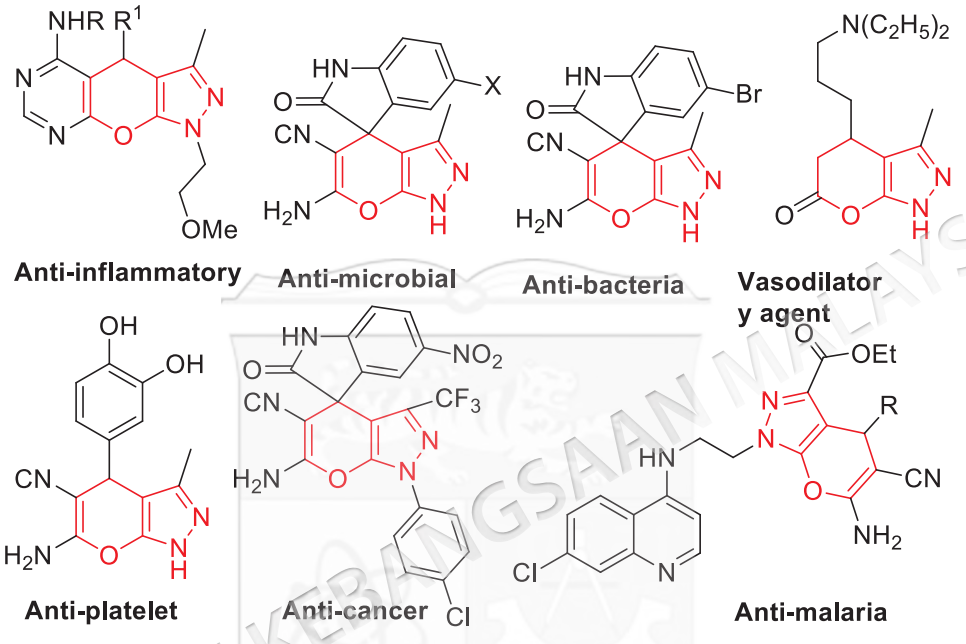

Figure 1.9 Biologically active pyrano[2,3-*c*]pyrazoles

The approach to drug design was used in the twentieth century with the concept of "one-target-one-drug" to discover novel drugs. However, this technique is still ineffective in treating a variety of diseases, including cancer, diabetes, and cardiovascular disease. In recent years, molecular hybridisation has become an important tool for biochemists in drug development. This molecular hybridisation involves covalent connections between two or more pharmacophores, each with antimalarial action. The resulting molecular hybrid may be no better than the parent drug in terms of efficacy.

1.1.3 *In Silico* Molecular Docking Study Methods

The complexity of every disease can be unravelled with the presence of *in silico* studies to see if the protein structure of the disease can be seen. Advances in biological

structuring provide many opportunities for computational biologists to design drug molecules with better biological activity and fewer side effects.

Molecular docking is the most well-known method for structure-based drug design. Molecular docking is a computational platform that maps ligands to proteins' 3D structures, resulting in stable complexes. Molecular docking has different uses and values in drug discovery and protein structure-activity investigations (Morris & Wilby 2008). This docking method examines the position of the drug binding to the protein to evaluate the drug's binding affinity and activity. Using a docking score system, a good binding site can predict the strength or affinity of the interaction between the ligand and the protein (Figure 1.10).

Molecular docking is the process by which two molecules engage with one another. Interaction forces can be classified into four types: electrostatic forces, electrodynamic forces, steric forces, and solvent-based forces. There are four necessary phases in molecular docking. The first step is to prepare the protein structure, which can be obtained from the Protein Data Bank (PDB). This structure must first be treated to remove water molecules from the protein, stabilise the charge, and generate side chains. The next step is to identify the active site on the processed protein. Next, ligands collected from various databases, such as ZINC and Pub Chem, can be prepared using ChemDraw software. Finally, the ligand and protein will be docked, and all interactions will be analysed using a docking scoring method.

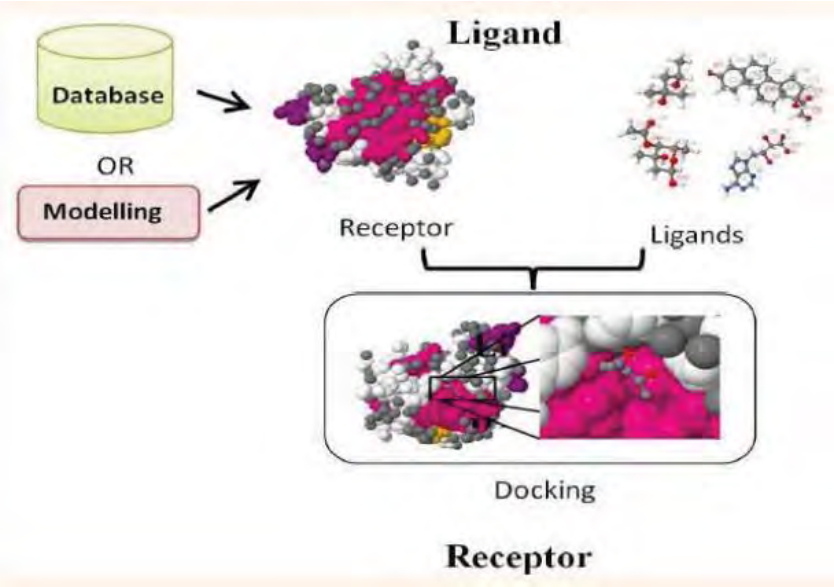

Figure 1.10 Flow chart of docking process between ligand and protein

Source: Chaudhary & Mishra 2016

The main goal of this molecular docking is to determine the molecular process using computer simulation and, acquire the ideal orientation to reduce free energy. The presence of contemporary bioinformatics information technologies can minimise the time required to develop effective medicines against *Plasmodium* parasites. During molecular docking investigations on *P. falciparum*, ligands bind to binding sites on the 3D structure of *P. falciparum*. Chloroquine, amodiaquine, quinine, and mefloquine compounds had lower affinity binding than the co-crystal structure of nicotinamide adenine dinucleotide (NADH) (Waingeh et al. 2013). The findings of this investigation indicate that all of these ligands are ineffective in suppressing *P. falciparum* because they are insufficient to be competitive inhibitors.

1.1.4 *In Vitro* Antimalarial Study Methods

Progress in malaria parasite culture is critical for understanding their biochemical, biological, immunological, and pharmacological features. The percentage of blood cells infected by the parasite and the total number of red blood cells in the culture influence the parasite's development and survival in static culture. A high number of parasite-infected blood cells (more than 10%) disrupts the parasite's growth, and only a few strains of parasites that are easy to culture can produce a proportion of parasite-infected blood cells of up to 30%.

In vitro study approaches towards *P. falciparum* have evolved, and several protocols have been utilised in these studies. However, the approach used in the *in vitro* cultivation of *P. falciparum* at the intra-erythrocyte level remains unchanged from that described by Trager and Jensen in 1976. This technique's approach involves the use of 4-(2-Hydroxyethyl)-1-piperazineethanesulfonic acid (HEPES), Roswell Park Memorial Institute (RPMI) culture media, human erythrocytes, and sodium bicarbonate. Several strategies were used to promote the growth of *P. falciparum's* asexual stage.

Plasmodium is a pathogen with a complex life cycle involving female mosquitos and the development of zoites to host cells at each stage. When sporozoites infiltrate the host, they infect hepatocytes and initiate an asexual cycle in the blood. In the early stages, *plasmodium* sporozoites will be injected into the host's dermis during blood-sucking process. At this point, the sporozoite will use gliding motility to reach the blood vessels. The lymphatic system removes and absorbs sporozoites that do not penetrate the host's dermis.

Sporozoites that have successfully entered the host's blood vessels will penetrate the host's liver through the distribution process. Several proteins are required in the distribution process, including SPECT (sporozoite microneme protein essential for traversal), SPECT2 (perforin-like protein 1, PLP1), CeiTOS (cell traversal protein for ookinetes and sporozoites), PL (phospholipase), and GEST (gamete egress and sporozoites traversal protein) (Cowman et al. 2016). The role of all proteins in cell dispersion is unknown. However, SPET2 has a membrane assault complex that punches a hole in the membrane. The sporozoite will then attack the hepatocyte once the host membrane has been penetrated. When a sporozoite is injected into the host's dermis, it is in transfer mode until it encounters a hepatocyte, which switches to attack mode. After infecting hepatocytes, these sporozoites will change stage (exo-erythrocytic) within 10-20 days and release 40,000 merozoites into the bloodstream. When this stage is reached, the liberated merozoites will quickly and dynamically invade the erythrocytes, resulting in cell division. Once the erythrocyte is attacked, cell division occurs in four stages over 48 hours.

Merozoites will target erythrocytes in the first stage and progress through various stages, including pre-invasion, active attack, and ekinocytosis, all within two minutes. Pre-attack is the initial engagement, while active attack involves intense interactions between merozoites and erythrocytes that produce host cell destruction. After the active attack phase, the merozoite membrane fuses with the erythrocyte, ensuring that the parasite accumulates in the erythrocyte. The parasite will lose its organelles (apical complex and surface coating) and transform into trophozoites (loop stage) in the following stage. The parasite will next progress to the schizont stage, when it will copy its deoxyribonucleic acid (DNA) multiple times before undergoing asynchronous mitotic division. Each schizont will produce 16-18 merozoites that will destroy the erythrocyte membrane and spread to normal red blood cells. Figure 1.11 depicts the life cycle of P. falciparum in erythrocytes.

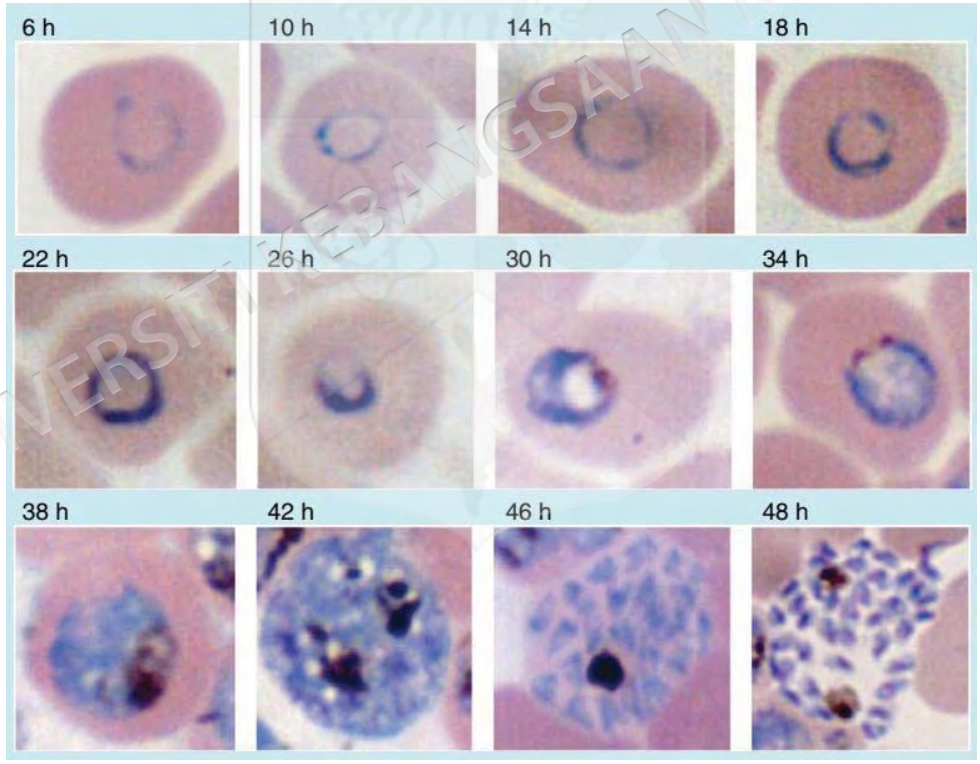

Figure 1.11 The life cycle of *Plasmodium falciparum* in erythrocytes

Source: Radfar et al. 2009

Trager and Jensen (1997) described two basic ways for *growing P. falciparum*: the wax jar approach and the continuous flow method. This wax jar method is utilised for parasites cultured in wax jars, with the culture media changing manually at least

once daily. Certain conditions must be met to promote good parasite growth in the wax jar, including a 3% carbon dioxide level and a 17% oxygen level. In contrast to the continuous flow approach commonly used to culture *P. falciparum*, new culture media are continuously added to ensure good parasite growth. This method is better then wax jars because it is more practical, as changing the media culture does not have to be done daily, and the flow of carbon dioxide gas at 7% and oxygen gas at 5% is continually channelled.

1.2 PROBLEM STATEMENT

Malaria is one of the most severe public health challenges worldwide. The disease is widespread in tropical and subtropical countries such as Indonesia, West Africa, Brazil, and Malaysia. One of the most important challenges in malaria control is the development of drug resistance in malaria parasites. The standard malaria treatment is artemisinin-combination therapy (ACT). Nonetheless, the *Plasmodium parasite's* significant resistance to previous drugs and low ACT efficacy demands fresh drug development. The discovery of effective, innovative, and inexpensive antimalarial drugs is important in fighting drug resistance, and the hybrid drug concept can be utilised to covalently combine two or more active pharmacophores that can act on many targets.

The development of novel antimalarial drugs that target the blood stages of the malaria parasite's life cycle is critical to achieving the goal of malaria suppression. Another method for discovering new metallodrugs is to bind an organic compound with known therapeutic value to a metal-containing fragment. According to SAR examinations on the 4-aminoquinoline scaffold, the 4-amino and 7-chloro groups in quinolines are essential for high-affinity binding to hematin and act by interfering with the parasite-feeding process. This is why the 4-aminoquinoline scaffold is still valuable for malaria drug discovery. Functionalized pyrano[2,3-*c*]pyrazole derivatives are highly explored and broadly studied and have a significant role in pharmaceuticals. Because of extensive synthetic utilities and potential biological activities, pyrano[2,3-*c*]pyrazoles have gained significant attention as an important class of heterocycles in organic synthesis and pharmaceutical industries. As a result, this research will

concentrate on developing pyrano[2,3-*c*]pyrazole-based 4-aminoquinoline derivatives as potential antimalarial agents. We choose pyrano[2,3-*c*]pyrazoles to improve the antimalarial efficacy of 4-aminoquinoline derivatives, by utilising the hybridisation concept.

1.3 RESEARCH OBJECTIVES

This study embarks on the following objectives:

1. To synthesise ethyl linker chain contained pyrano[2,3-*c*]pyrazole-based 4-aminoquinoline hybrids through a one-pot method followed by a nucleophilic substitution reaction.
2. To determine the ADMET properties and examine the molecular docking of synthesised hybrids utilising the *in-silico* approach.
3. To examine the heme detoxification of hybrid compounds.
4. To examine the anti-plasmodial effects of synthesised molecular hybrids utilising *in vitro P. falciparum* CQ-sensitive 3D7 and CQ-resistant K1 Strains.

1.4 RESEARCH SCOPE

The hybridisation of 4-aminoquinoline with pyrano[2,3-*c*]pyrazoles will increase the antimalarial potency of pyrano[2,3-*c*]pyrazole-4-aminoquinoline hybrids since pyranopyrazole derivatives have a wide range of therapeutic applications. Our lab recently reported a successful cascade process for conjugating pyrano[2,3-*c*]pyrazoles and 4-aminoquinoline as molecular hybrids for antimalarial agents. In this study, nineteen various substituted pyrano[2,3-*c*]pyrazoles were functionalised with the -NH of ethyl linker and the effect on antimalarial activity was studied. In this case, functionalising a heterocyclic component at the -NH of the ethyl linker may increase the compound's lipophilicity. All the synthesised hybrids were tested *in vitro* for antimalarial against *P. falciparum* CQ-sensitive (CQS) 3D7 and CQ-resistant (CQR) K1 strains and cytotoxicity against human normal liver WRL68 cell line, followed by molecular docking to predict absorption, distribution, metabolism, and excretion to identify newer targets of action. This study should result in a metabolically stable hybrid pyrano[2,3-*c*]pyrazole-4-aminoquinoline that could be used as a promising antimalarial agent.

CHAPTER II

LITERATURE REVIEW

2.1 METHOD FOR THE SYNTHESIS OF PYRANO[2,3-*C*]PYRAZOLES

Isomeric pyranopyrazole structure includes pyrano[4,3-*c*]pyrazole, pyrano[3,4-*c*]pyrazole, pyrano[2,3-*c*]pyrazole and pyrano[3,2-*c*]pyrazole (Figure 2.1). The formation of pyrano[2,3-*c*]pyrazole derivatives has been developed via different methods of multicomponent reactions (MCRs) either in two-, three- or four-component reactions (Otto & Engberts 2000; Shestopalov et al. 2003; Zonouz & Eskandari & Khavasi 2012). MCRs are considered convergent one-pot reaction protocol involving two or more of simple yet varied substrates to furnish archetypical molecules or complex materials with higher variability. Furthermore, MCR approaches also offered multiple advantages counting the elimination of difficult purification processes, the utility of easily available and flexible building blocks and also solvent and reagent economical purposes (Weber 2002).

Figure 2.1 Structures of isomeric pyranopyrazole

In organic chemistry, multicomponent reaction is one of the best methods for the synthesis of heterocycle compounds (Ivachtchenko et al. 2010). In the past decades, pyrano[2,3-*c*]pyrazoles were synthesized from a two-component type reaction of tetracyanoethylene and 3-methyl-1-phenylpyrazoline-5-one (Junek & Aigner 1973). Subsequently, Otto and Engberts (2000) successfully established a two-component Michael type reaction between malononitrile and 4-arylidiene-1-phenyl-1*H*-pyrazole-5-one catalyzed by a base for the construction of 4-aryl-pyrano[2,3-*c*]pyrazoles.

Furthermore, several research groups revealed that the Michael type of cyclization reaction can also archived smoothly with the aid of weak bases. Conversely, Shestopalov et al. (2003) demonstrated the three-component reaction of malononitriles, pyrazoline-5-ones and piperidin-4-ones catalyzed by a base (TEA) for the construction of spiro-pyrazolopyran derivatives **1** (Figure 2.2).

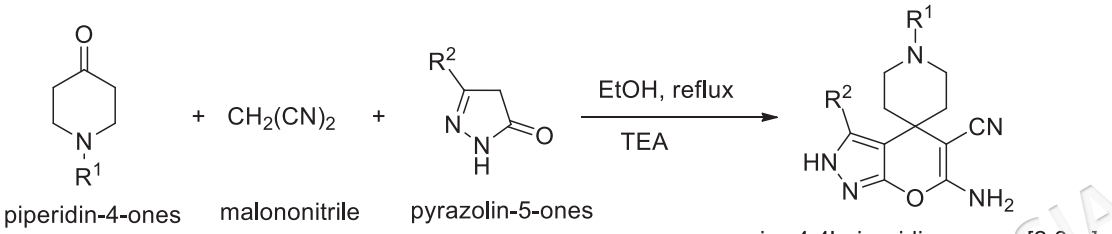

	R^1	R^2	Yield %		R^1	R^2	Yield %
1a.	H	Me	89	**1f.**	Me	Ph	51
1b.	H	Et	58	**1g.**	CH_2CH_2Ph	Me	79
1c.	Me	Me	73	**1h.**	C(O)ME	CH_2OMe	78
1d.	Et	Me	84	**1i.**	C(O)Me	*n*-Pr	65
1e.	Me	CH_2OMe	67	**1j.**	COOEt	CH_2OMe	64

Figure 2.2 Synthesis of spiro-pyrazolopyran derivatives

In pursuit of developing a green and economical synthesis of pyranopyrazole, Sonar et al. (2018) successfully synthesized pyrano[2,3-*c*]pyrazole hybrids **2** through a one-pot three component synthesis. It was reported that the three components used were malononitrile, aromatic aldehyde, and 3-methyl-1*H*-pyrazole-5(4*H*)-one, with triethanolamine as a catalyst (Figure 2.3)

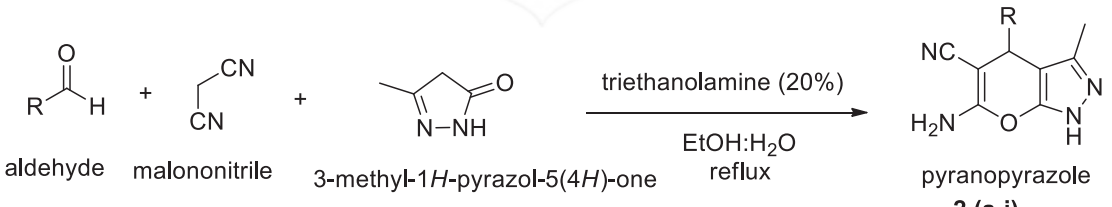

	R	Yield %		R	Yield %
2a.	Ph	90	**2f.**	4-BrPh	92
2b.	4-OHPh	85	**2g.**	4-NO_2Ph	87
2c.	4-OMePh	92	**2h.**	4-$N(Me)_2$Ph	82
2d.	4-FPh	93	**2i.**	2-ClPh	86
2e.	4-ClPh	91	**2j.**	2-furyl	81

Figure 2.3 Triethanolamine catalyzed formation of pyranopyrazoles

In a different progress, Zonouz and Eskandari and Khavasi (2012) successfully developed an efficient method for the four-component reaction of aromatic aldehydes, malononitrile, hydrazine hydrate and dimethyl acetylenedicarboxylate for the construction of 2,4-dihydropyrano[2,3-*c*]pyrazoles-3-carboxylates **3** in water (Figure 2.4).

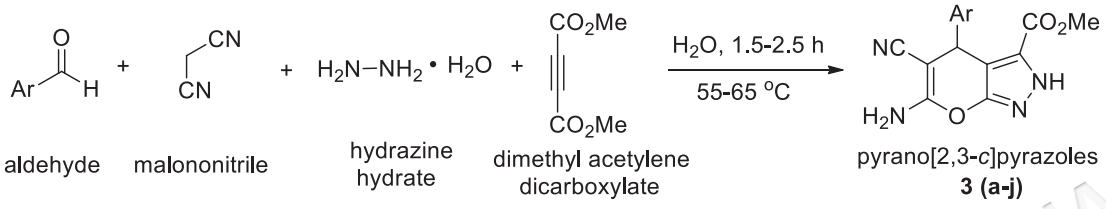

	Ar	Yield %		Ar	Yield %
3a.	Ph	78	**3f.**	2-NO_2Ph	64
3b.	2-MePh	75	**3g.**	3-NO_2Ph	66
3c.	3-MePh	70	**3h.**	4-NO_2Ph	76
3d.	3-BrPh	73	**3i.**	3-OHPh	84
3e.	4-BrPh	75	**3j.**	3-OMePh	75

Figure 2.4 Synthesis of pyrano[2,3-*c*]pyrazole derivatives

Kiyani et al. (2013) synthesized a series of pyrano[2,3-*c*]pyrazole hybrids **4** through the sodium benzoate catalyzed four-component reaction of equimolar amounts of ethyl acetoacetate, malononitrile, aldehyde and hydrazine hydrate in an aqueous medium at room temperature (Figure 2.5). A series of substituted aromatic aldehydes and phenylhydrazines were used to explore the synthesis reaction, which yielded a total of 17 derivatives.

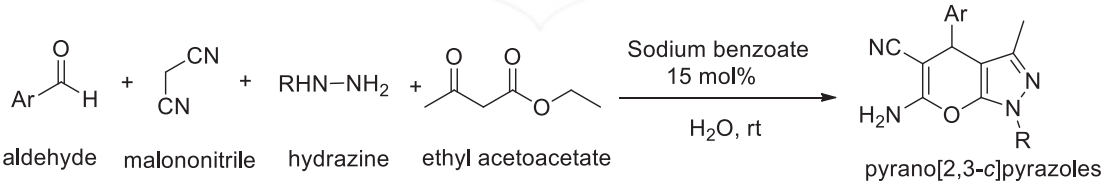

	R	Ar	Yield %
4a.	H	Ph	85
4b.	H	4-OHPh	90
4c.	H	4-OMePh	91
4d.	H	2-NO_2Ph	82
4e.	H	3-NO_2Ph	85
4f.	H	4-NO_2Ph	87
4g.	H	4-MePh	90
4h.	H	2-ClPh	84
4i.	H	3-ClPh	92

	R	Ar	Yield %
4j.	Ph	4-N(Me)$_2$Ph	94
4k.	Ph	Ph	82
4l.	Ph	4-NO_2Ph	83
4m.	Ph	3-NO_2Ph	78
4n.	Ph	4-MePh	84
4o.	Ph	4-OMePh	86
4p.	Ph	4-OHPh	85
4q	Ph	4-ClPh	79

Figure 2.5 Synthesis of pyrano[2,3-*c*]pyrazole derivatives catalyzed by sodium benzoate

Guo et al. (2013) also developed an efficient synthetic method for the construction of diverse pyranopyrazoles **5** by employing ethyl acetoacetate as the β-ketoester via meglumine promoted four-component reaction (Figure 2.6). To date, malanonitriles, aldehydes, β-ketoesters and hydrazines are the most common reagents involved in four-component reactions for the synthesis of pyranopyrazoles.

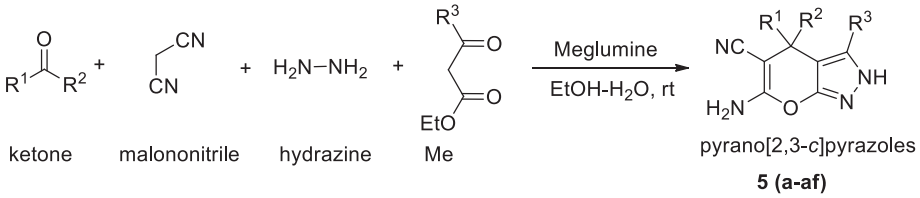

Carbonyl compounds (R^1 and R^2)	R^3	Yield %
5a. PhCHO	Me	95
5b. 2-$OCH_3C_6H_4CHO$	Me	90
5c. 4-$OCH_3C_6H_4CHO$	Me	91
5d. 4-$CH_3(CH_2)_2OC_6H_4CHO$	Me	92
5e. 4-$CH_3(CH_2)_4OC_6H_4CHO$	Me	93
5f. 2-OMe-5-$CHMe_2C_6H_3CHO$	Me	91
5g. 2,3,4-$(OMe)_3C_6H_2CHO$	Me	89
5h. 3-$CH_3C_6H_4CHO$	Me	90
5i. 4-$C(CH_3)_3C_6H_4CHO$	Me	91
5j. 4-$SCH_3C_6H_4CHO$	Me	90
5k. 4-OHC_6H_4CHO	Me	91
5l. 2-FC_6H_4CHO	Me	92
5m. 3-FC_6H_4CHO	Me	91
5n. 4-FC_6H_4CHO	Me	92
5o. 2-ClC_6H_4CHO	Me	90
5p. 3-ClC_6H_4CHO	Me	92

Carbonyl compounds (R^1 and R^2)	R^3	Yield %
5q. 4-ClC_6H_4CHO	Me	95
5r. 2,4-$Cl_2C_6H_3CHO$	Me	92
5s. 2-$NO_2C_6H_4CHO$	Me	92
5t. 4-$NO_2C_6H_4CHO$	Me	93
5u. 3-$CF_3C_6H_4CHO$	Me	94
5v. 4-$CF_3C_6H_4CHO$	Me	94
5w. 4-((4-Nitrobenzyl)oxy)benzaldehyde	Me	93
5x. Furan-2-carbaldehyde	Me	90
5y. Thiophene-2-carbaldehyde	Me	92
5z. Pyridine-4-carbaldehyde	Me	90
5aa. 1-Naphthaldehyde	Me	89
5ab. Decanal	Me	85
5ac. Cyclohexanecarbaldehyde	Me	86
5ad. PhCHO	Et	90
5ae. 4-$OCH_3C_6H_4CHO$	Et	90
5af. 4-ClC_6H_4CHO	Et	92

Figure 2.6 Synthesis of pyrano[2,3-*c*]pyrazoles

A novel synthetic route for the construction of pyrano[2,3-*c*]pyrazoles was accomplished through a domino one-pot, and the four-component reaction of malanonitrile, aldehyde, diethyl oxaloacetate and hydrazine in refluxing acidic ethanolic solution under the non-catalytic system (Gein & Zamaraeva & Kozulina 2014; Mohammat et al. 2018). In the first stage, the reaction between malononitrile and aldehyde will provide arylidenemalonodinitrile, and the simultaneous reaction between diethyloxalacetate sodium salt and hydrazine hydrate will furnish pyrazolone. In the second stage, pyrazolone reacts with arylidenemalononitrile through the Michael reaction to generate an intermediate that will undergo isomerization, followed by Thorpe-Ziegler cyclization to give pyranopyrazoles **6** (Figure 2.7). This procedure was practical, simple, rapid and environmentally friendly as it was carried out in an inexpensive solvent (ethanol) without any catalysts or chromatographic purification methods. It also provided products wiith good yields.

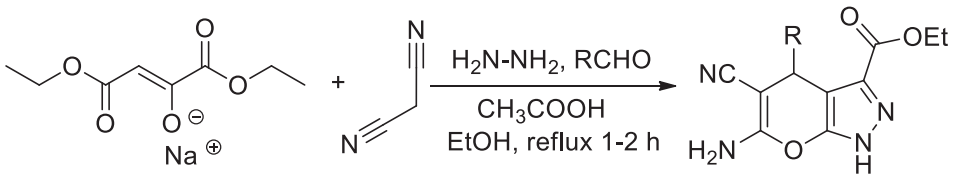

	R	Yield %		R	Yield %
6a.	Ph	82	**6i.**	3-Br-4-OHPh	73
6b.	4-OMePh	65	**6j.**	3-Cl-4-OHPh	50
6c.	4-OEtPh	60	**6k.**	4-CNPh	74
6d.	4-EtPh	69	**6l.**	2-furyl	63
6e.	4-NO_2Ph	75	**6m.**	2-thiophenyl	65
6f.	3-NO_2Ph	83	**6n.**	-CH_2-CHO	90
6g.	4-BrPh	73	**6o.**	*i*Pr-CHO	91
6h.	4-OHPh	57	**6p.**	-$(CH_2)_6$-CHO	11

Figure 2.7 Synthesis of pyrano[2,3-*c*]pyrazole derivatives

Recently, Maarop et al. (2020) synthesized a series of new dihydropyrano[2,3-*c*]pyrazole derivatives with reasonable yields replicating four-component and two-parallel reaction method as demonstrated by Gein and Zamaraeva and Kozulina 2014. However, upon varying the original reaction procedure to domino type reaction manner provided the dihydropyrano[2,3-*c*]pyrazoles up to excellent yields within 30 minutes. A possible reaction mechanism for the construction of pyrano[2,3-*c*]pyrazols was proposed (Figure 2.8). The reaction mechanism was initiated by the condensation reaction between diethyl oxaloacetate salt **7** and hydrazine **8** to generate intermediate A, which then underwent intramolecular nucleophilic cyclization to provide intermediate B. Subsequent dehydration of intermediate B generated the pyrazolone C, which then preceded tautomerization to provide more active enolic pyrazolone D. Subsequently, the Michael-type reaction between the resultant enolic pyrazolone D and pre-synthesized aryl/alkylidene malononitrile E generated intermediate F, which then preceded isomerization to generate compound G. Finally, Thorpe-Ziegler intramolecular cyclization of compound G yielded the final product dihydropyrano[2,3-*c*]pyrazol-3-carboxylates **9**.

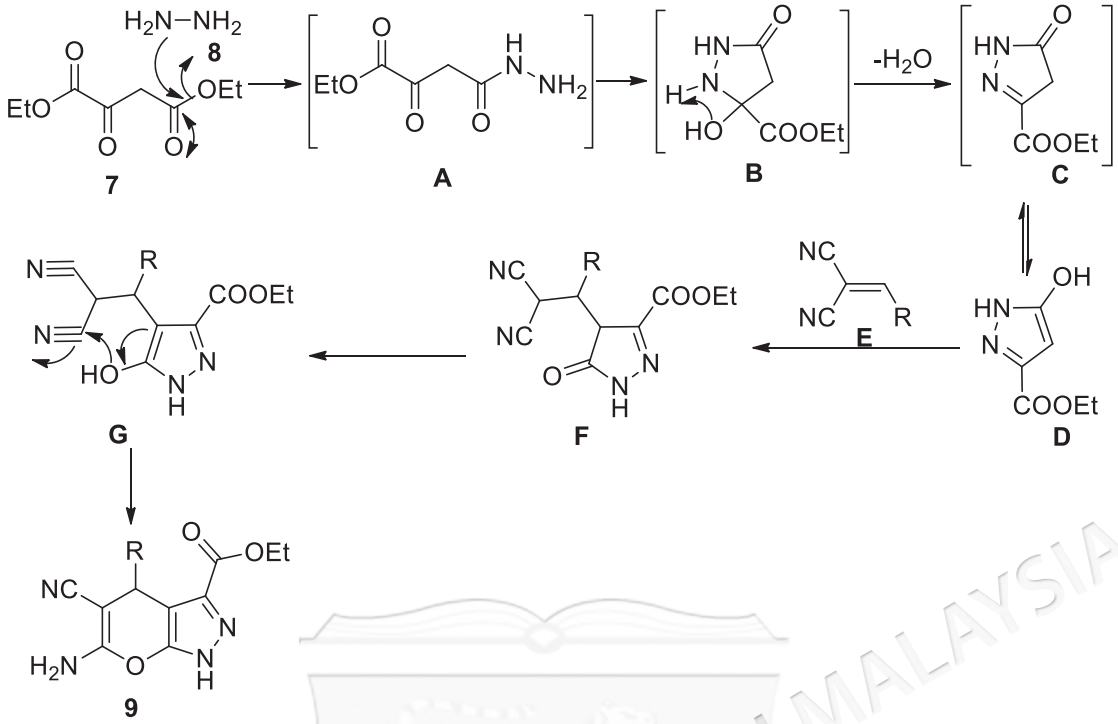

Figure 2.8 Possible reaction mechanism for the construction of pyrano[2,3-*c*]pyrazoles

2.2 METHOD FOR THE SYNTHESIS OF 4-AMINOQUINOLINE DERIVATIVES

Runge (1834) first obtained impure quinoline from coal tar. Later, Gerhardt (1842) obtained it from cinchonine and quinine as a degradation product. Coal tar also contains isoquinoline, alkyl isoquinoline and alkyl quinoline derivatives which are difficult to separate. Furthermore, satisfactory synthetic methods have not progressed for several years. Pure quinoline or benzo[b]pyridine **10** is a weak tertiary base. Several reduced quinoline derivatives are decahydroquinolines **11**, 1,2,3,4- tetrahydroquinoline **12** and 1,2-dihydroquinoline **13**. An important class of 1,2,3,4-tetrahydroquinoline derivatives **12** were commonly synthesized from the corresponding quinoline derivatives through direct reduction. Tin and hydrochloric acid readily reduce the quinoline to 1,2,3,4-tetrahydroquinoline **12**. 1,2-Dihydroquinoline **13** is a colourless solid, readily oxidized to the corresponding aromatic structure. The reduction reaction of quinoline derivatives with sodium in liquid ammonia or lithium aluminium hydride furnished the 1,2-dihydroquinoline derivatives **13**, formed as intermediates in the Skaurp synthesis (Figure 2.9).

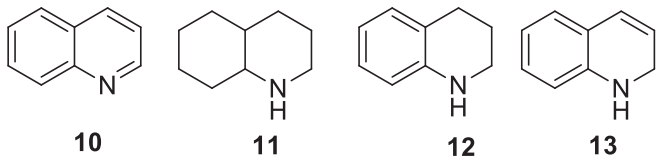

Figure 2.9 Quinoline and its reduced forms

Quinoline is an aromatic heterocyclic organic compound. It has a benzene ring fused with pyridine at two adjacent carbons. The synthetic methodology for constructing chloroquinoline derivatives is shown in Figure 2.10. Initially, 4-quinolinol 14 was transformed to 4-chloroquinoline intermediate **15** by employing the chlorinating agent phosphoryl oxychloride (Mao et al. 2007). The alkyl chain having 2/3/4 carbon atoms was linked to the 4-chloroquinoline **15** by reacting to aminoalcohols (butanolamine/propanolamine/ethanolamine) under the optimal reaction conditions to furnish quinoline aminoalcohol intermediate **16** (Guantai et al. 2011). Then, intermediate **16** was transformed to bromide derivative **17** by employing brominating agent HBr-H_2SO_4 (Cazelles et al. 2007).

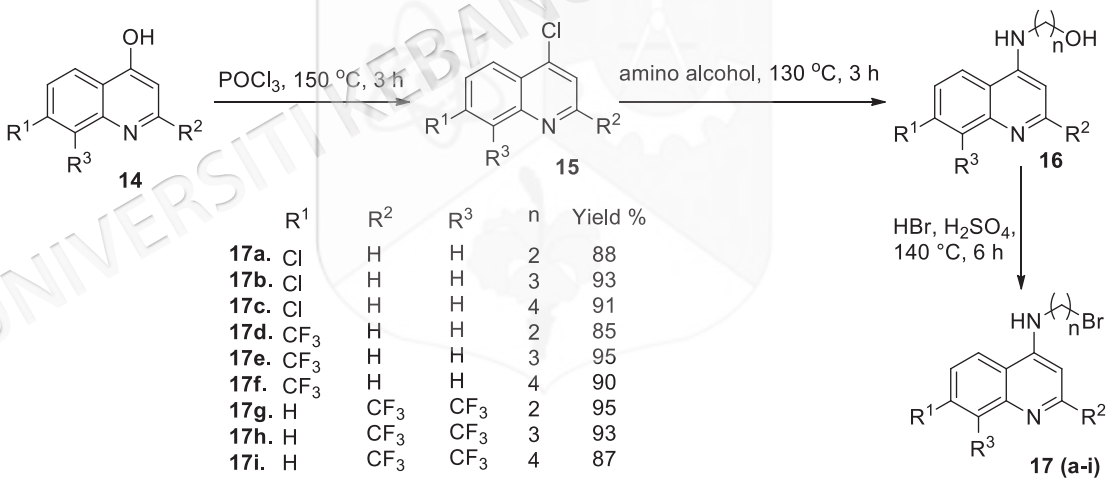

	R^1	R^2	R^3	n	Yield %
17a.	Cl	H	H	2	88
17b.	Cl	H	H	3	93
17c.	Cl	H	H	4	91
17d.	CF_3	H	H	2	85
17e.	CF_3	H	H	3	95
17f.	CF_3	H	H	4	90
17g.	H	CF_3	CF_3	2	95
17h.	H	CF_3	CF_3	3	93
17i.	H	CF_3	CF_3	4	87

Figure 2.10 Synthesis of chloroquinoline derivatives

2.3 METHOD FOR THE SYNTHESIS OF PYRANO[2,3-*C*]PYRAZOLE-4-AMINOQUINOLINE HYBRID COMPOUNDS

Many researchers developed synthetic methods for the construction of various 4-aminoquinoline derivatives hybridised with diverse heterocyclic moieties including artemisinin, adamantane, chalcone, ciprofloxacin, fluorene, guanylthiourea, harmine, imidazole, morpholine, nopol, pyrazoline, phthalimide, pyridine, pyrimidine,

piperidine, piperazine, quinoxaline, thiophene, triazolopyrimidine, triazole, and the metal complex. Widespread resistance of *P. falciparum* to artemisinin-based combination therapy is required to find a novel medicine. Since a wide range of therapeutic applications of pyranopyrazoles, the hybridization of pyrano[2,3-*c*]pyrazole derivatives **20** with 4-aminoquinolines **23** will supposedly enhance the antimalarial efficacy of pyrano[2,3-*c*]pyrazole-aminoquinolines **24**. Currently, a successful procedure for conjugating various pyrano[2,3-*c*]pyrazoles **20** and 4-aminoquinoline **23** as a molecular hybrid for an antimalarial agent was reported by our research group (Shamsuddin et al. 2021) (Figure 2.11).

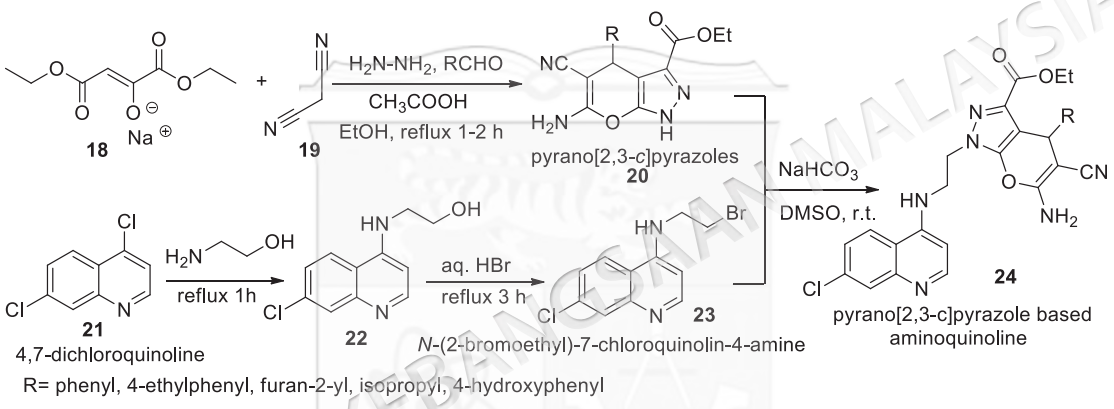

Figure 2.11 Synthesis of pyrano[2,3-*c*]pyrazole based aminoquinolines

A possible reaction mechanism for constructing 4-aminoquinoline-pyrano[2,3-*c*]pyrazole hybrid compounds was proposed (Figure 2.12). Initially, the elimination of acidic proton from the pyranopyrazole upon reaction with bicarbonate base generated the hybrid scaffold intermediate. The subsequent nucleophilic addition of the resultant pyrazolium anion intermediate to the 4-(bromoethylamino)-7-chloroquinoline via S_N2 reaction yielded the 4-aminoquinoline-pyrano[2,3-*c*]pyrazole hybrid. This elegant approach is simple, involving only a few steps to target hybrid molecules.

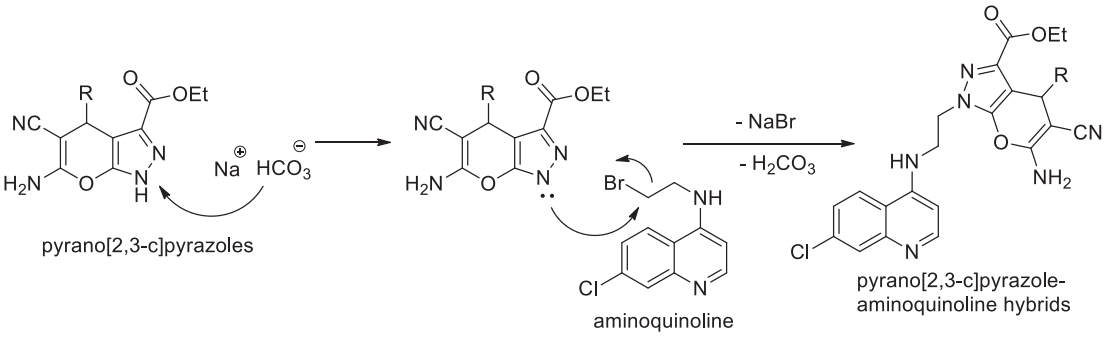

Figure 2.12 Plausible mechanism for the construction of pyrano[2,3-*c*]pyrazole-based aminoquinolines

2.4 *IN SILICO* ACTIVITY OF 4-AMINOQUINOLINE DERIVATIVES

Introducing a bioactive moiety to 4-aminoquinoline can enhance its antimalarial, anticancer, antiviral, and immunomodulatory properties. For example, introducing a pyridine or quinazoline moiety can increase its potency against *P. falciparum*. Introducing aryl or alkylamine moiety to 4-aminoquionilne can increase its potency against cancer cells. However, the same modifications can also lead to increased toxicity, particularly when they are close to other electron-withdrawing groups. However, the toxicity can also be influenced by the compound's physicochemical properties, such as its solubility, lipophilicity, bioavailability, pKa stability, and properties. For example, introducing hydrophilic groups to 4-aminoquinoline hybrids can increase their solubility and bioavailability and lead to decreased lipophilicity and increased toxicity. The solubility of 4-aminoquinoline hybrids is critical for their bioavailability and efficacy. SAR studies have shown that introducing hydrophilic groups, such as amino or hydroxyl groups, can increase the solubility of 4-aminoquinoline hybrids. Poorly soluble compounds can decrease bioavailability and efficacy, while highly soluble compounds can lead to rapid clearance and decreased half-life.

Furthermore, the pKa stability and properties of 4-aminoquinoline hybrids are critical for their biological activity. The pKa value of a compound determines its ionization state and ability to interact with biological targets. Compounds with a pKa value close to physiological pH of 7.4 are more likely to be in the ionized state, which can decrease their cell membrane permeability and decrease their bioavailability. SAR studies have shown that introducing certain bioactive moieties to 4-

aminoquinoline can influence pKa stability. The introduction of an amino group increases its pKa value but decreases its biological activity. Similarly, introducing an electron-withdrawing group, such as a nitro group, can decrease the pKa value but increase the biological activity of 4-aminoquinoline hybrids. Therefore, these hybrids' SAR, toxicity, biological potency and physicochemical properties are complex and dependent on various factors.

Thillainayagam et al. 2014 successfully conducted an *in silico* study on 4-aminoquinoline-chalcone hybrid compounds against *Plasmodium falciparum* lactate dehydrogenase enzyme, *Pf*LDH (PDB ID: 1LDG). In this study, thirty-eight 4-aminoquinoline-chalcon hybrid compounds were docked to *Pf*LDH's active site using SYBYL Surflex-Dock software. Following the docking investigation of these thirty-eight compounds, hybrid **25** revealed a good binding position with the best affinity bond of -161.6 kcal/mol. All hybrids showed the same bonding pattern as hybrid **25**. According to this study, compound **25**'s NH group on the side chain of LYS 267 and the carboxylic acid on the side chain of GLU 256 form two hydrogen bonds with the compound's oxygen and hydrogen atoms. The two hydrogen bonds have interaction bond distances of 2.1 Å and 2.9 Å (Figure 2.13).

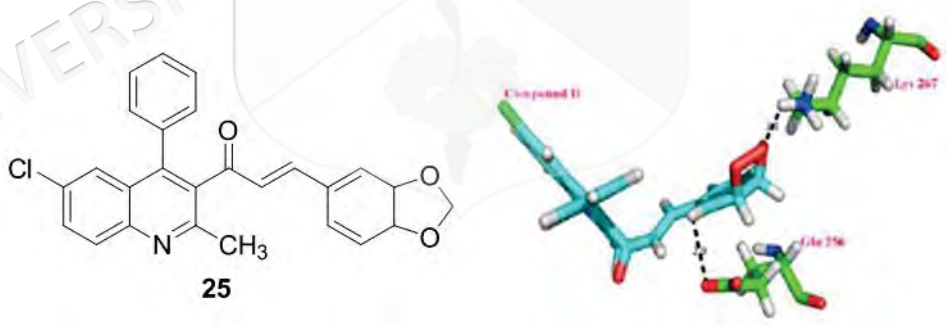

Figure 2.13 Structure of compound **25** and hydrogen bonding interactions at the active site of *Pf*LDH

Several studies have reported the *in silico* analysis of quinoline-derived compounds on *P. falciparum* strains. Cortopassi et al. 2011 conducted in silico studies and docked a quinoline derivative molecule (**26**) coupled to hematin dimer to *Pf*LDH. The Molegro Virtual Docker (MVD) software was utilised in this investigation to dock a chloroquinoline derivative (**26**) with Hematin, resulting in a complex with the *Pf*LDH

strain (PDB ID: 1LDG). The results of this investigation demonstrated that chloroquinoline compound (**26**) produces a lower value, -129.33 kcal/mol, than NADH, which is -241.54 kcal/mol. This study also shows why the complex formed by the interaction of chloroquine (**26**) and hematin has a greater docking value than NADH. This suggests that this compound can compete with NADH and inhibit *Pf*LDH. As a result of this docking investigation, four hydrogen bonds form between the complex compounds with the side chains of LYS 192, THR 101, ALA244, and HIS 243 and the active site of *Pf*LDH (Figure 2.14).

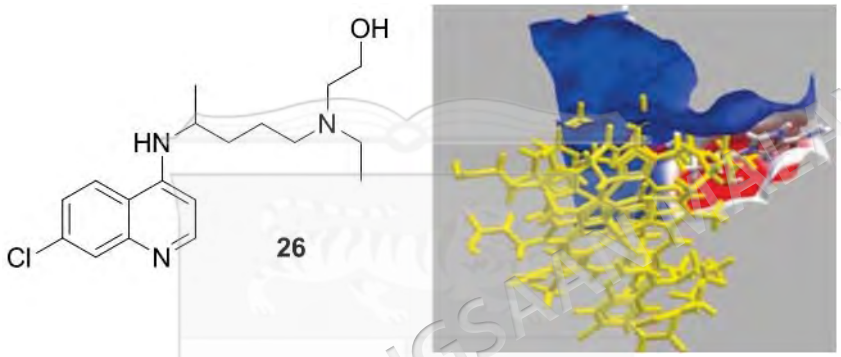

Figure 2.14 Structure of the chloroquinoline compound (**26**) used in the docking process with the active site of *Pf*LDH

The *in silico* method utilised to dock the quinoline hybrid compounds with *P. falciparum* was extensively studied. It allowed researchers to examine the compound's binding site to the protein and estimate its binding affinity and activity. Tripathi et al. 2017 docked a 4-aminoquinoline-pyrimidine hybrid to *P. falciparum* Dihydrofolate Reductase-Thimidylate synthetase, *Pf*DHFR-Ts (PDB ID: 3QG2) using Glide 5.8 software. This work also explains why *P. falciparum* requires Thymidylate Synthetase, a bifunctional enzyme. The findings of this study revealed that compound **27** (9.78kcal/mol) had the greatest docking value at the active site of *Pf*DHFR-Ts. This molecule interacts with the active level, forming two hydrogen bonds with the side chains of LEU 164 and ARG 122 (Figure 2.15).

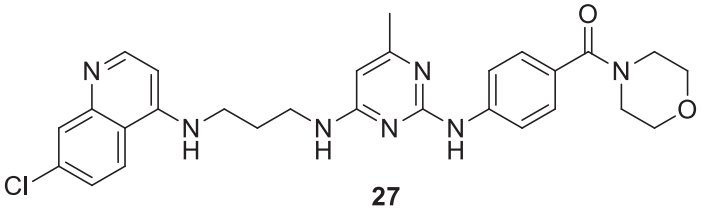

27

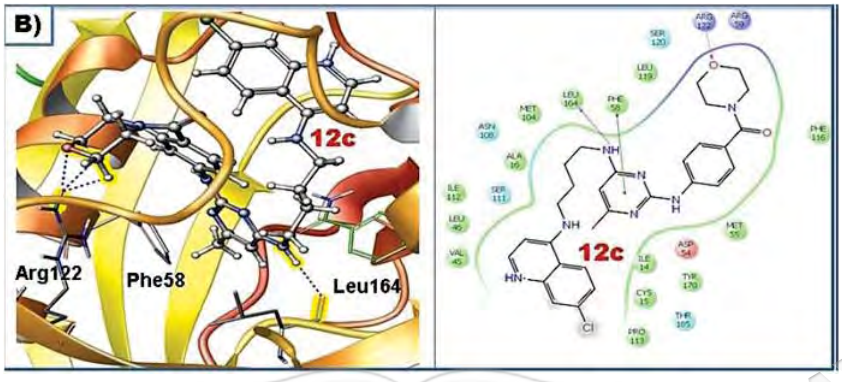

Figure 2.15 The docking position of compound **27** interacts with the active site of *Pf*DHFR-Ts (PDB ID: 3QG2)

2.5 *IN VITRO* ANTIMALARIAL ACTIVITY OF 4-AMINOQUINOLINE DERIVATIVES

For over five decades, 4-aminoquinoline hybrid compounds were the most promising antimalarial drugs available, and their chemistry, molecular docking, SARs, toxicity, and physicochemical properties have been extensively studied. (Bokosi & Ngoepe 2022; Hochegger et al. 2019; Palla et al. 2020; Ramírez et al. 2022; Ravindar et al. 2023; Singh & Chetia & Kumawat 2021).

2.5.1 Quinoxaline-4-aminoquinolines

Bonilla-Ramírez et al. (2018) synthesized a broad range of novel 4-aminoquinoline hybrid compounds having quinoxaline 1,4-di-*N*-oxide pharmacophores. They examined them for antimalarial activity against *P. falciparum* multidrug-resistant (FCR-3) and CQS (3D7) strains by employing CQ (IC_{50} 0.026 μM (3D7) and IC_{50} 0.207 μM (FCR-3)) as a standard drug. All the evaluated hybrids except **28c** showed sub-micromolar activity against the 3D7 clone (IC_{50}< 1 μM), whereas only **28b** and **28e** exhibited IC_{50} in the same range towards the FCR-3 clone. However, no compound performed better potently than standard CQ towards 3D7 and FCR-3 *P. falciparum* clones. All the examined hybrids exhibited low cytotoxicity towards the HepG2 cell line, with CC_{50} values ranging from 21 to 92 μM and only 1-6 times lower than the reference CQ. In

addition, all hybrids displayed high predicted gastrointestinal absorption, and none of the compounds violated either Veber's criteria (i.e., all except **28d** with 10 rotatable bonds) or Lipinski's rule of five (Figure 2.16).

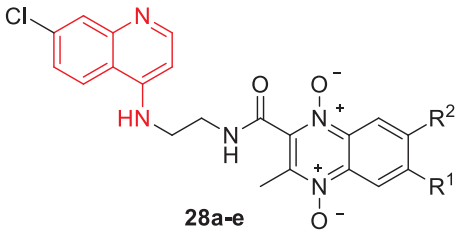

R^1/R^2	3D7 IC_{50} (μM)	FCR-3 IC_{50} (μM)	Cytotoxicity CC_{50} (μM)
a. H/H	0.78 ± 0.20	1.90 ± 0.72	58.22 ± 0.11
b. H/Cl	0.52 ± 0.11	0.40 ± 0.23	21.83 ± 0.28
c. H/OMe	2.11 ± 0.99	2.07 ± 0.12	92.69 ± 2.55
d. H/Me	0.57 ± 0.08	2.24 ± 0.67	31.41 ± 4.43
e. Me/Me	0.68 ± 0.25	0.90 ± 0.29	64.54 ± 5.07
CQ	0.026 ± 0.003	0.207 ± 0.015	137.42 ± 0.02

Figure 2.16 Antiplasmodial potency of quinoxaline-4-aminoquinolines against FCR-3 and 3D7 *P. falciparum* clones

2.5.2 Adamantane-4-aminoquinolines

Yvette et al. (2018) team identified a new class of antimalarials consisting of a wide variety of conjugated aza-adamantanol (**29**) and adamante-imine (**30**) 4-aminoquinolines. The constructed hybrids tested positive for antimalarial activity against CQS (NF54) and CQR (K1) *P. falciparum* clones. Among the series, only **30b** (IC_{50} = 5 nM) was more potent against the NF54 strain than the reference CQ (IC_{50} = 7.80 nM). In contrast, hybrids **29a**, **29b**, and **30a** exhibited a 3-4-fold higher antimalarial potency against the K1 clone than the reference CQ (IC_{50} = 300 nM). The hybrids with 2-to-3-carbon alkyl linkers from both series were the most potent against the NF54 and K1 clones. All conjugates displayed low cytotoxicity against the non-parasitic Chinese hamster ovarian (CHO) cell line, with IC_{50} values ranging from 37 to 279 μM (Figure 2.17).

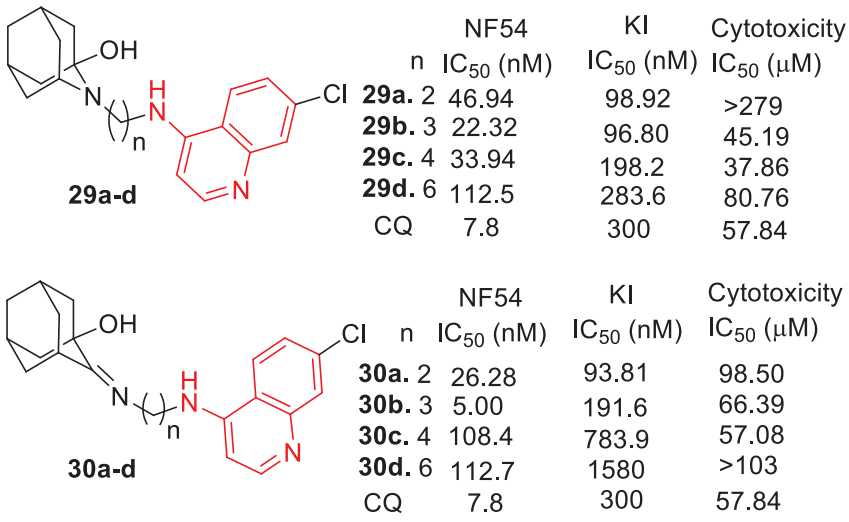

Figure 2.17 Antimalarial activity of adamantane-4-aminoquinolines towards NF54 and K1 *P. falciparum* clones

2.5.3 Artemisinin-4-aminoquinolines

Capci et al. (2019) synthesized alkydiesteramine thread 7-chloroquinoline derivatives hybridized with 3-hydroxy-desoxydihydroartemisinin core **31-33** and screened their antimalarial activity towards *P. falciparum* 3D7, Dd2, and K1 strains. Hybrid **32** containing artemisinin core tethered to 7-chloroquinoline bicycle via 3-(2-(methylamino)ethyl carbamoyl)propanoate moiety was a more potent counter of all three *P. falciparum* clones K1 (EC_{50} = 0.78 nM), 3D7 (EC_{50} = 2.7 nM), and Dd2 (EC_{50} = 1.0 nM) (Figure 2.18).

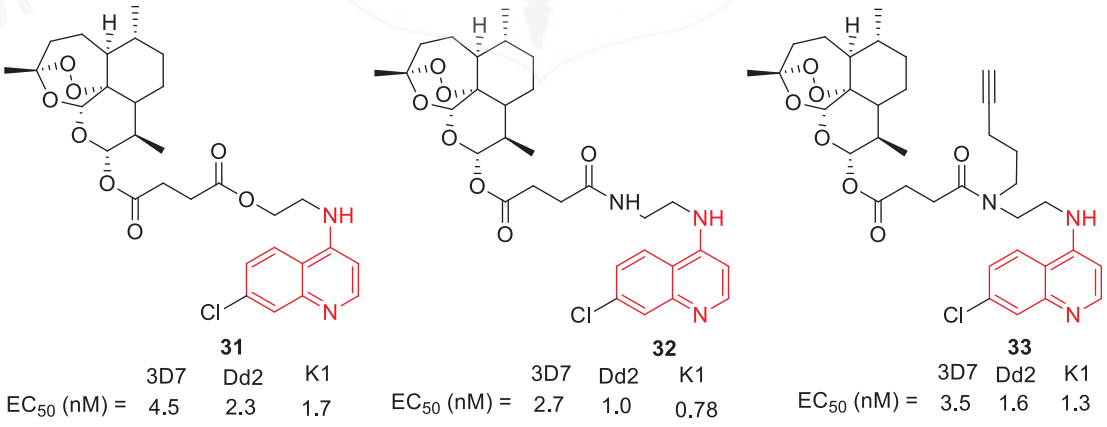

Figure 2.18 Antimalarial potency of artemisinin-4-aminoquinolines towards *P. falciparum* 3D7, Dd2, and K1 clones

Pepe et al. (2020) developed novel conjugates of 4-aminoquinolines hybridised with artemisinin core (**34-36**) and evaluated their antimalarial activity against the CQR *P. falciparum* FcB1/Colombia clone using CQ (IC_{50}; 72 nM) and Artemisinin (ART, IC_{50}; 55 nM) as reference drugs. Hybrid **36b** was comparable to ART, whereas the remaining hybrids exhibited lower inhibition values (11-33%) at 10 nM (Figure 2.19).

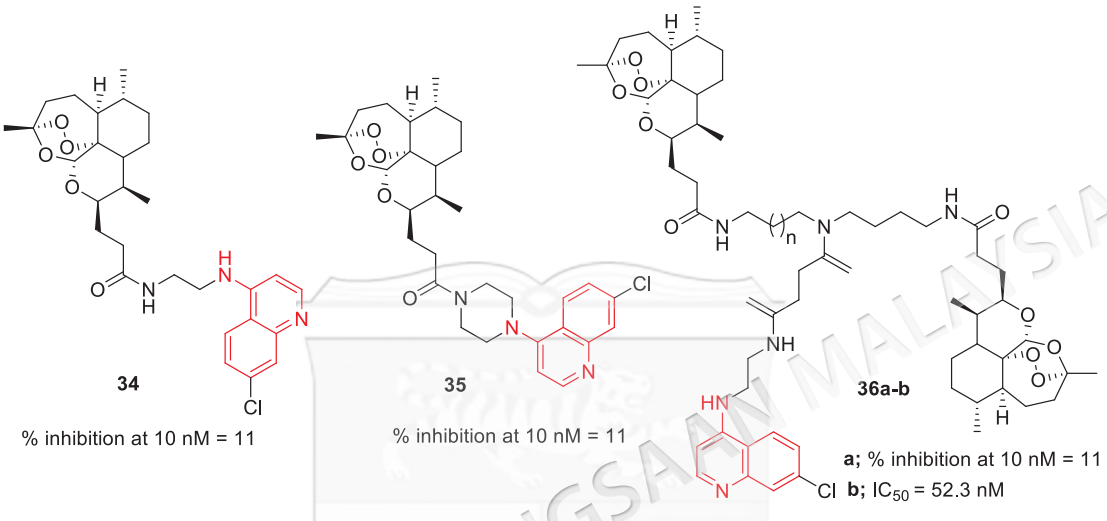

Figure 2.19 Antimalarial activity of artemisinin-4-aminoquinolines against *P. falciparum* FcB1/Colombia strain

2.5.4 Pyrimidine-4-aminoquinolines

A broad range of triazole-tethered pyrimidine-4-aminoquinoline derivatives was furnished by Chopra and Chibale and Singh (2018) and examined for *in vitro* potency towards NF54 (CQS) and Dd2 (CQR) clones of *P. falciparum* employing artesunate (ASN; IC_{50} < 5.202 µM (NF54) and 0.015 µM (Dd2)) and CQ (IC_{50} 0.018 µM (NF54) and 0.275 µM (Dd2)) for comparison. All the screened compounds except **37g** were identified as more potent towards the NF54 and Dd2 *P. falciparum* clones. The SAR studies showed that the compounds with three carbon methylene linkers between the 4-aminoquinoline and triazole moieties **37a-f** displayed better activity towards both NF54 and Dd2 clones than the hybrids with two carbon methylene linkers between the 4-aminoquinoline and triazole moieties **37g-l**. The most potent hybrid **37d** among the series towards the NF54 clone was less potent towards the Dd2 clone, whereas **37j** was more active than **37d** towards the Dd2 clone. Replacement of the methyl ester with ethyl and isopropyl esters enhanced activity towards the NF54 and Dd2 *P. falciparum* clones. Introducing a polar nitro substituent at the *para* position of C-6 phenyl substituent

improved the potency. However, replacing the C-6 phenyl substituent with methyl group resulted in a decrease in potency. All the compounds were tested for cytotoxicity against the mammalian Vero cell line, and the IC_{50} values (IC_{50}: 15-207 M) indicated that most of the conjugates exhibited no detectable cytotoxicity. The most active compound **37d** towards the NF54 clone showed a high selectivity index (SI = 317.50). The majority of active compounds **37a-f** (n = 3) possessed higher clog *P* and log D values than the hybrids **37g-l** (n = 2) (Figure 2.20).

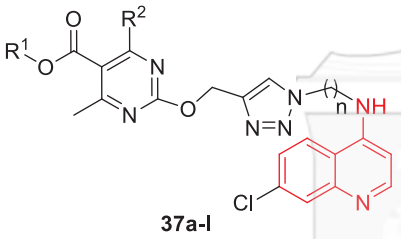

37a-l

	R^1	R^2	n	NF54 IC_{50} (μM)	Dd2 IC_{50} (μM)	Cytotoxicity IC_{50} (μM)
a.	CH_3	C_6H_5	3	1.01±0.10	1.65±0.22	155.65±1.55
b.	C_2H_5	C_6H_5	3	0.89±0.04	1.37±0.17	152.82±0.90
c.	*i*-C_3H_7	C_6H_5	3	0.33±0.03	0.61±0.01	28.52±3.40
d.	*i*-C_3H_7	*p*-$NO_2C_6H_4$	3	0.048±0.01	4.59±0.13	15.24±0.20
e.	*i*-C_3H_7	*o*-$NO_2C_6H_4$	3	0.60±0.04	0.86±0.06	23.35±1.1
f.	C_2H_5	CH_3	3	0.70±0.05	1.11±0.14	>201
g.	CH_3	C_6H_5	2	10.38±0.30	-	-
h.	C_2H_5	C_6H_5	2	1.49±0.10	2.52±0.29	149.40±2.50
i.	*i*-C_3H_7	C_6H_5	2	0.64±0.10	2.00±0.26	148.52±1.0
j.	*i*-C_3H_7	*p*-$NO_2C_6H_4$	2	0.18±0.02	0.99±0.06	149.87±2.8
k.	*i*-C_3H_7	*o*-$NO_2C_6H_4$	2	0.53±0.01	1.08±0.07	145.39±4.0
l.	C_2H_5	CH_3	2	2.49±0.20	8.14±0.17	>201
	CQ			0.018±0.002	0.275±0.02	-
	ASN			< 5.202	0.015±0.0001	-

Figure 2.20 Antiplasmodial potency of pyrimidine-4-aminoquinolines towards NF54 and Dd2 *P. falciparum* clones

Against W2 (CQR) and D6 (CQS) *P. falciparum* strains, Maurya et al. (2019) examined the antimalarial efficacy of pyrimidine-based 4-aminoquinolines having pyridyl (38) and thiophenyl (**39**) unit at the –NH group. Amongst, **39** showed 22-fold higher activity against the W2 strain than CQ (IC_{50}: 0.4215 μM), and **38** displayed higher activity against the D6 strain. The most active compounds were significantly non-cytotoxic against Vero cell lines (Figure 2.21). *In vitro*, Tripathi et al. (2019) hybrid **40** demonstrated 2.8 and 47.3-fold enhanced activity than the standard drugs ART and CQ, respectively, with an IC_{50} of 4.7 nM towards the Dd2 (CQR) strain (Figure 2.21). Against the NF54 (CQS) strain, Kayamba et al. (2021) hybrid **41** with 1,4-diamine butyl spacer between pyrimidine and chloroquine units and 4-hydroxyphenyl rings on pyrimidine moiety displayed superior potency (IC_{50}: 0.32 μM), with a favourable safety profile of 9.79 to HEK293 cell lines (Figure 2.21).

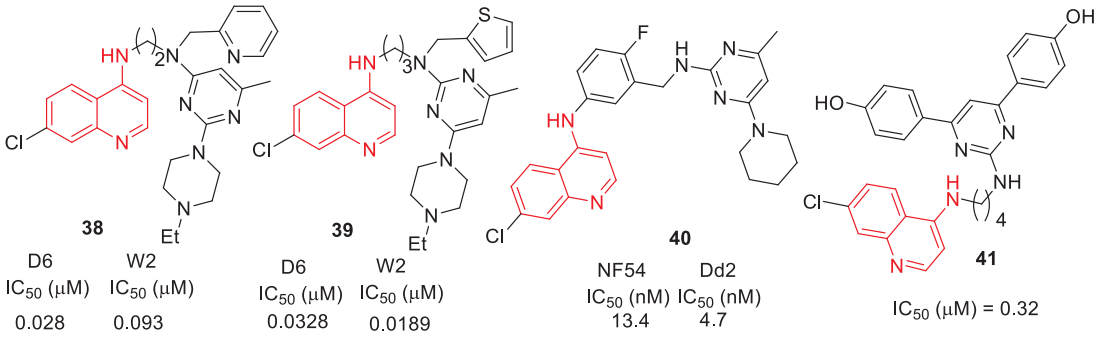

Figure 2.21 Antimalarial properties of 4-aminoquinoline-pyrimidines

2.5.5 Imidazole-4-aminoquinolines

A wide variety of 4-aminoquinolines hybridized with imidazole moiety was synthesized by Kondaparla et al. (2018) and evaluated for their antiplasmodial efficacy towards CQS (3D7) and CQR (K1) *P. falciparum* clones by utilizing CQ (IC_{50} 0.005 μM (3D7) and 0. 255 μM (K1)) as standard drug. All the synthesized hybrids displayed moderate to excellent antiplasmodial potency towards both 3D7 and K1 clones of *P. falciparum.* The SAR revealed that the nature of the substituent at imidazole moiety significantly affects the antiplasmodial potency of the tested hybrids, and bulky aromatic substituents are not suitable on the imidazole ring. Hybrids with electron-donating groups on the phenyl ring attached to imidazole moiety displayed lower potency towards the K1 strain than those having electron-withdrawing groups. Amongst the series, compound **42m** containing cyclopentyl ring at the fifth position of the imidazole moiety (IC_{50} = 0.079 μM) displayed the highest activity, followed by the hybrids substituted with tertiary butyl group **42i** (IC_{50} = 0.14 μM) and cyclohexyl ring **42q** (IC_{50} = 0.19 μM) at the fifth position of imidazole moiety counter to 3D7 clone of *P. falciparum*. Alkyl and cycloalkyl groups were the most favourable substituents in increasing antimalarial activity against the 3D7 clone. Towards the K1 strain, some tested hybrids (**42b**, **42d**, **42e**, and **42m**) exhibited comparable activity to standard CQ (Figure 2.22).

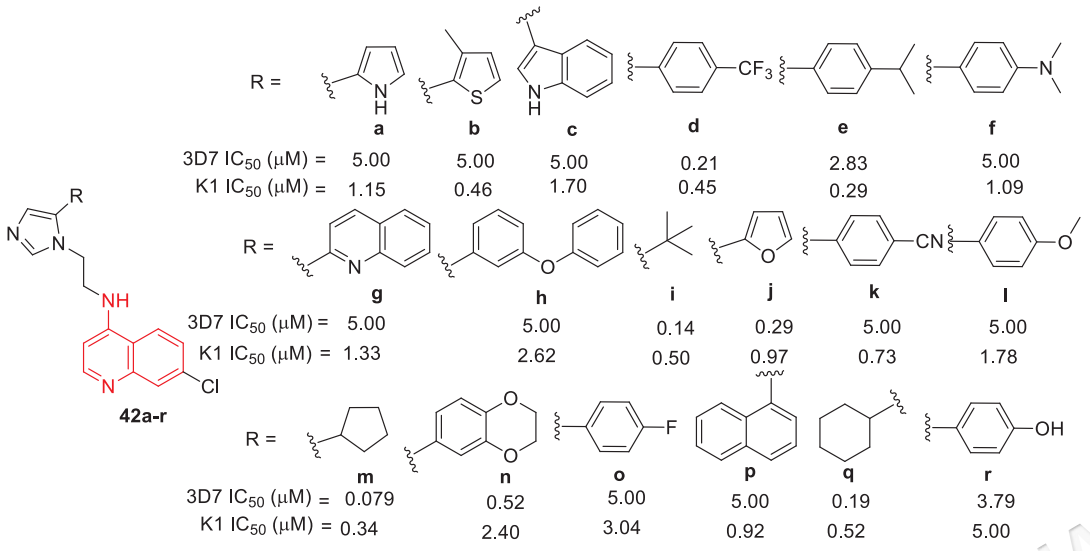

Figure 2.22 Antiplasmodial activity of imidazole-4-aminoquinolines towards 3D7 and K1 *P. falciparum* clones

2.5.6 Piperazine-4-aminoquinolines

Kondaparla et al. (2018) identified a variety of 4-aminoquinolines hybridised with piperazine scaffold **43** as antimalarial agents. Using CQ as the reference drug, they assessed their *in vitro* antimalarial potency against CQS (3D7) and CQR (K1) *P. falciparum* clones. All twenty-six compounds screened were less potent than the standard CQ (IC_{50} = 5 nM) against the 3D7 strain, whereas eight compounds were more potent than the standard CQ (IC_{50} = 255 nM) against the K1 clone. The most potent agent against 3D7 and K1 *P. falciparum* clones was hybrid **43l**, with IC_{50} values of 22.61 and 46.52 nM, respectively. According to the SAR results, the type of substitutions on the piperazine ring significantly affected the antimalarial activity of piperazine-4-aminoquinolines. 3D7/K1 dual inhibitory potency is facilitated by the isobutyl moiety at its 2-position to secondary amine and ethyl group on the 7-trifluoroquinoline cycle. Further, replacing the ethyl group with benzodioxole moiety has paved the way for selective K1 inhibitory potency. Nearly all the tested hybrids were less cytotoxic toward the Vero cells, and the fairly high SI ranged from 32.77 to 3,671.69. Most of the hybrids exhibited moderate to good binding scores with the heme (Figure 2.23**)**.

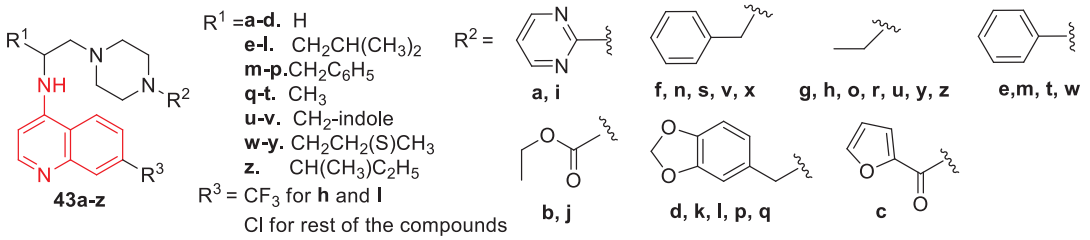

	3D7 IC50 (nM)	K1 IC50 (nM)		3D7 IC50 (nM)	K1 IC50 (nM)		3D7 IC50 (nM)	K1 IC50 (nM)		3D7 IC50 (nM)	K1 IC50 (nM)
a.	108.39	276.90	h.	24.55	797.67	o.	427.89	70.82	u.	4,150.08	>5,000
b.	899.23	161.80	i.	460.05	352.30	p.	757.38	89.0	v.	596.52	528.72
c.	993.50	4,231	j.	857.68	412.40	q.	108.10	71.39	w.	>5,000	>5,000
d.	521.20	46.50	k.	211.10	452.80	r.	126.54	362.28	x.	3,099.19	>5,000
e.	521.20	>1,000	l.	22.61	46.52	s.	404.80	84.01	y.	2,659	>5,000
f.	153.90	>1,000	m.	>1,000	1,100	t.	538.59	783.73	z.	113.76	502.10
g.	56.98	97.76	n.	>5,000	>5,000				CQ	5	225

Figure 2.23 Antimalarial potency of piperazine-4-aminoquinolines towards 3D7 and K1 *P. falciparum* clones

2.5.7 Pyridine-4-aminoquinolines

Remarkable antimalarial activity with 0.033 to <10 µM range of IC_{50} values against *P. falciparum* Dd2 strain has been demonstrated by pyridine conjugated 4-aminoquinoline hybrids of Huang et al. (2019). In comparison to standard CQ, hybrid **44** was discovered to be the most effective agent against the Dd2 strain among the series (Figure 2.24). Similar to this, de Silva et al. (2019) constructed 4-aminoquinolines substituted with a pyridine ring and tested them for in vitro efficacy against the *P. falciparum* W2 strain and *in vivo* activity against the mice infected with *P. berghei*. With 8.4 µM of IC_{50} value, hybrid **45** was proved to be an effective anti-*P. falciparum* drug showed superior activity against the mice infected with *P. berghei* five days after infection (Figure 2.24).

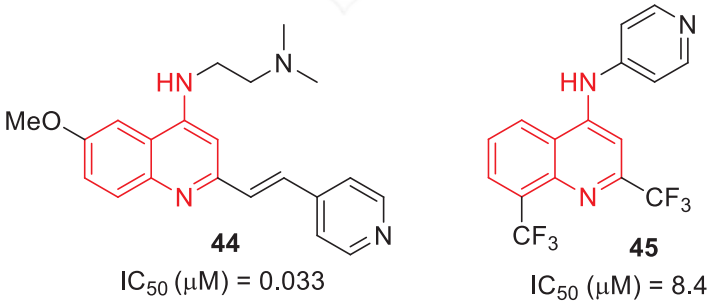

Figure 2.24 Antimalarial efficacy of 4-aminoquinoline-pyridines

Recently, the examination of the antimalarial efficacy of the furnished pyridine-4-aminoquinoline derivatives 46 towards the *P. falciparum* strain was carried out by Patel et al. (2022). CQ (IC_{50} = 0.06 µM) and QN (IC_{50} = 0.83 µM) were the reference

drugs employed in this examination. All the tested hybrids were less active toward the *P. falciparum* strain. The hybrids with –NHNH- (**46a** and **46b**) linkage were more potent than those with -NH- (**46c** and **46d**). All the hybrids performed with good binding affinity with shikimate kinase and hypoxanthineguanine phosphoribosyltransferase in the molecular docking studies; as such hybrid **46d** displayed the lowest (-9.2 kcal/mol) binding energy (Figure 2.25**)**.

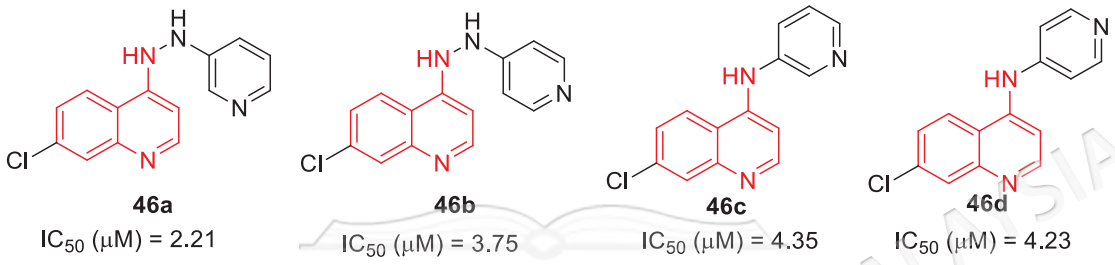

Figure 2.25 Antimalarial potency of pyridine-4-aminoquinolines towards *P. falciparum* strain

2.5.8 Phthalimide-4-aminoquinolines

Rani et al. (2018) reported the microwave-promoted construction of phthalimide containing 4-aminoquinoline derivatives to examine their anti-plasmodial potency counter to the CQR (W2) *P. falciparum* clone. Most furnished analogs were non-cytotoxic to J774 murine macrophage cell lines, and their SI ranges from 126 to 291 showed potent antimalarial actions with 0.10 to 7.55 μM ranges of IC_{50}values. According to the SAR studies, the halogen group on the phthalimide ring and the carbon chain length (n = 6, 8) between the two pharmacophores increased antiplasmodial potency. Introducing a tetrachloro and tetrabromo-phthalimide enhanced the potency profile even at shorter alkyl chain lengths. Among the series, compound **47w** with a tetra-bromophthalimide ring and hexyl chain as spacer emerged as the most active and non-toxic (IC_{50} = 29.11 μM) agent with 0.10 μM of IC_{50} value counter to the CQR (W2) clone of *P. falciparum* (Figure 2.26).

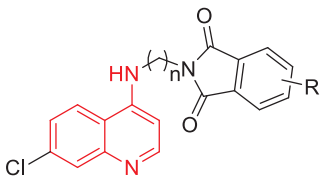

47a-y

	R	n	IC_{50} (μM)
a.	H	2	1.11 ± 0.01
b.	H	3	1.51 ± 0.02
c.	H	4	0.37 ± 0.05
d.	H	6	0.11 ± 0.004
e.	H	8	0.14 ± 0.01
f.	3-F	2	4.73 ± 0.8
g.	3-F	3	3.96 ± 0.17
h.	3-F	4	0.64 ± 0.11
i.	3-F	6	0.24 ± 0.01
j.	3-F	8	0.12 ± 0.0001
k.	4-F	2	4.56 ± 0.46
l.	4-F	3	1.19 ± 0.16
m.	4-F	4	0.42 ± 0.01
n.	4-F	6	0.12 ± 0.07
o.	4-F	8	0.17 ± 0.007
p.	3,4,5,6-Cl	2	0.21 ± 0.05
q.	3,4,5,6-Cl	3	0.57 ± 0.04
r.	3,4,5,6-Cl	4	0.27 ± 0.000002
s.	3,4,5,6-Cl	6	0.46 ± 0.00003
t.	3,4,5,6-Br	2	0.40 ± 0.03
u.	3,4,5,6-Br	3	3.76 ± 0.02
v.	3,4,5,6-Br	4	0.19 ± 0.03
w.	3,4,5,6-Br	6	0.10 ± 0.006
x.	3-NO_2	2	7.55 ± 0.30
y.	3-NO_2	6	0.15 ± 0.02
	CQ		0.077 ± 0.004
	ART		0.007 ± 0.0007

	Cytotoxicity IC_{50} (μM)
d.	14.34
j.	28.24
n.	15.16
w.	29.11

Figure 2.26 Antiplasmodial efficacy of 4-aminoquinoline-phthalimides towards the W2 clone of *P. falciparum*

Rani et al. (2019) examined anti-*P. falciparum* efficacy of C-5-substituted isoindoline-1,3-dione-4-aminoquinoline hybrids against W2 *P. falciparum* strain. With a diethylamino group on dioxoisoindoline moiety, **48** (IC_{50}: 0.097 μM) was discovered to be a promising non-cytotoxic drug with a selective index of > 2000 (Figure 2.27). The following year, the same group **(**Rani et al. 2020**)** examined anti-*P. falciparum* efficacy of cycloalkyl amine substituted 1,3-dioxoisoindoline-4-aminoquinoline hybrids against W2 strain. With a selectivity index >4200, **49** with propylamine linker between quinoline and dioxoisoindoline units and a hydroxyethyl piperazine group on dioxoisoindoline ring emerged as the most potent analog (IC_{50}: 0.006 μM) against W2 strain (Figure 2.27). Similarly, Shalini et al. (2020) investigated the anti-*P. falciparum* effects of naphthalimide hybridized 4-aminoquinoline derivatives towards the W2 strain. With a selectivity index >4000, **50** containing propylamine linker between quinoline and naphthalimide units and a hydroxyethyl piperazine group on naphthalimide ring was a promising candidate (IC_{50}: 15.445 nM) in the series (Figure 2.27). The same research team (Shalini et al. 2020) tested the anti-*P. falciparum* activity of another family of amide-linked naphthalimide-4-aminoquinoline hybrids against 3D7 and W2 strains. Hybrid **51** was the most potent towards both strains (Figure 2.27).

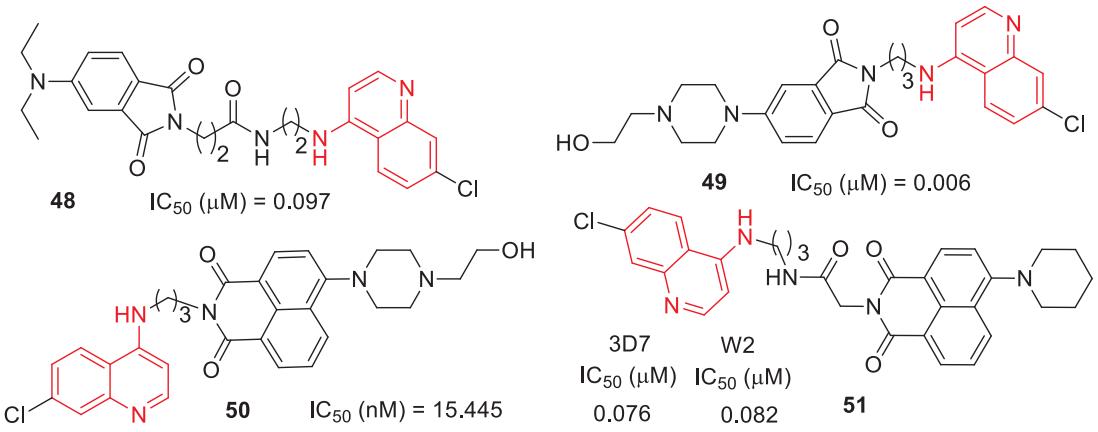

Figure 2.27 Antimalarial properties of 4-aminoquinoline-phthalimides

Sharma et al. (2022) recently produced a novel functionalized oxindole-4-aminoquinoline scaffold (**52** and **53**) as promising dual-function antiplasmodials and screened their *in vitro* potency. All of the produced hybrids demonstrated good to exceptional antiplasmodial activity against the CQR (W2) *P. falciparum* clone. The antiplasmodial efficacy of scaffolds was affected by the length of the alkyl chain, the type of spacer attached, and the nature of the substituent at the C-5 position of the oxindole unit, according to the results of SAR. Ten of the eighteen tested compounds were more potent than the standard CQ (IC_{50} = 213.8 nM). Remarkably, conjugates with acyclic amines as linkers (**52a-o)** were more potent than cyclic amine-containing compounds (**53a-c**). The aid of electron-withdrawing groups like Cl or Br on oxindole core (**52h**, **52j**, **52o**) enhanced the potencies than unsubstituted ones. The activity order with respect to the linker followed the order: n = 6 > 4 > 3 > 2 > 0. The most promising agent (**53o**) with 30.9 nM of IC_{50} value was seven-fold more potent than the reference CQ counter to the W2 clone of *P. falciparum*. The cytotoxicity of the most potent compounds, **52j** and **52o**, was tested against Vero cell lines and proved noncytotoxic, resulting in SI > 400 (Figure 2.28).

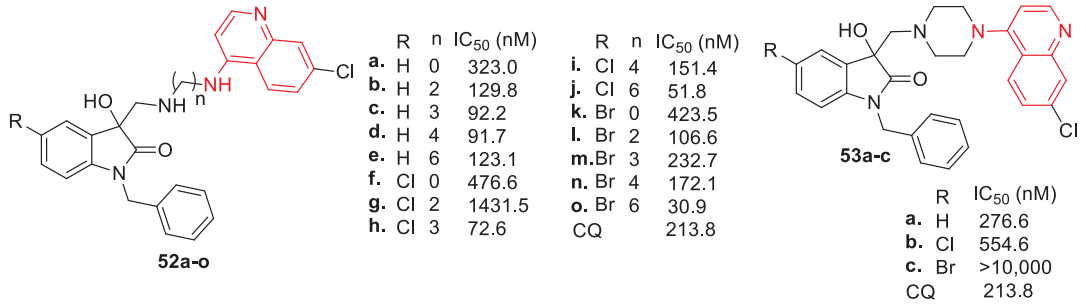

	R	n	IC_{50} (nM)
a.	H	0	323.0
b.	H	2	129.8
c.	H	3	92.2
d.	H	4	91.7
e.	H	6	123.1
f.	Cl	0	476.6
g.	Cl	2	1431.5
h.	Cl	3	72.6

	R	n	IC_{50} (nM)
i.	Cl	4	151.4
j.	Cl	6	51.8
k.	Br	0	423.5
l.	Br	2	106.6
m.	Br	3	232.7
n.	Br	4	172.1
o.	Br	6	30.9
CQ			213.8

	R	IC_{50} (nM)
a.	H	276.6
b.	Cl	554.6
c.	Br	>10,000
CQ		213.8

Figure 2.28 Antiplasmodial efficacy of oxindole-4-aminoquinolines towards W2 clone of *P. falciparum*

2.5.9 Triazole-4-aminoquinolines

In the search for new antimalarial agents, triazole-based aminoquinoline hybrids are desirable lead molecules (Ravindar et al. 2023). Triazole-tethered 4-aminoquinoline derivative **54**, synthesized by Rossier et al. (2019), was discovered to be 30-40 times more active than the cobalt complex counterpart against both the K1 and NF54 strains (Figure 2.29). One of the screened compounds of de Silva et al. (2019), **55** bearing methyl substituent on triazole nuclei, showed superior *in vitro* activity (IC_{50}: 0.083 µM) and emerged as the most promising agent against the mice infected with *P. berghei* on the 5th day after infection with favourable SI (132) and low cytotoxicity (IC_{50}: 127 µM) (Figure 2.29**)**. Among the Wadi et al. (2019) hybrids, the most active compound **56** towards the 3D7 strain with 40.00 nM of IC_{50} value was screened further counter to *P. falciparum* RKL-9 (CQR) strain. It was determined to be substantially more active (IC_{50}: 2.94 nM) than standard CQ (Figure 2.29**)**. Sharma et al. (2020) also investigated anti-*P. falciparum* effects of triazole-tethered tetrahydro-carboline-4-aminoquinoline hybrid compounds towards W2 strain, and **57** was discovered as the most promising candidate amongst (IC_{50}: 0.49 µM) with a SI > 300 on Vero cell (Figure 2.29**)**.

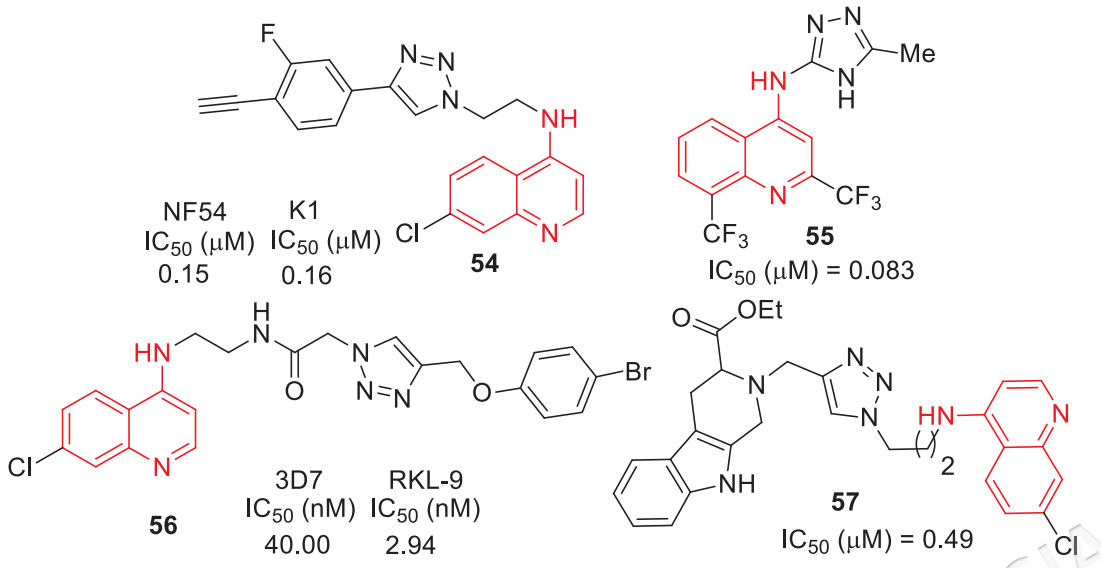

Figure 2.29 Antimalarial properties of 4-aminoquinoline-triazoles

Currently, the antiplasmodial activity of a library of 1*H*-1,2,3-triazole tethered 4-aminoquinoline-benzoxazole conjugates (58-65) was evaluated against W2 (CQR) and 3D7 (CQS) *P. falciparum* clones by utilizing CQ (IC_{50} = 0.024 μM towards 3D7, and IC_{50} = 0.475 μM towards W2) as a standard (Saini et al. 2021). All the compounds screened were less active than the standard CQ; the hybrids displayed IC_{50} values in the low micromolar range against the 3D7 and W2 strains and exhibited remarkable SAR. The alkyl spacer between the two moieties significantly increased the antiplasmodial potencies, with greater influence observed in hybrids **63a-b** than in hybrids **61a-b**. The promising 4-aminoquinoline-benzoxazole hybrid (**63a**) with ethyl spacer linker displayed 4.15 μM and 3.78 μM of IC_{50}values towards *P. falciparum* 3D7 and W2 clones, respectively, with lower cross-resistance with CQ. Inserting piperazyl-ethyl as a spacer decreased the potencies in the pioneer 64, confirming the favourable influence of flexible chains on quinoline moiety. At the same time, the corresponding oxaborole **65** exhibited moderate potencies counter to both the clones. The conjugates were non-cytotoxic towards mammalian Vero cell lines and showed SI in the range of 16.94–26.45 (Figure 2.30**)**.

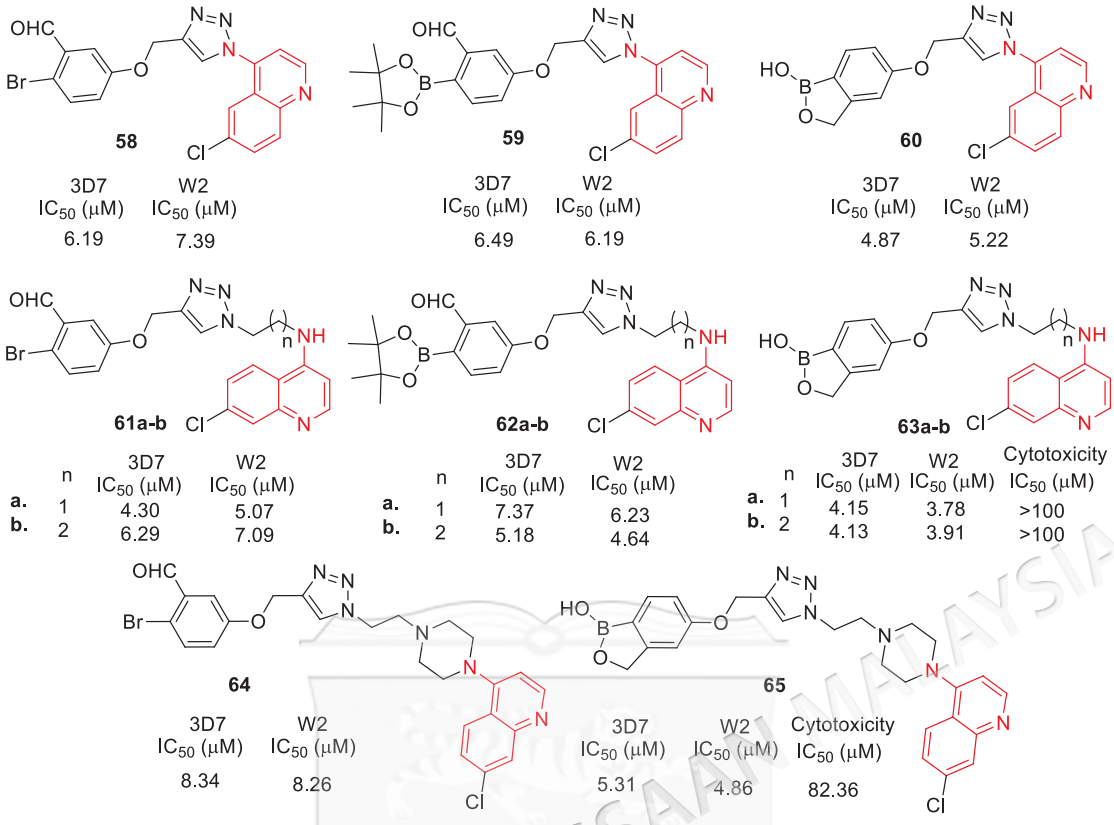

Figure 2.30 Antiplasmodial activity of triazole-4-aminoquinolines towards 3D7 and W2 clones of *P. falciparum*

2.5.10 Guanylthiourea-4-aminoquinolines

Guanylthiourea (GTU) was identified as a significant antimalarial unit, while 4-amino quinolone was already well-known for antimalarial potency. Molecules having GTU moiety and 4-aminoquinoline **66** have been synthesized and designed utilizing a molecular docking study with the *Pf*DHFR enzyme and heme unit (Bhagat et al. 2019). *In vitro* studies of these furnished hybrids showed potent antimalarial efficacy in the range of 0.61 to 7.55 μM for the D6 clone and 0.43 to 8.04 μM for the W2 clone. Compound **66c** was more potent towards D6 and W2 *P. falciparum* clones with 0.61 and 0.43 μM IC_{50} values, respectively. The SAR demonstrated that the chlorine substituent, a smaller group, in quinolone moiety plays a crucial role in increasing the potency. The carbon chain length (n = 4) was crucial for improving the potency. Replacement of the chlorine with trifluoromethyl, a bulky group, decreased activity towards both the clones. The hybrids, **66g-66i**, with two trifluoromethyl groups were the least potent among the series. At the highest concentrations tested, none of the hybrids were found to be cytotoxic to mammalian Vero cell lines. The required

interactions (Asp54 and Ile14) and docking score (-9.63 to -7.36 kcal/mmol) were comparable to WR99210 (-9.89 kcal/mol) as determined by molecular docking (Figure 2.31).

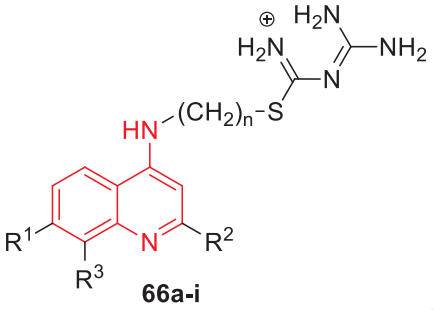

66a-i

	R^1	R^2	R^3	n	*Pf*D6 IC_{50} (μM)	*Pf*W2 IC_{50} (μM)	Cytotoxicity IC_{50} (μM)
a:	Cl	H	H	2	2.25	3.71	> 11.79
b:	Cl	H	H	3	1.56	2.13	> 11.39
c:	Cl	H	H	4	0.61	0.43	> 11.02
d:	CF_3	H	H	2	1.86	2.95	> 10.89
e:	CF_3	H	H	3	2.85	3.21	> 10.55
f:	CF_3	H	H	4	2.80	6.06	> 10.23
g:	H	CF_3	CF_3	2	7.55	8.04	> 9.42
h:	H	CF_3	CF_3	3	5.54	7.21	> 9.17
i:	H	CF_3	CF_3	4	> 8.93	> 8.93	> 8.93
Chloroquine					0.04	0.39	-
Pyrimethamine					0.01	-	18.12

Figure 2.31 Antimalarial potency of molecular hybrids based on 4-aminoquinoline and GTU against *Pf*D6 and *Pf*W2 *P. falciparum* clones

2.5.11 Morpholine-4-aminoquinolines

Hochegger et al. (2019) provided a wide range of morpholine-incorporated 4-aminoquinoline derivatives **67-69** to test in vitro activity against *P. falciparum* CQS (NF54) and CQR (K1) clones. All eight scaffolds examined had a high nM range against both strains. Only the hybrid **69a** containing a pyrrolidine moiety demonstrated excellent antimalarial activity against both NF54 (IC_{50}: 0.004 μM) and K1 (IC_{50}: 0.011 μM) *P. falciparum* strains, with SI values of 30775 and 11191, respectively (Figure 2.32). The SAR revealed propionamide analogues (**69a-d**) were more active against NF54 and K1 strains than acetamido analogues. The most potent hybrid **69a** further screened for physicochemical properties, displayed a lower log $D_{7.4}$ value (1.54) and higher ligand efficiency (LE = 0.338 kcal/mol/HA) along with far better permeability (P_e = 100.86 nm/s) (68a-c).

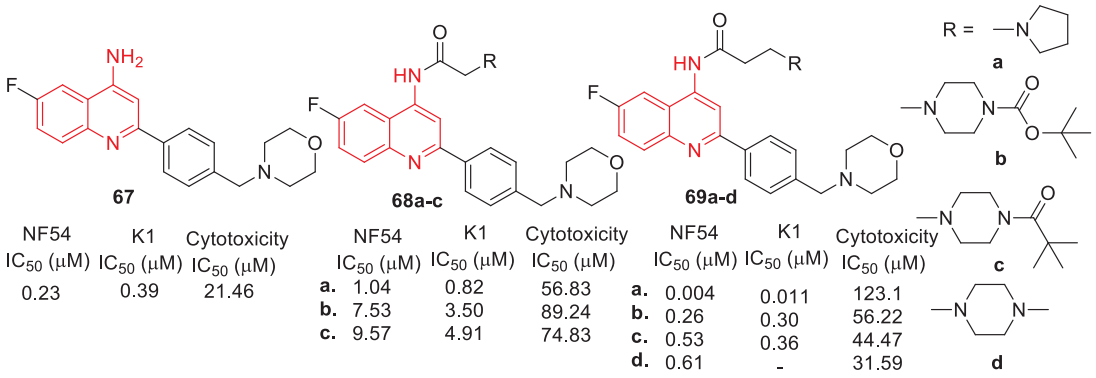

Figure 2.32 Antiplasmodial efficacy of morpholine-4-aminoquinolines towards *P. falciparum* NF54 and K1 clones

2.5.12 Nopol-4-aminoquinolines

Nyamwihura et al. (2021) conducted the screening of 4-aminoquinolines hybridized with nopol moiety (**70** and **71**) for their antimalarial potency towards CQS clone 3D7 and CQR clones NF54 and K1 by utilizing MQ (EC_{50} 2.33 μM (3D7), 0.003 μM (NF54) and 0.117 μM (K1)), CQ (EC_{50} 0.004 μM (3D7), 0.005 μM (NF54) and 0.212 μM (K1)) and ART (EC_{50}0.017 μM (NF54) and 0.11 μM (K1)) as standard drugs. The hybrid *N*-(7-chloroquinolin-4-yl)-2-((1*S*,5*R*)-6,6-dimethylbicyclo[3.1.1]hept-2-en-2-yl)acetamide (**71**) was found to be more potent than the hybrid 2-((1*S*,5*R*)-6,6-dimethylbicyclo[3.1.1]hept-2-en-2-yl)-*N*-(quinolin-4-yl)acetamide (**70**) towards all the *P. falciparum* clones (Figure 2.33).

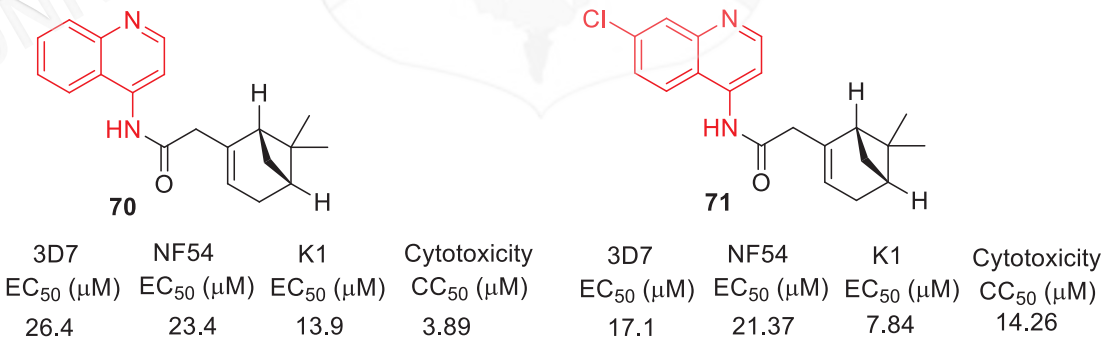

Figure 2.33 Antimalarial efficacy of nopol-4-aminoquinolines towards 3D7, NF54 and K1 *P. falciparum* strains

2.5.13 Ciprofloxacin-4-aminoquinolines

Dana et al. (2020) furnished a novel ciprofloxacin (CFX) based 4-aminoquinoline hybrid molecule **72** and tested *in vitro* activity towards CQR (K1) and CQS (3D7)

clones of *P. falciparum*. CQ and CFX were taken as controls. A potent ciprofloxacin-4-aminoquinoline-based antimalarial hybrid **72** was active at the first and second life cycles towards the K1 and 3D7 clones of *P. falciparum.* Still, it was also non-toxic to bacterial and mammalian systems up to 1 μM and 20 μM respectively. The antimalarial potency of hybrid **72** at both the life cycle was 2×10^2 - 7×10^2 -fold higher than the standard CFX. Hybrid **72** was also more active than CQ at the first life cycle toward the W2 *P. falciparum* clone (Figure 2.34**)**.

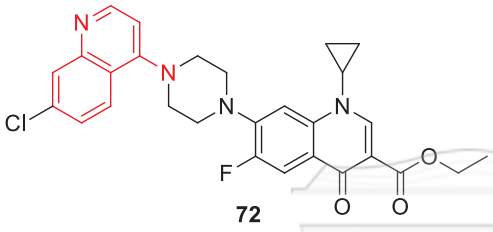

	1st life Cycle (48 h)		2nd life Cycle (96 h)	
	3D7	W2	3D7	W2
	IC_{50} (nM)	IC_{50} (nM)	IC_{50} (nM)	IC_{50} (nM)
	25.52	63.17	13.52	30.64
CQ	12.56	430.60	-	-
CFX	45350.0	37080.00	26260.00	22850.00

Figure 2.34 Antimalarial potency of ciprofloxacin-4-aminoquinolines towards 3D7 and W2 *P. falciparum* clones

2.5.14 Fluorene-4-aminoquinolines

Parth et al. (2022) identified a novel series of six fluorenes-incorporated 4-aminoquinoline hybrids (**73-78**) as promising antiplasmodial agents. They evaluated their *in vitro* activity against the CQS (NF54) clone of the human malaria parasite *P. falciparum*. The evaluation utilised the reference drug CQ (IC_{50} = 13.0 nM). All tested hybrids displayed blood stage activity against *P. falciparum*, with IC_{50} values ranging between 139 and 437 nM. The SAR uncovered that the nature of the linker between two pharmacophores and a substitution at the 9th position of the fluorene moiety significantly impacted the potency of the examined hybrids. The hybrids **73** and **74**, which contained an oxalamide linker, were more potent than the hybrids **77** and **78**, which contained an amide linker. The antiplasmodial activity of compounds containing a substituent at the 9th position of the fluorene moiety was greater than that of hybrids lacking this substitution. Increasing the length of the alkyl chain caused a sequential increase in activity. The most potent hybrid **76** showed binding to hemin (logK = 5.95) at pH 5.6, corresponding to the pH of the digestive vacuole of *P. falciparum* (Figure 2.35**)**.

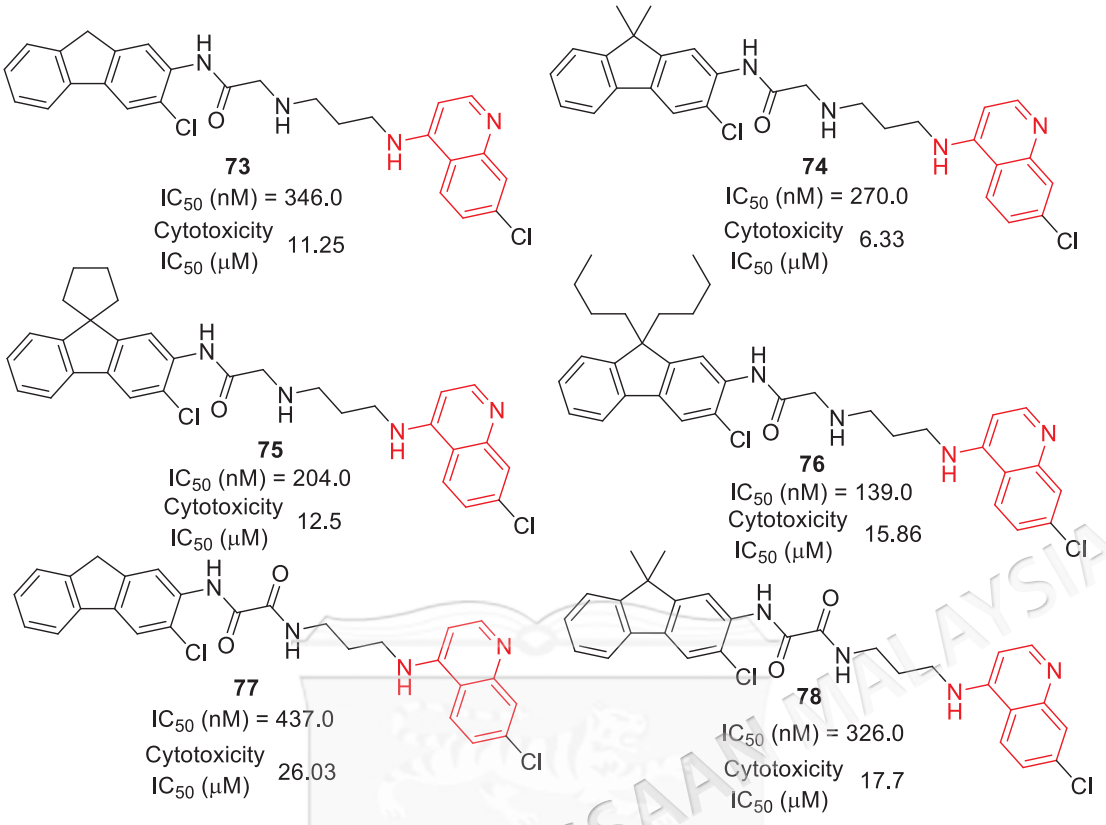

Figure 2.35 Antiplasmodial activity of fluorine-4-aminoquinolines against NF54 *P. falciparum* strain

2.5.15 Pyrazoline-4-aminoquinolines

A range of novel pyrazoline-4-aminoquinoline 7-chloro-*N*-[3 or 4-(4,5-dihydro-5-(phenyl-substituted)-1*H*-pyrazol-3-yl] phenyl) quinoline-4–amine hybrids (**79** and **80**) were also synthesized by Charris et al. (2019) to achieve an antimalarial potency. All provided hybrids were screened *in vitro* for their effects, such as -hematin formation inhibitors and *in vivo* in a murine model. In all experiments, CQ was utilised for comparison purposes. Most hybrids significantly inhibited hematin formation (% > 80). Some hybrids exhibited antimalarial activity comparable to that of CQ. The hybrids with 4′-phenyl substituted moiety were more potent than 3′-phenyl substituted moiety. Try methyl substituted anolog **79e** displayed higher potency among the 3′-phenyl substituted series, while 3,4-dimethoxy substituted hybrid **80c** proved more potent among the 4′-phenyl substituted series. Existing hybrids were evaluated *in vivo* as potential antimalarials in mice infected with *P. berghei* ANKA, a strain susceptible to chloroquine (Figure 2.36).

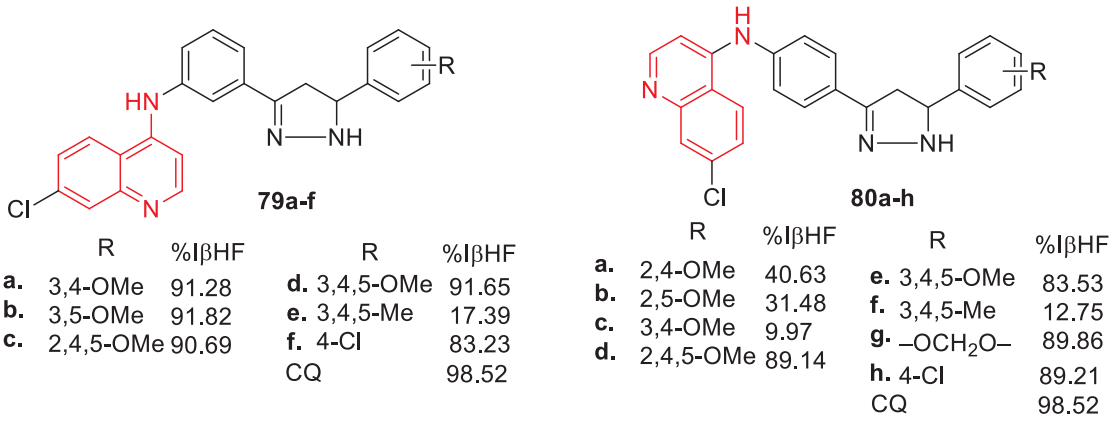

	R	%IβHF		R	%IβHF
a.	3,4-OMe	91.28	**d.**	3,4,5-OMe	91.65
b.	3,5-OMe	91.82	**e.**	3,4,5-Me	17.39
c.	2,4,5-OMe	90.69	**f.**	4-Cl	83.23
				CQ	98.52

	R	%IβHF		R	%IβHF
a.	2,4-OMe	40.63	**e.**	3,4,5-OMe	83.53
b.	2,5-OMe	31.48	**f.**	3,4,5-Me	12.75
c.	3,4-OMe	9.97	**g.**	$-OCH_2O-$	89.86
d.	2,4,5-OMe	89.14	**h.**	4-Cl	89.21
				CQ	98.52

Figure 2.36 Percentage of inhibition of β-hematin formation (% IβHF) of pyrazoline-4-aminoquinolines

2.5.16 The Metal Complex-4-aminoquinoline

Stringer et al. (2019) conducted anti-*P. falciparum* screening of cationic 1,3,5-triaza-phosphaadamantane (PTA) Ir(III) and Ru(II) (**81-82**), Rh(III) half-sandwich (**83**) (Stringer & Melis & Smith 2019) and Ferroquine(FQ)-derived (**84**) (Stringer & Wiesner & Smith 2019) 4-aminoquinoline complexes against K1 (CQR) and NF54 (CQS) strains. Amongst Ir(III) and Ru(II) species, non-benzylated compounds were less potent than the benzyl-PTA counterparts against both strains. Towards the K1 strain, all the Ru(II) species displayed reduced potency compared to the Ir(III) species. Against the NF54 strain, complex **81** (IC_{50}: 0.11 µM) of the Ir(III) series and complex **82** (IC_{50}: 0.10 µM) of the Ru(II) series were the most active candidates. Rh(III) complex **83** was active with a low nM range against the NF54 strain but disclosed cross-resistance against the K1 strain (IC_{50}: > 1000 nM). Among the Ferroquine-derived complexes, **84** was the most promising agent against NF54 and K1 strains with inhibitory concentrations of 0.305 µM and 0.328 µM, respectively (Figure 2.37)

Pereira et al. (2021) investigated anti-*P. falciparum* efficacy of metallic hybrid CQ and PQ linked by Au^I (**85**). Against the 3D7 strain, the CQPQ-Au^I complex was 50-fold more potent than PQ (IC_{50}: 1.1173 µM) and almost equipotent to CQ (IC_{50}: 0.018 µM). Against the W2 strain, the CQPQ-Au^I complex was as potent as PQ (IC_{50}: 0.1823 µM) and at very least twice as potent as CQ (IC_{50}: 0.460µM) (Figure 2.37**)**. In the following year, Sovari et al. (2022) identified triazole-4-aminoquinoline conjugated tricarbonyl rhenium metal species as effective antimalarial agents against *P. falciparum*

NF54 and K1 strains. The hybrid complex **86** was the most promising agent with the submicromolar range inhibitory potencies against both strains (Figure 2.37**)**.

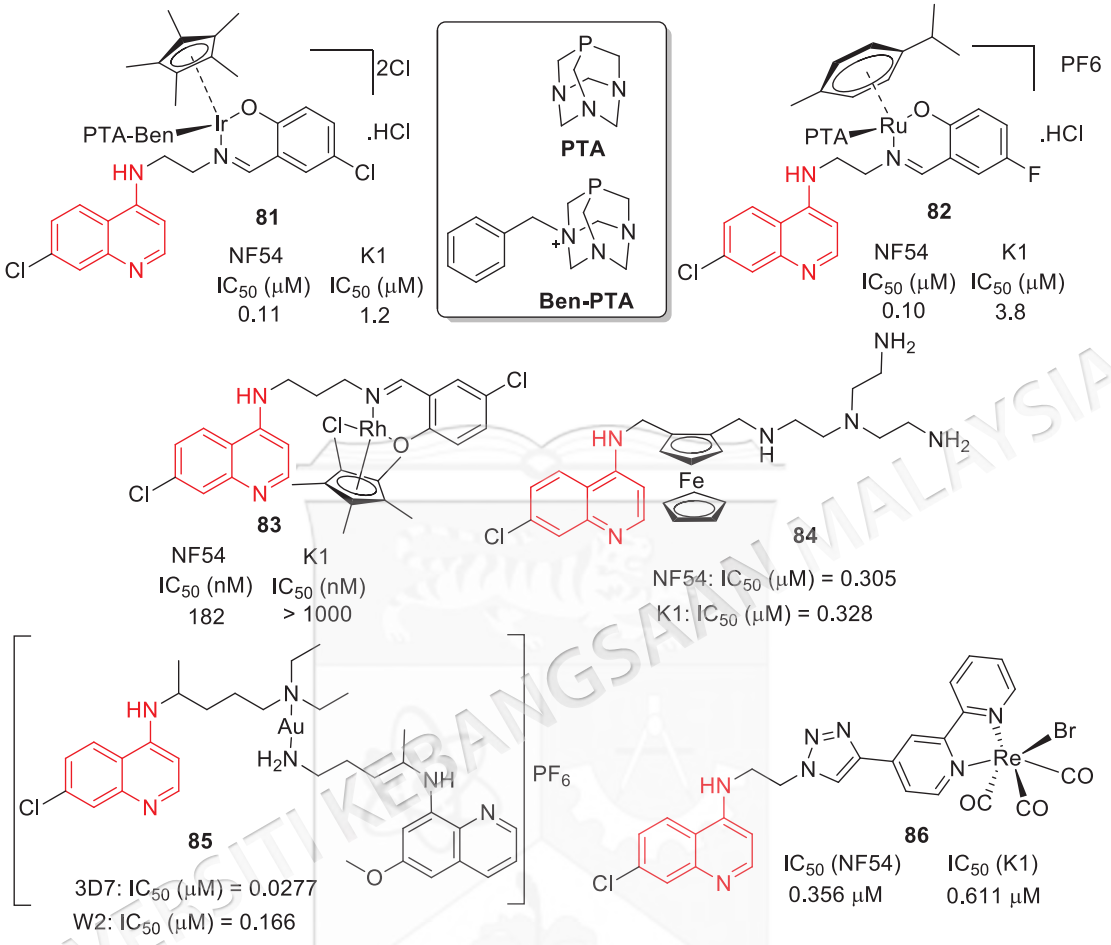

Figure 2.37 Antimalarial properties of various metal complex-4-aminoquinolines

Minic et al. (2020) developed another ferroquine-containing 4-aminoquinoline conjugate **87-90** and examined antimalarial activity counter to CQR (K1) and CQS (NF54) clones of the *P. falciparum*. CQ (IC_{50} 0.001 μM (NF54) and IC_{50} 0.167 μM (K1)) and FQ (IC_{50} 0.029 μM (NF54) and IC_{50} 0.039 μM (K1)) were utilized as standard drugs in the antiplasmodial assays. The SAR revealed better potencies were obtained when ferrocene is linked to the quinoline ring at position 4. The nature of the linker between ferroquine and 4-aminoquinoline pharmacophores significantly influenced the tested hybrids' potency. The ferrocene-containing heterotricyclic derivative, **90,** gave no significant activity. Among the series, complex **88** was the most promising antimalarial agent with 0.39 and 0.77 μM of IC_{50} values towards both the NF54 and K1 clones of *P. falciparum,* respectively. The most potent conjugates (**87-89**) were

examined for their cytotoxicity towards a mammalian cell line, CHO, and displayed a good cytotoxicity profile with lower activities, resulting in high selectivity indices (Figure 2.38**)**.

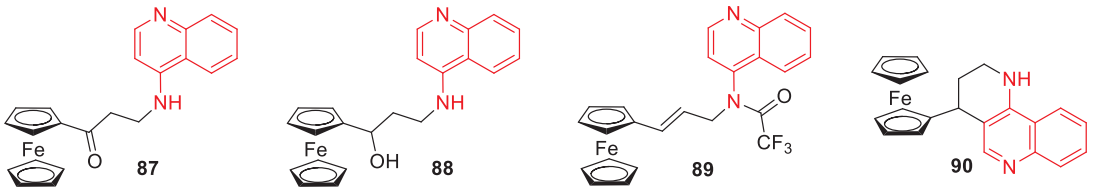

Figure 2.38 Antimalarial potency of Fe-containing 4-aminoquinolines towards NF54 and K1 *P. falciparum* strains

Various neutral and cationic Ir^{III} and Rh^{III} benzimidazole-4-aminoquinoline complexes were constructed, and their inhibitory potencies were examined counter to CQR (K1) and CQS (NF54) clones of the *P. falciparum* (Baartzes et al. 2020). CQ (IC_{50} 0.016 μM (NF54) and IC_{50} 0.164 μM (K1)) was employed as the control drug in the screening. Overall, the hybrid complexes showed better potency toward the NF54 clone of *P. falciparum*. The neutral CˆN-coordinated Ir^{III} and Rh^{III} complexes (**91** and **92**) were more active than their cationic NˆN-coordinated Ir^{III} and Rh^{III} counterparts (**93** and **94**) against both the clones. Among the neutral and cationic hybrid complexes, the Rh^{III} complexes (**92** and **94**) were more potent than the corresponding Ir^{III} complexes (**91** and **93**) towards the NF54 and K1 *P. falciparum* clones. From all the tested hybrids, trifluoromethyl-substituted neutral CˆN-coordinated Ir^{III} species **91c** was the most active towards the NF54 and K1 clones of *P. falciparum*. Low to no cytotoxicity towards the CHO cell line was observed for the screened potent hybrid complexes. Selected potent complexes displayed substantial inhibition of β-haematin formation in a cell-free NP-40 assay, suggesting an effect on the host haemoglobin degradation pathway as a potential contributing mechanism of action (Figure 2.39**)**.

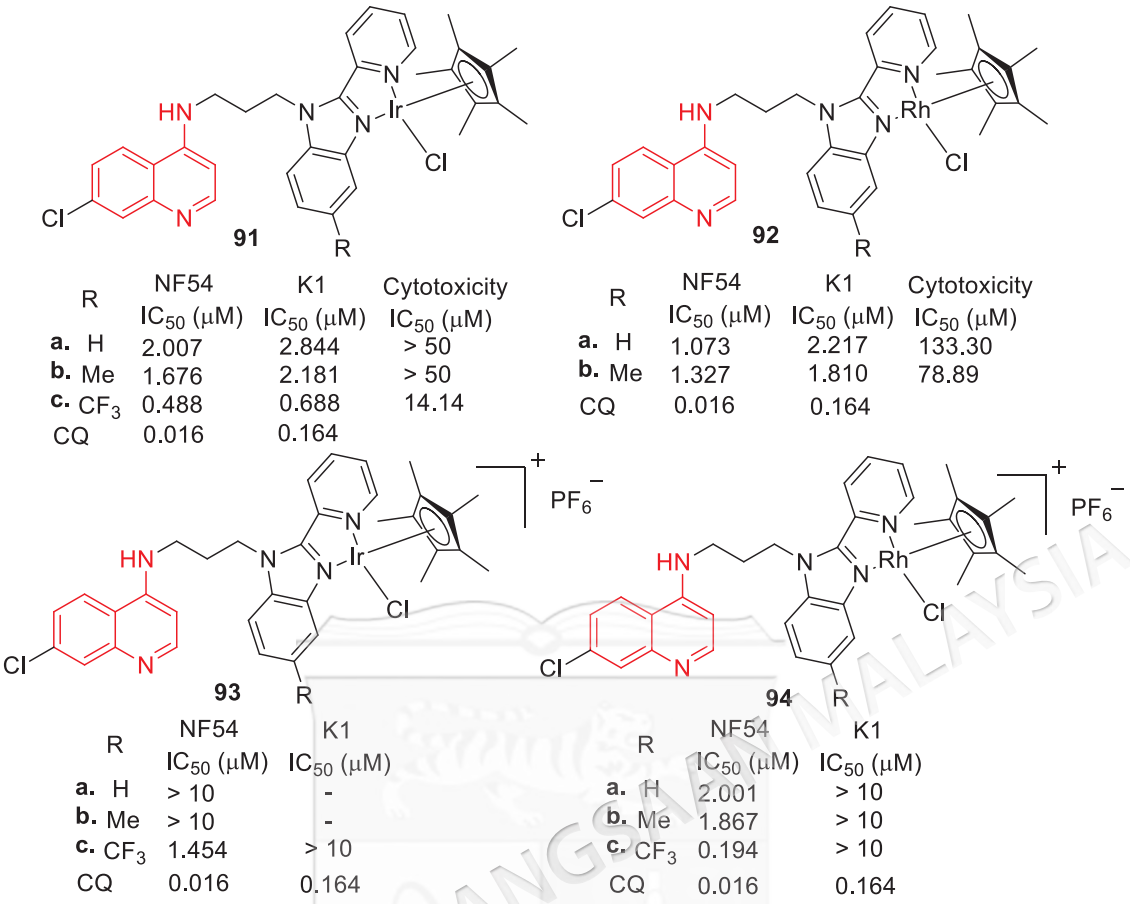

R	NF54 IC_{50} (μM)	K1 IC_{50} (μM)	Cytotoxicity IC_{50} (μM)
a. H	2.007	2.844	> 50
b. Me	1.676	2.181	> 50
c. CF_3	0.488	0.688	14.14
CQ	0.016	0.164	

R	NF54 IC_{50} (μM)	K1 IC_{50} (μM)	Cytotoxicity IC_{50} (μM)
a. H	1.073	2.217	133.30
b. Me	1.327	1.810	78.89
CQ	0.016	0.164	

R	NF54 IC_{50} (μM)	K1 IC_{50} (μM)
a. H	> 10	-
b. Me	> 10	-
c. CF_3	1.454	> 10
CQ	0.016	0.164

R	NF54 IC_{50} (μM)	K1 IC_{50} (μM)
a. H	2.001	> 10
b. Me	1.867	> 10
c. CF_3	0.194	> 10
CQ	0.016	0.164

Figure 2.39 Antiplasmodial activity of Rh/Ir-complex-4-aminoquinolines against NF54 and K1 *P. falciparum* strains

Baartrez et al. (2022) furnished the cationic Rh^{III} polypyridyl benzimidazole-4-aminoquinoline complexes **95** and screened them for their antiplasmodial potency towards the CQS (NF54) and CQR (K1) clones of *P. falciparum*. Selected potent hybrids significantly inhibited β-haematin formation in a cell-free NP-40 assay. All the tested hybrid complexes exhibited better potency towards both NF54 and K1 *P. falciparum* clones and were found to be slightly non-toxic counter to the Chinese hamster ovarian cell line (Figure 2.40).

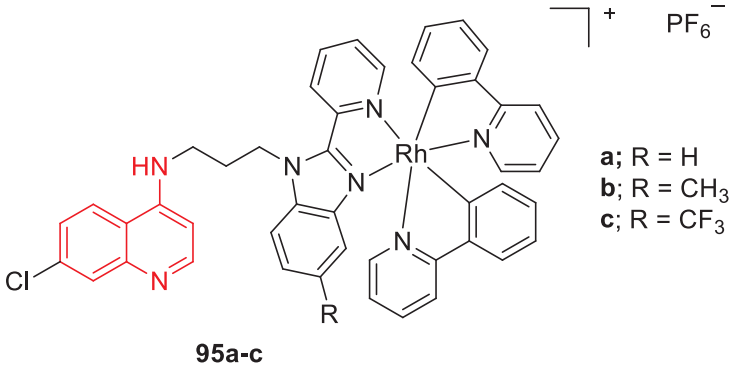

95a-c

Figure 2.40 Antimalarial activity of Rh-complex-4-aminoquinolines against NF54 and K1 *P. falciparum* strains

2.5.17 Miscellaneous 4-Aminoquinolines

Aiming to develop effective antimalarial agents, Van de Walle et al. (2020) tested anti-*P. falciparum* activity of piperidine-based 4-aminoquinoline hybrids towards K1 and NF54 strains. In the series, hybrid **96** was found to be equipotent to CQ (IC_{50}: 0.011 µM) against NF54 strain and higher active against K1 strain than CQ (IC_{50}: 0.167 µM) (Figure 2.41). Of the twenty-two hybrids tested by Vinindwa et al. (2021), chalcone-4-aminoquinoline molecular hybrids, **97a-b**, having a propyl linker were more active than the ethyl linker counterparts against the NF54 strain (Figure 2.41). When comparing the antimalarial activity of triazolopyrimidine-based 4-aminoquinoline hybrids furnished by Chowdhary et al. (2022), analog **98** with an octylamine linker between 4-aminoquinoline and triazolopyrimidine units was found to be a most potent candidate against both the W2 and 3D7 strains with IC_{50} values of 0.20 and 0.17 µM, respectively. It is worth mentioning that **98** showed a 3-fold enhanced activity compared to CQ against the W2 strain (Figure 2.41**)**.

Harmine-based 4-aminoquinolines were examined by Poje et al. (2022) for their antimalarial efficacy towards *P. falciparum* CQS 3D7 and CQR 7G8, K1, and Dd2 strains. The most effective hybrid, **99**, showed 5.5-fold enhanced activity than CQ against the 3D7 strain and 15.9-fold higher activity against all the CQR strains than CQ with high SI (4450) (Figure 2.41**)**. Srbljanovic et al. (2020) recognized thiophene and benzothiophene-based 4-aminoquinoline molecular hybrids as effective anti-*P. falciparum* agents against 3D7 and Dd2 strains. Only one of the tested hybrids, **100**, demonstrated comparable potency (IC_{50}: 18.77 nM) to CQ against the 3D7 strain,

whereas all of them were more potent against the Dd2 strain than CQ with lower IC_{50} values (Figure 2.41**)**.

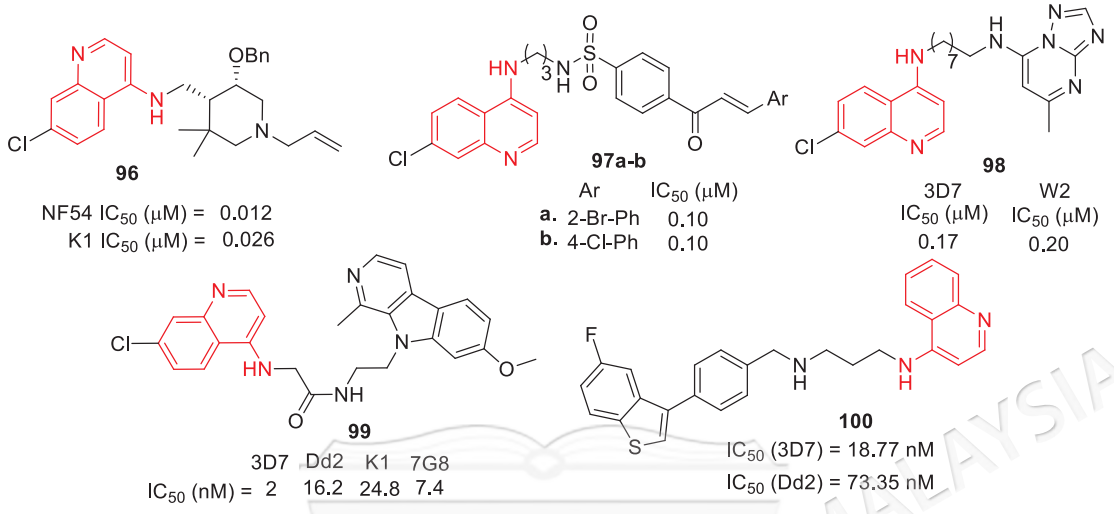

Figure 2.41 Antiplasmodial potency of 4-aminoquinolines hybridized with piperidine, chalcones, triazolopyrimidine, harmine, and thiophene

Ionic liquids produced from benchmark antimalarials are emerging as a unique approach to cost-effective drug rescue. The laureate salt of CQ (**101**) synthesized by Silva et al. (2020) was a promising ionic liquid against the *P. falciparum* Dd2 and 3D7 strains with IC_{50} values of 110 and 4 nM, respectively (Figure 2.42**)**. Among the series of Kalita et al. (2020), the inhibitory activity of hybrid **102** with *ortho*-hydroxy phenyl ring (IC_{50}: 0.0008 μM) was comparable to CQ against 3D7 and RKL9 strains (Figure 2.42**)**. Benzenesulfonamide-based 4-aminoquinoline hybrid **103** with the 2-naphthyl ring on the benzenesulfonamide unit emerged as the most promising candidate against the 3D7 strain (IC_{50} = 0.89 μM) among the series of Silveira et al. (2021) (Figure 2.42**)**.

Remarkable antimalarial activities with <1 μM of IC_{50} value were noticed against W2 strain in the case of 4-aminoquinolines incorporated with imines and hydrazones synthesized by Marinho et al. (2021). Hybrid **104** (IC_{50} = 0.215 μM) among the hydrazone series and 105 (IC_{50} = 0.145 μM) of the imine series were proved to be more active agents against the W2 strain (Figure 2.42**)**. The hybrids containing methyl group at 4-aminoquinoline nuclei were constructed by Tiwari et al. (2021) and examined for their anti-*P. falciparum* efficacy against K1 and 3D7 strains. The most promising agent, **106**, demonstrated lower IC_{50} values of 0.06 and 0.04 μM against K1

and 3D7 strains, respectively (Figure 2.42). Neto et al. (2022) identified dual hybrid 4-aminoquinolines as potential antimalarial agents. Of them, hybrid **107** showed nearly comparable activity to CQ (IC_{50} = 0.026 µM) against the 3D7 strain and hybrid 108 displayed 4-fold higher potency against the Dd2 strain (IC_{50} = 0.201 µM) than the reference CQ (IC_{50} 0.828 µM) (Figure 2.42**)**.

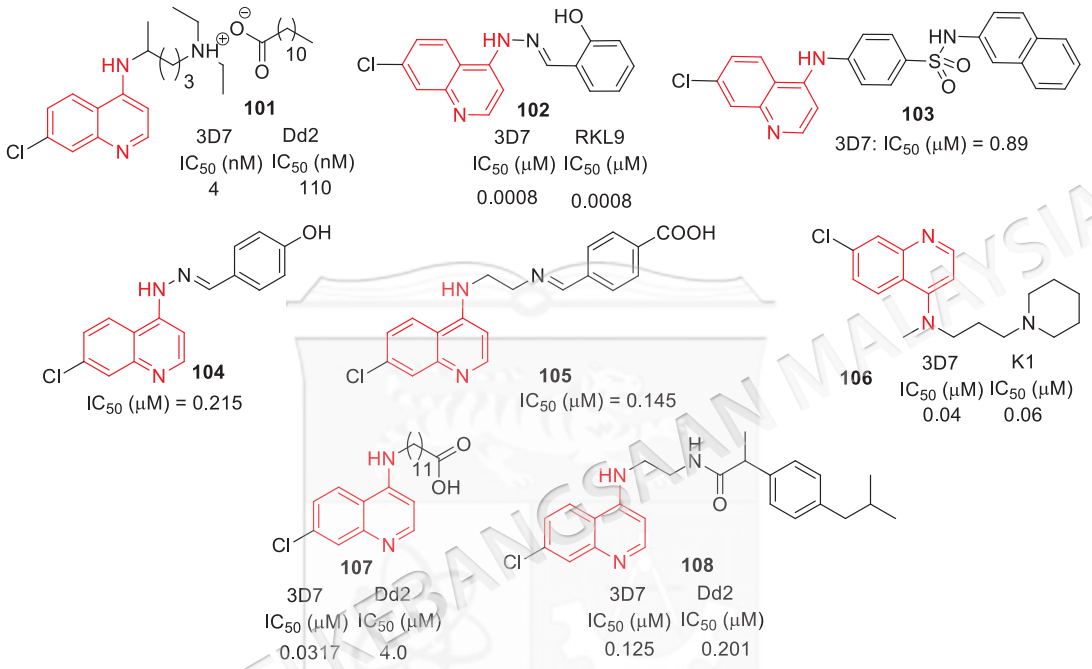

Figure 2.42 Antimalarial properties of 4-aminoquinolines

2.6 *IN VITRO* ANTIMALARIAL ACTIVITY OF PYRAZOLE DERIVATIVES

Pyrazole-incorporated hybrids are simple and effective scaffolds that considerably produce extremely effective and low-toxic antimalarial drugs (Ravindar et al. 2022; Shamsuddin et al. 2020). Pyrazole derivatives bearing quinoline, pyran, pyrazoline, pyridine, pyrimidine, imidazopyridazine, diazepine, curcumin, thiazole, benzothiazole, thiazolidine, triazine, oxadiazole, chalcone, furan, and aryl moiety are significant scaffolds in the advancement of novel antimalarial drugs.

2.6.1 Quinoline Containing Pyrazoles

A broad range of quinoline carboxylicacids containing substituted pyrazole derivatives was furnished and examined *in vitro* antimalarial potency counter to *P. falciparum* clone employing QN and CQ as reference drugs (Pandya & Patel & Desai 2019). All the

clubbed quinoine-pyrazoles **109-112** demonstrated excellent antimalarial potency against the *P. falciparum* clone with an IC_{50} value range between 0.036 and 1.55 µg/mL. Twenty-five of thirty-five synthesized were the most potent, with less than 1 µg mL-1 of IC_{50} values. Among them, compound **111g** emerged as more potent with IC_{50} 0.036 µg/ml, followed by **112f** and **111f** with 0.087 and 0.092 µg/mL of IC_{50} values, respectively, which were lower than that of standard agent QN (IC_{50} = 0.268 µg/mL). All other hybrids were not as potent as QN and CQ counter to the *P.falciparum* clone (Figure 2.43).

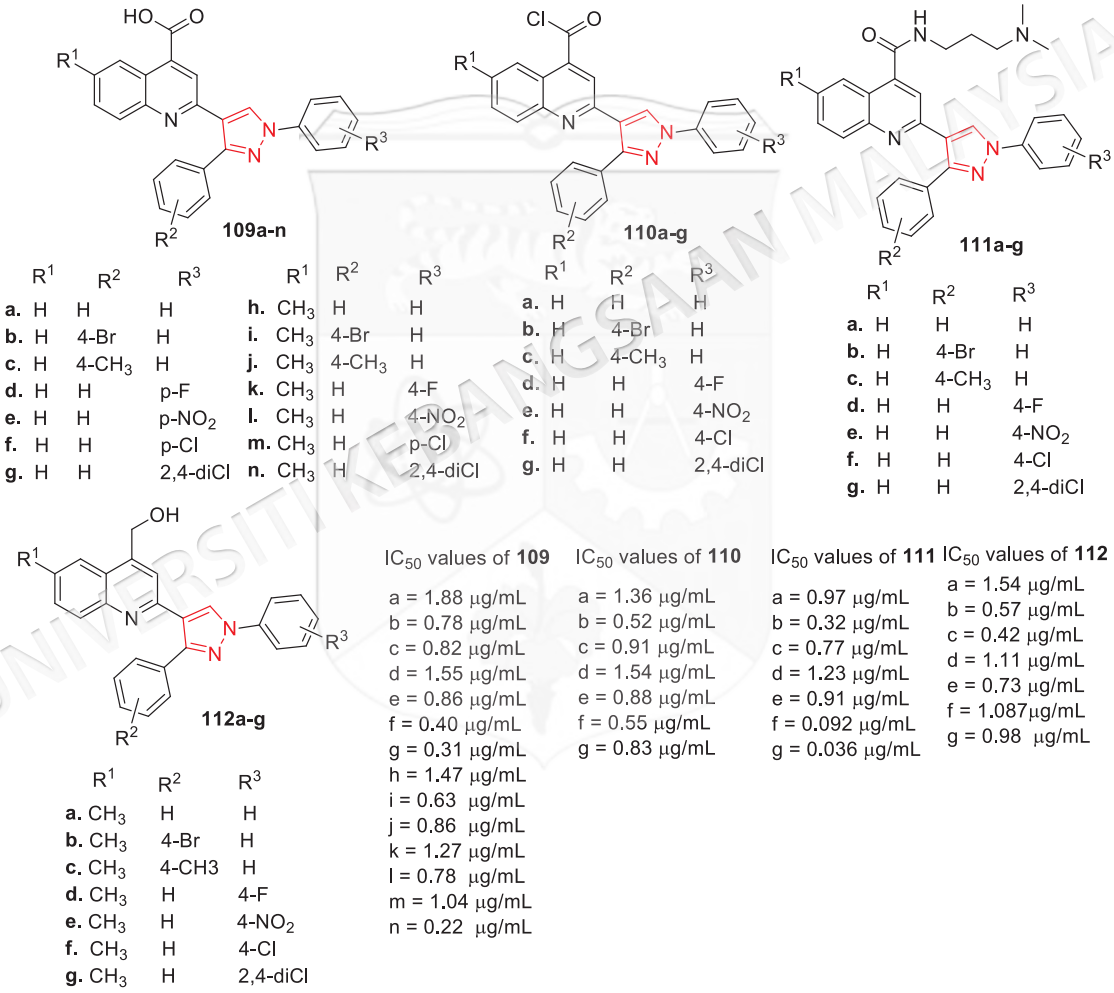

Figure 2.43 Antimalarial activity of quinolinein containing pyrazoles against *P. falciparum* strain

2.6.2 Pyran Containing Pyrazoles

Very recently, a range of pyrano[2,3-*c*]-pyrazole-5-carbonitriles **113** were synthesized and identified as antimalarial drugs and screened for their antimalarial potency counter

to the CQS (3D7) clone of *P. falciparum* employing QN (IC_{50} = 0.268 µg/mL) and CQ (IC_{50} = 0.020 µg/mL) as standard drugs (Parikh et al. 2022). All the ten constructed hybrids were found to be potent with a 0.027-2.09 µg/mL range of IC_{50} values, which is lower than the standard CQ. Compared to the standard QN drug, compounds **113a-d** displayed higher antimalarial activity, whereas **113e-j** was lower in antimalarial potency than the 3D7 *P. falciparum* clone. Among all, compound **113d** (IC_{50} = 0.027 µg/mL), having $–CF_3$ functional group, showed the highest activity, followed by **113c** (IC_{50} = 0.032 µg/mL) counter to the *P. falciparum* clone (Figure 2.44).

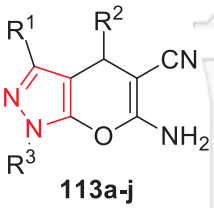

113a-j

	R^1	R^2	R^3	
a.	CF_3	Ph	Ph	(IC_{50} = 0.21 µg/mL)
b.	CF_3	4-BrPh	Ph	(IC_{50} = 0.26 µg/mL)
c.	CF_3	Ph	4-ClPh	(IC_{50} = 0.032 µg/mL)
d.	CF_3	4-OMePh	4-ClPh	(IC_{50} = 0.027 µg/mL)
e.	Me	Ph	3-NO_2Ph	(IC_{50} = 1.35 µg/mL)
f.	Me	3-Br-4-OMePh	3-NO_2Ph	(IC_{50} = 1.58 µg/mL)
g.	Me	4-NO_2Ph	3-NO_2Ph	(IC_{50} = 0.58 µg/mL)
h.	Me	4-OMePh	3-NO_2Ph	(IC_{50} = 1.24 µg/mL)
i.	Me	4-OHPh	3-NO_2Ph	(IC_{50} = 0.87 µg/mL)
j.	Me	5-Br-2-OHPh	3-NO_2Ph	(IC_{50} = 1.86 µg/mL)

Figure 2.44 Antimalarial activity of Pyran containing pyrazole derivatives against *P. falciparum* strain

2.6.3 Pyrazoline Containing Pyrazoles

Kumar et al. (2018) discovered various pyrazoline-pyrazole hybrids endowed with benzenesulfonamide **114.** Using CQ as a reference drug, they tested the *in vitro* antimalarial potency against CQR (RKL9) and CQS (3D7) *P. falciparum* strains. All the tested compounds (**114a-q**) were exhibited antimalarial potency against the 3D7 clone of *P. falciparum* with 1.38 to 6.67 µM range of EC_{50} values, whereas only selected compounds **114a-g** found to be potent counter to RKL-9 *P. falciparum* clone with the EC_{50} values range between 1.31 and 2.39 µM. Compared to their reference drug CQ, compounds **114a-g** exhibited higher potency against RKL-9 and 3D7 *P. falciparum* strains. *In vivo,* the antimalarial action of the most potent compound, **114f,** was tested against the *P. berghei* mouse model and demonstrated promising results with good mean survival days (Figure 2.45).

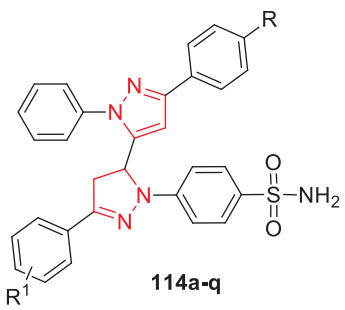

114a-q

	R	R^1	3D7 (EC_{50})	RLK-9 (EC_{50})		R	R^1	3D7 (EC_{50})
a.	H	4-OMe	1.42	1.78	**h.**	H	4-F	6.67
b.	4-F	4-OH	1.57	2.02	**i.**	H	4-Cl	3.35
c.	4-F	4-OMe	1.65	2.39	**j.**	H	4-OH	3.05
d.	4-Cl	4-OMe	1.61	2.12	**k.**	H	2,4-diCl	4.58
e.	4-Me	4-Me	1.43	1.64	**l.**	4-F	4-Br	3.08
f.	4-Me	4-OMe	1.38	1.31	**m.**	4-F	4-F	6.36
g.	4-Me	2,3-diOMe	1.61	1.55	**n.**	4-F	4-Me	2.23
					o.	4-Me	4-H	2.97
					p.	4-Cl	4-Cl	2.80
					q.	4-OMe	4-OMe	2.26

Figure 2.45 Antimalarial activity of pyrazoline-pyrazole hybrids against *P. berghei* and RKL9 and 3D7 strains of *P. falciparum*

Recently, Akolkar et al. (2022) have screened the antimalarial efficacy of pyrazoline containing pyrazole derivatives **115-118** counter to *P. falciparum* employing CQ and QN as standard drugs. Molecular hybrids of the benzene, pyrazoline, and thiophene, ring increased the antimalarial activity (Figure 2.46). Hybrids **116** and **117** were equipotent with 0.47 µM of IC_{50} value, lower than the standard quinine (IC_{50} = 0.83 µM). The inhibition potency **118** (IC_{50} = 0.21 µM) was 4-fold higher than the reference QN.

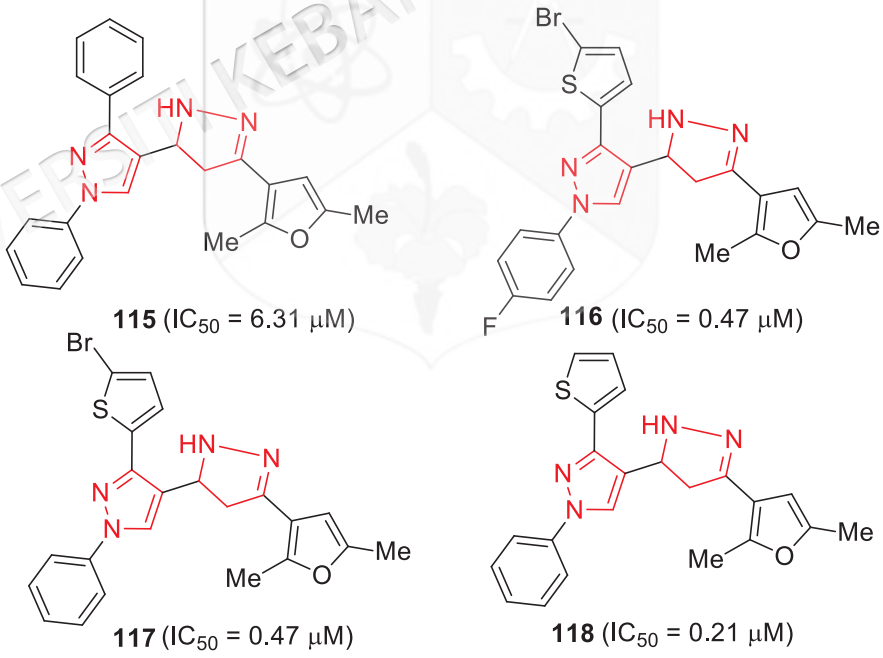

115 (IC_{50} = 6.31 µM)

116 (IC_{50} = 0.47 µM)

117 (IC_{50} = 0.47 µM)

118 (IC_{50} = 0.21 µM)

Figure 2.46 Antimalarial activity of pyrazoline containing pyrazoles as against *P. falciparum*

2.6.4 Pyridine Containing Pyrazoles

A novel series of acyl hydrazone-based molecular hybrids of 1,4-dihydropyridine and pyrazole **119** was identified as an antimalarial hybrid and tested for their *in vitro* antimalarial potency counter to CQS (3D7) *P. falciparum* strain employing chloroquine as reference compound (Kumar et al., 2017). All the screened compounds exhibited higher antimalarial potency (IC_{50} values range between 4.40 and 16.87 µM) than commercial drugs ART and CQ. Among all tested hybrids, compound **119g** was more potent with 4.40 µM of IC_{50} value (Figure 2.47).

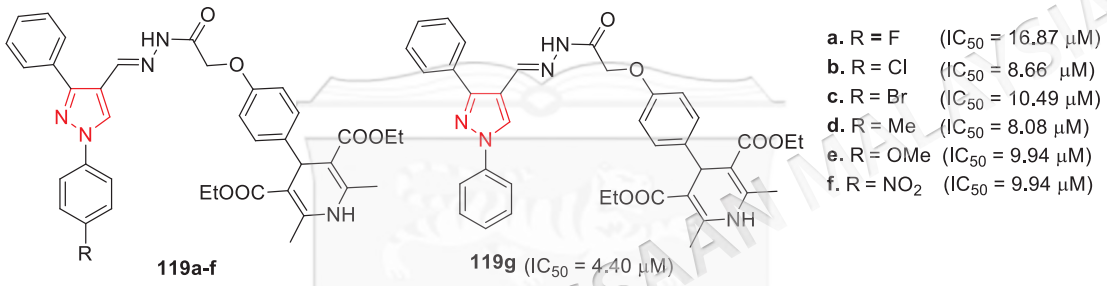

Figure 2.47 Antimalarial activity of acyl hydrazone substituted against the 3D7 *P. falciparum* strain

2.6.5 Pyrimidine Containing Pyrazoles

Azeredo et al. (2017) developed and synthesized the pyrazolopyrimidine derivatives incorporated with diverse arylamines at seventh position **120** and screened *in vitro* counter to CQR W2 *P. falciparum* clone *in vivo* counter to the *P. berghei*-infected mouse model, and *in vitro* as inhibitors of *Pf*DHODH. Out of fifteen hybrids synthesized, thirteen were active counter to *P. falciparum*, with IC_{50} value range between 1.2 and 92.4 µM. The *Pf*DHODH inhibition revealed that compounds with β-naphthylamine at the seventh position (**120n-o**) were the more potent. Hybrid **120o** exhibited higher and selective inhibitory activity (IC_{50} = 0.16µM), followed by **120n** and **120m**, with 4.0 and 6.0 µM of IC_{50} values, respectively. Hybrids **120n** and **120m** displayed low toxicity and higher SI values of 79.6 and 467.8, respectively. Hence, these hybrids were screened *in vivo* in *P. berghei*-infected mouse mode. On day 5, upon treatment at 5 mg/kg, administered orally, both hybrids reduced parasitemia by 50% (Figure 2.48).

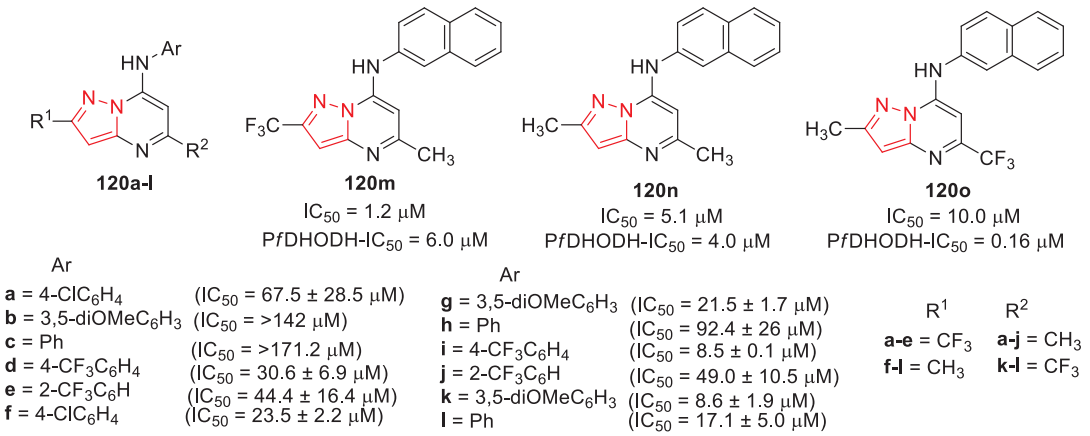

Figure 2.48 Antimalarial activity of 7-arylaminopyrazolo[1,5-*a*]pyrimidines against the W2 *P. falciparum* clone and *P. berghei*

The following year, a broad range of pyrazolopyrimidine derivatives conjugated with phenyl and benzenesulfonamide moieties having various substituents at the para-position **121** were furnished and screened *in vitro* counter to CQR W2 *P. falciparum* clone (Silvira et al. 2018). Out of nine hybrids synthesized, six demonstrated *in vitro* potency against the W2 *P. falciparum* strain, with an IC_{50} value range between 5.13 and 43.40 μM. Among them, hybrid **121c** emerged as the most active one with an IC_{50} of 5.13 μM, higher than the reference compound CQ (IC_{50} = 0.55 μM) and lower than the sulfadoxine (IC_{50} = 15.0 μM). Most synthesized hybrids displayed higher SI values than sulfadoxine, the standard agent (Figure 2.49).

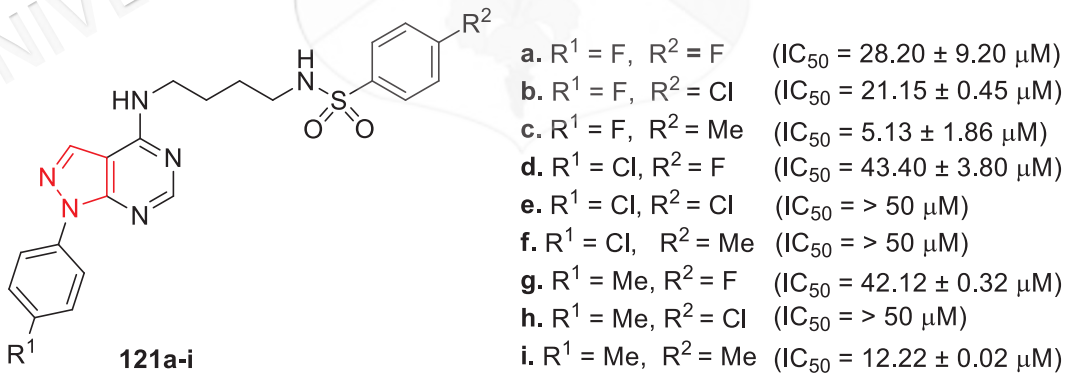

Figure 2.49 Antimalarial activity of pyrazolopyrimidine-benzenesulfonamide derivatives against the W2 *P. falciparum* strain

Further, imidazo[1,2-*a*]pyrimidine incorporated pyrazole derivatives **122-123** were designed and synthesized by Prasad & Kalola & Patel (2018) and screened antimalarial potency counter to *P. falciparum* employing chloroquine and quinine as

reference drugs. All the tested hybrids exhibited superior potency with the IC_{50} value range between 0.030 and 1.45 µg/ml. SAR studies showed that the hybrids having -F substituent at the *para* position of the phenyl ring (**122e** and **123e**) displayed excellent antimalarial activity with 0.030 and 0.041 µg mL^{-1}, respectively, whereas the hybrids with -Me group at the *para* position of the phenyl ring (**122b** and **123b**) demonstrated below average results with IC_{50} 1.84 and 1.50 µg mL^{-1}, respectively. Among the heterocyclic substituents at the sixth position of the pyrimidine ring, *N*-containing heterocycles demonstrated superior antimalarial activities than *S*-containing heterocycles (Figure 2.50).

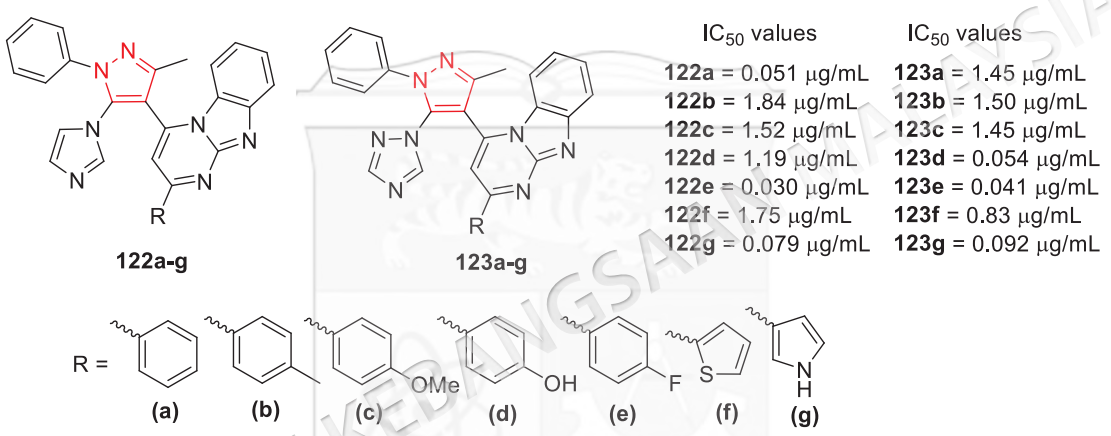

Figure 2.50 Antimalarial activity of imidazo[1,2-*a*]pyrimidine substituted pyrazoles against *P. falciparum*

2.6.6 Oxadiazole Containing Pyrazoles

The *in vitro* antimalarial potency of pyrazole acrylic acid-based oxadiazoles **124** counters to CQS (3D7) *P. falciparum* clone was tested by Verma et al. (2018) and displayed potent antimalarial activity with 0.245 to 3.507 µg/ml range of IC_{50} values. Four compounds, **124e**, **124q**, **124t**, and **124v**, out of twenty-four synthesized were the most potent, with less than 1 µg/ml of IC_{50} values (0.515, 0.489, 0.503, and 0.245 µg/ml, respectively). These four compounds were further examined for activity counter to CQR (RKL9) *P. falciparum* clone and showed an IC_{50} value of 1.1571, 0.902, 1.571, and 0.724 µg/ml, respectively (Figure 2.51).

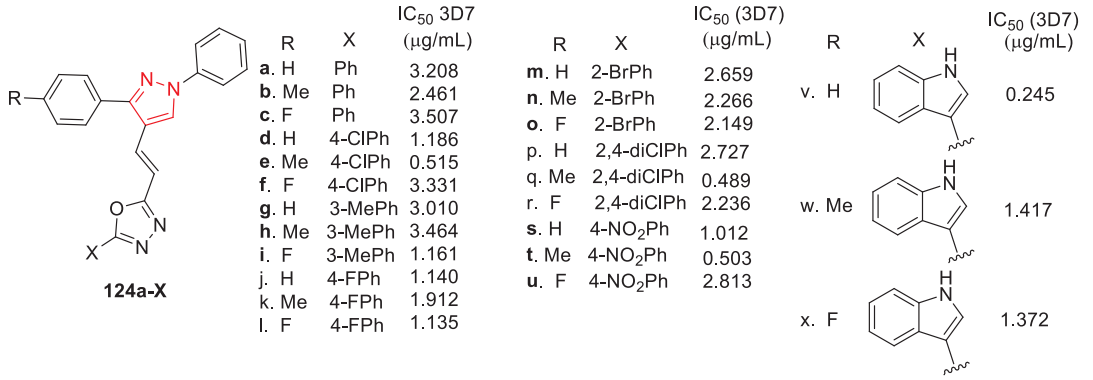

Figure 2.51 Antimalarial activity of pyrazole acrylic acid-based oxadiazole derivatives against 3D7 and RKL9 *P. falciparum* strains

Continuance of their interest in the antimalarial potency of pyrazole acrylic acid-based oxadiazole derivatives; an extension was carried out in the next year by Verma et al. (2019). All the furnished hybrids demonstrated potent antimalarial activity against the CQS (3D7) *P. falciparum* clone with an IC_{50} value range between 0.248 and 4.316 μg ml^{-1}. Out of eighteen compounds synthesized, six (**125a**, **125f**, **125g**, **125n**, **125o** and **125r**) were found to be the most potent with less than 1 μg/ml of IC_{50} values (0.886, 0.248, 0.647, 0.322, 0.582 and 0.494 μg ml^{-1}, respectively). Among them, compound **125f** has emerged as the most active one with an IC_{50} of 0.248 μg ml^{-1} followed by **125n** with an IC_{50} of 0.322 μg ml^{-1}. Both were lower than standard agent CQ (IC_{50} = 0.405 μg ml^{-1}) (Figure 2.52).

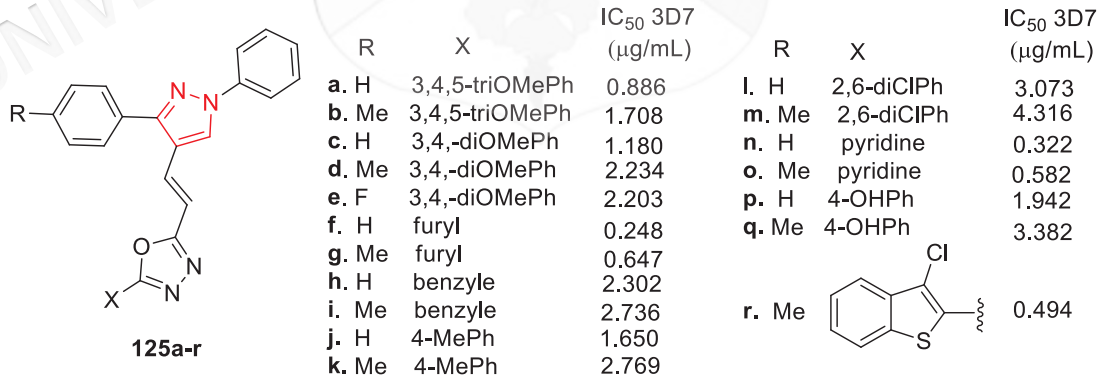

Figure 2.52 Antimalarial activity of pyrazole acrylic acid-based oxadiazole derivatives against the 3D7 *P. falciparum* strain

2.6.7 Curcumin Analogues Containing Pyrazoles

Balaji et al. (2015) also tested the *in vitro* antimalarial activity of several curcumin analogs having pyrazole ring **126**. All the examined compounds displayed

schizonticidal potency with an IC_{50} value range between 4.21 and 23.09 µM and parasiticidal activity with minimum killing concentrations (MKCs) ranging from 4.18 to 25.35 µM. Among the tested carboxamide (**126a-e**) and methanone (**126f-o**) analogs, compounds **126e** (IC_{50}; 9.87 µM) and **126o** (IC_{50}; 4.21 µM) exhibited maximum schizonticidal activity, respectively. Compound **126q** had a lesser schizonticidal activity with a 23.09 IC_{50} value among all the tested compounds (Figure 2.53).

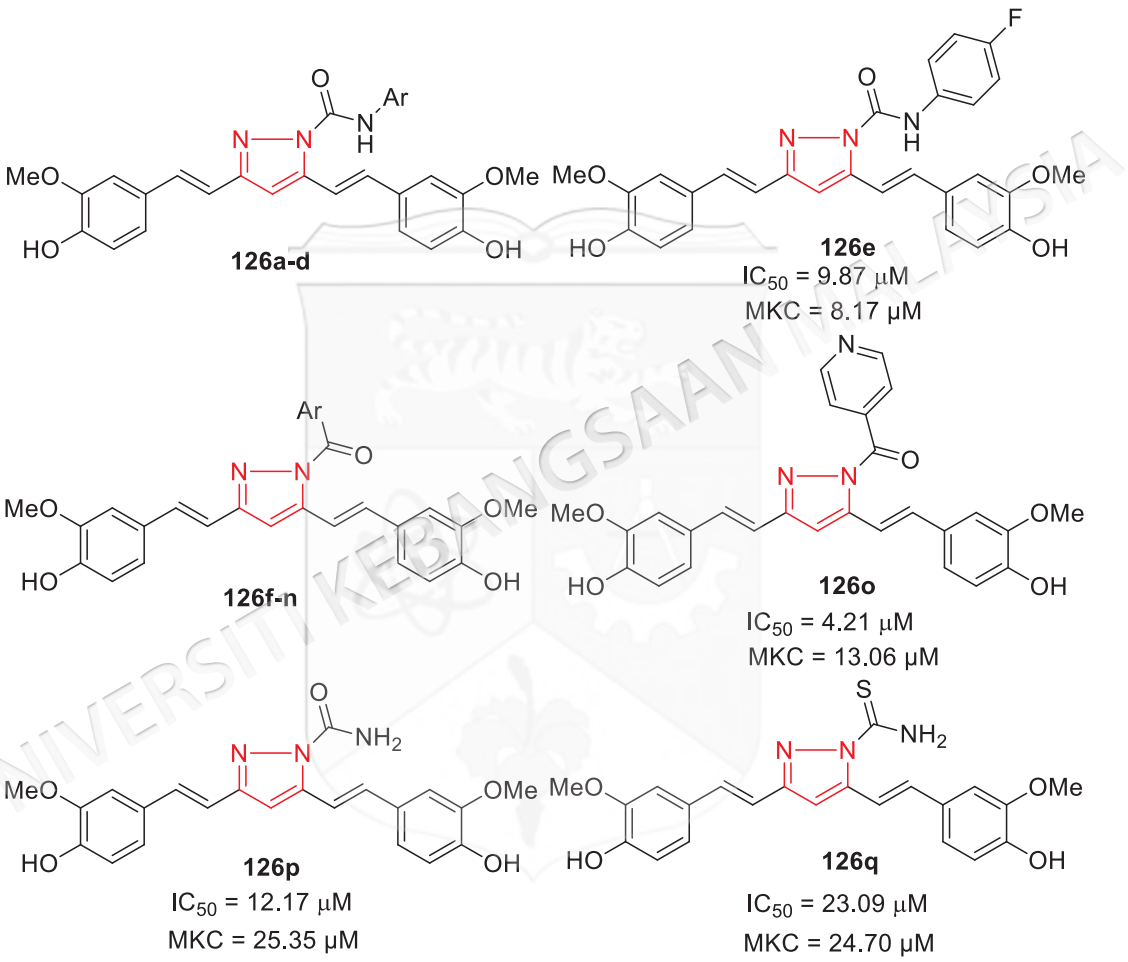

Figure 2.53 Antimalarial activity of curcumin analogs having pyrazole rings against *P. falciparum*

2.6.8 Chalcone Containing Pyrazoles

Chalcone (1,3-diaryl-2-propen-1-one) derivatives are simple and well-known analogs important progressing of highly active, less toxic antimalarials (Qin et al., 2020). Recently, Akolkar et al. (2020) have examined the antimalarial potency of chalcone containing pyrazole derivatives **127-130** counter to *P. falciparum* employing CQ and

quinine as standard drugs. All the tested hybrids displayed potency with an IC_{50} value range between 1.46 and 3.93 µM. The strongest potency was found in hybrid **127** with an IC_{50} 1.46 µM. (Figure 2.54).

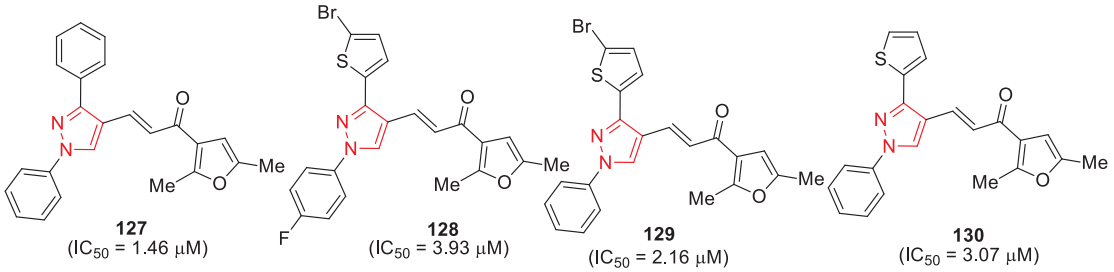

Figure 2.54 Antimalarial activity of compound **127** against *P. berghei* and compounds **128-130** against *P. falciparum*

2.6.9 Furan Containing Pyrazoles

Choudhary et al. (2022) furnished a wide variety of novel furan containing pyrazoles **131-133** and examined antiplasmodial potency based on *in vitro* antimalarial potency counter to the CQR (K1) *P. falciparum* strain. All the twenty-four furnished compounds displayed potent anti-plasmodial activity counter to the K1 clone of *P. falciparum*. Among the series **131a-h**, hybrids **131a**, **131d**, **131e**, **131f**, and **131g** exhibited very good activity with IC_{50}value <5 µg/ml, followed by hybrid **131b** with IC_{50} value <10 µg/ml, whereas hybrids **131c** and **131h** displayed lower antimalarial activity with IC_{50} value greater than 10 µg/ml. Similarly, hybrids **132d**, **132e**, **132f**, and **132g** displayed excellent antimalarial potency, while hybrids **132c** and **132h** were found to have poor activity. In addition, hybrids **133e**, **133f**, and **133g** also exhibited higher antimalarial potency, although hybrids **133b** and **133h** demonstrated a much lesser activity. According to the SAR studies, halogen as R substituent enhanced activity, whereas electron-donating or electron-withdrawing groups as R substituent reduced activity. Among all the twenty-four furnished hybrids, **132d** and **132g** have emerged as excellent antimalarial agents with IC_{50} values of 1.968 and 1.983 µg/mL, respectively (Figure 2.55).

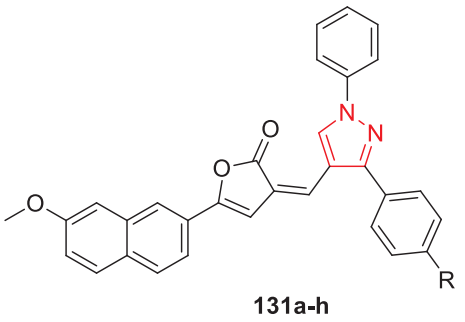

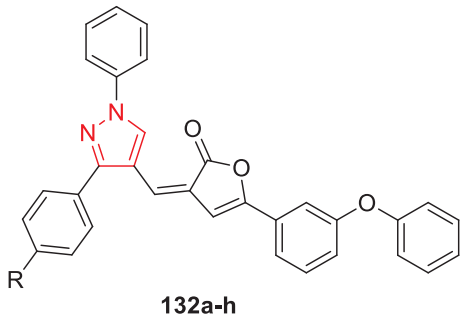

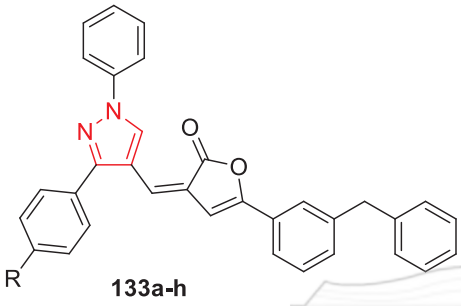

R	IC50 K1 (μg/mL)	R	IC50 K1 (μg/mL)	R	IC50 K1 (μg/mL)
131a. H	2.241	**132a**. H	8.271	**133a**. H	5.157
131b. Me	7.451	**132b**. Me	5.243	**133b**. Me	11.028
131c. OH	12.006	**132c**. OH	16.062	**133c**. OH	14.149
131d. OMe	2.258	**132d**. OMe	1.968	**133d**. OMe	7.251
131e. Cl	3.960	**132e**. Cl	3.251	**133e**. Cl	2.069
131f. F	2.238	**132f**. F	2.025	**133f**. F	2.358
131g. Br	3.125	**132g**. Br	1.983	**133g**. Br	2.473
131h. NO_2	15.406	**132h**. NO_2	23.792	**133h**. NO_2	16.837

Figure 2.55 Antimalarial activity of furan containing pyrazole derivatives against the K1 *P. falciparum* strain

2.6.10 Diazepine Containing Pyrazoles

A broad range of Pyrazolo[3,4-*b*][1,4]diazepine derivatives **134** was identified as antimalarial agents and screened *in vitro* antimalarial potency counter to *Plasmodium* parasite using CQ as the reference compound (Insuasty et al. 2015). All the tested compounds **134a-f** exhibited moderate *in vitro* antimalarial potency against the *Plasmodium* parasite, with the IC_{50} value range between 11.3 ± 2.3 and 18.9 ± 1.7μg mL^{-1}. Hybrid **134f** displayed an efficient antimalarial potency against the *Plasmodium* parasite with 11.3 ± 2.3 μg $mL^{-1}$of IC_{50} value (Figure 2.56).

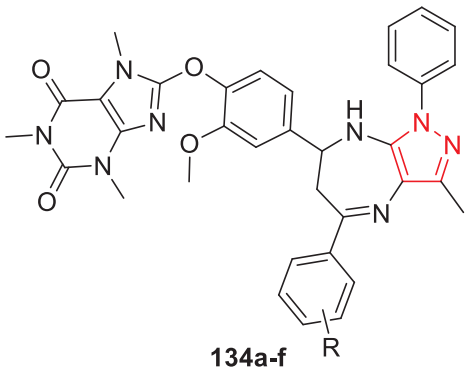

R	IC_{50} (μg/mL)
a. H	13.3 ± 1.9
b. 4-Cl	14.1 ± 2.1
C. 4-F	12.5 ± 2.4
d. 4-CH_3	12.3 ± 2.1
e. 4-OCH_3	13.1 ± 2.4
f. 3,4,5-triOCH_3	11.3 ± 2.3

Figure 2.56 Antimalarial activity of pyrazolo[3,4-*b*][1,4]diazepine derivatives against *Plasmodium* parasite

2.6.11 Thiazole Containing Pyrazoles

Cheuka et al. (2014) extend the construction of uncovered aminomethylthiazole pyrazole carboxamide derivatives **135-144** by replacing the pyrazole and thiazole cores. Among all the tested analogs, compound **138** exhibited better activity with a 1.84 µM IC_{50} value (Figure 2.57). However, all the synthesized compounds were shown lower *in vitro* antiplasmodial activity against CQS malaria parasite *P. falciparum* (NF54) with an IC_{50} value range between 1.84 and 67.5 µM.

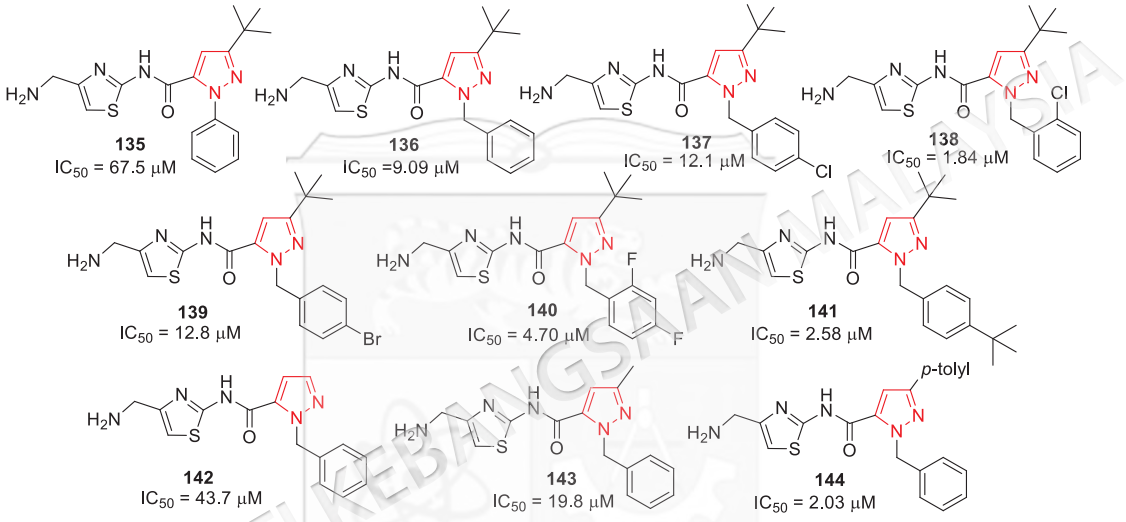

Figure 2.57 Antimalarial activity of aminomethylthiazole pyrazole carboxamide derivatives against the NF54 strain of *P. falciparum*

2.6.12 Benzothiazole Containing Pyrazoles

A wide variety of pyrazoles having benzenethiazole and iminium groups **145** were identified as antimalarial hybrids and tested *in vitro* antimalarial potency counter to CQS (3D7) *P. falciparum* clone (Aggarwal et al. 2018). Hybrids **145g-l** with Ar1 = 4-MePh exhibited higher antimalarial potency with EC_{50} values ranging from 1.953 to 3.518 µg/mL, whereas hybrids **145m-r** with Ar1 = 4-FPh and **145a-f** with Ar1 = Ph exhibited moderate (EC_{50} = 2.59-5.9 µg/mL) and lower (EC_{50} = 2.7-8.3 µg/mL) antimalarial activity, respectively. Among all the tested compounds, hybrid **145l** (Ar2 = 3-ClPh) was found to be the most active one with 1.953 µg/mL of E_{C50} value, followed by hybrid **145j** (Ar2 = 4-ClPh) with the EC_{50} of 1.98 µg/mL while hybrid **145a** (Ar2 = Ph) was found to be the least active one with 8.34 µg/mL of EC_{50} value (Figure 2.58).

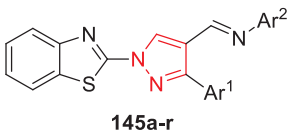

145a-r

Ar^1 = Ph	EC_{50} (μg/mL)	Ar^1 = 4-MePh	EC_{50} (μg/mL)	Ar^1 = 4-FPh	EC_{50} (μg/mL)
a. Ar^2 = Ph	8.342	**g.** Ar^2 = Ph	3.518	**m.** Ar^2 = Ph	5.920
b. Ar^2 = 4-MePh	2.760	**h.** Ar^2 = 4-MePh	2.241	**n.** Ar^2 = 4-MePh	2.726
c. Ar^2 = 4-OMePh	4.126	**i.** Ar^2 = 4-OMePh	3.923	**o.** Ar^2 = 4-OMePh	5.009
d. Ar^2 = 4-ClPh	2.769	**j.** Ar^2 = 4-ClPh	1.983	**p.** Ar^2 = 4-ClPh	5.009
e. Ar^2 = 2-ClPH	4.038	**k.** Ar^2 = 2-ClPH	2.621	**q.** Ar^2 = 2-ClPH	3.753
f. Ar^2 = 3-ClPh	2.702	**l.** Ar^2 = 3-ClPh	1.953	**r.** Ar^2 = 3-ClPh	2.621

Figure 2.58 Antimalarial activity of benzenethiazole-incorporated pyrazoles against the 3D7 strain of *P. falciparum*

2.6.13 Thiazolidine Containing Pyrazoles

Very recently, various pyrazole derivatives linked to thiazolidine moiety were developed and examined for their *in vivo* antimalarial potency counter to the *P. falciparum* clone (Bekhit et al. 2022). All the examined hybrids displayed considerable antimalarial potency with a minimum of 59.3% suppression and the lowest mean survival time of 8.71 days reported with hybrid **146a**. Among the studied compounds, **147a** and **147b** emerged as the most promising antimalarial agents with a maximum suppression of 95.35% and 96.51% and the highest mean survival time of 17.6 and 16.22 days, respectively (Figure 2.59).

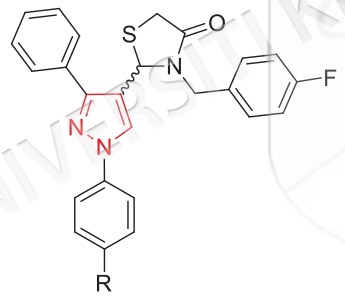

146a,b

a. R = H (59.30% suppression)
b. R = Me (69.77% suppression)

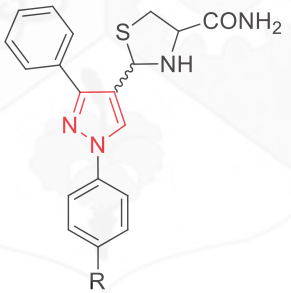

147a,b

a. R = H (95.35% suppression)
b. R = Me (96.51% suppression)

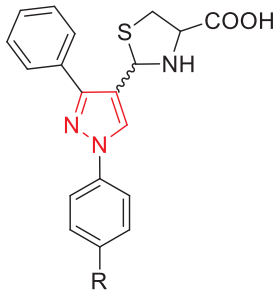

148a,b

a. R = H (69.77% suppression)
b. R = Me (74.42% suppression)

Figure 2.59 Antimalarial activity of thiazolidine-incorporated pyrazoles against *P. falciparum*

2.6.14 Triazine Containing Pyrazoles

Gogoi et al. (2020) examined the *in vitro* antimalarial potency of 1,3,5-triazine incorporated pyrazole derivatives **149** counter to the CQS (3D7) *P. falciparum* clone employing CQ as the standard agent. Out of ten hybrids synthesized, three hybrids **149e** (*p*-chlorophenyl amino-functionalized), **149g** (*p*-bromophenyl amino-functionalized),

and **149h** (*m*-chlorophenyl amino-functionalized) displayed considerable *in vitro* antimalarial potency counter to 3D7 *P. falciparum* clone with 53.85, 62.50, and 100 µg/mL of IC_{50} values, respectively. In contrast, other hybrids displayed no antimalarial potency (Figure 2.60).

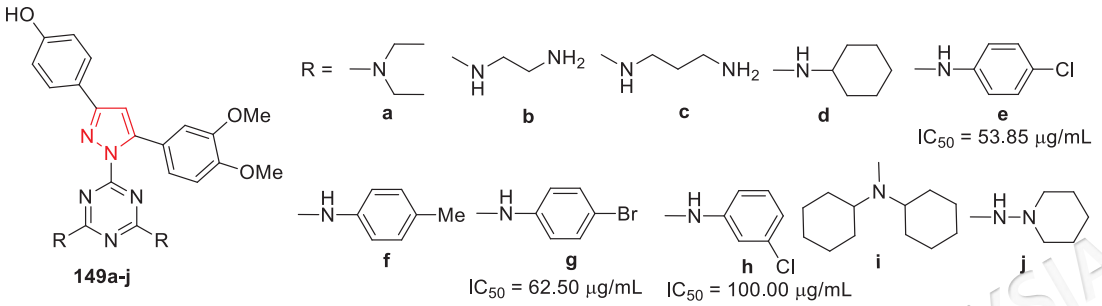

Figure 2.60 Antimalarial activity of 1,3,5-Triazine incorporated pyrazoles against the 3D7 *P. falciparum* clone

2.6.15 Miscellaneous Pyrazoles

A new class of 1,3,4-trisubstituted pyrazole derivatives was developed and studied *in vitro* antimalarial potency counter to CQR (RKL9) *P. falciparum* strain and antiplasmodial activity counter to *P. berghei* (Bekhit et al. 2018). Hybrids **152a-d**, were the most active antiplasmodial agents counter to *P. berghei*, with a higher percentage of inhibition range between 90-100%. The hybrid **152c** demonstrated superior antimalarial potency (IC50 = 0.0142 µM), 13-folder higher than standard CQ phosphate. The *in silico* studies of the most potent analogs counter to the quadruple and wild-type mutant *pf*DHFR-TS structures confirmed the antimalarial activity. Moreover, the hybrids demonstrated significant *in silico* drug-likeness and pharmacokinetics. RBC hemolysis assay and acute toxicity analysis showed satisfactory physiological tolerability of the most potent hybrids up to 150 mg kg^{-1} through the oral route and 75 mg kg^{-1} through the parenteral route (Figure 2.61).

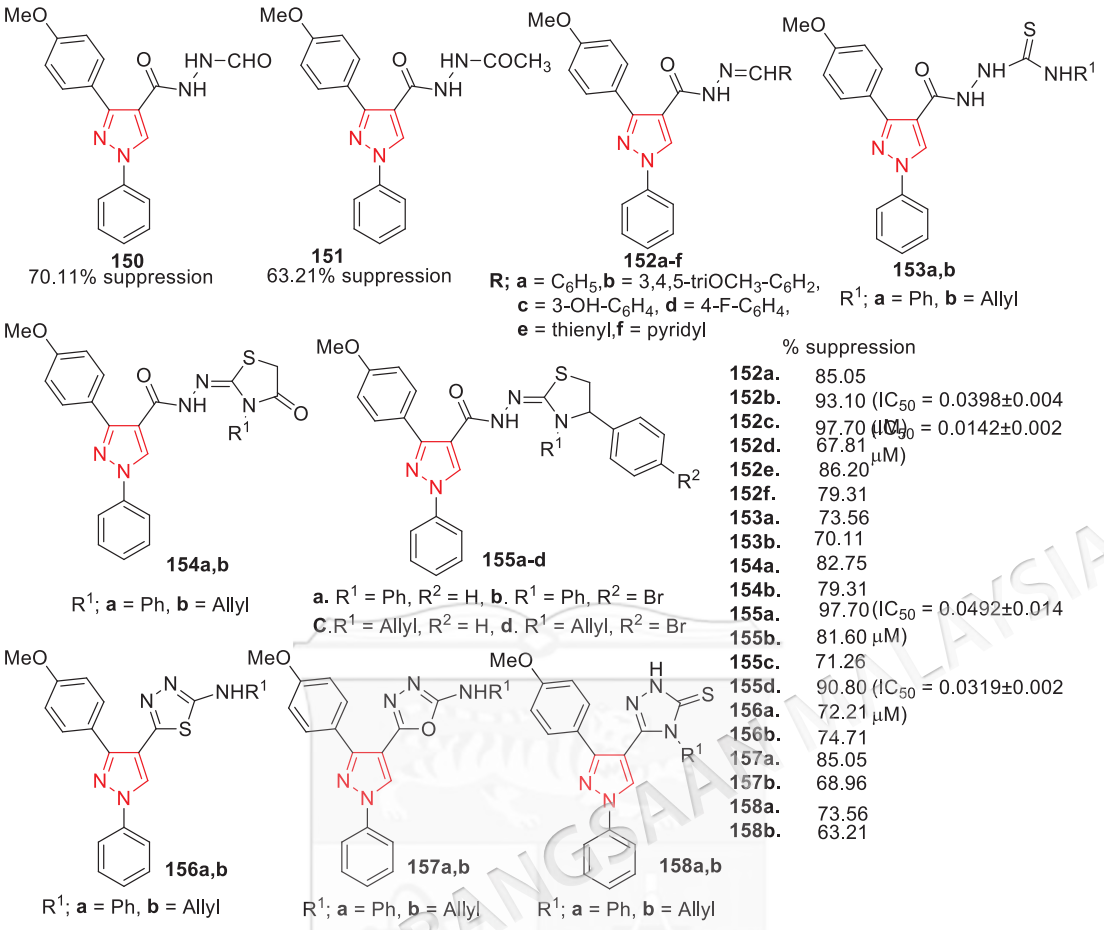

Figure 2.61 Antimalarial activity of 1,3,4-trisubstituted pyrazoles against *P. berghei* and RKL9 *P. falciparum* clone

In the same year, the *in vitro* antimalarial potency of pyrazole acrylic acid-based amide derivatives **159** counter to CQS (3D7) *P. falciparum* clone was tested and displayed potent antimalarial activity with 0.985 to 4.412 µg/mL range of IC_{50} values (Verma et al. 2018). Compound **159g** was further screened for activity counter to CQR (RKL9) *P. falciparum* clone and showed an IC_{50} value of 4.234 µg/mL (Figure 2.62). One compound, **159g** out of eight synthesized, was the most potent, with IC_{50} less than 1 µg/mL of IC_{50} value (0.985µg/mL).

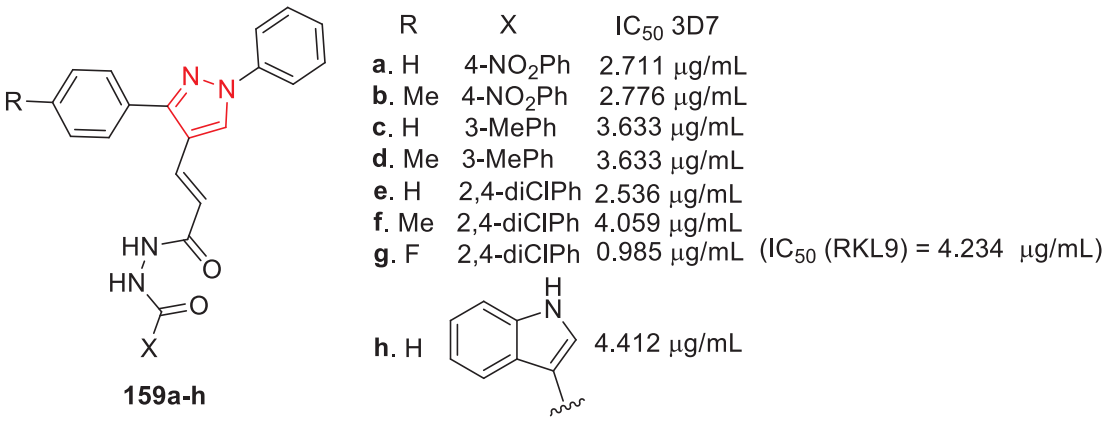

Figure 2.62 Antimalarial activity of pyrazole acrylic acid-based amide derivatives against 3D7 and RKL9 *P. falciparum* clones

The synthetic method for the construction of tetrahydro-1*H*,5*H*-pyrazolo[1,2-*a*]pyrazole-1-carboxylate derivatives **160** and **161** were reported by Strašek et al. (2019), and an assessment inhibition of dihydroorotate dehydrogenase of *Pf*DHODH was demonstrated. All the tested hybrids developed selectivity for *Pf*DHODH more than HsDHODH (Figure 2.63). Compound **161** was found to be the more active with an IC_{50} 2.9 μM.

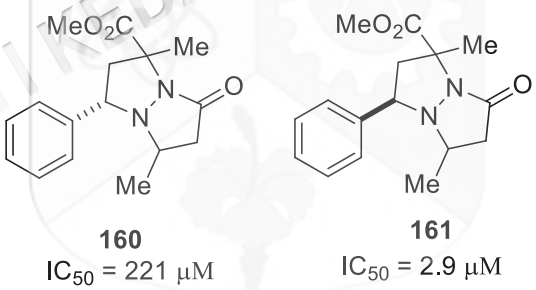

Figure 2.63 Antimalarial activity of tetrahydropyrazolo[1,2-*a*]pyrazole-1-carboxylates

2.7 *IN VITRO* ANTIMALARIAL ACTIVITY OF PYRANO[2,3-*C*]PYRAZOLE-4-AMINOQUINOLINE DERIVATIVES

The hybridization of 4-aminoquinoline with pyrano[2,3-*c*]pyrazoles will increase the antimalarial activity of pyrano[2,3-*c*]pyrazole-aminoquinoline hybrids since pyranopyrazole derivatives have a wide range of therapeutic applications. Recently, Shamsuddin et al. (2021) developed a novel hybridization method to synthesize 4-aminoquinoline-pyrano[2,3-*c*]pyrazole hybrids and screened their antimalarial efficacy towards CQS (3D7), and CQR (K1) strains of *P. falciparum*. For all the evaluations,

CQ (EC_{50} 0.002 µM (3D7) and 0.33 µM (K1)) and ART (EC_{50} 0.0001 µM (3D7) and 0.00017 µM (K1)) were utilized for comparison. All the synthesized hybrids were potent towards the 3D7 and K1 strains of *P. falciparum*. Data from antimalarial assessment revealed that the molecular compound **162** demonstrated better *in vitro* antimalarial activity towards both the 3D7 and K1 *P. falciparum* clones and displayed low to moderate cytotoxic activities, with CC_{50} ranging from 17 to 103 µM. The docking studies showed that hybrid **162b** evidenced the highest binding energy on *P. falciparum* lactate dehydrogenase (*Pf*LDH). This result suggested that *Pf*LDH is a potential molecular target of the furnished hybrid. Overall, all hybrids demonstrated a poor human absorption and low aqueous solubility. Notably, the in silico prediction showed that all the hybrids were hepatotoxic (Figure 2.64).

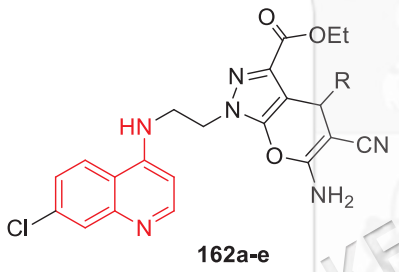

162a-e

		K1	3D7	Cytotoxicity
	R	EC_{50} (µM)	EC_{50} (µM)	CC_{50} (µM)
a.	Ph	0.25 ± 0.03	0.19 ± 0.07	102.54 ± 22.15
b.	4-EtPh	0.02 ± 0.01	0.0130 ± 0.0002	17.60 ± 1.50
c.	furyl	1.61 ± 0.15	0.113 ± 0.002	84.52 ± 6.45
d.	isopropyl	0.30 ± 0.01	3.39 ± 1.89	86.14 ± 7.33
e.	4-OHPh	7.12 ± 3.72	0.026 ± 0.009	9.24 ± 1.33
	CQ	0.33	0.002	138.40 ± 8.77
	ART	0.00017	0.0001	434.60 ± 64.21

Figure 2.64 Antimalarial activity of pyranopyrazole conjugated 4-aminoquinolines towards CQ^S (3D7) and CQ^R (K1) strains of *P. falciparum*

Bulky and lipophilic groups counting furan and phenyl increase the antimalarial potency against CQS strains in **162a**, **162b**, **162c** and **162e**. However, removing the phenyl group in **162d** reduces the compounds' activity. Contrarily, the furan substitutions at the 2nd position commonly reduce the activity against the CQR (K1) strain. Similarly, adding the hydroxyl group in **162e** unfavourably decreased the antimalarial activity. Alkyl substitutions in the para positions (**162b**) confer the best activity against CQR (K1) and CQS (3D7) strains (Figure 2.65).

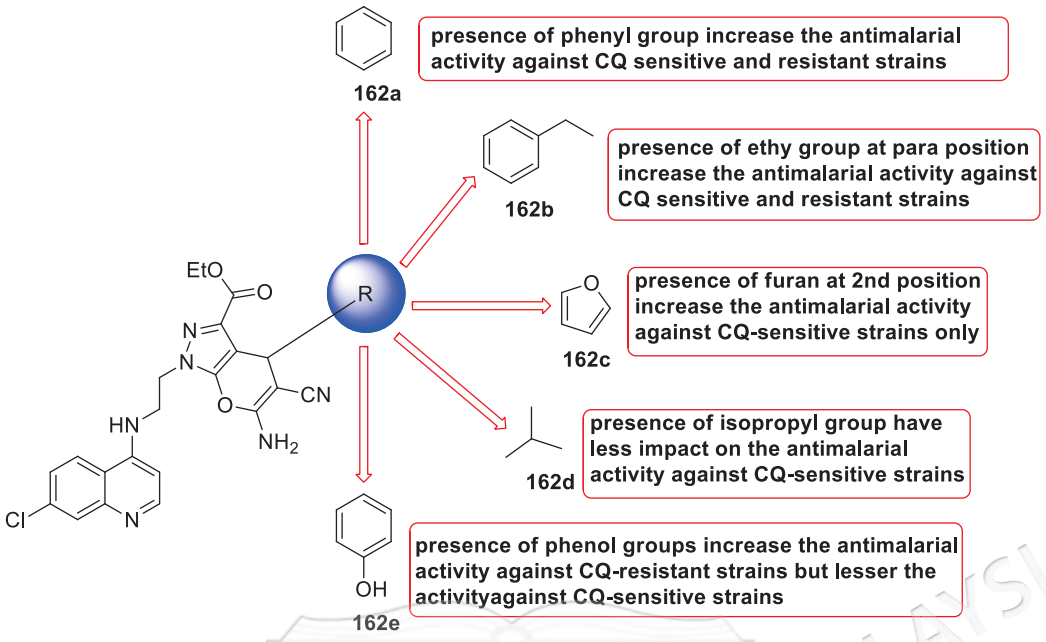

Figure 2.65 The SAR study of 4-aminoquinoline-pyrano[2,3*c*]pyrazole hybrid compounds

Source: Shamsuddin et al. 2021

2.8 CONCLUSION

In conclusion, out of a broad range of *N*-heterocyclic compounds used for antimalarial treatment, pyranopyrazole and 4-aminoquinoline bicycles are efficient moieties in the 21st century. Because of their simple chemistry, ease of synthesis, and a wide variety of biological applications in both natural and synthetic derivatives, these scaffolds are regarded as a biologically relevant active source with several therapeutic potentials including antimalarial activity. Considering the potent antimalarial activity of these scaffolds against both the CQS and CQR strains of *P. falciparum*, this study aimed to synthesize a novel series of pyrano[2,3-*c*]pyrazole-aminoquinoline hybrid compounds as antimalarial agents by covalently linking the moieties of various aromatic substituted pyrano[2,3-*c*]pyrazoles and 4-aminoquinoline *via* an ethyl linker. To achieve this goal, the prediction of good bioavailability using an *in silico* approach (ADMET/PK profile), molecular docking analysis on *Pf*LDH, heme detoxification, *in vitro* antimalarial potencies of all synthesized hybrids against CQS (3D7) and CQR (K1) strains of *P. falciparum* and cytotoxicity against human normal liver WRL68 cell line is carried out in this research.

CHAPTER III

RESEARCH METHODOLOGY

3.1 INTRODUCTION

This chapter discusses the meterials and methods used for the synthesis of 4-aminoquinolines, pyrano[2,3-*c*]pyrazoles, pyrano[2,3-*c*]pyrazole-4-aminoquinoline hybrids, and also *in silic* study methods, isothermal titration calorimetry methods, and *in vitro* study methods.

3.2 MATERIALS AND METHODS

All the solvents (dimethyl sulfoxide, ethyl acetate, n-hexane, toluene, dichloromethane, ethanol, and methanol) and chemicals were commercially available and did not require further purification. Activated charcoal (granulated), 4,7-dichloroquine 97%, monoethanolamine, hydrobromic acid 48%, acetic acid 98%, hydrazine solution 35 wt.% in H_2O, diethyl oxalacetate sodium salt 95%, malononitrile 99%, 4-methoxybenzaldehyde 99%, 3-hydroxybenzaldehyde 99%, 2-methoxybenzaldehyde 98%, 4-ethoxybenzaldehyde 99%, furan-2-carbaldehyde 99%, benzaldehyde 99%, 4-chlorobenzaldehyde 97%, 4-bromobenzaldehyde 99%, 3-nitrobenzaldehyde 99%, 4-nitrobenzaldehyde 98%, 2,4-dihydroxybenzaldehyde 98%, thiophene-2-carbaldehyde 98%, 3-bromo-4-dihydroxybenzaldehyde 97%, 4-formylbenzonitrile 98%, 3-ethoxybenzaldehyde 98%, 4-formylbenzoic acid 97%, 4-hydroxybenzaldehyde 99% 2-hydroxy-1-naphthaldehyde 99% and picolinaldehyde 99% were purchased from Sigma-Aldrich, Darmstadt, Germany and used without further purification unless stated.

Melting points were measured using the Stuart SMP40 instrument at room temperature till 300 ˚C. Elemental study was carried out by a Flash Elemental Analyzer 110 series (Selangor, Malaysia). The reaction progress was monitored using thin-layer

chromatography (TLC) on Merck Kieselgel (New Jersey, NJ, USA) $60F_{254}$, which was visualised with an ultraviolet lamp, and the hybrids were purified utilizing silica gel column chromatography.

Fourier transform infrared (FTIR) spectroscopy is a technique used to identify and confirm the presence of the significant functional groups of pyrano[2,3-c]pyrazoles-aminoquinolines hybrids. In this technique, infrared light source is used to quantify the frequency absorption in a molecule of the compounds showing the presence of functional groups such as amine (NH_2 and NH), cyano (CN), carbonyl (COOEt), and C=C, bonds present pyrano[2,3-*c*]pyrazoles-aminoquinoline hybrids. The FTIR spectra were taken in a wide spectral range of absorption frequency between 500-4000 cm^{-1}. In this study, attenuated total reflection (ATR) was employed in preparing the sample.

Nuclear magnetic resonance (NMR) spectroscopy is a preeminent technique which uses a component of electromagnetic radiation (radio frequency waves) to promote transitions between nuclear energy levels (Resonance) (Tognarelli et al. 2015). NMR is used in this study to elucidate the chemical structures of the pyrano[2,3-*c*]pyrazoles, aminoquinolines and pyrano[2,3-*c*]pyrazole-4-aminoquinoline hybrids. This technique offers complete analysis and interpretations of the entire spectrum with respect to the number and environment of proton and carbon in a compound. This spectroscopy technique was employed at frequency of 400 MHz and 100 MHz for ^{1}H and ^{13}C NMR, respectively. All the samples were dissolved in deuterated (DMSO-d_6 or chloroform-d_6) and processed using Mnova software. Generally, the combined data obtained from FTIR and NMR spectra is often adequate to confirm the identity and structure of the synthesised compounds.

3.3 GENERAL PROCEDURE FOR THE SYNTHESIS OF PYRANO[2,3-*C*]PYRAZOLE DERIVATIVES (20A-S)

Pyrano[2,3-*c*]pyrazole compounds **20a-s** were synthesized in moderate to good yields following the procedure described by Mohammat et al. (2018). To an oven-dried three-neck round-bottom flask (100 mL) with stirring bar charged 35% hydrazine solution (0.49 mL, 5.5 mmol) (**8**), with diethyloxalacetate sodium salt (1.15 g**,** 5.5 mmol) (**18),** 20 ml ethanol, and 1 ml of acetic acid. The reaction mixture was refluxed for 15 minutes.

Malononitrile (0.33 g, 5 mmol) (**19)** and carbonyl compound (5 mmol) were then added to the reaction mixture, and vigorously refluxed for additional 30 minutes. After completion of the reaction (monitoring by TLC), the reaction mixture was cooled to room temperature, and the resulting precipitate formed was filtered off and washed with water, dried, and recrystallized from methanol (Figure 3.1).

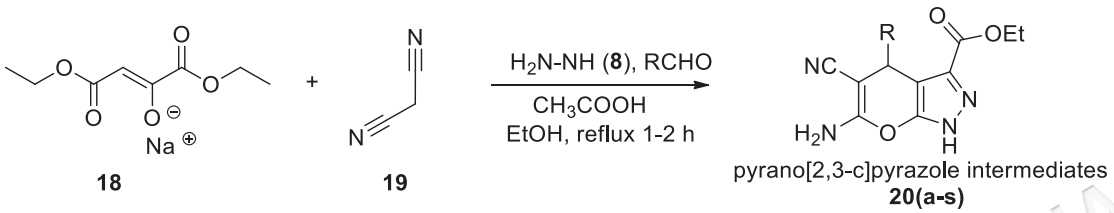

Figure 3.1 Pyrano[2,3-*c*]pyrazoles synthesis

3.3.1 Synthesis of ethyl 6-amino-5-cyano-4-(4-methoxyphenyl)-1,4-dihydropyrano[2,3-*c*]pyrazole-3-carboxylate (20a)

The synthesis method of the pyrano[2,3-*c*]pyrazole compound **20a** is the same as described in subsection 3.3, using a mixture of hydrazine solution 35% (0.49 mL, 5.5 mmol) (**8**), sodium diethyloxalacetate solution (1.15 g, 5.5 mmol) (**18**), 1 mL of Acetic acid, 20 mL of ethanol, Malanonitrile (0.33 g, 5 mmol) (**19**) and 4-methoxybenzaldehyde (0.68 gr, 5 mmol), to yield a white solid (64%). Melting point: 235-236 ^{o}C; ^{1}H NMR (400 MHz, DMSO) δ 13.68 (s, 1H), 7.01 (dt, J = 9.6, 2.8 Hz, 2H), 6.96 (s, 2H), 6.84 (dt, J = 9.6, 3.2 Hz, 2H), 4.70 (s, 1H), 4.11 (q, J = 6.8 Hz, 2H), 3.71 (s, 3H), 1.10 (t, J = 6.8 Hz, 3H); ^{13}C NMR (100 MHz, DMSO): δ 160.4, 158.6, 158.4, 137.6, 130.4, 129.4, 128.8, 120.8, 114.9, 114.0, 104.5, 61.3, 58.7, 55.5, 36.7, 14.3. IR results are identical with Mohammat et al. (2018).

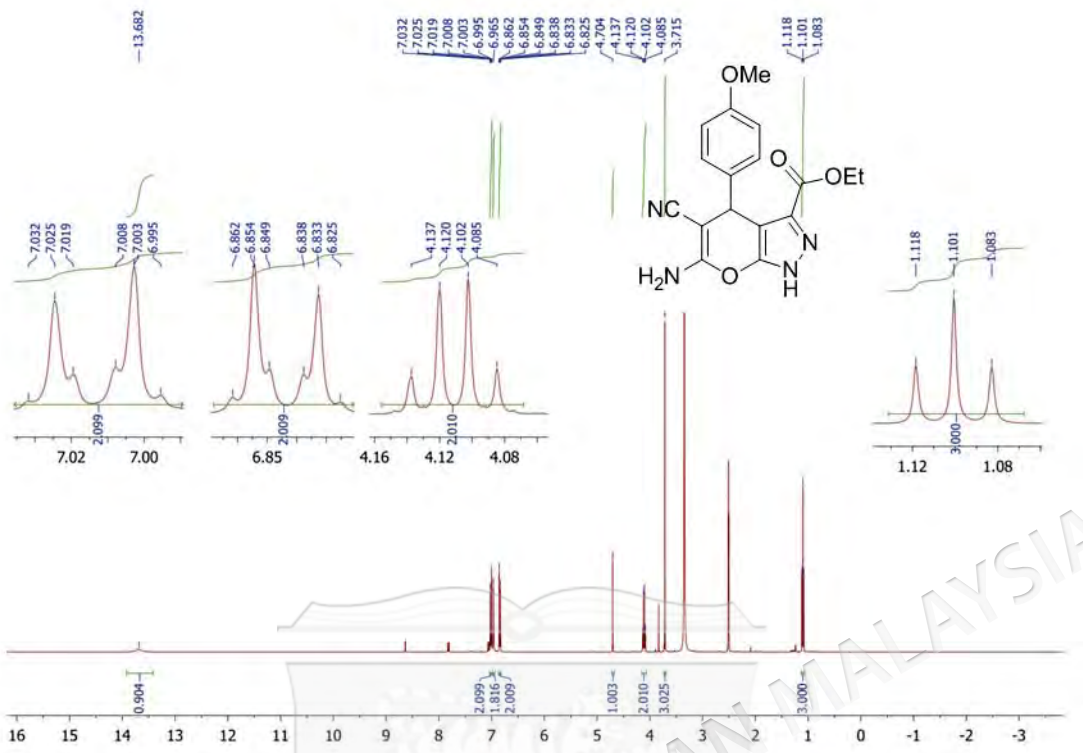

Figure 3.2 ^{1}H NMR spectrum of compound **20a**

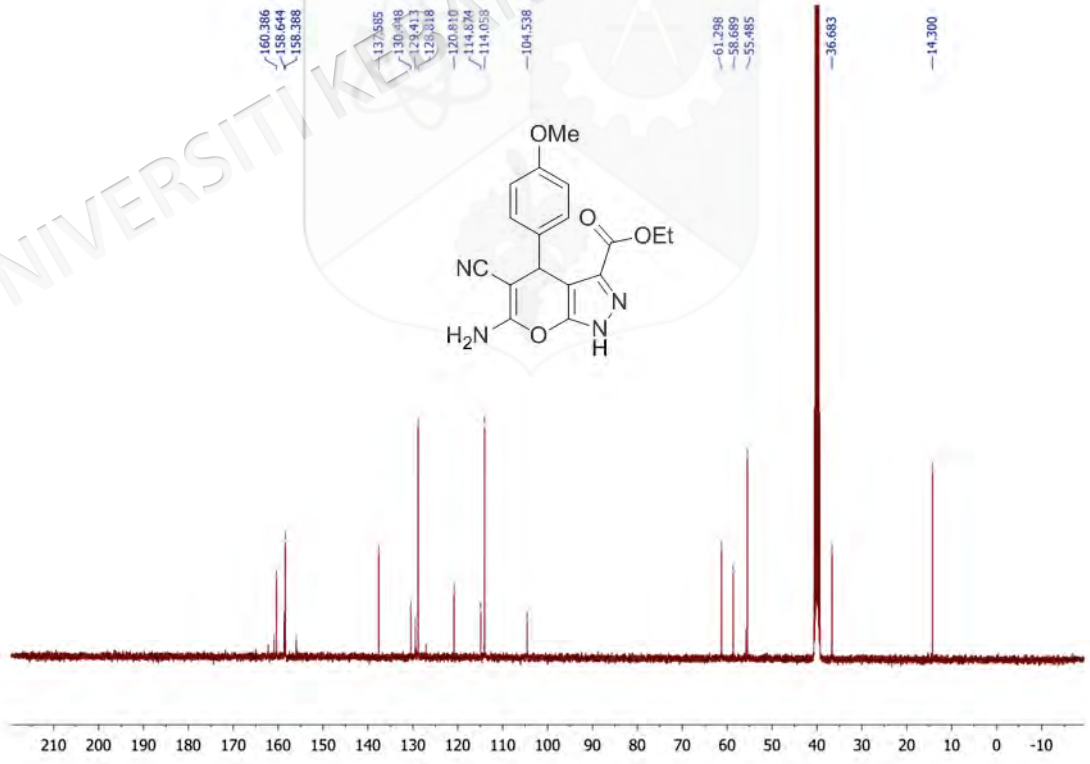

Figure 3.3 ^{13}C NMR spectrum of compound **20a**

3.3.2 Synthesis of ethyl 6-amino-5-cyano-4-(3-hydroxyphenyl)-1,4-dihydropyrano[2,3-*c*]pyrazole-3-carboxylate (20b)

The synthesis method of the pyrano[2,3-*c*]pyrazole compound **20b** is the same as described in subsection 3.3, using a mixture of hydrazine solution 35% (0.49 mL, 5.5 mmol) (**8**), sodium diethyloxalacetate solution (1.15 g, 5.5 mmol) (**18**), 1 mL of Acetic acid, 20 mL of ethanol, Malanonitrile (0.33 g, 5 mmol) (**19**) and 3-hydroxybenzaldehyde (0.61 gr, 5 mmol), to yield a white solid (64%). a white solid (56%). Melting point: 237-238 ºC; IR cm^{-1}: 3438 (NH_2), 3300 (NH), 2186 (CN), 1718 (COOEt), 1636 (C=C); ^{1}H NMR (400 MHz, DMSO) δ 13.71 (s, 1H), 9.26 (s, 1H), 7.07 (t, J = 7.6 Hz, 1H), 6.99 (s, 2H), 6.58 (ddd, J = 8, 2.4, 0.8 Hz, 1H), 6.54 (d, J = 7.6 Hz, 1H), 6.47 (t, J = 2 Hz, 1H), 4.64 (s, 1H), 4.12 (q, J = 7.2 Hz, 2H), 1.10 (t, J = 7.2 Hz, 3H); ^{13}C NMR (100 MHz, DMSO): δ 160.5, 158.7, 157.7, 156.1, 146.8, 129.6, 129.5, 120.8, 118.5, 114.6, 114.1, 104.3, 61.3, 58.4, 37.4, 14.3.

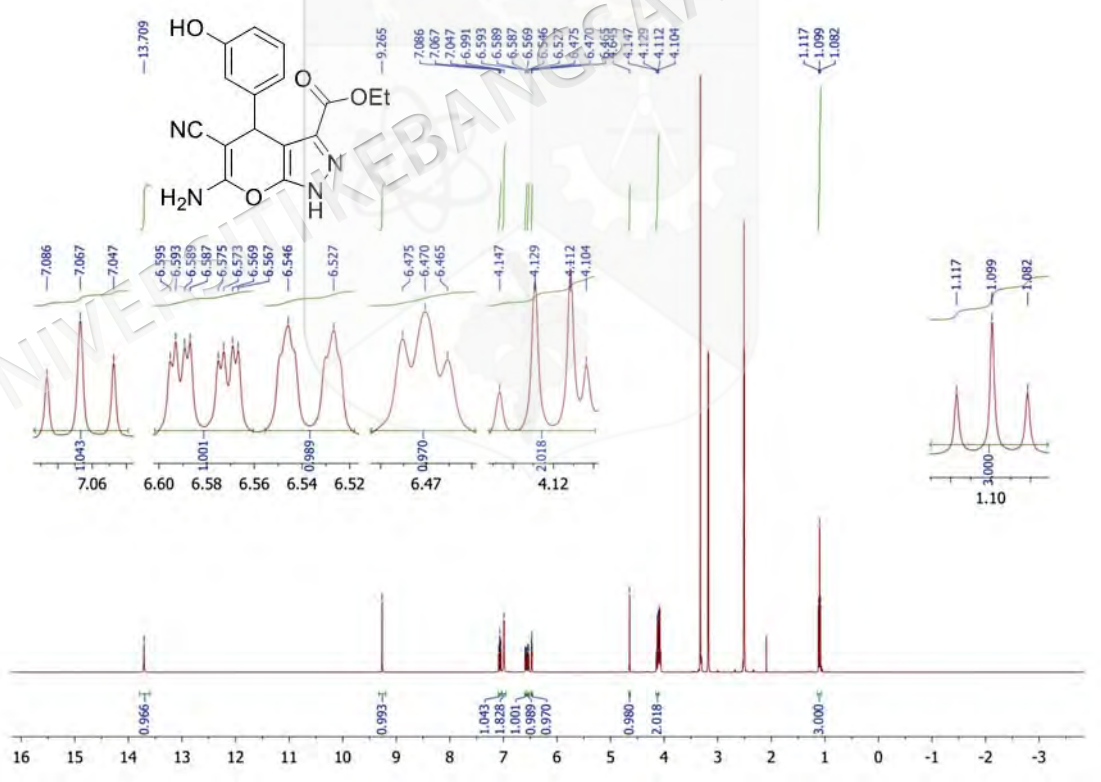

Figure 3.4 ^{1}H NMR spectrum of compound **20b**

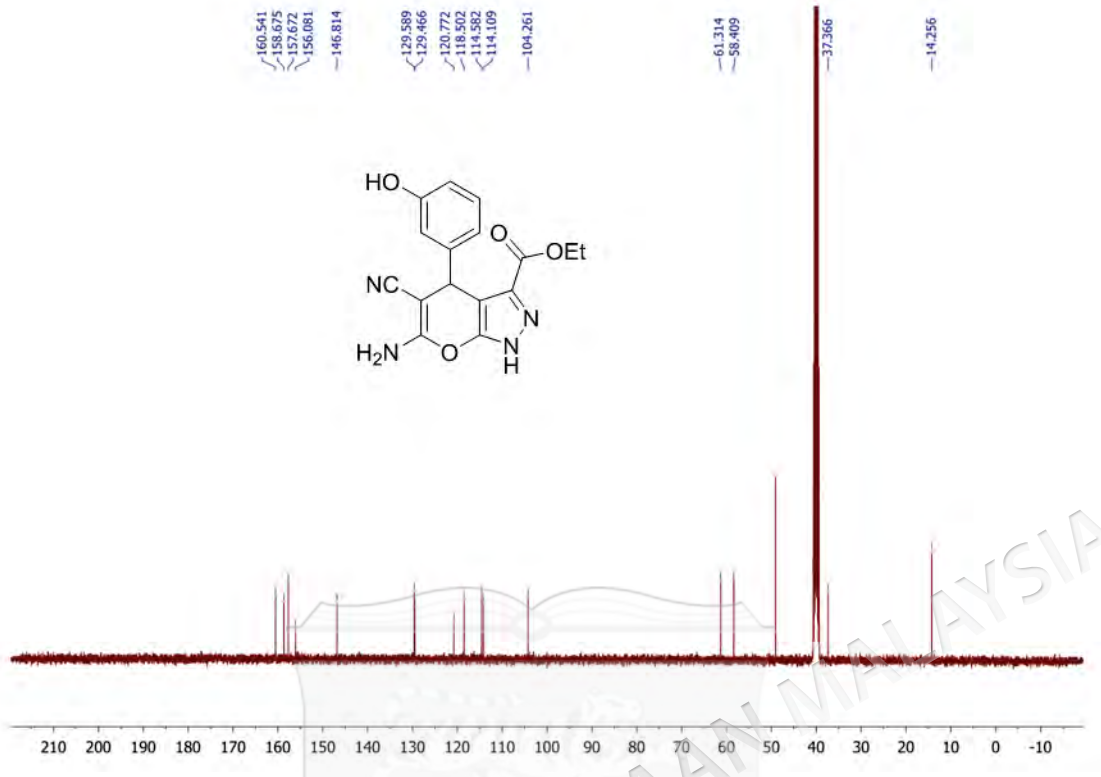

Figure 3.5 ^{13}C NMR spectrum of compound **20b**

3.3.3 Synthesis of ethyl 6-amino-5-cyano-4-(2-methoxyphenyl)-1,4-dihydropyrano[2,3-*c*]pyrazole-3-carboxylate (20c)

The synthesis method of the pyrano[2,3-*c*]pyrazole compound **20c** is the same as described in subsection 3.3, using a mixture of hydrazine solution 35% (0.49 mL, 5.5 mmol) (**8**), sodium diethyloxalacetate solution (1.15 g, 5.5 mmol) (**18**), 1 mL of Acetic acid, 20 mL of ethanol, Malanonitrile (0.33 g, 5 mmol) (**19**) and 2-methoxybenzaldehyde (0.68 gr, 5 mmol), to yield a White solid (76%). Melting point: 212-213 ^{o}C; IR cm^{-1}: 3412 (NH_2), 3390 (NH), 2189 (CN), 1718 (COOEt), 1647 (C=C); ^{1}H NMR (400 MHz, DMSO) δ 13.57 (s, 1H), 7.21-7.16 (m, 1H), 6.96 (d, J = 7.6 Hz, 1H), 6.90 (dd, J = 7.6, 1.6 Hz, 1H), 6.86-6.83 (m, 3H), 5.06 (s, 1H), 4.08 (q, J = 5.2 Hz, 2H), 3.71 (s, 3H), 1.03 (t, J = 7.2 Hz, 3H); ^{13}C NMR (100 MHz, DMSO): δ 161.1, 158.8, 157.1, 156.8, 132.9, 129.3, 129.1, 128.4, 120.8, 120.7, 111.9, 104.1, 61.1, 57.3, 56.0, 32.1, 14.1.

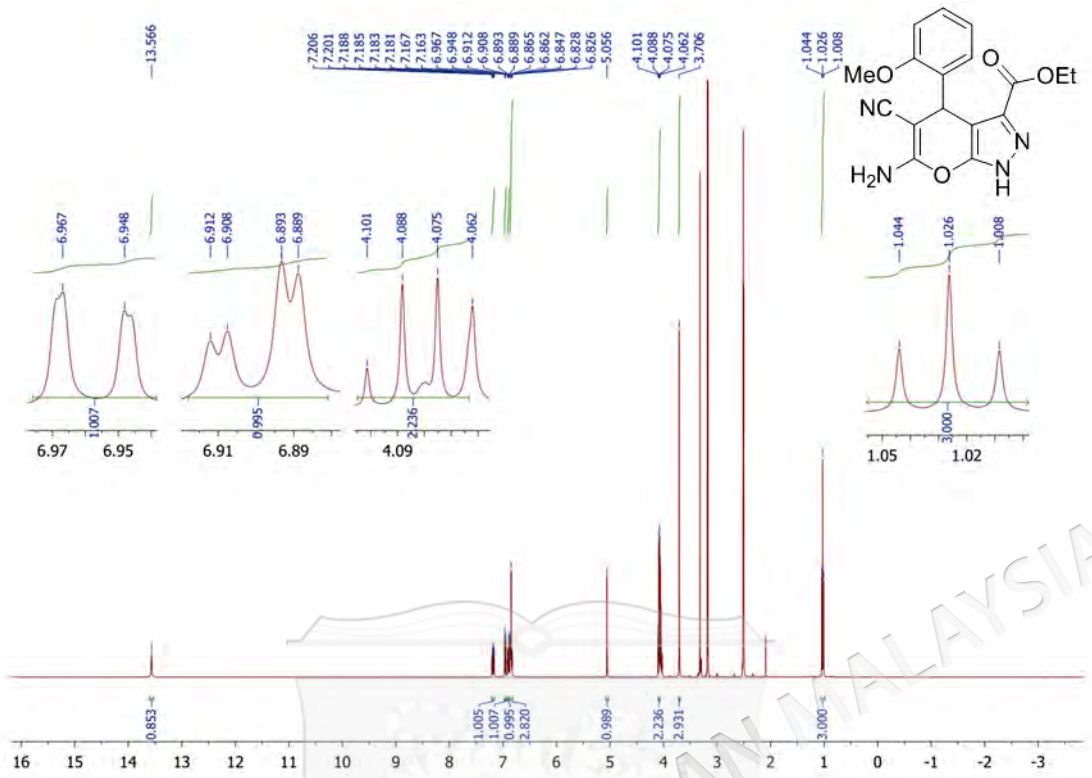

Figure 3.6 ^{1}H NMR spectrum of compound **20c**

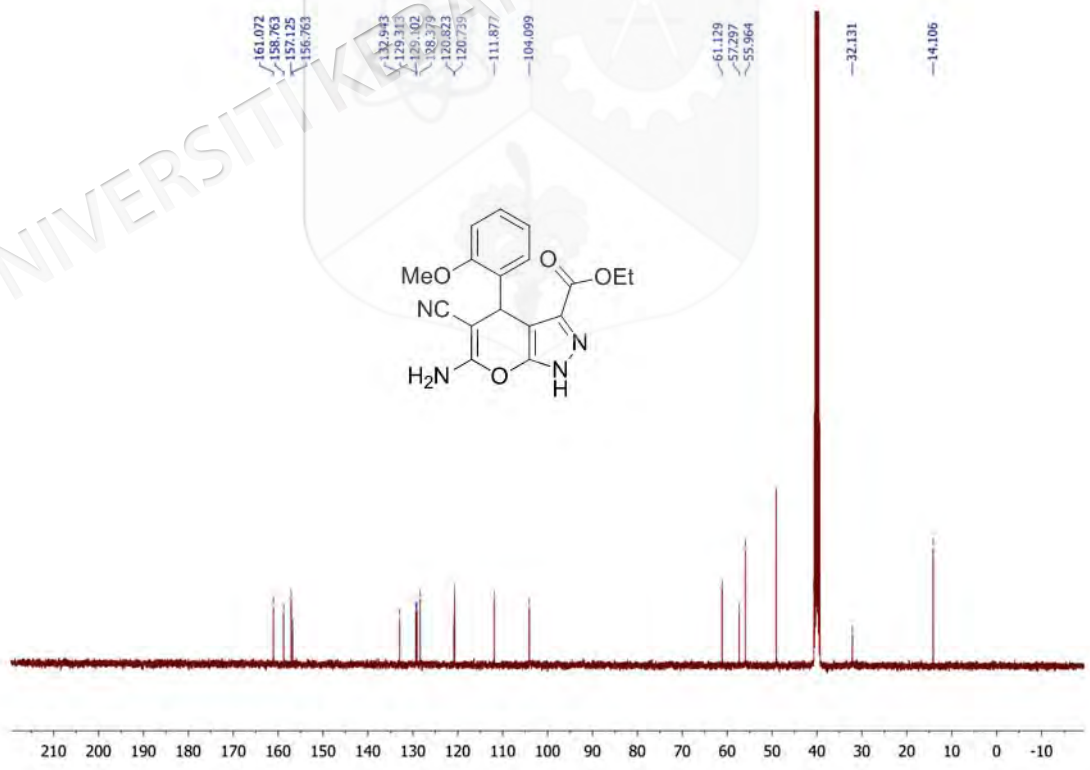

Figure 3.7 ^{13}C NMR spectrum of compound **20c**

3.3.4 Synthesis of ethyl 6-amino-5-cyano-4-(4-ethoxyphenyl)-1,4-dihydropyrano[2,3-*c*]pyrazole-3-carboxylate (20d)

The synthesis method of the pyrano[2,3-*c*]pyrazole compound **20d** is the same as described in subsection 3.3, using a mixture of hydrazine solution 35% (0.49 mL, 5.5 mmol) (**8**), sodium diethyloxalacetate solution (1.15 g, 5.5 mmol) (**18**), 1 mL of Acetic acid, 20 mL of ethanol, Malanonitrile (0.33 g, 5 mmol) (**19**) and 4-ethoxybenzaldehyde (0.75 gr, 5 mmol), to yield a yellowish white solid (85%). Melting point: 210-211 ^{o}C; ^{1}H NMR (400 MHz, DMSO) δ 13.67 (s, 1H), 7.01-6.96 (m, 4H), 6.82 (dt, *J* = 9.6, 2.8 Hz, 2H), 4.70 (s, 1H), 4.11 (q, *J* = 6.8 Hz, 2H), 3.97 (q, *J* = 6.8 Hz, 2H), 1.30 (t, *J* = 7.2 Hz, 3H), 1.10 (t, *J* = 6.8 Hz, 3H); ^{13}C NMR (100 MHz, DMSO): δ 160.4, 158.7, 157.7, 156.0, 137.5, 129.4, 128.4, 120.8, 114.5, 104.6, 63.4, 61.3, 58.7, 36.7, 15.1, 14.3. IR results are identical with Mohammat et al. (2018).

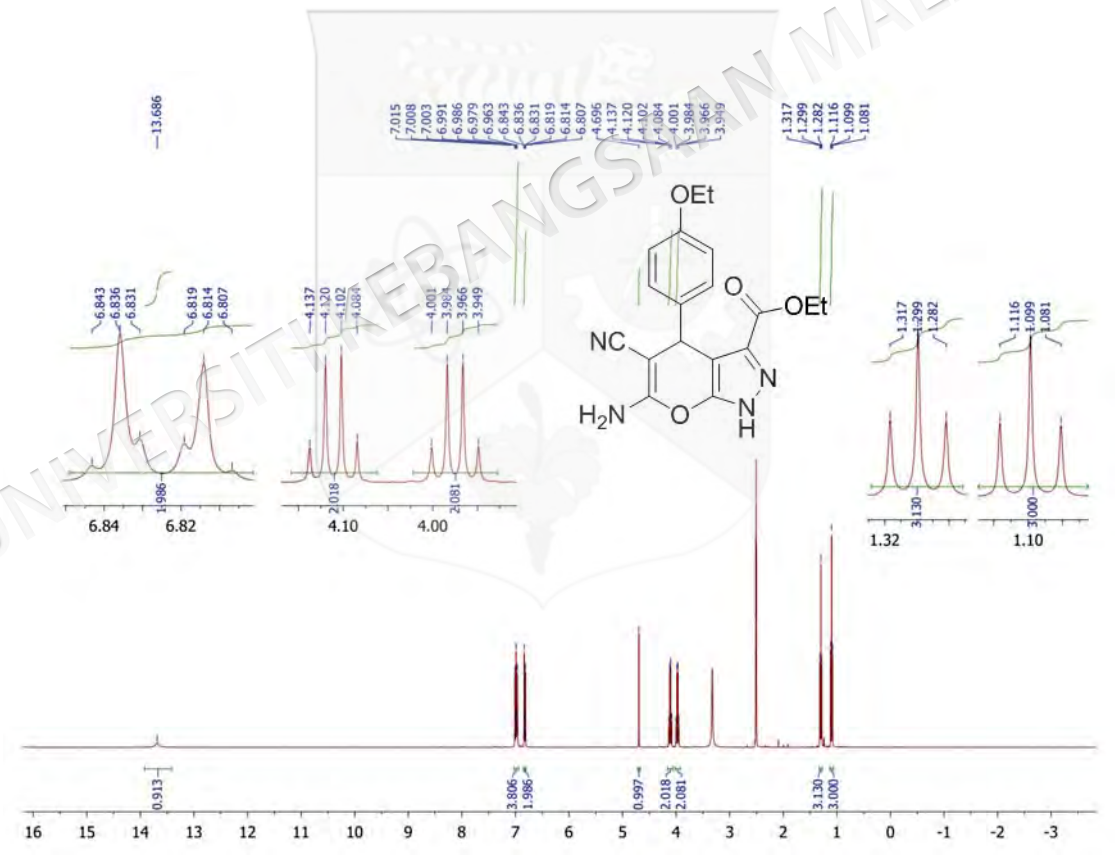

Figure 3.8 ^{1}H NMR spectrum of compound **20d**

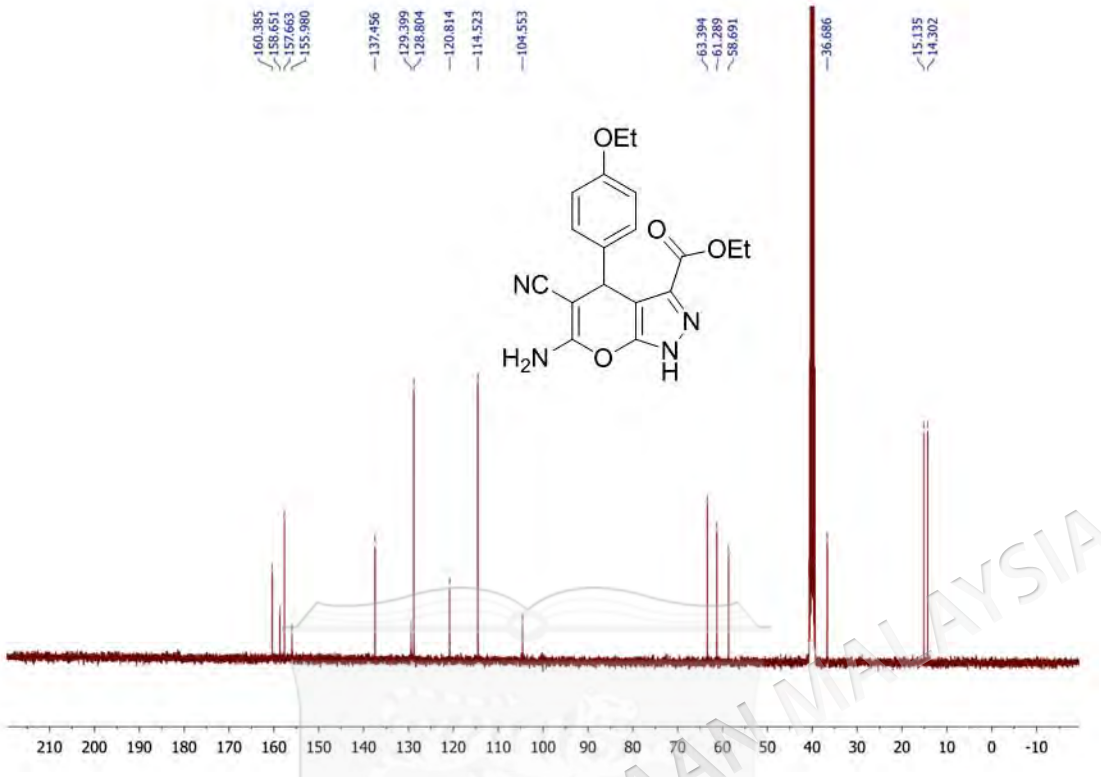

Figure 3.9 ^{13}C NMR spectrum of compound **20d**

3.3.5 Synthesis of ethyl 6-amino-5-cyano-4-(furan-2-yl)-1,4-dihydropyrano[2,3-*c*]pyrazole-3-carboxylate (20e)

The synthesis method of the pyrano[2,3-*c*]pyrazole compound **20e** is the same as described in subsection 3.3, using a mixture of hydrazine solution 35% (0.49 mL, 5.5 mmol) (**8**), sodium diethyloxalacetate solution (1.15 g, 5.5 mmol) (**18**), 1 mL of Acetic acid, 20 mL of ethanol, Malanonitrile (0.33 g, 5 mmol) (**19**) and furan-2-carbaldehyde (0.48 gr, 5 mmol), to yield a brown solid (61%). Melting point: 218-219 ^{o}C; ^{1}H NMR (400 MHz, DMSO) δ 13.77 (s, 1H), 7.48 (q, *J* = 0.8 Hz, 1H), 7.10 (s, 2H), 6.35 (q, *J* = 2 Hz, 1H), 6.12 (d, *J* = 3.2 Hz, 1H), 4.93 (s, 1H), 4.22-4.15 (m, 2H), 1.17 (t, *J* = 7.2 Hz, 3H); ^{13}C NMR (100 MHz, DMSO): δ 161.3, 158.7, 155.9, 142.3, 129.7, 120.6, 110.8, 105.9, 101.5, 61.4, 55.3, 31.2, 14.3. IR results are identical with Mohammat et al. (2018).

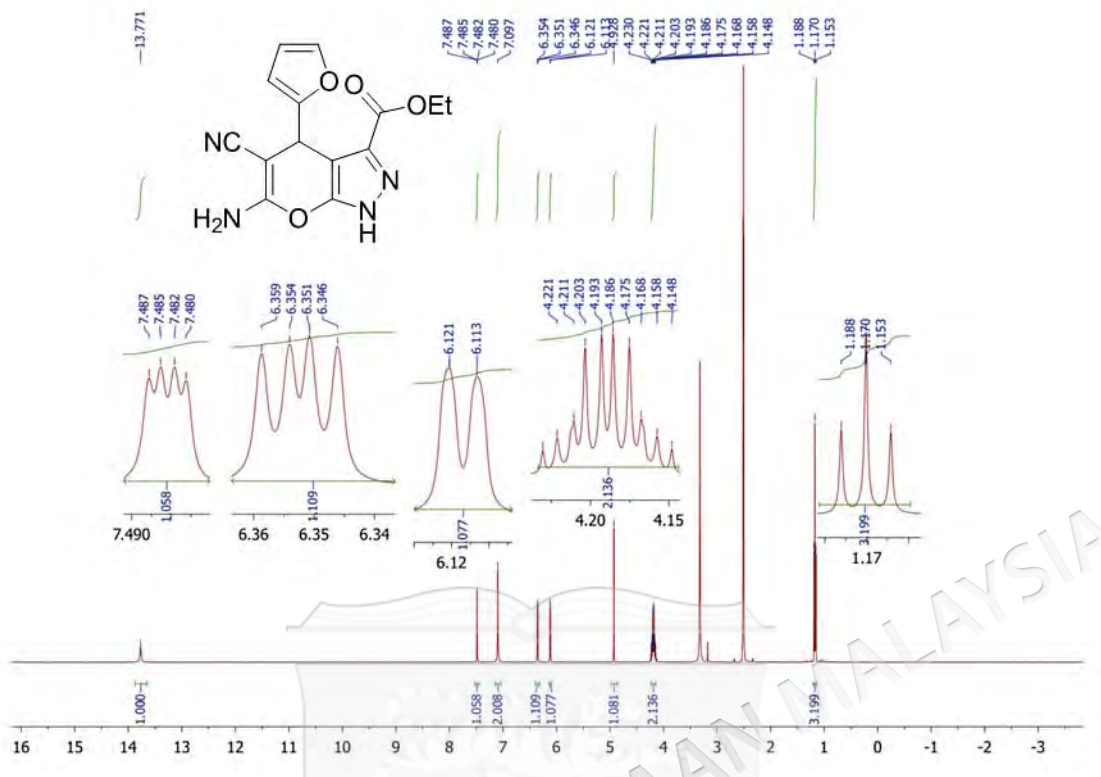

Figure 3.10 ^{1}H NMR spectrum of compound **20e**

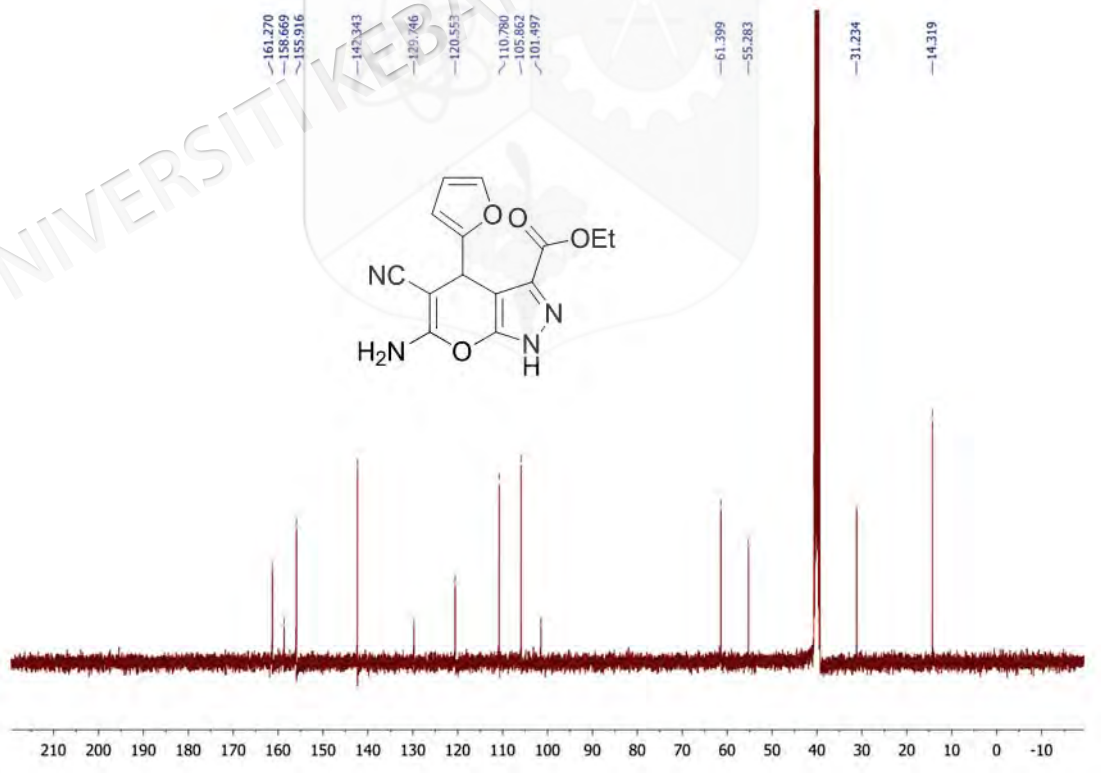

Figure 3.11 ^{13}C NMR spectrum of compound **20e**

3.3.6 Synthesis of ethyl 6-amino-5-cyano-4-phenyl-1,4-dihydropyrano[2,3-*c*]pyrazole-3-carboxylate (20f)

The synthesis method of the pyrano[2,3-*c*]pyrazole compound **20f** is the same as described in subsection 3.3, using a mixture of hydrazine solution 35% (0.49 mL, 5.5 mmol) (**8**), sodium diethyloxalacetate solution (1.15 g, 5.5 mmol) (**18**), 1 mL of Acetic acid, 20 mL of ethanol, Malanonitrile (0.33 g, 5 mmol) (**19**) and benzaldehyde (1.06 gr, 5 mmol), to yield a white solid (66%). Melting point: 226-227 ^{o}C; ^{1}H NMR (400 MHz, DMSO) δ 13.72 (s, 1H), 7.31-7.27 (m, 2H), 7.22-7.18 (m, 1H), 7.18 (s, 2H), 7.11-7.09 (m, 2H), 4.76 (s, 1H), 4.09 (q, *J* = 6.8 Hz, 2H), 1.05 (t, *J* = 7.2 Hz, 3H); ^{13}C NMR (100 MHz, DMSO): δ 160.5, 158.6, 156.1, 145.4, 129.5, 128.7, 127.8, 127.1, 120.7, 104.1, 61.3, 58.4, 37.4, 14.2. IR results are identical with Mohammat et al. (2018).

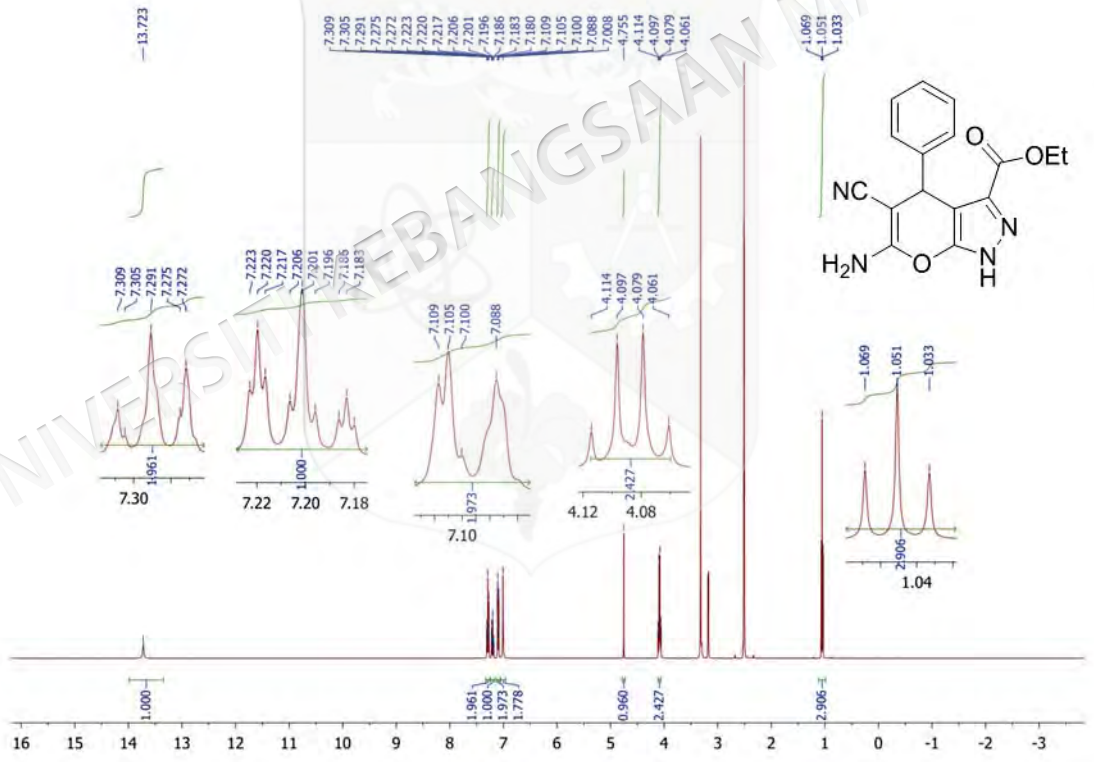

Figure 3.12 ^{1}H NMR spectrum of compound **20f**

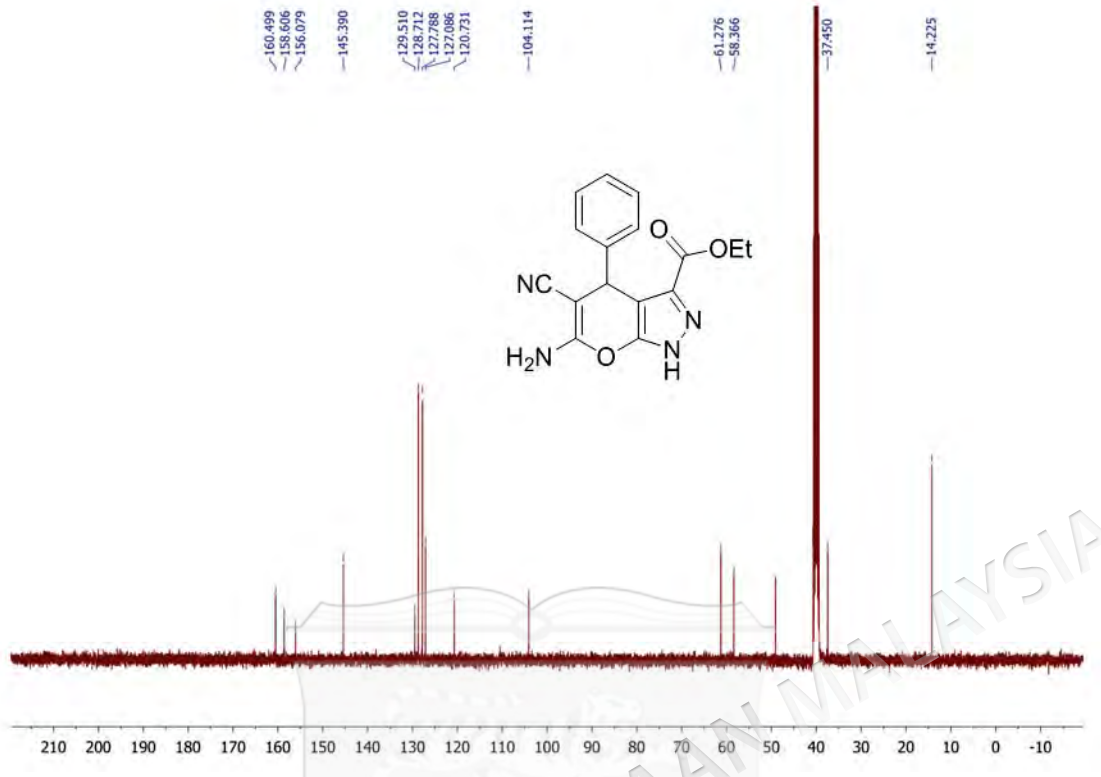

Figure 3.13 ^{13}C NMR spectrum of compound **20f**

3.3.7 Synthesis of ethyl 6-amino-4-(4-chlorophenyl)-5-cyano-1,4-dihydropyrano[2,3-*c*]pyrazole-3-carboxylate (20g)

The synthesis method of the pyrano[2,3-*c*]pyrazole compound **20g** is the same as described in subsection 3.3, using a mixture of hydrazine solution 35% (0.49 mL, 5.5 mmol) (**8**), sodium diethyloxalacetate solution (1.15 g, 5.5 mmol) (**18**), 1 mL of Acetic acid, 20 mL of ethanol, Malanonitrile (0.33 g, 5 mmol) (**19**) and 4-chlorobenzaldehyde (0.70 gr, 5 mmol), to yield a white solid (74%) Melting point: 228-230 ºC; IR cm^{-1}: 3390 (NH_2), 3145 (NH), 2173 (CN), 1731 (COOEt), 1641 (C=C); ^{1}H NMR (400 MHz, DMSO) δ 13.77 (s, 1H), 7.35 (dt, *J* = 9.2, 2.8 Hz, 2H), 7.13 (dt, *J* = 9.2, 2.4 Hz, 2H), 7.06 (s, 2H), 4.79 (s, 1H), 4.10 (q, *J* = 6.8 Hz, 2H), 1.07 (t, *J* = 6.8 Hz, 3H); ^{13}C NMR (100 MHz, DMSO): δ 160.5, 158.5, 156.0, 144.4, 131.6, 129.7, 129.6, 128.7, 120.6, 103.6, 61.4, 57.9, 36.8, 14.3.

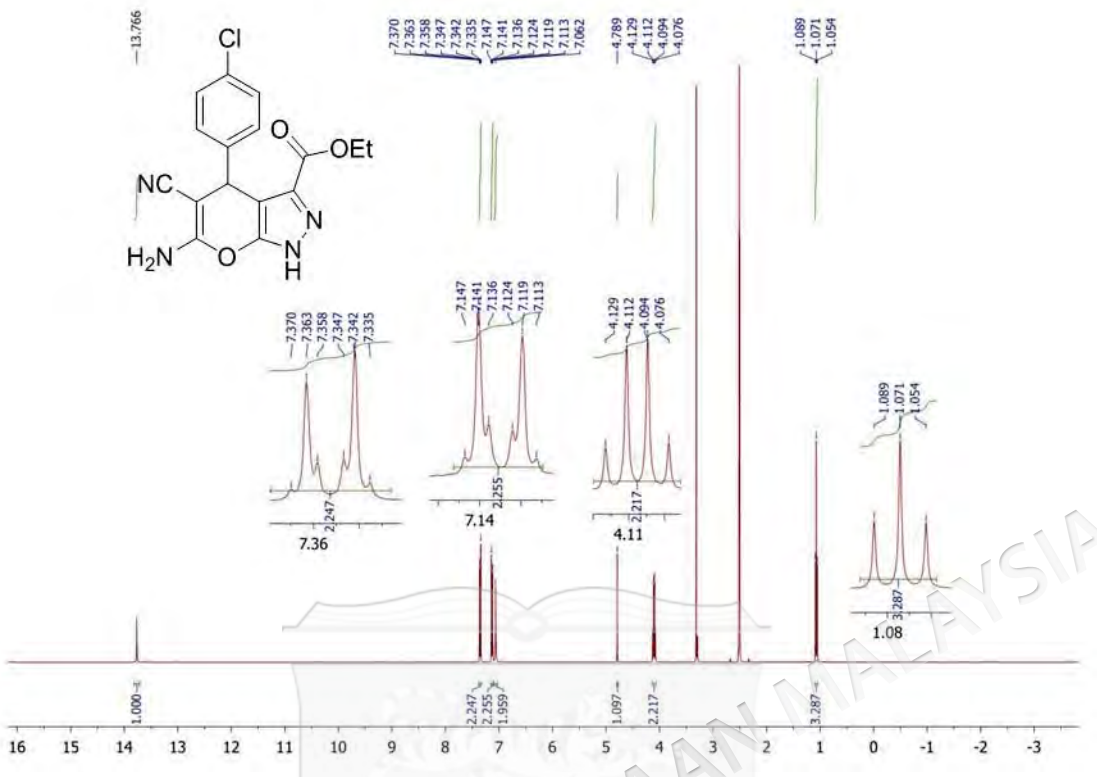

Figure 3.14 ^{1}H NMR spectrum of compound **20g**

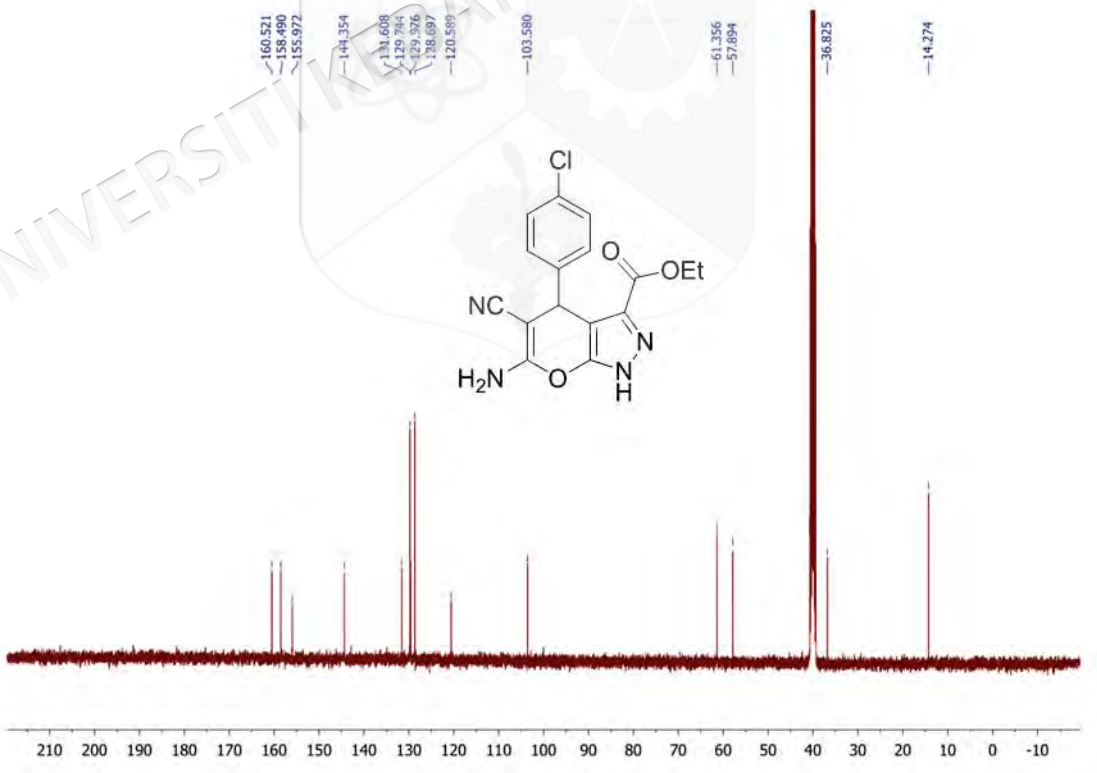

Figure 3.15 ^{13}C NMR spectrum of compound **20g**

3.3.8 Synthesis of ethyl 6-amino-4-(4-bromophenyl)-5-cyano-1,4-dihydropyrano[2,3-*c*]pyrazole-3-carboxylate (20h)

The synthesis method of the pyrano[2,3-*c*]pyrazole compound **20h** is the same as described in subsection 3.3, using a mixture of hydrazine solution 35% (0.49 mL, 5.5 mmol) (**8**), sodium diethyloxalacetate solution (1.15 g, 5.5 mmol) (**18**), 1 mL of Acetic acid, 20 mL of ethanol, Malanonitrile (0.33 g, 5 mmol) (**19**) and 4-bromobenzaldehyde (0.92 gr, 5 mmol), to yield a white solid (71%). Melting point: 221-222 ^{o}C; ^{1}H NMR (400 MHz, DMSO) δ 13.77 (s, 1H), 7.49 (dt, *J* = 9.2, 2.4 Hz, 2H), 7.09-7.06 (m, 4H), 4.77 (s, 1H), 4.10 (q, *J* = 6.8 Hz, 2H), 1.07 (t, *J* = 6.8 Hz, 3H); ^{13}C NMR (100 MHz, DMSO): δ 160.5, 158.5, 156.0, 144.8, 131.6, 130.1, 129.6, 120.6, 120.1, 103.5, 61.4, 57.8, 36.9, 14.3. IR results are identical with Mohammat et al. (2018).

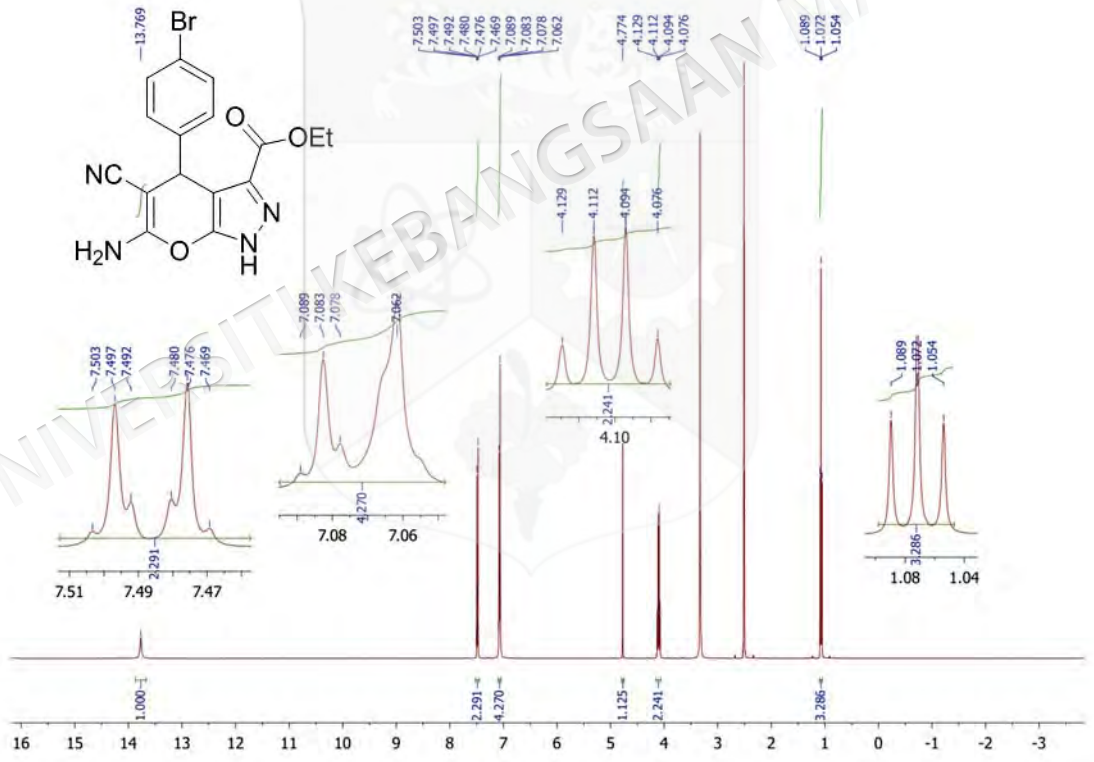

Figure 3.16 ^{1}H NMR spectrum of compound **20h**

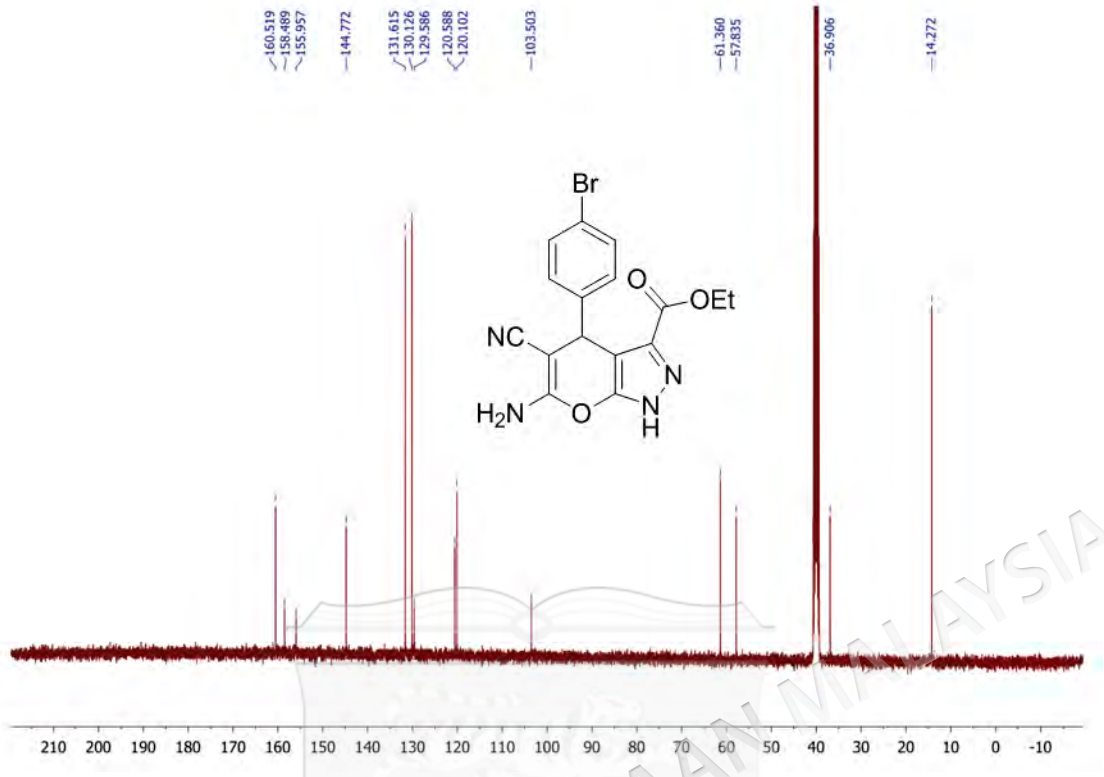

Figure 3.17 ^{13}C NMR spectrum of compound **20h**

3.3.9 Synthesis of ethyl 6-amino-5-cyano-4-(3-nitrophenyl)-1,4-dihydropyrano[2,3-*c*]pyrazole-3-carboxylate (20i)

The synthesis method of the pyrano[2,3-*c*]pyrazole compound **20i** is the same as described in subsection 3.3, using a mixture of hydrazine solution 35% (0.49 mL, 5.5 mmol) (**8**), sodium diethyloxalacetate solution (1.15 g, 5.5 mmol) (**18**), 1 mL of Acetic acid, 20 mL of ethanol, Malanonitrile (0.33 g, 5 mmol) (**19**) and 3-nitrobenzaldehyde (0.75 gr, 5 mmol), to yield a yellow solid (70%). Melting point: 224-225 ºC; ^{1}H NMR (400 MHz, DMSO) δ 13.85 (s, 1H), 8.11 (dt, *J* = 6.4, 2.8 Hz, 1H), 7.98-7.97 (m, 1H), 7.65-7.60 (m, 2H), 7.17 (s, 2H), 5.03 (s, 1H), 4.08 (q, *J* = 6.8 Hz, 2H), 1.04 (t, *J* = 7.2 Hz, 3H); ^{13}C NMR (100 MHz, DMSO): δ 160.7, 158.4, 155.9, 148.1, 147.5, 134.9, 130.5, 129.8, 122.4, 122.3, 120.4, 102.8, 61.4, 57.3, 36.9, 14.2. IR results are identical with Mohammat et al. (2018).

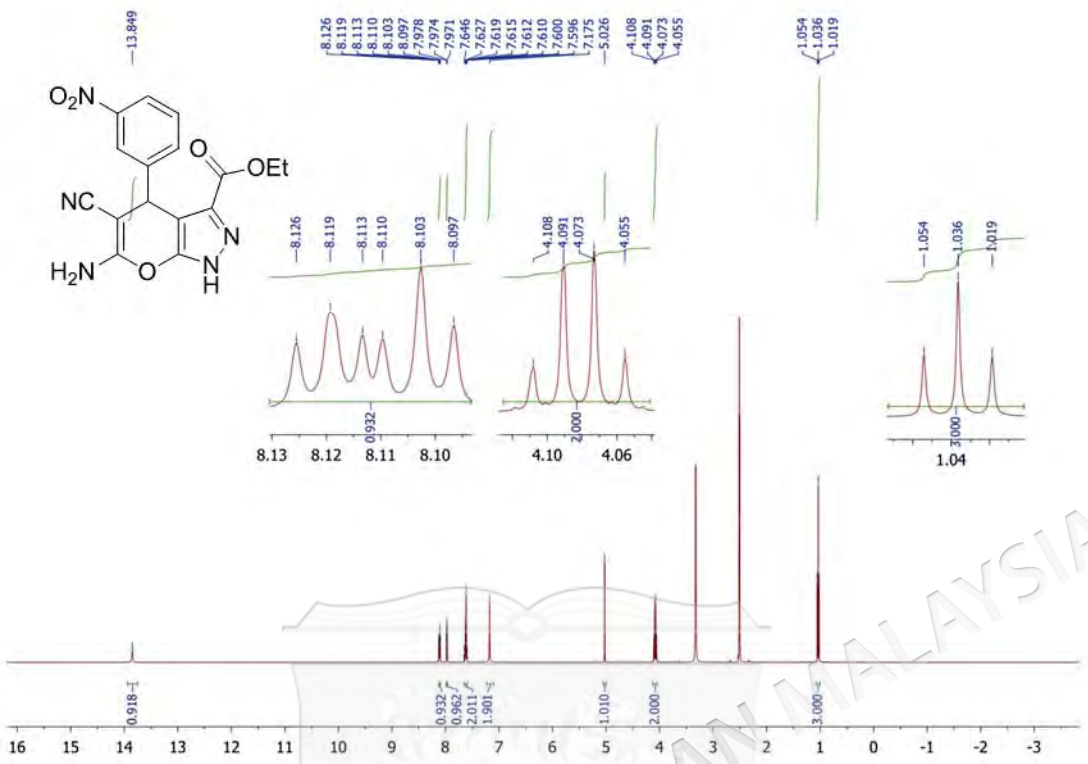

Figure 3.18 ^{1}H NMR spectrum of compound **20i**

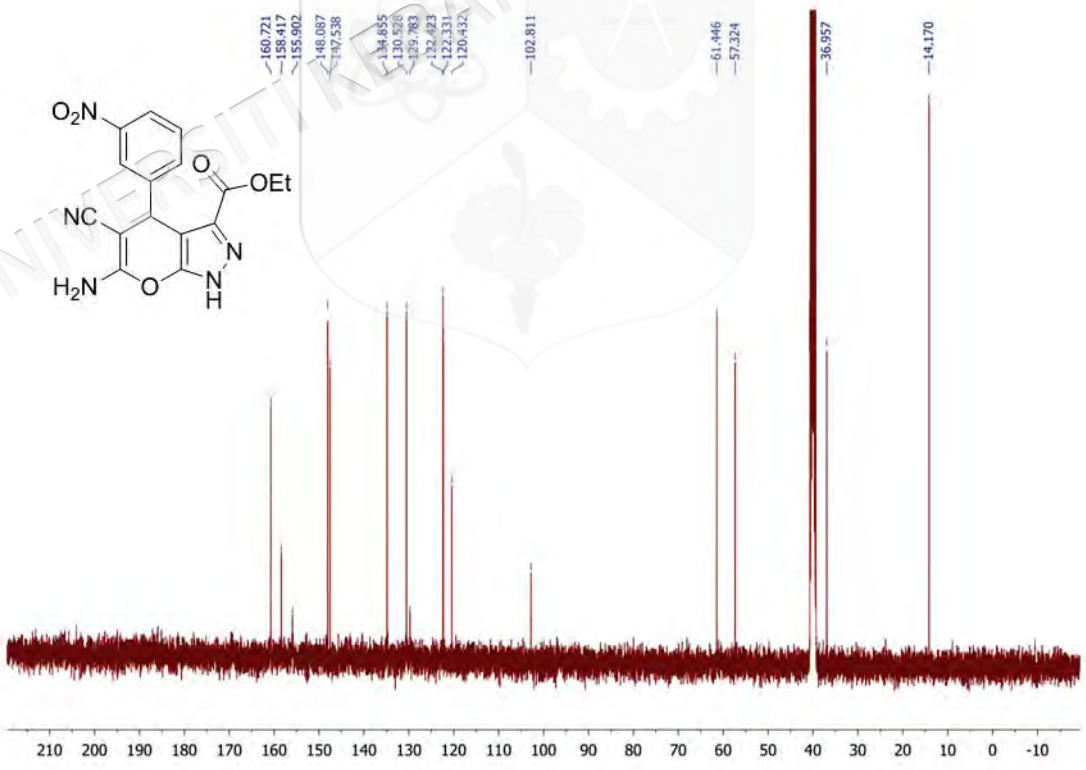

Figure 3.19 ^{13}C NMR spectrum of compound **20i**

3.3.10 Synthesis of ethyl 6-amino-5-cyano-4-(4-nitrophenyl)-1,4-dihydropyrano[2,3-*c*]pyrazole-3-carboxylate (20j)

The synthesis method of the pyrano[2,3-*c*]pyrazole compound **20j** is the same as described in 3.3, using a mixture of hydrazine solution 35% (0.49 mL, 5.5 mmol) (**8**), sodium diethyloxalacetate solution (1.15 g, 5.5 mmol) (**18**), 1 mL of Acetic acid, 20 mL of ethanol, Malanonitrile (0.33 g, 5 mmol) (**19**) and 4-nitrobenzaldehyde (0.75 gr, 5 mmol), to yield a yellow solid (74%). Melting point: 235-237 ^{o}C; ^{1}H NMR (400 MHz, DMSO) δ 13.85 (s, 1H), 8.18 (dt, *J* = 9.2, 2.4 Hz, 2H), 7.40 (dt, *J* = 9.6, 2.8 Hz, 2H), 7.18 (s, 2H), 4.97 (s, 1H), 4.08 (q, *J* = 7.2 Hz, 2H), 1.05 (t, *J* = 7.2 Hz, 3H); ^{13}C NMR (100 MHz, DMSO): δ 160.7, 158.4, 156.0, 152.7, 146.7, 129.8, 129.3, 124.1, 120.4, 102.8, 61.4, 57.1, 37.1, 14.3. IR results are identical with Mohammat et al. (2018).

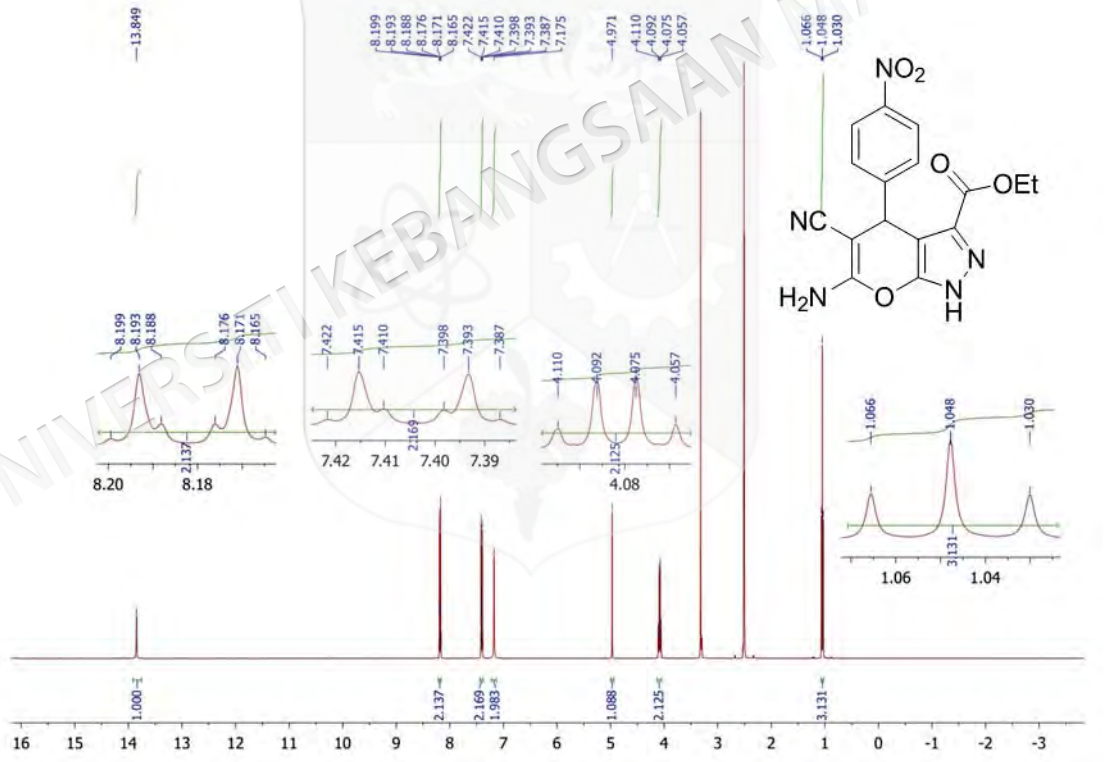

Figure 3.20 ^{1}H NMR spectrum of compound **20j**

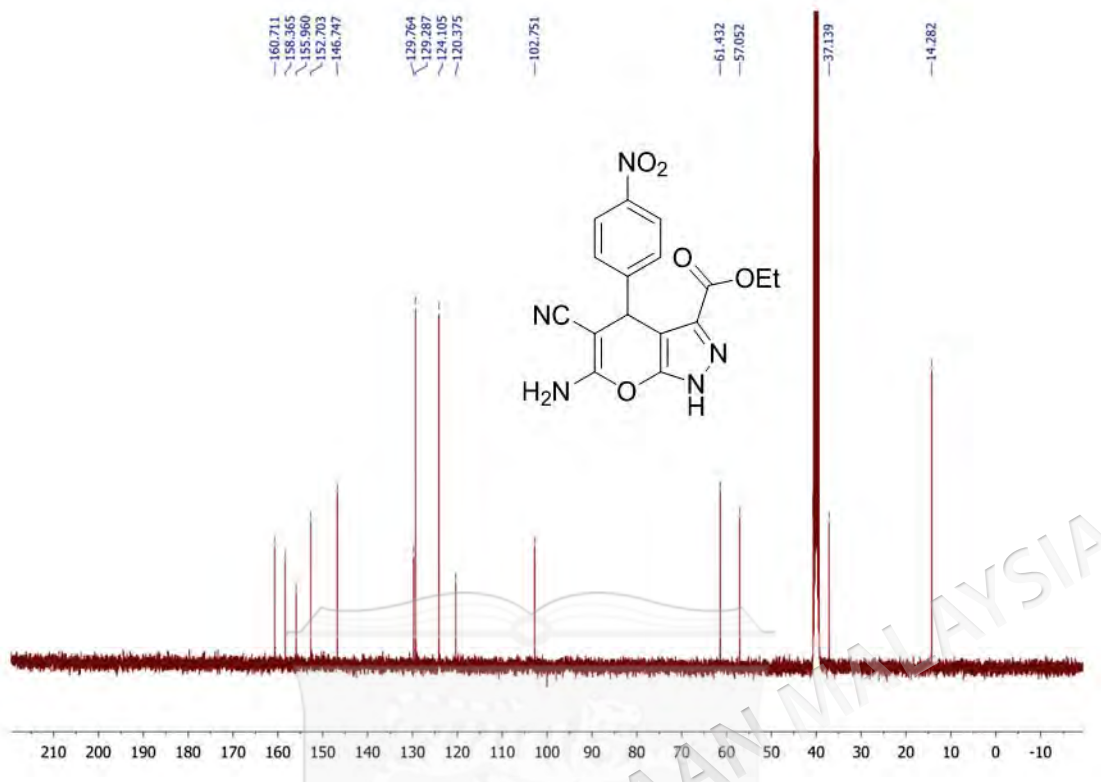

Figure 3.21 ^{13}C NMR spectrum of compound **20j**

3.3.11 Synthesis of ethyl 6-amino-5-cyano-4-(2,4-dihydroxyphenyl)-1,4-dihydropyrano[2,3-*c*]pyrazole-3-carboxylate (20k)

The synthesis method of the pyrano[2,3-*c*]pyrazole compound **20k** is the same as described in subsection 3.3, using a mixture of hydrazine solution 35% (0.49 mL, 5.5 mmol) (**8**), sodium diethyloxalacetate solution (1.15 g, 5.5 mmol) (**18**), 1 mL of Acetic acid, 20 mL of ethanol, Malanonitrile (0.33 g, 5 mmol) (**19**) and 2,4-dihydroxibenzaldehyde (0.69 gr, 5 mmol), to yield a orange solid (42%). Melting point: 281-282 ^{o}C; IR cm^{-1}: 3479 (NH_2), 3358 (NH), 2212 (CN), 1720 (COOEt), 1636 (C=C); ^{1}H NMR (400 MHz, DMSO) δ 12.66 (s, 1H), 9.50 (s, 1H), 6.78 (d, *J* = 8.4 Hz, 1H), 6.42 (dd, *J* = 8.4, 2.8 Hz, 1H), 6.38 (d, *J* = 2.4 Hz, 1H), 6.327 (s, 2H), 5.94 (s, 1H), 5.28 (s, 1H), 4.34 (d, *J* = 6.4 Hz, 2H), 1.31 (t, *J* = 7.2 Hz, 3H); ^{13}C NMR (100 MHz, DMSO): δ 159.7, 159.4, 157.3, 156.8, 151.3, 130.1, 116.9, 113.4, 111.8, 102.6, 89.0, 71.0, 61.5, 27.2, 14.5.

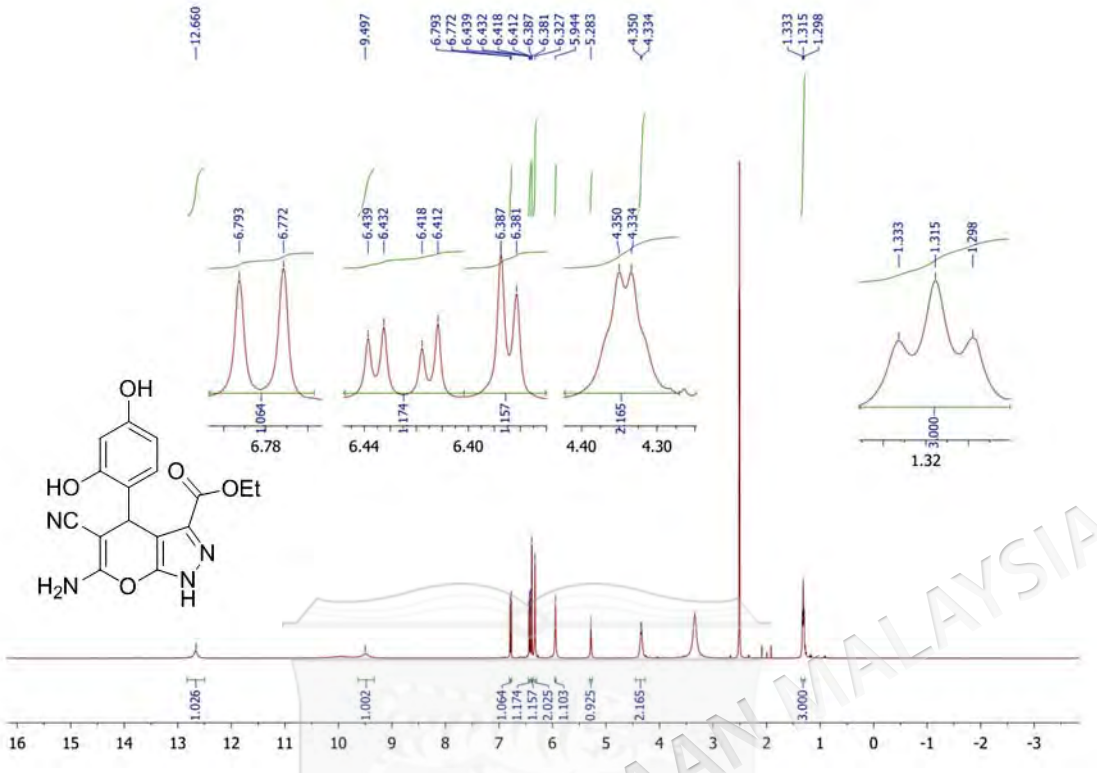

Figure 3.22 ^{1}H NMR spectrum of compound **20k**

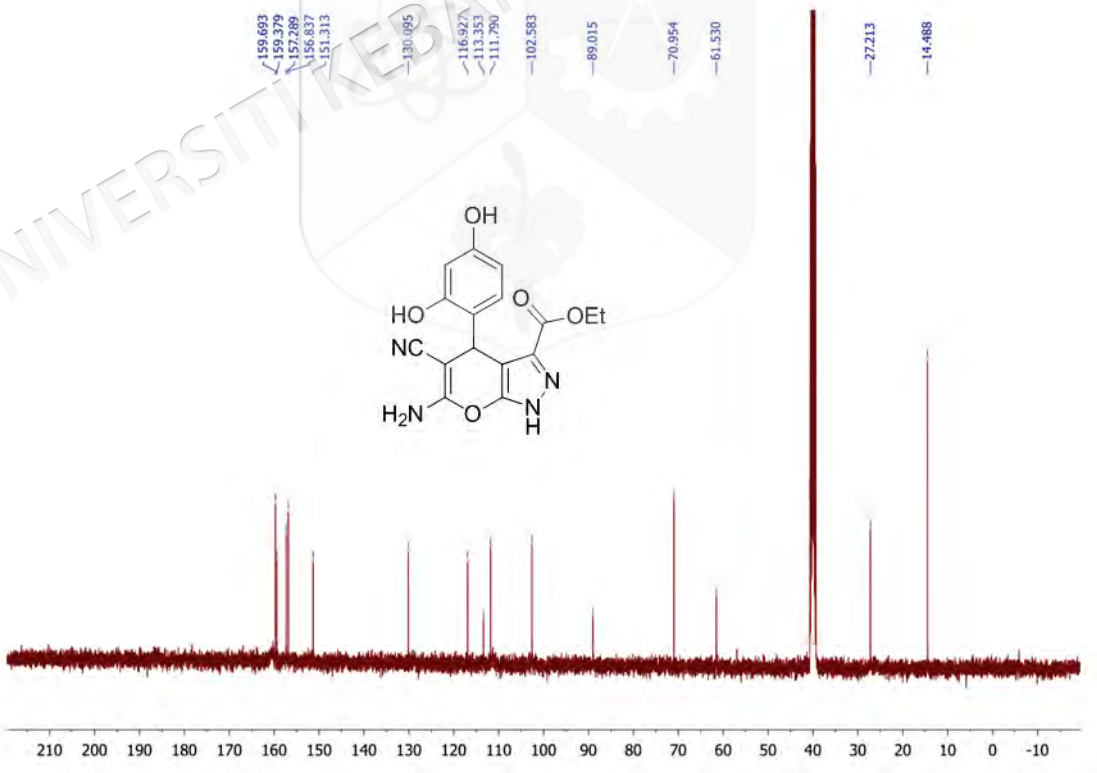

Figure 3.23 ^{13}C NMR spectrum of compound **20k**

3.3.12 Synthesis of ethyl 6-amino-5-cyano-4-(thiophen-2-yl)-1,4-dihydropyrano[2,3-*c*]pyrazole-3-carboxylate (20l)

The synthesis method of the pyrano[2,3-*c*]pyrazole compound **20l** is the same as described in subsection 3.3, using a mixture of hydrazine solution 35% (0.49 mL, 5.5 mmol) (**8**), sodium diethyloxalacetate solution (1.15 g, 5.5 mmol) (**18**), 1 mL of Acetic acid, 20 mL of ethanol, Malanonitrile (0.33 g, 5 mmol) (**19**) and thiophene-2-carbaldehyde (0.56 gr, 5 mmol), to yield a yellow solid (60%). Melting point: 205-207 ^{o}C; ^{1}H NMR (400 MHz, DMSO) δ 13.80 (s, 1H), 7.34-7.32 (m, 1H), 7.11 (s, 2H), 6.93-6.91 (m, 2H), 5.13 (s, 1H), 4.22-4.16 (m, 2H), 1.14 (t, *J* = 7.2 Hz, 3H); ^{13}C NMR (100 MHz, DMSO): δ 160.7, 158.6, 155.4, 149.9, 129.7, 127.1, 125.0, 120.7, 104.2, 61.5, 58.2, 32.6, 14.3. IR results are identical with Mohammat et al. (2018).

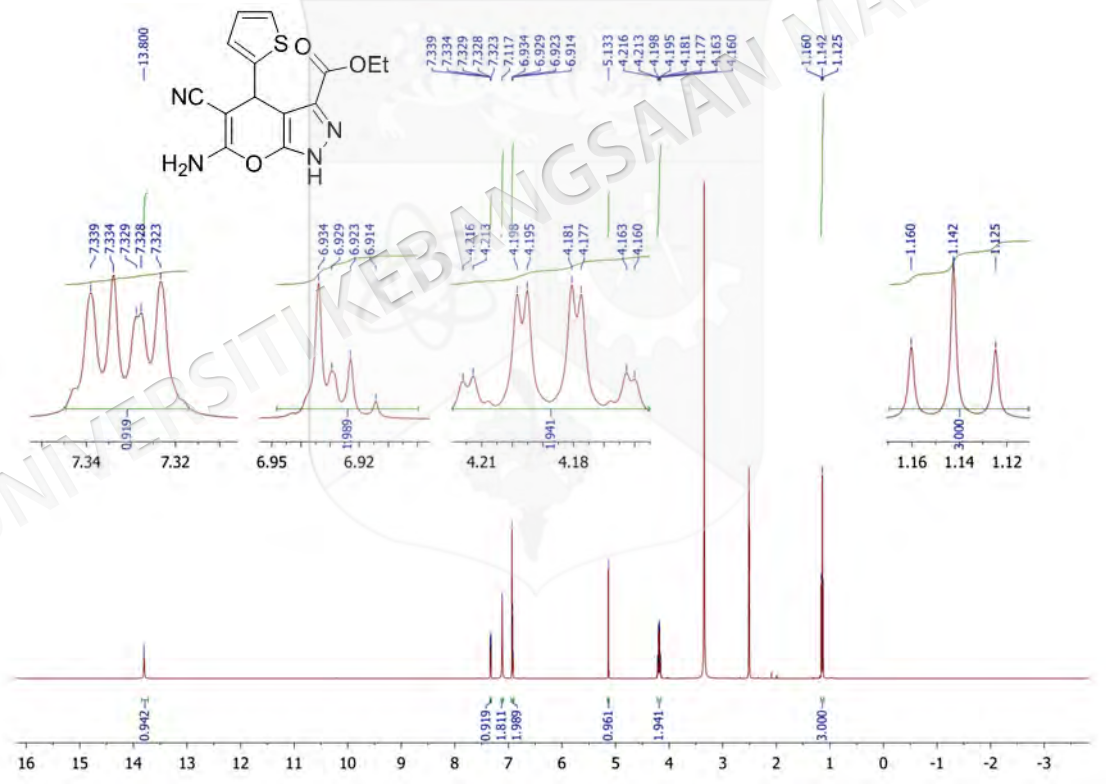

Figure 3.24 ^{1}H NMR spectrum of compound **20l**

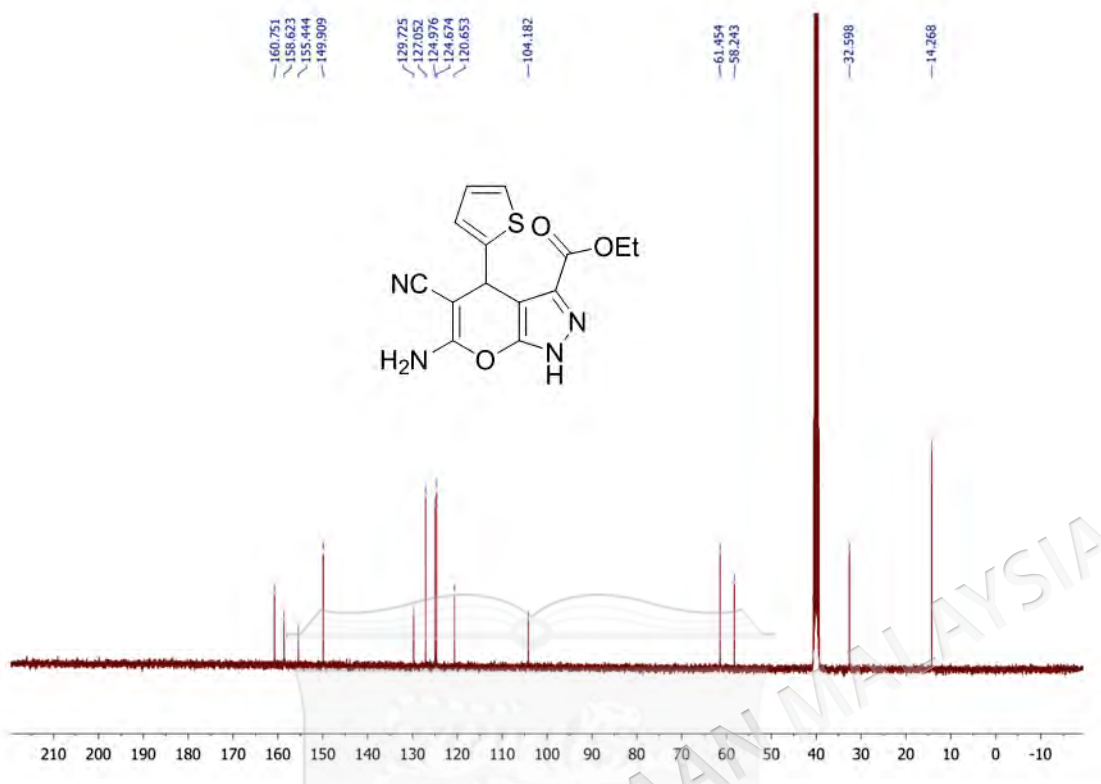

Figure 3.25 ^{13}C NMR spectrum of compound **20l**

3.3.13 Synthesis ethyl 6-amino-4-(3-bromo-4-hydroxyphenyl)-5-cyano-1,4-dihydropyrano[2,3-*c*]pyrazole-3-carboxylate (20m)

The synthesis method of the pyrano[2,3-*c*]pyrazole compound **20m** is the same as described in subsection 3.3, using a mixture of hydrazine solution 35% (0.49 mL, 5.5 mmol) (**8**), sodium diethyloxalacetate solution (1.15 g, 5.5 mmol) (**18**), 1 mL of Acetic acid, 20 mL of ethanol, Malanonitrile (0.33 g, 5 mmol) (**19**) and 3-bromo-4-hydroxibenzaldehyde (1.0 gr, 5 mmol), to yield a white solid (76%). Melting point: 224-225 ^{o}C; ^{1}H NMR (400 MHz, DMSO) δ 13.73 (s, 1H), 10.12 (s, 1H), 7.20 (d, *J* = 1.6 Hz, 1H); 7.01 (s, 2H), 6.90-6.85 (m, 2H), 4.68 (s, 1H), 4.16-4.10 (m, 2H), 1.13 (t, *J* = 7.2 Hz, 3H); ^{13}C NMR (100 MHz, DMSO): δ 160.4, 158.6, 155.4, 153.1, 137.7, 132.1, 129.5, 128.1, 120.7, 116.7, 109.1, 104.1, 61.4, 58.3, 36.3, 14.3. IR results are identical with Mohammat et al. (2018).

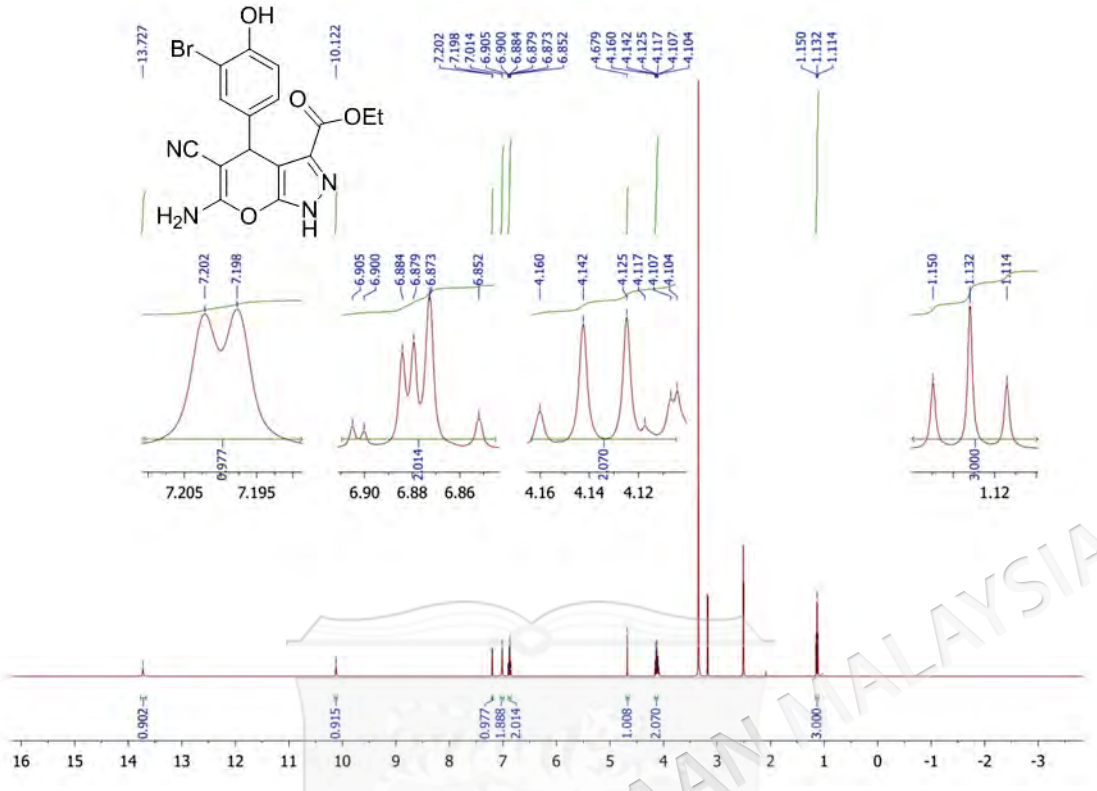

Figure 3.26 ^{1}H NMR spectrum of compound **20m**

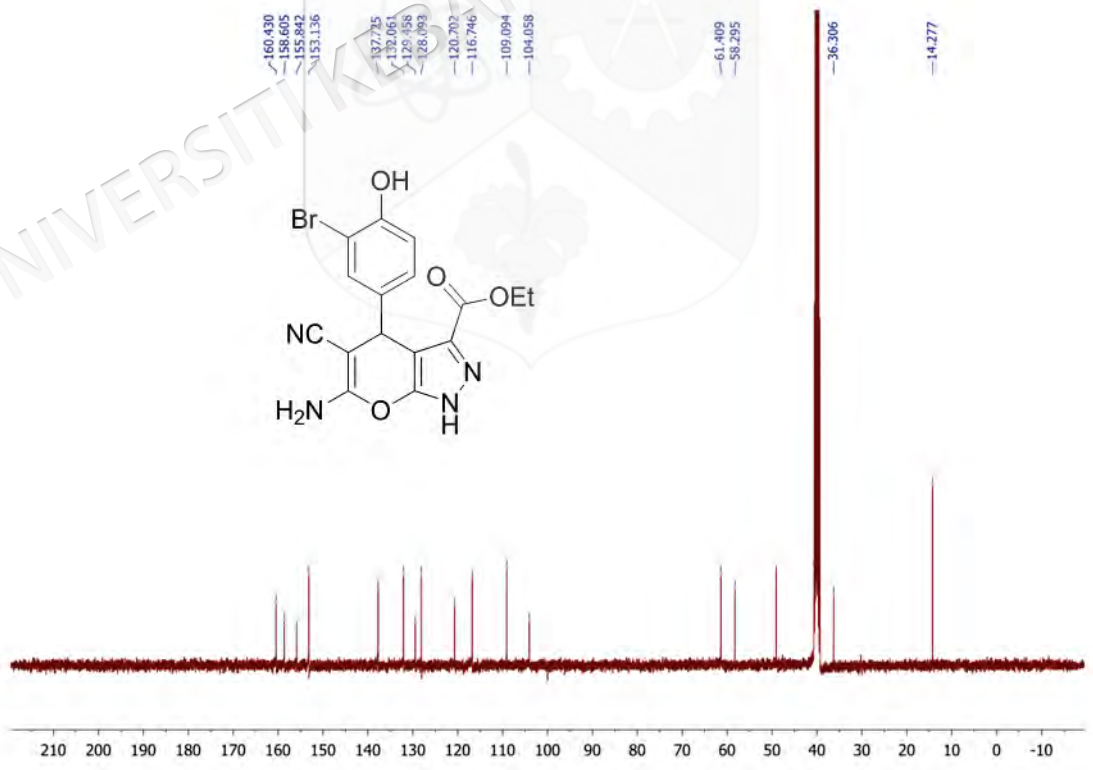

Figure 3.27 ^{13}C NMR spectrum of compound **20m**

3.3.14 Synthesis of ethyl 6-amino-5-cyano-4-(4-cyanophenyl)-1,4-dihydropyrano[2,3-*c*]pyrazole-3-carboxylate (20n)

The synthesis method of the pyrano[2,3-*c*]pyrazole compound **20n** is the same as described in subsection 3.3, using a mixture of hydrazine solution 35% (0.49 mL, 5.5 mmol) (**8**), sodium diethyloxalacetate solution (1.15 g, 5.5 mmol) (**18**), 1 mL of Acetic acid, 20 mL of ethanol, Malanonitrile (0.33 g, 5 mmol) (**19**) and 4-formylbenzonitrile (0.65 gr, 5 mmol), to yield a yellow solid (68%). Melting point: 218-221 ^{o}C; ^{1}H NMR (400 MHz, DMSO) δ 13.83 (s, 1H), 7.77 (dt, *J* = 8.4, 2 Hz, 2H); 7.31 (dt, *J* = 8.4, 2 Hz, 2H); 7.14 (s, 2H), 4.90 (s, 1H), 4.08 (q, *J* = 7.2 Hz, 2H), 1.03 (t, *J* = 6.8 Hz, 3H); ^{13}C NMR (100 MHz, DMSO): δ 160.7, 158.4, 156.0, 150.7, 132.8, 129.7, 129.0, 120.4, 119.2, 110.0, 102.8, 61.4, 57.2, 37.4, 14.2. IR results are identical with Mohammat et al. (2018).

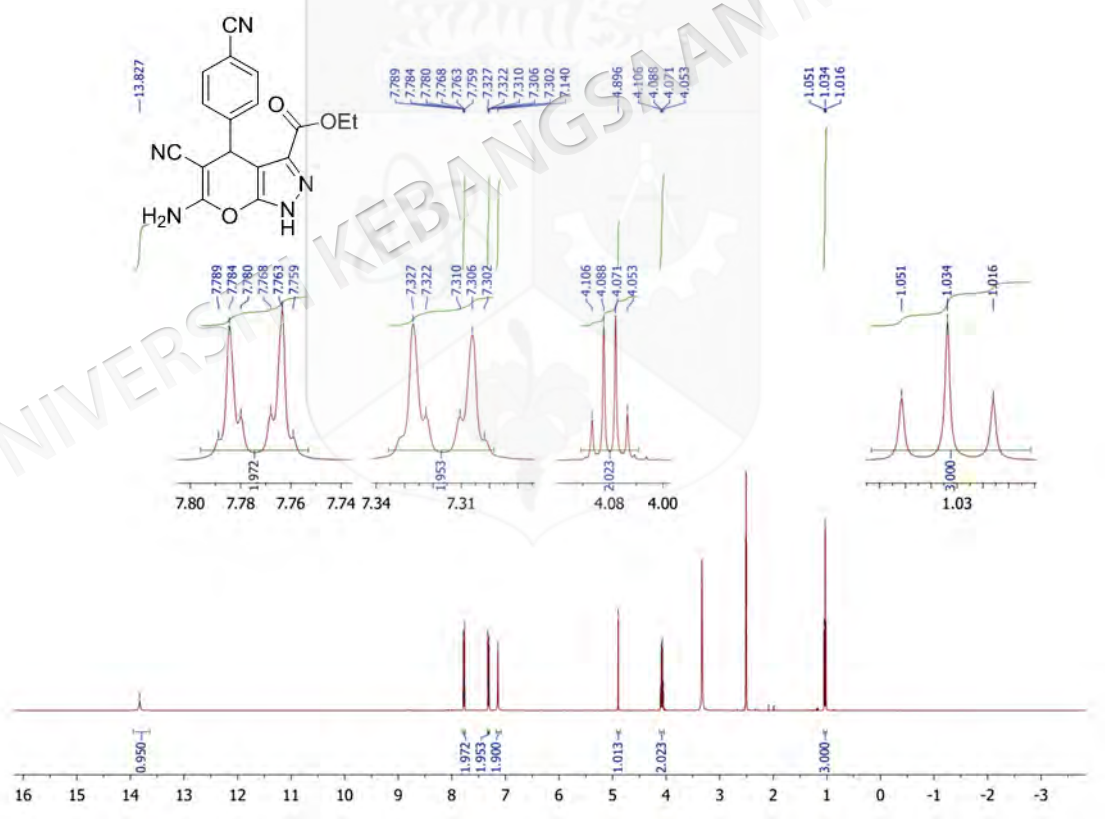

Figure 3.28 ^{1}H NMR spectrum of compound **20n**

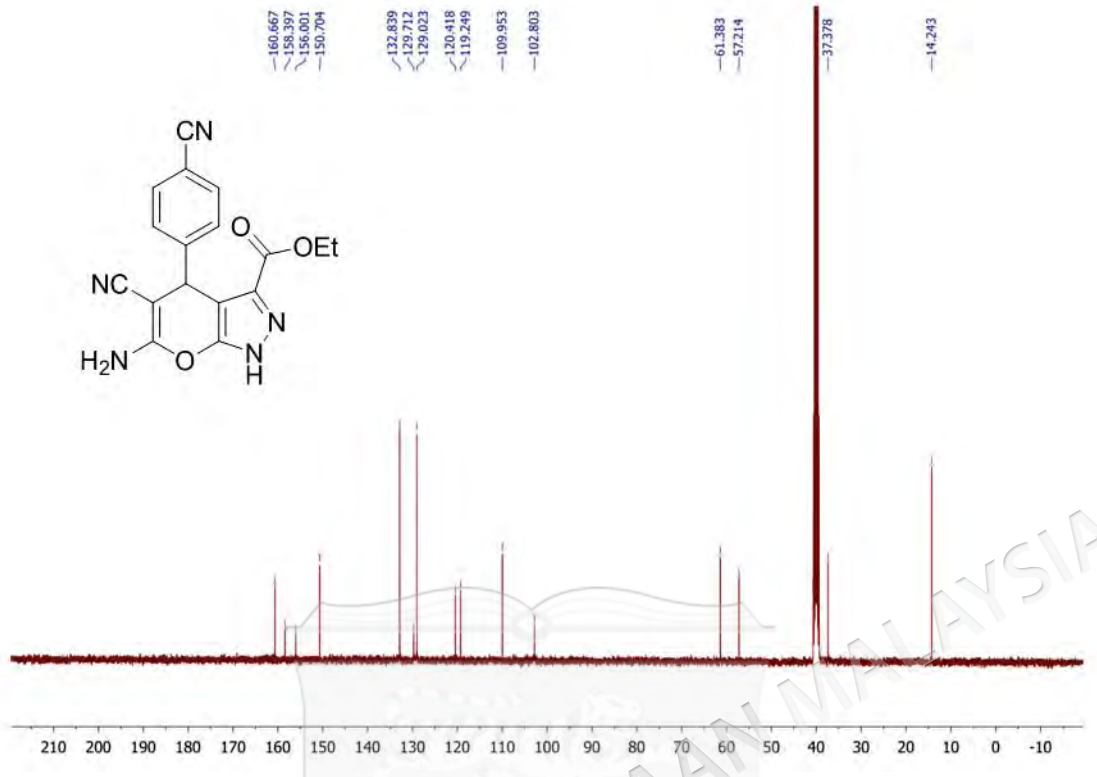

Figure 3.29 ^{13}C NMR spectrum of compound **20n**

3.3.15 Synthesis of ethyl 6-amino-5-cyano-4-(3-ethoxyphenyl)-1,4-dihydropyrano[2,3-*c*]pyrazole-3-carboxylate (20o)

The synthesis method of the pyrano[2,3-*c*]pyrazole compound **20o** is the same as described in subsection 3.3, using a mixture of hydrazine solution 35% (0.49 mL, 5.5 mmol) (**8**), sodium diethyloxalacetate solution (1.15 g, 5.5 mmol) (**18**), 1 mL of Acetic acid, 20 mL of ethanol, Malanonitrile (0.33 g, 5 mmol) (**19**) and 3-ethoxybenzaldehyde (0.75 gr, 5 mmol), to yield a yellowish white solid (55%). Melting point: 211-212 ºC; IR cm^{-1}: 3319 (NH_2), 3179 (NH), 2189 (CN), 1729 (COOEt), 1654 (C=C); ^{1}H NMR (400 MHz, DMSO) δ 13.73 (s, 1H), 7.19 (t, *J* = 8 Hz, 1H), 7.01 (s, 2H), 6.76 (dd, *J* = 8, 2.4 Hz, 1H), 6.64-6.61 (m, 2H), 4.72 (s, 1H), 4.11 (q, *J* = 7.2 Hz, 2H), 3.97 (q, *J* = 7.2 Hz, 2H), 1.30 (t, *J* = 7.2 Hz, 3H), 1.07 (t, *J* = 7.2 Hz, 3H); ^{13}C NMR (100 MHz, DMSO): δ 160.6, 158.8, 158.6, 156.1, 146.9, 129.8, 129.5, 120.7, 119.8, 114.4, 112.5, 104.0, 63.3, 61.3, 58.2, 37.3, 15.1, 14.2.

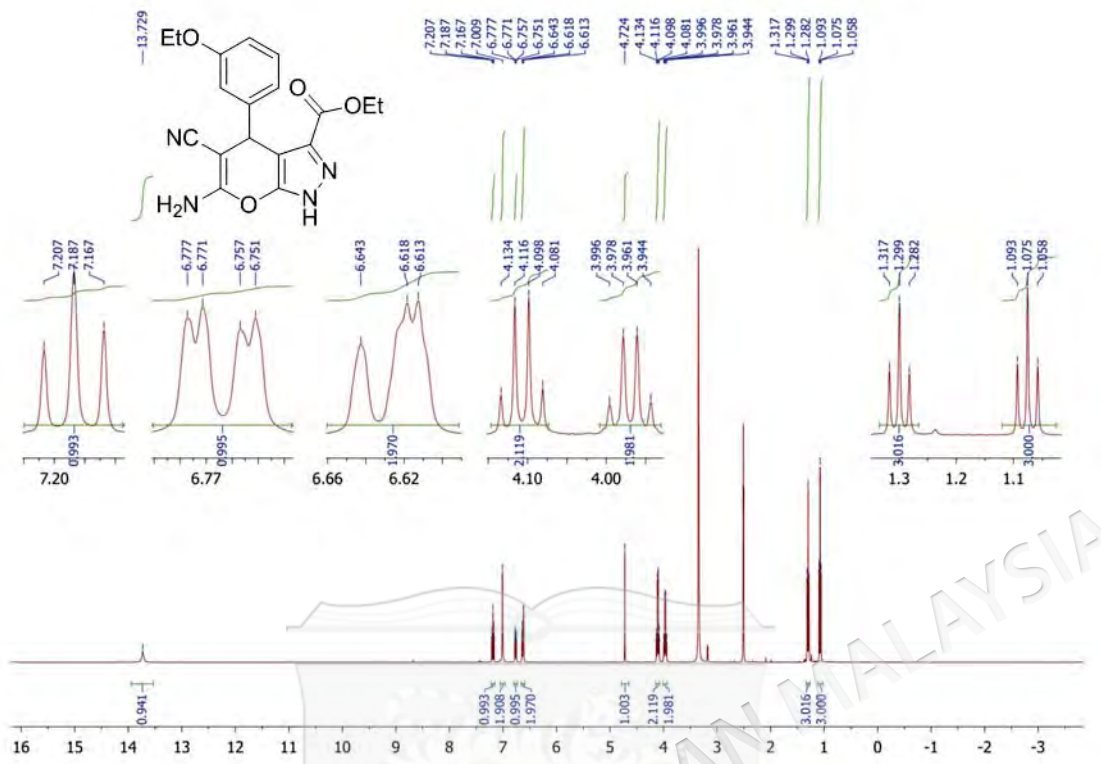

Figure 3.30 ^{1}H NMR spectrum of compound **20o**

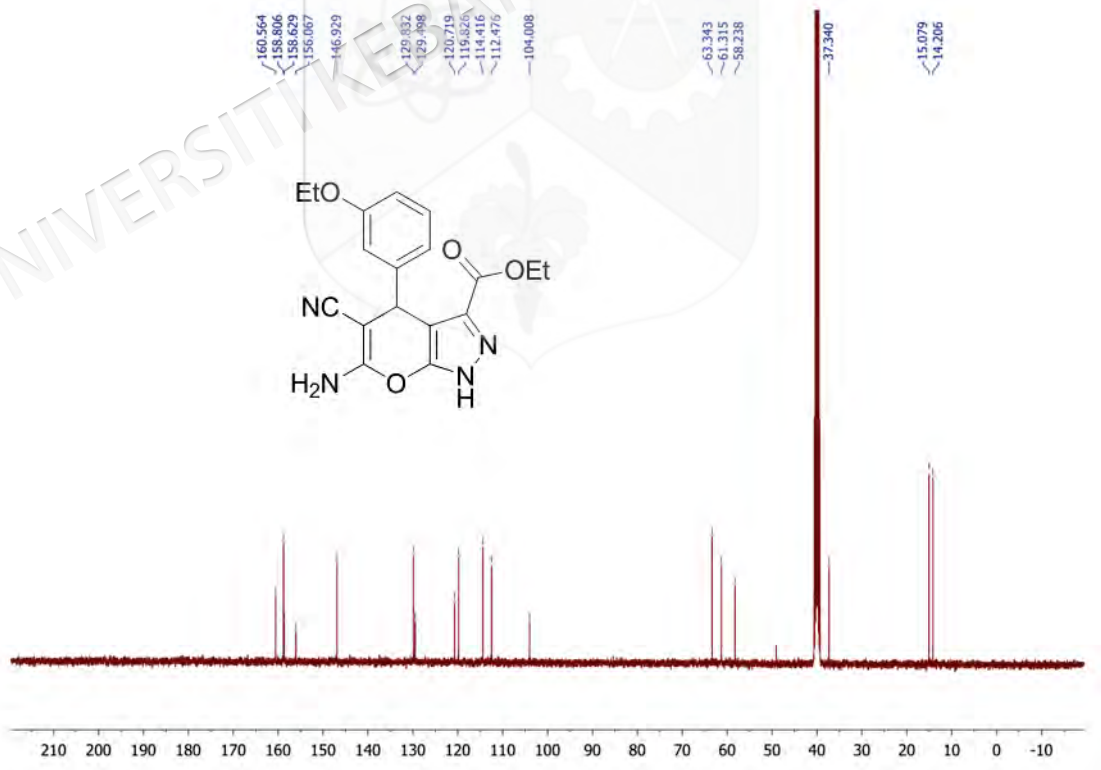

Figure 3.31 ^{13}C NMR spectrum of compound **20o**

3.3.16 Synthesis of 4-(6-amino-5-cyano-3-(ethoxycarbonyl)-1,4-dihydropyrano[2,3-*c*]pyrazol-4-yl)benzoic acid (20p)

The synthesis method of the pyrano[2,3-*c*]pyrazole compound **20p** is the same as described in subsection 3.3, using a mixture of hydrazine solution 35% (0.49 mL, 5.5 mmol) (**8**), sodium diethyloxalacetate solution (1.15 g, 5.5 mmol) (**18**), 1 mL of Acetic acid, 20 mL of ethanol, Malanonitrile (0.33 g, 5 mmol) (**19**) and 4-formylbenzoic acid (0.75 gr, 5 mmol), to yield a brownish white solid (84%). Melting point: 242-244 ^{o}C; IR cm^{-1}: 3321 (NH_2), 3175 (NH), 2189 (CN), 1718 (COOEt), 1641 (C=C); ^{1}H NMR (400 MHz, DMSO) δ 7.84 (d, *J* = 8 Hz, 2H), 7.12 (d, *J* = 8 Hz, 2H), 7.04 (s, 2H), 4.80 (s, 1H), 4.08 (q, *J* = 6.8 Hz, 2H), 1.90 (s, 1H), 1.04 (t, *J* = 7.2 Hz, 3H); ^{13}C NMR (100 MHz, DMSO): δ 160.5, 158.5, 155.9, 129.8, 128.9, 128.1, 127.7, 120.6, 103.5, 61.3, 57.9, 37.3, 21.7, 14.7, 14.2.

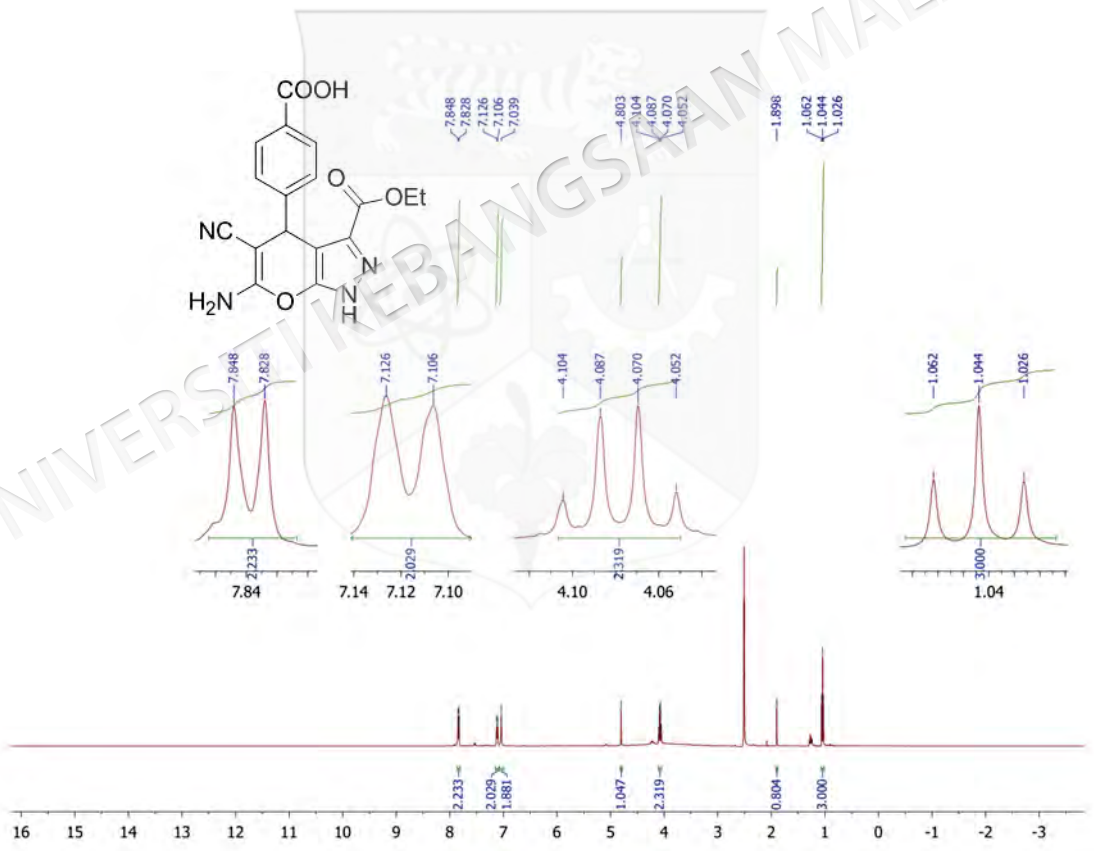

Figure 3.32 ^{1}H NMR spectrum of compound **20p**

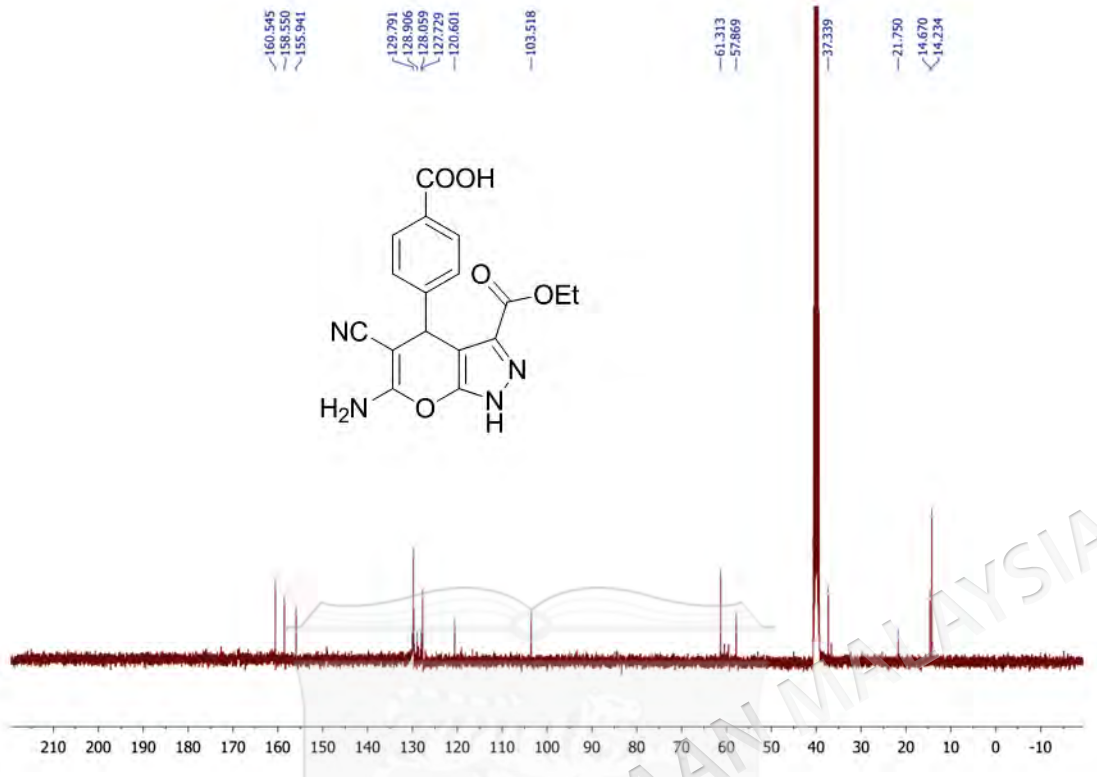

Figure 3.33 ^{13}C NMR spectrum of compound **20p**

3.3.17 Synthesis ethyl 6-amino-5-cyano-4-(4-hydroxyphenyl)-1,4-dihydropyrano[2,3-*c*]pyrazole-3-carboxylate (20q)

The synthesis method of the pyrano[2,3-*c*]pyrazole compound **20q** is the same as described in subsection 3.3, using a mixture of hydrazine solution 35% (0.49 mL, 5.5 mmol) (**8**), sodium diethyloxalacetate solution (1.15 g, 5.5 mmol) (**18**), 1 mL of Acetic acid, 20 mL of ethanol, Malanonitrile (0.33 g, 5 mmol) (**19**) and 4-hydroxybenzaldehyde (0.61 gr, 5 mmol), to yield a white solid (55%). Melting point: 217-218 ºC; ^{1}H NMR (400 MHz, DMSO) δ 13.66 (s, 1H), 9.24 (s, 1H), 6.94 (s, 2H), 6.89 (dt, *J* = 9.6, 2.8 Hz, 2H), 6.66 (dt, *J* = 9.2, 2.8 Hz, 2H), 4.64 (s, 1H), 4.12 (q, *J* = 7.2 Hz, 2H), 1.10 (t, *J* = 7.2 Hz, 3H); ^{13}C NMR (100 MHz, DMSO): δ 160.3, 158.7, 156.4, 156.0, 135.9, 129.4, 128.7, 120.9, 115.4, 104.8, 61.3, 58.9, 36.7, 14.3. IR results are identical with Mohammat et al. (2018).

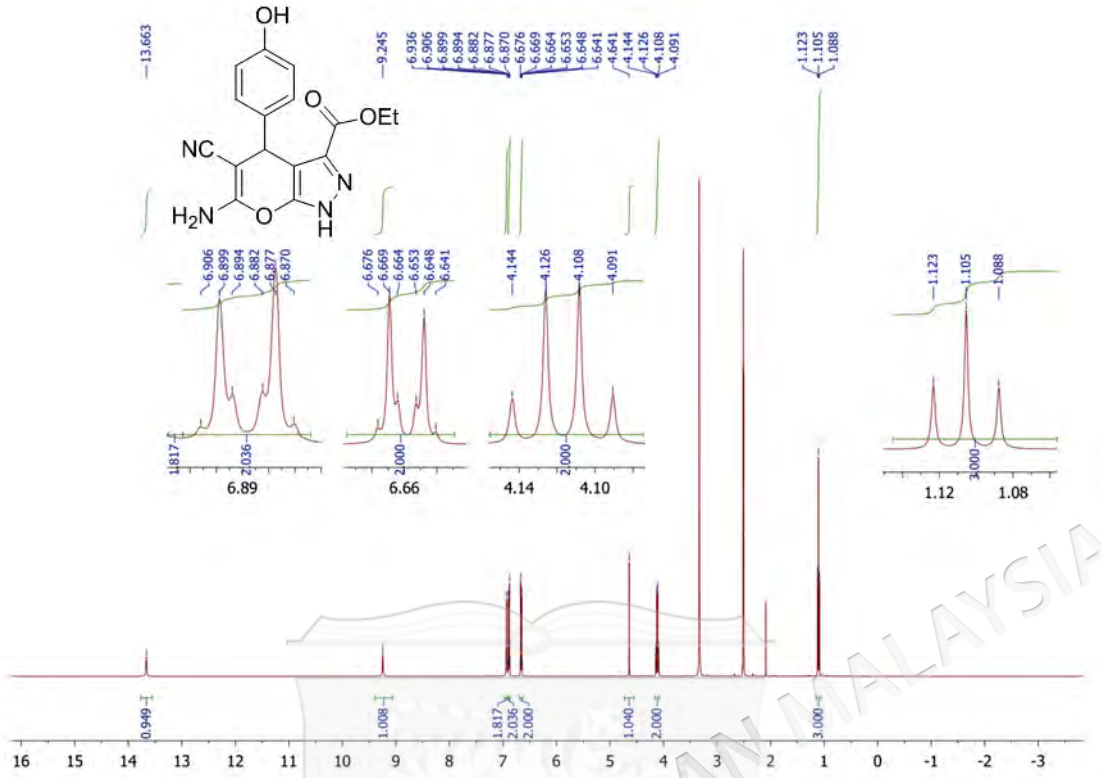

Figure 3.34 ^{1}H NMR spectrum of compound **20q**

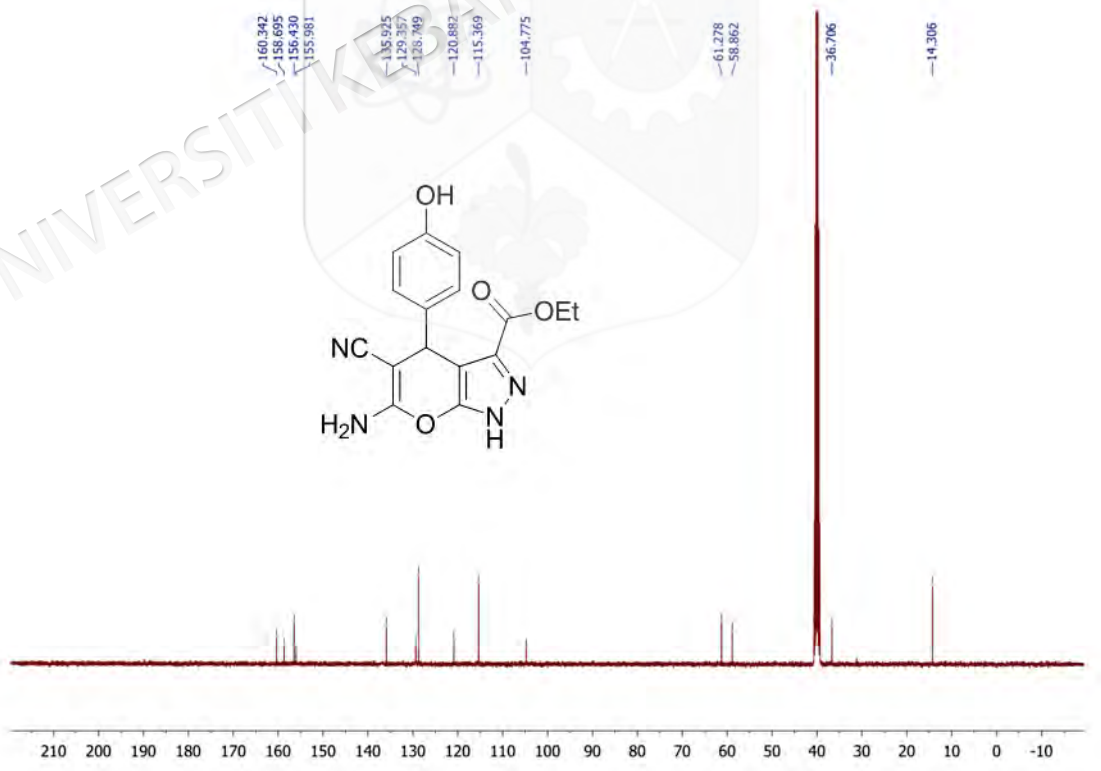

Figure 3.35 ^{13}C NMR spectrum of compound **20q**

3.3.18 Synthesis of ethyl 6-amino-5-cyano-4-(2-hydroxynaphthalen-1-yl)-1,4-dihydropyrano[2,3-*c*]pyrazole-3-carboxylate (20r)

The synthesis method of the pyrano[2,3-*c*]pyrazole compound **20r** is the same as described in subsection 3.3, using a mixture of hydrazine solution 35% (0.49 mL, 5.5 mmol) (**8**), sodium diethyloxalacetate solution (1.15 g, 5.5 mmol) (**18**), 1 mL of Acetic acid, 20 mL of ethanol, Malanonitrile (0.33 g, 5 mmol) (**19**) and 2-hydroxy-1-naphthaldehyde (0.86 gr, 5 mmol), to yield a yellow solid (52%). Melting point: 231-233 ^{o}C; IR cm^{-1}: 3393 (NH_2), 3173 (NH), 2197 (CN), 1720 (COOEt), 1654 (C=C); ^{1}H NMR (400 MHz, DMSO) δ 12.63 (s, 1H), 7.94-7.84 (m, 4H), 7.47-7.36 (m, 2H), 7.22 (d, J = 9.6, Hz, 1H), 6.78 (s, 2H), 5.72 (s, 1H), 4.40 (s, 2H), 1.37 (s, 3H); ^{13}C NMR (100 MHz, DMSO): δ 160.6, 159.8, 156.9, 147.6, 131.1, 129.1, 127.3, 125.0, 123.3, 121.1, 117.9, 117.2, 114.3, 71.3, 61.2, 55.5, 27.3, 25.5, 14.6.

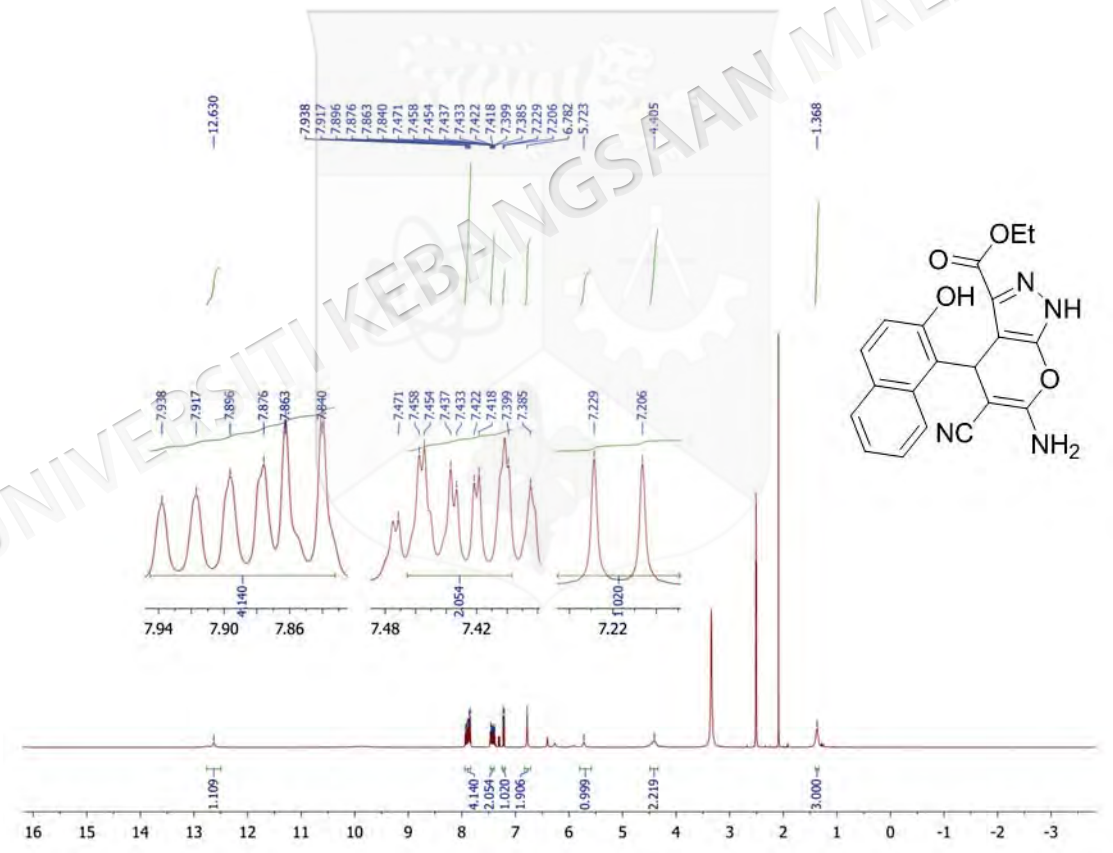

Figure 3.36 ^{1}H NMR spectrum of compound **20r**

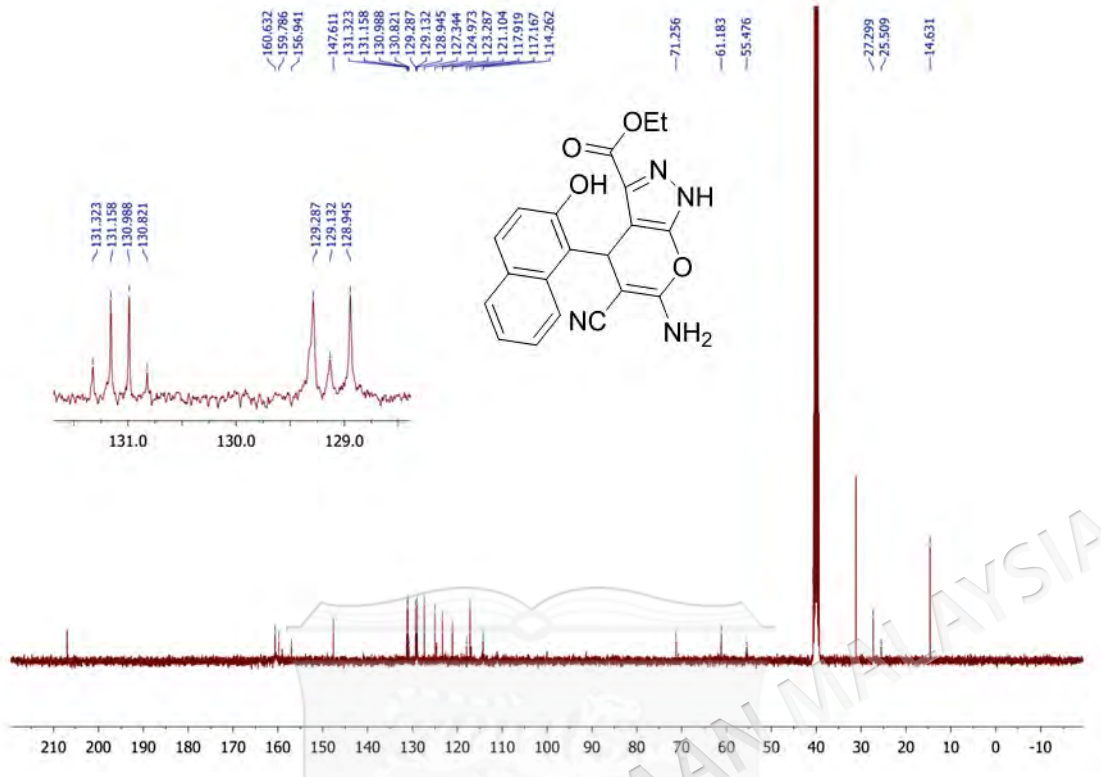

Figure 3.37 ^{13}C NMR spectrum of compound **20r**

3.3.19 Synthesis of ethyl 6-amino-5-cyano-4-(pyridin-2-yl)-1,4-dihydropyrano[2,3-*c*]pyrazole-3-carboxylate (20s)

The synthesis method of the pyrano[2,3-*c*]pyrazole compound **20s** is the same as described in subsection 3.3, using a mixture of hydrazine solution 35% (0.49 mL, 5.5 mmol) (**8**), sodium diethyloxalacetate solution (1.15 g, 5.5 mmol) (**18**), 1 mL of Acetic acid, 20 mL of ethanol, Malanonitrile (0.33 g, 5 mmol) (**19**) and picolinaldehyde (0.53 gr, 5 mmol), to yield a brown solid (54%). Melting point: 289-291 ºC; IR cm^{-1}: 3404 (NH_2), 3313 (NH), 2212 (CN), 1723 (COOEt), 1626 (C=C); ^{1}H NMR (400 MHz, DMSO) δ 12.85 (s, 1H), 7.82 (d, *J* = 6.8 Hz, 1H), 6.94 (d, *J* = 9.2 Hz, 1H), 6.54-6.45 (m, 2H), 6.13 (s, 2H), 4.16 (q, *J* = 7.2 Hz, 2H), 3.18 (s, 1H), 1.15 (t, *J* = 7.2 Hz, 3H); ^{13}C NMR (100 MHz, DMSO): δ 154.9, 150.4, 138.0, 130.0, 123.3, 121.2, 120.4, 117.5, 115.8, 111.4, 101.6, 80.3, 60.8, 49.1, 14.3.

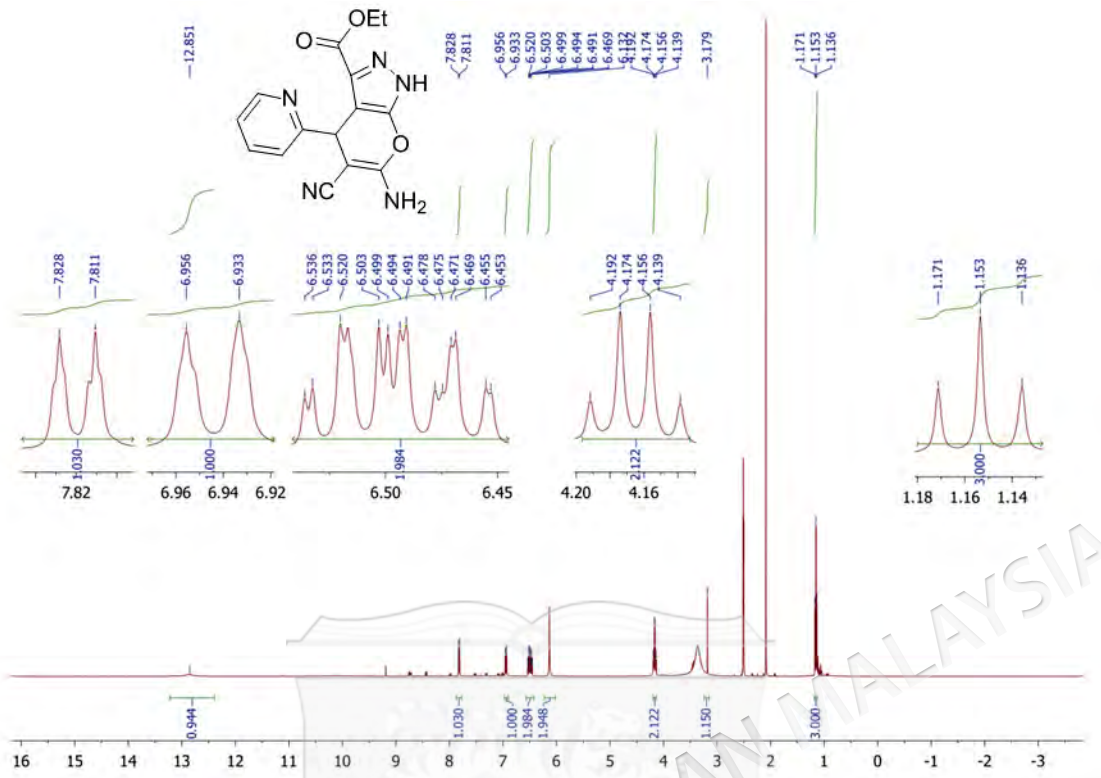

Figure 3.38 ^{1}H NMR spectrum of compound **20s**

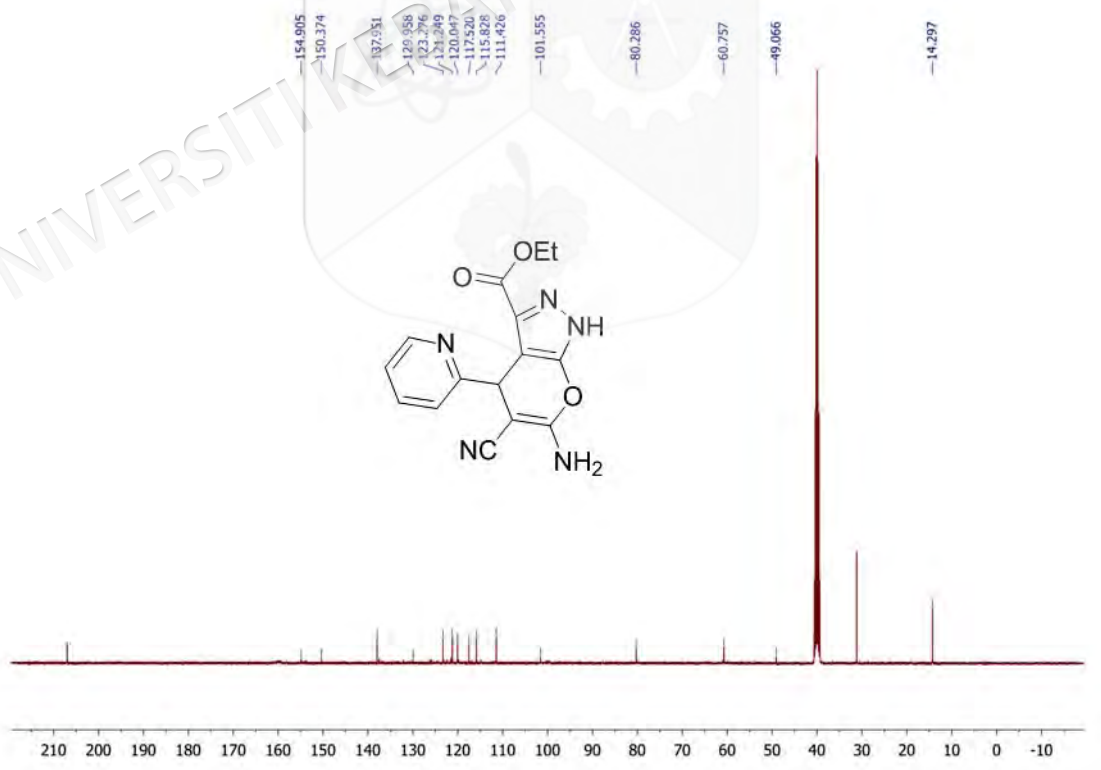

Figure 3.39 ^{13}C NMR spectrum of compound **20s**

3.4 GENERAL PROCEDURE FOR THE SYNTHESIS OF 4-(ETHANOLAMINO)-7-CHLOROQUINE (22)

In a three-neck round-bottom flask, a mixture of 4,7-dichloroquinoline (2 g, 10 mmol) (**21**) and aminoethanol (10 mL) was heated for 5 h at 130 ºC. The mixture was then allowed to cool at room temperature and poured into cold water during which the compound precipitated. The precipitate was filtered and dried under vacuum to get 2-((7-chloroquinolin-4-yl)amino)ethan-1-ol (**22**) as a white solid in 94% yield (Figure 3.40) (Guantai et al. 2011). Melting point: 210-211 ºC; ^{1}H NMR (400 MHz, DMSO) δ 8.37 (d, *J* = 5.6 Hz, 1H), 8.26 (d, *J* = 8.8 Hz, 1H), 7.78 (d, *J* = 2 Hz, 1H), 7.45 (dd, *J* = 9.2, 2.4 Hz, 1H), 7.25 (t, *J* = 5.6 Hz, 1H), 6.51 (d, *J* = 5.2 Hz, 1H), 4.88 (s, 1H), 3.66 (s, 2H), 3.37 (t, *J* = 5.6 Hz, 2H); ^{13}C NMR (100 MHz, DMSO): δ 152.4, 150.7, 149.6, 133.8, 127.9, 124.5, 124.5, 117.9, 99.2, 59.2, 45.6.

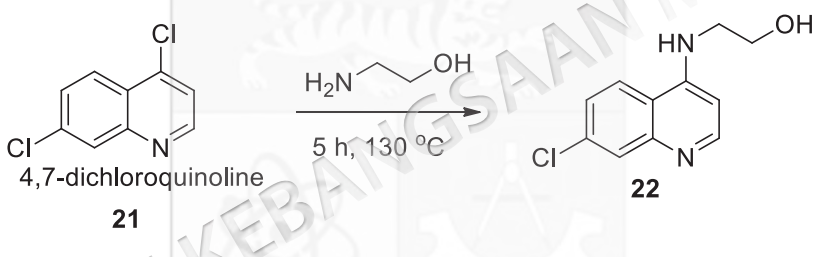

Figure 3.40 4-(Ethanolamino)-7-chloroquine synthesis

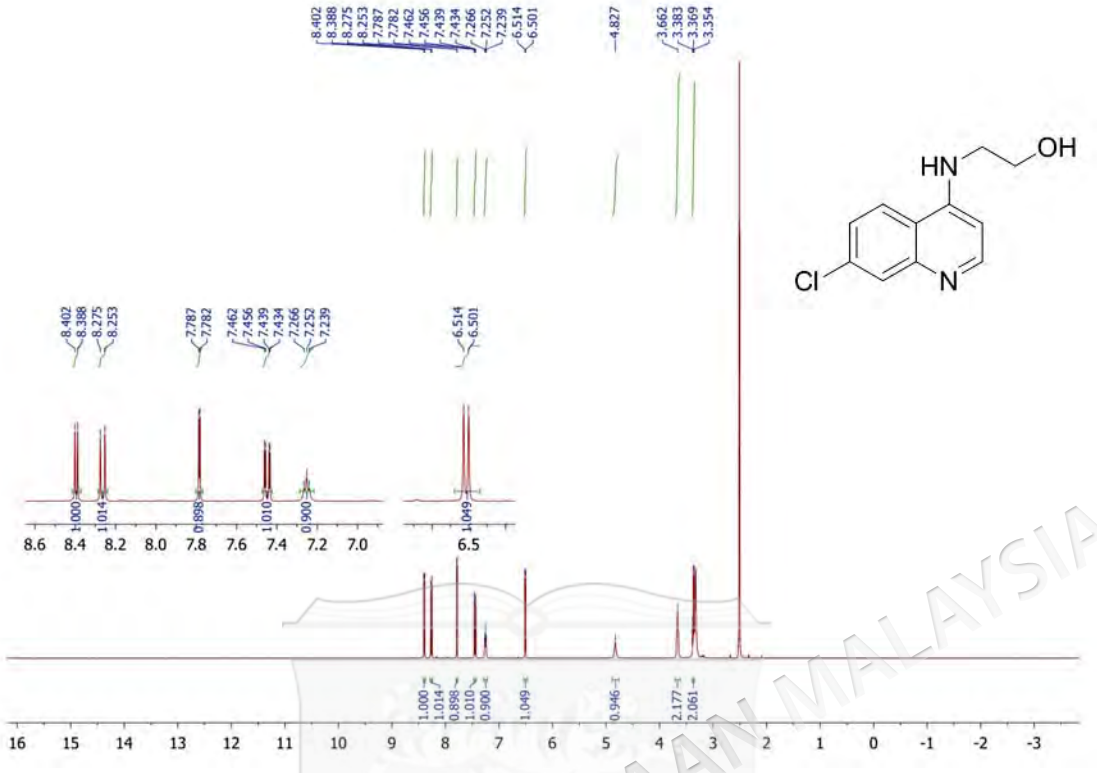

Figure 3.41 ^{1}H NMR spectrum of compound **22**

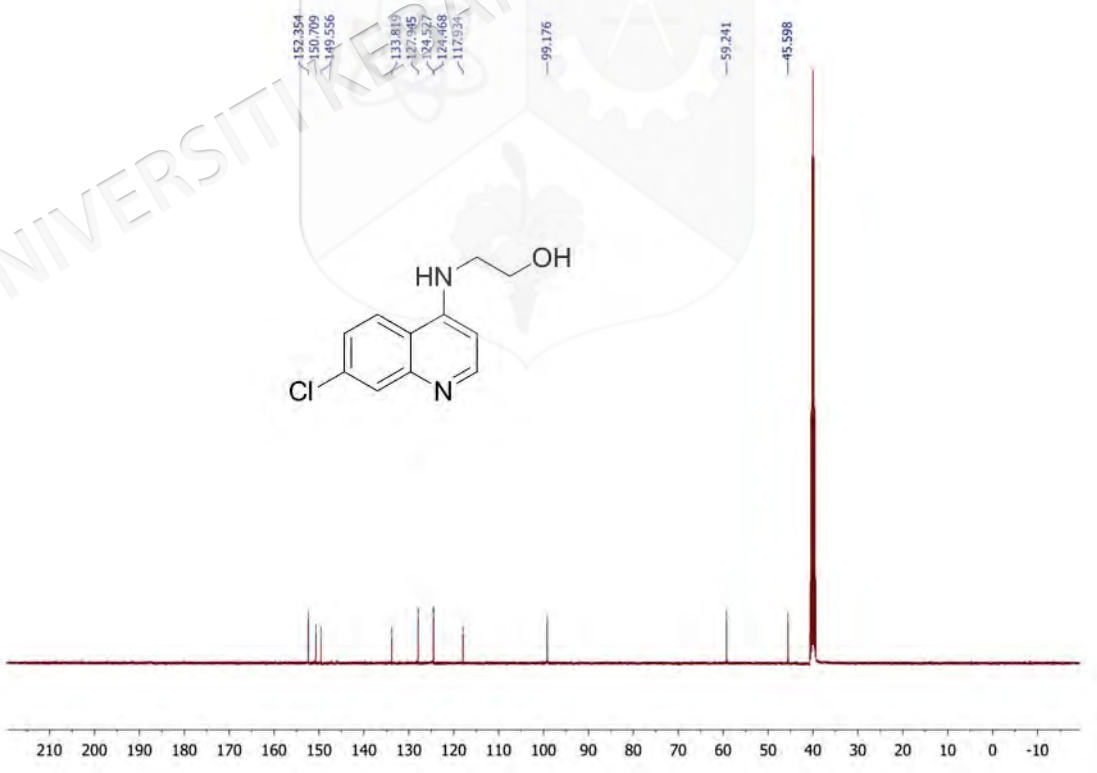

Figure 3.42 ^{13}C NMR spectrum of compound **22**

3.5 GENERAL PROCEDURE FOR THE SYNTHESIS OF 4-(BROMOMETHYLAMINO)-7-CHLOROQUINE (23)

Under cold conditions, hydrobromic acid (0.88 mL, 16.2 mmol) and sulphuric acid (0.29 mL, 5.5 mmol) was added slowly to **22** (0.58 g 2.6 mmol). The reaction was then refluxed for 4 h at 165 ºC, and the progress of the reaction was monitored using TLC. The reaction medium was quenched by adding $NaHCO_3$ solution dropwise and the pH was adjusted around 7. The reaction mixture was then extracted with dichloromethane dried over Na_2SO_4 and concentrated under vacuum to obtain the corresponding product **23** in 70% yield as a white solid (Figure 3.43) (Cazelles et al. 2011). Melting point: 140-141 ºC; ^{1}H NMR (400 MHz, DMSO) δ 8.44 (d, *J* = 5.2 Hz, 1H), 8.25 (d, *J* = 8.8 Hz, 1H), 7.82 (d, *J* = 2.4 Hz, 1H), 7.50 (dd, *J* = 9.2, 2.4 Hz, 1H), 6.59 (d, *J* = 5.6 Hz, 1H), 3.77-3.70 (m, 4H), 3.33 (s, 1H); ^{13}C NMR (100 MHz, DMSO): δ 151.8, 149.9, 146.4, 135.4, 125.7, 125.6, 124.8, 117.3, 99.4, 44.7, 31.6.

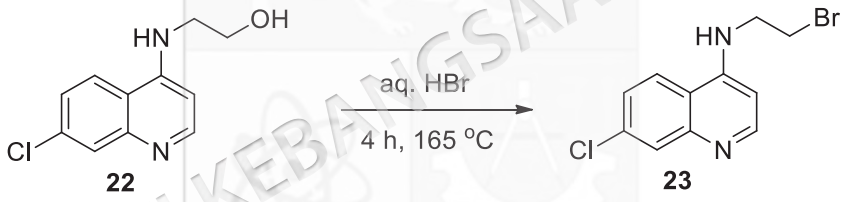

Figure 3.43 4-(Bromoethylamino)-7-chloroquinoline synthesis

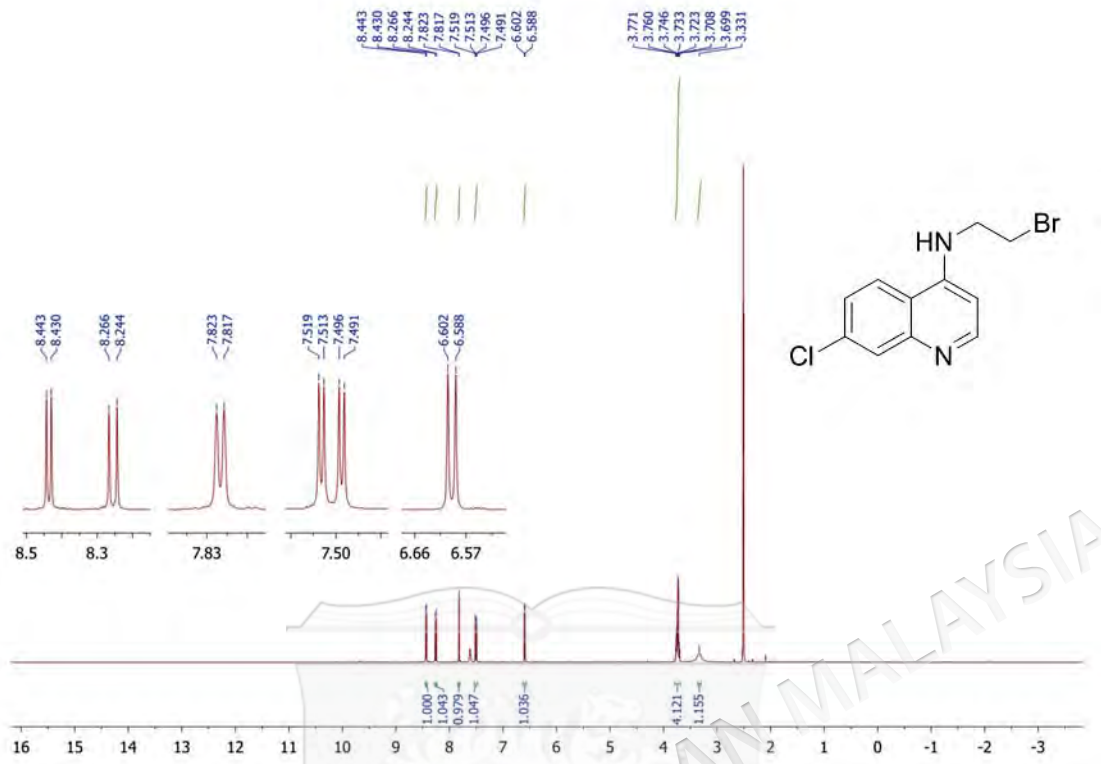

Figure 3.44 ^{1}H NMR spectrum of compound **23**

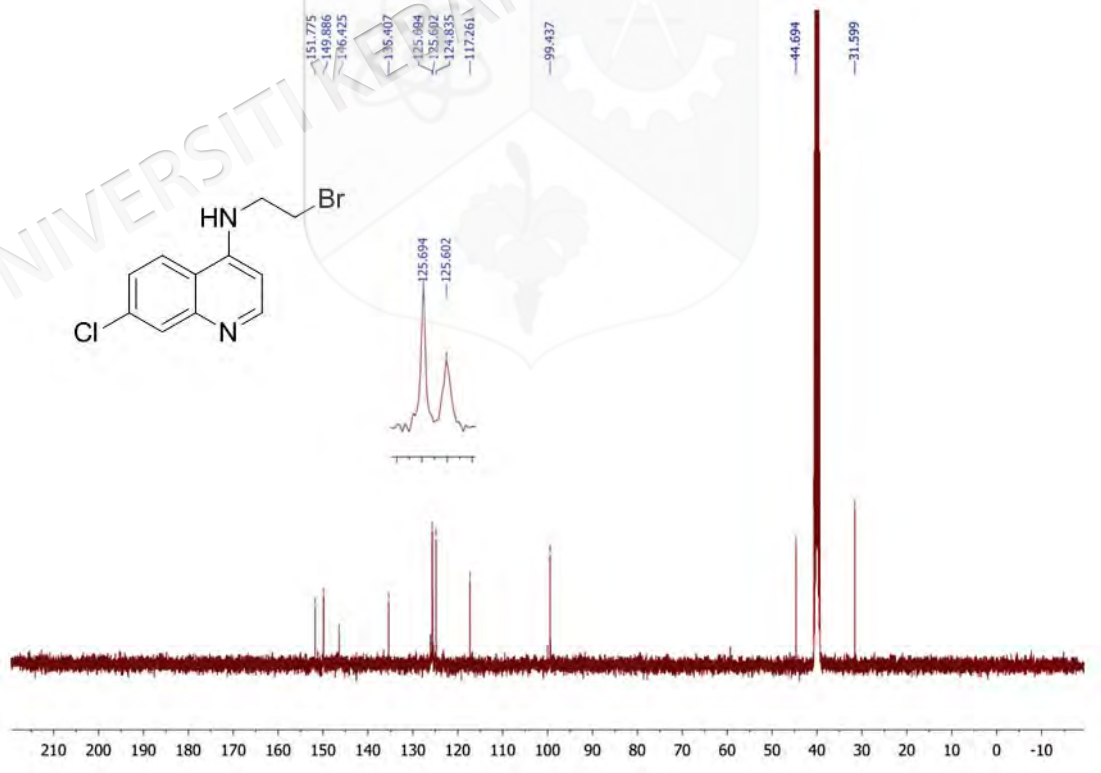

Figure 3.45 ^{13}C NMR spectrum of compound **23**

3.6 GENERAL PROCEDURE FOR THE SYNTHESIS OF PYRANO[2,3-*C*]PYRAZOLE-4-AMINOQUINOLINES (24A-S)

To a mixture of desired pyrano[2,3-*c*]pyrazole **20a–s** compounds (5 mmol) and 4-(bromoethylamino)-7-chloroquinoline (1.43 g, 5 mmol) (**23)** in DMSO, sodium bicarbonate (0.84 g, 10 mmol) was added and vigorously stirred for 24 h at 30–40 ˚C. After cooling to room temperature, the mixture was extracted using 80 mL of brine and 20 mL of ethyl acetate, the organic layer was separated, and then concentrated through rotary evaporator. Finally, a mixture of ethyl acetate:hexane (3:1) was used to purify all the synthesized hybrid compounds through the silica column chromatography (Figure 3.46) (Shamsuddin et al. 2021).

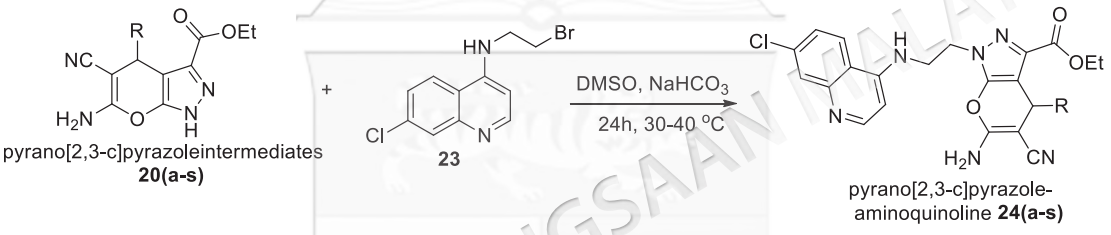

Figure 3.46 Synthesis of pyrano[2,3-*c*]pyrazole-aminoquinoline hybrids

3.6.1 Synthesis of ethyl 6-amino-1-(2-((7-chloroquinolin-4-yl)amino)ethyl)-5-cyano-4-(4-methoxyphenyl)-1,4-dihydropyrano[2,3-*c*]pyrazole-3-carboxylate (24a)

The reaction between pyrano[2,3-*c*]pyrazole **20a** (1.7g, 5 mmol) and 4-(bromoethylamino)-7-chloroquinoline (1.43g, 5 mmol) (**23**) afforded pyrano[2,3-*c*]pyrazole-aminoquinoline hybrid compound **24a** as a brown solid with 25% yield and melting range of 169-171 ºC. IR cm^{-1}: 3354 (NH_2), 3229 (NH), 2187 (CN), 1718 (COOEt), 1640 (C=C); ^{1}H NMR (400 MHz, DMSO) δ 8.43 (d, *J* = 5.6 Hz, 1H), 8.10 (d, *J* = 9.2 Hz, 1H), 7.82 (d, *J* = 2 Hz, 1H), 7.48 (dd, *J* = 8.8, 2 Hz, 1H), 7.33 (dt, *J* = 9.6, 2.8 Hz, 1H), 7.01-6.99 (m, 2H), 6.91 (dt, *J* = 9.2, 2.8 Hz, 2H), 6.79 (dt, *J* = 9.2, 2.8 Hz, 2H), 6.55 (d, *J* = 5.6 Hz, 1H), 4.70-4.65 (m, 2H), 4.61 (s, 1H), 3.81 (s, 1H), 3.72 (s, 3H), 1.92 (s, 3H), 0.77 (t, *J* = 6.8 Hz, 3H); ^{13}C NMR (100 MHz, DMSO): δ 172.5, 161.4, 158.6, 158.3, 154.7, 137.4, 131.1, 128.6, 128.3, 124.6, 119.5, 117.3, 117.0, 114.2, 114.0, 105.9, 61.3, 58.8, 55.7, 55.5, 41.2, 37.0, 36.7, 24.1, 21.5, 13.7. HRMS calcd. for $C_{28}H_{25}ClN_6O_4$: *m/z* 544.1626; found: *m/z* 545.1679 (M^+).

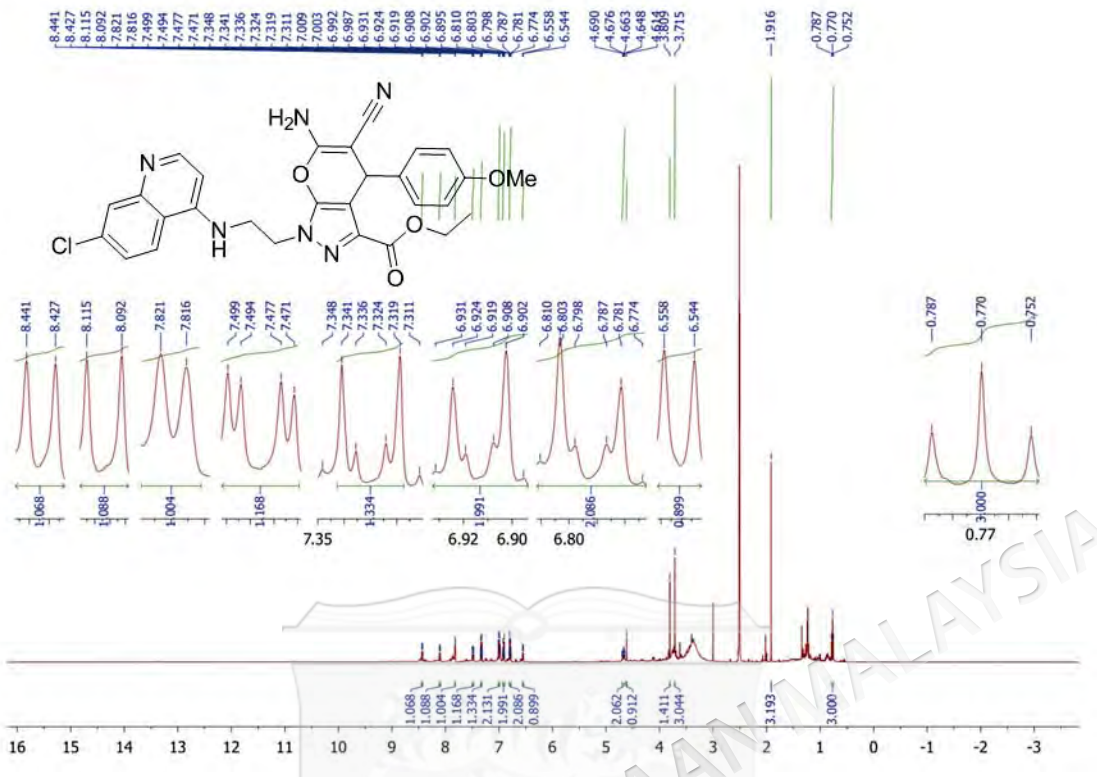

Figure 3.47 ^{1}H NMR spectrum of hybrid **24a**

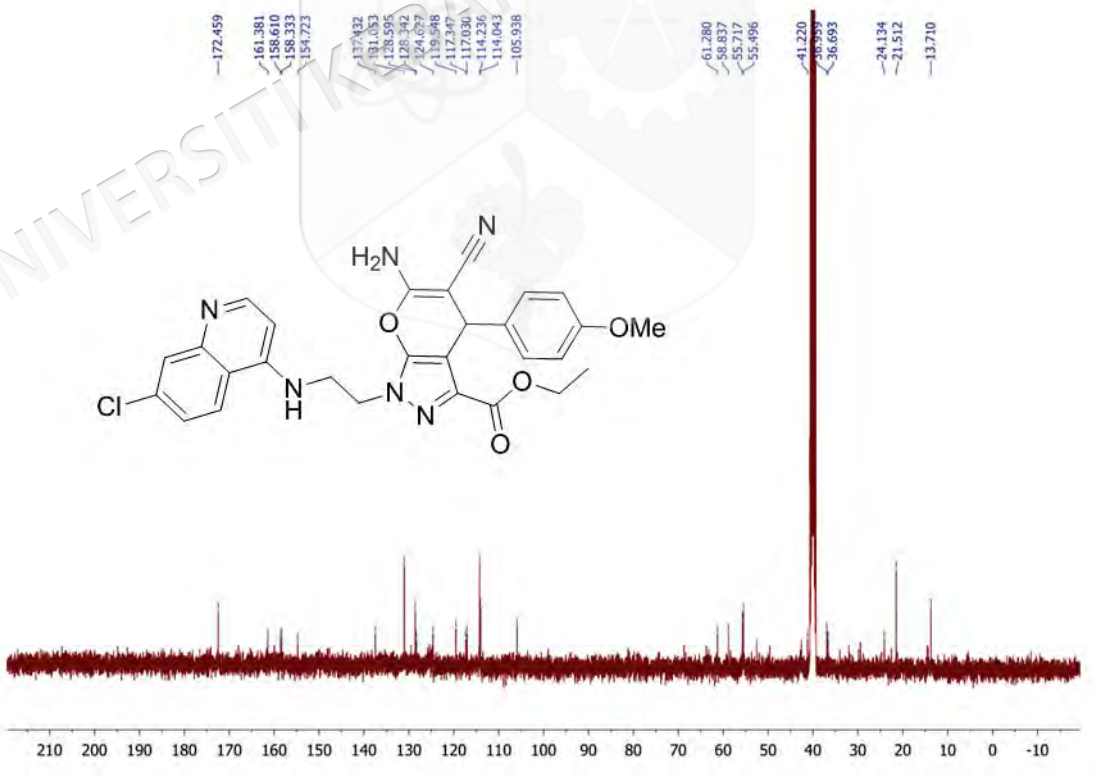

Figure 3.48 ^{13}C NMR spectrum of hybrid **24a**

3.6.2 Synthesis of ethyl 6-amino-1-(2-((7-chloroquinolin-4-yl)amino)ethyl)-5-cyano-4-(3-hydroxyphenyl)-1,4-dihydropyrano[2,3-*c*]pyrazole-3-carboxylate (24b)

The reaction between pyrano[2,3-*c*]pyrazole **20b** (1,63g, 5 mmol) and 4-(bromoethylamino)-7-chloroquinoline (1.43g, 5 mmol) (**23**) afforded pyrano[2,3-*c*]pyrazole-aminoquinoline hybrid compound **24b** as a brown solid with 24% yield and melting range of 199-201 ^{o}C. IR cm^{-1}: 3388 (NH_2), 3311 (NH), 2200 (CN), 1733 (COOEt), 1619 (C=C); ^{1}H NMR (400 MHz, DMSO) δ 9.370 (s, 1H), 8.39 (d, *J* = 5.2 Hz, 1H), 8.07 (d, *J* = 9.2 Hz, 1H), 7.79 (d, *J* = 2.4 Hz, 1H), 7.47-7.42 (m, 2H), 7.06-7.01 (m, 3H), 6.58 (ddd, *J* = 8, 2.4, 0.8 Hz, 1H), 6.45 (d, *J* = 5.6 Hz, 1H), 6.46-6.44 (m, 2H), 4.74 (q, *J* = 6.8 Hz, 1H), 4.58-4.53 (m, 2H), 3.76-3.69 (m, 4H), 0.83 (t, *J* = 7.2 Hz, 3H); ^{13}C NMR (100 MHz, DMSO): δ 160.2, 158.7, 157.7, 154.7, 151.7, 150.4, 148.9, 146.6, 134.1, 129.7, 129.5, 127.4, 124.9, 124.4, 118.2, 117.8, 114.5, 114.1, 105.7, 99.1, 61.3, 58.5, 49.7, 42.7, 37.7, 13.7.

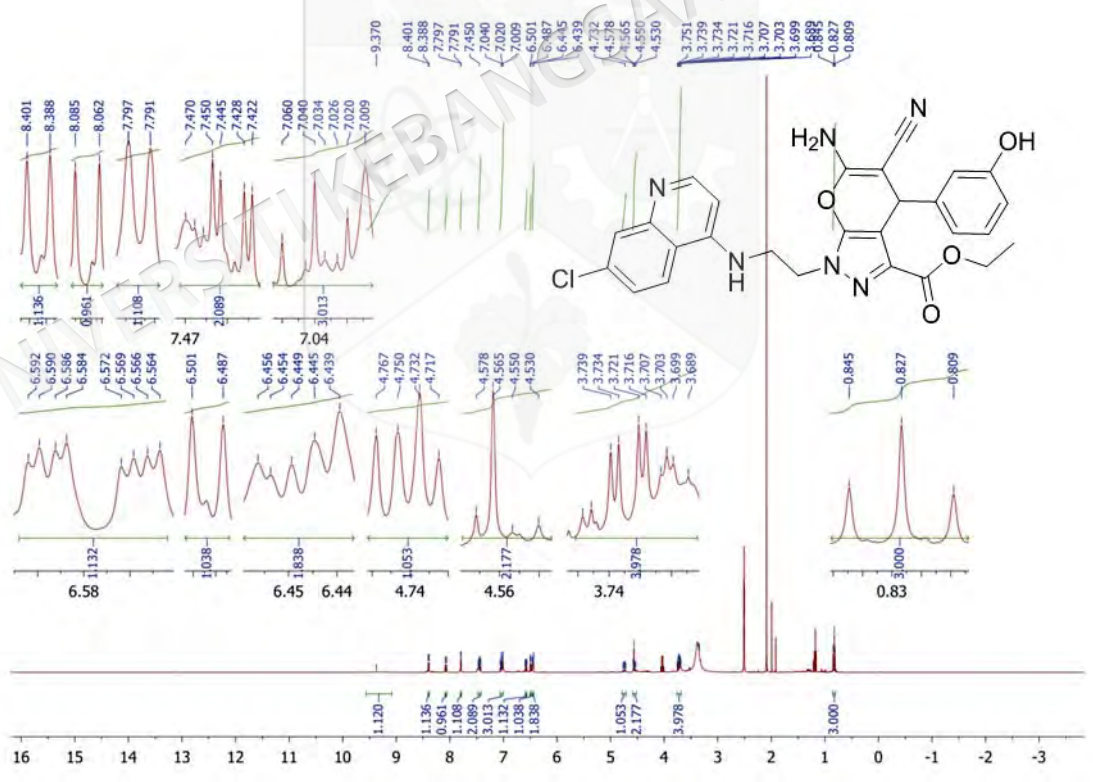

Figure 3.49 ^{1}H NMR spectrum of hybrid **24b**

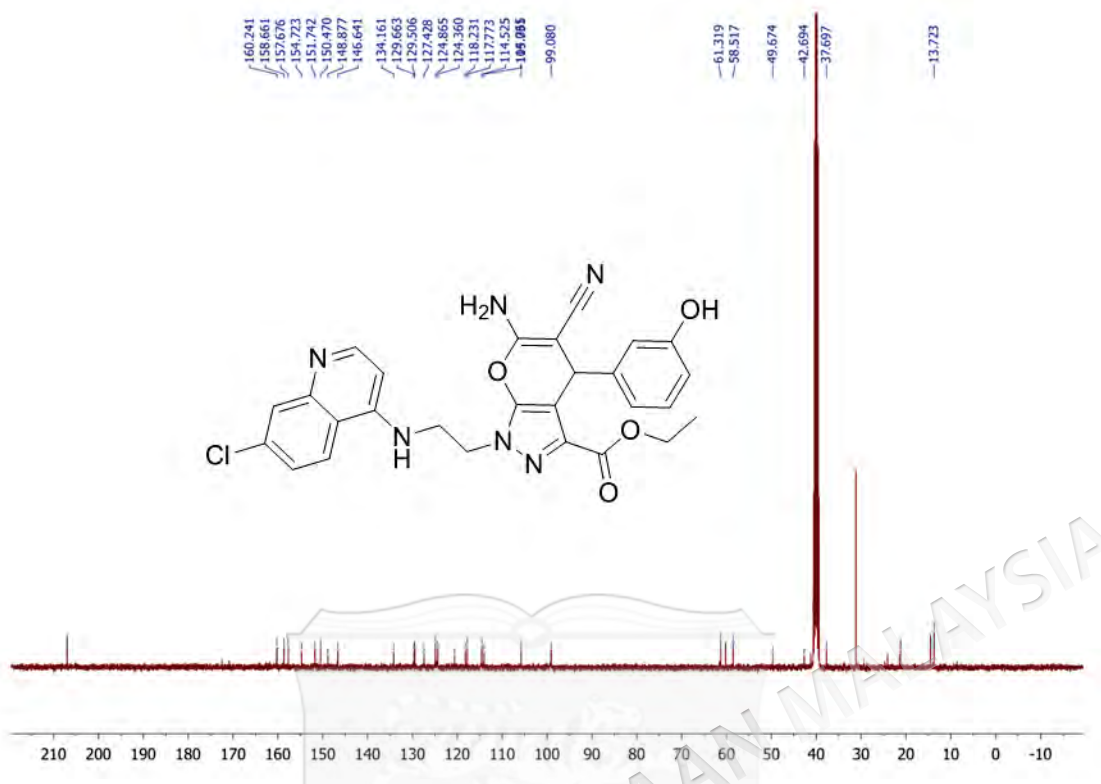

Figure 3.50 ^{13}C NMR spectrum of hybrid **24b**

3.6.3 Synthesis of ethyl 6-amino-1-(2-((7-chloroquinolin-4-yl)amino)ethyl)-5-cyano-4-(2-methoxyphenyl)-1,4-dihydropyrano[2,3-*c*]pyrazole-3-carboxylate (24c)

The reaction between pyrano[2,3-*c*]pyrazole **20c** (1.70g, 5 mmol) and 4-(bromoethylamino)-7-chloroquinoline (1.43g, 5 mmol) (**23**) afforded pyrano[2,3-*c*]pyrazole-aminoquinoline hybrid compound **24c** as a brown solid with 10% yield and melting range of 180-182 ^{o}C. IR cm^{-1}: 3347 (NH_2), 3278 (NH), 2146 (CN), 1722 (COOEt), 1640 (C=C); ^{1}H NMR (400 MHz, DMSO) δ 8.42 (d, *J* = 5.6 Hz, 1H), 8.26 (d, *J* = 9.2 Hz, 1H), 7.81 (d, *J* = 2.4 Hz, 1H), 7.58 (t, *J* = 5.2 Hz, 1H), 7.47 (dd, *J* = 9.2, 2.4 Hz, 1H), 7.27 (dd, *J* = 7.6, 1.6 Hz, 1H), 7.22-7.18 (m, 1H), 6.98 (d, *J* = 8.4 Hz, 1H), 6.67 (d, *J* = 5.6 Hz, 1H), 6.62 (td, *J* = 14.8, 7.6, 0.8 Hz, 1H), 5.57 (s, 2H), 6.46-6.44 (m, 2H), 4.48-4.43 (m, 1H), 4.33-4.28 (m, 2H), 3.768 (s, 4H), 1.92 (s, 3H), 1.27 (t, *J* = 7.2 Hz, 3H); ^{13}C NMR (100 MHz, DMSO): δ 172.5, 159.2, 156.9, 152.1, 150.5, 149.3, 134.0, 131.6, 129.8, 128.9, 127.8, 126.0, 124.7, 124.4, 120.7, 117.9, 111.7, 104.1, 99.2, 67.1, 61.6, 55.9, 41.9, 34.8, 31.1, 26.9, 21.5, 14.4.

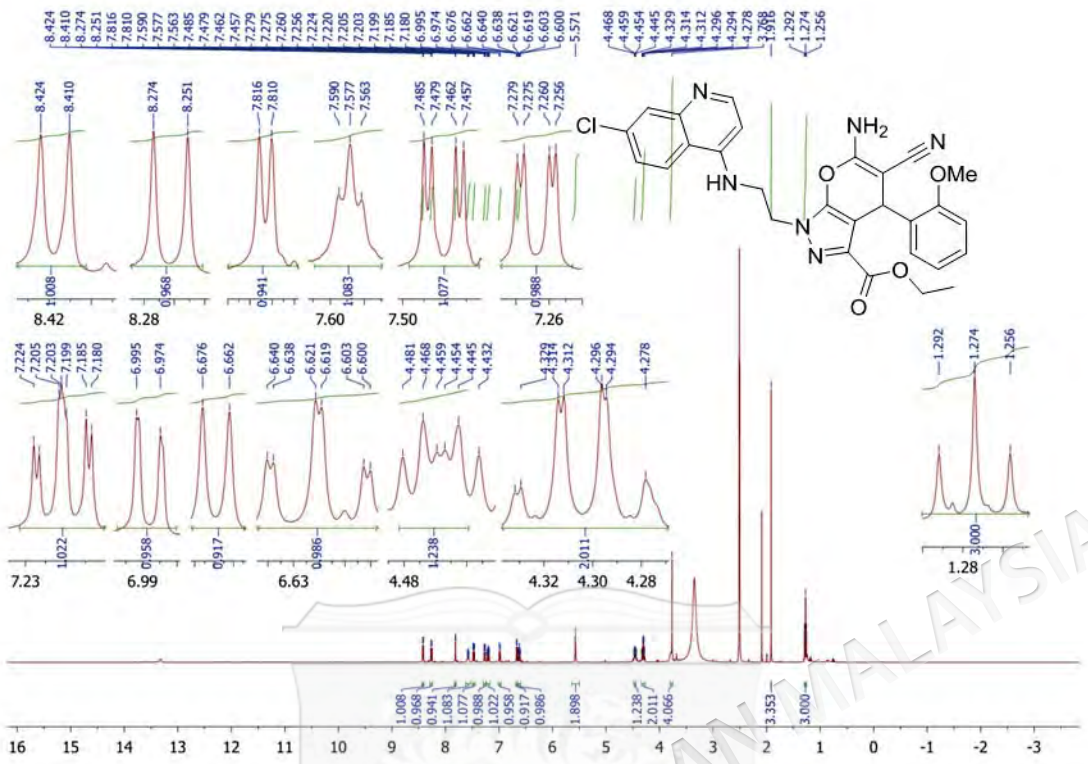

Figure 3.51 ^{1}H NMR spectrum of hybrid **24c**

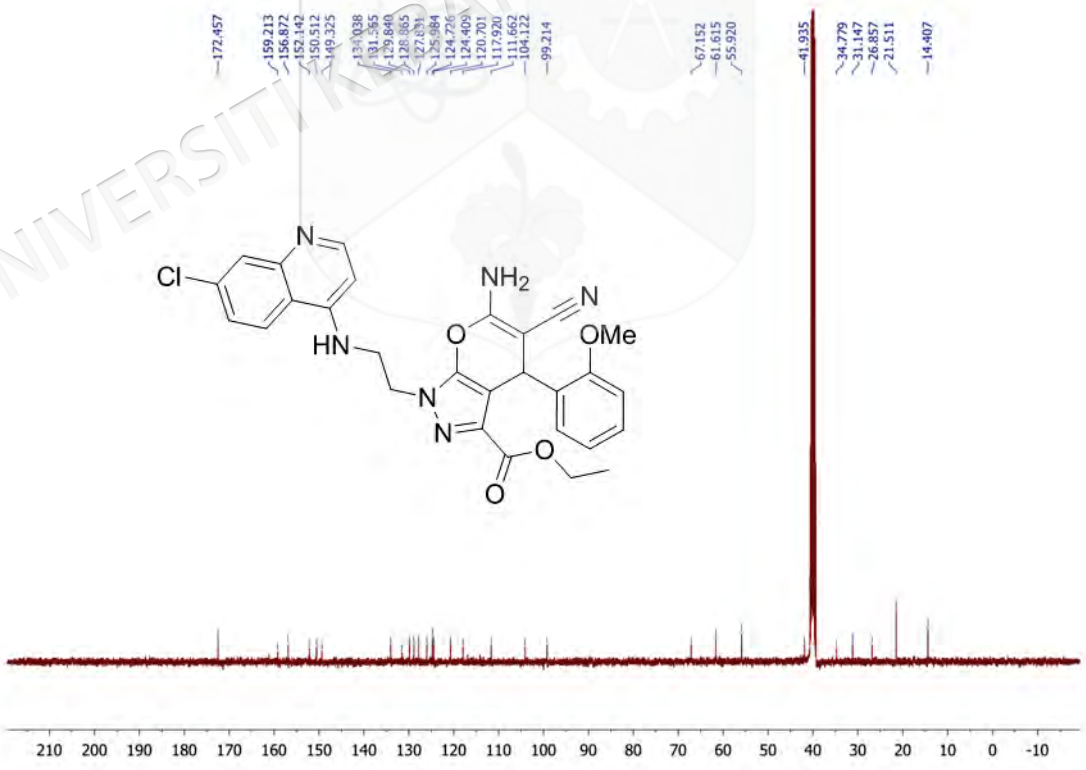

Figure 3.52 ^{13}C NMR spectrum of hybrid **24c**

3.6.4 Synthesis of ethyl 6-amino-1-(2-((7-chloroquinolin-4-yl)amino)ethyl)-5-cyano-4-(4-ethoxyphenyl)-1,4-dihydropyrano[2,3-*c*]pyrazole-3-carboxylate (24d)

The reaction between pyrano[2,3-*c*]pyrazole **20d** (1.77g, 5 mmol) and 4-(bromoethylamino)-7-chloroquinoline (1.43g, 5 mmol) (**23**) afforded pyrano[2,3-*c*]pyrazole-aminoquinoline hybrid compound **24d** as a brown solid with 14% yield and melting range of 201-203 °C. IR cm^{-1}: 3382 (NH_2), 3354 (NH), 2189 (CN), 1718 (COOEt), 1640 (C=C); ^{1}H NMR (400 MHz, DMSO) δ 8.38 (d, *J* = 5.2 Hz, 1H), 8.04 (d, *J* = 9.2 Hz, 1H), 7.79 (d, *J* = 2.4 Hz, 1H), 7.22 (d, *J* = 8.8 Hz, 1H), 6.97 (s, 2H), 6.89 (dt, *J* = 9.6, 2.8 Hz, 2H), 6.77 (dt, *J* = 9.6, 2.8 Hz, 2H), 6.52 (d, *J* = 8.8 Hz, 1H), 6.67 (d, *J* = 5.6 Hz, 1H), 4.70-4.63 (m, 2H), 4.60 (s, 1H), 3.96 (q, *J* = 7.2 Hz, 2H), 3.73-3.67 (m, 4H), 1.30 (t, *J* = 4 Hz, 3H), 0.76 (t, *J* = 7.2 Hz, 3H); ^{13}C NMR (100 MHz, DMSO): δ 160.0, 158.6, 157.6, 154.7, 151.7, 150.4, 148.9, 137.3, 134.1, 129.6, 128.6, 127.4, 124.8, 124.4, 120.7, 117.7, 114.5, 105.8, 99.0, 63.4, 61.2, 58.9, 49.7, 42.7, 37.0, 15.1, 13.7. HRMS calcd. for $C_{29}H_{27}ClN_6O_4$: *m/z* 558.1782; found: *m/z* 559.1802 (M^+).

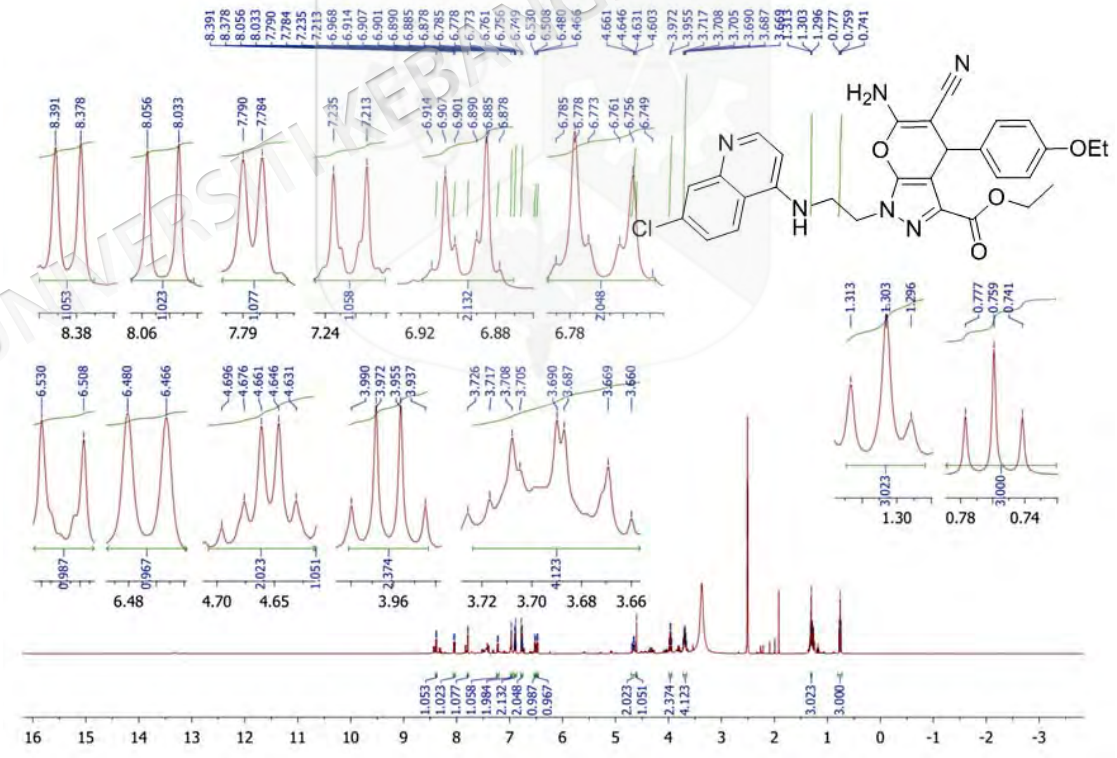

Figure 3.53 ^{1}H NMR spectrum of hybrid **24d**

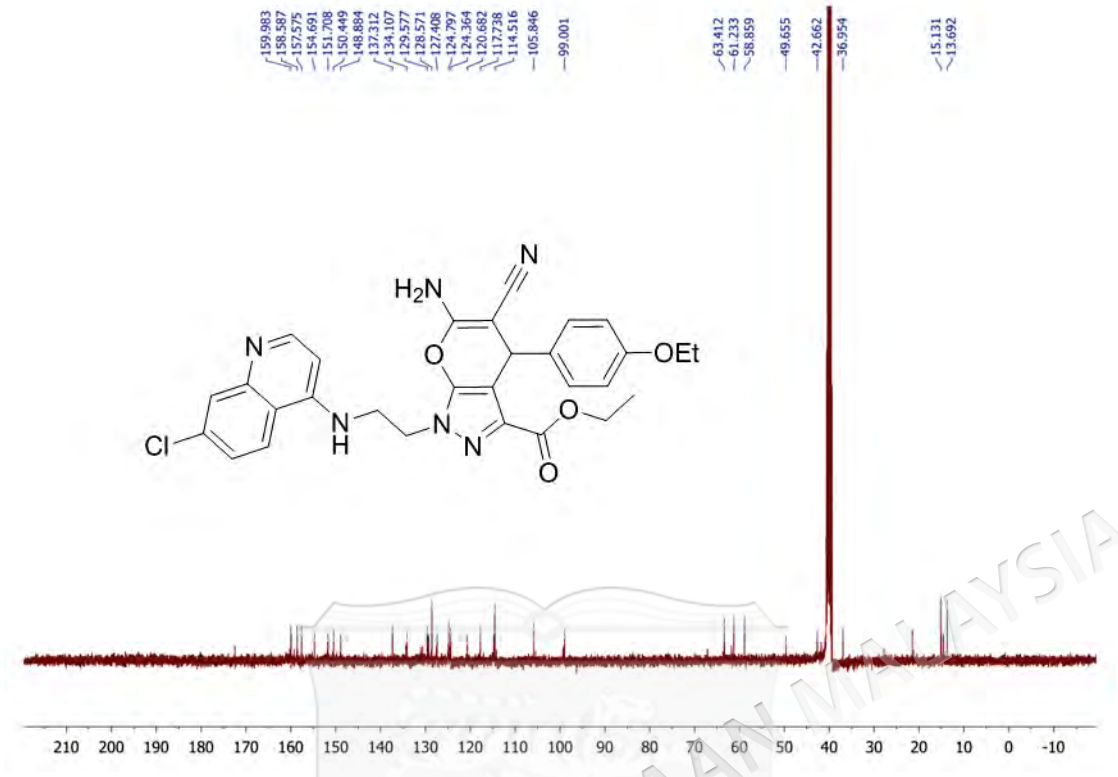

Figure 3.54 ^{13}C NMR spectrum of hybrid **24d**

3.6.5 Synthesis of ethyl 6-amino-1-(2-((7-chloroquinolin-4-yl)amino)ethyl)-5-cyano-4-(furan-2-yl)-1,4-dihydropyrano[2,3-*c*]pyrazole-3-carboxylate (24e)

The reaction between pyrano[2,3-*c*]pyrazole **20e** (1.5g, 5 mmol) and 4-(bromoethylamino)-7-chloroquinoline (1.43g, 5 mmol) (**23**) afforded pyrano[2,3-*c*]pyrazole-aminoquinoline hybrid compound **24e** as a brown solid with 22% yield and melting range of 232-234 ºC. ^{1}H NMR (400 MHz, DMSO) δ 8.40 (d, *J* = 5.6 Hz, 1H), 8.09 (d, *J* = 9.2 Hz, 1H), 7.80 (d, *J* = 2 Hz, 1H), 7.53 (t, *J* = 6 Hz, 1H), 7.48-7.45 (m, 2H), 7.13 (s, 2H), 6.50 (d, *J* = 5.6 Hz, 1H), 6.32 (q, *J* = 2 Hz, 1H), 6.01 (d, *J* = 2.8 Hz, 1H), 4.835 (s, 1H), 4.77-4.70 (m, 1H), 4.61-4.55 (m, 1H), 3.87-3.78 (m, 2H), 3.71 (t, *J* = 5.6 Hz, 2H), 0.91 (t, *J* = 7.2 Hz, 3H); ^{13}C NMR (100 MHz, DMSO): δ 161.1, 158.6, 156.1, 154.6, 151.4, 150.7, 146.9, 142.3, 129.7, 127.1, 125.0, 124.4, 120.5, 117.7, 110.8, 105.6, 103.1, 99.1, 61.4, 55.3, 49.7, 42.7, 31.5, 13.8. IR and MS results are identical with Shamsuddin et al. (2021).

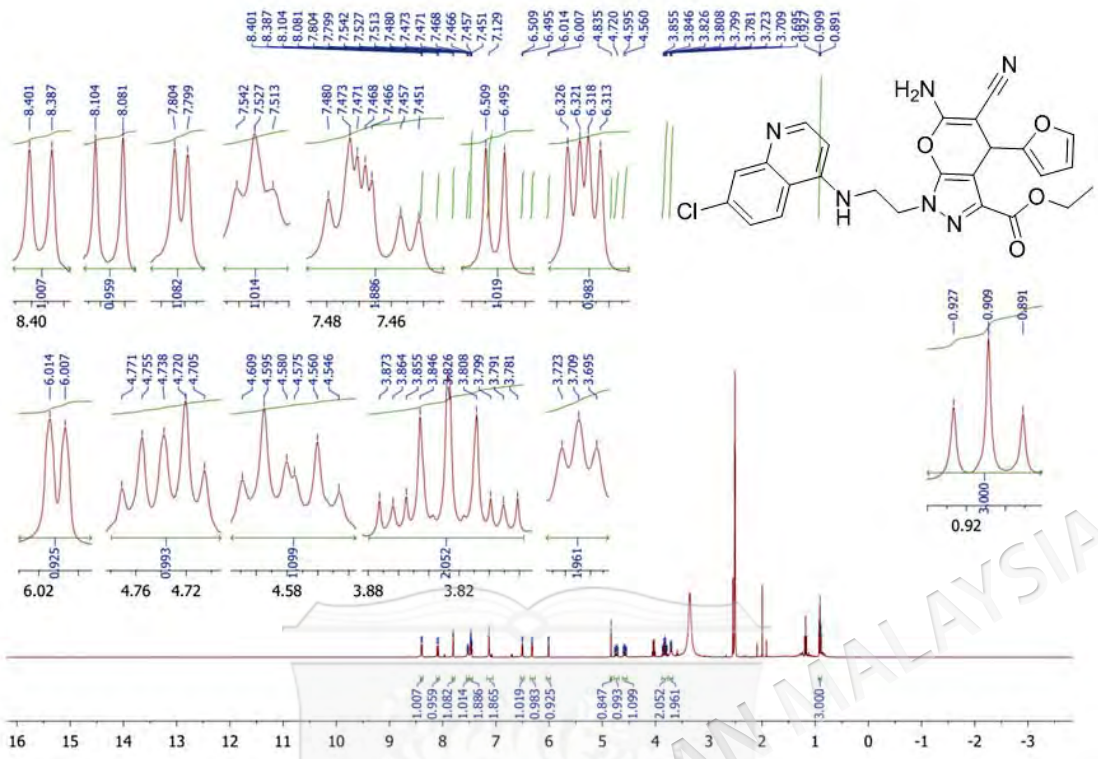

Figure 3.55 ^{1}H NMR spectrum of hybrid **24e**

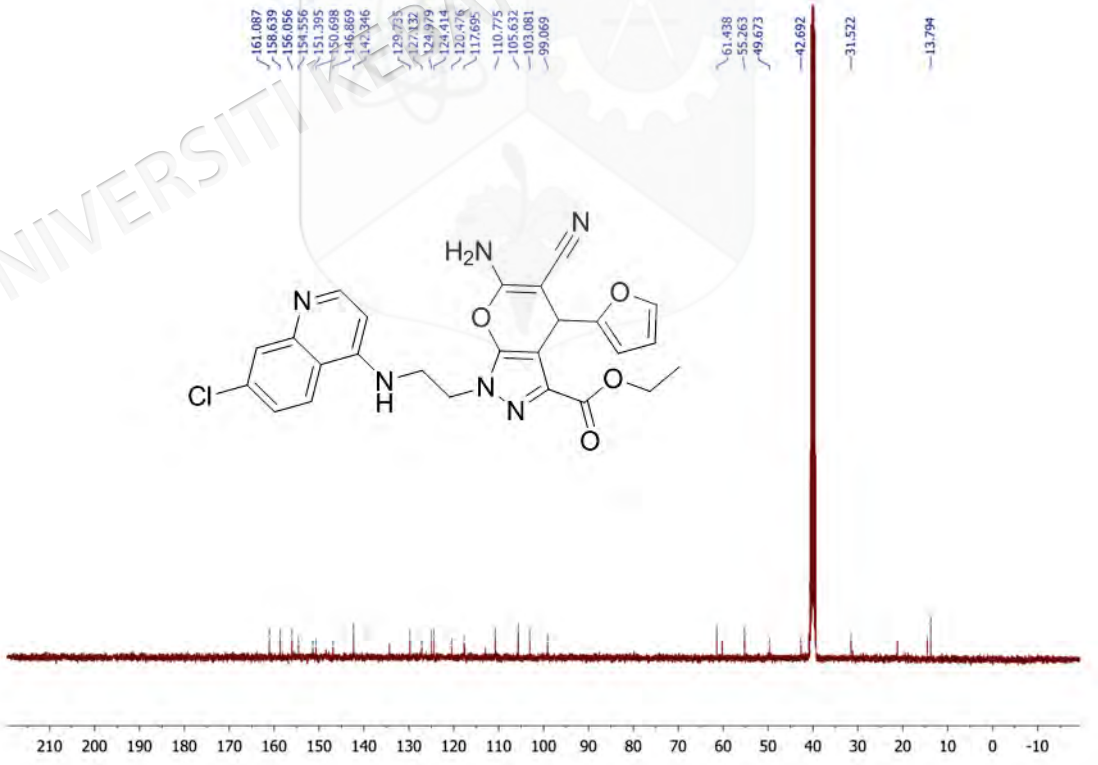

Figure 3.56 ^{13}C NMR spectrum of hybrid **24e**

3.6.6 Synthesis of ethyl 6-amino-1-(2-((7-chloroquinolin-4-yl)amino)ethyl)-5-cyano-4-phenyl-1,4-dihydropyrano[2,3-*c*]pyrazole-3-carboxylate (24f)

The reaction between pyrano[2,3-*c*]pyrazole **20f** (1.55g, 5 mmol) and 4-(bromoethylamino)-7-chloroquinoline (1.43g, 5 mmol) (**23**) afforded pyrano[2,3-*c*]pyrazole-aminoquinoline hybrid compound **24f** as a yellow solid with 18% yield and melting range of 145-147 ºC. ^{1}H NMR (400 MHz, DMSO) δ 8.39 (d, *J* = 5.6 Hz, 1H), 8.06 (d, *J* = 8.8 Hz, 1H), 7.79 (d, *J* = 2 Hz, 1H), 7.50 (t, *J* = 5.6 Hz, 1H), 7.42 (dd, *J* = 9.2, 2.4 Hz, 1H), 7.26 (t, *J* = 7.2 Hz, 2H), 7.19 (dt, *J* = 6.4, 1.2 Hz, 1H), 7.02 (dd, *J* = 6, 1.6 Hz, 4H), 6.49 (d, *J* = 5.6 Hz, 1H), 4.74-4.69 (m, 1H), 4.67 (s, 1H), 4.62 (q, *J* = 6 Hz, 1H), 3.72-3.62 (m, 4H), 0.74 (t, *J* = 6.8 Hz, 3H); ^{13}C NMR (100 MHz, DMSO): δ 160.1, 158.6, 154.8, 151.7, 150.5, 148.9, 145.2, 134.1, 129.6, 128.7, 127.6, 127.4, 127.0, 124.8, 124.4, 120.6, 117.8, 105.5, 99.0, 61.2, 58.5, 49.7, 42.6, 37.7, 13.6. IR and MS results are identical with Shamsuddin et al. (2021).

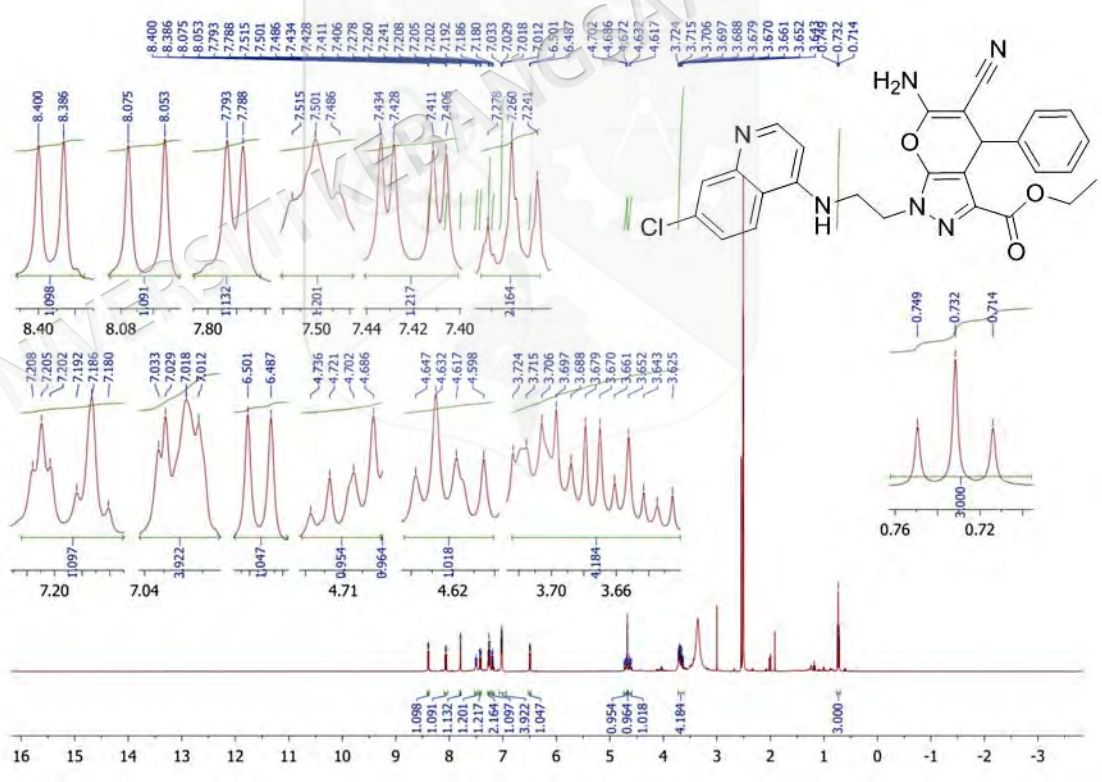

Figure 3.57 ^{1}H NMR spectrum of hybrid **24f**

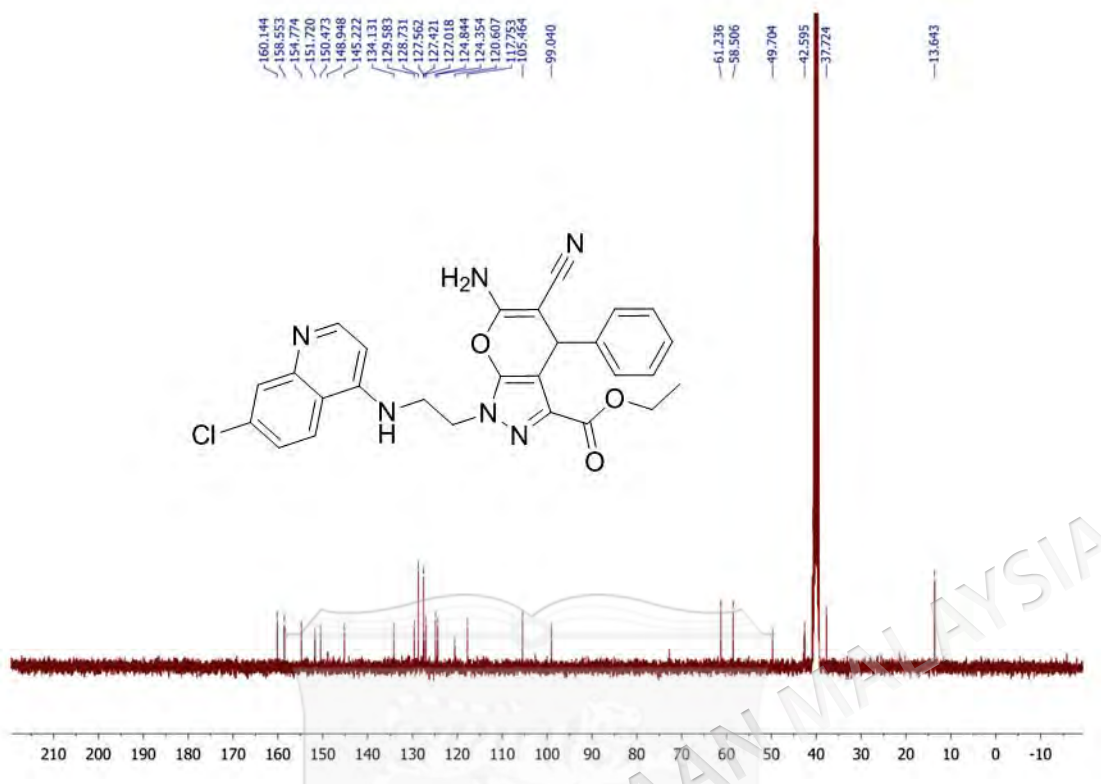

Figure 3.58 ^{13}C NMR spectrum of hybrid **24f**

3.6.7 Synthesis of ethyl 6-amino-4-(4-chlorophenyl)-1-(2-((7-chloroquinolin-4-yl)amino)ethyl)-5-cyano-1,4-dihydropyrano[2,3-*c*]pyrazole-3-carboxylate (24g)

The reaction between pyrano[2,3-*c*]pyrazole **20g** (1.72g, 5 mmol) and 4-(bromoethylamino)-7-chloroquinoline (1.43g, 5 mmol) (**23**) afforded pyrano[2,3-*c*]pyrazole-aminoquinoline hybrid compound **24g** as a brown solid with 23% yield and melting range of 157-159 ^{o}C. IR cm^{-1}: 3408 (NH_2), 3311 (NH), 2191 (CN), 1720 (COOEt), 1641 (C=C); ^{1}H NMR (400 MHz, DMSO) δ 8.38 (d, *J* = 5.2 Hz, 1H), 8.06 (d, *J* = 9.2 Hz, 1H), 7.78 (d, *J* = 2.4 Hz, 1H), 7.48 (s, 1H),7.37 (dd, *J* = 9.2, 2 Hz, 1H), 7.31 (d, *J* = 8.4 Hz, 2H), 7.05 (t, *J* = 8.8 Hz, 4H), 6.47 (d, *J* = 5.6 Hz, 1H), 4.71-4.62 (m, 3H), 3.71-3.60 (m, 4H), 0.69 (t, *J* = 6.8 Hz, 3H); ^{13}C NMR (100 MHz, DMSO): δ 160.1, 158.4, 154.7, 151.9, 150.3, 144.3, 134.0, 131.5, 129.7, 129.5, 128.7, 127.6, 124.7, 124.4, 120.5, 117.8, 104.9, 99.0, 61.2, 58.0, 49.7, 42.6, 37.1, 31.2, 13.6. HRMS calcd. for $C_{27}H_{22}Cl_2N_6O_3$: *m/z* 548.1130; found: *m/z* 549.1151 (M^+).

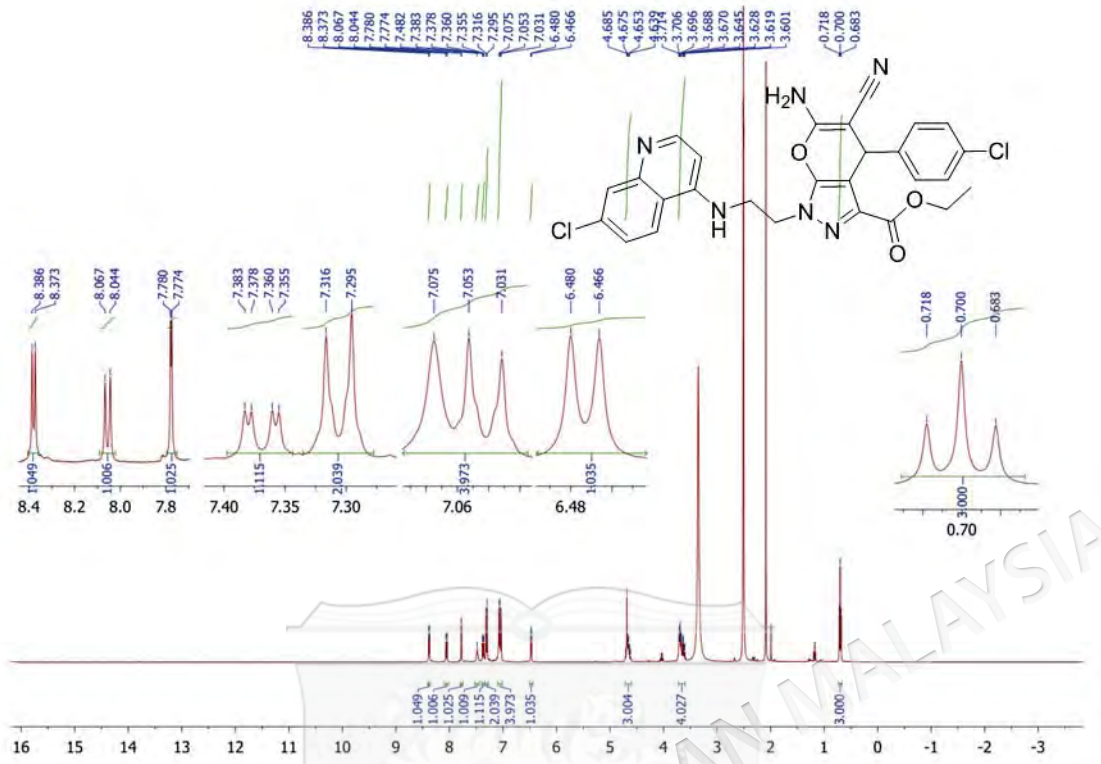

Figure 3.59 ^{1}H NMR spectrum of hybrid **24g**

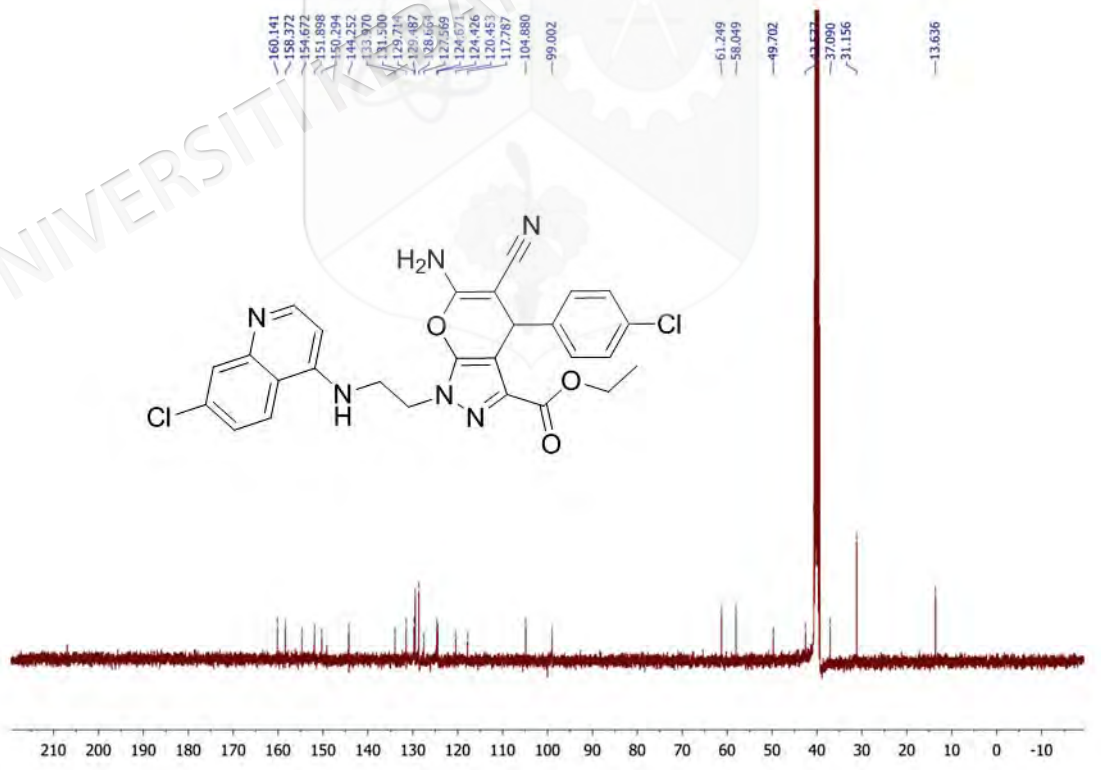

Figure 3.60 ^{13}C NMR spectrum of hybrid **24g**

3.6.8 Synthesis of ethyl 6-amino-4-(4-bromophenyl)-1-(2-((7-chloroquinolin-4-yl)amino)ethyl)-5-cyano-1,4-dihydropyrano[2,3-*c*]pyrazole-3-carboxylate (24h)

The reaction between pyrano[2,3-*c*]pyrazole **20h** (1.94g, 5 mmol) and 4-(bromoethylamino)-7-chloroquinoline (1.43g, 5 mmol) (**23**) afforded pyrano[2,3-*c*]pyrazole-aminoquinoline hybrid compound **24h** as a light pink solid with 29% yield and melting range of 171-173 ºC. IR cm^{-1}: 3408 (NH_2), 3382 (NH), 2186 (CN), 1699 (COOEt), 1638 (C=C); ^{1}H NMR (400 MHz, DMSO) δ 8.38 (d, *J* = 5.2 Hz, 1H), 8.00 (d, *J* = 9.2 Hz, 1H), 7.77 (d, *J* = 2 Hz, 1H), 7.44 (dt, *J* = 9.2, 2.4 Hz, 2H), 7.38-7.33 (m, 2H), 7.07 (s, 2H), 6.98 (dt, *J* = 9.2, 2.4 Hz, 2H), 6.48 (d, *J* = 5.6 Hz, 1H), 4.73-4.68 (m, 1H), 4.67 (s, 1H), 4.65-4.60 (m, 1H), 3.72-3.58 (m, 4H), 0.69 (t, *J* = 6.8 Hz, 3H); ^{13}C NMR (100 MHz, DMSO): δ 160.1, 158.4, 154.7, 152.2, 150.1, 149.4, 144.7, 133.9, 131.6, 129.9, 129.7, 127.8, 124.6, 124.2, 120.4, 120.0, 117.8, 104.8, 99.0, 61.2, 58.0, 49.7, 42.6, 37.2, 13.6. HRMS calcd. for $C_{27}H_{22}BrClN_6O_3$: *m/z* 592.0625; found: *m/z* 593.0745 (M^+).

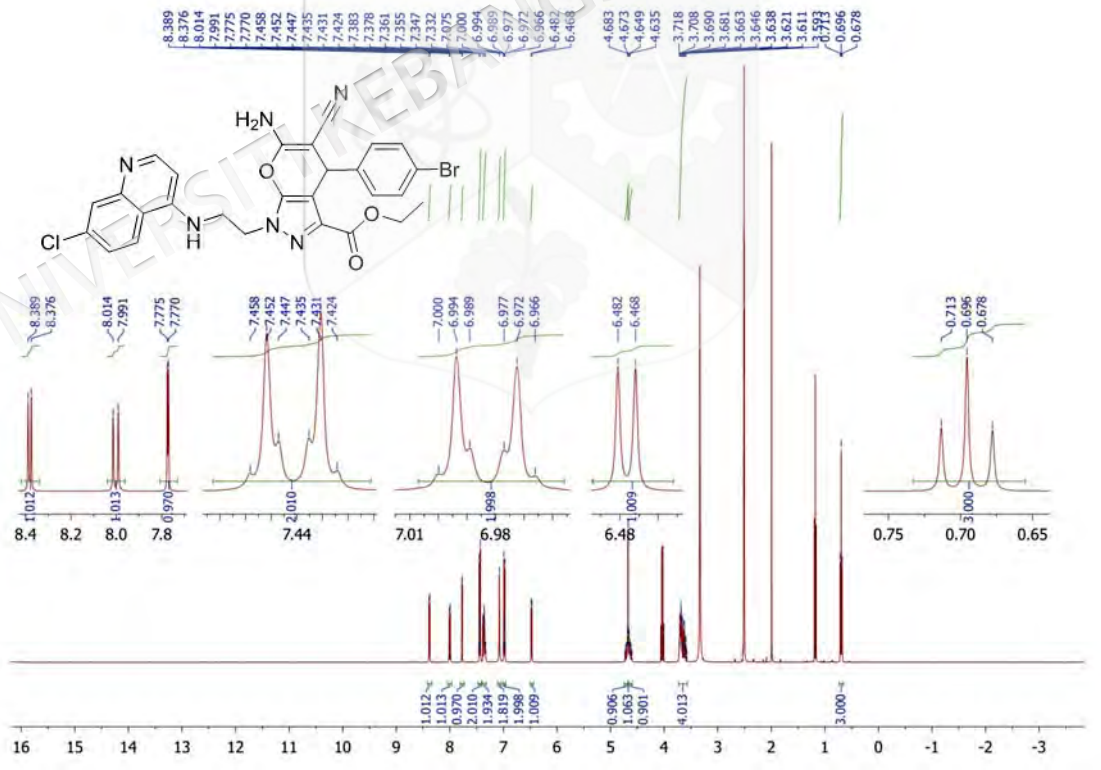

Figure 3.61 ^{1}H NMR spectrum of hybrid **24h**

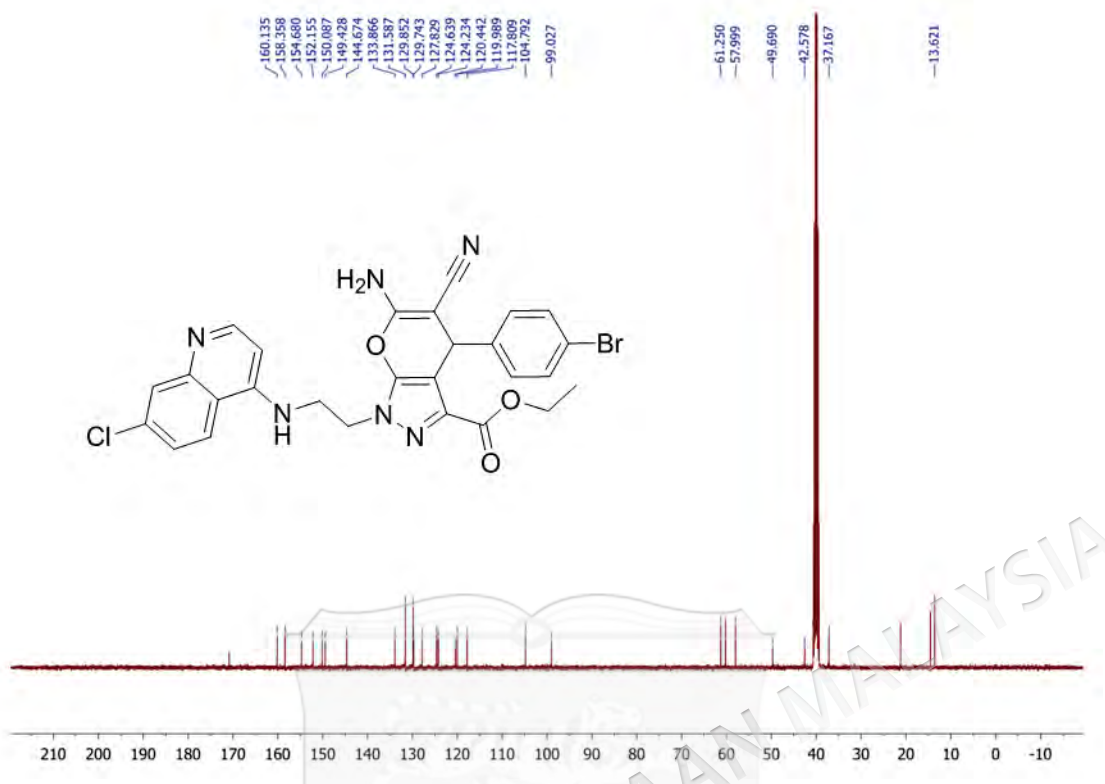

Figure 3.62 ^{13}C NMR spectrum of hybrid **24h**

3.6.9 Synthesis of ethyl 6-amino-1-(2-((7-chloroquinolin-4-yl)amino)ethyl)-5-cyano-4-(3-nitrophenyl)-1,4-dihydropyrano[2,3-*c*]pyrazole-3-carboxylate (24i)

The reaction between pyrano[2,3-*c*]pyrazole **20i** (1.77g, 5 mmol) and 4-(bromoethylamino)-7-chloroquinoline (1.43g, 5 mmol) (**23**) afforded pyrano[2,3-*c*]pyrazole-aminoquinoline hybrid compound **24i** as a yellow solid with 12% yield and melting range of 214-215 ^{o}C. IR cm^{-1}: 3458 (NH_2), 3319 (NH), 2195 (CN), 1731 (COOEt), 1636 (C=C); ^{1}H NMR (400 MHz, DMSO) δ 8.49 (d, *J* = 6 Hz, 1H), 8.34 (ddd, *J* = 8.4, 2.4, 1.2 Hz, 1H), 8.24 (t, *J* = 1.6 Hz, 1H), 8.13-8.11 (m, 1H), 7.96 (t, *J* = 2 Hz, 1H), 7.88 (ddd, *J* = 7.6, 1.6, 1.2 Hz, 1H), 7.83 (d, *J* = 2.4, 1H), 7.78 (t, *J* = 8.4, 1H), 7.61 (t, *J* = 7.6, 1H), 7.54 (d, *J* = 1.2, 1H), 7.19 (s, 1H), 6.68 (d, *J* = 6.4, 1H), 4.95 (s, 1H), 4.71 (q, *J* = 6, 2H), 3.78-3.65 (m, 4H), 0.70 (t, *J* = 7.2 Hz, 3H); ^{13}C NMR (100 MHz, DMSO): δ 165.2, 160.4, 158.3, 154.6, 148.1, 147.5, 138.4, 135.8, 134.6, 130.9, 129.7, 126.1, 125.3, 124.9, 123.9, 122.4, 120.3, 118.8, 116.1, 104.5, 100.0, 61.5, 57.5, 53.7, 37.2, 21.5, 13.6.

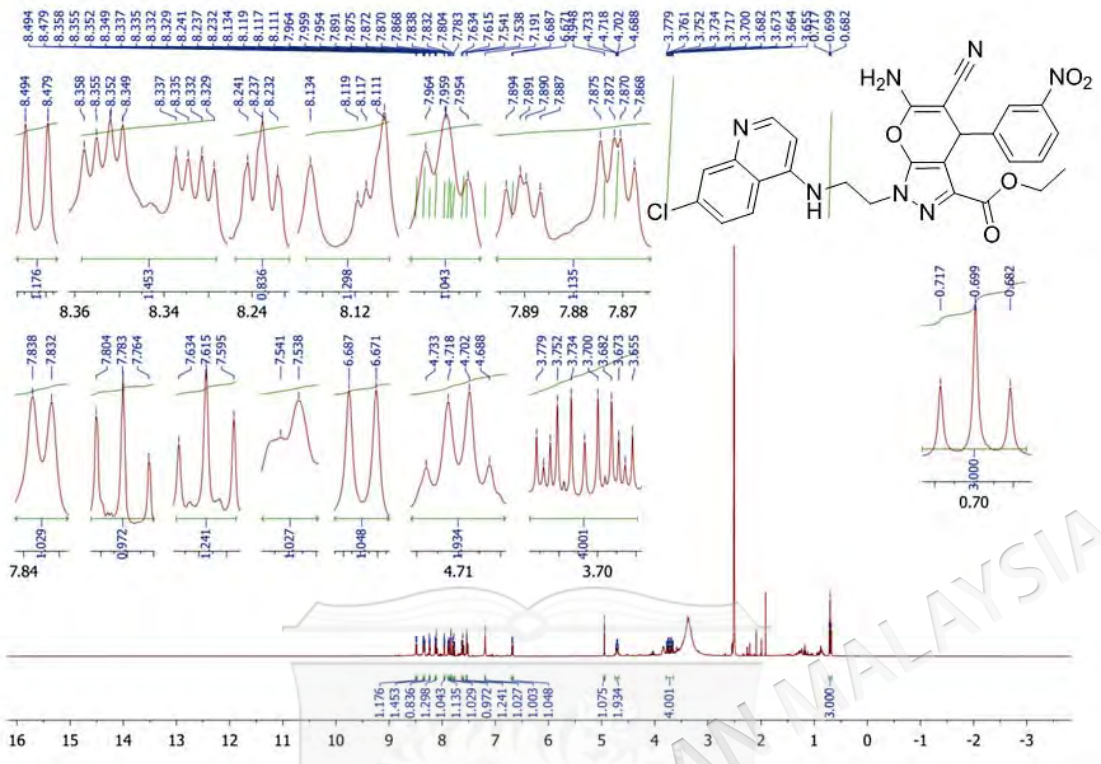

Figure 3.63 ^{1}H NMR spectrum of hybrid **24i**

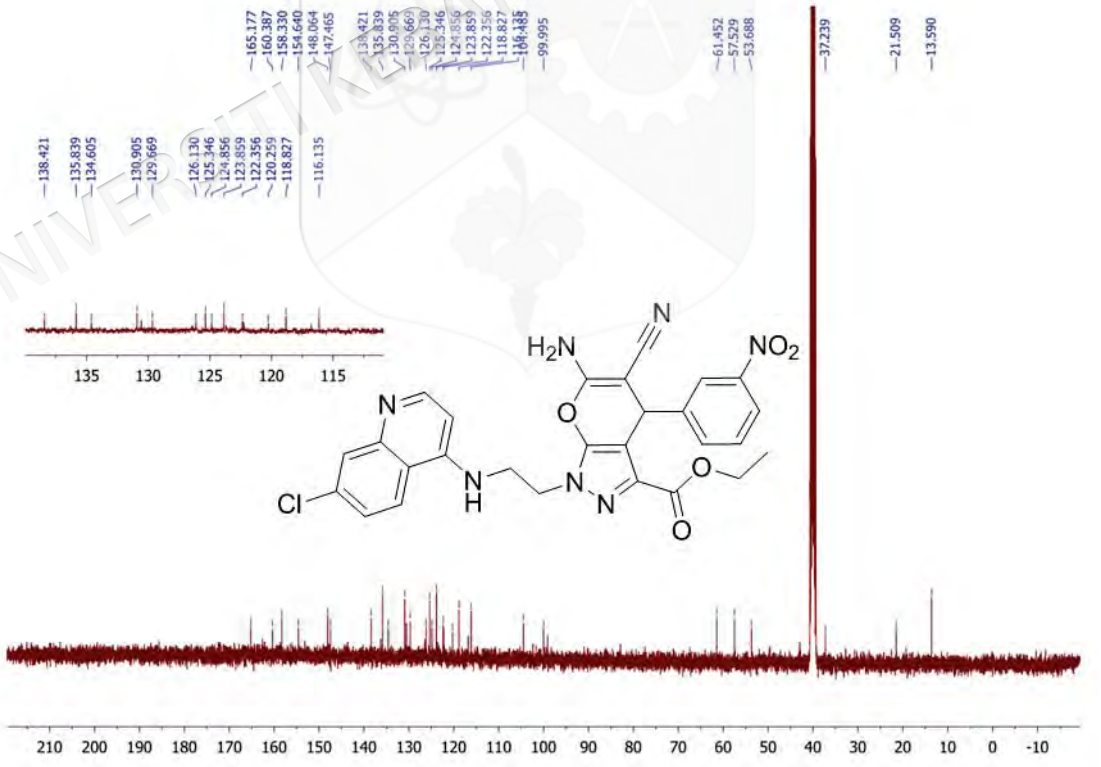

Figure 3.64 ^{13}C NMR spectrum of hybrid **24i**

3.6.10 Synthesis of ethyl 6-amino-1-(2-((7-chloroquinolin-4-yl)amino)ethyl)-5-cyano-4-(4-nitrophenyl)-1,4-dihydropyrano[2,3-*c*]pyrazole-3-carboxylate (24j)

The reaction between pyrano[2,3-*c*]pyrazole **20j** (1.77g, 5 mmol) and 4-(bromoethylamino)-7-chloroquinoline (1.43g, 5 mmol) (**23**) afforded pyrano[2,3-*c*]pyrazole-aminoquinoline hybrid compound **24j** as a yellow solid with 38% yield and melting range of 198-200 °C. IR cm^{-1}: 3410 (NH_2), 3311 (NH), 2191 (CN), 1697 (COOEt), 1645 (C=C); ^{1}H NMR (400 MHz, DMSO) δ 8.39 (d, *J* = 5.2 Hz, 1H), 8.13 (dt, *J* = 9.2, 2.4 Hz, 2H), 8.01 (d, *J* = 9.2 Hz, 1H), 7.76 (d, *J* = 2.4, 1H), 7.38-7.32 (m, 2H), 7.30 (dt, *J* = 9.6, 2.8 Hz, 2H), 7.18 (s, 2H), 6.47 (d, *J* = 5.6 Hz, 1H), 4.86 (s, 1H), 4.79-4.72 (m, 1H), 4.65-4.59 (m, 1H), 3.72-3.57 (m, 4H), 0.63 (t, *J* = 7.2 Hz, 3H); ^{13}C NMR (100 MHz, DMSO): δ 160.4, 158.2, 154.7, 152.7, 152.1, 150.1, 149.3, 146.6, 133.9, 129.9, 129.0, 127.8, 124.6, 124.2, 124.1, 120.2, 117.8, 104.0, 99.0, 61.3, 57.2, 49.8, 42.6, 37.4, 13.6. HRMS calcd. for $C_{27}H_{22}ClN_7O_5$: *m/z* 559.1371; found: *m/z* 560.1443 (M^+).

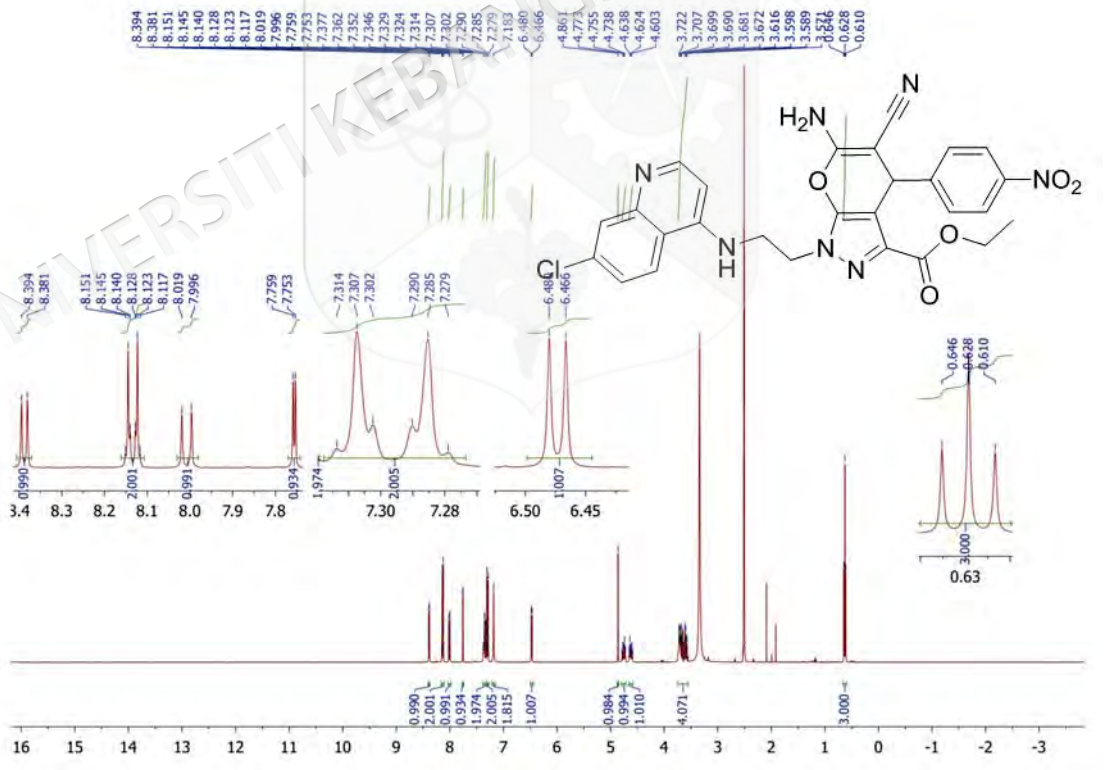

Figure 3.65 ^{1}H NMR spectrum of hybrid **24j**

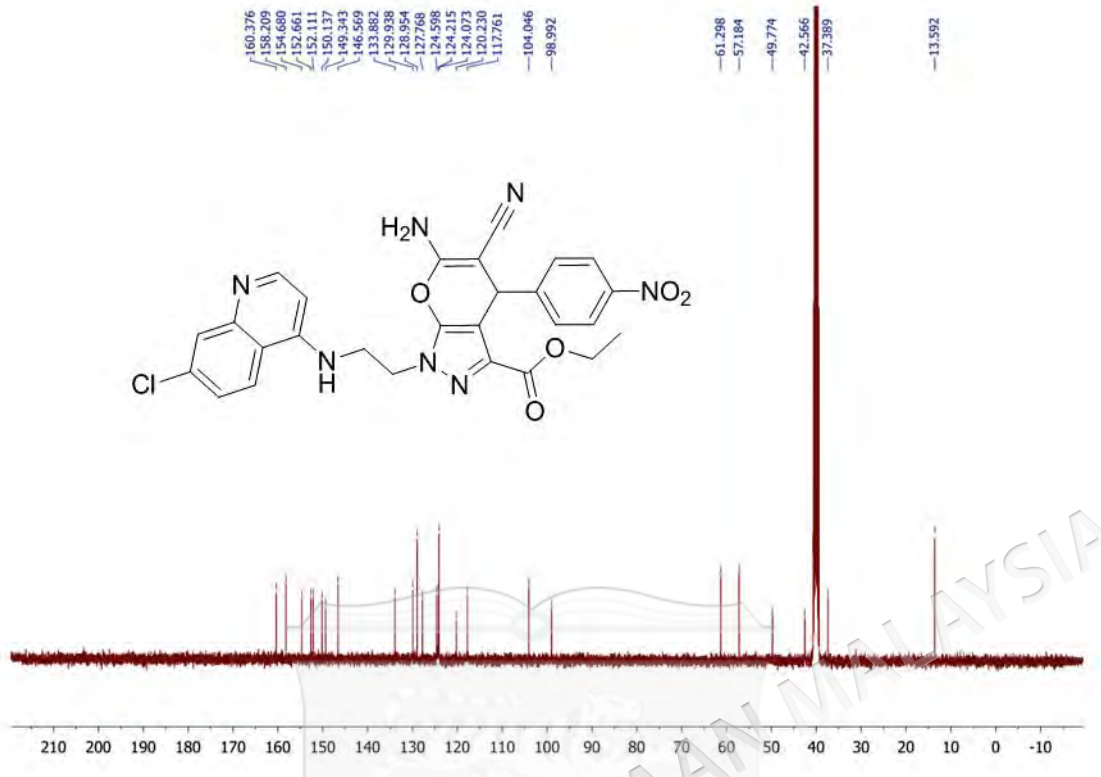

Figure 3.66 ^{13}C NMR spectrum of hybrid **24j**

3.6.11 Synthesis of ethyl 6-amino-1-(2-((7-chloroquinolin-4-yl)amino)ethyl)-5-cyano-4-(2,4-dihydroxyphenyl)-1,4-dihydropyrano[2,3-*c*]pyrazole-3-carboxylate (24k)

The reaction between pyrano[2,3-*c*]pyrazole **20k** (1.71g, 5 mmol) and 4-(bromoethylamino)-7-chloroquinoline (1.43g, 5 mmol) (**23**) afforded pyrano[2,3-*c*]pyrazole-aminoquinoline hybrid compound **24k** as a brown solid with 13% yield and melting range of 278-279 ^{o}C. IR cm^{-1}: 3403 (NH_2), 3354 (NH), 2214 (CN), 1705 (COOEt), 1630 (C=C); ^{1}H NMR (400 MHz, DMSO) δ 13.08 (s, 1H), 9.56 (s, 1H), 8.43 (d, *J* = 5.2 Hz, 1H), 8.17 (d, *J* = 9.2 Hz, 1H), 7.81 (d, *J* = 2.4 Hz, 1H), 7.49 (dd, *J* = 8.8, 2.4 Hz, 1H), 7.15 (s, 1H), 6.84 (d, *J* = 8.8 Hz, 1H), 6.44-6.42 (m, 5H), 5.98 (s, 2H), 5.36 (s, 1H), 4.40 (q, *J* = 6.8 Hz, 2H), 4.12-4.06 (m, 2H), 1.35 (t, *J* = 7.2 Hz, 3H); ^{13}C NMR (100 MHz, DMSO): δ 160.9, 159.8, 157.6, 156.9, 152.4, 151.4, 150.3, 149.3, 134.0, 130.2, 127.9, 124.9, 124.4, 117.8, 116.9, 113.1, 112.6, 112.0, 102.6, 99.2, 88.8, 71.0, 67.0, 61.9, 41.8, 27.2, 14.5. HRMS calcd. for $C_{25}H_{21}ClN_6O_3S$: *m/z* 546.1418; found: *m/z* 547.7913 (M^+).

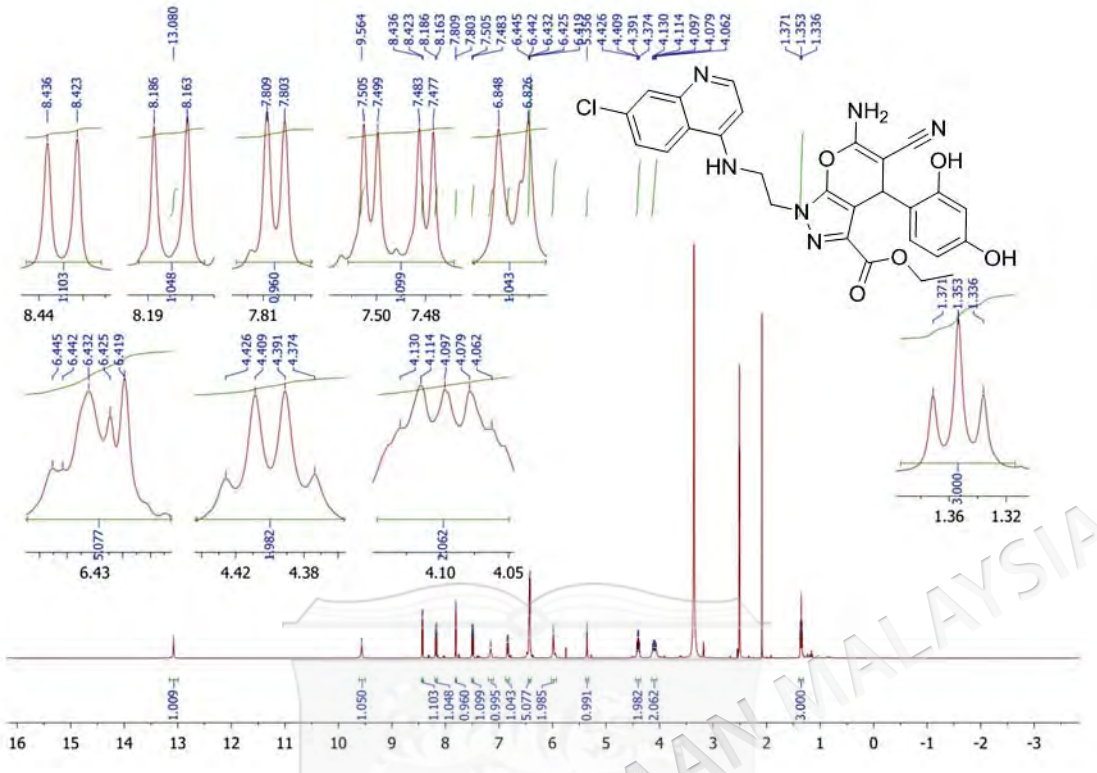

Figure 3.67 ^{1}H NMR spectrum of hybrid **24k**

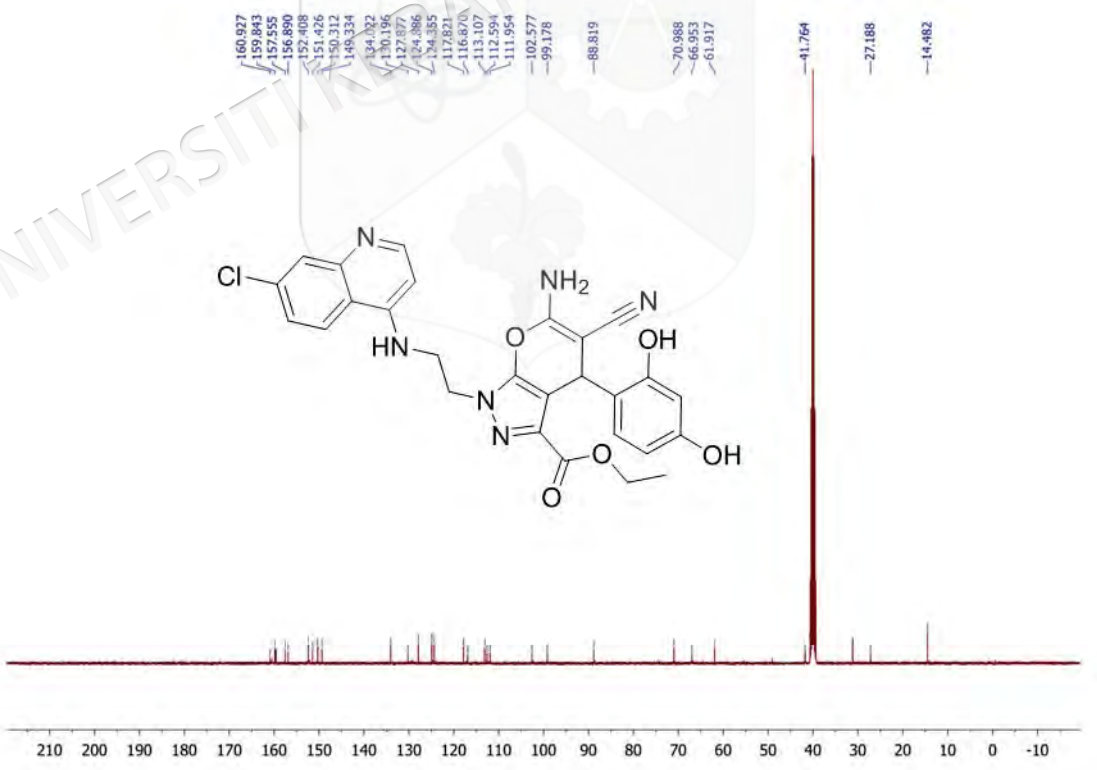

Figure 3.68 ^{13}C NMR spectrum of hybrid **24k**

3.6.12 Synthesis of ethyl 6-amino-1-(2-((7-chloroquinolin-4-yl)amino)ethyl)-5-cyano-4-(thiophen-2-yl)-1,4-dihydropyrano[2,3-*c*]pyrazole-3-carboxylate (24l)

The reaction between pyrano[2,3-*c*]pyrazole **20l** (1.58g, 5 mmol) and 4-(bromoethylamino)-7-chloroquinoline (1.43g, 5 mmol) (**23**) afforded pyrano[2,3-*c*]pyrazole-aminoquinoline hybrid compound **24l** as a brown solid with 36% yield and melting range of 239-240 °C. IR cm^{-1}: 3423 (NH_2), 3326 (NH), 2189 (CN), 1720 (COOEt), 1671 (C=C); ^{1}H NMR (400 MHz, DMSO) δ 8.38 (d, *J* = 5.6 Hz, 1H), 8.09 (d, *J* = 8.8 Hz, 1H), 7.80 (d, *J* = 2 Hz, 1H), 7.45 (dd, *J* = 9.2, 2.4 Hz, 2H), 7.30 (dd, *J* = 5.2, 1.2 Hz, 1H), 7.14 (s, 2H), 6.89 (q, *J* = 3.6 Hz, 1H), 6.82-6.81 (m, 1H), 6.48 (d, *J* = 5.6 Hz, 1H), 5.03 (s, 1H), 4.78-4.71 (m, 1H), 4.61-4.55 (m, 1H), 3.83-3.68 (m, 4H), 0.87 (t, *J* = 7.2 Hz, 3H); ^{13}C NMR (100 MHz, DMSO): δ 160.6, 158.6, 154.1, 151.8, 150.4, 149.5, 149.0, 134.1, 129.8, 127.6, 127.0, 124.9, 124.8, 124.5, 124.4, 120.6, 117.8, 105.6, 99.1, 61.5, 58.2, 49.8, 42.7, 32.9, 13.7. HRMS calcd. for $C_{25}H_{21}ClN_6O_3S$: *m/z* 520.1084; found: *m/z* 521.1203 (M^+).

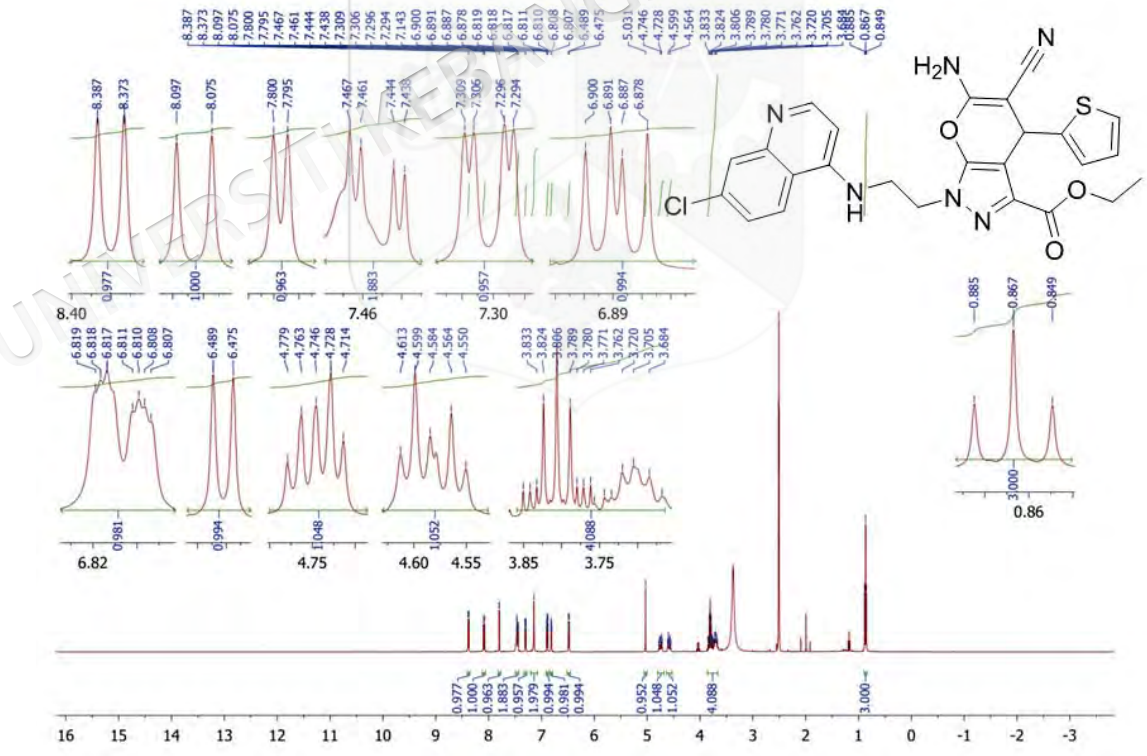

Figure 3.69 ^{1}H NMR spectrum of hybrid **24l**

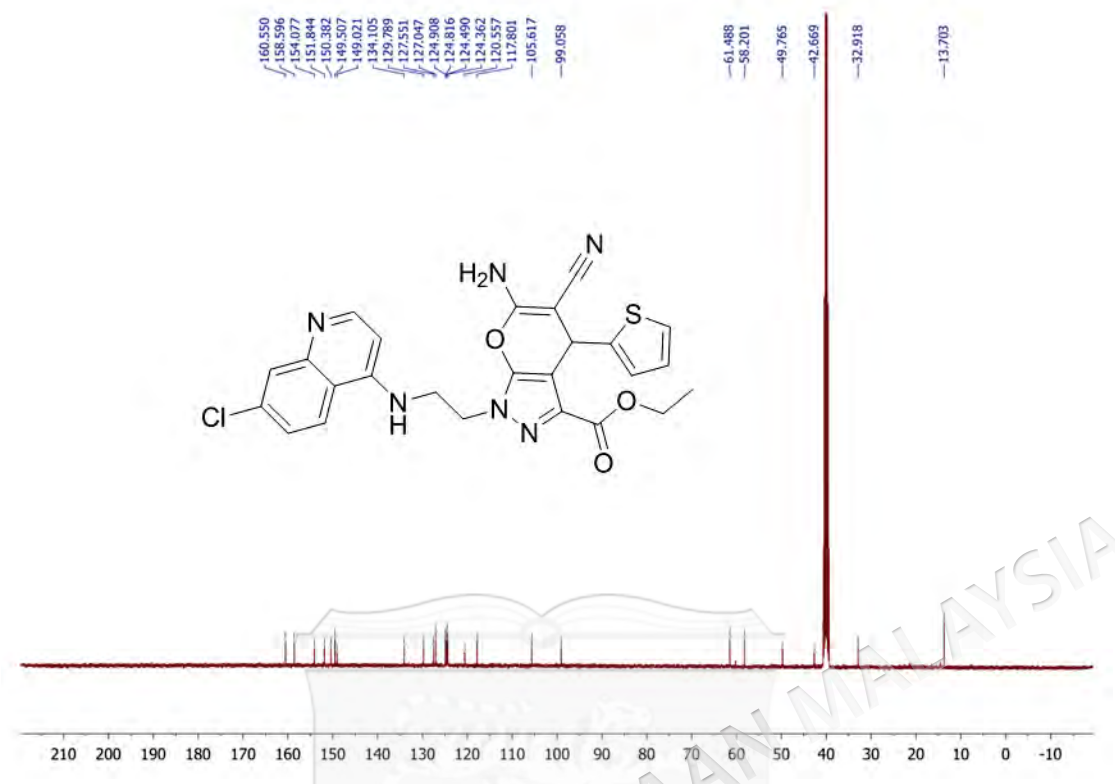

Figure 3.70 ^{13}C NMR spectrum of hybrid **24l**

3.6.13 Synthesis of ethyl 6-amino-4-(3-bromo-4-hydroxyphenyl)-1-(2-((7-chloroquinolin-4-yl)amino)ethyl)-5-cyano-1,4-dihydropyrano[2,3-*c*]pyrazole-3-carboxylate (24m)

The reaction between pyrano[2,3-*c*]pyrazole **20m** (2.02g, 5 mmol) and 4-(bromoethylamino)-7-chloroquinoline (1.43g, 5 mmol) (**23**) afforded pyrano[2,3-*c*]pyrazole-aminoquinoline hybrid compound **24m** as a brown solid with 25% yield and melting range of 217-219 ^{o}C. IR cm^{-1}: 3393 (NH_2), 3339 (NH), 2197 (CN), 1708 (COOEt), 1647 (C=C); ^{1}H NMR (400 MHz, DMSO) δ 10.13 (s, 1H), 8.39 (d, *J* = 5.2 Hz, 1H), 8.02 (d, *J* = 9.2 Hz, 1H), 7.78 (d, *J* = 2.4 Hz, 1H), 7.40 (dd, *J* = 8.8, 2 Hz, 2H), 7.18 (d, *J* = 2 Hz, 1H), 7.03 (s, 2H), 6.87-6.85 (m, 1H), 6.81 (dd, *J* = 8.4, 2 Hz, 1H), 6.48 (d, *J* = 5.6 Hz, 1H), 4.68 (q, *J* = 8 Hz, 1H), 4.60-4.57 (m, 2H), 3.73-3.66 (m, 4H), 0.82 (t, *J* = 7.2 Hz, 3H); ^{13}C NMR (100 MHz, DMSO): δ 160.1, 158.6, 154.5, 153.1, 152.1, 150.2, 149.3, 137.6, 133.9, 131.9, 129.6, 127.9, 124.7, 124.3, 120.6, 117.8, 116.7, 109.1, 105.4, 99.1, 61.3, 58.5, 49.7, 42.6, 36.6, 13.7. HRMS calcd. for $C_{27}H_{22}BrClN_6O_4$: *m/z* 608.0574; found: *m/z* 609.0661 (M^+).

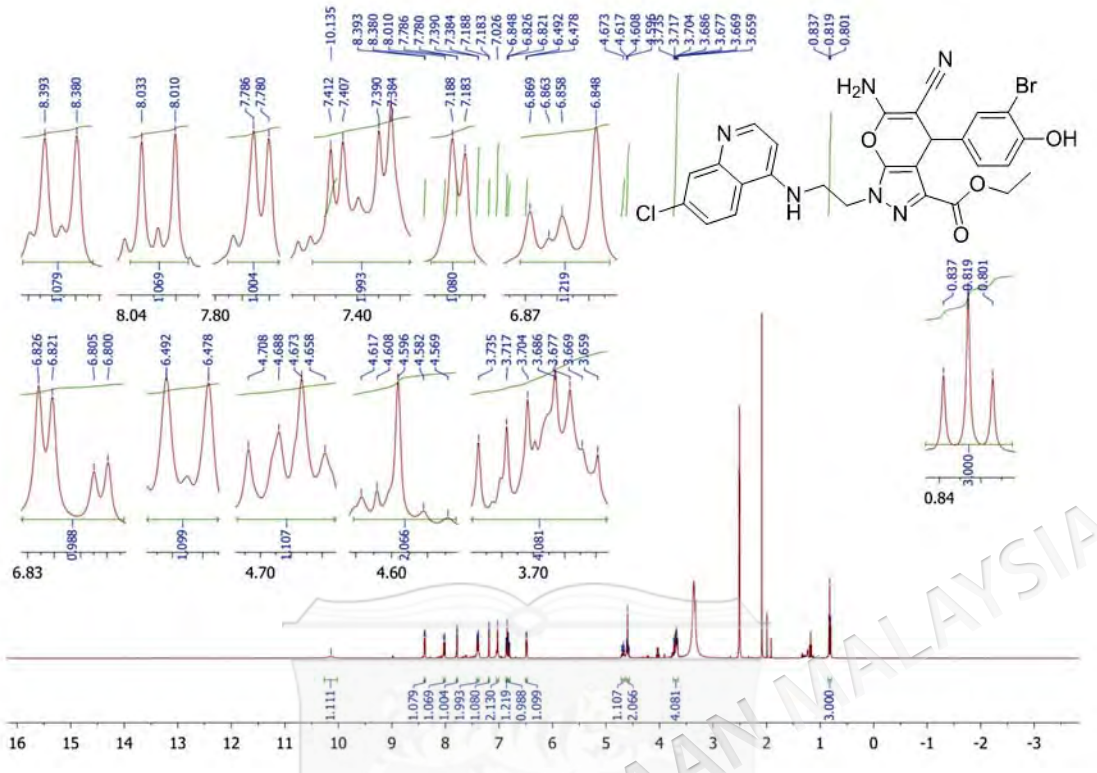

Figure 3.71 ^{1}H NMR spectrum of hybrid **24m**

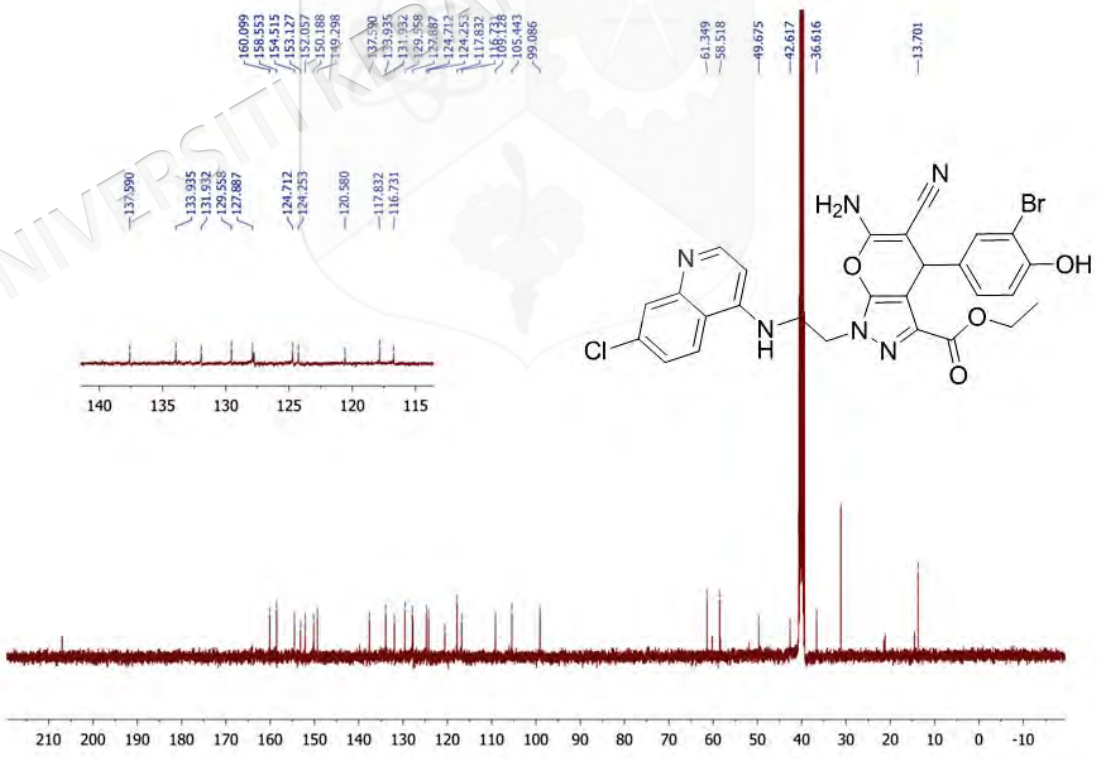

Figure 3.72 ^{13}C NMR spectrum of hybrid **24m**

3.6.14 Synthesis of ethyl 6-amino-1-(2-((7-chloroquinolin-4-yl)amino)ethyl)-5-cyano-4-(4-cyanophenyl)-1,4-dihydropyrano[2,3-*c*]pyrazole-3-carboxylate (24n)

The reaction between pyrano[2,3-*c*]pyrazole **20n** (1.67g, 5 mmol) and 4-(bromoethylamino)-7-chloroquinoline (1.43g, 5 mmol) (**23**) afforded pyrano[2,3-*c*]pyrazole-aminoquinoline hybrid compound **24n** as a yellow solid with 49% yield and melting range of 199-201 ^{o}C. IR cm^{-1}: 3390 (NH_2), 3319 (NH), 2197 (CN), 1723 (COOEt), 1647 (C=C); ^{1}H NMR (400 MHz, DMSO) δ 8.39 (d, *J* = 5.6 Hz, 1H), 8.01 (d, *J* = 9.2 Hz, 1H), 7.77 (d, *J* = 2.4 Hz, 1H), 7.73 (d, *J* = 8 Hz, 2H), 7.43 (t, *J* = 5.6 Hz, 1H), 7.38 (dd, *J* = 9.2, 2.4 Hz, 1H), 7.23 (d, *J* = 8.4 Hz, 2H), 7.145 (s, 2H), 6.49 (d, *J* = 5.6 Hz, 1H), 4.72 (q, *J* = 7.6 Hz, 1H), 4.66-4.61 (m, 2H), 3.72-3.56 (m, 4H), 0.63 (t, *J* = 7.2 Hz, 3H); ^{13}C NMR (100 MHz, DMSO): δ 160.3, 158.2, 154.7, 151.7, 150.6, 150.4, 148.8, 134.1, 132.8, 129.9, 128.7, 127.4, 124.8, 124.3, 120.3, 117.7, 109.8, 104.1, 99.0, 61.3, 57.4, 49.7, 42.6, 37.6, 13.6. HRMS calcd. for $C_{28}H_{22}ClN_7O_3$: *m/z* 539.1473; found: *m/z* 540.1505 (M^+).

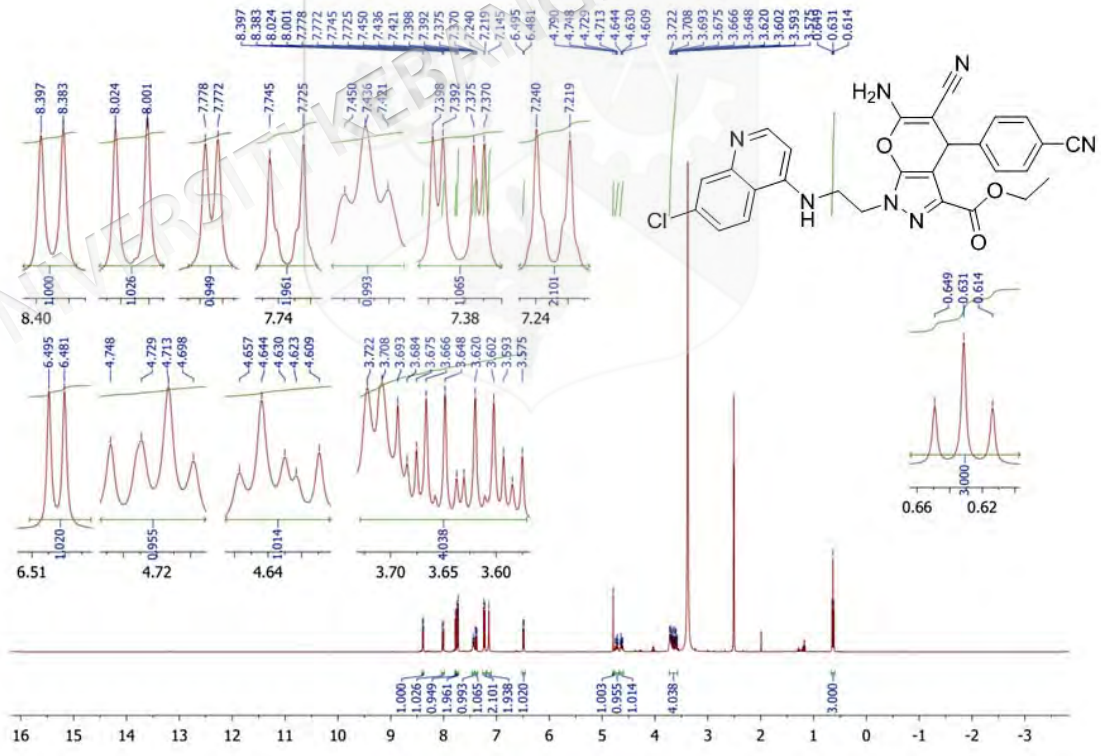

Figure 3.73 ^{1}H NMR spectrum of hybrid **24n**

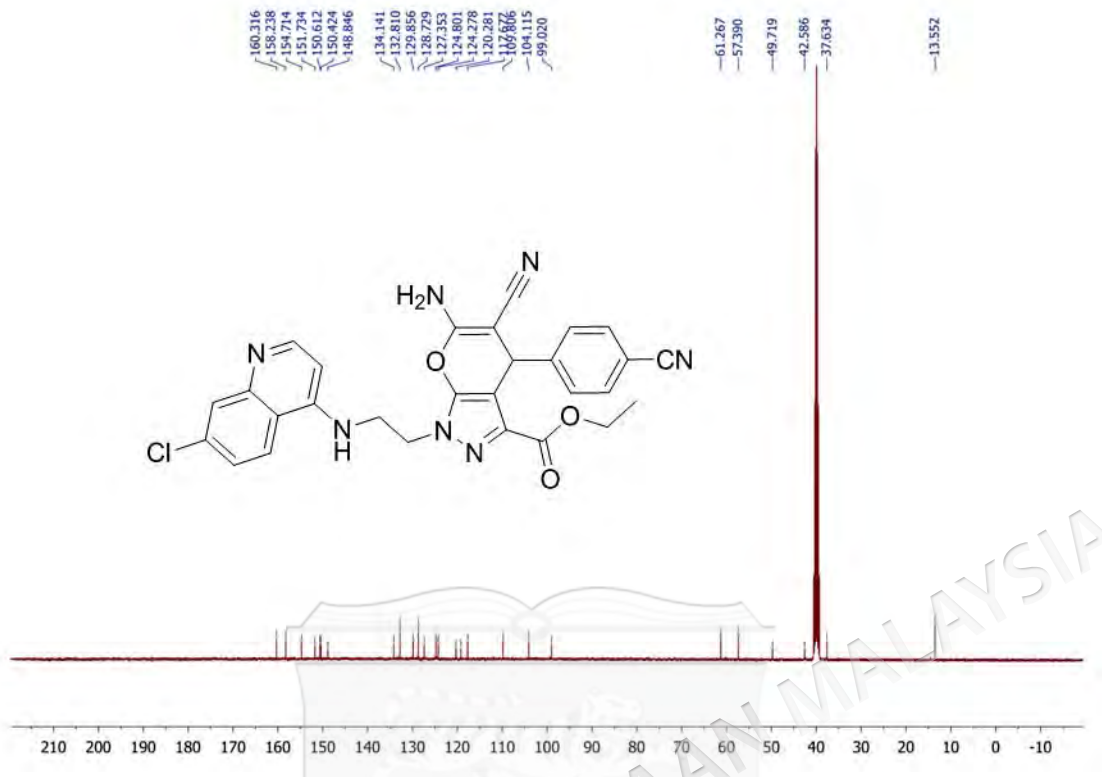

Figure 3.74 ^{13}C NMR spectrum of hybrid **24n**

3.6.15 Synthesis of ethyl 6-amino-1-(2-((7-chloroquinolin-4-yl)amino)ethyl)-5-cyano-4-(3-ethoxyphenyl)-1,4-dihydropyrano[2,3-*c*]pyrazole-3-carboxylate (24o)

The reaction between pyrano[2,3-*c*]pyrazole **20o** (1.77g, 5 mmol) and 4-(bromoethylamino)-7-chloroquinoline (1.43g, 5 mmol) (**23**) afforded pyrano[2,3-*c*]pyrazole-aminoquinoline hybrid compound **24o** as a brown solid with 31% yield and melting range of 179-180 ^{o}C. IR cm^{-1}: 3421 (NH_2), 3334 (NH), 2189 (CN), 1720 (COOEt), 1641 (C=C); ^{1}H NMR (400 MHz, DMSO) δ 8.39 (d, *J* = 5.6 Hz, 1H), 8.05 (d, *J* = 9.2 Hz, 1H), 7.79 (d, *J* = 2.4 Hz, 1H), 7.40 (dd, *J* = 8.8, 2.4 Hz, 2H), 7.17 (q, *J* = 8 Hz, 1H), 7.02 (s, 2H), 6.77 (ddd, *J* = 8.4, 2.8, 0.8 Hz, 1H), 6.62 (t, *J* = 2 Hz, 1H), 6.59-6.54 (m, 1H), 6.48 (d, *J* = 5.6 Hz, 1H), 4.75-4.69 (m, 1H), 4.65 (s, 1H), 4.62-4.56 (m, 1H), 3.76-3.69 (m, 6H), 0.79 (t, *J* = 7.2 Hz, 3H); ^{13}C NMR (100 MHz, DMSO): δ 160.2, 159.5, 158.6, 154.7, 152.0, 150.3, 149.2, 146.8, 134.0, 129.9, 129.6, 127.7, 124.7, 124.3, 120.6, 119.7, 117.8, 113.9, 111.9, 105.4, 99.1, 61.3, 58.4, 55.4, 49.7, 42.6, 37.7, 15.1, 13.7.

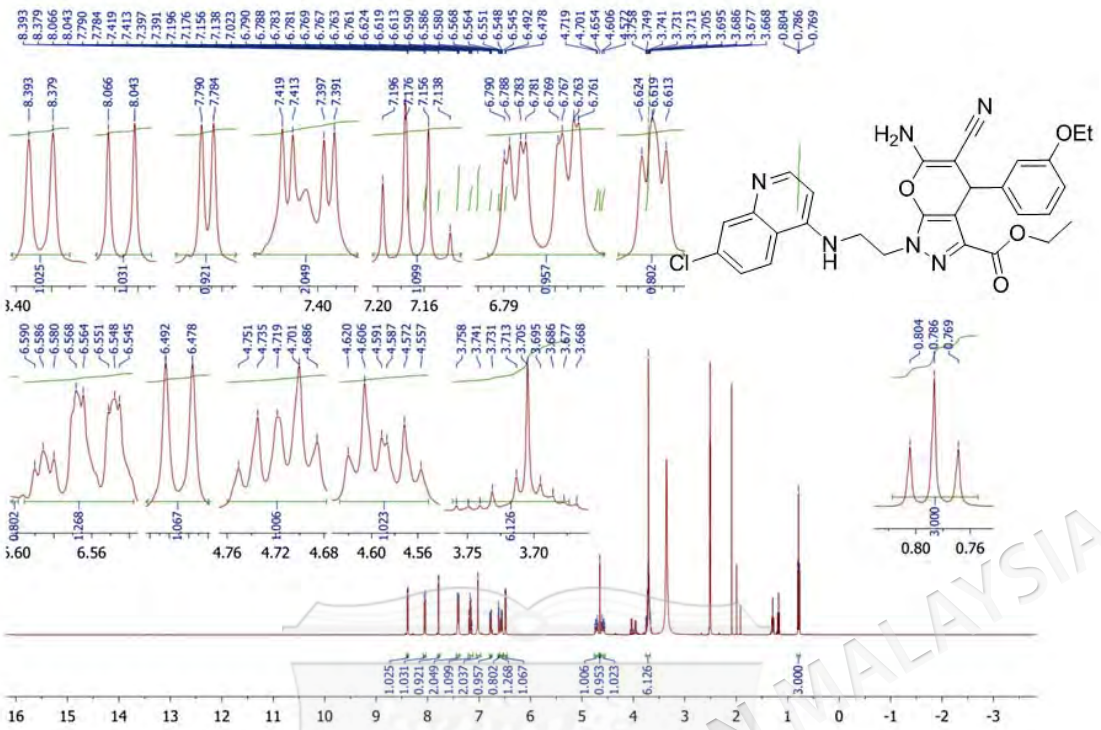

Figure 3.75 ^{1}H NMR spectrum of hybrid **24o**

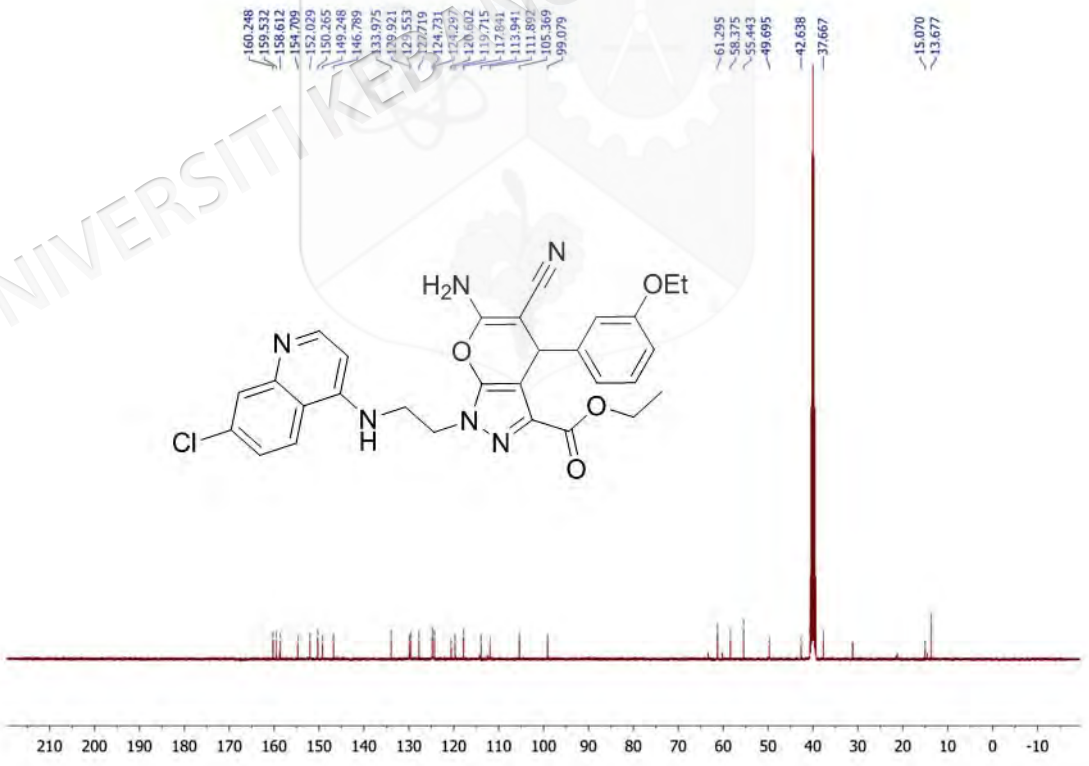

Figure 3.76 ^{13}C NMR spectrum of hybrid **24o**

3.6.16 Synthesis of 4-(6-amino-1-(2-((7-chloroquinolin-4-yl)amino)ethyl)-5-cyano-3-(ethoxycarbonyl)-1,4-dihydropyrano[2,3-*c*]pyrazol-4-yl)benzoic acid (24p)

The reaction between pyrano[2,3-*c*]pyrazole **20p** (1.77g, 5 mmol) and 4-(bromoethylamino)-7-chloroquinoline (1.43g, 5 mmol) (**23**) afforded pyrano[2,3-*c*]pyrazole-aminoquinoline hybrid compound **24p** as a brown solid with 42% yield and melting range of 211-212 °C. IR cm^{-1}: 3334 (NH_2), 3132 (NH), 2191 (CN), 1720 (COOEt), 1612 (C=C); ^{1}H NMR (400 MHz, DMSO) δ 8.39 (d, *J* = 5.2 Hz, 1H), 8.13 (dt, *J* = 9.2, 2.4 Hz, 2H), 8.01 (d, *J* = 9.2 Hz, 1H), 7.76 (d, *J* = 2.4 Hz, 1H), 7.38-7.32 (m, 2H), 7.30 (dt, *J* = 9.6, 2.8 Hz, 2H), 7.18 (s, 2H), 6.47 (d, *J* = 5.6 Hz, 1H), 4.86 (s, 1H), 4.79-4.72 (m, 1H), 4.65-4.59 (m, 1H), 3.72-3.57 (m, 4H), 0.63 (t, *J* = 7.2 Hz, 3H); ^{13}C NMR (100 MHz, DMSO): δ 166.7, 165.7, 152.9, 148.8, 141.7, 135.7, 131.4, 129.9, 129.7, 129.4, 125.7, 125.6, 125.4, 125.1, 125.0, 124.7, 118.9, 117.1, 116.3, 99.3, 63.2, 55.4, 53.2, 45.9, 42.0, 13.6. HRMS calcd. for $C_{25}H_{21}ClN_6O_3S$: *m/z* 558.1418; found: *m/z* 560.3309 (M^+).

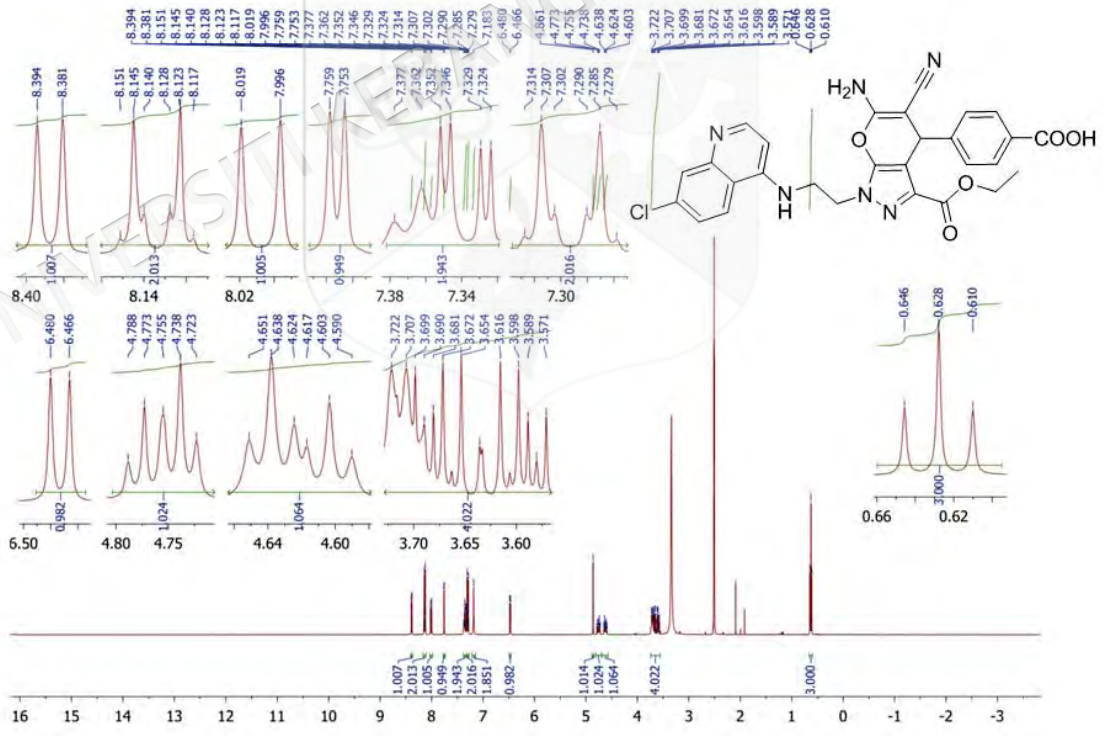

Figure 3.77 ^{1}H NMR spectrum of hybrid **24p**

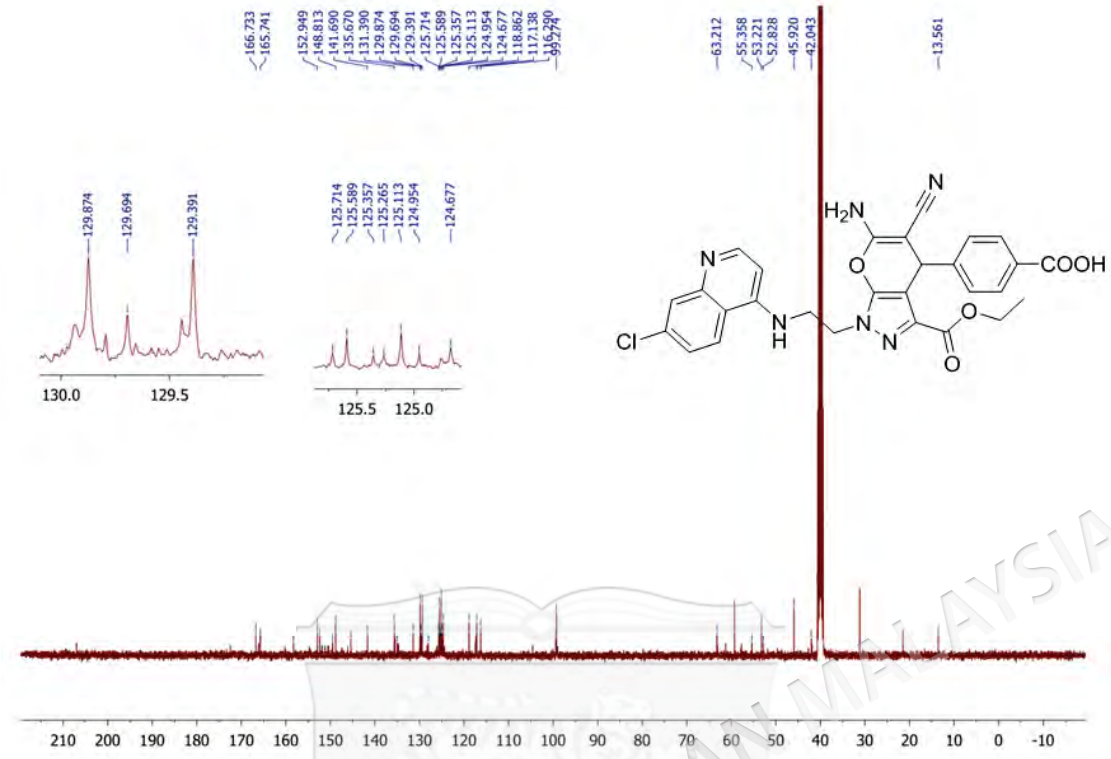

Figure 3.78 ^{13}C NMR spectrum of hybrid **24p**

3.6.17 Synthesis of ethyl 6-amino-1-(2-((7-chloroquinolin-4-yl)amino)ethyl)-5-cyano-4-(4-hydroxyphenyl)-1,4-dihydropyrano[2,3-*c*]pyrazole-3-carboxylate (24q)

The reaction between pyrano[2,3-*c*]pyrazole **20q** (1.63g, 5 mmol) and 4-(bromoethylamino)-7-chloroquinoline (1.43g, 5 mmol) (**23**) afforded pyrano[2,3-*c*]pyrazole-aminoquinoline hybrid compound **24q** as a brown solid with 19% yield and melting range of 233-234 ºC. ^{1}H NMR (400 MHz, DMSO) δ 9.26 (s, 1H), 8.38 (d, *J* = 5.6 Hz, 1H), 8.05 (d, *J* = 9.2 Hz, 1H), 7.79 (d, *J* = 2.4 Hz, 1H), 7.42 (dd, *J* = 9.2, 2.4 Hz, 1H), 6.94 (s, 2H), 6.82 (d, *J* = 8.4 Hz, 2H), 6.64 (d, *J* = 8.4 Hz, 2H), 6.47 (d, *J* = 5.6 Hz, 1H), 4.73-4.57 (m, 2H), 4.56 (s, 1H), 3.74-3.65 (m, 4H), 0.80 (t, *J* = 7.2 Hz, 3H); ^{13}C NMR (100 MHz, DMSO): δ 160.0, 158.7, 156.4, 154.7, 151.9, 150.4, 149.0, 135.8, 134.1, 129.5, 128.5, 127.6, 124.8, 124.3, 120.8, 117.8, 115.4, 106.1, 99.1, 61.3, 59.1, 49.7, 42.7, 37.0, 13.7. IR and MS results are identical with Shamsuddin et al. (2021).

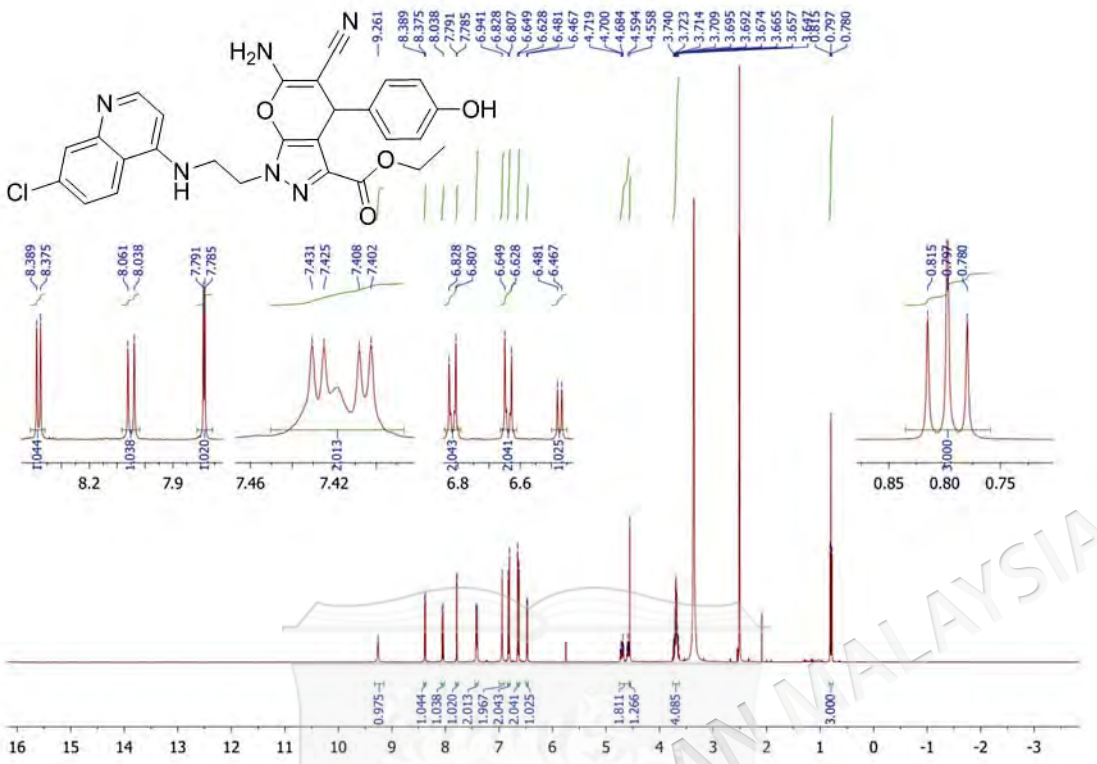

Figure 3.79 ^{1}H NMR spectrum of hybrid **24q**

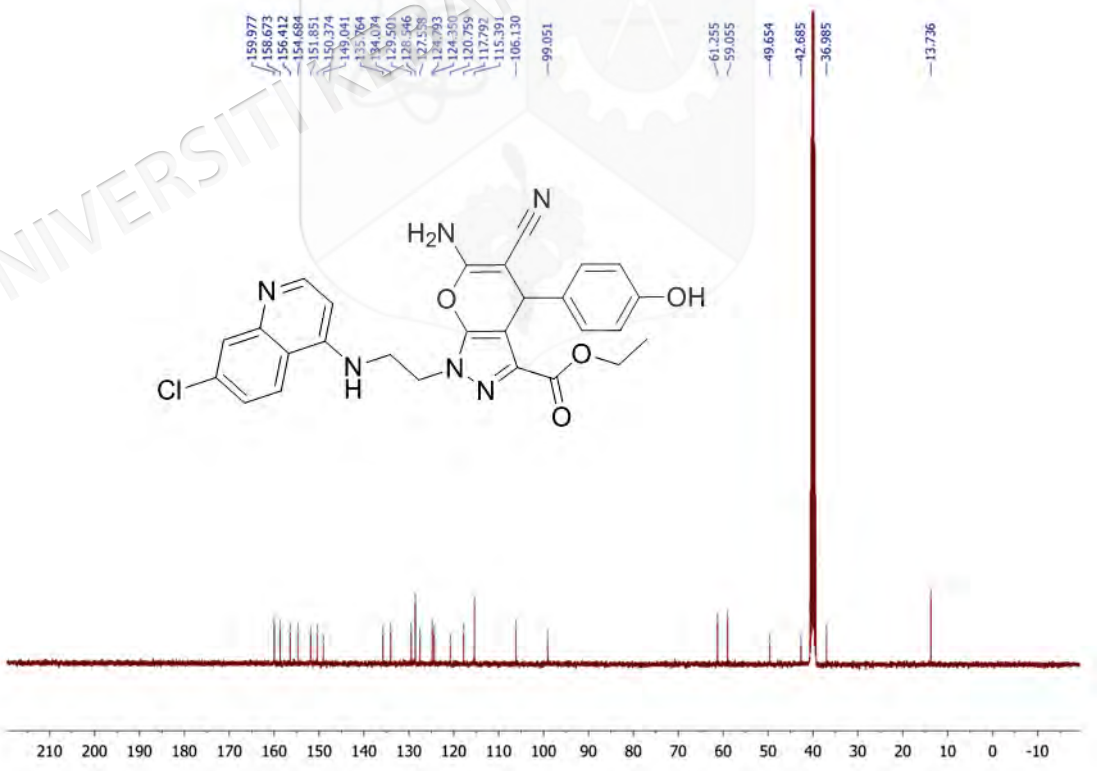

Figure 3.80 ^{13}C NMR spectrum of hybrid **24q**

3.6.18 Synthesis of ethyl 6-amino-1-(2-((7-chloroquinolin-4-yl)amino)ethyl)-5-cyano-4-(2-hydroxynaphthalen-1-yl)-1,4-dihydropyrano[2,3-*c*]pyrazole-3-carboxylate (24r)

The reaction between pyrano[2,3-*c*]pyrazole **20r** (1.88g, 5 mmol) and 4-(bromoethylamino)-7-chloroquinoline (1.43g, 5 mmol) (**23**) afforded pyrano[2,3-*c*]pyrazole-aminoquinoline hybrid compound **24r** as a brown solid with 36% yield and melting range of 252-253 ºC. IR cm^{-1}: 3436 (NH_2), 3306 (NH), 2180 (CN), 1722 (COOEt), 1654 (C=C); ^{1}H NMR (400 MHz, DMSO) δ 8.40 (d, *J* = 5.2 Hz, 1H), 8.08 (d, *J* = 9.2 Hz, 1H), 7.89-7.83 (m, 2H), 7.81 (d, *J* = 2.4 Hz, 1H), 7.69 (d, *J* = 8.8 Hz, 1H), 7.44 (dd, *J* = 9.2, 2.4 Hz, 1H), 7.40-7.37 (m, 2H), 7.13 (s, 1H), 7.04 (d, *J* = 8.8 Hz, 1H), 6.88 (s, 2H), 6.39 (d, *J* = 4.4 Hz, 1H), 5,75 (s, 1H), 4.47-4.04 (m, 5H), 1.39 (t, *J* = 6.8 Hz, 3H); 13C NMR (100 MHz, DMSO): δ 160.8, 160.0, 152.3, 150.4, 149.3, 147.7, 134.0, 131.0, 130.9, 129.5, 129.0, 127.8, 127.4, 125.0, 124.7, 124.5, 123.1, 121.0, 117.8, 116.9, 113.9, 112.1, 99.1, 66.6, 61.5, 55.4, 42.1, 27.3, 14.6.

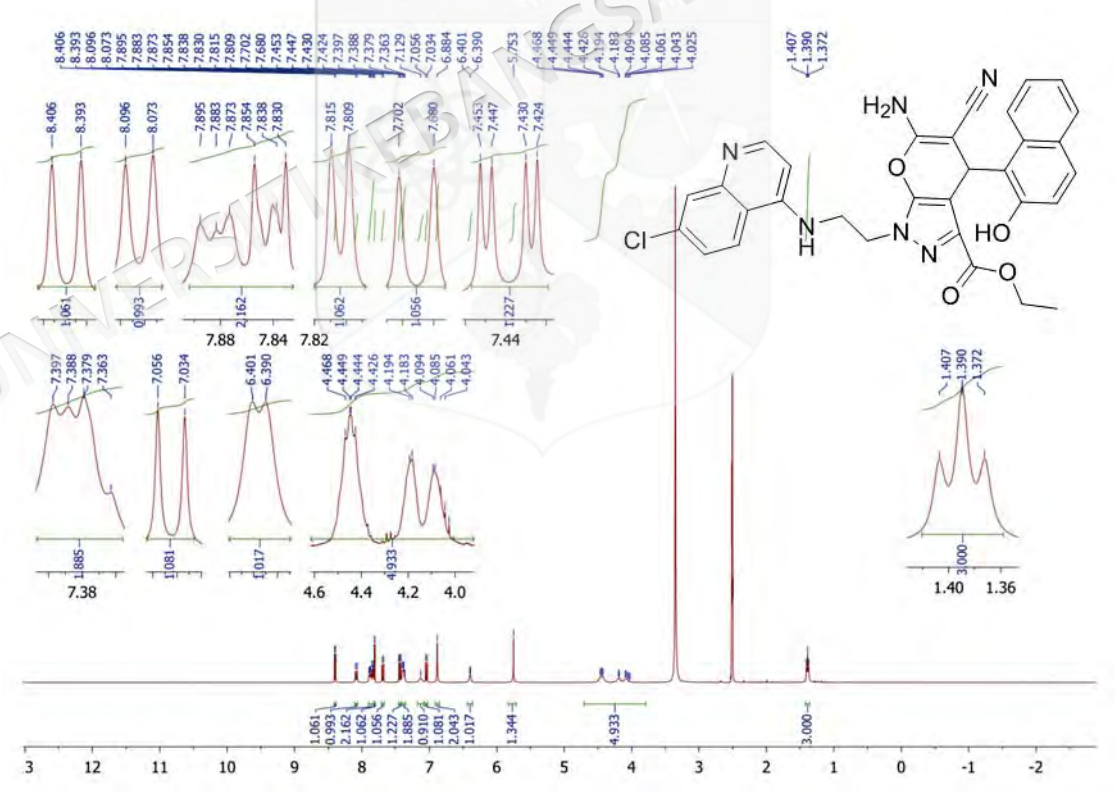

Figure 3.81 ^{1}H NMR spectrum of hybrid **24r**

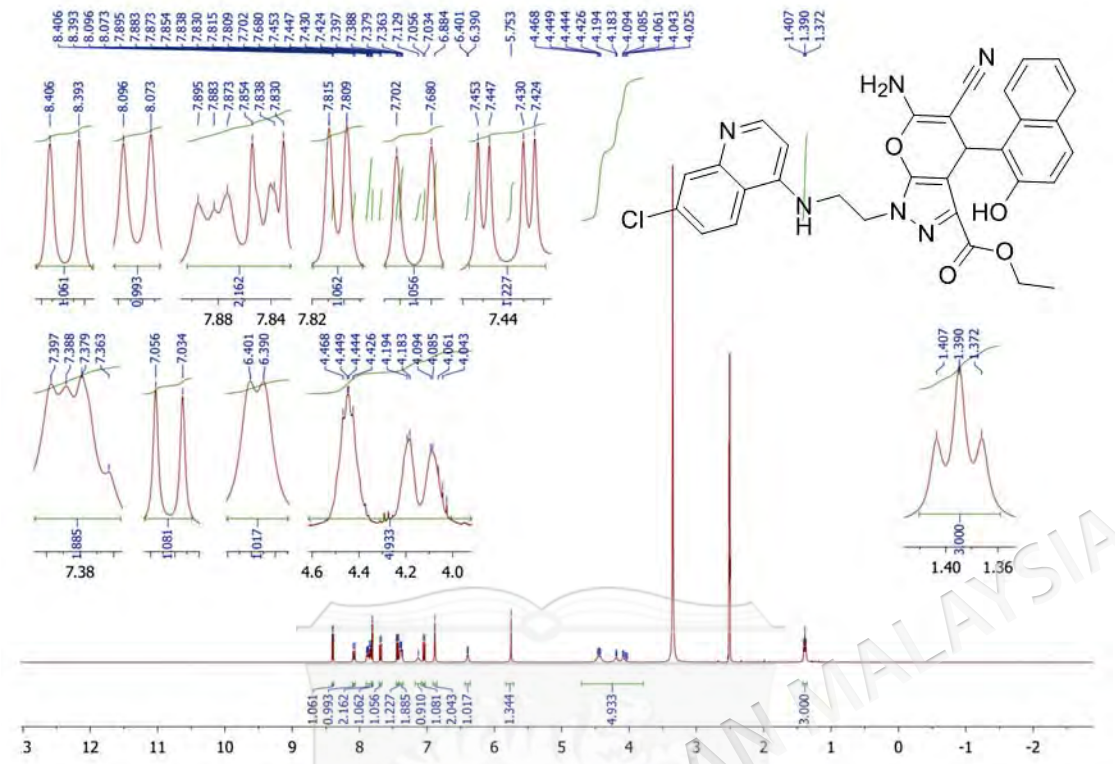

Figure 3.82 ^{13}C NMR spectrum of hybrid **24r**

3.6.19 Synthesis of ethyl 6-amino-1-(2-((7-chloroquinolin-4-yl)amino)ethyl)-5-cyano-4-(pyridin-2-yl)-1,4-dihydropyrano[2,3-*c*]pyrazole-3-carboxylate (24s)

The reaction between pyrano[2,3-*c*]pyrazole **20s** (1.55g, 5 mmol) and 4-(bromoethylamino)-7-chloroquinoline (1.43g, 5 mmol) (**23**) afforded pyrano[2,3-*c*]pyrazole-aminoquinoline hybrid compound **24s** as a brown solid with 24% yield and melting range of 202-204. IR cm^{-1}: 3356 (NH_2), 3257 (NH), 2215 (CN), 1720 (COOEt), 1613 (C=C); ^{1}H NMR (400 MHz, DMSO) δ 8.36-8.29 (m, 3H), 7.85 (d, *J* = 2 Hz, 1H), 7.77 (d, *J* = 7.2 Hz, 1H), 7.60 (dd, *J* = 8.8, 2 Hz, 1H), 6.93 (d, *J* = 9.2 Hz, 1H), 6.67 (d, *J* = 6.4 Hz, 2H), 6.41 (td, *J* = 7.2, 0.8 Hz, 1H), 6.15 (t, *J* = 6.4 Hz, 2H), 4.58-4.47 (m, 4H), 4.19 (q, *J* = 7.2 Hz, 3H), 4.21-3.98 (m, 2H), 1.39 (t, *J* = 6.8 Hz, 3H); 13C NMR (100 MHz, DMSO): δ 172.5, 161.2, 160.8, 158.1, 151.7, 149.7, 137.9, 127.5, 126.2, 125.9, 125.2, 123.9, 116.9, 114.7, 114.1, 102.1, 99.3, 84.7, 81.6, 78.4, 68.1, 67.0, 61.9, 42.3, 21.5, 14.0.

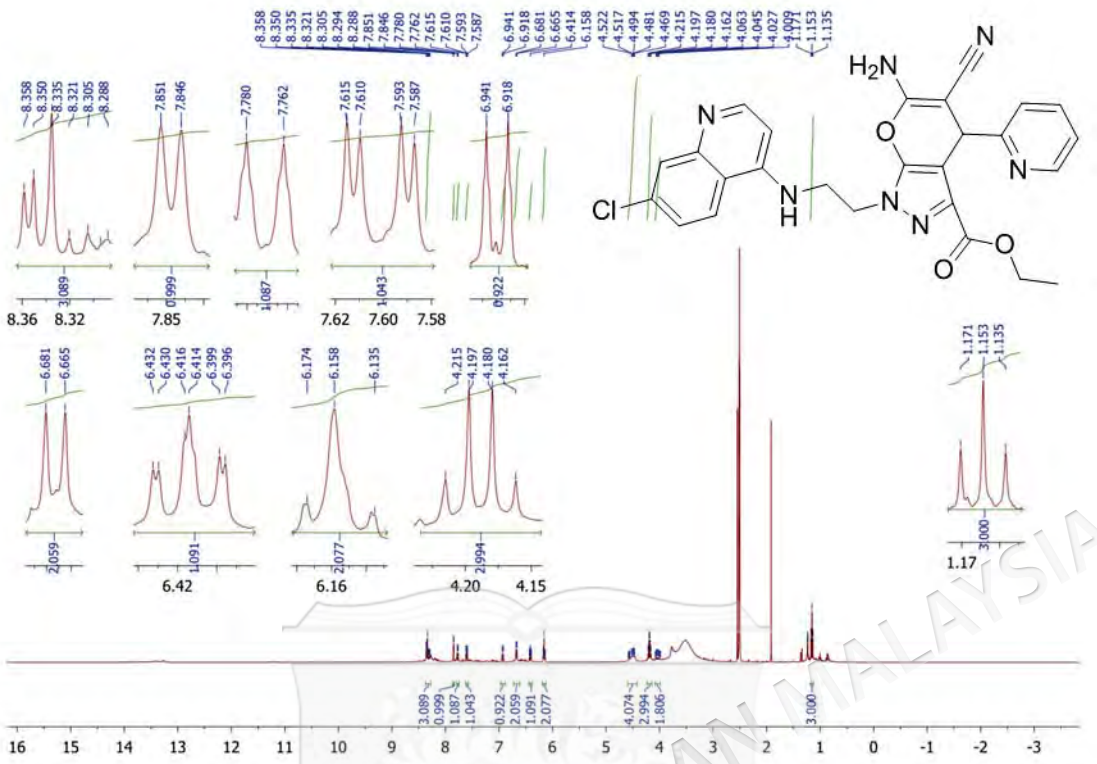

Figure 3.83 ^{1}H NMR spectrum of hybrid **24s**

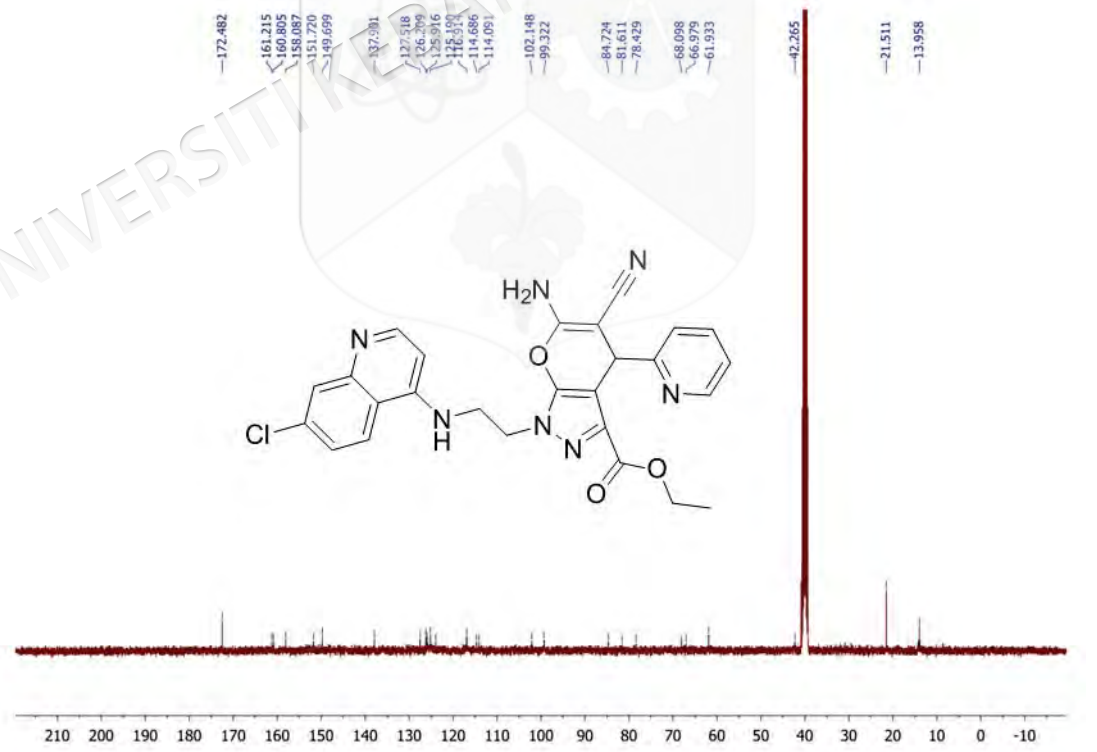

Figure 3.84 ^{13}C NMR spectrum of hybrid **24s**

3.7 *IN SILICO* STUDY METHODS

3.7.1 Physicochemical and ADMET Filtration

Physiochemical properties are one of the filters to assess the drug-like nature of compounds. ChemDraw Ultra 12.0 was used to draw the 2D chemical structures of all 19 designed pyrano[2,3-c]pyrazole-4-aminoquinoline hybrid compounds (**24a-s**) to create the Simplified Molecular Input Line Entry System (SMILES). OpenBabel 3.1.1 was then used to convert the SMILES to the Symyx Spatial Data File (SDF) format prior to being imported as an input file into the FAF-Drugs4 Web Server (http://mobyle.rpbs.univ-paris-diderot.fr/cgi-bin/portal.py?form=FAF-%20Drugs4#forms::FAFDrugs4), as advised by the FAF-Drugs4 Bank Formatter (https://mobyle.rpbs.univ-paris-diderot.fr/cgi-bin/portal.py?form=FAF-%20Drugs4#forms::FAFDrugs4). Finally, by inserting the current SMILES into SwissADME (https://admet.scbdd.com/ChemAGG/index/) and the ADMETlab 2.0 web server (https://admet.scbdd.com/calcpre/index/), ADMET profiles could be produced.

3.7.2 Molecular Docking

The X-ray crystallographic structure of *Pf*LDH was acquired from the Protein Data Bank (PDB ID: 1CET) with a resolution of 2.05 Å (Read et al. 1999). Initial 2D structures of the hybrid compounds were crafted using ChemDraw and subsequently transformed into 3D structures *via* Chem3D, with further refinement through energy minimization using the MM2 force field. AutoDock Tools 1.5.7 (Sanner 1999) was utilized in preparing the protein and ligands structures for docking. The protein crystal structure underwent removal of ligands and water molecules to serve as the docking receptor. Further, polar hydrogens were added, and Kollman united partial atom charges were assigned to the protein coordinates. Nonpolar hydrogens were merged for the ligands, rotatable bonds were defined, and Gasteiger charges were computed. Both protein and ligand data files were then converted into the pdbqt format for subsequent docking analysis.

The co-crystallized ligand, CQ, was first re-docked at the cofactor binding site of *Pf*LDH to evaluate the relico-crystallised docking process. Following this, the docking of all hybrid compounds (**24a-4s**) was docked at the same site. PyMOL (http://www.pymol.org/) and BIOVIA Discovery Studio Visualizer 4.5 (BIOVIA, Dassault Systèmes, 2021) identified the amino acids present within this site. The docking coordinates were centered at x = 36.302, y = 11.09, and z = 19.234, with a box dimension of 40 × 40 × 40 points and 0.375 Å spacing. Molecular docking of the hybrid compounds to *Pf*LDH was executed using AutoDock4.2 (Morris et al. 2009), employing the Lamarckian genetic algorithm search engine with 100 search runs and a population size of 150. Additional parameters were specified, including a maximum of 27000 generations, mutation rate of 0.02, crossover operator weight of 0.8, and elitism set at 1. Each ligand underwent 100 docking simulations, and subsequent clustering analysis, with a root-mean-square deviation tolerance set at 2.0 Å. Upon completion, the most favorable docking conformation with the lowest binding energy was selected for further analysis to elucidate the binding energy and the intermolecular interactions involved using AutoDock Tools and BIOVIA Discovery Studio Visualizer, respectively.

3.8 ISOTHERMAL TITRATION CALORIMETRY METHODS

The isothermal titration calorimetry (ITC) method was carried out in collaboration with the Department of Biological Sciences and Biotechnology, Faculty of Science and Technology, Universiti Kebangsaan Malaysia. Since ITC is expensive and time-consuming, we have screened the potential compounds (**24a**, **24g**, **24h**, **24j**, and **24q**) instead of trying all available compounds. A Nano isothermal titration calorimetry microcalorimeter (TA Instruments, New Castle, DE, USA) was used to study the interaction between five hybrid compounds (**24a**, **24g**, **24h**, **24j**, and **24q**) and hemin at 37 °C. Stock solutions of the hybrids (2 mg/ml) were prepared by dissolution in DMSO, while a 0.5 mg/mL hemin solution was prepared in 0.5 M NaOH. These stock solutions were diluted with 10 mM sodium phosphate buffer, pH 7.4 while ensuring that the final samples contained 0.5 M NaOH and approximately 3% DMSO. Prior to the titration experiments, all samples were degassed under vacuum for 10 minutes. For the titration, 20 µM hemin was loaded into the sample cell, while the reference cell contained only deionized water. A 250 µL syringe containing the hybrid compound (100 µM) was

introduced into the microcalorimeter. The titration protocol involved 16 consecutive injections of 15 μL of the titrant into the sample cell with an interval of 400 s between injections, all while maintaining a stirring speed of 200 rpm to ensure thorough mixing of the solutions. Control experiments were performed by injecting the ligand into the buffer solution under similar conditions to account for the heat generated by dilution and solution mixing. The data obtained from these experiments were processed and analyzed using the NanoAnalyze software (v3.3.0), utilizing an independent binding model.

3.9 *IN VITRO* EVALUATION METHODS

The analysis in this section uses pyrano[2,3-*c*]pyrazole utilising quinoline hybrid compounds (**24a-s**) to perform antiplasmodium assays and cytotoxicity assays against *P. falciparum* CQ-sensitive 3D7, CQ-resistant K1 strains and human normal liver WRL68 cell line, respectively. Several steps are carried out when making an antiplasmodium test, namely the culturing of the parasite strain 3D7 and K1, the parasite incubation with the hybrid compound and the Schizont maturation assay. Next, the cytotoxicity test started with culturing the human normal liver WRL68 cell line, incubating the human normal liver WRL68 cell line with hybrid compounds and MTT assay. Finally, the SI values were determined based on the IC_{50} values from the Schizont maturation and MTT assays to assess the level of inhibition of the hybrid compounds against *P. falciparum* without causing toxicity to the normal human liver WRL68 cell line. The *in vitro* method was carried out in collaboration with the Department of Parasitology, Faculty of Medicine, University of Malaya.

3.9.1 Cytotoxic Evaluation Methods

A human normal liver WRL68 cell line (ATCC: CL-48) was purchased from the American Type Culture Collection (ATCC). The cell lines were cultivated in MEM medium (supplemented with 5% of FBS and 1% of penicillin–streptomycin) in a tissueculture flask (T25) (Nunc, USA) at 37 °C and 5% CO_2 in a sterile incubator. When the cells reached confluency, the media were removed and washed with phosphate buffer saline (PBS, Gibco, USA). Cells were detached by adding trypsin (Gibco, USA)

and incubated for 5–10 minutes at 37 °C. The cell suspension was transferred into a 15 mL sterile tube and centrifuged at 300 x *g* for 5 minutes.

An assay using 3-[4,5-dimethyl thiazol-2-yl] 2,5-diphenyl tetrazolium bromide (MTT; Merck) was carried out to measure the cytotoxicity activity of the compounds. The cells were seeded in 96-well flat-bottomed plates (Eppendorf) at a density of 5×104 cells per well in a final volume of 100 µl/well. After 24 h incubation at 37 ºC with 5% CO_2, the cells were treated with 2 µl of a serial dilution of the compounds at concentrations starting from 0.3 µg/ml to 99 µg/ml (concentration of extract in the well). The serial concentrations were added into the wells shown as in Table 3.1. After 72 h of incubation, 50 µl MTT solution (2 mg/ml) was added to each well and further incubated for 4 h at 37 ºC. Then, 200 µl of DMSO was added to each well to dissolve the MTT crystals and their absorbance was recorded at 570 nm using an enzyme-linked immunosorbent assay (ELISA) plate reader. Each experiment was performed in triplicates. The percentage of cell viability was determined using the following formula:

$$\text{Percentage of cell viability (\%)} = \frac{\text{Absorbance of treated cells (Compounds)}}{\text{Absorbance of DMSO}} \times 100$$

The IC_{50} values of the treated cells were determined by plotting a graph of cell's viability versus extract concentration.

Table 3.1 Serial concentration of tested compound

Stock extract concentration (mg/ml)	Concentration of extract in the well (mg/ml)	Concentration of extract in the well (µg/ml)
10.000	0.0990	99.00
5.000	0.0495	49.50
2.500	0.0248	24.80
1.250	0.0124	12.40
0.625	0.0062	6.20
0.313	0.0031	3.10
0.156	0.00155	1.55
0.078	0.00077	0.77
0.039	0.00039	0.39

3.9.2 Antiplasmodium Evaluation Methods

This section outlines the methodology for *in vitro* antiplasmodial activity studies involving screening synthesized for antimalarial efficacy using the schizont maturation inhibition assay. The methodology is divided into three parts; *P. falciparum* cultures, continuous culture maintenance for sustained parasite supply, and the subsequent schizont maturation inhibition assay following the establishment of robust cultures.

a. *In vitro* cultivation of *P. falciparum*

The CQ-sensitive strain (3D7) of *P. falciparum* was sourced from Professor Lau Yee Ling at the Department of Parasitology, University of Malaya. In contrast, the CQ-resistant strain (K1) was obtained from the Institute for Medical Research (IMR), Setia Alam, Selangor. *P. falciparum* culture was cultivated and maintained following the procedure described by Trager and Jensen with minor modifications (Trager & Jensen 1976).

The culture medium preparation consisted of Roswell Park Memorial Institute (RPMI)-1640 media supplemented with AlbuMax-II (20%), L-glutamine, hypoxanthine, D-glucose, and sodium bicarbonate. The medium's pH was adjusted around 7.25 - 7.30 by adding 10M sodium hydroxide. Subsequently, the medium was sterilized *via* vacuum filtration, using a poly ether sulfone (PES) membrane filter with a porosity of 0.22 μm. Both resistant and sensitive strains of *P. falciparum* were cultured in B+ erythrocytes in the prepared RPMI-1640 medium in a culture flask (Figure 3.85). The culture flask is then placed in a candle jar and incubated at 37 °C.

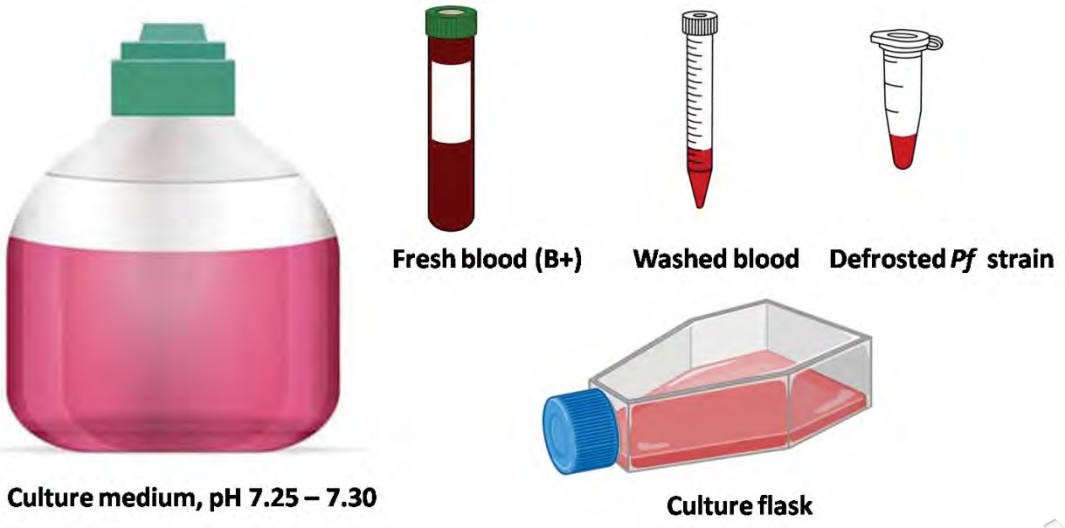

Figure 3.85 The culture medium preparation

The candle jar setup includes a culture flask with the parasite culture medium, a candle, and a dampened tissue in a petri dish for humidity control. The method, utilizing a vacuum desiccator made of heavy glass, maintains oxygen at 17% and carbon dioxide at 3% (Trager & Jensen 1977). Figure 3.86 depicts the candle jar setup before being placed in an incubator at 37 °C.

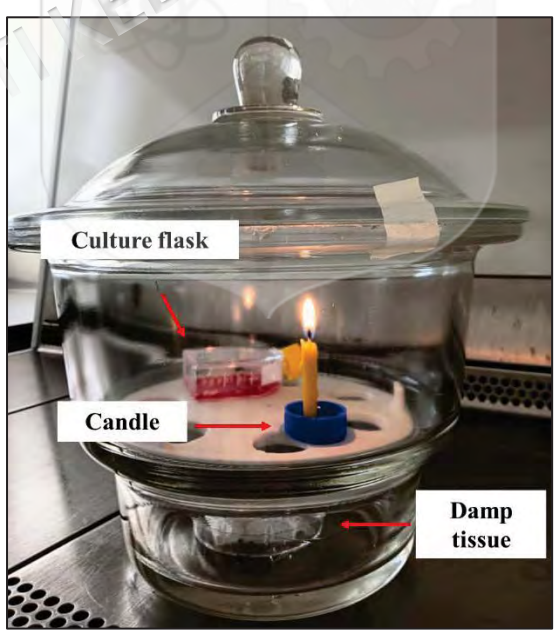

Figure 3.86 The candle jar setup for *P. Falciparum* culture cultivation

b. Continuous maintenance of *P. falciparum* culture

Parasite growth and multiplication are monitored at 48-hour intervals through microscopic examination of Giemsa-stained, thin-smeared slides. Parasitaemia, representing the percentage of infected erythrocytes, is consistently monitored and maintained within the 2% to 4% range (Figure 3.87). Simultaneously, the haematocrit level is upheld at 2%. The percentage of parasitaemia is calculated using the following formula:

$$\text{Parasitaemia (\%)} = \frac{Number\ of\ infected\ red\ blood\ cells}{Mean\ number\ of\ red\ blood\ cells \times number\ of\ fields\ under\ microscope} \times 100$$

The haematocrit levels are calculated as the ratio of the volume of red blood cells to the total culture volume, expressed as a percentage in the following formula:

$$\text{Haematocrit (\%)} = \frac{Volume\ of\ red\ blood\ cells}{Total\ culture\ volume} \times 100$$

Depending on the parasitaemia level observed, the parasite culture medium is managed by either solely replacing the existing medium or by introducing new red blood cells concurrently. This adaptive approach allows for adjusting parasitaemia levels, ensuring optimal conditions for cultivating the parasite culture.

Volume of RBC (uL) in different culture volume

Culture volume	5 mL	7 mL	10 mL	12 mL	15 mL	20 mL	25 mL	30 mL	50 mL
1.5% hct	75	105	150	180	225	300	375	450	750
2% hct	100	140	200	240	300	400	500	600	1mL
3% hct	150	210	300	360	450	600	750	900	1.5mL
4% hct	200	280	400	480	600	800	1mL	1.2mL	2mL
5% hct	250	350	500	600	750	1mL	1.25mL	1.5mL	2.5mL

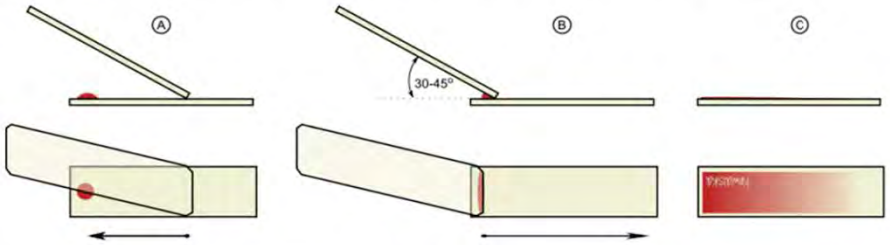

0.5mL Giemsa stain + 3.5mL PBS (12.5%) **dipped in MeOH prior to staining**

Figure 3.87 Monitering of parasite growth through microscopic examination of Giemsa-stained thin-smeared slides.

c. Schizont maturation inhibition assay

Prior to the inhibition assay experiment, the culture is synchronised using D-sorbitol to obtain predominantly ring-stage parasites. The culture is treated with an equal volume of aqueous 5% D-sorbitol for 5 minutes (Lambros & Vanderberg 1979). Subsequently, after centrifugation, the pellet is suspended in complete medium after two washes with incomplete RPMI-1640 medium. The parasitaemia level is adjusted using the same method for culture maintenance to obtain the synchronised culture with 0.5% ring stage, which then utilised for the inhibition assay.

Stock solutions for the test compounds were individually prepared by weighing 1 mg of each compound and dissolving them in approximately 50-100 µL of dimethylsulfoxide (DMSO). Subsequently, the solutions were diluted with culture medium to achieve a concentration of 1 mg/mL. The test compounds underwent further dilution across a range from 0.0001 to 100 µg/mL, while the reference drug, chloroquine

diphosphate, was serially diluted from 0.00001 to 10 µg/mL. Following this, 50 µL of serial dilutions of all compounds were dispensed in triplicates into 96-well plates. Then, 150 µL of the synchronised culture was added to each well, resulting in a final volume of 200 µL with a final hematocrit of 2% and 0.5% ring stage parasites (Faith et al. 2013). The positive control wells contained the synchronizsed ring stage culture, serving as an indicator for monitoring the normal growth of parasites. In contrast, the negative control wells consisted solely of uninfected erythrocytes in culture medium to monitor possible contamination. The 96-well plate setup is shown in Figure 3.88.

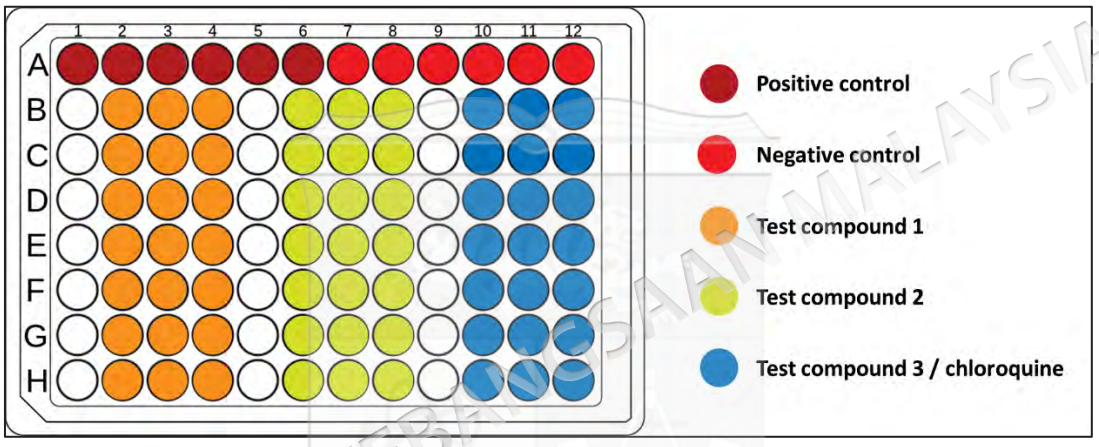

Figure 3.88 The 96-well plate setup for schizont maturation inhibition assay

The drugs plates are placed within the candle jar and then in an incubator set at 37°C. Incubation of the drug plates extends for 33-42 hours or until 50% of the ring stage parasites undergo maturation to schizonts (monitored using the thin smear method) (Figure 3.89). Post-incubation, the plates are inclined at an approximate angle of 45° for around 30 min, allowing the supernatant to separate from the erythrocyte mixture. Subsequently, thick blood smears are crafted for each concentration using the erythrocytes remaining in the fluid. After thorough drying, the smears are stained with a 10% Giemsa solution (Kosaisavee et al. 2006) and examined under a light microscope.

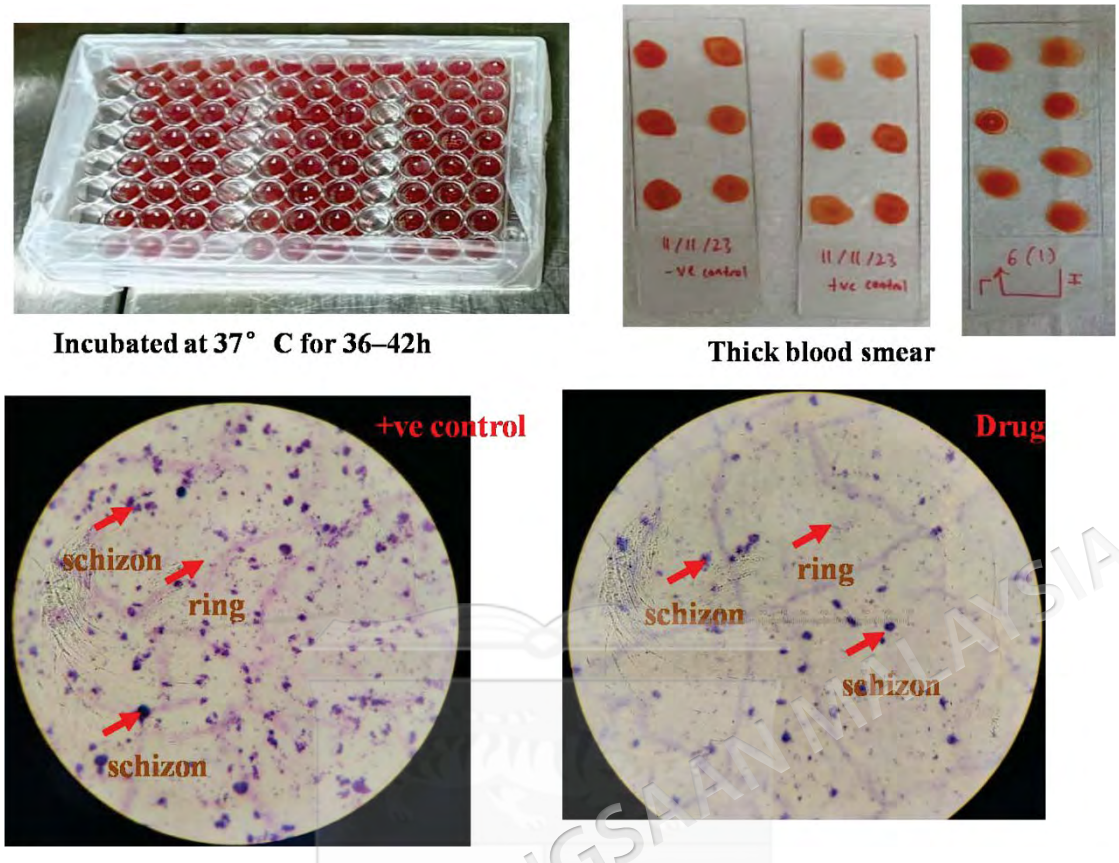

Figure 3.89 Results after incubation of the drug plates for 33-42 hours or until getting 50% of the schizont stage parasites

Microscopic evaluation involved counting the number of schizonts with three or more nuclei among 200 asexual parasites in each thick film (Russell et al. 2008). The inhibition of parasite growth in the treated groups was determined using the following Equation:

$$\text{Inhibition } (\% = (1 - \frac{Number\ of\ schizonts\ in\ test\ wells}{Number\ of\ schizonts\ in\ positive\ wells} \times 100$$

The 50% inhibitory concentration (IC_{50}) for all compounds was calculated by estimating values from the graph plotted with the inhibition (%) data using GraphPad Prism 7 software (Graphpad software Inc., CA, USA).

3.9.3 Selectivity and Resistance Indexes Calculation

The pyrano[2,3-c]pyrazole-aminoquinoline hybrid compounds' selectivity index (SI) was calculated as a ratio of the values from the IC_{50} of cytotoxicity and the IC_{50} of

antimalarial activity. Strong and selective antimalarial drugs are test with pure substances with SI > 100 (Sarr et al. 2011). The ratio of the IC_{50} for the resistant strain to the sensitive strain (CQR/CQS) is known as the resistance index (RI). The ratio of the antimalarial activity against the CQ-resistant strain to that against the CQ-sensitive strain is measured quantitatively, known as the RI. A reduced RI index indicates a compound's efficacy against CQ-resistant malarial parasites (Iwaniuk et al. 2009).

CHAPTER IV

RESULTS AND DISCUSSION

4.1 INTRODUCTION

This chapter discusses the research results that have been carried out in the process of studying the synthesis of 4-aminoquinolines, pyrano[2,3-*c*]pyrazoles, pyrano[2,3-*c*]pyrazole-4-aminoquinoline hybrids. The results of the *in silico* study of the hybrid compounds against the *Pf*LDH, heme detoxification and the antiplasmodium test and cytotoxicity test of the hybrid compounds against *P. falciparum* CQ-sensitive 3D7, CQ-resistant K1 strains and human normal liver WRL68 cell line, respectively are discussed in this chapter.

4.2 SYNTHESIS OF PYRANO[2,3-*C*]PYRAZOLE-4-AMINOQUINOLINES

4.2.1 Synthesis of Pyrano[2,3-*c*]pyrazole Derived Compounds (20a-s)

In the first step, the ester group of sodium diethyloxalacetate reacted with the nucleophilic group of hydrazine solution in the presence of acetic acid (a catalyst which helps the sodium diethyloxalacetate to dissolve in the ethanol solvent) to provide an intermediate A, which then underwent elimination to give an intermediate B with a simultaneous release of an ethoxide anion. The subsequent deprotonation of intermediate B resulted in intermediate C, which underwent intramolecular cyclization reactions (D and E) to furnish intermediate F and water molecules as a by-product.

In the next step, the deprotonation of malanonitrile by the resultant water molecule generates the carbide anion intermediate G, which subsequently reacts with aldehyde to form an intermediate H. The subsequent protonation of intermediate H generates an intermediate I. The alcoholic group of the resultant intermediate I

abstract the proton of adjacent aliphatic carbon to form oxonium anion intermediate J, which finally underwent dehydration to provide intermediate K and the regeneration of water molecules as a by-product.

In the final step, the resultant intermediates F and K undergo an addition reaction to provide intermediate L, which underwent deprotonation by the base to furnish anion intermediate M. Finally, the intramolecular cyclization of the resultant anion intermediate M yielded the corresponding pyrano[2,3-*c*]pyrazole compound (1a-s). Figure 4.1 describes the synthesis mechanism of the pyranopyrazole compound (**20a-s**).

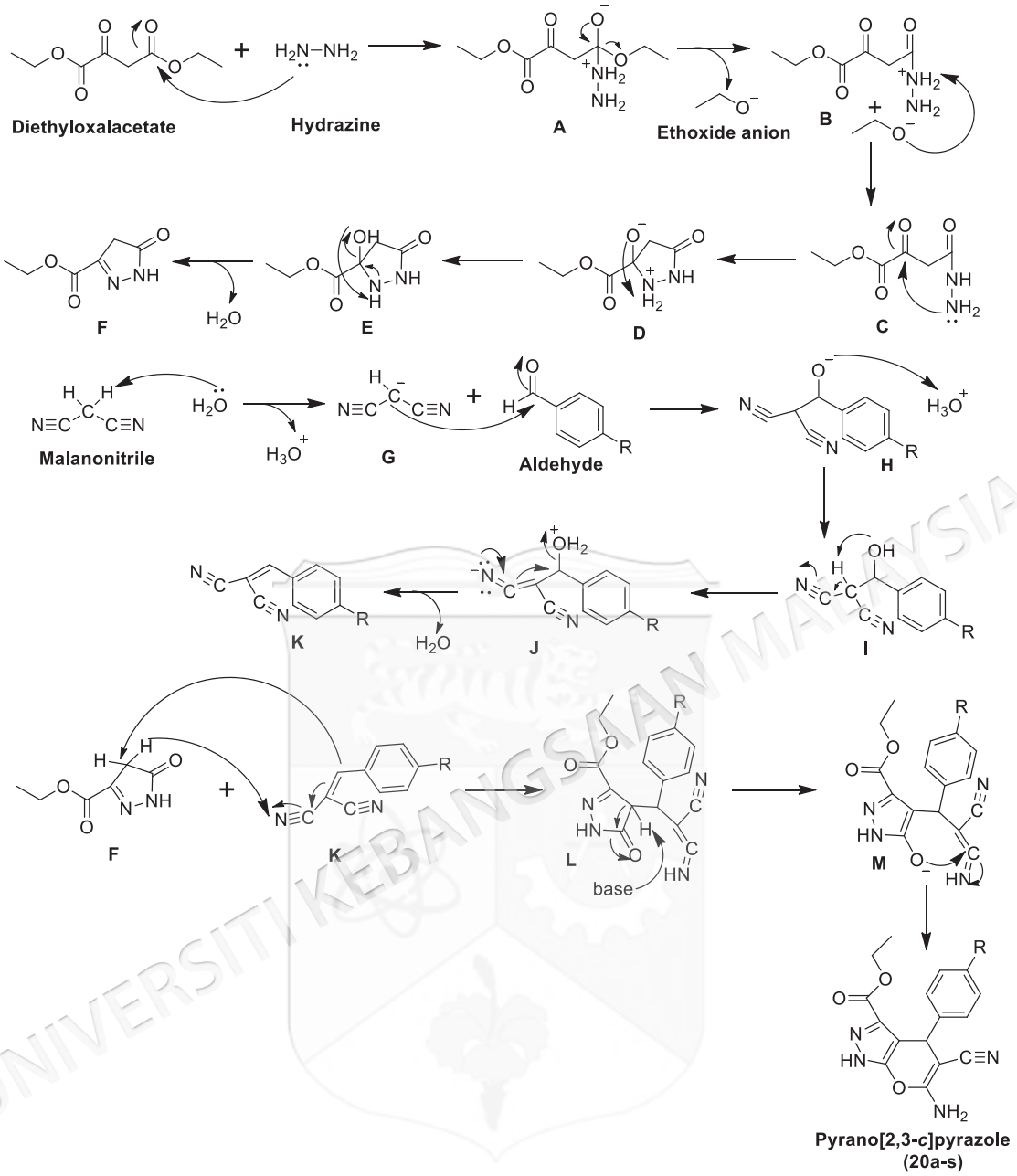

Figure 4.1 Plausible mechanism of pyrano[2,3-*c*]pyrazoles synthesis

As shown in Table 4.1, the yield percentage of pyrano[2,3-*c*]pyrazole compounds revealed that the aromatic compounds of aldehydes containing electron-withdrawing groups provided a higher yield percentage of the pyrano[2,3-*c*]pyrazole compounds than the aromatic compounds of aldehydes having electron-donating groups. Aromatic aldehyde compounds with an electron-donating group will activate the aromatic ring by increasing the electron density on the aromatic ring through the inductive donating effect. Electron-donating substituent groups will increase the electron density at the *ortho* and *para* positions. This will cause the carbonyl in the

aromatic aldehyde to be weakly electrophilic and give a low yield percentage compared to aromatic aldehydes containing electron-withdrawing groups. Figure 4.2 describes the effect of substituent groups on the aromaticity of aldehydes. A study by Mohammat et al. (2018) also stated that increasing the length of the aliphatic chain results in a reduced yield percentage due to the tendency to undergo aldol self-condensation or Cannizzoro-type reactions.

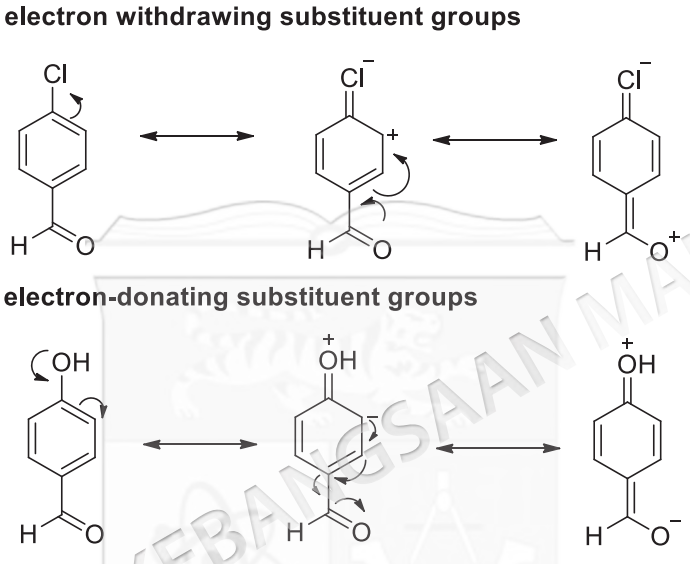

Figure 4.2 Effects of substituent groups on aldehydes

Table 4.1 Yield percentage of pyrano[2,3-*c*]pyrazole compounds

Entry	Carbonyl compound	Product	Time (min)	Yield (%)	Melting point (ºC)
20a	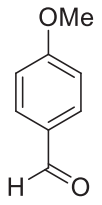	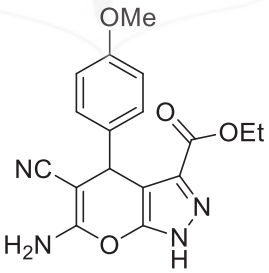	30	64	235-236
20b	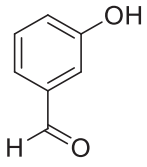	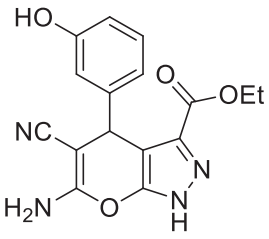	30	56	237-238

To be continued…

Continuation…

20c	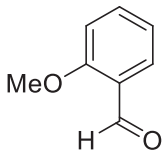	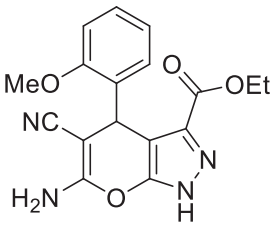	30	76	212-213
20d	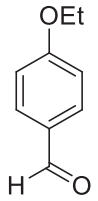	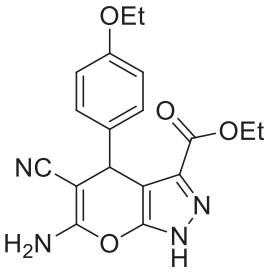	30	85	210-211
20e	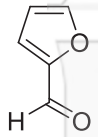	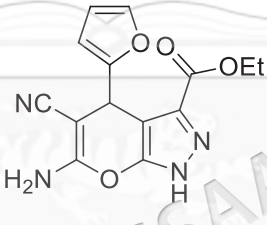	30	61	218-219
20f	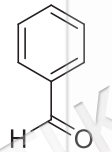	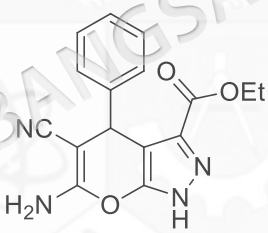	30	66	226-227
20g	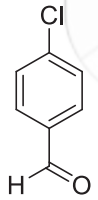	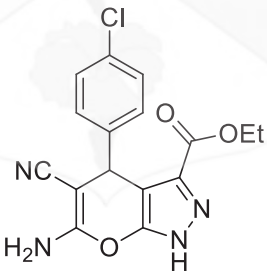	30	74	228-230
20h	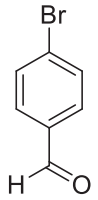	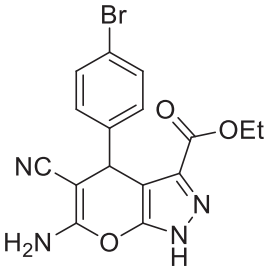	30	71	221-222

To be continued…

Continuation…

20i	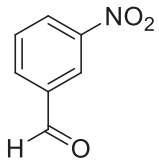	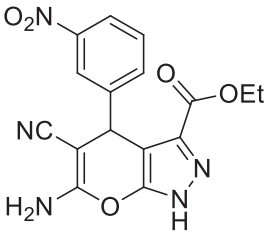	30	70	224-225
20j	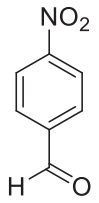	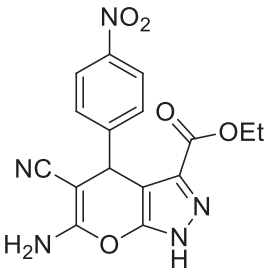	30	74	235-237
20k	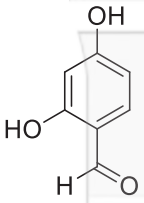	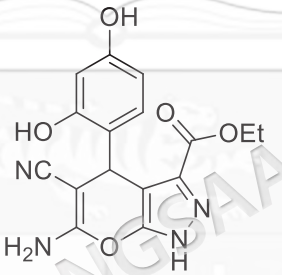	30	42	281-282
20l	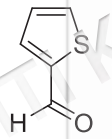	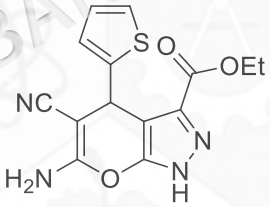	30	60	205-207
20m	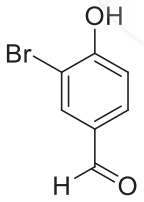	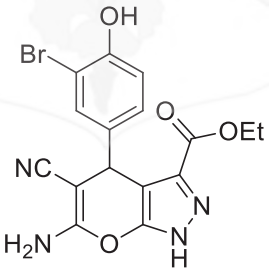	30	76	224-225
20n	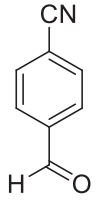	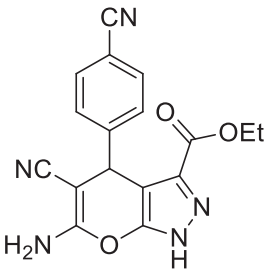	30	68	218-221

To be continued…

Continuation…

20o	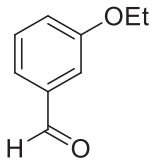	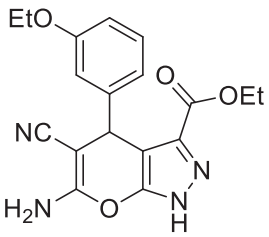	30	55	211-212
20p	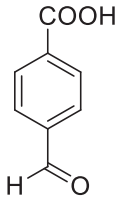	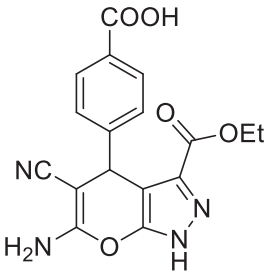	30	84	242-244
20q	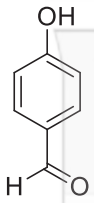	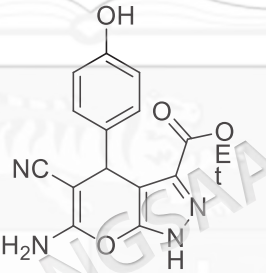	30	55	217-218
20r	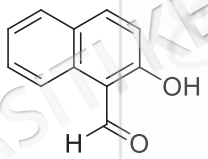	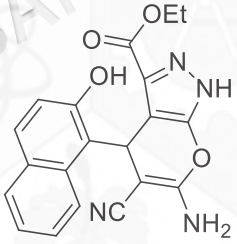	30	52	231-233
20s	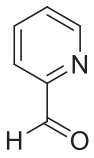	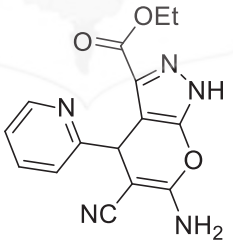	30	54	289-291

4.2.2 Synthesis of 4-(bromoethylamino)-7-chloroquinoline (23)

Initially, the alkyl chain containing 2 carbon atoms was linked to the 4,7-chloroquinoline moiety **21** by reacting to amino alcohol (ethanolamine) under neat conditions to provide 4-(ethanolamine)-7-chloroquine intermediate **22** with a much higher yield (94%) (Guantai et al. 2011). Finally, the intermediate **22** was successfully transformed to 4-(bromoethylamino)-7-chloroquinoline **23,** in moderate yield (70%)

under established reaction conditions utilizing HBr-H_2SO_4 as brominating agent (Cazelles et al. 2011) (Figure 4.3).

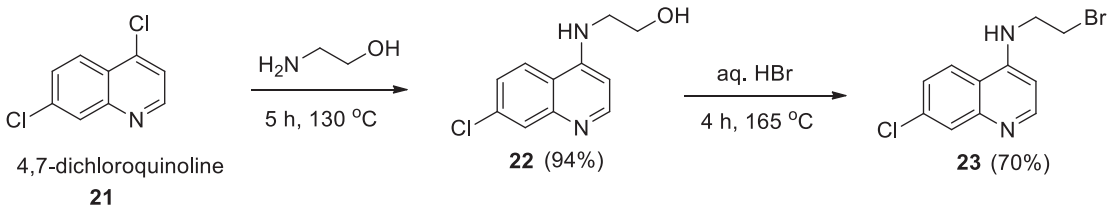

Figure 4.3 4-(Bromoethylamino)-7-chloroquinoline synthesis

4.2.3 Synthesis of Pyrano[2,3-*c*]pyrazole-4-aminoquinoline Hybrid Compounds (24a-s)

Having secured the synthesis of **20a-s** and **23**, the formation of intended pyrano[2,3-*c*]pyrazole-4-aminoquinoline hybrid compounds (**24a-s**) was carried out by the hybridization of pyranopyrazole derivatives (**20a-s**) with 4-(bromoethylamino)-7-chloroquine (**23**) at 30-40 °C under basic conditions, employing DMSO as a solvent (Shamsuddin et al., 2021). A possible reaction mechanism of pyrano[2,3-*c*]pyrazole-4-aminoquinoline hybrid compounds synthesis is depicted in Figure 4.4. Initially, the elimination of acidic proton from the pyrano[2,3-*c*]pyrazole **20** upon reaction with the base, generated the hybrid scaffold intermediate. The subsequent nucleophilic addition of the resultant pyrazolium anion intermediate to the 4-aminoquinoline derivative **23** via S_N2 reaction yielded the corresponding hybrid **24**. This elegant approach is simple, involving only a few steps to target hybrid molecules.

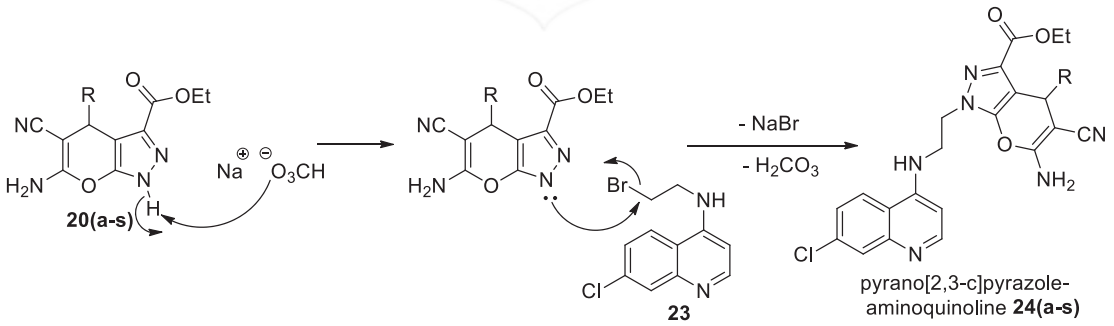

Figure 4.4 Possible reaction mechanism of pyrano[2,3-*c*]pyrazole-aminoquinoline hybrids synthesis

After completion of the reaction, the reaction mixture was left to cool at room temperature and extracted using a mixture of 20 mL of ethyl acetate and 80 mL of brine

in a separatory funnel. Brine facilitates the process of compound purification because DMSO will miscible in brine and the compound will dissolve on the organic layer. The organic layer was separated and concentrated using a rotary evaporator. Finally, all the synthesised hybrid compounds (Table 4.2) were purified using silica column chromatography by elution with a mixture of ethyl acetate: hexane (3:1). Poor to moderate yields were observed in the case of all the purified hybrid compounds. Among all, high yields were observed for hybrids containing electron-withdrawing groups, such as –CN (2**4n,** 49%), –COOH (2**4p,** 42%), and –NO_2 (2**4j,** 38%) at the *para* position of the phenyl ring attached to the pyranopyrazole moiety. Notably, the synthesis of hybrid compounds containing *O*-heterocycle (**24e**), *S*-heterocycle (**24l**,), and *N*-heterocycle (**24e**, 22%) were achieved from the corresponding pyrano[2,3-*c*]pyrazoles in considerable yields (22% to 36%). Lower yields were obtained in the case of hybrids with *ortho*-methoxy (**24c**), *meta*-nitro (**24i**), and *ortho,para*-dihydroxy (**24k**) phenyl rings (10% to 13%).

Table 4.2 Yield percentage of pyrano[2,3-*c*]pyrazole-aminoquinoline hybrids

Entry	Product	Time (hrs)	Yield (%)	Melting point (ºC)
24a	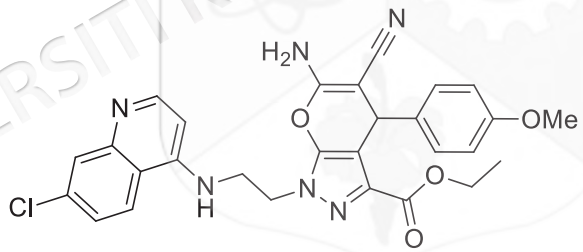	24	25	169-171
24b	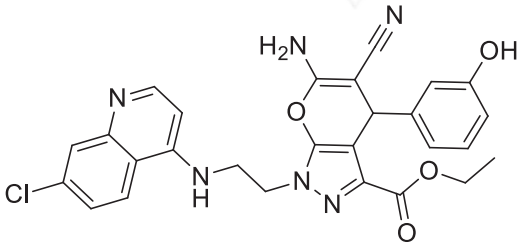	24	24	199-201

To be continued…

Continuation…

24c	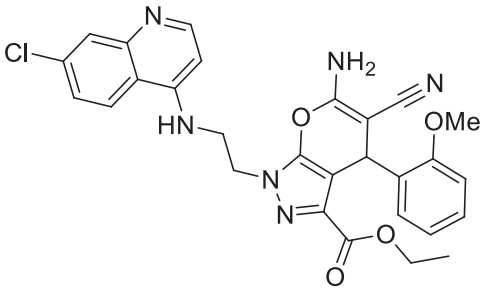	24	10	180-182
24d	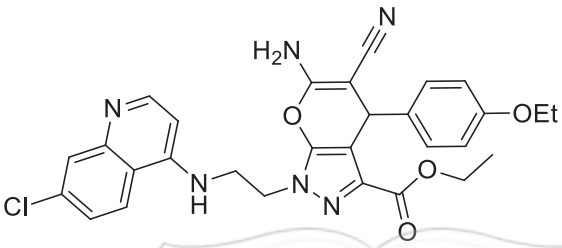	24	14	201-203
24e	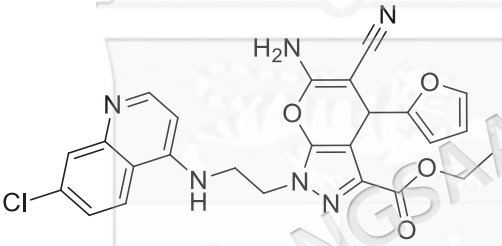	24	22	232-234
24f	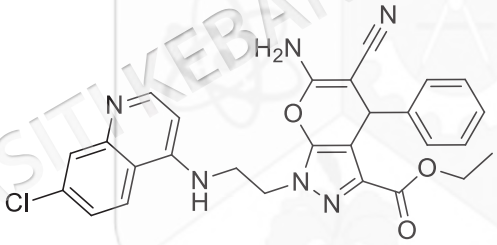	24	18	145-147
24g	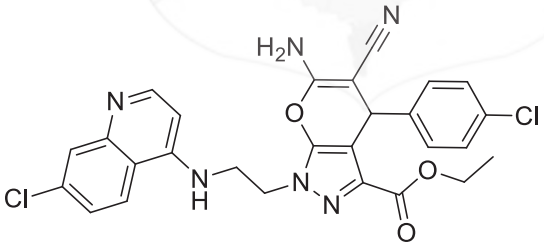	24	23	157-159
24h	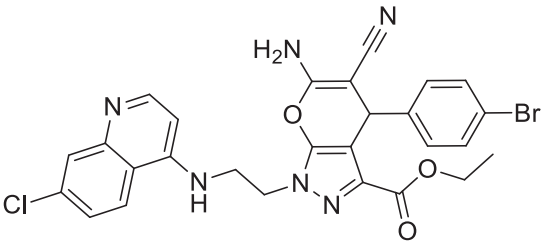	24	29	171-173

To be continued…

Continuation…

24i	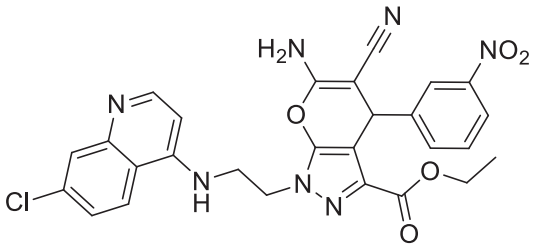	24	12	214-215
24j	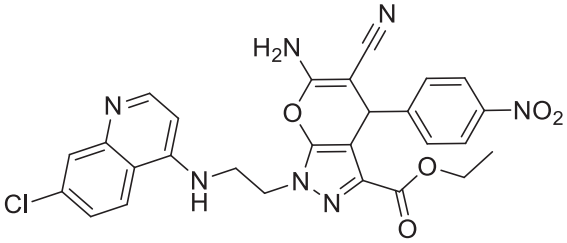	24	38	198-200
24k	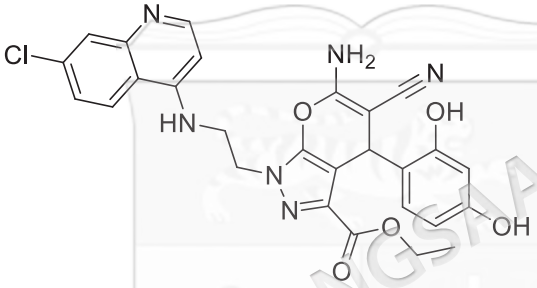	24	13	278-279
24l	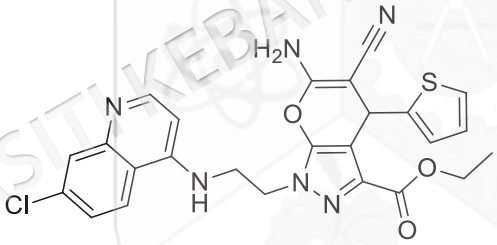	24	36	239-240
4m	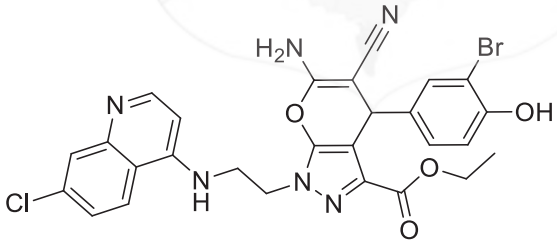	24	25	217-219
24n	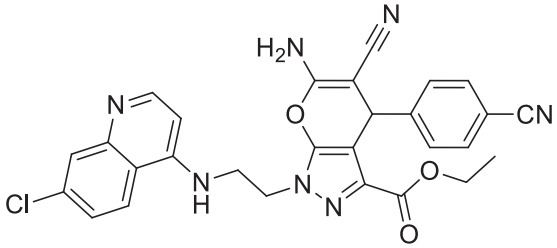	24	49	119-201

To be continued…

Continuation…

24o	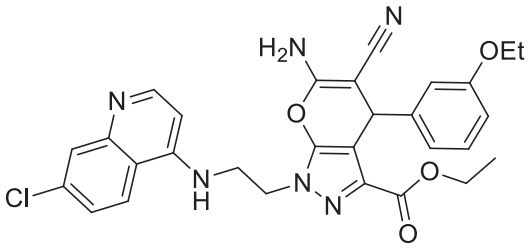	24	31	179-180
24p	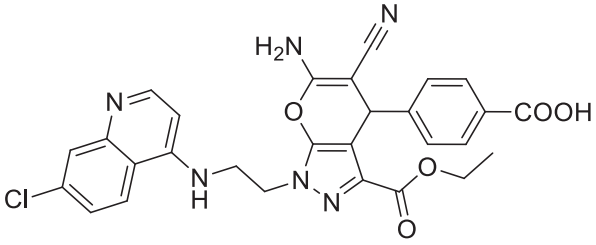	24	42	212-213
24q	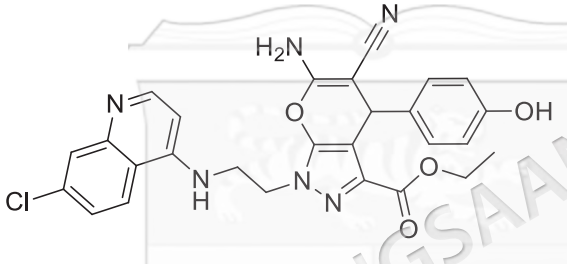	24	19	233-234
24r	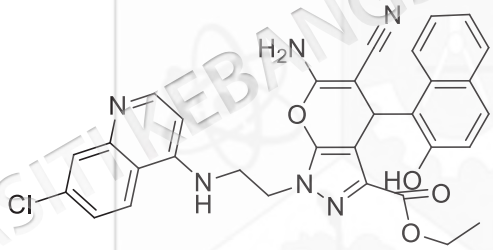	24	36	252-253
24s	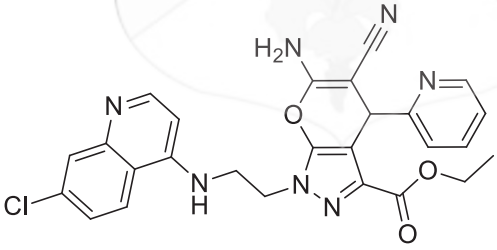	24	24	202-204

4.3 *IN SILICO* STUDY OF PYRANO[2,3-*C*]PYRAZOLE-4-AMINOQUINOLINES

In order to identify viable drug candidates at a reasonable cost during the drug discovery and development process, computer-aided drug design (CADD) is essential (Brogi et al. 2020). These computational techniques, namely molecular docking and *in silico* filtering, are crucial for the rational development of novel, safe drug candidates. They also help determine the binding energy of protein-ligand complexes through scoring

functions, structurally map the binding positions of compounds within the cavities of proteins-of-interest, and identify the best-scored compounds for synthesis and biological assay validation. In order to pre-screen the compounds for drug-like qualities, all designed pyrano[2,3-*c*]pyrazole-4-aminoquinoline hybrid compounds (**24a-s**) underwent *in silico* studies before molecular docking, including physicochemical, and absorption, distribution, metabolism, excretion, and toxicity (ADMET) predictions.

4.3.1 Physicochemical and ADMET Properties

Predicting physiochemical characteristics is crucial in determining drug-likeness, prioritizing potential drugs among a group of developed molecules, and eliminating substances that might be hazardous to human health or the environment. As illustrated in Table 4.3, physiochemical characteristics, such as Lipinski's Rule of 5 (RO5), which includes hydrogen bond acceptor (HBA), hydrogen bond donor (HBD), octanol-water partition coefficient (logP), molecular weight (MW), as well as non-rotational bonding (NRB) and total polar surface area (TPSA), can be generated with FAFDrug4. The term "RO5" refers to a set of parameters that, when combined, can be used to determine whether a certain drug candidate has problems with permeability and absorption (Fernandes et al. 2016; Lipinski et al. 1997). According to this rule, a compound cannot break more than one criterion: HBA ≤ 10, HBD ≤ 5, log P ≤ 5, and MW ≤ 500. All the proposed pyrano[2,3-*c*]pyrazole-4-aminoquinoline hybrid compounds (**24a-s**) violate RO5 (MW ≥ 500) (Table 4.3).

Additionally, the VEBER-based drug-likeness prediction stipulates that TPSA ≤140 and NRB ≤10 are necessary to pre-selection oral active compounds. Furthermore, the EGAN rule-based prediction of oral bioavailability listed the following criteria: (a) good bioavailability for drugs with -1 ≥ log P ≤ 6 and 0 ≥ TPSA ≤132 $Å^2$ (Craciun & Modra & Isvoran 2015) and (b) good orally available drugs with TPSA ≤130 $Å^2$, -1≤ log P ≤ 5.8, (Gurung & Bhattacharjee & Ali 2016). Table 4.4 illustrates the predicted oral bioavailability for all hybrid compounds (**24a-s**), which correlates with VEBER and EGAN rules.

Table 4.3 Physiochemical properties of hybrid compounds (**24a-s**)

Compound	MW (g/mol)	HBD	HBA	MLogP	RO5 violation	TPSA (Å)	NRB
24a	544.989	2	7	2.29	1	137.31	9
24b	530.962	3	7	2.09	1	148.31	8
24c	544.989	2	7	2.29	1	137.31	9
24d	559.015	2	7	2.48	1	137.31	10
24e	504.925	2	7	1.46	1	141.22	8
24f	514.962	2	6	2.49	1	128.08	8
24g	549.408	2	6	3.06	1	128.08	8
24h	593.859	2	6	3.15	1	128.08	8
24i	559.960	2	8	1.79	1	173.90	9
24j	559.960	2	8	1.79	1	173.90	9
24k	546.961	4	8	1.60	1	168.54	8
24l	520.990	2	6	2.23	1	156.32	8
24m	609.858	3	7	2.65	1	148.31	8
24n	539.972	2	7	1.95	1	151.87	8
24o	559.015	2	7	2.48	1	137.31	10
24p	558.972	3	8	2.00	1	165.38	9
24q	530.962	3	7	2.09	1	148.31	8
24r	581.021	3	7	2.69	1	148.31	8
24s	515.951	2	7	1.63	1	140.97	8

An additional factor that affects the prediction of optimal drug bioavailability is the carbon fraction sp^3 (Fsp^3). A molecule's spatial complexity and carbon saturation can be estimated using the percentage of sp^3-hybridized carbons (Fsp^3) about its overall carbon content (Lovering & Bikker & Humblet 2009). A drug candidate's clinical success rate is higher and its solubility is projected to be better with a higher Fsp^3 value (Wei et al. 2020). Unfortunately, very low solubility was predicted for all designed pyrano[2,3-*c*]pyrazole-4-aminoquinoline hybrid compounds. This could be solved by hydrolyzing the ester group to a carboxylic acid. Table 4.4 summarizes all proposed hybrid compounds' logS and Fsp^3 values (**24a-s**).

Predicting the viability and drug-likeness of therapeutic candidates during the early phases of drug discovery and development also relies extensively on *in silico* screening of ADMET characteristics. Since ADMET is frequently used to describe the

mechanisms of intestinal wall passage, intercompartmental movement, drug metabolism, excretion, and transport, as well as the pharmacokinetic characteristics of compounds, its properties help scientists understand the safety and efficacy aspects of a drug candidate (Doogue & Polasek 2013). Table 4.4 lists the anticipated ADMET characteristics of hybrid compounds (**24a-s**), such as protein plasma binding (PPB), inhibition of CYP2C19, blood-brain barrier (BBB), and inhibition of P-glycoprotein (PgP).

BBB is a significant factor frequently connected to the central nervous system (CNS)-based drug delivery pathway. To limit negative effects on the CNS, it makes sense that drugs that target the CNS would have a higher BBB penetration than those that target peripheral organs. Weak BBB absorption to the CNS <0.1, moderate BBB penetration to the CNS, 0.1 < BBB <2.0, and strong BBB penetration to the CNS >2.0, are the three categories into which BBB penetration falls (Jokipii et al. 1977). The entire hybrid compounds (**24a-s**), according to our data (Table 4.4), have a weak BBB penetration.

Furthermore, a CYP2C19 inhibitor should raise the drug's plasma levels because the CYP2C19 or cytochrome P450 enzyme metabolizes the drug in humans (Dean et al. 2012). CYP inhibitors such as felbamate and oxcarbazepine have been demonstrated in earlier research to be efficacious AEDs. Sixteen of the ninteen hybrid compounds are anticipated to be CYP2C19 inhibitors, indicating their potential as AEDs (Table 4.4). Consequently, assessing the inhibitory qualities of CYP2C19 is essential in the search for novel AED candidates.

PgP belongs to the ATP-binding cassette transporters (ABC) class, broadly dispersed in the intestinal epithelium and involved in the translocation of various of substances across cell membranes (Sonia & Sharma 2014). According to recent research, the endothelial cells of the BBB of epilepsy patients overexpress PgP. Several AEDs may be PgP substrates or inhibitors, according to certain studies, which raises the idea that PgP is a major factor in medication resistance in refractory epilepsy patients. Based on Table 4.4, all the hybrid compounds, except **24p**, were predicted to be PgP inhibitors, suggesting they could be effective AEDs.

On the other hand, when utilizing drugs that block transporters and metabolizing enzymes, which may cause an unpleasant reaction, PPB is helps estimate the quantity of a drug that is unbound per effective concentration (Bohnert & Gan 2013). PPB can be classified as (a) substances that are highly bound (PPB >90%) and (b) compounds that are weakly bound (PPB <90%). As shown in Table 4.3, every proposed hybrid compound, except **24k** and **24p**, exhibited a substantial binding affinity with protein plasma. More importantly, the *in silico* prediction revealed that all hybrid compounds (**24a-s**) are hepatotoxic (Table 4.4).

Table 4.4 Drug likeness and ADMET properties of hybrid compounds (**24a-s**)

	VEBER violation	**EGAN violation**	**LogS**	**Fsp^3**	**BBB**	**CYP2C19 inhibition**	**PgP inhibition**	**PPB**	**Hepatotoxicity**
24a	0	1	-6.15	0.21	-0.976	Inhibitor	Inhibitor	98.168	Toxic
24b	1	1	-5.94	0.19	-1.552	Inhibitor	Inhibitor	99.714	Toxic
24c	0	1	-6.15	0.21	-1.011	Inhibitor	Inhibitor	98.979	Toxic
24d	0	1	-6.40	0.24	-0.972	Inhibitor	Inhibitor	98.966	Toxic
24e	1	1	-5.44	0.20	-1.083	Inhibitor	Inhibitor	95.259	Toxic
24f	0	0	-6.07	0.19	-0.783	Inhibitor	Inhibitor	96.742	Toxic
24g	0	0	-6.67	0.19	-0.951	Inhibitor	Inhibitor	97.815	Toxic
24h	0	0	-6.99	0.19	-0.959	Inhibitor	Inhibitor	97.551	Toxic
24i	1	1	-6.15	0.19	-1.256	Inhibitor	Inhibitor	93.643	Toxic
24j	1	1	-6.15	0.19	-1.249	Inhibitor	Inhibitor	93.56	Toxic
24k	1	1	-5.80	0.19	-1.811	Non-inhibitor	Inhibitor	89.4	Toxic
24l	1	1	-5.93	0.20	-0.969	Inhibitor	Inhibitor	97.01	Toxic
24m	1	1	-6.86	0.19	-1.741	Inhibitor	Inhibitor	94.614	Toxic
24n	1	1	-6.03	0.18	-0.953	Inhibitor	Inhibitor	94.346	Toxic
24o	0	1	-6.40	0.24	-0.954	Inhibitor	Inhibitor	100	Toxic
24p	1	1	-5.95	0.18	-1.779	Non-inhibitor	Non-inhibitor	68.159	Toxic
24q	1	1	-5.94	0.18	-1.566	Inhibitor	Inhibitor	93.718	Toxic
24r	1	1	-7.07	0.16	-1.562	Non-inhibitor	Inhibitor	100	Toxic
24s	1	1	-5.43	0.19	-1.106	Inhibitor	Inhibitor	100	Toxic

4.3.2 Molecular Docking

In the context of drug discovery, molecular docking plays a vital role in the identification and optimization of lead compounds. By simulating the molecular interactions between ligands and proteins, docking studies identify of key binding residues and elucidate structural features essential for ligand recognition and binding (Muhammed & Aki-Yalcin 2024; Pinzi & Rastelli 2019). In this study, docking simulations were utilized to predict the binding orientations of chloroquine (CQ) and a series of 19 hybrid compounds within the cofactor binding site of the *Pf*LDH enzyme, contributing to an improved comprehension of their prospective pharmacological effects.

The molecular docking simulations unveiled a spectrum of binding energies and distinct conformations for CQ and various hybrid compounds against the target protein, signifying diverse potential interactions. A molecular docking study shows that CQ manifested a moderate affinity towards *Pf*LDH enzyme, with a binding energy of -5.68 kcal/mol. It displayed versatility in binding, adopting 12 distinct conformations across the docking process (Figure 4.5), and indicative of its adaptability to different regions within the protein's active site. In contrast, the hybrid compounds exhibited a greater diversity, forming over 28 distinct clusters, as illustrated in (Figure 4.5). These clusters displayed various binding energies, containing fewer ligand conformations (<23). Notably, compounds **24a-s** had a disparity between the cluster with the lowest binding energy and the most populated cluster, indicating that the most energetically favourable ligand configuration did not prevail throughout the simulations.

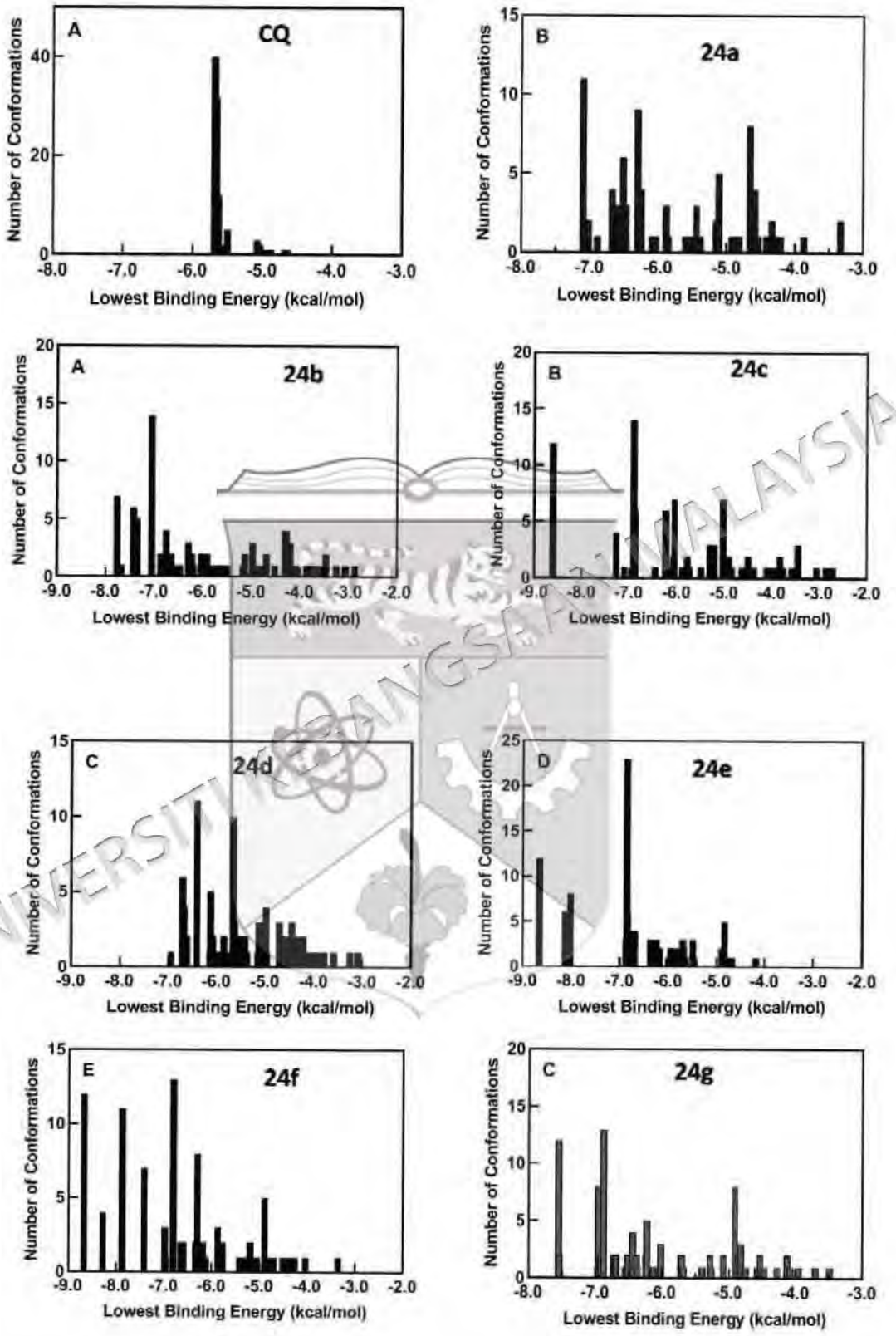

To be continued…

Continuation…

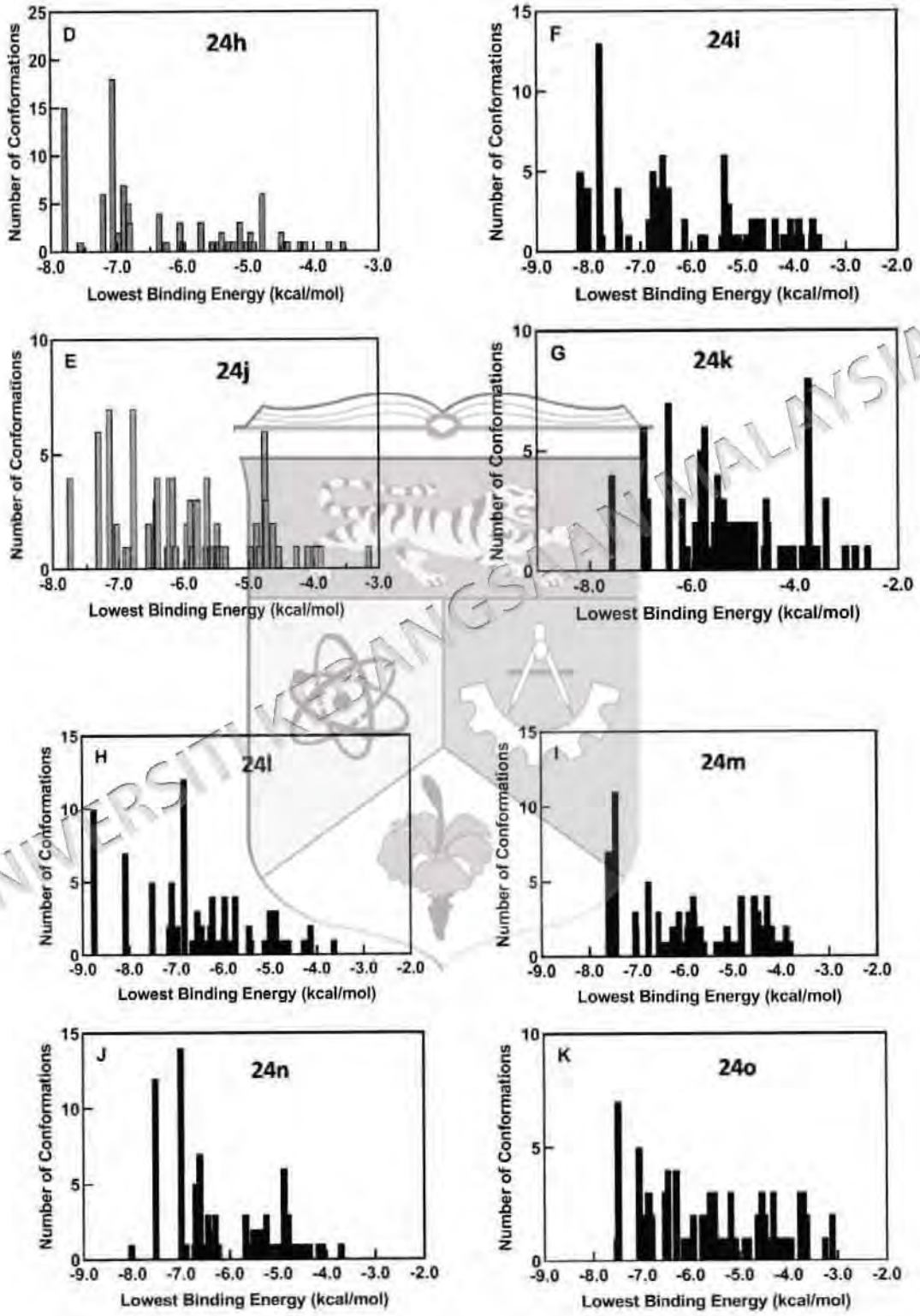

To be continued...

Continuation...

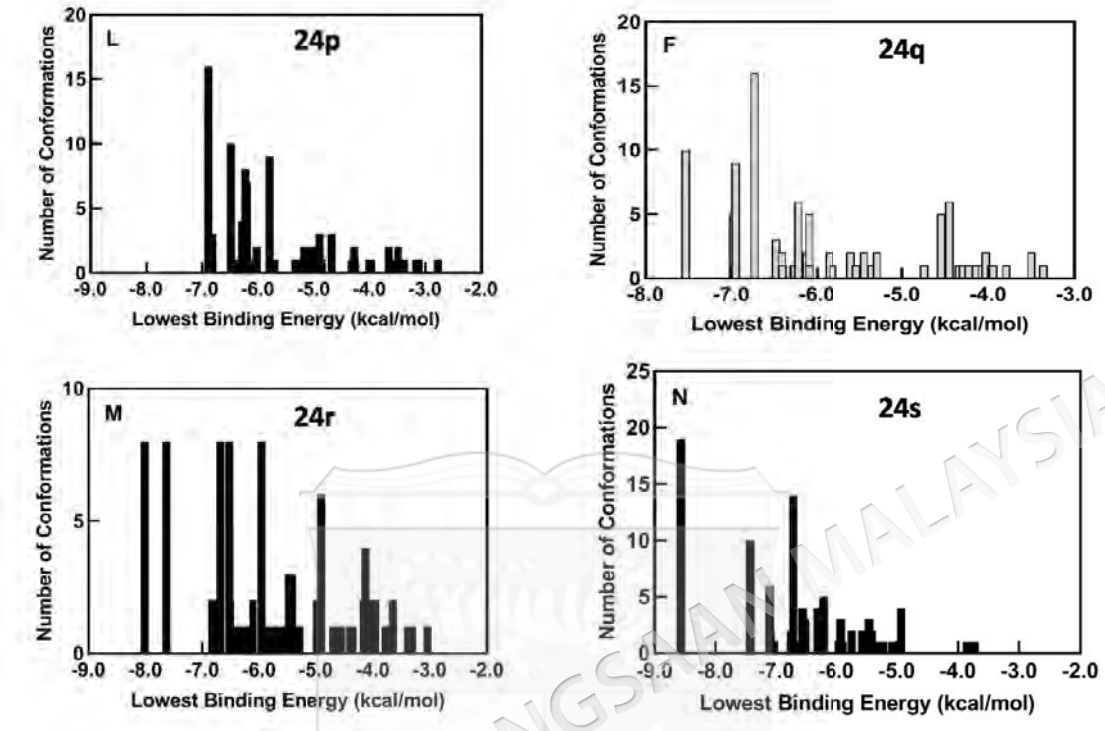

Figure 4.5 Cluster analysis of the docking of CQ and (F) **24a-s** to the cofactor binding site of *Pf*LDH (1CET), with outcomes generated from a total of 100 runs

The most stable ligand–*Pf*LDH complex for the above nineteen compounds was then visualized and further examined employing BIOVIA Discovery Studio Visualizer to determine the intermolecular interaction involved in the complexation (Table 4.5). The *Pf*LDH enzyme features a critical cofactor binding pocket encompassing key amino acid residues such as Val-26, Phe-52, Ile-54, Ala-98, Phe-100, Ile-119, and Glu-122 (Read et al. 1999, Zakaria & Lam & Hassan 2020).

Table 4.5 Intermolecular forces involved in the interactions of *Pf*LDH (1CET) with CQ and the hybrids **24a-s**

Compound	Binding energy (kcal/mol)	Type of interaction	Bond type	Interacting residues
CQ	-5.68	Hydrogen bond	Conventional	Glu-122
		Hydrophobic interaction	π-σ	Ile-54, Ala-98, Ile-119
			Alkyl	Ala-98, Ile-119
			π-alkyl	Val-26, Phe-52, Tyr-85, Lys-118
		Van der Waals forces		Gly-27, Asp-53, Phe-100, Ile-123

To be continued…

Continuation…

24a	-7.10	Hydrogen bond	Conventional	Tyr-85
		Hydrophobic interaction	π-σ	Ile-119
			π-π T-shaped	Phe-100
			Alkyl	Ile-54, Phe-100
			π-alkyl	Ile-54, Phe-100, Leu-115, Lys-118
		Electrostatic interaction	π-anion	Glu-122
		Van der Waals forces		Val-26, Asp53, Ala-98, Ile123
24b	-7.76	Hydrogen bond	Conventional	Tyr-85, Leu-115, Lys-118, Glu-122
		Hydrophobic interaction	π-σ	Ala-98
			π-alkyl	Ile-54, Phe-100, Leu-115, Lys-118
		Electrostatic interaction	π-anion	Asp-53, Glu-122
		Van der Waals forces		Gly-27, Phe-52, Phe-100, Asn-116, Ile123
24c	-8.60	Hydrogen bond	Conventional	Tyr-85, Glu-122
			Carbon	Ile-119
		Hydrophobic interaction	π-σ	Ala-98
			π-alkyl	Val-26, Ile-54, Leu-115, Lys-118, Ile-119
		Electrostatic interaction	π-anion	Glu-122
		Van der Waals forces		Gly-27, Phe-52, Asp-53, Phe-100, Ile-123
24d	-6.94	Hydrogen bond	Conventional	Glu-122
		Hydrophobic interaction	π-σ	Phe-100
			π-π T-shaped	Tyr-85
			Alkyl	Ile-54, Phe-100, Leu-115, His-126
			π-alkyl	Ile-54, Lys-118. Ile-119
		Electrostatic interaction	π-anion	Glu-122
		Van der Waals forces		Phe-52, Asn-83, Thr-84
24e	-8.66	Hydrogen bond	Conventional	Tyr-85, Glu-122
			Carbon	Ile-119
		Hydrophobic interaction	π-σ	Ile-54, Ala-98
			π-π T-shaped	Phe-100
			Alkyl	Lys-118
			π-alkyl	Ile-54, Leu-115, Lys-118, Ile-119
		Van der Waals forces		Val-26, Gly-27, Phe-52, Ile-119, Ile-123
24f	-8.67	Hydrogen bond	Conventional	Tyr-85
		Hydrophobic interaction	π-σ	Ala-98
			π-π T-shaped	Phe-100
			Alkyl	Lys-118
			π-alkyl	Ile-54, Leu-115, Lys-118, Ile-119

To be continued…

Continuation…

		Van der Waals forces		Val-26, Gly-27, Phe-52, Asp-53, Glu-122, Ile-123
24g	-7.55	Hydrogen bond	Conventional	Tyr-85
			Carbon	Asp-53
		Hydrophobic interaction	π-σ	Ile-119
			Alkyl	Ile-54, Phe-100, Leu-115, Lys-118, Ile-119
			π-alkyl	Ile-54, Lys-118, Ile-119
		Electrostatic interaction	π-anion	Glu-122
		Van der Waals forces		Val-26, Ala-98, Leu-115, Ile-123
24h	-7.79	Hydrogen bond	Conventional	Tyr-85
			Carbon	Asp-53
		Hydrophobic interaction	π-σ	Ile-119
			Alkyl	Ile-54, Phe-100, Leu-115, Ile-119
			π-alkyl	Ile-54, Leu-115, Lys-118
		Electrostatic interaction	π-anion	Glu-122
			π-cation	Lys-118
		Van der Waals forces		Val-26, Ala-98, Ile-123
24i	-8.16	Hydrogen bond	Conventional	Gly-27, Tyr-85, Leu-115, Glu-122
			Carbon	Glu-122
		Hydrophobic interaction	π-σ	Ile-54, Ala-98
			Alkyl	Ile-54
			π-alkyl	Val-26, Ile-54, Lys-118, Ile-119
		Electrostatic interaction	π-anion	Glu-122
		Van der Waals forces		Phe-52, Asp-53, Val-55, Phe-100, Asn-116, Ile-123
24j	-7.73	Hydrogen bond	Conventional	Gly-99, Lys-118, Glu-122 (2)
		Hydrophobic interaction	π-σ	Ile-119
			π-π T-shaped	Phe-100
			Alkyl	Ile-54, Tyr-85, Ala-98, Phe-100, Leu-115, Ile-119, Ile-123
			π-alkyl	Ile-54, Ala-98, Phe-100
		Van der Waals forces		Phe-52
24k	-7.56	Hydrogen bond	Conventional	Asp-53, Gly-99, Tyr-85
			Carbon	Asp-53
		Hydrophobic interaction	π-σ	Ile-119
			Alkyl	Phe-100, Ile-115
			π-alkyl	Ile-54, Ala-98, Leu-115, Lys-118, Ile-119
		Van der Waals forces		Val-26, Gly-27, Phe-52, Val-55, Glu-122, Ile-123
24l	-8.75	Hydrogen bond	Conventional	Tyr-85
			Carbon	Phe-52, Ile-119

To be continued…

Continuation…

		Hydrophobic interaction	π-σ	Ala-98
			π-sulfur	Phe-100
			π-π T-shaped	Phe-100
			Alkyl	Lys-118
			π-alkyl	Ile-54, Leu-115, Lys-118. Ile-119
		Electrostatic interaction	π-anion	Glu-122
		Van der Waals forces		Val-26, Gly-27, Asp-53, Ile-123
24m	-7.60	Hydrogen bond	Conventional Carbon	Tyr-85, Gly-99 Asp-53
		Hydrophobic interaction	π-σ	Ile-119
			Alkyl	Ile-54, Phe-100, Ile-115
			π-alkyl	Ile-54, Ala-98, Phe-100, Leu-115, Lys-118, Ile-119
		Van der Waals forces		Val-26, Gly-27, Phe-52, Ile-123
24n	-8.02	Hydrogen bond	Conventional Carbon	Tyr-85, Lys-118, Glu-122 Leu-115, Glu-122
		Hydrophobic interaction	π-σ	Ile-54, Ala-98
			Alkyl	Phe-100, Lys-118
			π-alkyl	Ile-54, Lys-118, Ile-119
		Electrostatic interaction	π-anion	Asp-53
		Van der Waals forces		Val-26, Gly-27, Phe-52, Ile-123
24o	-7.52	Hydrogen bond	Carbon	Ile-119
		Hydrophobic interaction	π-σ	Ala-98
			π-π T-shaped	Phe-100
			Alkyl	Ala-98, Lys-118
			π-alkyl	Ile-54, Ala-98, Leu-115, Lys-118. Ile-119
		Electrostatic interaction	π-anion	Asp-53, Glu-122
		Van der Waals forces		Gly-27, Ser-28, Phe-52, Tyr-85
24p	-6.89	Hydrogen bond	Conventional	Tyr-85, Glu-122
		Hydrophobic interaction	π-σ	Ile-119
			Alkyl	Val-26, Phe-52, Ile-54, Lys-118
			π-alkyl	Phe-52, Ile-54
		Electrostatic interaction	π-anion	Glu-122
		Van der Waals forces		Gly-27, Asp-53, Asn-83, Phe-100, Leu-115, Ile-123, His-126
24q	-7.53	Hydrogen bond	Conventional Carbon	Tyr-85, Leu-115 Glu-122
		Hydrophobic interaction	π-σ	Ala-98
			π-πT-shaped	Phe-100
			Alkyl	Ile-54
			π-alkyl	Ile-54, Leu-115, Lys-118, Ile-119

To be continued…

Continuation…

		Van der Waals forces		Val-26, Gly-27, Phe-52, Asp-53, Asn-116, Ile-123
24r	-8.01	Hydrogen bond	Conventional	Tyr-85, Glu-122
		Hydrophobic interaction	π-σ	Ile-54, Ala-98
			Alkyl	Phe-100, Leu-115
			π-alkyl	Ile-54, Lys-118, Ile-119
		Van der Waals forces		Val-26, Gly-27, Phe-52, Asp-53, Ile-123
24s	-8.57	Hydrogen bond	Conventional	Tyr-85
			Carbon	Glu-122
		Hydrophobic interaction	π-σ	Ala-98
			π-πT-shaped	Phe-100
			π-alkyl	Ile-54, Leu-115, Lys-118. Ile-119
		Electrostatic interaction	π-anion	Glu-122
		Van der Waals forces		Val-26, Gly-27, Phe-52, Asp-53, Ile-123

For the CQ–*Pf*LDH complex (Figure 4.6), the formation of only a single hydrogen bond with Glu-122 was predicted. Thus, the stability of the interaction is significantly contributed by the collective presence of the various hydrophobic forces listed in Table 4.5. The π-σ interactions involved the association between the π electrons of CQ and the σ electrons of carbon-hydrogen (C-H) bonds in Ile-54, Ala-98, and Ile-119. Further, alkyl and π-alkyl interactions encompassed the nonpolar hydrophobic contacts between CQ and the alkyl groups of the amino acid residues at the binding site (Gómez-Jeria et al. 2020). Additionally, Van der Waals forces also partially contributed towards enhancing the stability of the complex.

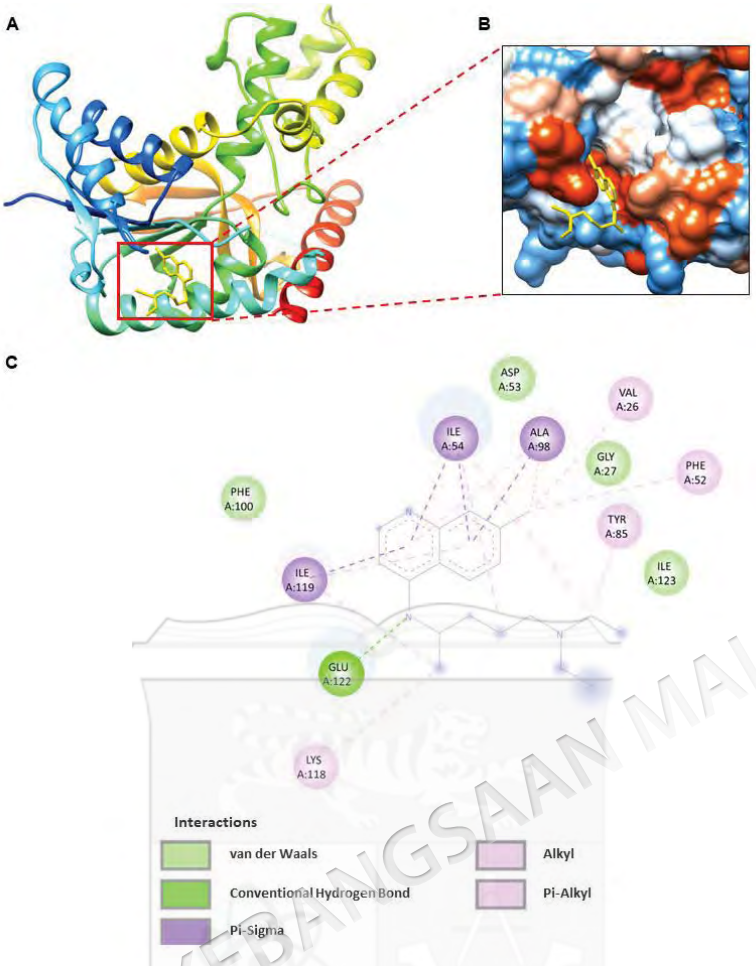

Figure 4.6 (A) Predicted orientation of the lower binding energy (–5.68 kcal/mol) conformation of CQ (rendered in ball and stick) on the *Pf*LDH enzyme. (B) Zoomed-in view of the cofactor binding site. (C) Schematic diagram of the intermolecular forces involved in the *Pf*LDH –CQ interaction

Among the hybrid compounds examined, **24l** exhibited the lowest binding energy with a remarkable value of -8.75 kcal/mol (Figure 4.7). Firstly, conventional hydrogen bonds formed with Tyr-85 are crucial in stabilizing the complex by facilitating direct interactions between hydrogen and oxygen atoms. Carbon hydrogen bonds with Phe-52 and Ile-119 also contribute to the binding by forming stabilizing interactions between carbon and hydrogen atoms. Hydrophobic interactions, including π-σ Ala-98, π-sulfur with Phe-100, and π-π T-shaped with Phe-100, enhance the stability of the complex by promoting interactions between hydrophobic regions of the ligand and protein. Alkyl interactions with Lys-118 and π-alkyl interactions involving Ile-54, Leu-115, and Ile-119 further contribute to the hydrophobic interactions, strengthening the binding affinity.

Compounds, an electrostatic interaction in the form of π-anion with Glu-122 enhances the stability of the complex through attraction between oppositely charged residues. Furthermore, van der Waals forces involving Val-26, Gly-27, Asp-53, and Ile-123 provide additional stabilization by promoting interactions between non-polar groups. Compared to other hybrid compounds and CQ, **24l** exhibits all types of interactions and uniquely features a π-sulfur interaction, absent in other compounds. This distinctive interaction likely contributes significantly to its highest binding energy with *Pf*LDH.

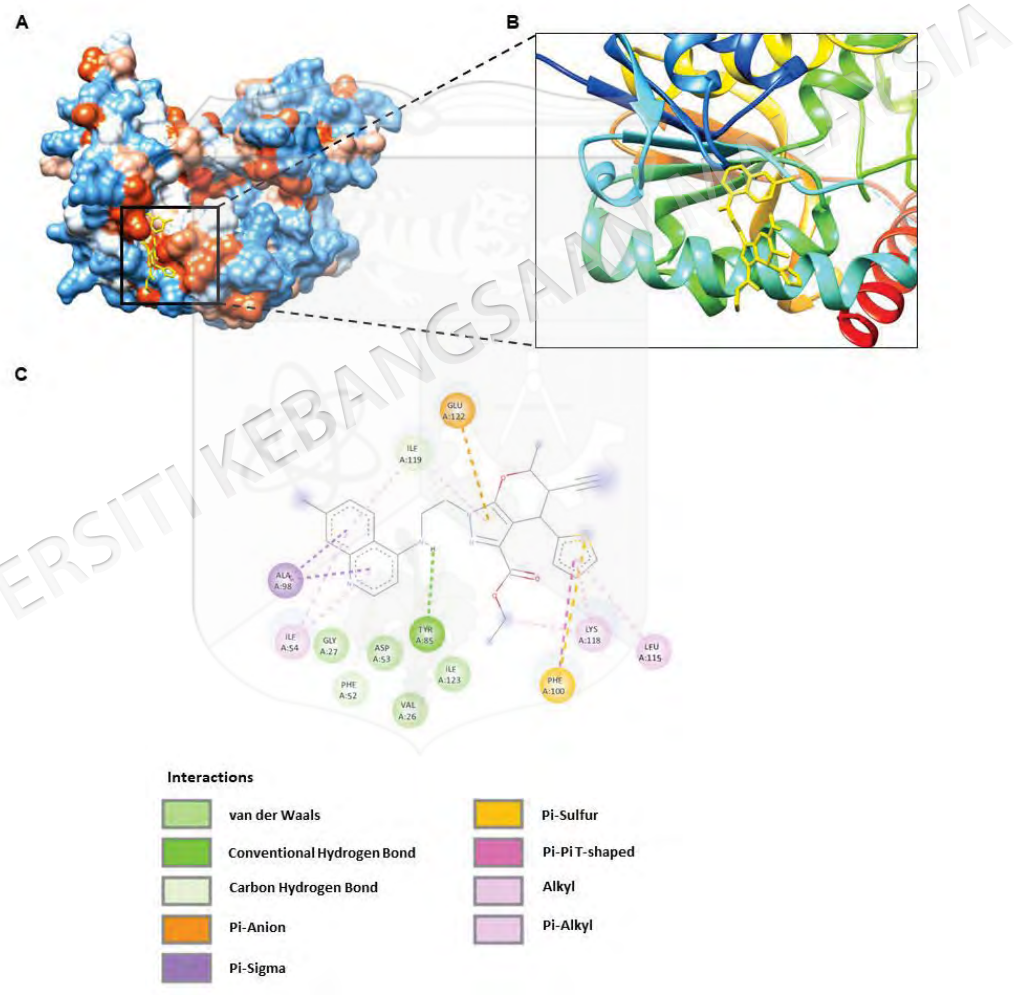

Figure 4.7 (A) Predicted orientation of the lowest docking energy (–8.75 kcal/mol) conformation of **24l** on the *Pf*LDH enzyme as depicted via a 3D hydrophobicity surface representation. (B) Close-up view of the binding site. (C) Schematic diagram of the intermolecular forces involved in the *Pf*LDH –**24l** interaction

Moreover, **24c**, **24e**, **24f**, and **24s** demonstrated notable binding energies ranging from -8.57 to -8.67 kcal/mol, indicating a strong affinity for *Pf*LDH (Figures 4.8-4.11).

They exhibited varying numbers of distinct conformations (28 to 40) (Figure 4.5), suggesting their versatility in adopting multiple binding modes within the protein's active site. These compounds engage in diverse interactions with specific amino acid residues of *Pf*LDH. They include conventional hydrogen bonds with Tyr-85 and Glu-122 and carbon-hydrogen bonds with Phe-52 and Ile-119. Additionally, hydrophobic interactions, such as π-σ interactions with Ala-98, π-π T-shaped interactions with Phe-100, and alkyl interactions with Lys-118 and Ile-119, play crucial roles in stabilizing the protein-ligand complex. Furthermore, electrostatic interactions involving π-anion interactions with Glu-122 and van der Waals forces with Gly-27, Phe-52, Asp-53, and Ile-123 were noted. As the other hybrids, alkyl and π-alkyl interactions play pivotal roles in stabilizing the **24c**, **24e**, **24f**, and **24s**-*Pf*LDH complex.

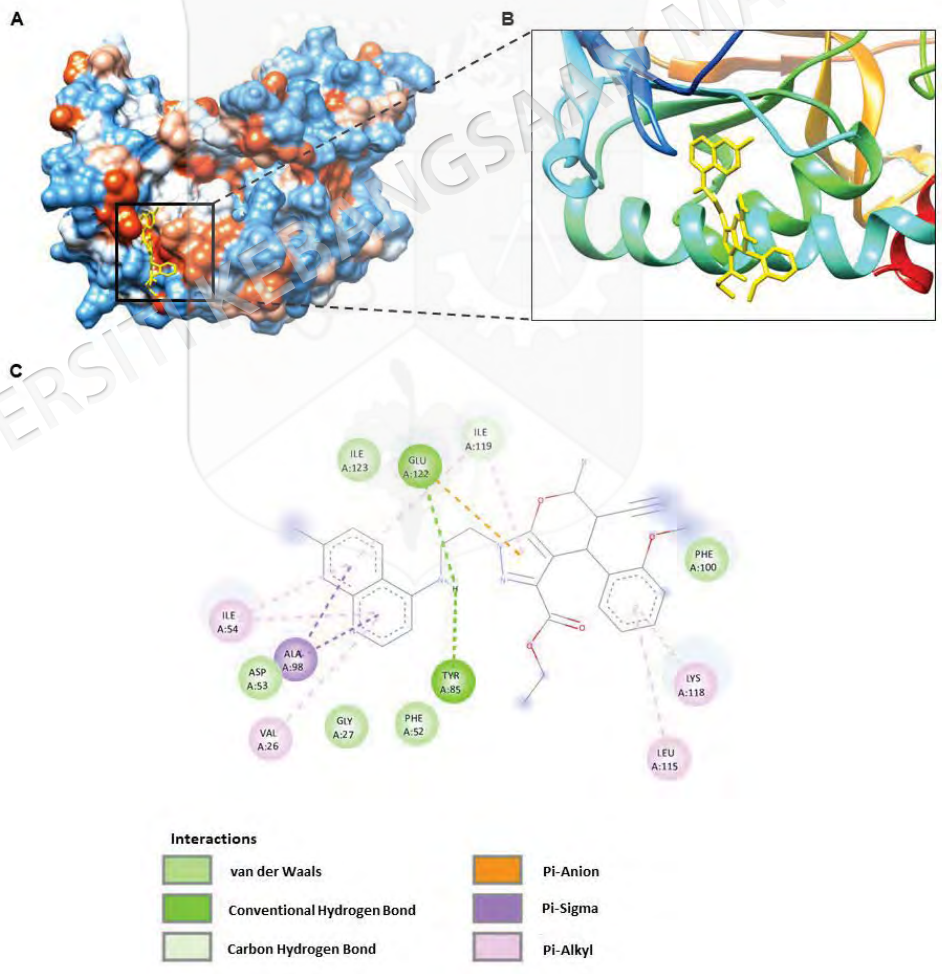

Figure 4.8 (A) Predicted orientation of the lowest docking energy (–8.60 kcal/mol) conformation of **24c** on the *Pf*LDH enzyme as depicted via a 3D hydrophobicity surface representation. (B) Close-up view of the binding site. (C) Schematic diagram of the intermolecular forces involved in the *Pf*LDH –**24c** interaction

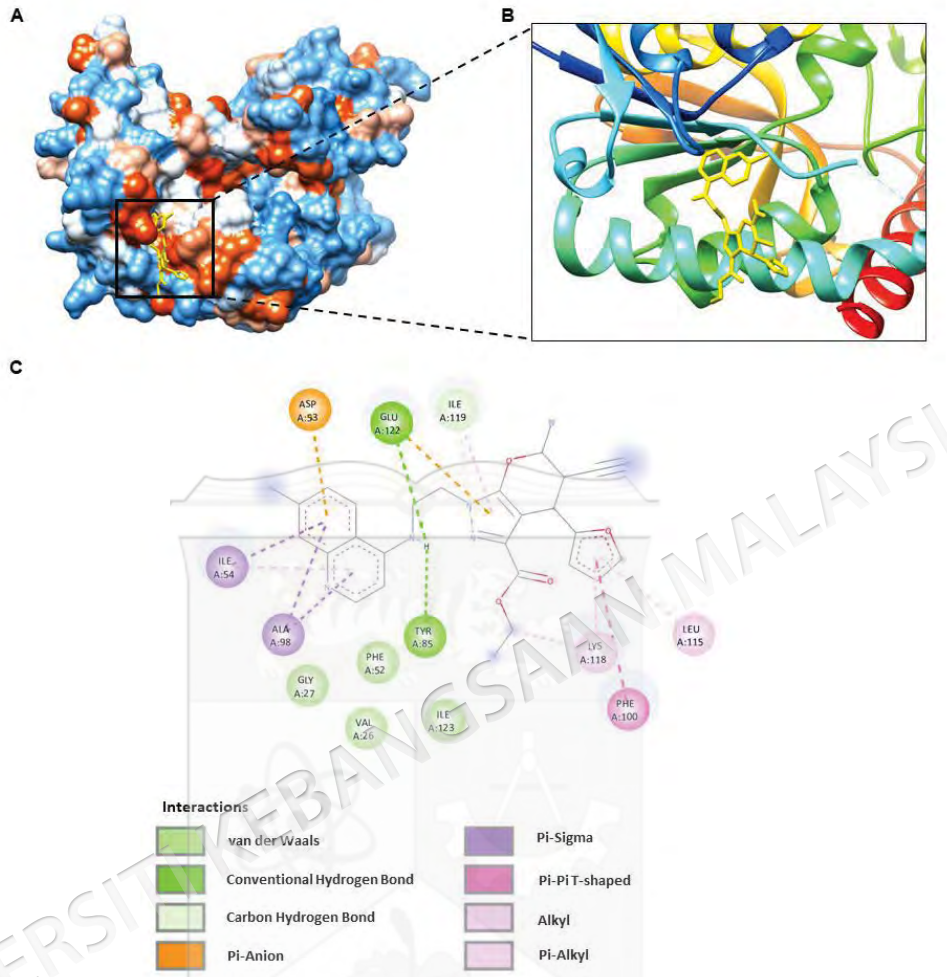

Figure 4.9 (A) Predicted orientation of the lowest docking energy (–8.66 kcal/mol) conformation of **24e** on the *Pf*LDH enzyme as depicted via a 3D hydrophobicity surface representation. (B) Close-up view of the binding site. (C) Schematic diagram of the intermolecular forces involved in the *Pf*LDH –**24e** interaction

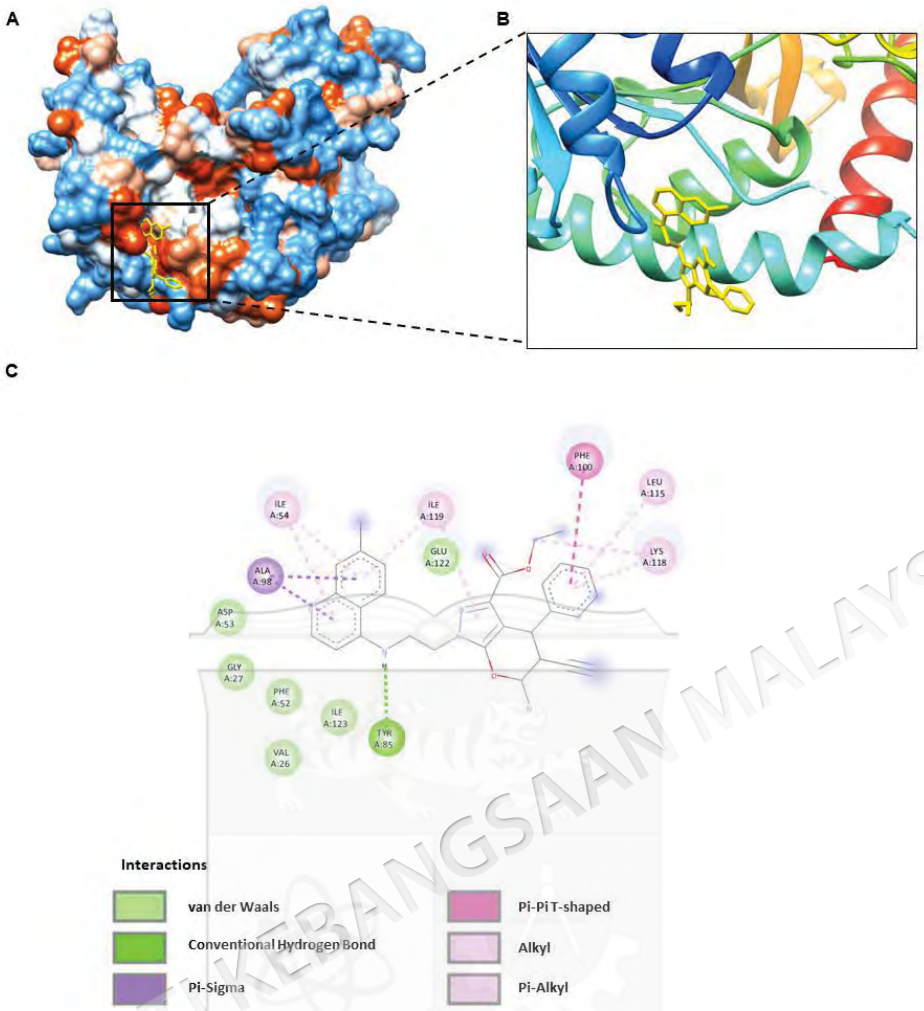

Figure 4.10 (A) Predicted orientation of the lowest docking energy (–8.67 kcal/mol) conformation of **24f** on the *Pf*LDH enzyme as depicted via a 3D hydrophobicity surface representation. (B) Close-up view of the binding site. (C) Schematic diagram of the intermolecular forces involved in the *Pf*LDH –**24f** interaction

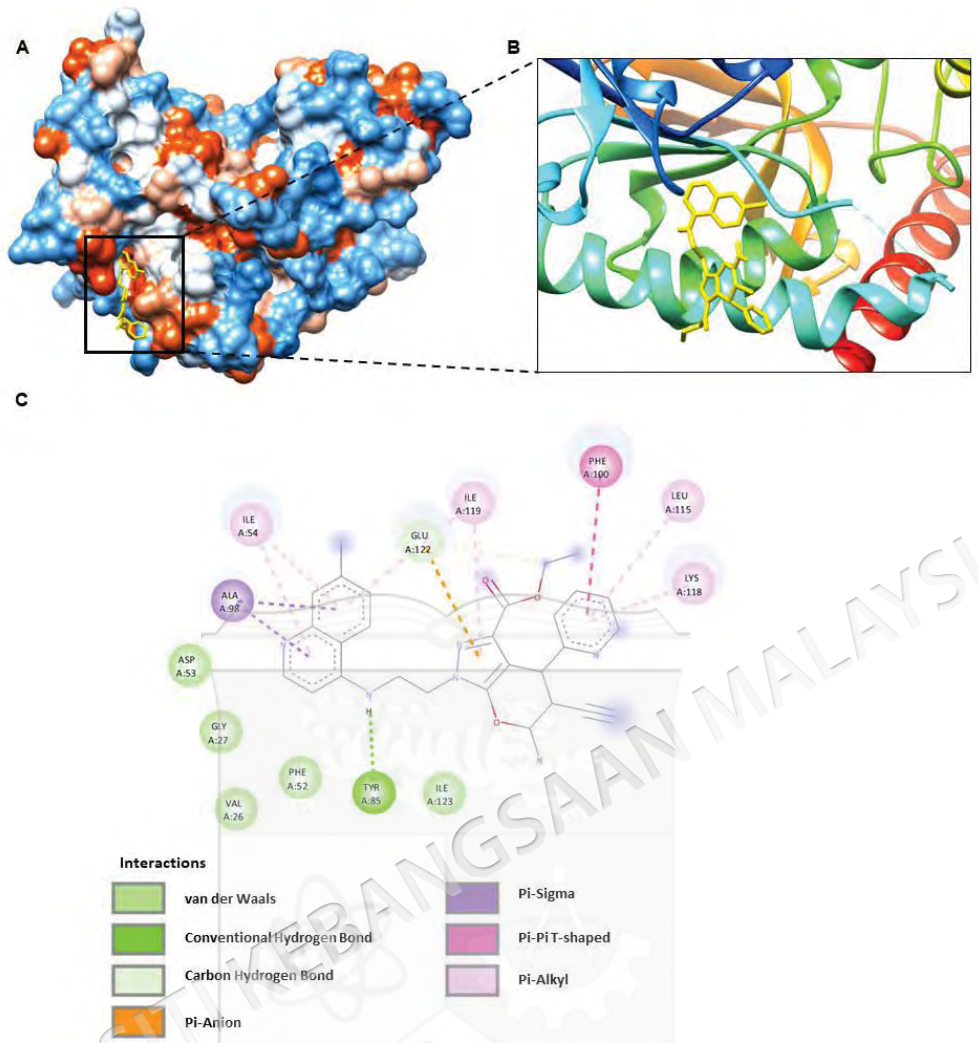

Figure 4.11 (A) Predicted orientation of the lowest docking energy (–8.57 kcal/mol) conformation of **24s** on the *Pf*LDH enzyme as depicted via a 3D hydrophobicity surface representation. (B) Close-up view of the binding site. (C) Schematic diagram of the intermolecular forces involved in the *Pf*LDH –**24s** interaction

On the other hand, **24p** exhibited the weakest binding energy with *Pf*LDH among the compounds, with a binding energy of -6.89 kcal/mol (Figure 4.12). Despite its weaker binding affinity compared to other compounds, **24p** still interacted with *Pf*LDH through various interaction types, including hydrogen bonds, hydrophobic interactions, alkyl interactions, electrostatic interactions, and van der Waals forces. These interactions primarily involved residues Tyr-85, Glu-122, Ala-98, Val-26, Phe-52, Ile-54, Lys-118, and Ile-123. Although **24p** displayed lower binding energy, multiple interaction types suggest potential binding flexibility and the ability to form stable complexes with *Pf*LDH. Further optimization of **24p** or exploration of its

structural derivatives may enhance its binding affinity and efficacy as an antimalarial agent.

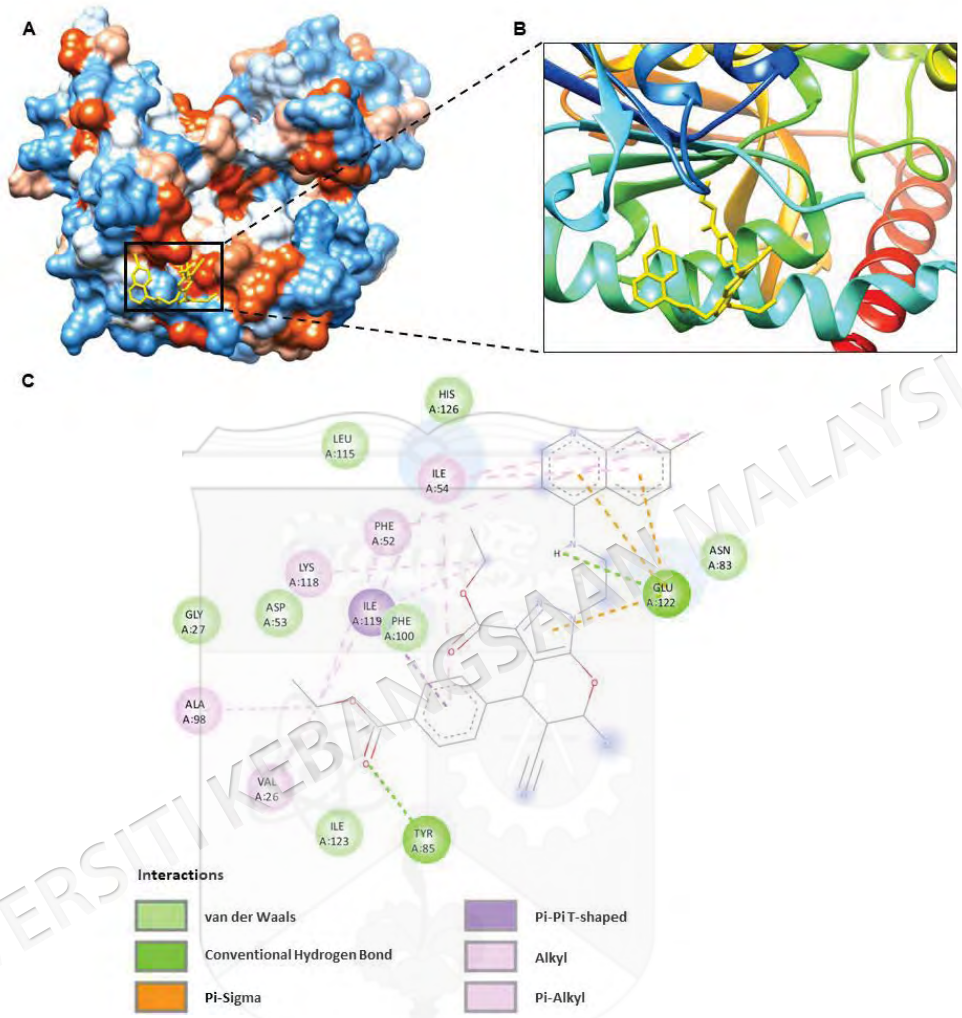

Figure 4.12 (A) Predicted orientation of the lowest docking energy (–6.89 kcal/mol) conformation of **24p** on the *Pf*LDH enzyme as depicted via a 3D hydrophobicity surface representation. (B) Close-up view of the binding site. (C) Schematic diagram of the intermolecular forces involved in the *Pf*LDH –**24p** interaction

While the rest of the hybrid compounds (**24a-b**, **24d**, **24g-k**, **24m-o**, **24q**, and **24r**) exhibited relatively higher (less negative) binding energies than **24c, 24e, 24f, 24l,** and **24s**, they still demonstrated favourable interactions with *Pf*LDH (Figures 4.13–4.25). Hydrogen bonds, hydrophobic contacts, electrostatic interactions, and van der Waals forces all contributed to the stability of the docked conformers. However, the absence of certain key interactions as observed in **24c, 24e, 24f, 24l,** and **24s** may explain the slightly increased binding energies.

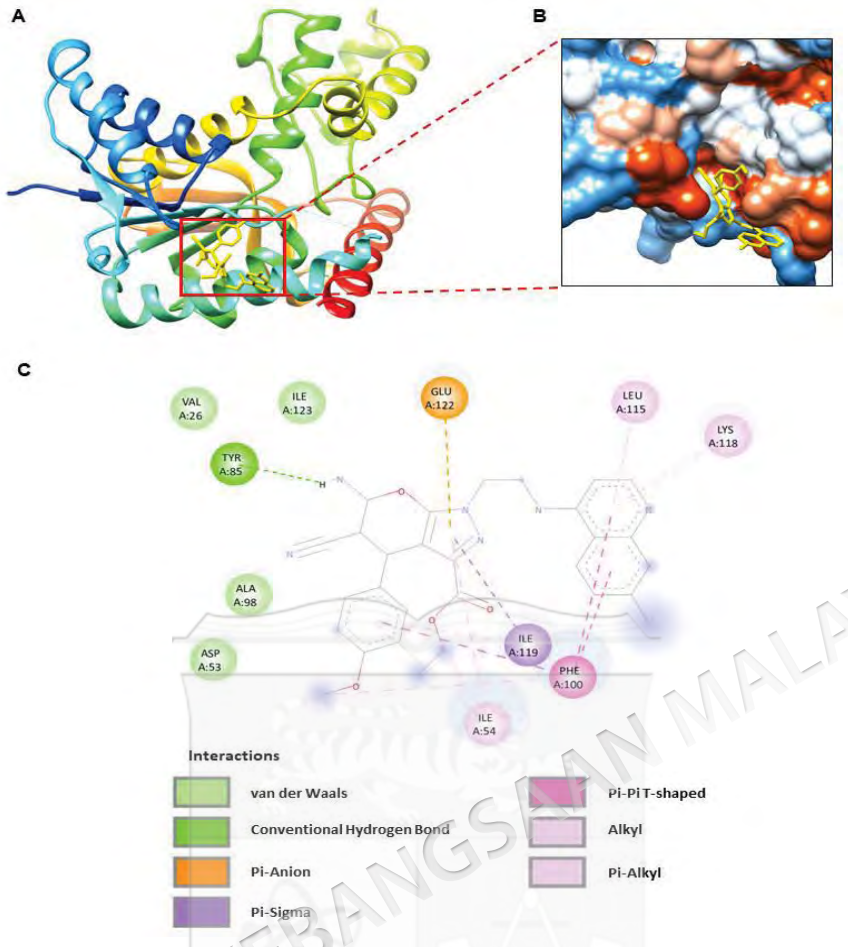

Figure 4.13 (A) Predicted orientation of the lowest docking energy (–7.10kcal/mol) conformation of **24a** (rendered in ball and stick) on the *Pf*LDH enzyme. (B) Zoomed-in view of the cofactor binding site. (C) Schematic diagram of the intermolecular forces involved in the *Pf*LDH –**24a** interaction

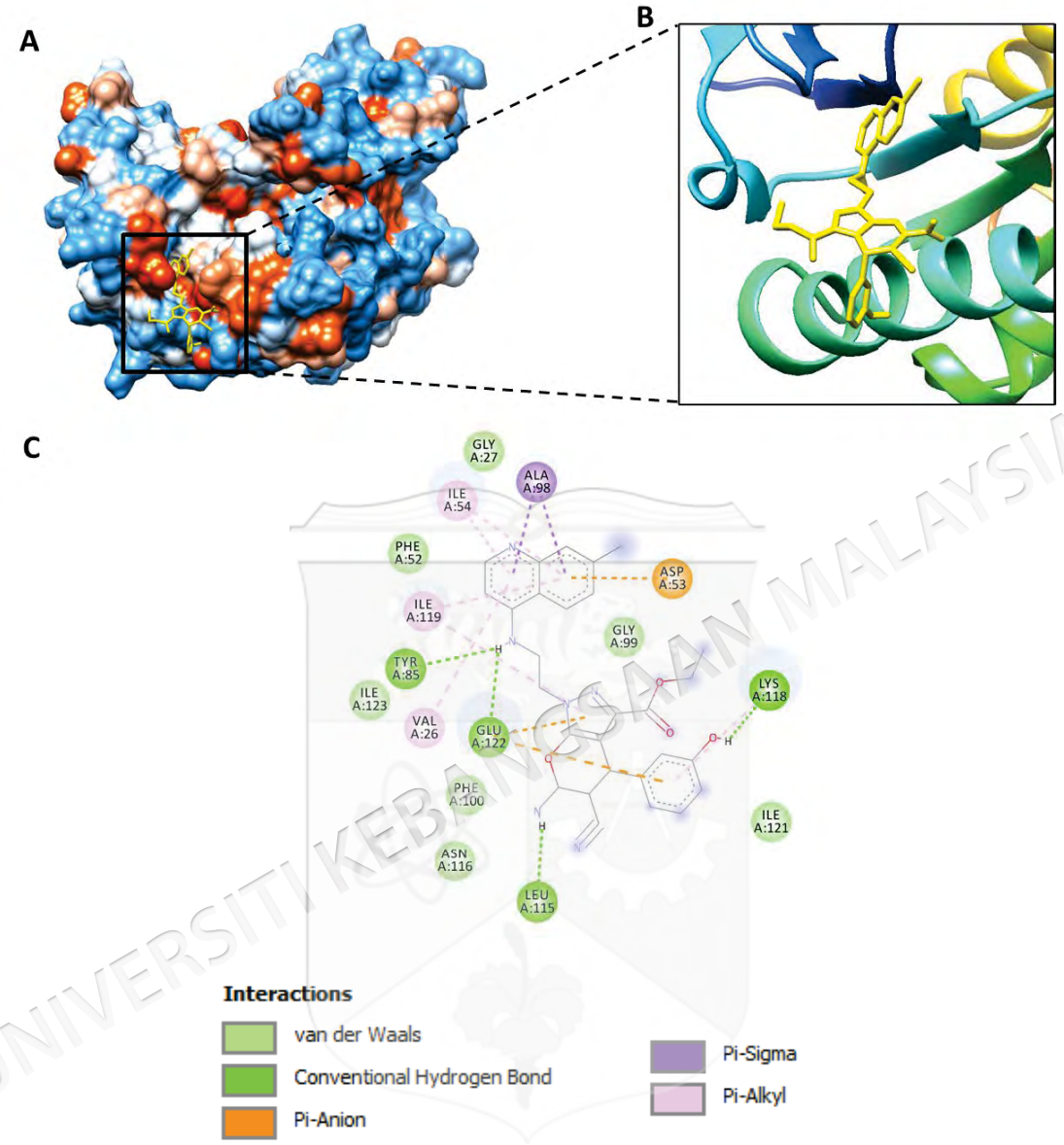

Figure 4.14 (A) Predicted orientation of the lowest docking energy (–7.76 kcal/mol) conformation of **24b** on the *Pf*LDH enzyme as depicted via a 3D hydrophobicity surface representation. (B) Close-up view of the binding site. (C) Schematic diagram of the intermolecular forces involved in the *Pf*LDH –**24b** interaction

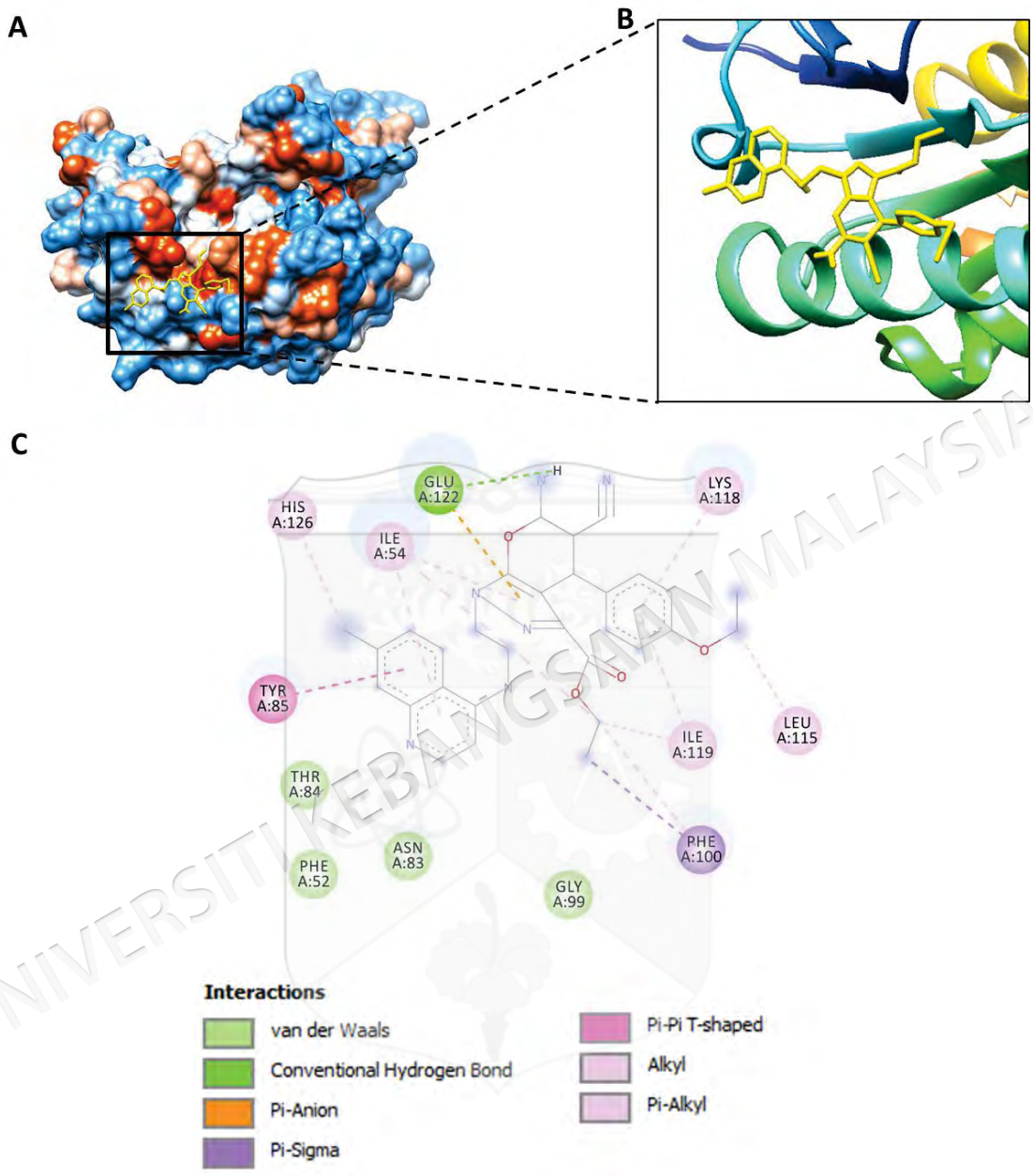

Figure 4.15 (A) Predicted orientation of the lowest docking energy (–6.94 kcal/mol) conformation of **24d** on the *Pf*LDH enzyme as depicted via a 3D hydrophobicity surface representation. (B) Close-up view of the binding site. (C) Schematic diagram of the intermolecular forces involved in the *Pf*LDH –**24d** interaction

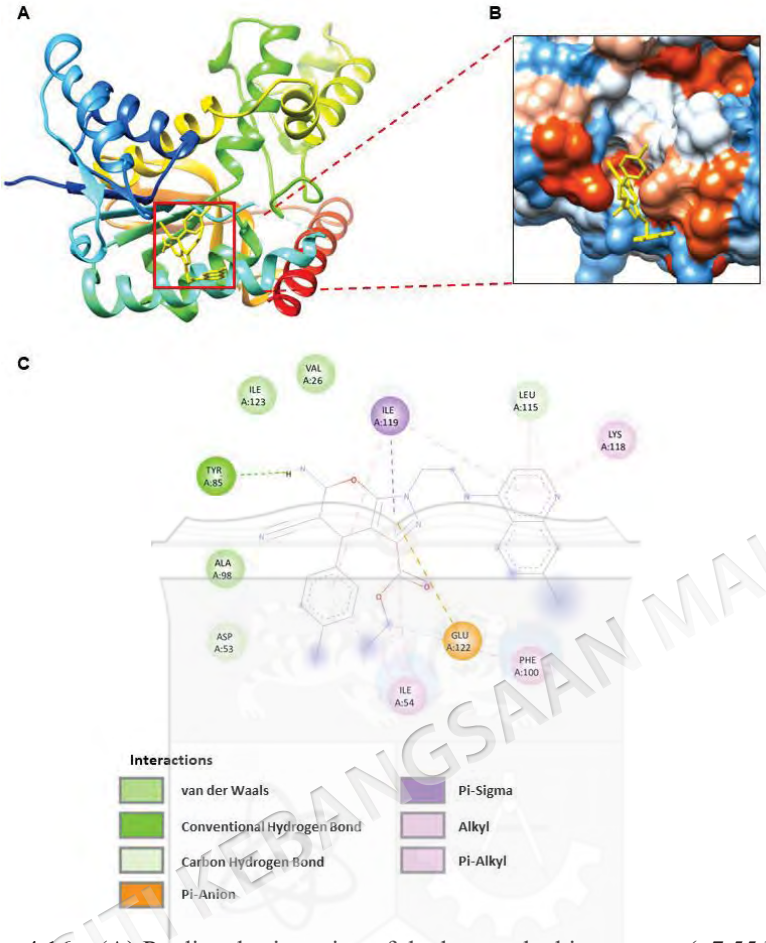

Figure 4.16 (A) Predicted orientation of the lowest docking energy (–7.55 kcal/mol) conformation of **24g** (rendered in ball and stick) on the *Pf*LDH enzyme. (B) Zoomed-in view of the cofactor binding site. (C) Schematic diagram of the intermolecular forces involved in the *Pf*LDH –**24g** interaction

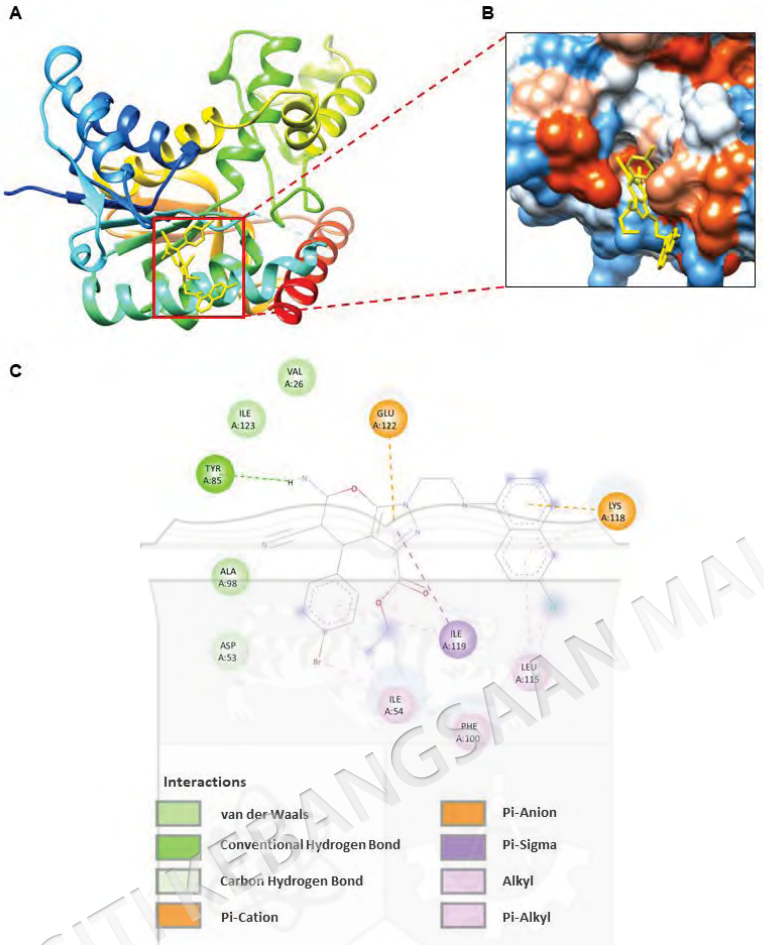

Figure 4.17 (A) Predicted orientation of the lowest docking energy (–7.79 kcal/mol) conformation of **24h** (rendered in ball and stick) on the *Pf*LDH enzyme. (B) Zoomed-in view of the cofactor binding site. (C) Schematic diagram of the intermolecular forces involved in the *Pf*LDH –**24h** interaction

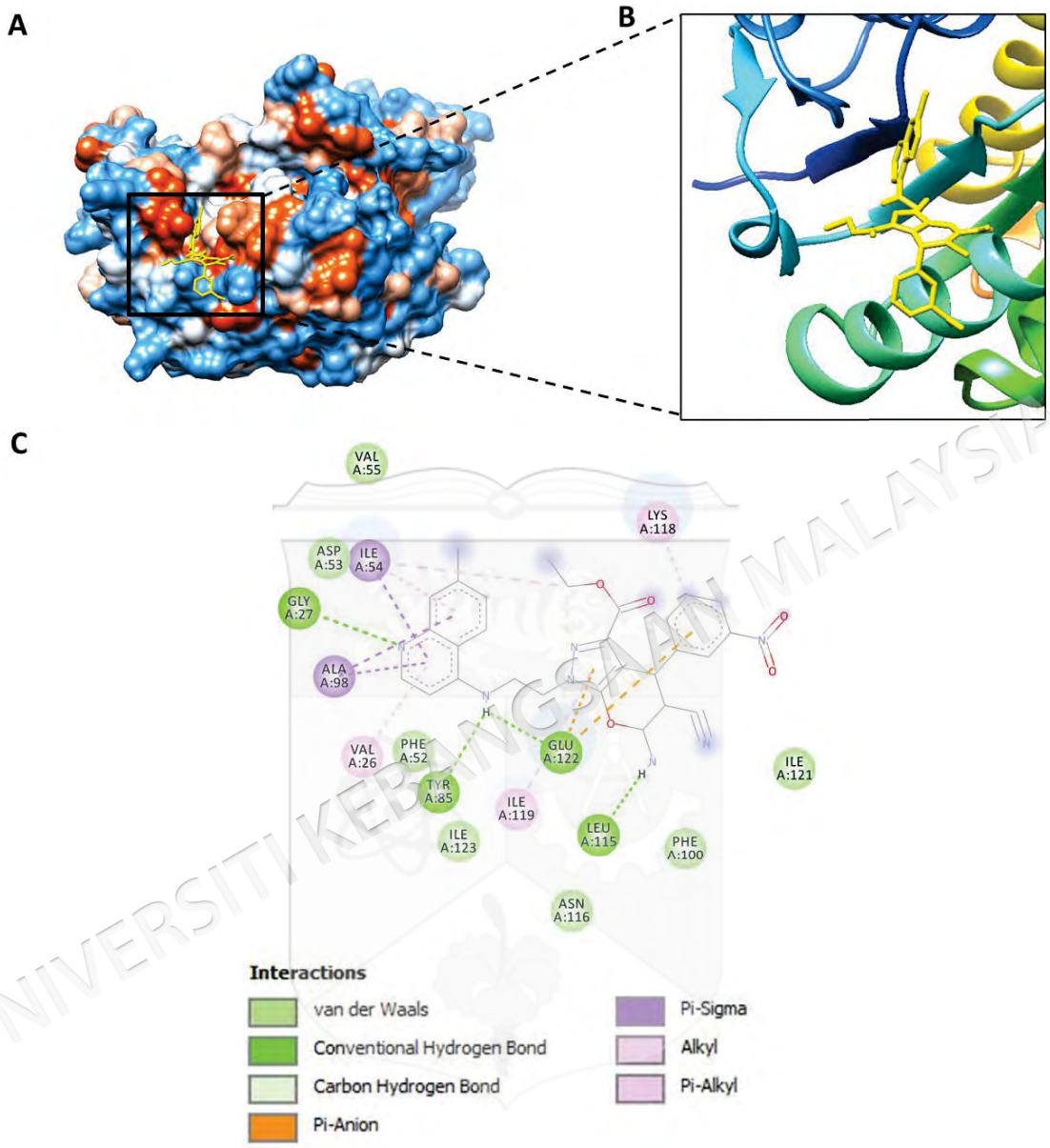

Figure 4.18 (A) Predicted orientation of the lowest docking energy (–8.16 kcal/mol) conformation of **24i** on the *Pf*LDH enzyme as depicted via a 3D hydrophobicity surface representation. (B) Close-up view of the binding site. (C) Schematic diagram of the intermolecular forces involved in the *Pf*LDH –**24i** interaction

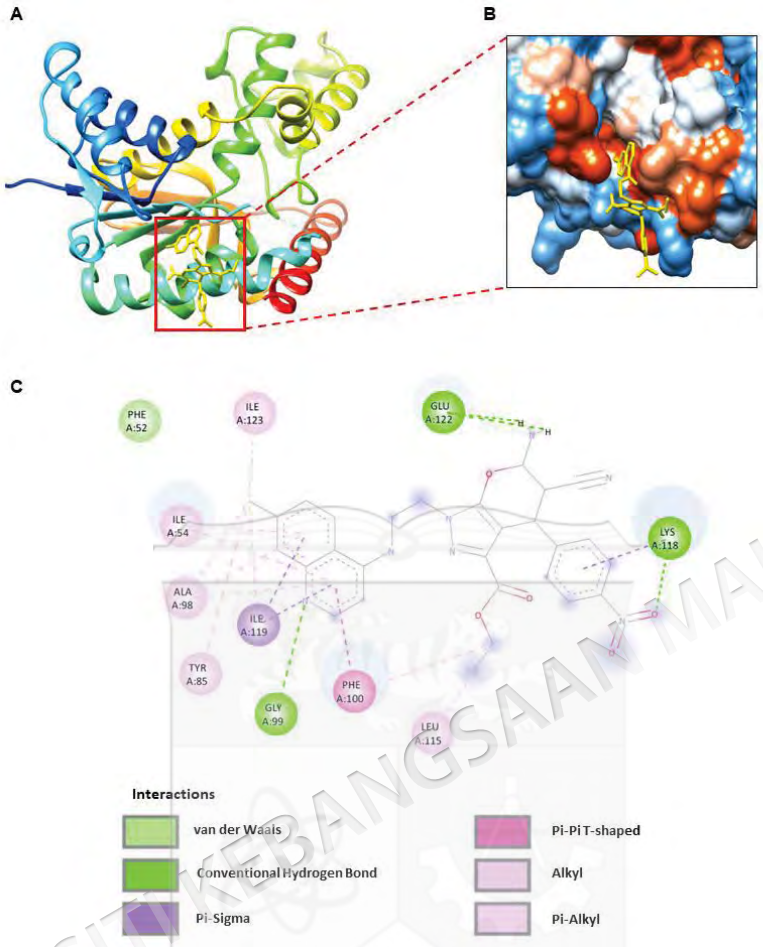

Figure 4.19 (A) Predicted orientation of the lowest docking energy (–7.73 kcal/mol) conformation of **24j** (rendered in ball and stick) on the *Pf*LDH enzyme. (B) Zoomed-in view of the cofactor binding site. (C) Schematic diagram of the intermolecular forces involved in the *Pf*LDH –**24j** interaction

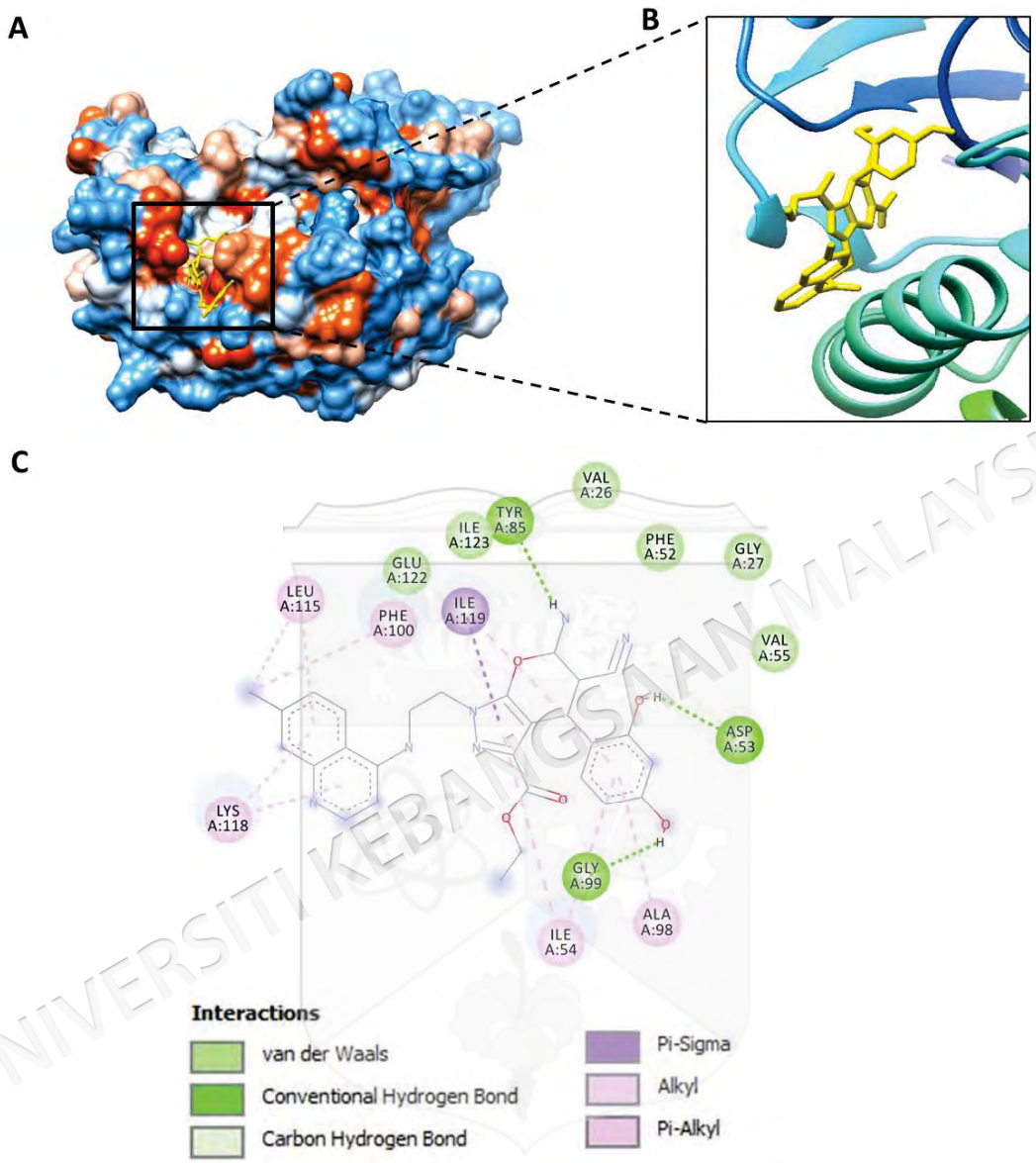

Figure 4.20 (A) Predicted orientation of the lowest docking energy (–7.56 kcal/mol) conformation of **24k** on the *Pf*LDH enzyme as depicted via a 3D hydrophobicity surface representation. (B) Close-up view of the binding site. (C) Schematic diagram of the intermolecular forces involved in the *Pf*LDH –**24k** interaction

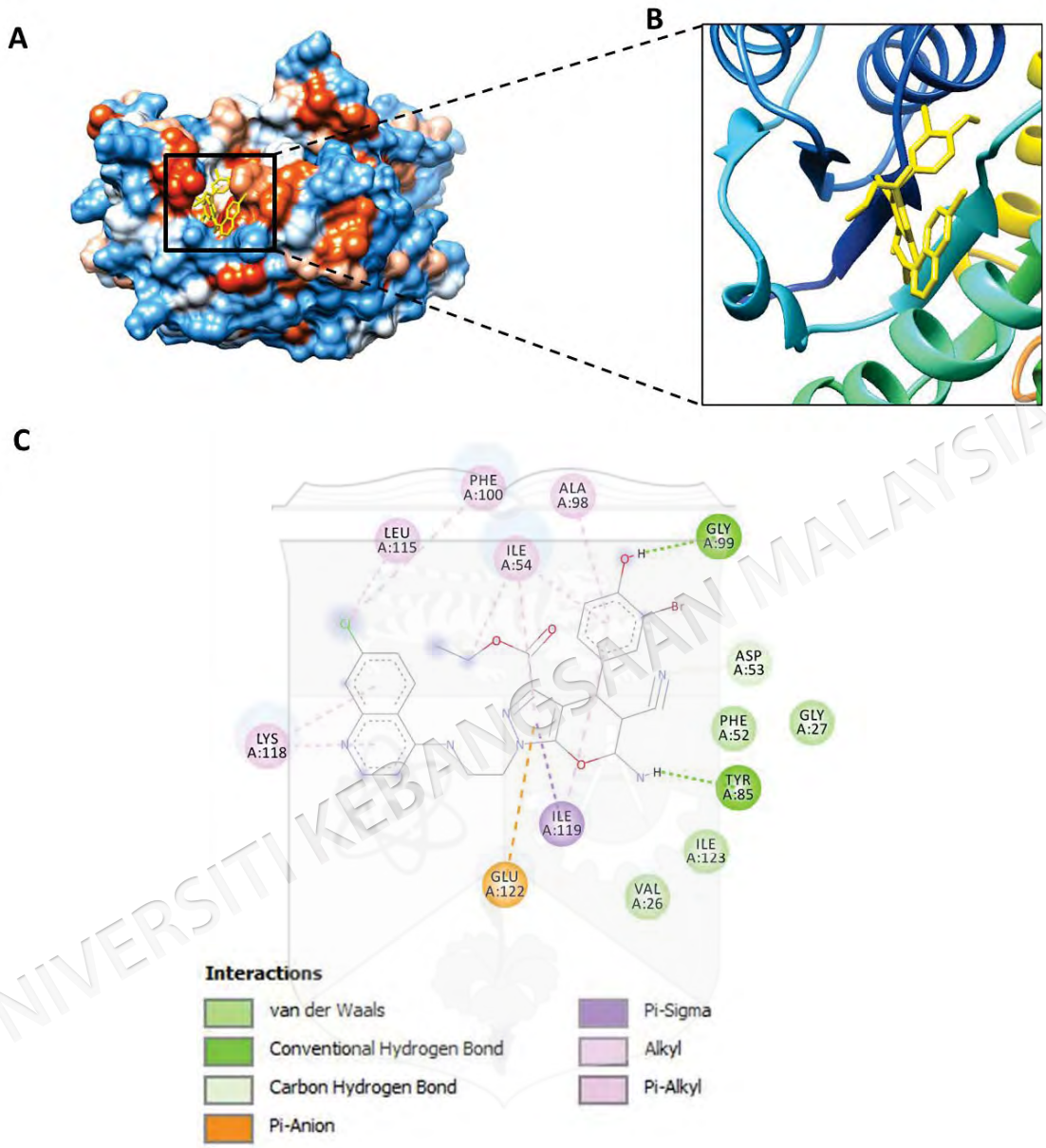

Figure 4.21 (A) Predicted orientation of the lowest docking energy (–7.60 kcal/mol) conformation of **24m** on the *Pf*LDH enzyme as depicted via a 3D hydrophobicity surface representation. (B) Close-up view of the binding site. (C) Schematic diagram of the intermolecular forces involved in the *Pf*LDH –**24m** interaction

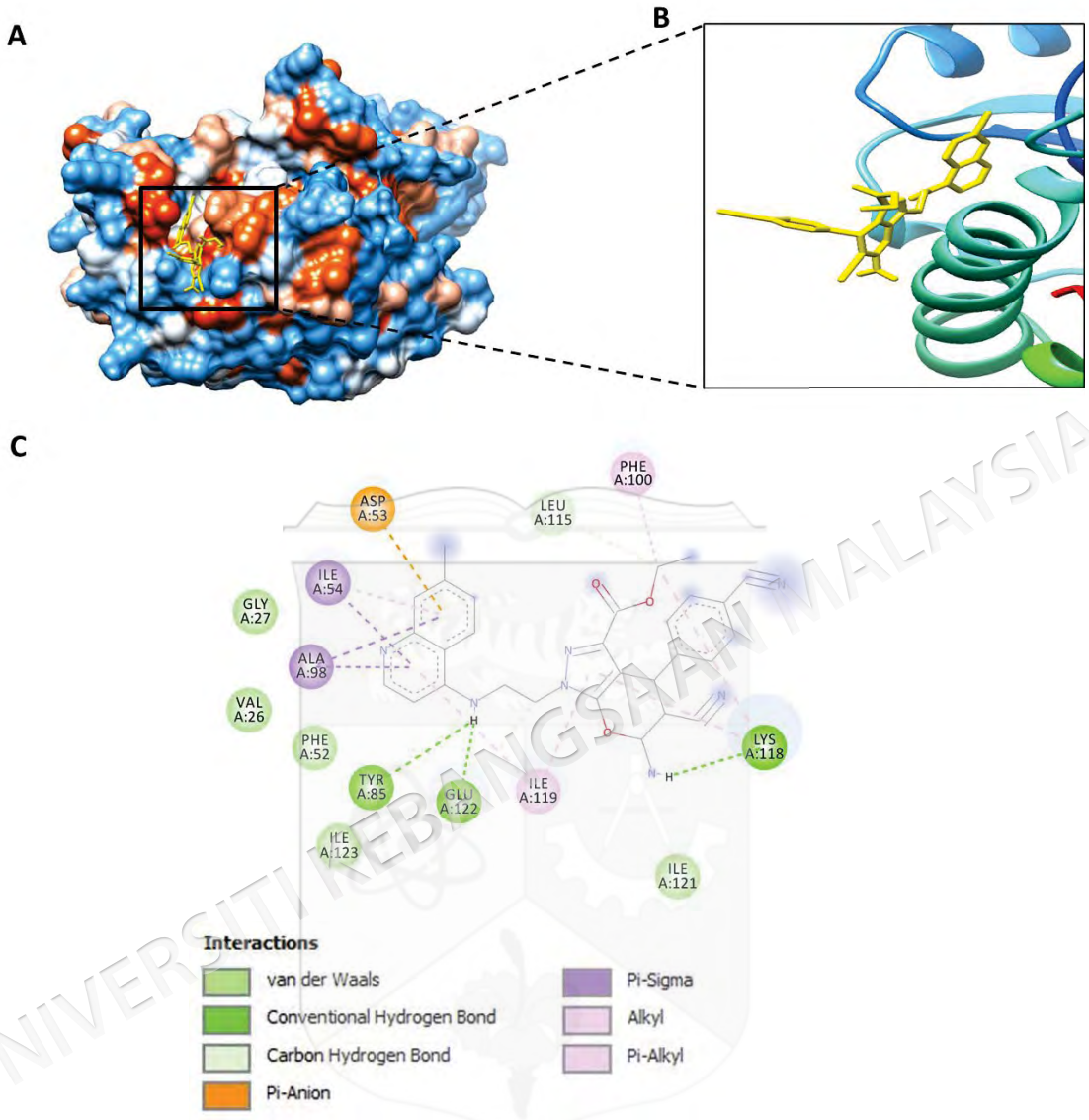

Figure 4.22 (A) Predicted orientation of the lowest docking energy (–8.02 kcal/mol) conformation of **24n** on the *Pf*LDH enzyme as depicted via a 3D hydrophobicity surface representation. (B) Close-up view of the binding site. (C) Schematic diagram of the intermolecular forces involved in the *Pf*LDH –**24n** interaction

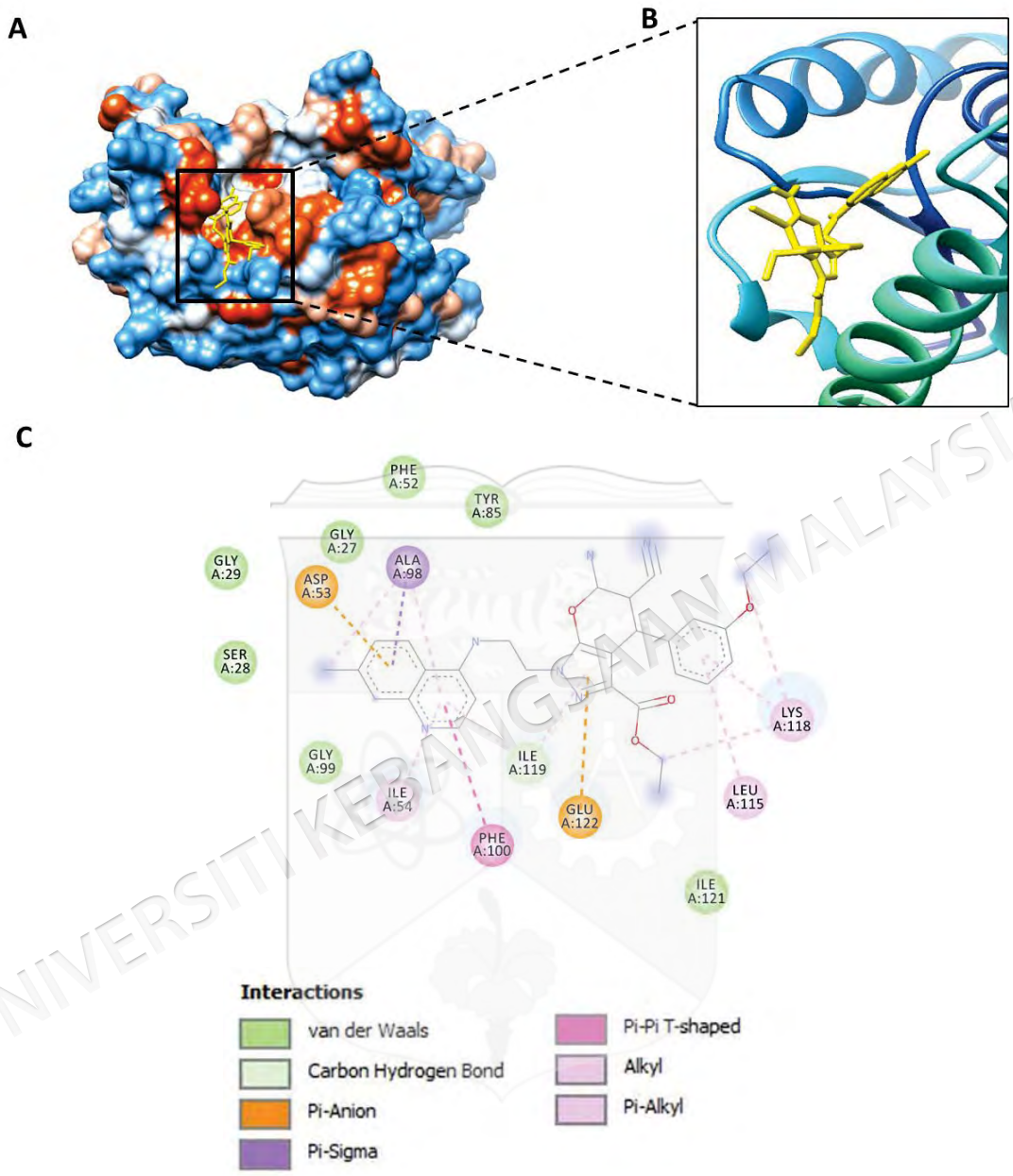

Figure 4.23 (A) Predicted orientation of the lowest docking energy (–8.01 kcal/mol) conformation of **24o** on the *Pf*LDH enzyme as depicted via a 3D hydrophobicity surface representation. (B) Close-up view of the binding site. (C) Schematic diagram of the intermolecular forces involved in the *Pf*LDH –**24o** interaction

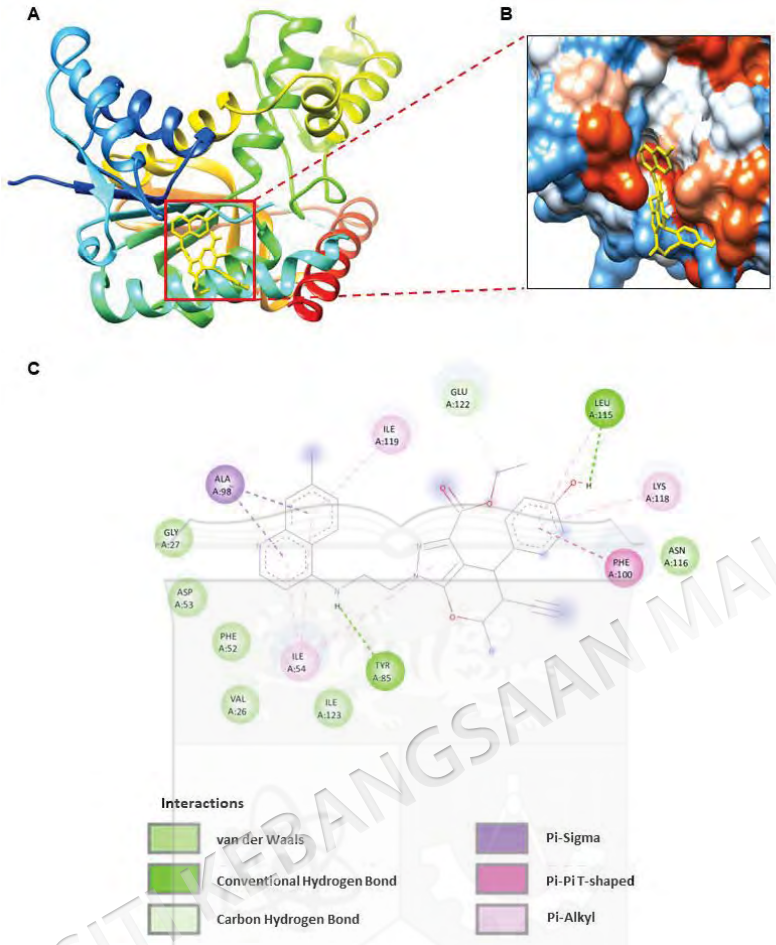

Figure 4.24 (A) Predicted orientation of the lowest docking energy (–7.53 kcal/mol) conformation of **24q** (rendered in ball and stick) on the *Pf*LDH enzyme. (B) Zoomed-in view of the cofactor binding site. (C) Schematic diagram of the intermolecular forces involved in the *Pf*LDH –**24q** interaction

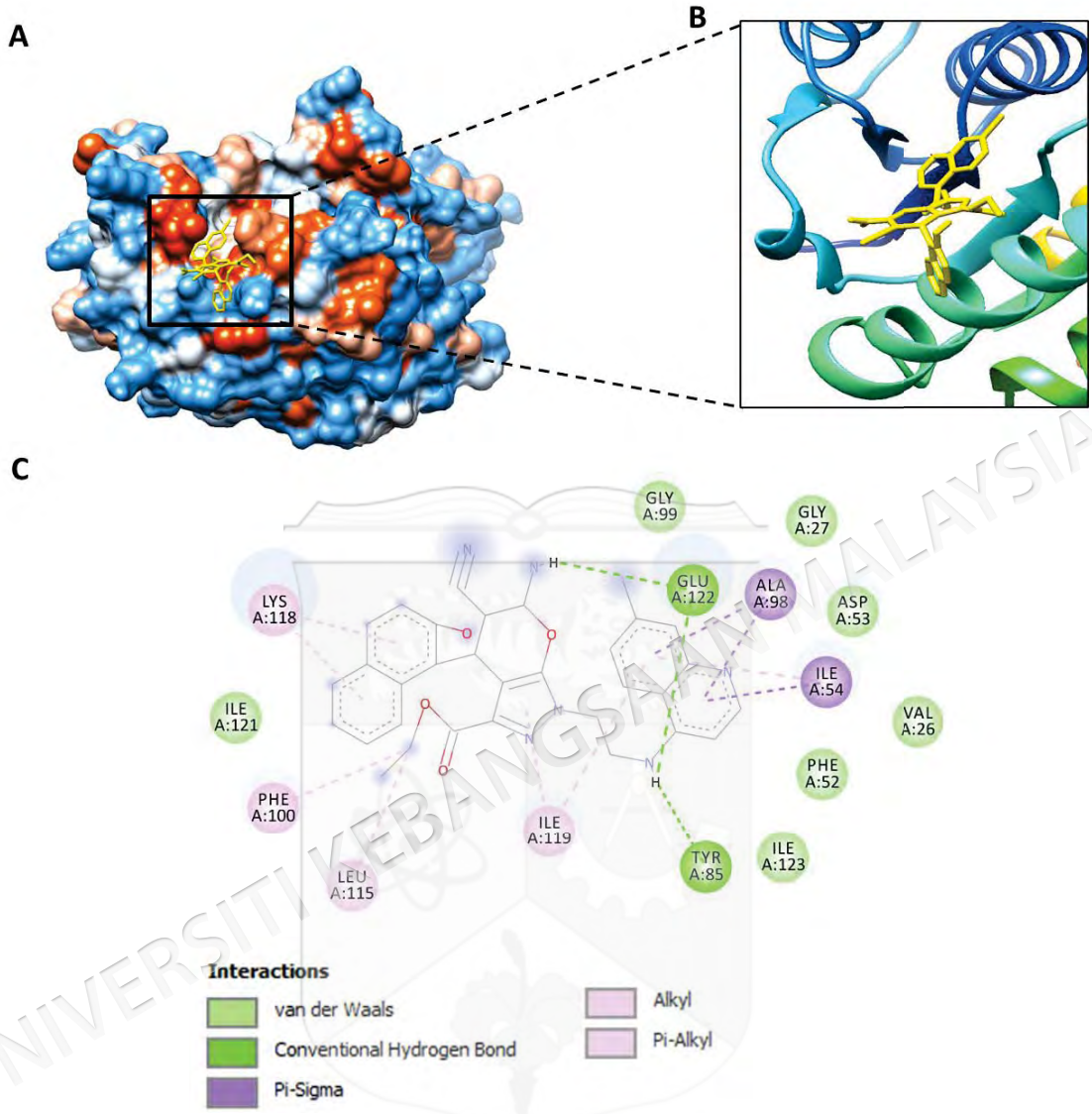

Figure 4.25 (A) Predicted orientation of the lowest docking energy (–8.01 kcal/mol) conformation of **24r** on the *Pf*LDH enzyme as depicted via a 3D hydrophobicity surface representation. (B) Close-up view of the binding site. (C) Schematic diagram of the intermolecular forces involved in the *Pf*LDH –**24r** interaction

4.4 ISOTHERMAL TITRATION CALORIMETRY MEASUREMENTS

Additionally, the study explored the interaction between five hybrids (**24a**, **24g**, **24h**, **24j** and **24q)** and hemin, a pivotal component in the heme detoxification pathway of malaria parasites. The interaction between the hybrids and hemin was examined by employing ITC to evaluate their inhibition potential against heme detoxification. This technique measures the heat generated or absorbed during molecular binding events, which can be employed to quantify the binding affinity, K_a (Du et al. 2016). The ITC

profiles of the interactions between hemin and compounds **24a**, **24g**, **24h**, **24j** and **24q** as illustrated in Figure 4.26. In Table 4.6, the K_a values of the hybrids ranged from 10^4 to 10^6 M^{-1}, with **24a** and **24g** exhibiting notably stronger affinity to hemin compared to compounds **24h**, **24j** and **24q**. This variation in affinity towards hemin suggests distinct binding modes of the hybrids and sheds light on the structural nuances that influence the interactions of these compounds with hemin.

One mechanism of action of antimalarial drugs such as CQ, artemisinin, and their derivatives is binding to heme, which prevents the formation of heme crystals known as hemozoin. This leads to the accumulation of the toxic heme in the digestive vacuole, thus killing the *Plasmodium* parasite (Wicht & Mok & Fidock, 2020). Hence, the ability of compounds to bind favourably to heme can be used to evaluate their potential as antimalarial agents. Our results indicate that, **24a** and **24g**, as distinguished by their strong heme binding affinity, could effectively disrupt the formation of hemozoin crystals and intervene in the heme detoxification process within the parasite. This information is valuable in understanding the molecular interactions involved in the action of antimalarial drugs and can be used to optimize the design of drug candidates for enhanced efficacy.

The thermodynamic parameters of the interactions were depicted in Table 4.6. All synthesized hybrid compounds exhibit exothermic reactions (negative ΔH), indicating heat release upon binding to hemin and the formation of intermolecular forces between the molecules. Furthermore, for each of these interactions, the entropy changes (ΔS) were negative, implying a reduction in disorder resulting from hydrogen bonds and specific Van der Waals interactions constraining the molecules. The spontaneity of these processes is reflected by the negative ΔG values. Among the studied compounds, **24a** and **24b** which showed the highest affinity towards hemin, also exhibited the most negative ΔG values, suggesting the most stable and favourable interactions with hemin. Interestingly, the interaction of the synthesized hybrids with hemin was enthalpy driven, as opposed to the entropy driven binding of chloroquine to hematin (Vippagunta et al. 2000), presumably due to the additional pyrano[2,3-c]pyrazole group. These findings indicate that these compounds can effectively interact

with heme and disrupting its detoxification in *Plasmodium* parasites, thereby exerting antimalarial effects.

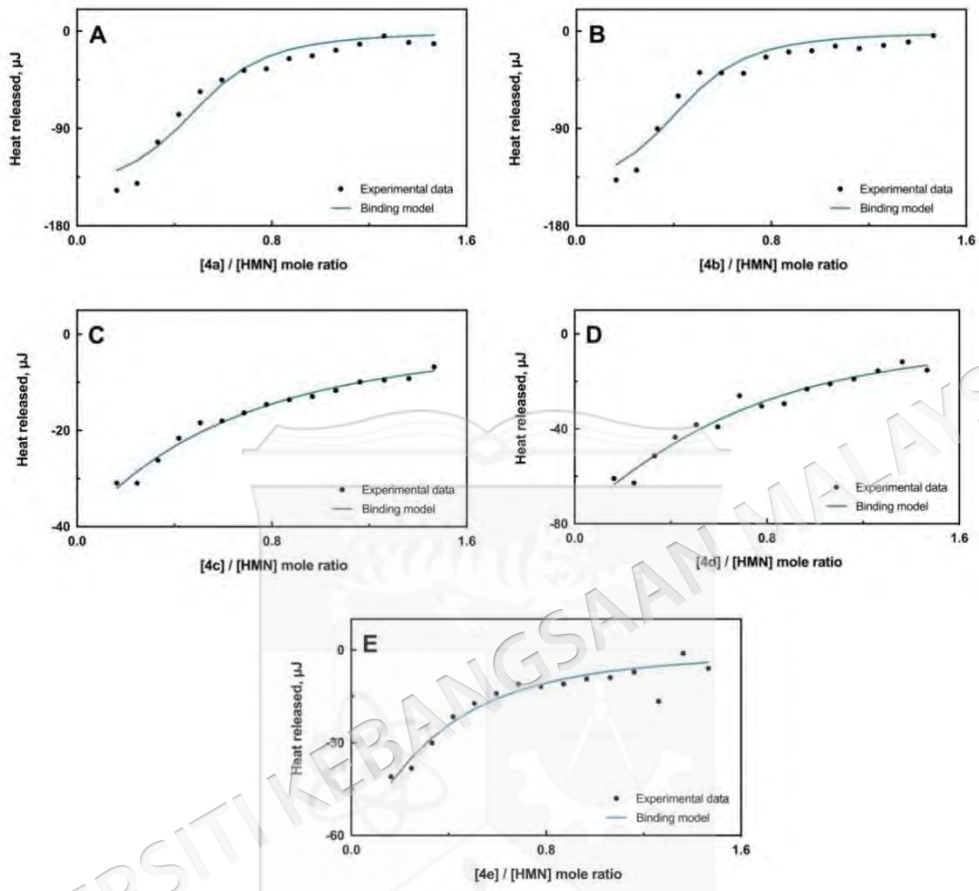

Figure 4.26 Isothermal titration calorimetric was obtained upon the titration of hemin with the different hybrids (A: **24a**, B: **24g**, C: **24h**, D: **24j**, and E: **24q**). The solid line represents the best fit to the measured heat values based on the independent binding model

Table 4.6 Binding affinity and thermodynamic parameters of the interaction between the synthesized hybrids and hemin at 37 °C, derived from ITC analysis

Complex	**Ka (M^{-1})**	**ΔH (kJ mol^{-1})**	**ΔS(J mol^{-1} K^{-1})**	**ΔS(J mol^{-1} K^{-1})**
CQ–hematin	(3.2±0.7)×105	50.208	-59.03	-59.03
24a–hemin	(1.43±0.60)×106	(-71.66±6.68)	(-215.50±11.31)	(-215.50±11.31)
24g–hemin	(1.64±0.97)×106	(-100 ± 0.00)	(-204.25±3.75)	(-204.25±3.75)
24h–hemin	(7.45±3.42)×104	(-100 ± 0.00)	(-229.60±2.80)	(-229.60±2.80)
24j–hemin	(3.37±3.54)×105	(-81.04±4.47)	(-203.48±17.20)	(-203.48±17.20)
24q–hemin	(1.85±0.56)×105	(-96.55±3.45)	(-210.65±9.35)	(-210.65±9.35)

4.5 *IN VITRO* STUDY OF PYRANO[2,3-C]PYRAZOLE-4-AMINOQUINOLINES

4.5.1 Cytotoxicity

Based on the study of Tanamatayarat et al. 2010, the cytotoxicity of pure compounds is considered highly toxic when IC_{50} values ≤ 20 μM, moderately toxic when IC_{50} values range from 21 to 50 μM, and low toxic when IC_{50} values > 50 μM. The IC_{50} values can be measured through a curve-shaped graph plotted based on the cytotoxicity test results.

As shown in table 4.7, majority of the hybrids with *para*-substituted phenyl ring (**24a**, **24j**, **20m**, **24n**, and **24p**), meta-substituted phenyl ring (**24b**), heterocyclic scaffold **(24l** and **24s**), and unsubstituted phenyl ring (**24f**) on pyrano[2,3-c]pyrazole moiety displayed low toxicity against a human normal liver WRL68 cell line with the IC_{50} value of 130.72±13.36, 56.896±1.77, 61.57±5.03, >183.34, 86.48±27.22, 68.61±5.06, 59.48±1.31, 90.47±0.47, and 81.54±7.11 μM, respectively. Significantly, the hybrids containing *para*-ethoxy (**24d**, IC_{50} = 6.98±0.40 μM), *para*-chloro (**24g**, IC_{50} = 12.12±0.37 μM), *para*-bromo (**24h**, IC_{50} = 5.85 ±0.34 μM) substituted pheny rig, and *ortho*-hydroxy substituted naphthyl ring (**24r**) on pyrano[2,3-c]pyrazole unit were found to be higher.toxic. In contrast, the rest of the hybrid compounds were moderately toxic against a human normal liver WRL68 cell line with IC_{50} values ranging from 20.91±0.56 to 48.59±4.22 μM.

Table 4.7 Cytotoxicity values of hybrid compounds **24a-s** against a human normal liver WRL68 cell line

Compound	Molecular Weight (g/mol)	Cytotoxicity values IC_{50} (μM) ± SD	Activity
24a	544.989	130.72±13.36	low toxicity
24b	530.962	68.61±5.06	low toxicity
24c	544.989	26.11±2.20	Moderately toxic
24d	559.015	6.98±0.40	highly toxic
24e	504.925	47.59±7.53	Moderately toxic
24f	514.962	81.54±7.11	low toxicity
24g	549.408	12.12±0.37	highly toxic

To be continued…

Continuation…

24h	593.859	5.85 ±0.34	highly toxic
24i	559.960	35.43±0.69	Moderately toxic
24j	559.960	56.896±1.77,	low toxicity
24k	546.961	23.22 ±2.41	Moderately toxic
24l	520.990	59.48±1.31	low toxicity
24m	609.858	61.57±5.03	low toxicity
24n	539.972	>183.34	low toxicity
24o	559.015	20.91±0.56	Moderately toxic
24p	558.972	86.48±27.22	low toxicity
24q	530.962	48.59±4.22	Moderately toxic
24r	581.021	6.69±0.53	highly toxic
24s	515.951	90.47±0.47	low toxicity
CQDP	515.86	60.64±1.13	low toxicity

4.5.2 Antimalarial Activity

According to the study of Dolabela et al. 2008, the antimalarial efficacy of pure compounds is considered as potent when IC_{50} values ≤ 1 μM, active is from 2 to 20 μM, moderately active when IC_{50} values range from 21 to 100 μM, weak when IC_{50} values range is from 101 to 200 μM, and inactive when IC_{50} values >200 μM. The IC_{50} values can be measured through a curve-shaped graph plotted using the GraphPad Prism 7 software (GraphPad Software Inc., CA, USA) based on the antimalarial test results.

The examinations on the antimalarial efficacy of all the synthesized hybrid compounds (**24a-s**) and the standard drug CQDP against both the CQS (3D7) and CQR (K1) *P. falciparum* strains were performed in triplicates by schizont maturation inhibition assay (SMIA). Table 4.8 presented the antimalarial activities of all hybrid compounds **24a-s** and the CQDP against both strains. It was concluded that all the tested hybrid compounds (**24a-s**) were potent against both the CQS 3D7 (IC_{50} values ranging from 0.0151 ± 0.004 to 0.301 ± 0.07 μM) and CQR K1 (IC_{50} values ranging from 0.01895 ± 0.014 to 2.746± 1.214 μM) *P. falciparum* parasites. All the tested hybrid compounds exhibited lower potentency compared to the standard drug CQDP (IC_{50} = 0.002 ± 0.0001) against the CQS (3D7) strain. In contrast, nine of the nineteen hybrids (**24d**, **24g**, **24h**, **24i**, **24l**, **24n**, **24o**, **24r** and **24s**) displayed superior antimalarial activity

than the CQDP (IC_{50} = 0.1195± 0.042) against the CQR (K1) *P. falciparum* strain. Among all the tested hybrids, **24c** against the 3D7 strain and **24h** against the K1 strain were proved to be the most promising antimalarial agents with 0.0151 ± 0.004 and 0.01895 ± 0.014 μM of IC_{50} values, respectively, while **24r** aginst the 3D7 strian and **24q** against the K1 strain showed lower antimalarial activity with 0.301 ± 0.07 and 2.746± 1.214 μM of IC_{50} values, respectively.

Table 4.8 Antimalarial activities of hybrid compounds **24a-s** against CQ-sensitive (3D7) and CQ-resistance (K1) *P.falciparum* strains

	Antimalarial activity		**Cytotoxic activity**	**Selectivity Index (SI)** $(\frac{IC_{50}\ MTT}{IC_{50}\ SMIA})$		**Resistance Index (RI)** $(\frac{IC_{50}\ K1}{IC_{50}\ 3D7})$
Compound	**3D7 IC_{50} (μM) ± SD**	**K1 IC_{50} (μM) ± SD**	**IC_{50} (μM) ± SD**	**3D7**	**K1**	
24a	0.021 ± 0.005	0.2543±0.091	130.72 ±13.36	6224	514	12.1
24b	0.0173 ±0.002	1.340±0.294	68.61±5.06	3965	51	77.46
24c	0.0151 ± 0.004	0.5916±0.305	26.11±2.20	1729	44	39.18
24d	0.024± 0.0005	0.0858±0.058	6.98±0.40	290	81	3.57
24e	0.0248 ± 0.008	0.2069± 0.1026	47.59±7.53	1918	230	8.34
24f	0.0187 ± 0.004	0.4187± 0.1803	81.54±7.11	4360	195	22.39
24g	0.0259 ± 0.01	0.048± 0.022	12.12±0.37	467	252	1.85
24h	0.0328 ± 0.013	0.01895± 0.014	5.85 ±0.34	178	309	0.58
24i	0.028 ± 0.01	0.1064± 0.029	35.43±0.69	1265	333	3.8
24j	0.1009± 0.015	0.2942± 0.052	56.896±1.77,	563	193	2.92

To be continued…

Continuation…

24k	0.0190 ± 0.008	0.2495± 0.081	23.22 ±2.41	1222	93	13.13
24l	0.0231± 0.002	0.03744± 0.0191	59.48±1.31	2574	1589	1.62
24m	0.0232 ± 0.011	0.2319± 0.1668	61.57±5.03	2653	265	10.0
24n	0.0194± 0.008	0.0373± 0.028	>183.34	>9450	>4915	1.92
24o	0.0679 ± 0.006	0.02566± 0.018	20.91±0.56	308	815	0.38
24p	0.038 ± 0.02	0.2103± 0.1275	86.48±27.22	2275	411	5.53
24q	0.0152 ± 0.006	2.746± 1.214	48.59±4.22	3196	18	180.66
24r	0.301 ± 0.07	0.0202± 0.010	6.69±0.53	22	334	0.07
24s	0.0208±0.007	0.02396± 0.012	90.47±0.47	4349	3775	1.15
CQDP	0.002 ± 0.0001	0.1195± 0.042	60.64±1.13	30320	507	59.75

The data obtained from the schizontical antimalarial test and the cytotoxic test was used to determine the selectivity index (SI) values of the pyranopyrazole-aminoquinoline hybrid compounds (**24a-s**) and the standard drug CQDP. The SI value is intended to determine the ability of a hybrid compound that has been tested to inhibit parasite growth without causing cytotoxicity. At a SI value exceeding 10, antimalarial activity is classified as selective against the tested parasite (Sarr et al. 2011). As shown in Table 4.8, all hybrid compounds (**24a-s**) and the reference drug CQDP showed an SI value of greater than 10 against both the CQS (3D7) and CQR (K1) *P. falciparum* strains. Against the CQS (3D7) strain, the most promising antimalarial agents, **24c** and **24q,** were proved to be the most selective agents, displaying 1729 and 3196 SI values, respectively, whereas the most potent antimalarial agent against the CQR (K1) strain, **24h**, was found to be the most selective agent with 309 of SI value. Notably, the lower

potent antimalarial agents **24r** against the 3D7 strain and **24q** against the K1 strain were the selective hybrid compounds inhibiting *P. falciparum* parasites with SI values of 22 and 18, respectively.

The resistance index (RI) value aims to determine the resistance level of *P. falciprarum* to the tested hybrid compounds. According to the study of Nzila and Mwai 2010, an RI value of less than 10 is a low resistance level to the tested drug compound. As depicted in Table 4.8, twelve of nineteen hybrid compounds exhibited an RI value of less than 10. Remarkably, the most potent antimalarial agent against the CQS (3D7) strain, **24q**, displayed the highest RI value (180.66). In contrast, the lower potent antimalarial agent against the CQS (3D7) strain, **24r**, exhibited the lowest RI value (0.07) among the series.

The results of this study can be concluded that the results of the *In vitro* studies can be linked to the *In silico* studies that have been conducted where all pyrano[2,3-*c*]pyrazole-4-aminoquinoline hybrid compounds (**24a-s**) gave good results in inhibiting both the 3D7 and K1 *P. falciparum* strains. Hybrid compounds **24c** and **24q** were the compounds that provided good antimalarial activity with moderate to low cytotoxicity, showing the best selectivity to inhibit *P. falciparum* at high levels of resistance compared to the rest of the hybrid compounds. Based on *In silico* studies, pyrano[2,3-*c*]pyrazole-4-aminoquinoline hybrid compounds containing unsubstituted (**24f**), *ortho*-substituted (**24c** and **24r**), and *meta*-substituted (**24i**) aromatic units, and *O*-heterocyclic (**24e**), *S*-heterocyclic (**24l**) and *N*-heterocyclic (**24s**) units on pyranopyrazole ring gave higher binding values compared to the rest hybrid compounds. *In vitro* studies also showed the same results. When comparing the results of the pyrano[2,3-*c*]pyrazole-4-aminoquinoline hybrid compounds (**24a-s**) with CQDP, better results than all the hybrid compounds were observed in the case of CQDP against the CQS (3D7) strain and nine of the nineteen hybrid compounds displayed better results than the CQDP against the CQR (K1) strain.

CHAPTER V

CONCLUSION

5.1 SUMMARY

In this research, nineteen pyrano[2,3-*c*]pyrazole-4-aminoquinoline hybrid compounds have been successfully synthesizsed and characterised, consisting of sixteen new and three known hybrid compounds. The pyrano[2,3-*c*]pyrazole-4-aminoquinoline hybrid compounds (**24a-s**) were synthesised through the hybridisation between pyrano[2,3-*c*]pyrazoles (**20a-s**) and 4-(bromoethylamino)-7-chloroquine (**23**) at room temperature under basic conditions, employing DMSO as a solvent, and characterised using Fourier Transform Infrared Spectroscopy (FTIR) and Nuclear Magnetic Resonance (NMR). The synthesised pyrano[2,3-*c*]pyrazole-4-aminoquinoline hybrid compounds demonstrated lower to moderate percentages of yields ranging from 10% to 49%. Pyrano[2,3-*c*]pyrazole-4-aminoquinoline hybrids are potential compounds containing *O*-heterocyclic, *S*-heterocyclic, *N*-heterocyclic, and aromatic scaffolds with electron-withdrawing and electron-donating functional groups such as nitro, halo, cyano, carbonyl and hydroxyl respectively.

Consequently, an *in silico* study was conducted, including predictions on physicochemical and absorption, distribution, metabolism, excretion, and toxicity (ADMET). In general, all the proposed hybrid compounds violate RO5 (MW ≥ 500), and the majority of hybrids are predicted to have VEBER violations (TPSA>140) and EGAN violations (TPSA>132). Unfortunately, very low solubility was predicted for all designed hybrid compounds. This could be solved by hydrolysing the ester group to a carboxylic acid. The hybrid compounds have weak blood-brain barrier (BBB) penetration. Sixteen of nineteen hybrid compounds are anticipated to be CYP2C19 inhibitors, while all the hybrid compounds, except **24p**, were predicted to be PgP inhibitors, indicating their potential as AEDs. In terms of protein plasma binding (PPB)

capability, every proposed hybrid compound, except **24k** and **24p**, exhibited a substantial binding affinity with protein plasma. More importantly, the *in silico* prediction revealed that all hybrid compounds are generally hepatotoxic.

Furthermore, molecular docking analysis was conducted to predict the binding orientations of a series of 19 hybrid compounds and the reference CQ within the cofactor binding site of the *Pf*LDH enzyme, contributing to an improved comprehension of their prospective pharmacological effects. The molecular docking analysis revealed that all hybrid compounds exhibited stronger binding energies with *Pf*LDH than the reference CQ. The diverse interactions observed between the hybrid compounds and specific amino acid residues of *Pf*LDH underscore their potential as effective enzyme activity inhibitors. Among the hybrid compounds tested, **24l** demonstrated the lowest binding energy with a remarkable value of -8.75 kcal/mol, while **24p** exhibited the weakest binding energy with *Pf*LDH (-6.89 kcal/mol). Compared to other hybrid compounds and CQ, **24l** exhibits all types of interactions and uniquely features a π-sulfur interaction, absent in other compounds. This distinctive interaction likely contributes significantly to its highest binding energy with *Pf*LDH. Despite its weaker binding affinity compared to other compounds, **24p** still interacted with *Pf*LDH through various interaction types, including hydrogen bonds, hydrophobic interactions, alkyl interactions, electrostatic interactions, and van der Waals forces. Further optimisation of **24p** or exploration of its structural derivatives may enhance its binding affinity and efficacy as an antimalarial agent.

In addition, heme detoxification is a unique target for antimalarial drugs. Heme was identified as a target of chloroquine and was found to inhibit hemozoin formation, leading to membrane damage. Hemozoin formation is a prominent process in blood-stage malaria parasites and remains a viable drug target. Several heme-binding antimalarial compounds that inhibit hemozoin formation have been discovered. Therefore, compounds that show heme detoxification results can be evaluated for their potential as antimalarial agents. This study studied the interaction between the five hybrid compounds (**24a**, **24g**, **24h**, **24j** and **24q)** and hemin using isothermal titration calorimetry (ITC) to evaluate their inhibition potential against heme detoxification. Our results indicate that **24a** (K_a = (1.43±0.60 ×10^6 M^{-1}) and **24g** (K_a = (1.64±0.97 ×10^6 M^{-}

[1]), as distinguished by their strong heme binding affinity, would be able to effectively disrupt the formation of hemozoin crystals and intervene in the heme detoxification process within the parasite. This information is valuable in understanding the molecular interactions involved in the action of antimalarial drugs and can be used to optimise the design of drug candidates for enhanced efficacy.

Moreover, the cytotoxic evaluation against a human normal liver WRL68 cell line revealed that the majority of the hybrids with heterocyclic scaffolds, unsubstituted phenyl ring, *meta*- and *para*-substituted phenyl ring on the pyrano[2,3-*c*]pyrazole moiety displayed low toxicity. The examinations on the antimalarial efficacy of all the synthesised hybrid compounds against the CQ-sensitive (3D7) and CQ-resistant (K1) *P. falciparum* strains showed that all the tested hybrids were potent and gave an SI value of >10 against both the *P. falciparum* parasites. Twelve of the nineteen hybrid compounds exhibited an RI value <10. Against the CQS (3D7) strain, the most potent antimalarial agents, **24c** and **24q,** were proved to be the most selective agents, displaying 1729 and 3196 of SI values, respectively, where as the most promising antimalarial agent against the CQR (K1) strain, **24h**, was found to be the most selective agent with 309 of SI value. Remarkably, the most potent antimalarial agent against the CQS (3D7) strain, **24q**, displayed the highest RI value (180.66). In contrast, the lower potent antimalarial agent against the CQS (3D7) strain, **24r**, exhibited the lowest RI value (0.07) among the series.

The results of this study can be concluded that hybrid compounds **24c** and **24q** were the compounds that provided good antimalarial activity with moderate to low cytotoxicity, showing the best selectivity to inhibit *P. falciparum* at high levels of resistance compared to the rest of the hybrid compounds. These findings highlight the promising therapeutic potential of these hybrid compounds against malaria, warranting further experimental validation and development as antimalarial agents. Figure 5.1 depicts the objectives achived in this research work.

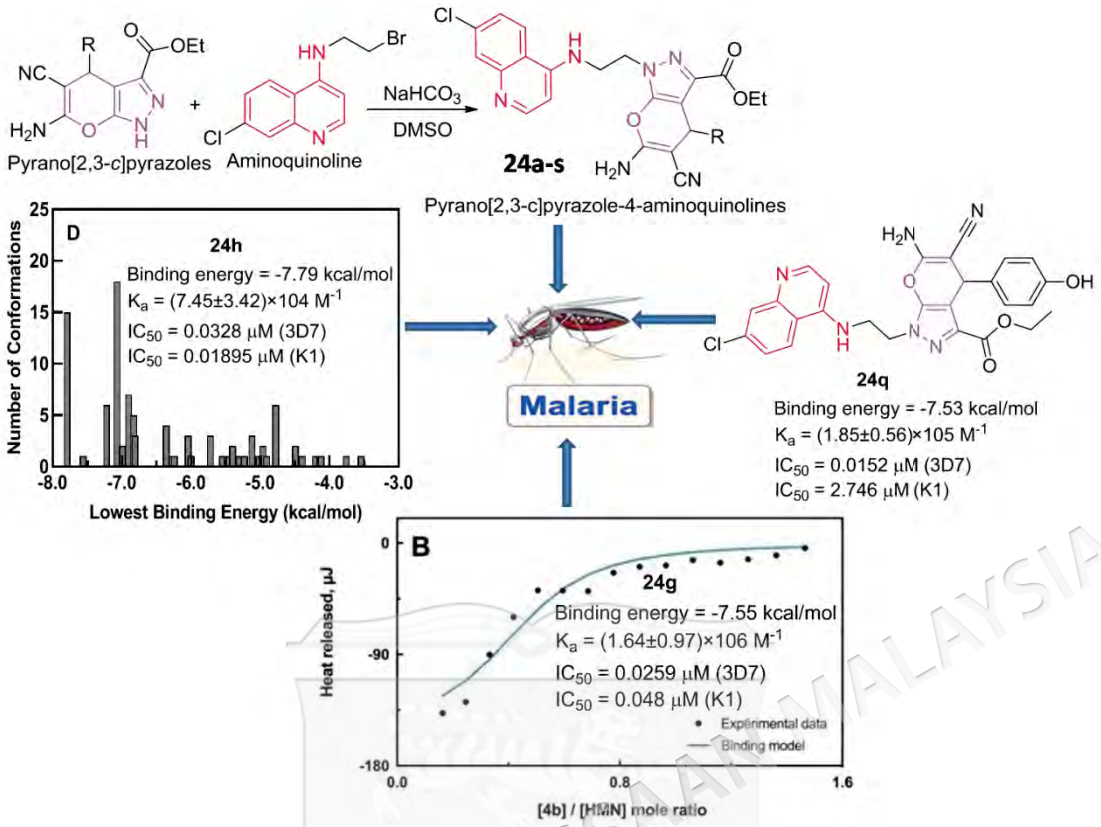

Figure 5.1 The objectives achived in this research work

5.2 FUTURE STUDIES

Pyrano[2,3-*c*]pyrazole and aminoquinoline moieties are potent in various applications and the pyrano[2,3-*c*]pyrazole-4-aminoquinoline hybrid compounds are great to be explored for other biological applications and detections. The pyrano[2,3-*c*]pyrazole-aminoquinoline hybrid compounds should be continued by synthesising more potential compounds with more reactive functional groups such as amine, amide, acid anhydride, acyl chloride, and various carbonyl groups. Computational studies like molecular dynamic simulations of pyrano[2,3-*c*]pyrazole-4-aminoquinoline hybrid compounds must be conducted as a preliminary study to understand the capabilities of the compound for other biological applications including antimalarial activities. Cytotoxic evaluations on other cells, such as human embryonic kidney cells (HEK293T), should be conducted to learn more about the toxic level of the pyrano[2,3-*c*]pyrazole-4-aminoquinoline hybrid compounds. Overall, the reported pyrano[2,3-*c*]pyrazole-4-aminoquinoline hybrid compounds (**24a-s**) exhibited potent antimalarial activity against both the CQS (3D7) and CQR (K1) *P. falciparum* strains. This creates new insights into the development of promising antimalarial agents, which can be explored further.

Moreover, the development of novel pyrano[2,3-*c*]pyrazole-4-aminoquinoline hybrid compounds can be explored for other biological applications, including antimalarial activity.

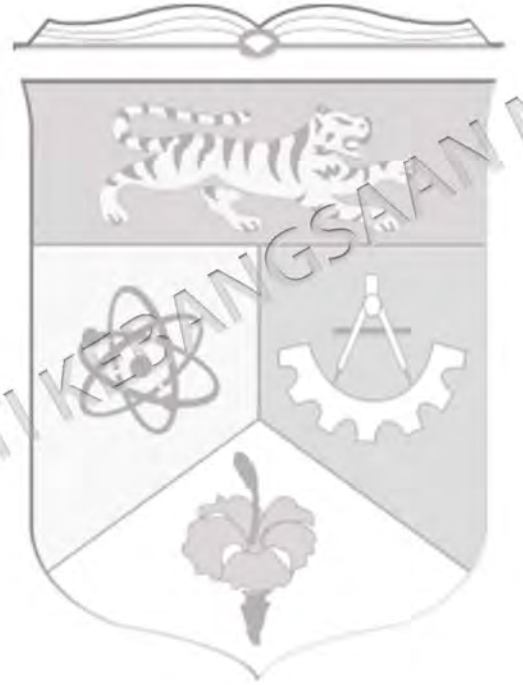

REFERENCES

Abdi, B., Fekadu, M., Zeleke, D., Eswaramoorthy, R. & Melaku, Y. 2021. Synthesis and evaluation of the antibacterial and antioxidant activities of some novel chloroquinoline analogs. *Journal of Chemistry* 2021: 2408006.

Abdullah, M. A., Lee, Y. -R., Mastuki, S. N., Leong, S. W., Wan Ibrahim, W. N., Mohammad Latif, M. A., Ramli, A. N. M., Mohd Aluwi, M. F. F., Mohd Faudzi, S. M. & Kim, C.- H. 2020. Development of diarylpentadienone analogues as alpha-glucosidase inhibitor: synthesis, *in vitro* biological and *in vivo* toxicity evaluations, and molecular docking analysis. *Bioorganic Chemistry* 104: 104277.

Aboelnaga, A. & EL-Sayed, T. H. 2018. Click synthesis of new 7-chloroquinoline derivatives by using ultrasound irradiation and evaluation of their biological activity. *Green Chemistry Letters & Reviews* 11: 254-263.

Adeleke, A. A., Zamisa, S. J., Islam, M. S., Olofinsan, K., Salau, V. F., Mocktar, C. & Omondi, B. 2021. Quinoline Functionalized Schiff Base Silver (I) Complexes: Interactions with Biomolecules and *In Vitro* Cytotoxicity, Antioxidant and Antimicrobial Activities. *Molecules* 26(5): 1205.

Agarwal, D., Sharma, M., Dixit, S. K., Dutta, R. K., Singh, A. K., Gupta, R. D. & Awasthi, S. K. 2015. *In vitro* synergistic effect of fluoroquinolone analogues in combination with artemisinin against *Plasmodium falciparum*; their antiplasmodial action in rodent malaria model. *Malaria Journal* 14(1): 48.

Aggarwal, S., Paliwal, D., Kaushik, D., Gupta, G. K. & Kumar, A. 2018. Pyrazole schiff base hybrids as anti-malarial agents: Synthesis, *in vitro* screening and computational study. *Combinatorial Chemistry & High Throughput Screening* 21(3): 194-203.

Aguiara, A. C. C., Murceb, E., Cortopassic, W. A., Pimentelb, A. S., Almeidad, M. M. F. S., Barrosd, D. C. S., Guedesd, J. S., Meneghettid, M. R. & Krettli, A. U. 2018. Chloroquine analogs as antimalarial candidates with potent *in vitro* and *in vivo* activity. *International Journal for Parasitology: Drugs and Drug Resistance* 8(3): 459-464.

Ahluwalia, V. K., Dahiya, A. & Garg, V. 1997. Reaction of 5-amino-4-formyl-3-methyl(or phenyl)-1-phenyl-1H-pyrazoles with active methylene compounds: Synthesis of fused heterocyclic rings. *Indian Journal of Chemistry -Section B* 36(1): 88-90.

Akolkar, H. N., Dengale, S. G., Deshmukh, K. K., Karale, B. K., Darekar, N. R., Khedkar, V. M. & Shaikh, M. H. 2020. Design, synthesis and biological evaluation of novel furan & thiophene containing pyrazolyl pyrazolines as antimalarial agents. *Polycyclinic Aromatic Compounds* 42(5): 1959-1979.

Alonso, P. L. & Tanner, M. 2013. Public health challenges and prospects for malaria control and elimination. *Nature Medicine* 19(2): 150-155.

Alven, S. & Aderibigbe, B. 2019. Combination Therapy Strategies for the Treatment of Malaria. *Molecules* 24(19): 3601.

Ashley, E. A., Phyo, A. P. & Woodrow, C. J. 2018. Malaria. *The Lancet* 391: 1608.

Azeredo, L. F. S. P., Coutinho, J. P., Jabor, V. A. P., Feliciano, P. R., Nonato, M. C., Kaiser, C. R., Menezes, C. M. S., Hammes, A. S. O., Caffarena, E. R., Hoelz, L. V. B., de Souza, N. B., Pereira, G. A. N., Ceravolo, I. P., Krettli, A. U. & Boechat, N. 2017. Evaluation of 7-arylaminopyrazolo[1,5-a]pyrimidines as anti-*Plasmodium falciparum*, antimalarial, and *Pf*-dihydroorotate dehydrogenase inhibitors. *European Journal of Medicinal Chemistry* 126, 72-83.

Baartzes, N., Combrinck, J., Chibale, K. & Smith, G.S. 2022. Heteroleptic Rh(III) phenylpyridyl complexes based on an aminoquinoline-benzimidazole hybrid scaffold: Antiplasmodial evaluation and mechanistic insights. *Journal of Organometalic Chemistry* 975: 122419.

Baartzes, N., Jordaan, A., Warner, D. F., Combrinck, J., Taylor, D., Chibale, K. & Smith, G. S. 2020. Antimicrobial evaluation of neutral and cationic iridium(III) and rhodium(III) aminoquinoline-benzimidazole hybrid complexes. *European Journal of Medicinal Chemistry* 206: 112694.

Balaji, S. N., Ahsan, M. J., Jadav, S. S. & Trivedi, V. 2015. Molecular modelling, synthesis, and antimalarial potentials of curcumin analogues containing heterocyclic ring. *Arabian Journal of Chemistry* 12(8): 2492-2500.

Bekhit, A. A., Nasralla, S. N., Bekhit, S. A. & Bekhit, A. E. A. 2022. Novel dual acting antimalarial antileishmanial agents derived from pyrazole moiety. *Biointerface Ressearch in Applied Chemistry* 12(5): 6225-6233.

Bekhit, A. A., Nasralla, S. N., El-Agroudy, E. J., Hamouda, N., El-Fattah, A. A., Bekhit, S. A., Amagase, K. & Ibrahim, T. M. 2022. Investigation of the anti-inflammatory and analgesic activities of promising pyrazole derivative. *European Journal of Pharmaceutical sciences* 168: 106080.

Bekhit, A. A., Saudi, M. N., Hassan, A. M. M., Fahmy, S. M., Ibrahim, T. M., Ghareeb, D., El-Seidy, A. M., Nasralla, S. N. & Bekhit, A. E. A., 2018. Synthesis, *in silico* experiments and biological evaluation of 1,3,4-trisubstituted pyrazole derivatives as antimalarial agents. *European Journal of Medicinal Chemistry* 163, 353-366.

Bhagat, S., Arfeen, M., Das, G., Ramkumar, M., Khan, S. I., Tekwani, B. L. & Bharatam P. V. 2019. Design, synthesis and biological evaluation of 4-aminoquinoline-guanylthiourea derivatives as antimalarial agents. *Bioorganic Chemistry* 91: 103094.

Birkholtz, L. M., Bornman, R., Focke, W., Mutero, C. & de Jager, C. 2012. Sustainable malaria control: Transdisciplinary approaches for translational applications. *Malaria Journal* 11: 431.

Biswas, S. K. & Das, D. 2022. One-pot synthesis of pyrano[2,3-*c*]pyrazole derivatives via multicomponent reactions (MCRs) and their applications in medicinal chemistry. *Mini-Reviews in Organic Chemistry* 19: 552-568.

Boger, D., Fink, B. & Hedrick, M. 2000. Total Synthesis of Distamycin A and 2640 Analogues: A Solution-Phase Combinatorial Approach to the Discovery of New, Bioactive DNA Binding Agents and Development of a Rapid, High-Throughput Screen for Determining Relative DNA Binding Affinity or DNA Bindi. *Journal of the American Chemical Society* 122: 6382-6394.

Bohnert, T. & Gan, L. -S. 2013. Plasma protein binding: from discovery to development. *Journal of Pharmacological Sciences* 102(9): 2953-2994.

Bokosi, F. R. B. & Ngoepe, M. P. 2022. Synthesis, *in silico* docking studies, and antiplasmodial activity of hybrid molecules bearing 7-substituted 4-aminoquinoline moiety and cinnamic acid derivatives. *Chemical Biology & Drug Desin* 100(1): 41-50.

Bonilla-Ramírez, L., Rios, A., Quiliano, M., Ramírez-Calderon, G., Beltrán-Hortelano, I., Franetich, J. F., Corcuera, L., Bordessoulles, M., Vettorazzi, A., López de Cerain, A., Aldana, I., Mazier, D., Pabón, A. & Galiano, S. 2018. Novel antimalarial chloroquine- and primaquine-quinoxaline 1,4-di-N-oxide hybrids: Design, synthesis, *Plasmodium* life cycle stage profile, and preliminary toxicity studies. *European Journal of Medicinal Chemistry* 158: 68-81.

Brogi, S., Ramalho, T. C., Kuca, K., Medina-Franco, J. L. & Valko, M. 2020. Editorial: *In silico* methods for drug design and discovery. *Frontier Chemistry* 8: 612

Brucoli, F., Hawkins, R. M., James, C. H., Wells, G., Jenkins, T. C., Ellis, T., Hartley, J.A., Howard, P.W. & Thurston, D.E. 2011. Novel C8-linked pyrrolobenzodiazepine (PBD)- heterocycle conjugates that recognize DNA sequences containing an inverted CCAAT box. *Bioorganic & Medicinal Chemistry Letters* 21(12): 3780-3783.

Cazelles, J., Cosledan, F., Meunier, B. et al. 2011. Dual molecules containing peroxy derivative, the synthesis and therapeutic applications thereof, Sanofi-Aventis, Paris (FR).

Capci, A., Lorion, M. M., Wang, H., Simon, N., Leidenberger, M., Silva, M. C. B., Moreira, D. R. M., Zhu, Y., Meng, Y., Chen, J. Y., Lee, Y. M., Friedrich, O., Kappes, B., Wang, J., Ackermann, L. & Tsogoeva, S. B. 2019. Artemisinin–(Iso)quinoline Hybrids by C-H Activation and Click Chemistry: Combating Multidrug-Resistant Malaria. *Angewandte Chemie International Edition* 58(37): 13066-13079.

Charris, J. E., Monasterios, M. C., Acosta, M. E., Rodríguez, M. A., Gamboa, N. D., Martínez, G. P., Rojas, H. R., Mijares, M. R. & De Sanctis, J. B. 2019. Antimalarial, antiproliferative, and apoptotic activity of quinoline-chalcone and quinoline-pyrazoline hybrids. A dual action. *Medicinal Chemistry Research* 28: 2050-2066.

Cheuka, P. M., Cabrera, D. G., Paquet, T. & Chibale, K. 2014. Structure-activity relationship studies of antiplasmodial aminomethylthiazoles. *Bioorganic & Medicinal Chemistry Letters* 24(22): 5207-5211.

Choudhary, D., Rani, I., Monga, J., Goyal, R., Husain, A., Garg, P. & Khokra, S.L. 2022. Pyrazole based furanone hybrids as novel antimalarial: A combined experimental, pharmacological and computational study. *Central Nervous System Agents Medicinal Chemistry* 22(1): 39-56.

Chopra, R., Chibale, K. & Singh, K. 2018. Pyrimidine-chloroquinoline hybrids: Synthesis and antiplasmodial activity. *European Journal of Medicinal Chemistry* 148: 39-53.

Chowdhary, S., Shalini, Mosnier, J., Fonta, I., Pradines, B., Cele, N., Seboletswe, P., Singh, P. & Kumar, V. 2022. Synthesis, Anti-Plasmodial Activities, and Mechanistic Insights of 4-Aminoquinoline-Triazolopyrimidine Hybrids. *ACS Medicinal Chemistry Letters* 13(7): 1068-1076.

Chaudhary, K. K. & Mishra, N. 2016. A Review on Molecular Docking: Novel Tool for Drug Discovery. *JSM Chem* 4(3): 1029.

Coban, C. 2020. The host targeting effect of chloroquine in malaria. *Current Opinion in Immunology* 66: 98.

Cortopassi, W. A., Oliveira, A. A., Guimarães, A. P., Rennó, M. N., Krettli, A. U. & França, T. C. C. 2011. Docking studies on the binding of quinoline derivatives and hematin to *plasmodium falciparum* lactate dehydrogenase. *Journal of Biomolecular Structure and Dynamics* 29(1): 207-218.

Costa, C. A., Lopes, R. M., Ferraz, L. S., Esteves, G. N. N., Di Iorio, J. F., Souza, A. A., de Oliveira, I. M., Manarin, F., Judice, W. A. S., Stefani, H. A. & Rodrigues, T. 2020. Cytotoxicity of 4-substituted quinoline derivatives: Anticancer and antileishmanial potential. *Bioorganic & Medicinal Chemistry* 28(11): 115511.

Cowman, A. F., Healer, J., Marapana, D. & Marsh, K. 2016. Review Malaria : *Biology and Diseas Cell* 167(3): 610-624.

Craciun, D., Modra, D. & Isvoran, A. 2015. ADME-Tox profiles of some food additives and pesticides. *AIP Conference Proceedings* 1694(1): 040007.

Crockett, M. & Kain, K. C. 2007. Tafenoquine: a promising new antimalarial agent. *Expert Opinion on Investigational Drugs* 16(5): 705-715.

Dana, S., Valissery, P., Kumar, S., Gurung, S. K., Mondal, N., Dhar, S. K. & Mukhopadhyay, P. 2020. Synthesis of novel Ciprofloxacin-based hybrid molecules toward potent Antimalarial activity. *ACS Medicinal Chemistry Letters* 11(7): 1450-1456.

Da Silva, R. M., Gandi, M.O., Mendonça, J. S., Carvalho, A. S., Coutinho, J. P., Aguiar, A. C., Krettli, A. U. & Boechat, N. 2019. New hybrid trifluoromethylquinolines as antiplasmodium agents. *Bioorganic & Medicinal Chemistry* 27: 1002-1008.

De, D., Krogstad, F. M., Byers, L. D. & Krogstad, D. J. 1998. Structure-activity relationships for antiplasmodial activity among 7-substituted 4-aminoquinolines. *Journal of Medicinal Chemistry* 41(25): 4918-4926.

De Walle, T. V., Boone, M., Puyvelde, J. V., Combrinck, J., Smith, P. J., Chibale, K., Mangelinckx, S. & D'hooghe, M. 2020. Synthesis and biological evaluation of novel quinoline-piperidine scaffolds as antiplasmodium agents. *European Journal of Medicinal Chemistry* 198: 112330.

Dean, L. & Kane, M. Omeprazole therapy and CYP2C19 genotype, in: Pratt, V. M., Scott, S. A., Pirmohamed, M., Esquivel, B., Kane, M. S., Kattman, B. L. & Malheiro (Eds.), A. J. 2012. Medical Genetics Summaries, National Center for Biotechnology Information (US), Bethesda (MD). PMID: 28520353.

Dian, N. D., Salleh, A. F. M., Rahim, M. A. F. A., Munajat, M. B., Manap, S. N. A. A., Ghazali, N., Hassan, N. W. & Idris, Z. M. 2021. Malaria Cases in a Tertiary Hospital in Kuala Lumpur, Malaysia: A 16-Year (2005–2020) Retrospective Review. *Tropical Medicine and Infectious Disease* 6: 177.

Dolabela, M., Oliveira, S., Nascimento, J., Peres, J., Wagner, H., Povoa, M., & Oliveira, A. 2008. *In vitro* antiplasmodial activity of extract and constituents from Esenbeckia febrifuga, a plant traditionally used to treat malaria in the Brazilian Amazon. *Phytomedicine* 15(5): 367-372.

Doogue, M. P. & Polasek, T. M. 2013. The ABCD of clinical pharmacokinetics. *Therapeutic Advances in Drug Safety* 4(1): 5-7.

Dorababu, A. 2021. Quinoline: A promising scaffold in recent antiprotozoal drug discovery. *ChemistrySelect* 6(9): 2164-2177.

Du, X., Li, Y., Xia, Y. -L., Ai, S. -M., Liang, J., Sang, P., Ji, X.-L. & Liu, S. -Q. 2016. Insights into protein–ligand interactions: mechanisms, models, and methods. *International Journal of Molecular Sciences*. 17(2), 144.

Faheem, Dey, S., Johri, S., Abirami, M., Kumar, B. K., Taramelli, D., Basilico, N.; Balana-Fouce, R., Sekhar, K. V. G. C. & Murugesan, S. 2022. Search for structurally diverse heterocyclic analogs as dual-acting antimalarial and antileishmanial agents: An overview. *European Journal of Medicinal Chemistry* 4: 100031.

Fatih, F. A., Staines, H. M., Siner, A. Ahmed, M. A., Woon, L. C., Pasini, E. M., HM Kocken, C., Singh, B., Cox-Singh, J. & Krishna, S. 2013. Susceptibility of human *Plasmodium knowlesi* infections to anti-malarials. *Malaria Journal* 12(1): 425.

Fan, Y. -L., Cheng, X. -W., Wu, J. -B., Zhang, F. -Z., Xu, Z. & Feng, L. -S. Antiplasmodial and antimalarial activities of quinolone derivatives: An overview. *European Journal of Medicinal Chemistry* 146: 1.

Fernandes, B. T., Segretti, C. F. M., Polli, C. M. & Parise-Filho, R. 2016. Analysis of the applicability and use of Lipinski's rule for central nervous system drugs. *Letters in Drug Design and Discovery* 13(10): 999-1006.

Fernando, D., Rodrigo, C. & Rajapakse, S. 2011. Primaquine in vivax malaria: an update and review on management issues. *Malaria Journal* 10(2011): 351

Fidock, D. A., Rosenthal, P. J., Croft, S.L., Brun, R. & Nwaka, S. 2004. Antimalarial drug discovery: efficacy models for compound screening. *Nature Reviwes Drug Discovery* 3(6): 509-520.

Firestone, T. M., Oyewole, O. O., Reid, S. P. & Ng, C. L. 2021. Repurposing Quinoline and Artemisinin Antimalarials as Therapeutics for SARS-CoV-2: Rationale and Implications. *ACS Pharmacology & Translational Science* 4(2): 613-623.

Foloppe, N., Fisher, L. M., Howes, R., Potter, A., Robertson, A. G. S. & Surgenor, A. E. 2006. Identification of chemically diverse Chk1 inhibitors by receptor-based virtual screening. *Bioorganic & Medicinal Chemistry* 14(14): 4792-4802.

Franco, J., Medeiros, A., Benitez, D., Perelmuter, K., Serra, G., Comini, M. A. Scarone, L. 2016. *In vitro* activity and mode of action of distamycin analogues against African trypanosomes. *European Journal of Medicinal Chemistry* 126: 776-778.

Gamo, F. J., Sanz, L. M., Vidal, J. et al. 2010. Thousands of chemical starting points for antimalarial lead identification. *Nature* 465(7296): 305-310.

García-Cañaveras, J. C., Lancho, O., Ducker, G. S., Ghergurovich, J. M., Xu, X., da Silva-Diz, V., Minuzzo, S., Indraccolo, S., Kim, H., Herranz, D. & Rabinowitz, J. D. 2021. SHMT inhibition is effective and synergizes with methotrexate in T-cell acute lymphoblastic leukemia. *Leukemia* 35: 377-388.

Gein, V. L., Zamaraeva, T. M. & Kozulina, I. V. 2014. New synthesis of ethyl 6-amino-4-aryl-5-cyano-1,4-dihydropyrano[2,3-c]pyrazole-3-carboxy lates. *Russian Journal of Organic Chemistry* 50(5): 691-693.

Gerhardt, C. H. 1842. *Ann Chemi Phys* 7: 25.

Gil, J. P. 2008. Amodiaquine pharmacogenetics. *Pharmacogenomics* 9(10): 1385-1390.

Gogoi, P., Shakya, A., Ghosh, S. K., Gogoi, N., Gahtori, P., Singh, N., Bhattacharyya, D. R., Singh, U. P. & Bhat, H. R. 2020. *In silico* study, synthesis, and evaluation of the antimalarial activity of hybrid dimethoxy pyrazole 1,3,5-triazine derivatives. *Journal of Biochemical and Molecular Toxicology* 35(3): 22682.

Gómez-Jeria, J.-S., Robles-Navarro, A., Kpotin, G., Gómez-Jeria, J.S., Kpotin, G.A., Garrido-Sáez, N. & Gatica-Díaz, N. 2020. Some remarks about the relationships between the common skeleton concept within the Klopman-Peradejordi-Gómez QSAR method and the weak molecule-site interactions. *Chemistry Research Journal* 5(2): 32-52.

Guantai, E. M., Ncokazi, K., Egan, T. J., Gut, J.; Rosenthal, P. J., Bhampidipati, R., Kopinathan, A., Smith, P. J. & Chibale, K. 2011. Enone- and chalcone-chloroquinoline hybrid analogues: *in silico* guided design, synthesis, antiplasmodial activity, *in vitro* metabolism, and mechanistic studies. *Journal of Medicinal Chemistry* 54(10): 3637-3649.

Guo, R. Y., An, Z. M., Mo, L. P., Yang, S. T., Liu, H. X., Wang, S. X. & Zhang, Z. H. 2013. Meglumine promoted one-pot, four-component synthesis of pyranopyrazole derivatives. *Tetrahedron* 69: 9931-9938.

Gurung, A. B., Bhattacharjee, A. & Ali, M. A. 2016. Exploring the physicochemical profile and the binding patterns of selected novel anticancer Himalayan plant derived active compounds with macromolecular targets. *Informatics in Medicine Unlocked* 5: 1-14.

Hasan, A., Mazumder, H. H., Chowdhury, A. S., Datta, A. & Khan, A. 2015. Moleculardocking study of malaria drug target enzyme transketolase in *Plasmodium falciparum* 3D7 portends the novel approach to its treatment. *Source Code for Biology and Medicine* 10(7): 1-14.

Hochegger, P., Faist, J., Seebacher, W., Saf, R., Mäser, P., Kaiser, M. & Weis, R. 2019. Synthesis and structure-activity relationships for new 6-fluoroquinoline derivatives with antiplasmodial activity. *Bioorganic & Medicinal Chemistry* 27(10): 2052-2065.

Huang, G., Solano, C.M., Su, Y., Ezzat, N., Matsui, S., Huang, L., Chakrabarti, D. & Yuan, Y. 2019. Microwave-assisted, rapid synthesis of 2-vinylquinolines and evaluation of their antimalarial activity. *Tetrahedron Letter* 60(26): 1736-1740.

Insuasty, B., Ramirez, J., Beceraa, D., Echeverry, C., Quiroga, J., Abonia, R., Robledo, S.M., Velez, I.D., Upegui, Y., Munoz, J.A., Ospina, V., Nogueras, M. & Cobo, J. 2015. An efficient synthesis of new caffiene-based chalcones, pyrazolines and pyrazolo[3,4-b][1,4]diazepines as potential antimalarial, antitrypanosomal and antileishmanial agents. *European Journal of Medicinal Chemistry* 93: 401-413.

Ivachtchenko, A. V., Ivanenkov, Y. A., Kysil, V. M., Krasavin, M. Y. & Ilyin, A.P. 2010. Multicomponent reactions of isocyanides in the synthesis of heterocycles. *Russian Chemical Reviews* 79(9): 861-893.

Iwaniuk, D. P., Whetmore, E. D., Rosa, N., Ekoue-Kovi, K., Alumasa, J., de Dios, A. C., Roepe, P. D. & Wolf, C. 2009. Synthesis and antimalarial activity of new chloroquine analogues carrying a multifunctional linear side chain. *Bioorganic & Medicinal Chemistry* 17: 6560-6566.

Jokipii, A. M. M., Myllyla, V. V., Hokkanen, E. & Jokipii, L. 1977. Penetration of the blood brain barrier by metronidazole and tinidazole. *Journal of Antimicrobial. Chemotherapy* 3(3): 239-245.

Junek, H. & Aigner, H. 1973. Synthesen mit nitrilen, XXXV. Reaktionen von tetracyanäthylen mit heterocyclen. *Chemische Berichet* 106: 914-921.

Kalaria, P. N, Karad, S. C & Raval, D. K. 2018. A review on diverse heterocyclic compounds as the privileged scaffolds in antimalarial drug discovery. *European Journal of Medicinal Chemistry* 158: 917-936.

Kalita1, J., Chetia1, D. & Rudrapal, M. 2020. Design, Synthesis, Antimalarial Activity and Docking Study of 7-Chloro-4-(2-(substituted benzylidene)hydrazineyl)quinolines. *Medicinal Chemistry* 16(7): 928-937.

Kamath, P. R., Sunil, D. & Ajees, A. A. 2016. Synthesis of indole–quinoline–oxadiazoles: Their anticancer potential and computational tubulin binding studies. *Research on Chemical Intermediates* 42(6): 5899-5914.

Kaur, K., Jain, M., Kaur, T. & Jain, R. 2009. Antimalarials from nature, *Bioorganic & Medicinal Chemistry* 17: 3229-3256.

Kaur, K., Jain, M., Reddy, R. P. & Jain, R. 2010. Quinolines and structurally related heterocycles as antimalarials. *European Journal of Medicinal Chemistry* 45(8): 3245-3264.

Kaur, R. & Kumar, K. 2021. Synthetic and medicinal perspective of quinolines as antiviral agents. *European Journal of Medicinal Chemistry* 215: 113220.

Kayamba, F., Malimabe, T., Ademola, I. K., Pooe, O. J., Kushwaha, N. D., Mahlalela, M., van Zyl, R. L., Gordon, M., Mudau, P. T., Zininga, T., Shonhai, A., Nyamori, V. O & Karpoormath, R. 2021. Design and synthesis of quinoline-pyrimidine inspired hybrids as potential plasmodial inhibitors. *European Journal of Medicinal Chemistry* 217: 113330.

Kekeli, E. K., Kimberly, Y., Daniel, P. I., Jayakumar, K. N. & Christian W. 2009. Synthesis and antimalarial activity of new 4-amino-7-chloroquinolyl amides, sulfonamides, ureas and thioureas. *Bioorganic & Medicinal Chemistry* 17(1): 270-283.

Kiyani, H., Samimi, H. A., Ghorbani, F. & Esmaieli, S. 2013. One-pot, four-component synthesis of pyrano[2,3-c]pyrazoles catalyzed by sodium benzoate in aqueous medium. *Current Chemistry Letters* 2(4): 197-206.

Kondaparla, S., Debnath, U., Soni, A., Dola, V. R., Sinha, M., Srivastava, K., Puri, S. K. & Katti, S. B. 2018. Synthesis, Biological Evaluation, and Molecular Modeling Studies of Chiral Chloroquine Analogues as Antimalarial Agents. *Antimicrobial Agents and Chemotherapy* 62(12): e02347-17.

Kondaparla, S., Manhas, A., Dola, V. R., Srivastava, K., Puri, S. K. & Katti, S. B. 2018. Design, Synthesis and Antiplasmodial activity of novel imidazole derivatives based on 7-chloro-4-aminoquinoline. *Bioorganic Chemistry* 80: 204-211.

Kondaparla, S., Soni, A., Manhas, A., Srivasta, K., Puri, S. K. & Katti, S. B. 2017. Antimalarial activity of novel 4-aminoquinolines active against drug-resistant strains. *Bioorganic Chemistry* 70: 74-85.

Kosaisavee, V., Suwanarusk, R., Nosten, F., Kyle, D. E., Barrends, M., Jones, J., Price, R., Russell, B. & Lek-Uthai, U. 2006. *Plasmodium vivax*: isotopic, PicoGreen, and microscopic assays for measuring chloroquine sensitivity in fresh and cryopreserved isolates, *Experimental Parasitology* 114(1) :34e39.

Kucharski, D. J., Jaszczak, M. K. & Boratyński, P. J. 2022. A review of modifications of quinoline antimalarials: mefloquine and (hydroxy)chloroquine. *Molecules* 27(3): 1003.

Kumar, S., Bhardwaj, T. R., Prasad, D. N. & Singh, R. K. 2018. Drug targets for resistant malaria: Historic to future perspectives. *Biomedicine & Pharmacotheraphy* 104: 8-27.

Kumar, G., Tanwer, O., Kumar, J., Akhter, M., Sharma, S., Pillai, C. R., Alam, M. M. & Zama, M. S. 2018. Pyrazole-pyrazoline as promising novel antimalarial agents: A mechanistic study. *European Journal of Medicinal Chemistry* 149: 139-147.

Kumar, P., Kadyan, K., Duhan, M., Sindhu, J., Singh, V. & Saharan, B.S. 2017. Design, synthesis, conformational and molecular docking study of some novel acyl hydrazone based molecular hybrids as antimalarial and antimicrobial agents. *Chemistry Central Journal* 11(1) 115.

Kuo, S. C., Huang, L. J. & Nakamura, H. 1984. Studies on heterocyclic compounds. 6. Synthesis and analgesic and antiinflammatory activities of 3,4-dimethylpyrano[2,3-c]pyrazol-6-one derivatives. *Journal of Medicinal Chemistry* 27(4); 539-544.

Lambros, C., & Vanderberg, J. P., 1979. Synchronization of *Plasmodium falciparum* erythrocytic stages in cultur. Journal of Parasitology 65(3): 418-420.

Lawrenson, A. S., Cooper, D. L., O'Neill, P. M. & Berry, N. G. 2018. Study of the antimalarial activity of 4-aminoquinoline compounds against chloroquine-sensitive and chloroquine-resistant parasite strains. *Journal of Molecular Modeling* 24(9): 237.

Leven, M., Held, J., Duffy, S., Avelar, L. A. A., Meister, S., Delves, M., Plouffe, D., Kuna, K., Tschan, S., Avery, V. M., Winzeler, E. A., Mordmüller, B. & Kurz, T. 2019. Novel 8-aminoquinolines containing an aminoxyalkyl side chain exert in vitro dual-stage antiplasmodial activity. *ChemMedChem* 14(4): 501-511.

Lipinski, C. A., Lombardo, F., Dominy, B. W. & P. J. 1997. Feeney, Experimental and computational approaches to estimate solubility and permeability in drug discovery and development settings. *Advanced drug delivery reviews* 23(1): 3-25.

Loeb, F., Clark, W. M., Coateny, G. R., Coggeshall, L. T., Dieuaide, F. R., Dochez, A. R., Hankansson, E. G., Marshall Jr, E. K., Marvel, C. S., McCoy, O. R., Sapero, J. J., Sebrell, W. H., Shannon, J. A. & Carden Jr, G. A. 1946. Activity of a new antimalarial agent, chloroquine (SN 7618): statement approved by the board for

coordination of malarial studies. *Journal of American Medicinal Association* 130: 1069.

Lovering, F., Bikker, J. & Humblet, C. 2009. Escape from flatland: increasing saturation as an approach to improving clinical success. *Journal of Medicinal Chemistry* 52(21): 6752-6756.

Maarop, M. S., Rashid, F. N. A. A., Mohammat, M. F., Shaameri, Z., Johari, S. A., Isa, M. M. & Low A. L. M. 2020. New access to pyrano[2,3-*c*]pyrazole-3-carboxylates via domino four-component reaction and their antimicrobial activity. *Indonesian journal of Chemistry* 20(1): 60-71.

Mahmud, A. W., Shallangwa, G. A. & Uzairu, A. 2020. *In silico* modeling of tetraoxane-8- aminoquinoline hybrids active against *Plasmodium falciparum*. *Beni-Suef University Journal of Basic and Applied Sciences* 9: 19.

Makler, M. T. & Hinrichs, D. J. 1993. Measurement of the lactate dehydrogenase activity of *Plasmodium falciparum* as an assessment of parasitemia. *American Journal of Tropical Medicine and Hygiene* 48: 205-210.

Malaria vaccine: WHO position paper, Wkly. Epidemiol. Rec. 2016. 91(4): 33-52.

Mandha, S. R., Siliveri, S., Alla, M., Bommena, V.R., Bommineni, M.R. & Balasubramanian, S. 2012. Eco-friendly synthesis and biological evaluation of substituted pyrano[2,3-*c*]pyrazoles. *Bioorganic & Medicinal Chemistry Letters* 22(16): 5272-5278.

Manohar, S., Khan, S. I. & Rawat, D. S. 2010. Synthesis, antimalarial activity, and cytotoxicity of 4-aminoquinoline-triazine conjugates. *Bioorganic and Medicinal Chemistry Letters* 20(1): 322-325.

Manohar, S., Rajesh, C., Khan, S. I., Tekwani, B. L. & Rawat, D. S. 2012. Novel 4-aminoquinoline-pyrimidine based hybrids with improved *in vitro* and *in vivo* antimalarial activity. *ACS Medicinal Chemistry Letters* 3(7): 555-559.

Mao, J., Wang, Y., Wan, B., Kozikowski, A. P. & Franzblau, S. G. 2007. Design, synthesis, and pharmacological evaluation of mefloquine-based ligands as novel antituberculosis agents. *ChemMedChem* 2(11): 1624-30.

Marinho, J. A. et al. 2021. *In Vitro* and *in Vivo* Antiplasmodial Activity of Novel Quinoline Derivative Compounds by Molecular Hybridization. *European Journal of Medicinal Chemistry* 215: 113271.

Maurya, S. S., Bahuguna, A., Khan, S. I., Kumar, D., Kholiya, R. & Rawat, D. S. 2019. N-substituted aminoquinoline-pyrimidine hybrids: Synthesis, *in vitro* antimalarial activity evaluation and docking studies. *European Journal of Medicinal Chemistry* 162: 277-289.

Meunier, B. 2008. Hybrid molecules with a dual mode of action: Dream or reality? *Accounts of Chemical Research* 41(1): 69-77.

Minic, A., de Walle, T. V., Hecke, K. V., Combrinck, J., Smith, P. J., Chibale, K. & D'hooghe, M. 2020. Design and synthesis of novel ferrocene-quinoline conjugates and evaluation of their electrochemical and antiplasmodium properties. *European Journal of Medicinal Chemistry* 187: 111963.

Ministry of Health Malaysia. Guidelines for malaria vector control in Malaysia. Putrajaya, Malaysia: Ministry of Health Malaysia; 2022.

Miotto, O., Almagro-Garcia, J., Manske, M., MacInnis, B., Campino, S., Rockett, K. A. & Sreng, S. 2013. Multiple populations of artemisinin-resistant *Plasmodium falciparum* in Cambodia. *Nature Genetics* 45: 648-655.

Mistry, P. T., Kamdar, N. R., Haveliwala, D. D. & Patel, S. K. 2012. Synthesis, characterization, and *in vitro* biological studies of some novel pyran fused pyrimidone derivatives. *Journal of Heterocyclic Chemistry* 49(2): 349-357.

Mohammat, M. F., Maarop, M. S., Shaameri, Z., Wibowo, A., Johari, S. A. & Hamzah, A. S. 2018. Practical synthesis and electronic study of non-spiro and spiropyrano[2,3-c]pyrazole-3-carboxyate derivatives via uncatalyzed domino one-pot, four-component reactions. *Organic Communications* 11: 149-162.

Morphy, R. & Rankovic, Z. 2005. Designed multiple ligands. An emerging drug discovery paradigm. *Journal of Medicinal Chemistry* 48(21): 6523-6543.

Morris, G. M., Huey, R., Lindstrom, W., Sanner, M. F., Belew, R. K., Goodsell, D. S. & Olson, A. J. 2009. AutoDock4 and AutoDockTools4: automated docking with selective receptor flexibility. *Journal of Computational Chemistry* 30(16): 2785–2791.

Morris, G. M. & Lim-wilby, M. 2008. Methods in Molecular Biology. New Jersey: Humana Press.

Mosmann, T. 1983. Rapid colorimetric assay for cellular growth and survival: application to proliferation and cytotoxicity assays. *Journal of Immunological Methods* 65(1-2): 55-63.

Muhammed, M. T. & Aki-Yalcin, E. 2024. Molecular docking: Principles, advances, and its applications in drug discovery. *Letters in Drug Design & Discovery* 21(3): 480-495.

Narasimhan, V. & Attaran, A. 2003. Roll Back Malaria? The scarcity of international aid for malaria control. *Malaria Journal* 2(1): 8.

Neto, G. J. S., Silva, L. R., de Omena, R. J. M., Aguiar, A. C. C., Annunciato, Y., Rossetto, B. S., Gazarini, M. L., Heimfarth, L., Quintans-Junior, L. J., da Silva-Junior, E. F. & Meneghetti, M. R. 2022. Dual quinoline-hybrid compounds with antimalarial activity against *Plasmodium falciparum* parasites. *New Journal of Chemistry* 46: 6502-6518.

Nkhoma, S., Molyneux, M. & Ward, S. 2007. *In vitro* anti-malarial susceptibility profile and prcrt/pfmdr-1 genotypes of *Plasmodium falciparum* field isolates from

Malawi. *American Journal of Tropical Medicine and Hygiene* 76 (6): 1107-1112.

Nqoro, X. & Aderibigbe, B. A. 2020. 4-Aminoquinoline-ferrocene Hybrids as Potential Antimalarials. *Recent patents on Anti-infective Drug Discovery* 15(2): 157-172.

Nuwaha, F. 2001. The challenge of chloroquineresistant malaria in sub-Saharan Africa. *Health Policy Plan* 16(1): 1-12.

Nyamwihura, R. J., Zhang, H., Collins, J. T., Crown, O. & Ogungbe, I. V. 2021. Nopol-Based Quinoline Derivatives as Antiplasmodial Agents. *Molecules* 26(4): 1008.

Nzila, A., & Mwai, L. 2010. *In vitro* selection of *Plasmodium falciparum* drug-resistant parasite lines. *Journal of Antimicrobial Chemotheraphy* 65(3): 390-398.

Okombo, J. & Chibale, K. 2018. Recent updates in the discovery and development of novel antimalarial drug candidates. *Medicinal Chemistry Communications* 9(3): 437-453.

Otto, S. & Engberts, J. B. F. N. 2000. Diels Alder reactions in water. *Pure and Applied Chemistry* 72(7): 1365-1372.

Palla, D., Antoniou, A. I., Baltas, M., Menendez, C., Grellier, P., Mouray, E. & Athanassopoulos, C. M. 2020. Synthesis and Antiplasmodial Activity of Novel Fosmidomycin Derivatives and Conjugates with Artemisinin and Aminochloroquinoline. *Molecules* 25(20): 4858.

Pandey, A. V., Bisht, H., Babbarwal, V. K., Srivastava, J., Pandey, K. C. & Chauhan, V. S. 2001. Mechanism of malarial haem detoxifica tion inhibition by chloroquine. *Biochemical Journal* 355: 333-338.

Pandya, K. M., Patel, A. H. & Desai, P. S. 2020. Development of antimicrobial, antimalarial and antitubercular compounds based on a quinoline-pyrazole clubbed scaffold derived via Doebner reaction. 3: 89-98.

Parikh, P. H., Timaniya, J. B., Patel, M. J. & Patel, K. P. 2022. Microwave-assisted synthesis of pyrano[2,3-*c*]-pyrazole derivatives and their anti-microbial, anti-malarial, anti-tubercular, and anti-cancer activities. *Journal of Molecular Structure* 1249, 131605.

Parth, Kaur, N., Korkor, C., Mobin, S. M., Chibale, K. & Singh, K. 2022. Fluorene-Chloroquine Hybrids: Synthesis, *in vitro* Antiplasmodial Activity, and Inhibition of Heme Detoxification Machinery of *Plasmodium falciparum*. *ChemMedChem* 17(19): e202200414.

Patel, A. J., Patel, M. P., Dholakia, A. B., Patel, V. C. & Patel, D. S. 2022. Antitubercular, Antimalarial Activity and Molecular Docking Study of New Synthesized 7- Chloroquinoline Derivatives. *Polycyclinic Aromatic Compounds* 42: 4717-4725.

Pavic, K., Perkovic, I., Pospisilova, S., Machado, M., Fontinha, D., Prudencio, M., Jampilek, J., Coffey, A., Endersen, L., Rimac, H. & Zorc, B. l. 2018. Primaquine hybrids as promising antimycobacterial and antimalarial agents. *European Journal of Medicinal Chemistry* 143: 769-779.

Pawar, P., Mane, B., Salve, M. & Bafana, S. 2017. Synthesis and anticonvulsant activity of n-substituted-7-hydroxy-4-methyl-2-oxa-quinoline derivatives. *International Journal of Drug Research and Technology* 3(3): 60-66.

Payne, D. 1987. Spread of chloroquine resistance in *Plasmodium falciparum*. *Parasitol Today* 3(8): 241-246.

Pepe, D. A., Toumpa, D., André-Barrès, C., Menendez, C., Mouray, E., Baltas, M., Grellier, P., Papaioannou, D. & Athanassopoulos, C. M. 2020. Synthesis of novel G factor- or chloroquine-artemisinin hybrids and conjugates with potent antiplasmodial activity. *ACS Medicinal Chemistry Letters* 11(5): 921-927.

Pereira, C. S., Quadros, H. C., Moreira, D. R. M., Castro, W., Silva, R. I. S. D. D. D., Soares, M. B. P., Fontinha, D., Prudêncio, M., Schmitz, V., Santos, H. F. D., Gendrot, M., Fonta, I., Mosnier, J., Pradines, B. & Navarro, M. 2021. A Novel Hybrid of Chloroquine and Primaquine Linked by Gold(I): Multitarget and Multiphase Antiplasmodial Agent. *ChemMedChem* 16(4): 662-678.

Pinzi, L. & Rastelli, G. 2019. Molecular docking: shifting paradigms in drug discovery. *International Journal of Molecular Sciences* 20(18): 4331.

Poje, G., de Carvalho, L. P., Held, J., Moita, D., Prudˆencio, M., Perkovi´c, I., Tandari´c, T., Vianello, R. & Raji´c, Z. 2022. Design and synthesis of harmiquins, harmine and chloroquine hybrids as potent antiplasmodial agents. *European Journal of Medicinal Chemistry* 238: 114408.

Poonam, Gupta, Y., Gupta, N., Singh, H., Wu, L., Chhikra, B. S., Rawat, M. & Rathi, B. 2018. Multistage inhibitors of the malaria parasite: emerging hope for chemoprotection and malaria eradication. *Medicinal Research Reviews* 38(5): 1511-1535.

Prasad, P., Kalola, A. G. & Patel, M. P. 2018. Microwave assisted one-pot synthetic route to imidazo[1,2-a]pyrimidine derivatives of imidazo/triazole clubbed pyrazole and their pharmacological screening. *New Journal of Chemistry* 42: 12666-12676.

Qin, H. -L., Zhang, Z. -W., Lekkala, R., Alsulami, H. & Rakesh, K. P. 2020. Chalcone hybrids as privileged scaffolds in antimalarial drug discovery: A key review. *European Journal of Medicinal Chemistry* 193: 112215.

Radfar, A., Méndez, D., Moneriz, C., Linares, M., Marín-garcía, P., Puyet, A., Diez, A. & Bautista, J. M. 2009. Synchronous culture of *Plasmodium falciparum* at high parasitemia levels. *Nature Protocols* 4(12): 1899–1915.

Raj, R., Gut, J., Rosenthal, P. J. & Kumar, V. 2014. 1H-1,2,3-Triazole-tethered isatin-7-chloroquinoline and 3-hydroxy-indole-7-chloroquin oline conjugates:

Synthesis and antimalarial evaluation. *Bioorganic & Medicinal Chemistry Letters* 24: 756-759.

Raj, R., Land, K. M. & Kumar, V. 2015. 4-Aminoquinoline-Hybridization en Route Towards the Development of RSC Advances. *RSC Advances* 5: 82676-82698.

Ramasamy, R. & Surendran, S. N. 2012. Global climate change and its potential impact on disease transmission by salinity-tolerant mosquito vectors in coastal zones. *Frontiers in Physiology* 3: 1-14.

Ramiz, M. M. M., Hafiz, I. S. A., Rahim, M. A. M. A. & Gaber, H. M. 2012. Pyrazolones as building blocks in heterocyclic synthesis: Synthesis of new pyrazolopyran, pyrazolopyridazine and pyrazole derivatives of expected antifungicidal activity. *Journal of the Chinese Chemical Society* 59(1): 72-80.

Ramírez, H., Fernandez-Moreira, E., Rodrigues, J. R., Mijares, M. R., Ángel, J.E. & Charris, J.E. 2022. Synthesis and *in silico* ADME/Tox profiling studies of heterocyclic hybrids based on chloroquine scaffolds with potential antimalarial activity. *Parasitology Research* 121(1): 441-451.

Rani, A., Kumar, S., Legac, J., Adeniyi, A. A., Awolade, P., Singh, P., Rosenthal, P.J. & Kumar, V. 2020. Design, synthesis, heme binding and density functional theory studies of isoindoline-dione-4-aminoquinolines as potential antiplasmodials. *Future Medicinal Chemistry* 12(3): 193-205.

Rani, A., Legac, J., Rosenthal, P. J. & Kumar, V. 2019. Substituted 1,3-dioxoisoindoline-4-aminoquinolines coupled via amide linkers: Synthesis, antiplasmodial and cytotoxic evaluation. *Bioorganic Chemistry* 88: 102912.

Rani, A., Singh, A., Gut, J., Rosenthal, P. J. & Kumar, V. 2018. Microwave-promoted facile access to 4-aminoquinolinephthalimides: Synthesis and anti-plasmodial evaluation. *European Journal of Medicinal Chemistry* 143: 150.

Rathod, G. K., Jain, M., Sharma, K. K., Das, S., Basak, A. & Jain. R. 2022. New structural classes of antimalarials. *European Journal of Medicinal Chemistry* 242: 114653.

Ravindar, L., Hasbullah, S. A., Rakesh, K. P. & Hassan, N. I. 2022. Pyrazole and pyrazoline derivatives as antimalarial agents: A key review. *European Journal of Pharmaceutical Science* 183: 106365.

Ravindar, L., Hasbullah, S. A., Rakesh, K. P. & Hassan, N. I. 2023. Recent developments in antimalarial activities of 4-aminoquinoline derivatives. *European Journal of Medicinal Chemistry* 256: 115458.

Ravindar, L., Hasbullah, S. A., Rakesh, K. P. & Hassan, N. I. 2023. Triazole hybrid compounds: A new frontier in malaria treatment. *European Journal of Medicinal Chemistry* 259: 115694.

Read, J. A., Wilkinson, K. W., Tranter, R., Sessions, R. B. & Brady, R. L. 1999. Chloroquine binds in the cofactor binding site of *Plasmodium falciparum* lactate dehydrogenase. *The Journal of biological chemistry* 274(15): 10213-10218.

Rossier, J., Sovari, S. N., Pavic, A., Vojnovic, S., Stringer, T., Bättig, S., Smith, G. S., Nikodinovic-Runic, J. & Zobi, F. 2019. Antiplasmodial Activity and *In Vivo* Bio-Distribution of Chloroquine Molecules Released with a 4-(4-Ethynylphenyl)-Triazole Moiety from Organometallo-Cobalamins. *Molecules* 24(12): 2310.

Roy, D., Anas, M., Manhas, A., Saha, S., Kumar, N. & Panda, G. 2022. Synthesis, biological evaluation, Structure-Activity relationship studies of quinoline-imidazole derivatives as potent antimalarial agents. *Bioorganic Chemistry* 121: 105671.

Runge F.F. 1834. *Ann Physik Und Chem* 31: 65.

Russell, B., Chalfein, F., Prasetyorini, B., Kenangalem, E., Piera, K., Suwanarusk, R., Brockman, A., Prayoga, P., Sugiarto, P., Cheng, Q., Tjitra, E., Anstey, N. M. & Price, R. N. 2008. Determinants of *in vitro* drug susceptibility testing of *Plasmodium vivax*. *Antimicrobial Agents Chemotheraphy* 52(3): 1040e1045.

Saeedi, M., Rastegari, A., Hariri, R., Mirfazli, S. S., Mahdavi, M., Edraki, N., Firuzi, O. & Akbarzadeh, T. 2020. Design and synthesis of novel arylisoxazole-chromenone carboxamides: Investigation of biological activities associated with Alzheimer's disease. *Chemistry & Biodiversity* 17(5): e1900746.

Sahu, R., Walker, L. A. & Tekwani, B. L. 2014. *In vitro* and *in vivo* anti-malarial activity of tigecycline, a glycylcycline antibiotic, in combination with chloroquine. *Malaria Journal* 13(1): 414.

Saini, A., Kumar, S., Raj, R., Chowdhary, S., Gendrot, M., Mosnier, J., Fonta, I., Pradines, B. & Kumar, V. 2021. Synthesis and antiplasmodial evaluation of 1H-1,2,3-triazole grafted 4-aminoquinoline-benzoxaborole hybrids and benzoxaborole analogues. *Bioorganic Chemistry* 109: 104733.

Sanner, M. F. 1999. Python: a programming language for software integration and development. *Journal of molecular graphics & modelling* 17(1): 57-61.

Sarr, S. O., Perrotey, S., Fall, I., Ennahar, S., Zhao, M., Diop, Y. M., Candolfi, E. & Marchioni, E. 2011. Icacina senegalensis (Icacinaceae), traditionally used for the treatment of malaria, inhibits *in vitro Plasmodium falciparum* growth without host cell toxicity. *Malaria Joural* 10: 85-95.

Sashidhara, K. V., Kumar, M., Modukuri, R. K., Srivastava, R. K., Soni, A., Srivastava, K., Singh, S. V., Saxena, J. K., Gauniyal, H. M. & Puri, S. K. 2012. Antiplasmodial activity of novel keto-enamine chalconechloroquine based hybrid pharmacophores. *Bioorganic & Medicinal Chemistry* 20(9): 2971-81

Satasia, S. P., Kalaria, P. N. & Raval, D. K. 2014. Catalytic regioselective Synthesis of pyrazole based pyrido[2,3-d]pyrimidine-diones and their biological evaluation. *Organic & Biomolecular Chemistry* 12(11): 1751-1758.

Shalini, Kumar, S., Gendrot, M., Fonta, I., Mosnier, J., Cele, N., Awolade, P., Singh, P., Pradines, B. & Kumar, V. 2020. Amide Tethered 4-Aminoquinoline-naphthalimide Hybrids: A New Class of Possible Dual Function Antiplasmodials. *ACS Medicinal Chemistry Letter*s 11(12): 2544-552.

Shalini, Legac, J., Adeniyi, A. A., Kisten, P., Rosenthal, P. J., Singh, P. & Kumar, V. 2020. Functionalized Naphthalimide-4-aminoquinoline Conjugates as Promising Antiplasmodials, with Mechanistic Insights, *ACS Medicinal Chemistry Letters* 11(12): 154-161.

Shamsuddin, M. A., Ali, A. H., Zakaria, N. H., Mohammat, M. F., Hamzah, A. S., Shaameri, Z., Lam, K. W., Mark-Lee, W. F., Agustar, H. K., Mohd Abd Razak, M. R., Latip, J. & Hassan, N. I. 2021. Synthesis, molecular docking, and antimalarial activity of hybrid 4-aminoquinoline-pyrano[2,3-c]pyrazole derivatives. *Pharmaceuticals*. 14: 1174-1190.

Shamsuddin, M. A., Zakaria1, N. H., Mohammat, M. F., Syahri, J., Latip, J. & Hassan, N. I. 2020. Synthesis and Molecular Docking Studies of Pyrano[2,3-c] Pyrazole-3-Carboxylates as Potential Inhibitors of *Plasmodium Falciparum*. *Malaysian Journal of Chemistry* 22: 52-61.

Sharma, B., Kaur, S., Legac, J., Rosenthal, P. J. & Kumar, V. 2020. Synthesis, anti-plasmodial and cytotoxic evaluation of 1H-1,2,3-triazole/acyl hydrazide integrated tetrahydro-β-carboline-4-aminoquinoline conjugates. *Bioorganic & Medicinal Chemistry Letters* 30(2): 126810.

Sharma, B., Legac, J., Cele, N., Awolade, P., Rosenthal, P. J., Singh, P. & Kumar, V. 2022. Functionalized 3-hydroxy-3-aminoquinoline-oxindole hybrids as promising dual-function anti-plasmodials. *European Journal of Medicinal Chemistry Reports* 5: 100052.

Shestopalov, A. M., Emeliyanova, Y. M., Shestopalov, A. A., Rodinovskaya, L. A., Niazimbetova, Z. I. & Evans, D. H. 2003. Cross-condensation of derivatives of cyanoacetic acid and carbonyl compounds. Part 1: Single-stage synthesis of 1′-substituted 6-aminospiro-4-(piperidine-4′)-2H,4H-pyrano[2,3-c]pyrazole-5-carbonitriles. *Tetrahedron* 59(38): 7491-7496.

Shruthi, T. G., Eswaran, S., Shivarudraiah, P., Narayanan, S. & Subramanian, S. 2019. Synthesis, antituberculosis studies and biological evaluation of new quinoline derivatives carrying 1,2,4-oxadiazole moiety. Bioorg. *Bioorganic & Medicinal Chemistry Letters* 29(1): 97-102.

Silva, A. T., Lobo, L., Oliveira, I. S., Gomes, J., Teixeira, C., Nogueira, F., Marques, E. F., Ferraz, R. & Gomes, P. 2020. Building on Surface-Active Ionic Liquids for the Rescuing of the Antimalarial Drug Chloroquine. *International Journal of Molecular Science* 21(15): 5334.

Silveira, F. F., de Souza, J. O., Hoelz, L. V. B., Campos, V. R., Jabor, V. A. P., Aguiar, A. C. C., Nonato, M. C., Albuquerque, M. G., Guido, R. V. C., Boechat, N. & Pinheiro, L. C. S. 2021. Comparative study between the anti-*P. falciparum* activity of triazolopyrimidine, pyrazolopyrimidine and quinoline derivatives and the identification of new PfDHODH inhibitors. *European Journal of Medicinal Chemistry* 209: 112941.

Silveira, F. F., Feitosa, L. M., Mafra, J. C. M., Ferreira, M. L. G., Rogerio, K. R., Carvalho, L. J. M., Boechat, N. & Pinheiro, L. C. S. 2018. Synthesis and anti-*Plasmodium falciparum* evaluation of novel pyrazolopyrimidine derivatives. *Medicinal Chemistry Research* 27: 1876-1884.

Singh, B., Chetia, D. & Kumawat, M. K. 2021. Synthesis and *in vitro* antimalarial activity evaluation of some new 1,2-diaminopropane side-chain-modified 4-aminoquinoline mannich bases. *Pharmaceutical Chemistry Journal* 55(2): 724-731.

Singh, S., Sharma, N., Upadhyay, C., Kumar, S., Rathi, B. & Poonam. 2018. Small molecules effective against liver and blood stage malarial infection. *Current Topics in Medicinal Chemistry* 18(23): 2008-2021.

Sonar, J. P., Pardeshi, S. D., Dokhe, S. A., Zine, A. M., Pawar, R. P. & Thore, S. N. 2018. An efficient protocol for the one-pot synthesis of pyranopyrazoles in aqueous medium using triethanolamine as a catalyst. *Archives of Organic and Inorganic Chemical Sciences* 3(1): 3-6.

Sonia, T. A. & Sharma, C. P. 2014. Oral Delivery of Insulin, Woodhead Publishing Series in Biomedicine. *Woodhead Publishing* 1: 128-129.

Sovari, S. N., Golding, T. M., Mbaba, M., Mohunlal, R., Egan, T. J. & Smith, G. S. 2022. Fabio Zobi, Rhenium(I) derivatives of aminoquinoline and imidazolopiperidine-based ligands: Synthesis, *in vitro* and *in silico* biological evaluation against *Plasmodium falciparum*. *Journal of Inorganic Biochemistry* 234: 111905.

Srbljanovic, J., Bobic, B., Štajner, T., Uzelac, A., Opsenica, I., Terzic-Jovanovic, N., Bauman, N., Šolaja, B. A. & Djurkovic-Djakovic, O. 2020. Aminoquinolines afford resistance to cerebral malaria in susceptible mice. *Journal of Global Antimicrobial Resistance* 23: 20-25.

Strasek, N., Lavrencic, L., Ostrek, A., Slapsak, D., Groselj, U., Klemencic, M., Zugelj, H. B., Wagger, J., Novinec, M. & Svete, J. 2019. Tetrahydro-1H,5H-pyrazolo[1,2-a]pyrazole-1-carboxylates as inhibitors of *Plasmodium falciparum* dihydroorotate dehydrogenase. *Bioorganic Chemistry* 89: 102982.

Stringer, T., Melis, D. R. & Smith, G. S. 2019. N,O-chelating quinoline-based half-sandwich organorhodium and -iridium complexes: synthesis, antiplasmodial activity and preliminary evaluation as transfer hydrogenation catalysts for the reduction of NAD+. *Dalton Transactions* 48(35): 13143-13148.

Stringer, T., Quintero, M. A. S., Wiesner, L., Smith, G. S. & Nordlander, E. 2019. Evaluation of PTA-derived ruthenium(II) and iridium(III) quinoline complexes against chloroquine-sensitive and resistant strains of the *Plasmodium falciparum* malaria parasite. *Journal of Inorganic Biochemistry* 191: 164-173.

Stringer, T., Wiesner, L. & Smith, G. S. 2019. Ferroquine-derived polyamines that target resistant *Plasmodium falciparum*. *European Journal of Medicinal Chemistry* 179: 78-83.

Sun, B., Liu, K., Han, J., Zhao, L., Su, X., Lin, B., Zhao, D. -M. & Cheng, M. -S. 2015. Design, synthesis, and biological evaluation of amide imidazole derivatives as novel metabolic enzyme CYP26A1 inhibitors. *Bioorganic & Medicinal Chemistry* 23(20): 6763-6773.

Talundzic, E., Okoth, S. A., Congpuong, K., Plucinski, M. M., Morton, L., Goldman, I. F., Kachur, P. S., Wongsrichanalai, C., Satimai, W., Barnwell, J. W. & Udhayakumar, V. 2015. Selection and Spread of Artemisinin-Resistant Alleles in Thailand Prior to the Global Artemisinin Resistance Containment Campaign. *PLOS Pathogens* 11(4): e1004789.

Thillainayagam, M., Pandian, L. & Murugan, K. K. 2014. *In silico* analysis reveals the anti-malarial potential of quinolinyl chalcone derivatives. *Journal of Biomolecular Structure and Dynamics* 33(5): 37-41.

Trager, W. & Jensen, J. 1976. Human malaria parasites in continuous culture. *Science* 193(4254): 673-676.

Trager, W. & Jensen, J. B. 1977. Cultivation of erythrocytic stages. *Bulletin of the World Health Organisation* 55(2-3): 361-365.

Tripathi, M., Khan, S., Ponnan, P., Kholiya, R. & Rawat, D. 2017. Aminoquinoline-Pyrimidine-Modified Anilines: Synthesis, *In Vitro* Antiplasmodial Activity, Cytotoxicity, Mechanistic Studies and ADME Predictions. *ChemistrySelect* 2: 9074-9083.

Teixeira, C., Vale, N., Pérez, B., Gomes, A., Gomes, J. R. B. & Gomes, P. 2014. Recycling Classical Drugs for Malaria. *Chemical Reviews* 114(22): 11164-11220.

Tibon, N. S., Ng, C. H. & Cheong, S. L. 2020. Current progress in antimalarial pharmacotherapy and multi-target drug discovery. *European Journal of Medicinal Chemistry* 188: 111983.

Tiwari, V. S., Joshi, P., Yadav, K., Sharma, A., Chowdhury, S., Manhas, A., Kumar, N., Tripathi, R. & Haq, W. 2021. Synthesis and Antimalarial Activity of 4-Methylaminoquinoline Compounds against Drug-Resistant Parasite. ACS Omega 6(20): 12984-12994.

Tognarelli, J. M., Dawood, M., Shariff, M., Grover, V. P. B., Crossey, M. M., Cox, I. J.,Taylor-Robinson, S. D., & McPhail, M. 2015. Magnetic Resonance

Spectroscopy:Principles and Techniques: Lessons for Clinicians. *Journal of Clinical and Experimental Hepatology* 5(4): 320–328.

Tripathi, M., Taylor, D., Khan, S. I., Tekwani, B. L., Ponnan, P., Das, U. S., Velpandian, T. & Rawat, D. S. 2019. Hybridization of fluoro-amodiaquine (FAQ) with pyrimidines: Synthesis and antimalarial efficacy of FAQ-pyrimidines. *ACS Medicinal Chemistry Letters* 10(5): 714-719.

Uddin, A., Chawla, M., Irfan, I., Mahajan, S., Singh, S. & Abid, M. 2021. Medicinal Chemistry Updates on Quinoline- and Endoperoxide-Based Hybrids with Potent Antimalarial Activity. *RSC Medicinal Chemistry* 12: 24-42.

Valverde, E. A., Romero, A. H., Acosta, M. E., Gamboa, N., Henriques, G., Rodrigues, J. R., Ciangherotti, C. & opez, S. E. L. 2018. Synthesis, β-hematin inhibition studies and antimalarial evaluation of new dehydroxy isoquine derivatives against *Plasmodium berghei*: A promising antimalarial agent. *European Journal of Medicinal Chemistry* 148: 498-506.

Vandekerckhove, S. & D'Hooghe, M. 2015. Quinoline-based antimalarial hybrid compounds. *Bioorganic & Medicinal Chemistry* 23(16): 5098-119.

Vangapandu, S., Jain, M., Kaur, K., Patil, P., Patel, S. R. & Jain, R. 2007. Recent advances in antimalarial drug development. *Medicinal Research Reviews* 27(1): 65-107.

Verma, G., Chashoo, G., Ali, A., Khan, M. F., Akhtar, W., Ali, I., Akhtar, M., Alam, M. M. & Shaquiquzzaman, M. 2018. Synthesis of pyrazole acrylic acid based oxadiazole and amide derivatives as antimalarial and anticancer agents. *Bioorganic Chemistry* 77: 106-124.

Verma, G., Khan, M. F., Nainwal, L. M., Ishaq, M., Akhter, M., Bakht, A., Anwer, T., Afrin, F., Islamuddin, M., Husain, I., Alam, M. M. & Shaquiquzzaman, M. 2019. Targeting malaria and leishmaniasis: Synthesis and pharmacological evaluation of novel pyrazole 1,3,4-oxadiazole hybrids. Part II, *Bioorganic Chemistry* 89: 102986.

Vinindwa, B., Dziwornu, G. A. & Masamba, W. 2021. Synthesis and Evaluation of Chalcone-Quinoline Based Molecular Hybrids as Potential Anti-Malarial Agents. *Molecules* 26(13): 4093.

Vippagunta, S.R., Dorn, A., Ridley, R.G. & Vennerstrom, J.L. 2000. Characterization of chloroquine-hematin W-oxo dimer binding by isothermal titration calorimetry, Biochimica et Biophysica Acta 1475: 133-140.

Wadi, I., Prasad, D., Batra, N., Srivastava, K., Anvikar, A. R., Valecha, N. & Nath, M. 2019. Targeting Asexual and Sexual Blood Stages of Human Malaria Parasite *P. falciparum* with 7-Chloroquinoline Based [1,2,3]-Triazoles. *ChemMedChem* 14(4): 484-493.

Waingeh, V. F., Groves, A. T. & Eberle, J. A. 2013. Binding of Quinoline-Based Inhibitors to *Plasmodium falciparum* Lactate Dehydrogenase : A Molecular Docking Study. *Open Journal of Biophysics* 3: 285-290.

Wang, J. L., Liu, D., Zheng, Z. J., Shan, S., Han, X., Srinivasula, S. M., Croce, C. M. Alnemri, E. S. & Huang, Z. 2009. Structure-based discovery of an organic compound that binds Bcl-2-protien and induces apoptosis of tumor cell. *Proceedings of the National Academy of Sciences of the United States of America* 97(13): 7124-7129.

Weber, L. 2002. Multi-component reactions and evolutionary chemistry. *Drug Discovery Today* 7(2): 143-147.

Wei, W., Cherukupalli, S., Jing, L., Liu, X. & Zhan, P. 2020. Fsp3: a new parameter for drug-likeness. *Drug Discovary* 25(10): 1839-1845.

Wellems, T. E. & Plowe, C. V. 2001. Chloroquine-Resistant Malaria. *The Journal of Infectious Diseases* 184(6): 770-776.

Wells, T. N., Hooft van Huijsduijnen, R. & Van Voorhis, W. C. 2015. Malaria medicines: a glass half full?. *Nature Review Drug Discovery* 14(6): 424-442.

Wicht, K. J., Mok, S. & Fidock, D. A. 2020. Molecular mechanisms of drug resistance in *Plasmodium falciparum* malaria. *Annual Review of Microbiology* 74(1): 431-454.

White, N. J. 2010. Artemisinin resistance--the clock is ticking. *Lancet* 376(9758): 2051-2052.

Witschel, M. C., Rottmann, M., Schwab, A., Leartsakulpanich, U., Chitnumsub, P., Seet, M., Tonazzi, S., Schwertz, G., Stelzer, F., Mietzner, T., McNamara, C., Thater, F., Freymond, C., Jaruwat, A., Pinthong, C., Riangrungroj, P., Oufir, M., Hamburger, M., Mäser, P., Sanz-Alonso, L. M., Charman, S., Wittlin, S., Yuthavong, Y., Chaiyen, P. & Diederich, F. 2015. Inhibitors of plasmodial serine hydroxymethyltransferase (SHMT): Cocrystal structures of pyrazolopyrans with potent blood- and liver-stage activities. *Journal of Medicinal Chemistry* 58: 3117-3130.

World malaria report 2018, World Health Organization, Geneva, 2018, p. 166.

World Health Organization (WHO), World Malaria Report 2023, Geneva, 2023. https://www.who.int/teams/global-malaria-programme/reports/world-malariareport-2023.

Yeung, S., Pongtavornpinyo, W., Hastings, I. M., Mils, J. A. & Whit, N. J. 2004. Antimalarial drug resistance, artemisinin-based combination therapy, and the contribution of modeling to elucidating policy choices. *American Journal of Tropical Medicine and Hygiene* 71(2): 179-186.

Yvette, O. M., Malan, S. F., Taylor, D., Kapp, E. & Joubert, J. 2018. Adamantane amine-linked chloroquinoline derivatives as chloroquine resistance modulating

agents in *Plasmodium falciparum*. *Bioorganic & Medicinal Chemistry Letters* 28(8): 1287-1291.

Zakaria, N. H., Lam, K. W. & Hassan, N. I. 2020. Molecular docking study of the interactions between *Plasmodium falciparum* lactate dehydrogenase and 4-aminoquinoline hybrids. *Sains Malaysiana* 49(8): 1905-1913.

Zhao, S., Zhao, L., Zhang, X., Liu, C., Hao, C., Xie, H., Sun, B., Zhao, D. & Cheng, M. 2016. Design, synthesis, and structure-activity relationship studies of benzothiazole derivatives as antifungal agents. *European Journal of Medicinal Chemistry* 123: 514-522.

Zhao, S., Zhang, X., Wei, P., Su, X., Zhao, L., Wu, M., Hao, C., Liu, C., Zhao, D. & Cheng, M. 2017. Design, synthesis and evaluation of aromatic heterocyclic derivatives as potent antifungal agents. *European Journal of Medicinal Chemistry* 137: 96-107.

Zhou, S., Liao, H., Liu, M., Feng, G., Fu, B., Li, R., Cheng, M., Zhao, Y. & Gong, P. 2014. Discovery and biological evaluation of novel 6,7-disubstituted-4-(2-fluorophenoxy)quinoline derivatives possessing 1,2,3-triazole-4-carboxamide moiety as c-Met kinase inhibitors. *Bioorganic & Medicinal Chemistry* 22(22): 6438-6452.

Zhou, W., Wang, H., Yang, Y., Chen, Z. -S., Zou, C. & Zhang, J. 2020. Chloroquine against malaria, cancers and viral diseases. *Drug Discovery* 25(11): 2012-2022.

Zonouz, A. M., Eskandari, I. & Khavasi, H. R. 2012. A green and convenient approach for the synthesis of methyl 6-amino-5-cyano-4-aryl-2,4-dihydropyrano [2,3-c]pyrazole-3-carboxylates via a one-pot, multicomponent reaction in water. *Tetrahedron Letters* 53(41): 5519-5522.

APPENDIX A1

FT-IR SPECTRUM OF PYRANO[2,3-*C*]PYRAZOLE-4-AMINOQUINOLINE 24A

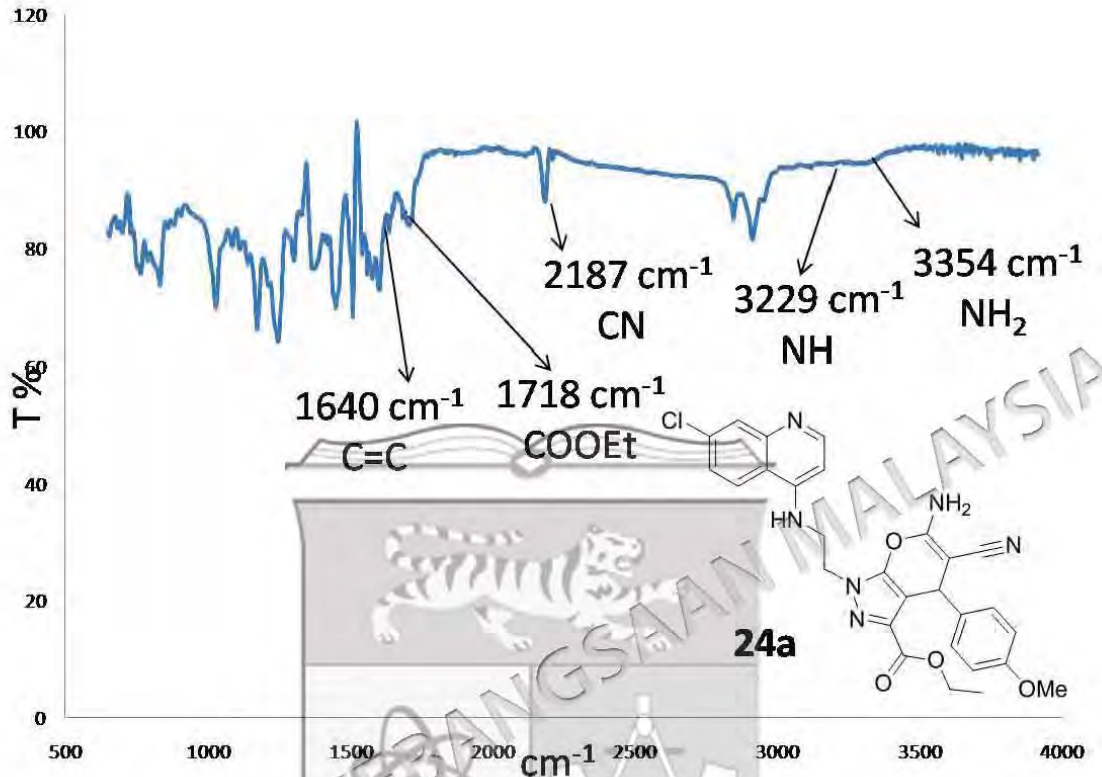

APPENDIX A2

FT-IR SPECTRUM OF PYRANO[2,3-*C*]PYRAZOLE-4-AMINOQUINOLINE 24B

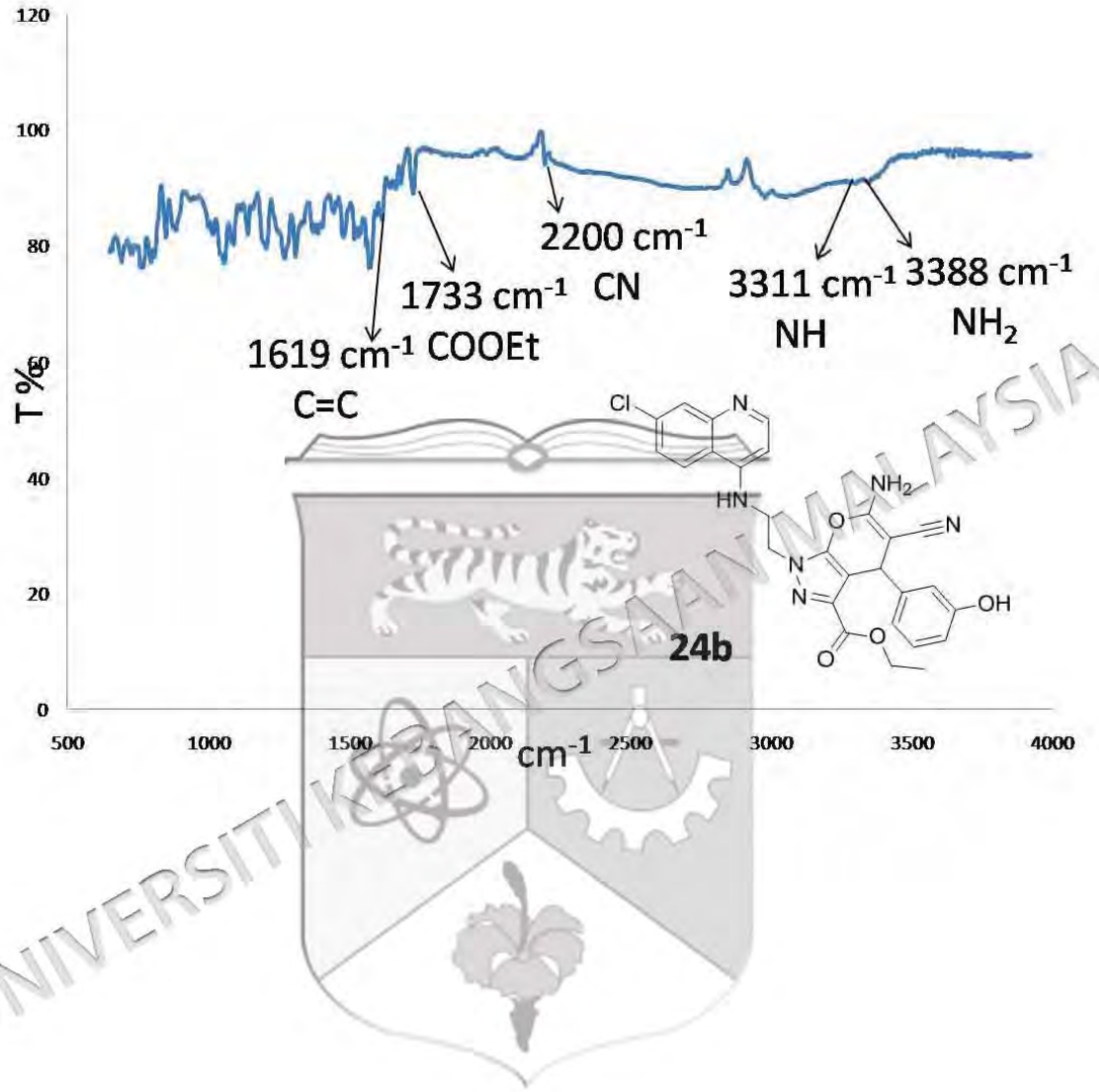

APPENDIX A3

FT-IR SPECTRUM OF PYRANO[2,3-*C*]PYRAZOLE-4-AMINOQUINOLINE 24C

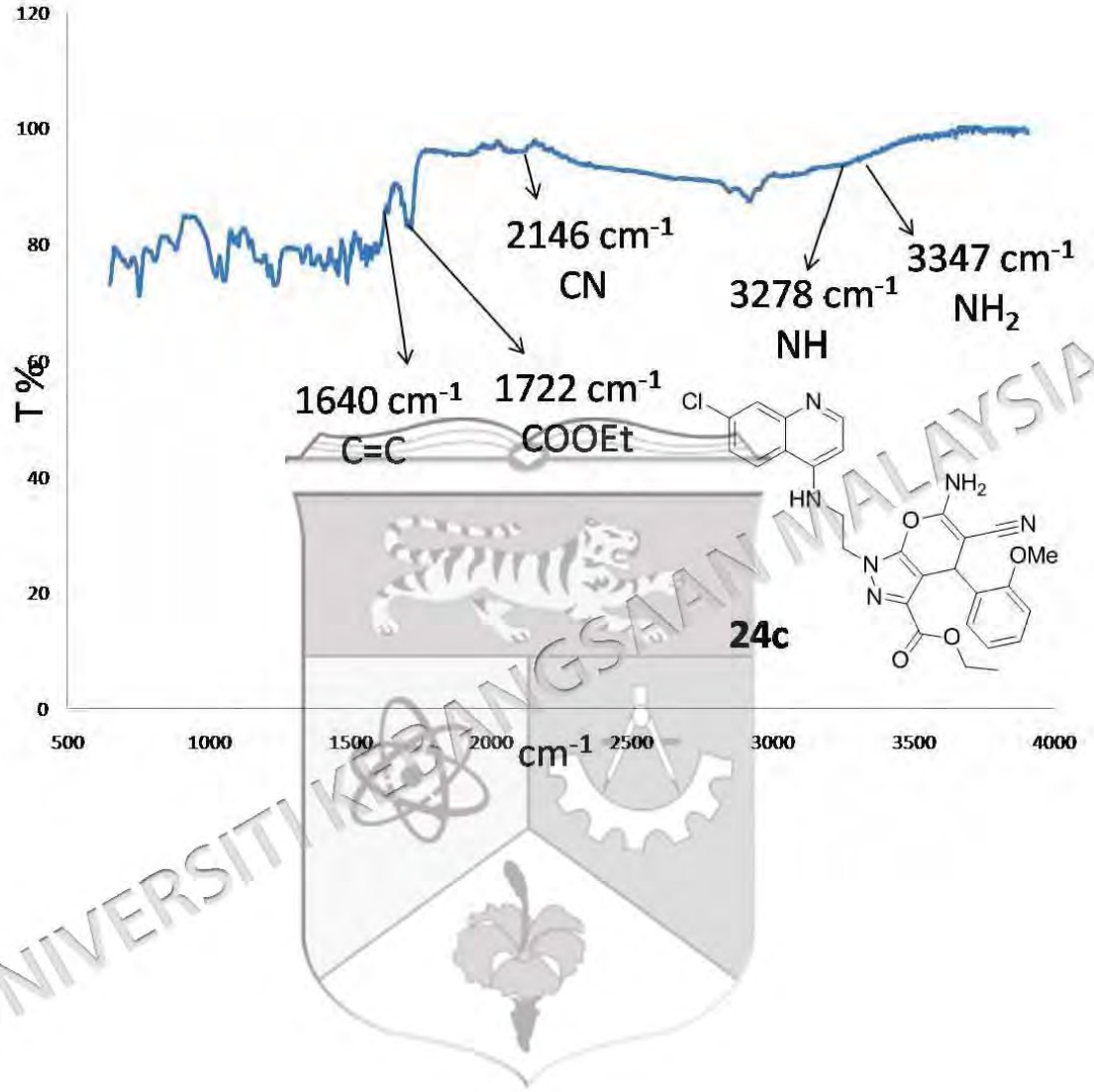

APPENDIX A4

FT-IR SPECTRUM OF PYRANO[2,3-*C*]PYRAZOLE-4-AMINOQUINOLINE 24D

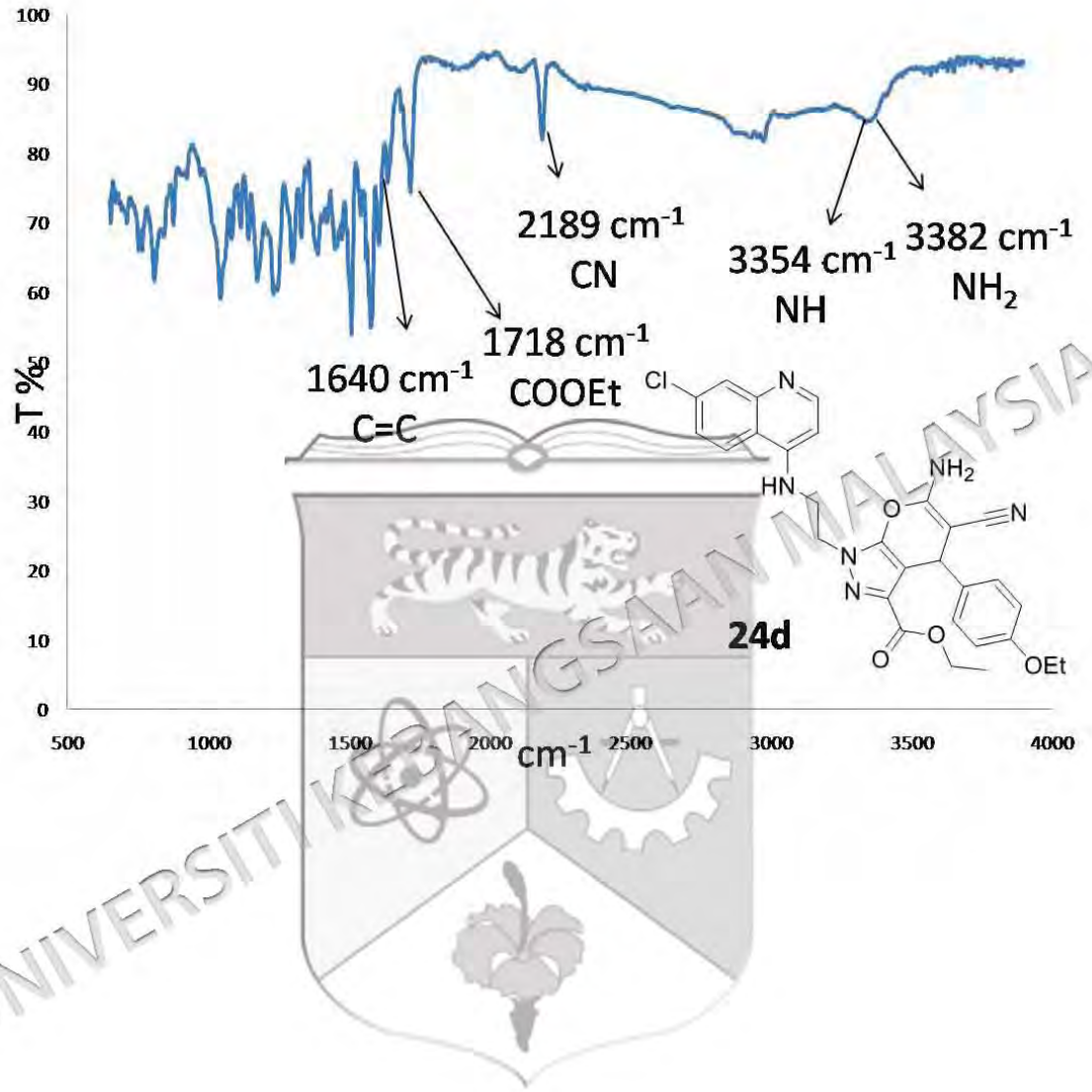

APPENDIX A5

FT-IR SPECTRUM OF PYRANO[2,3-*C*]PYRAZOLE-4-AMINOQUINOLINE 24G

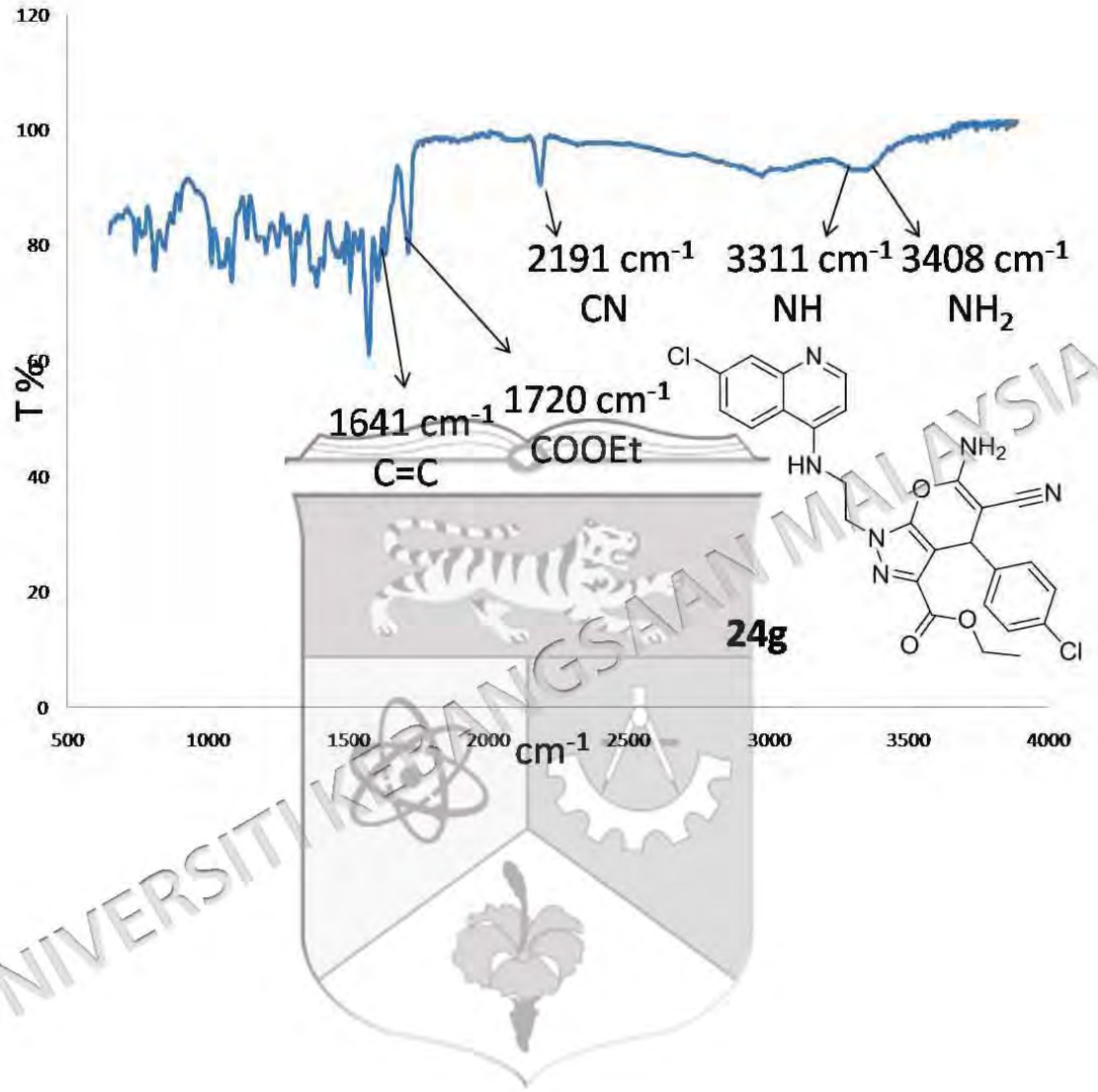

APPENDIX A6

FT-IR SPECTRUM OF PYRANO[2,3-*C*]PYRAZOLE-4-AMINOQUINOLINE 24H

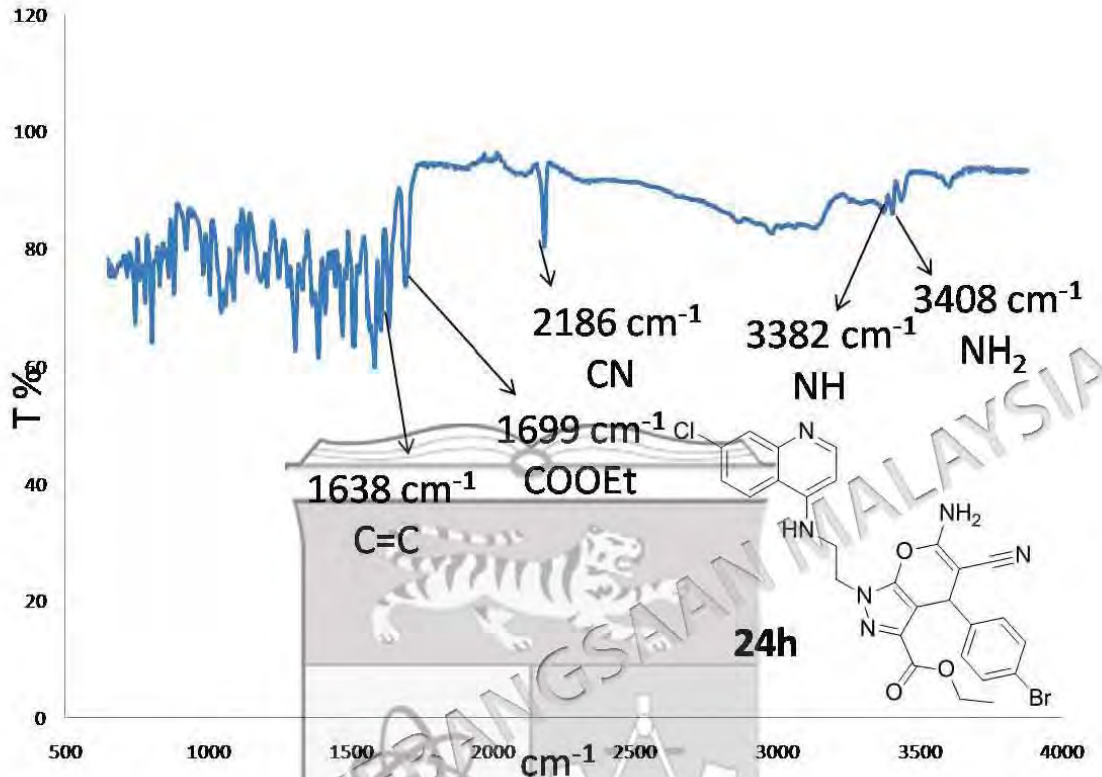

APPENDIX A7

FT-IR SPECTRUM OF PYRANO[2,3-*C*]PYRAZOLE-4-AMINOQUINOLINE 24I

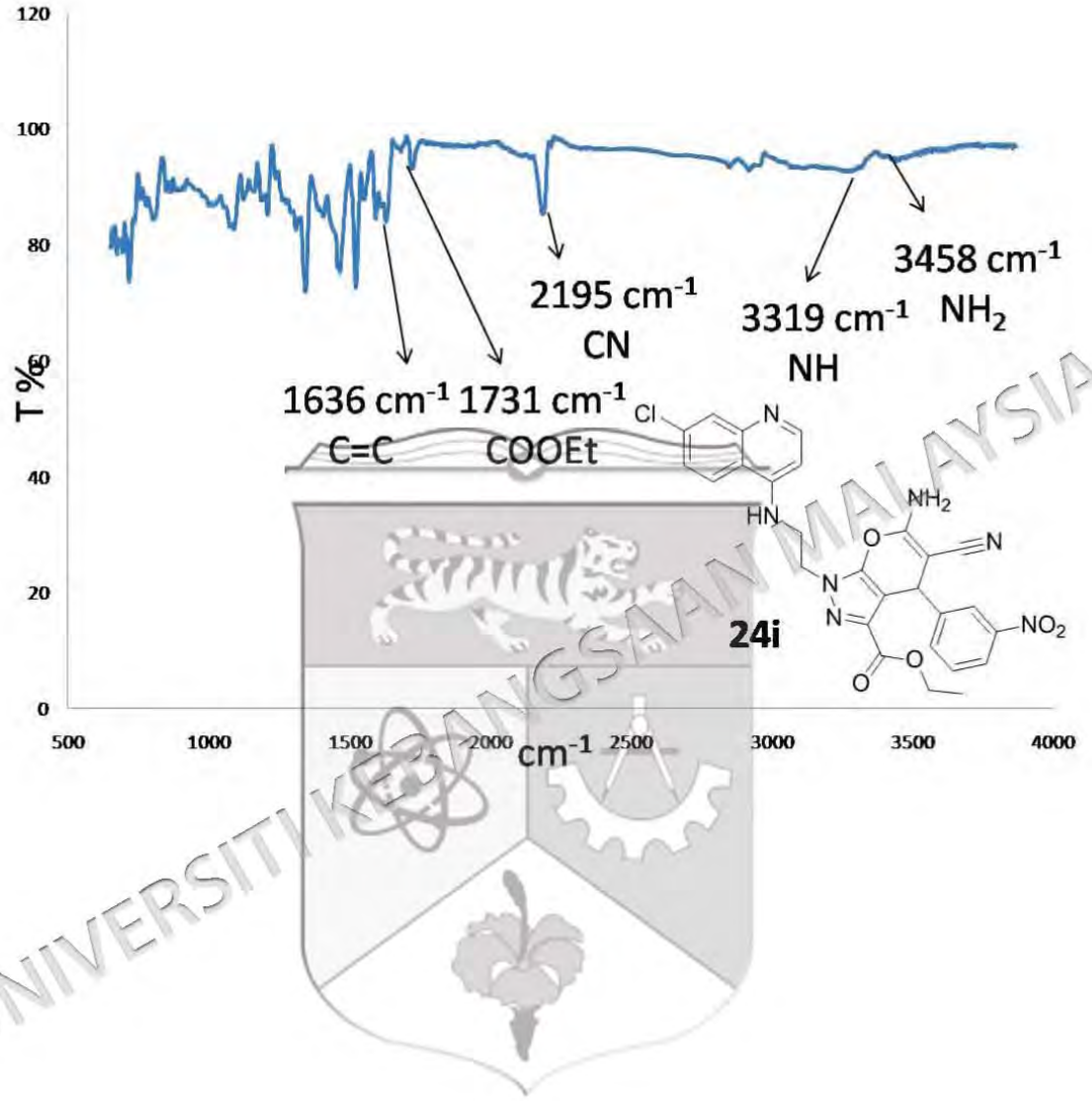

APPENDIX A8

FT-IR SPECTRUM OF PYRANO[2,3-*C*]PYRAZOLE-4-AMINOQUINOLINE 24J

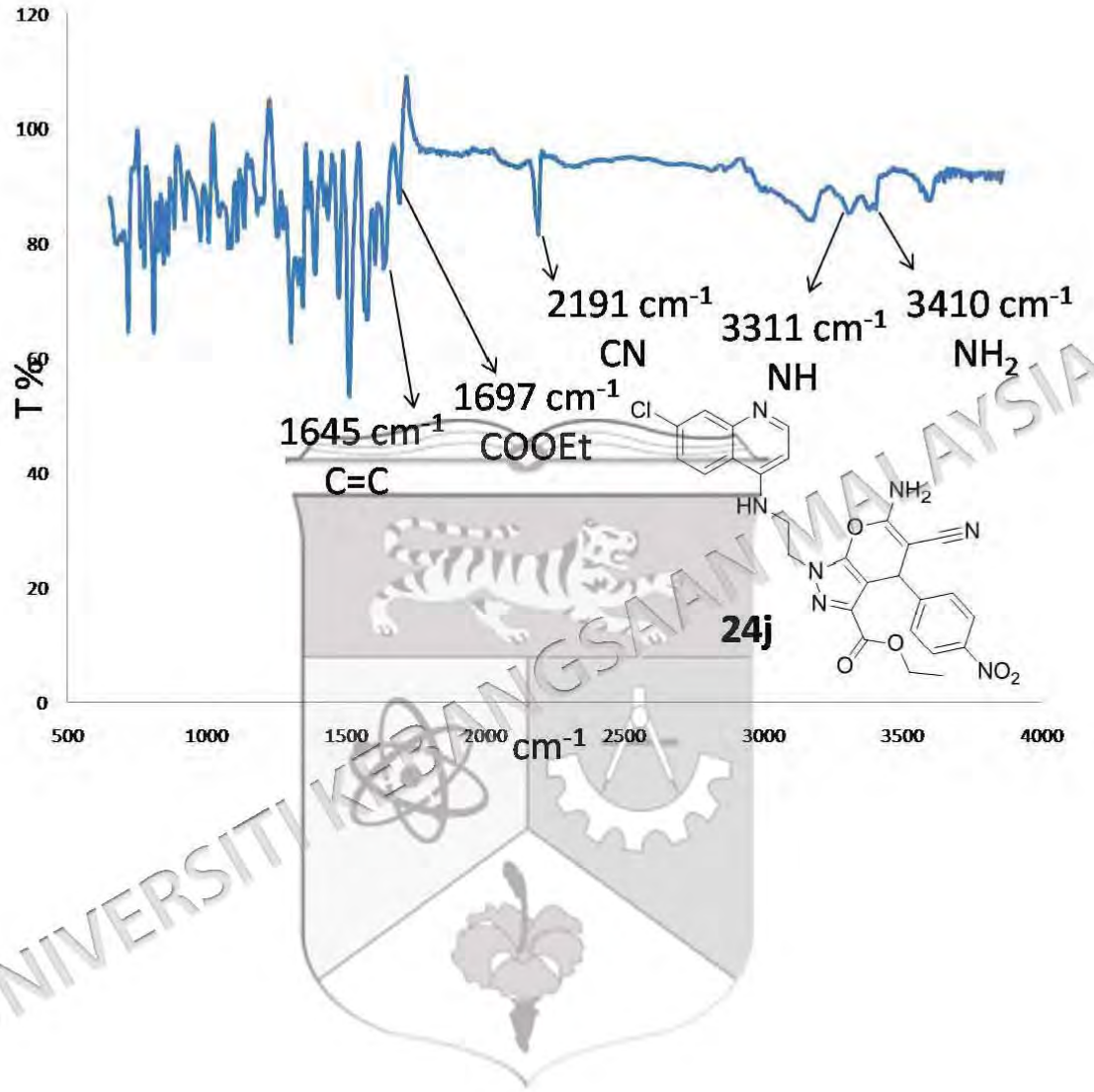

APPENDIX A9

FT-IR SPECTRUM OF PYRANO[2,3-*C*]PYRAZOLE-4-AMINOQUINOLINE 24K

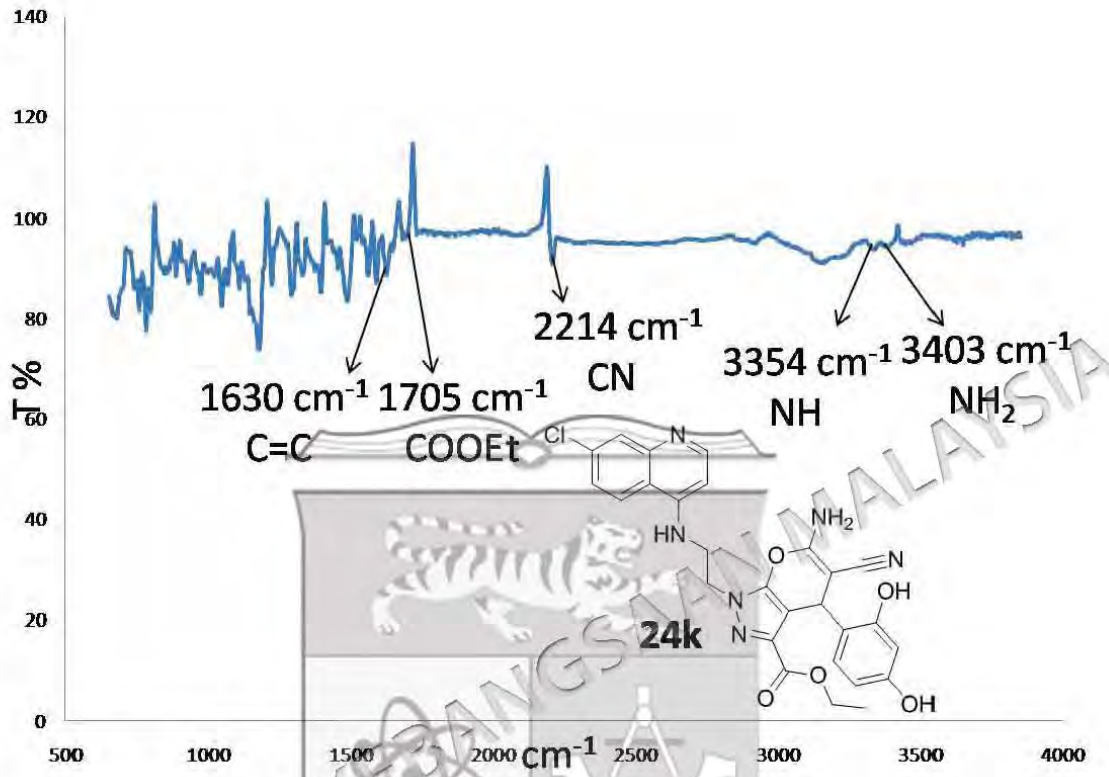

APPENDIX A10

FT-IR SPECTRUM OF PYRANO[2,3-*C*]PYRAZOLE-4-AMINOQUINOLINE 24L

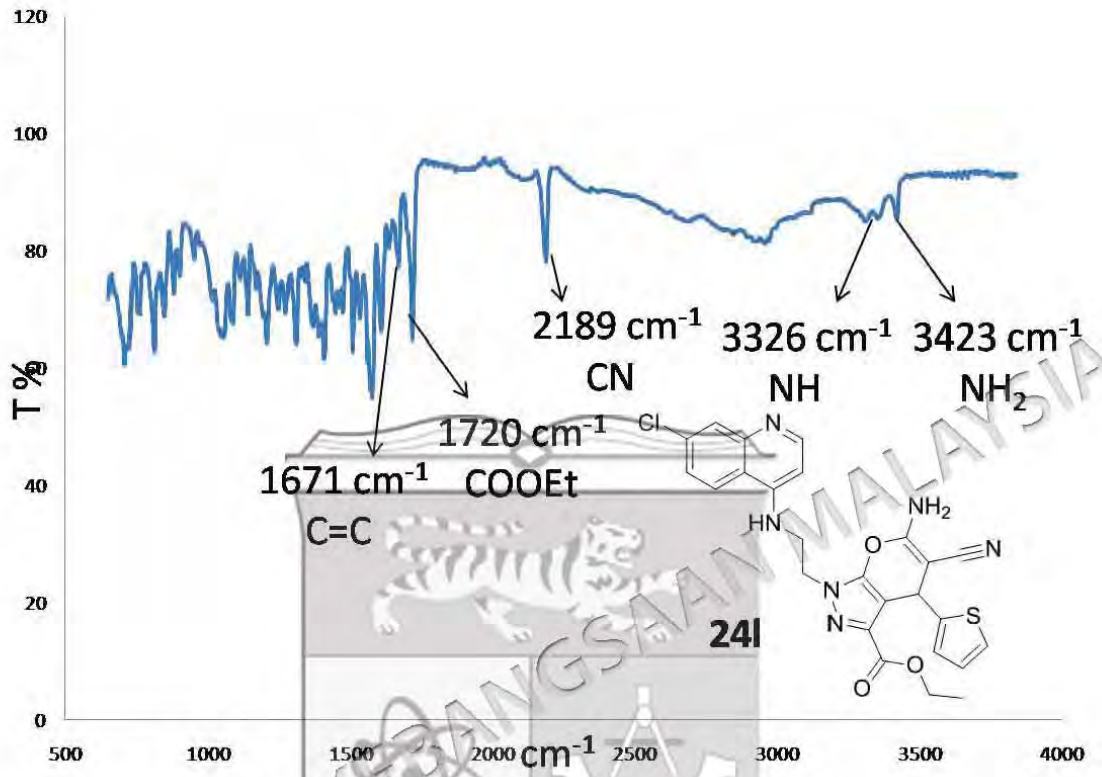

APPENDIX A11

FT-IR SPECTRUM OF PYRANO[2,3-*C*]PYRAZOLE-4-AMINOQUINOLINE 24M

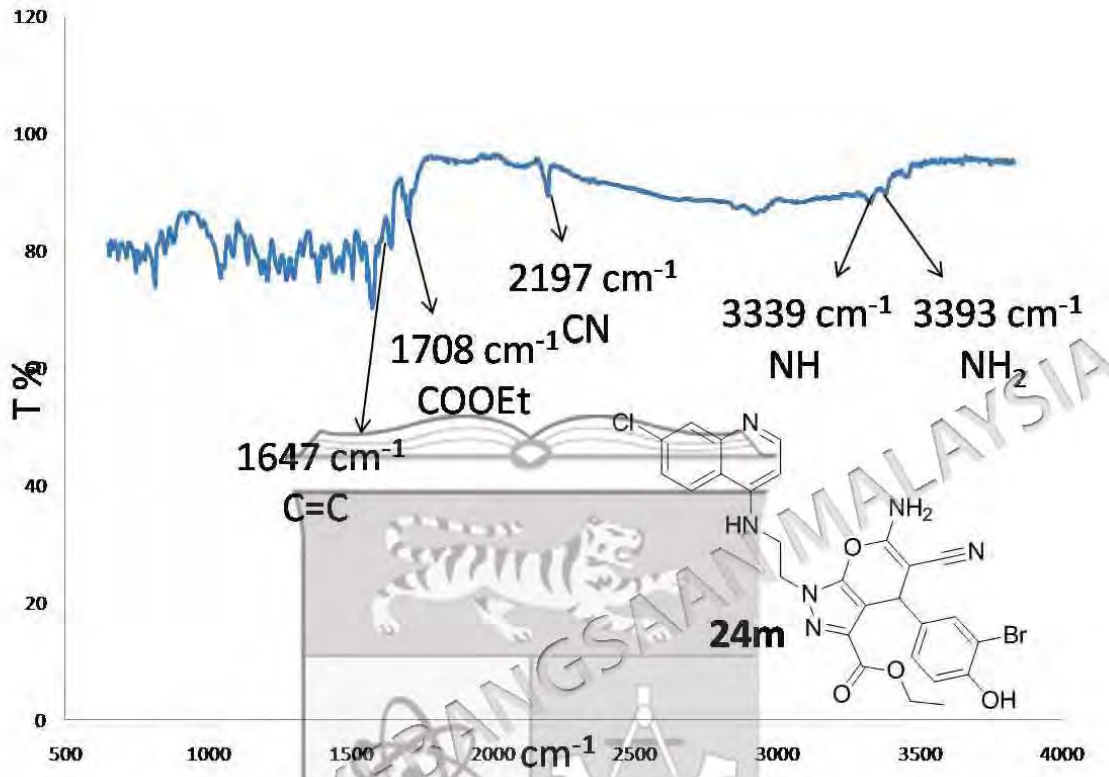

APPENDIX A12

FT-IR SPECTRUM OF PYRANO[2,3-*C*]PYRAZOLE-4-AMINOQUINOLINE 24N

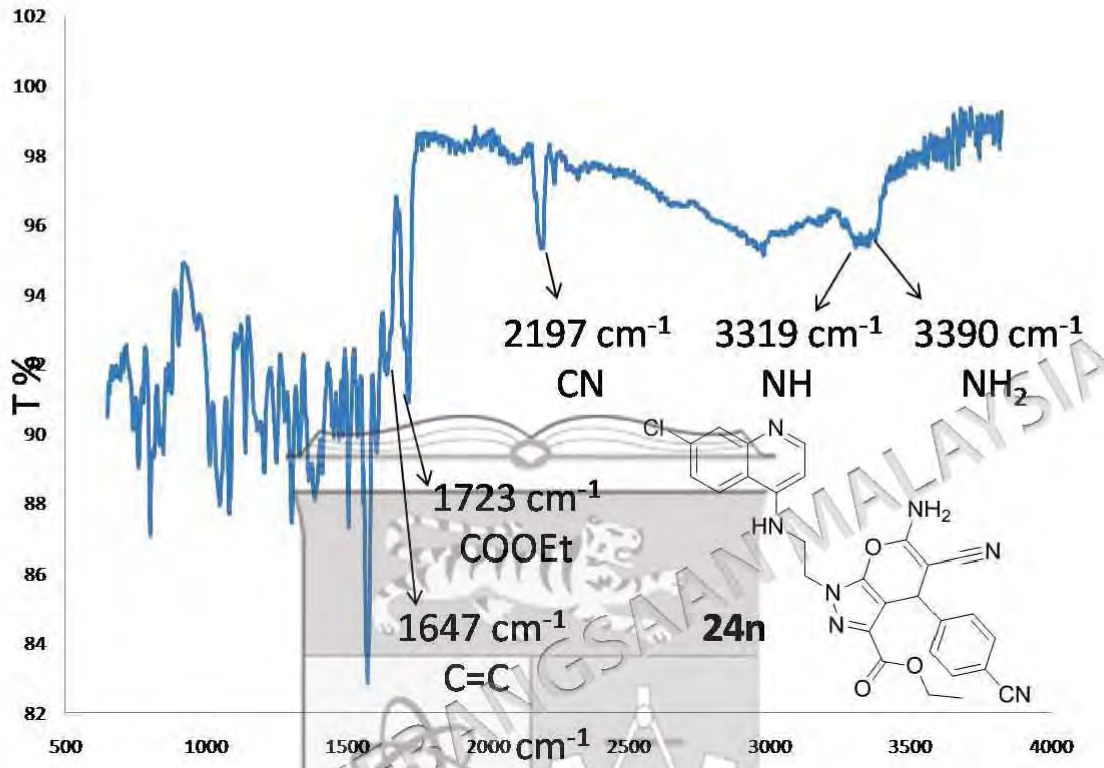

APPENDIX A13

FT-IR SPECTRUM OF PYRANO[2,3-*C*]PYRAZOLE-4-AMINOQUINOLINE 24O

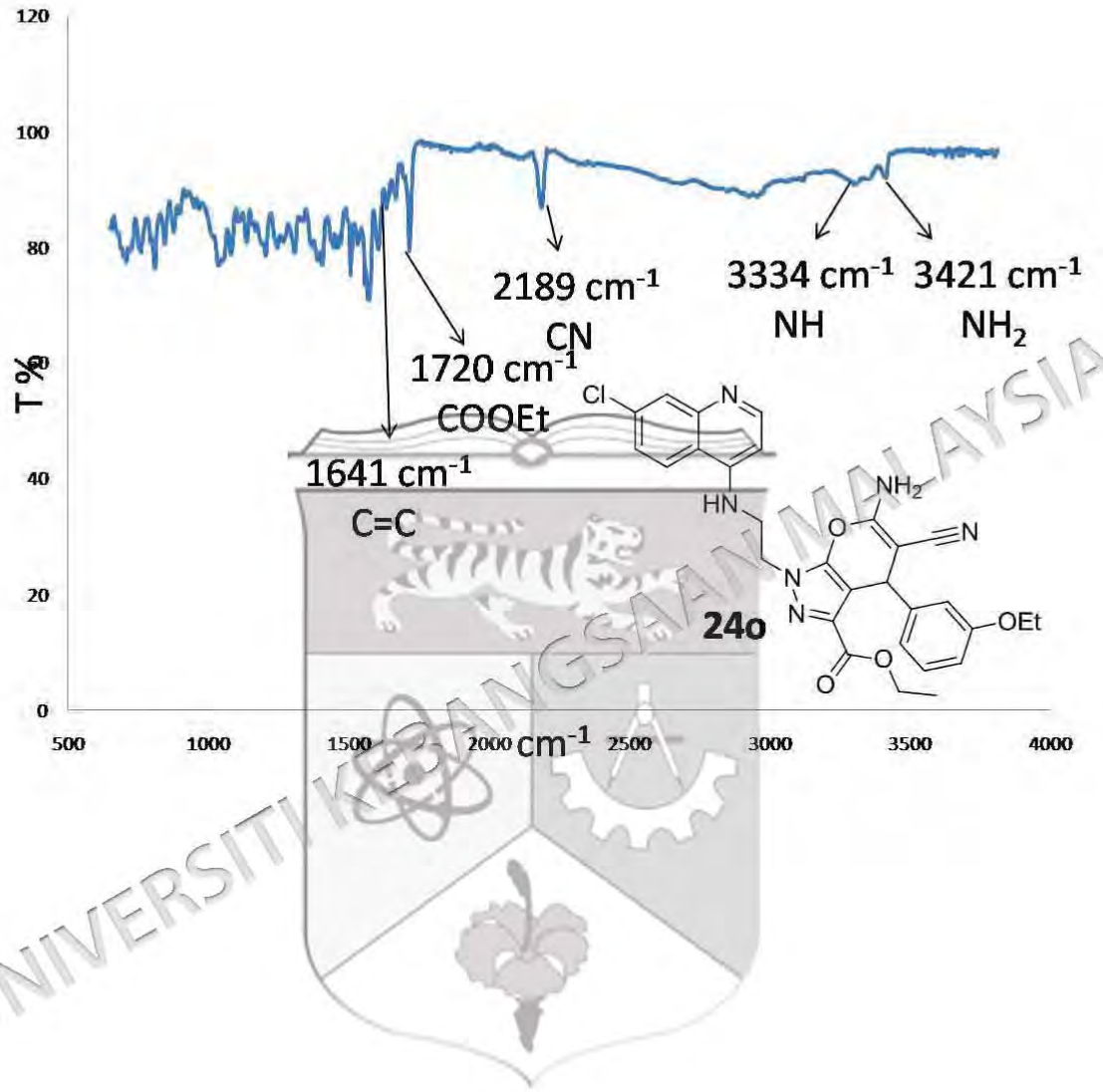

APPENDIX A14

FT-IR SPECTRUM OF PYRANO[2,3-C]PYRAZOLE-4-AMINOQUINOLINE 24P

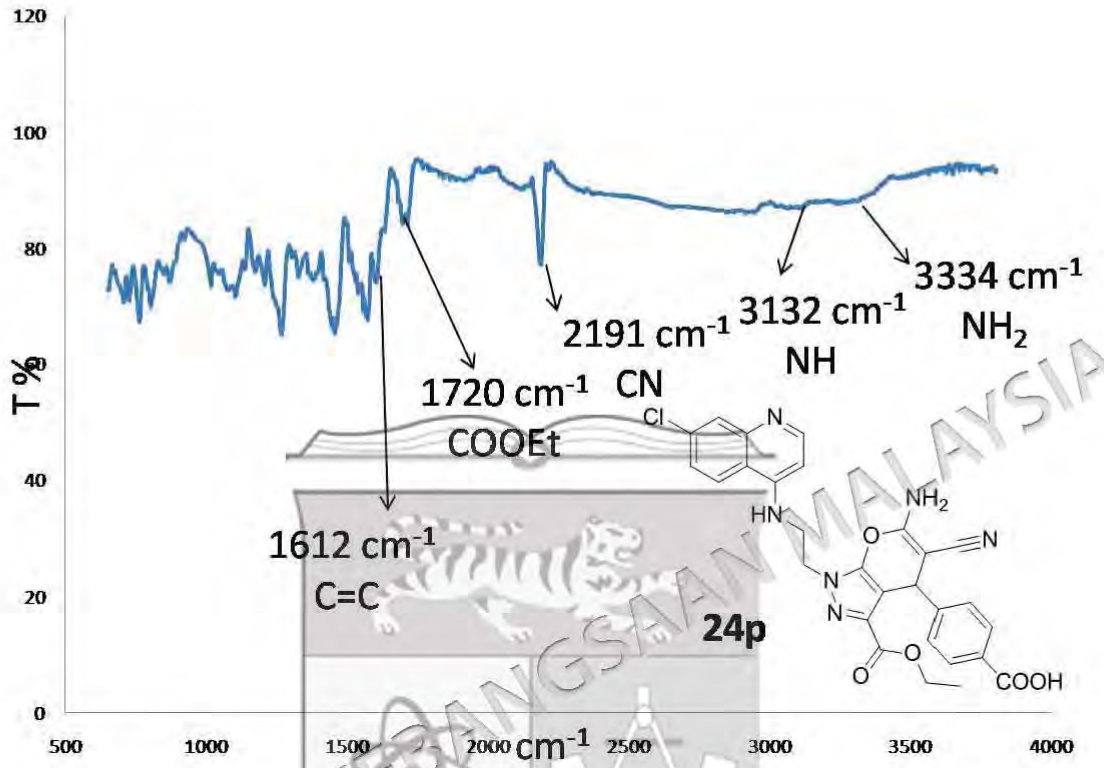

APPENDIX A15

FT-IR SPECTRUM OF PYRANO[2,3-*C*]PYRAZOLE-4-AMINOQUINOLINE 24R

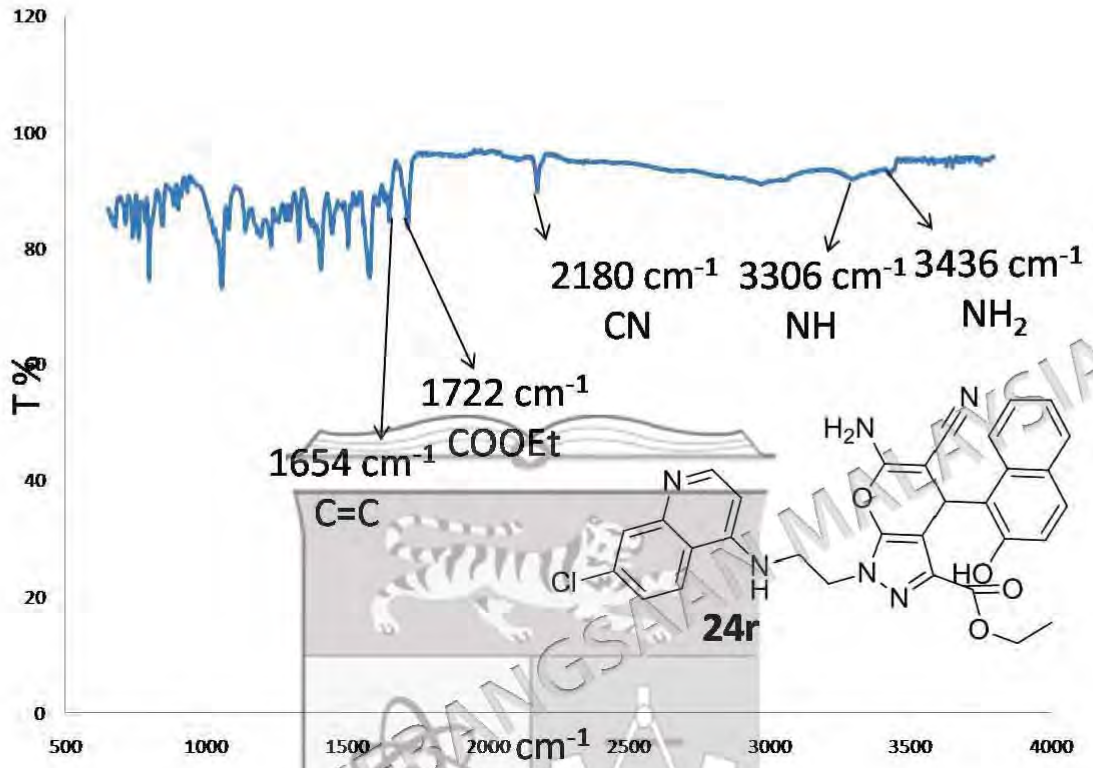

APPENDIX A16

FT-IR SPECTRUM OF PYRANO[2,3-*C*]PYRAZOLE-4-AMINOQUINOLINE 24S

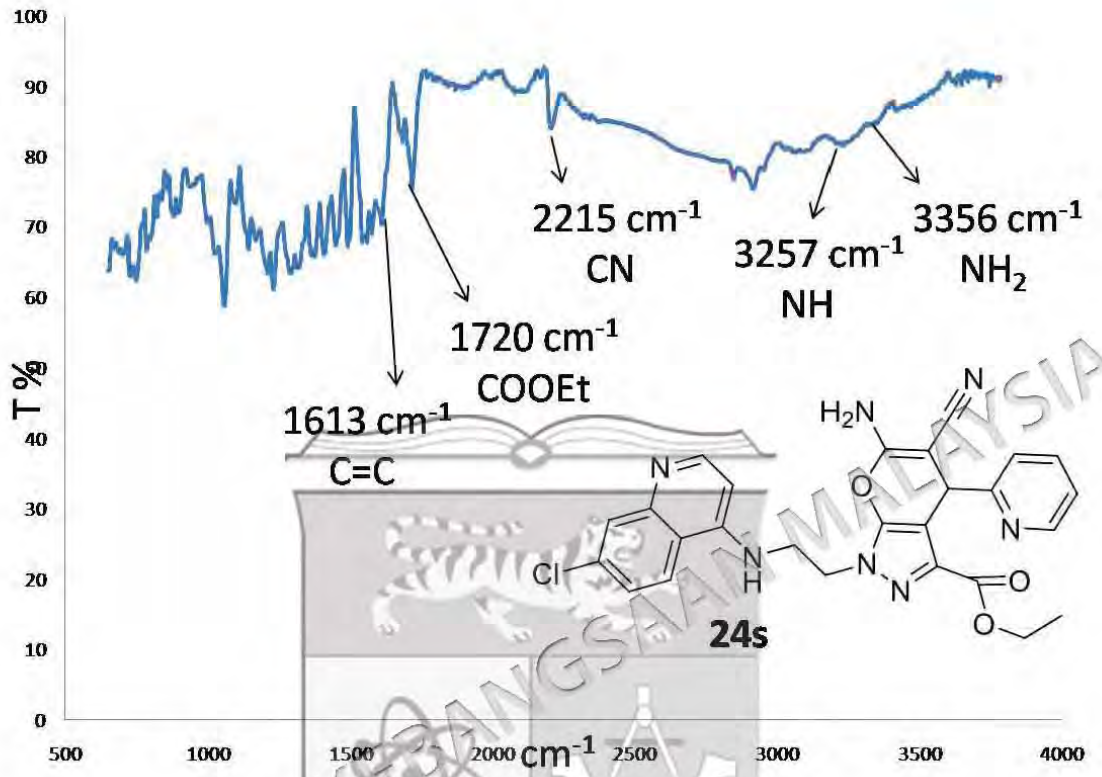

APPENDIX B1

MASS SPECTRUM OF PYRANO[2,3-*C*]PYRAZOLE-4-AMINOQUINOLINE 24A

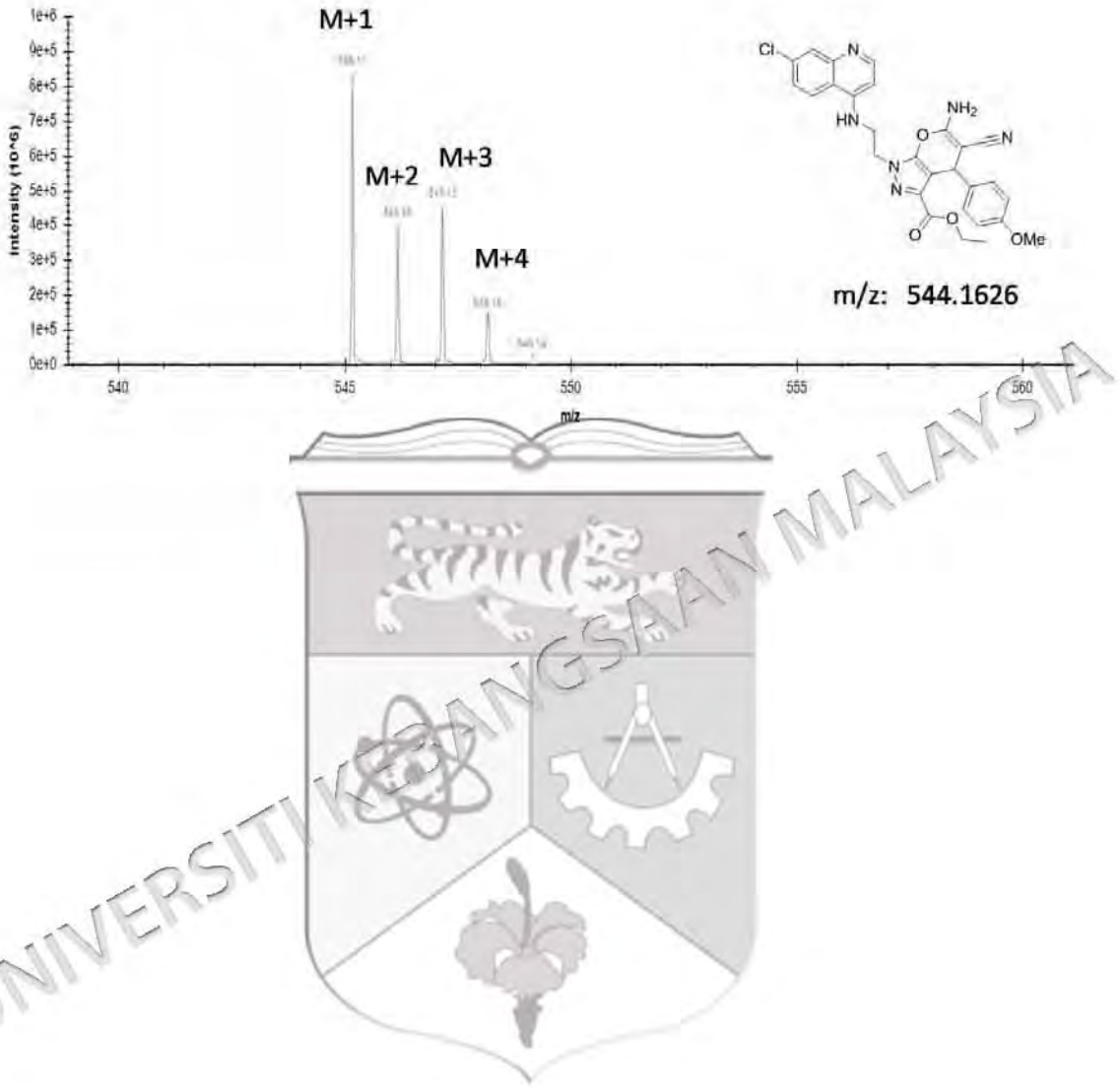

APPENDIX B2

MASS SPECTRUM OF PYRANO[2,3-*C*]PYRAZOLE-4-AMINOQUINOLINE 24D

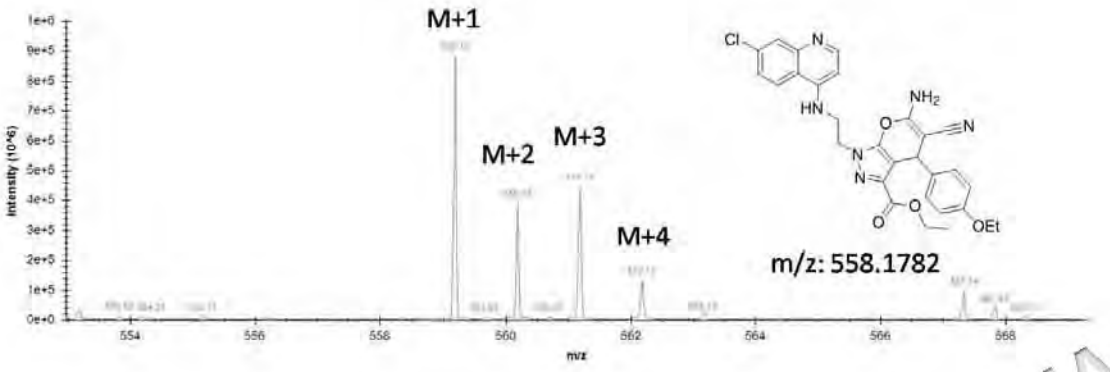

APPENDIX B3

MASS SPECTRUM OF PYRANO[2,3-*C*]PYRAZOLE-4-AMINOQUINOLINE 24G

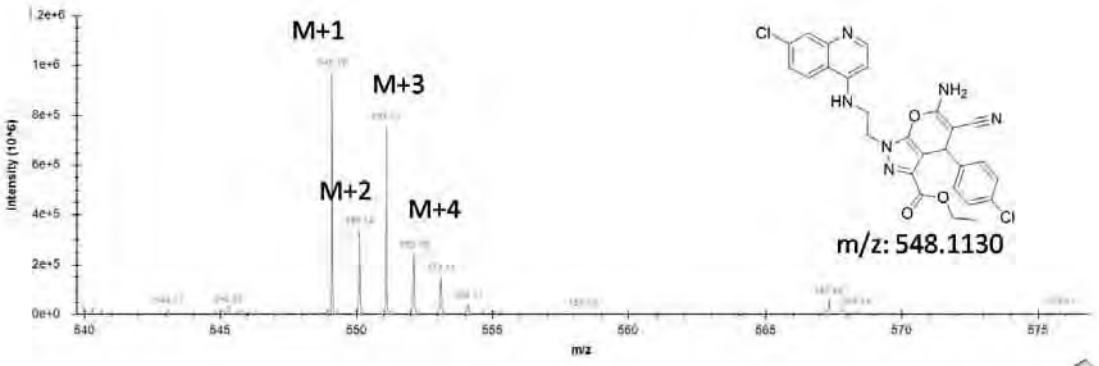

APPENDIX B4

MASS SPECTRUM OF PYRANO[2,3-*C*]PYRAZOLE-4-AMINOQUINOLINE 24H

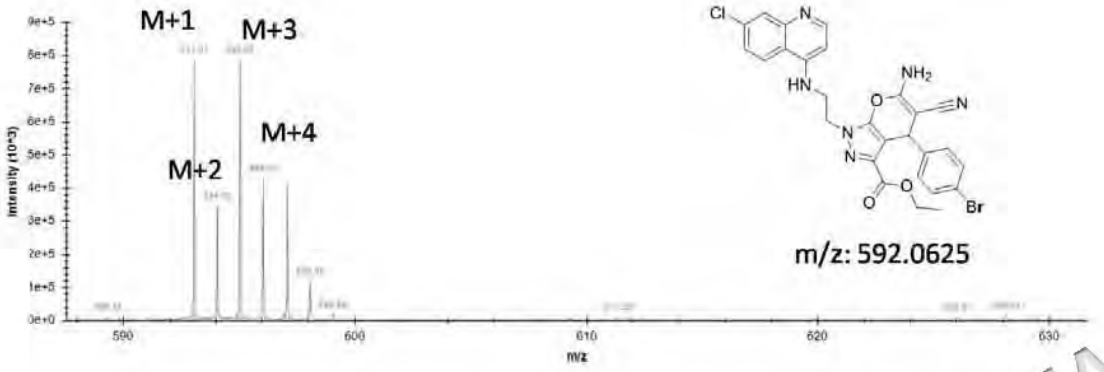

APPENDIX B5

MASS SPECTRUM OF PYRANO[2,3-*C*]PYRAZOLE-4-AMINOQUINOLINE 24J

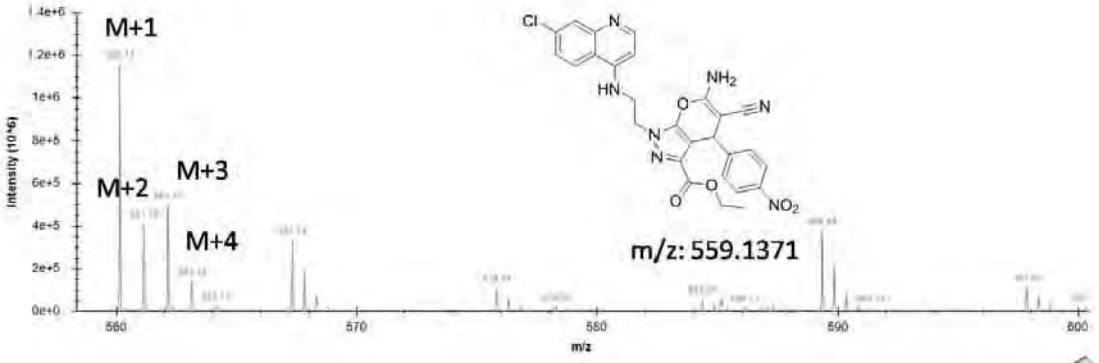

APPENDIX B6

MASS SPECTRUM OF PYRANO[2,3-*C*]PYRAZOLE-4-AMINOQUINOLINE 24K

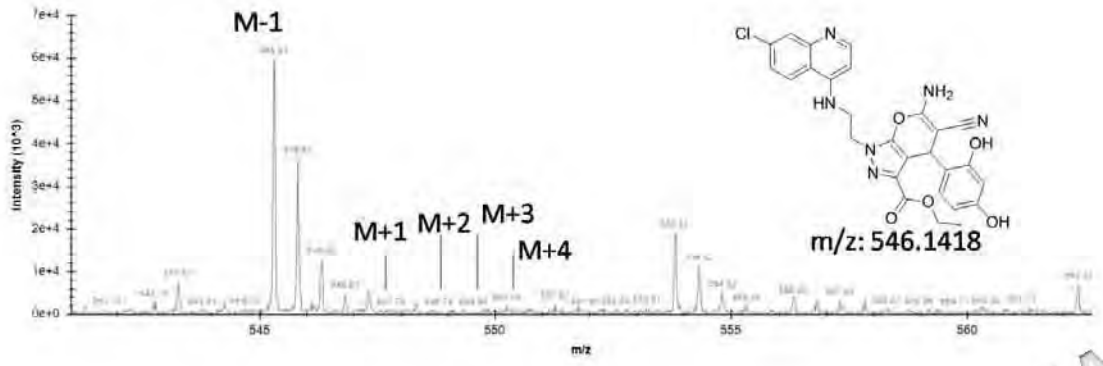

APPENDIX B7

MASS SPECTRUM OF PYRANO[2,3-*C*]PYRAZOLE-4-AMINOQUINOLINE 24L

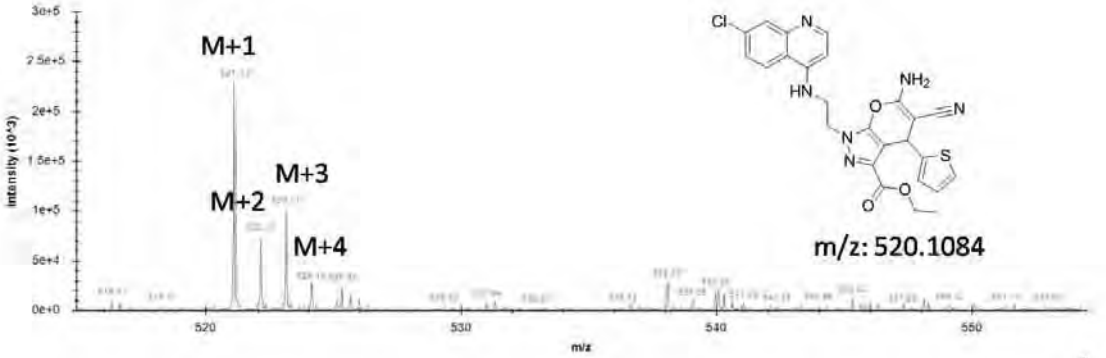

APPENDIX B8

MASS SPECTRUM OF PYRANO[2,3-*C*]PYRAZOLE-4-AMINOQUINOLINE 24M

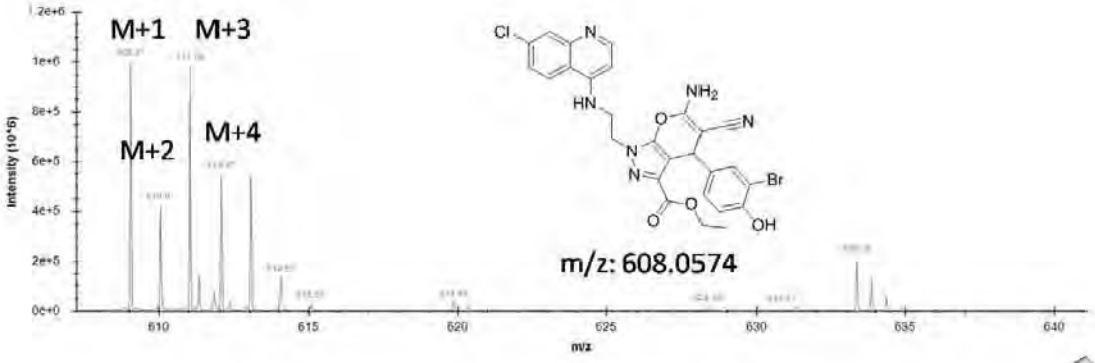

APPENDIX B9

MASS SPECTRUM OF PYRANO[2,3-C]PYRAZOLE-4-AMINOQUINOLINE 24N

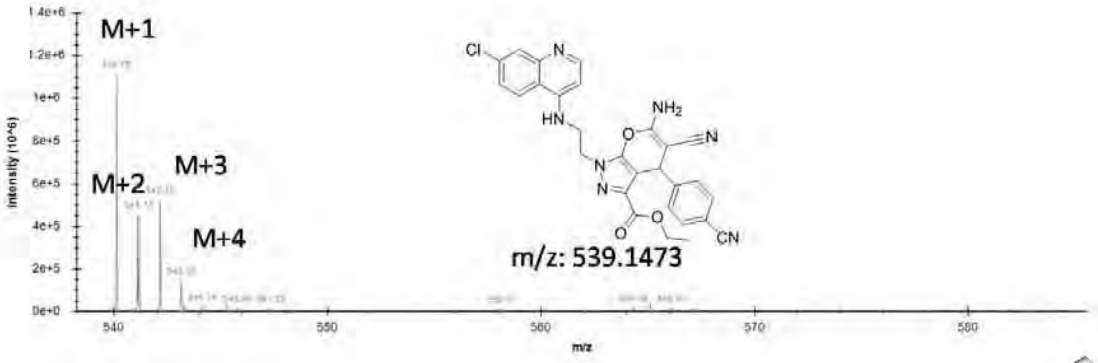

APPENDIX B10

MASS SPECTRUM OF PYRANO[2,3-*C*]PYRAZOLE-4-AMINOQUINOLINE 24P

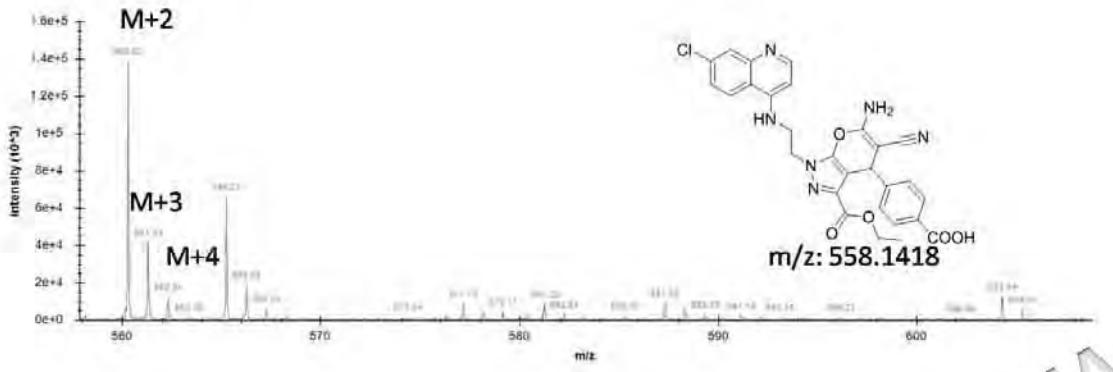

APPENDIX C1

CURVE GRAPH DEPICTING CYTOTOXICITY VALU OF PYRANO[2,3-*C*]PYRAZOLE-4-AMINOQUINOLINE 24A

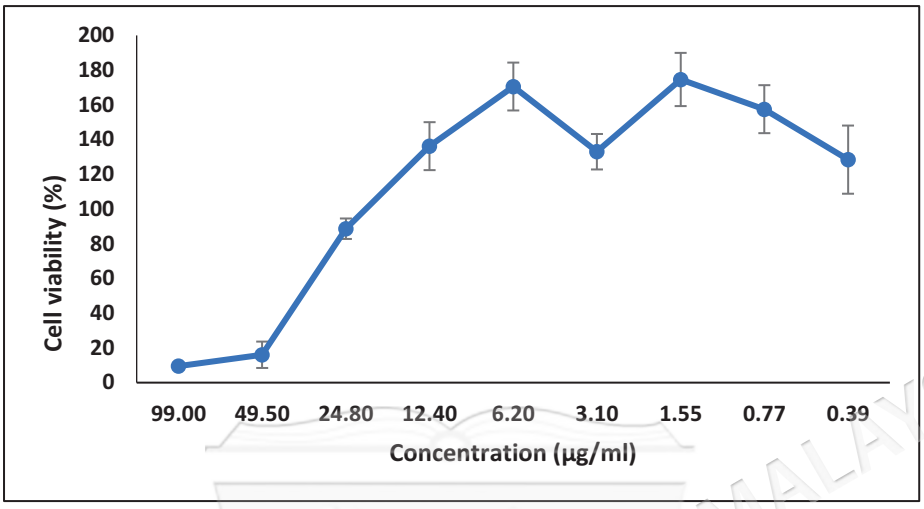

APPENDIX C2

CURVE GRAPH DEPICTING CYTOTOXICITY VALU OF PYRANO[2,3-*C*]PYRAZOLE-4-AMINOQUINOLINE 24B

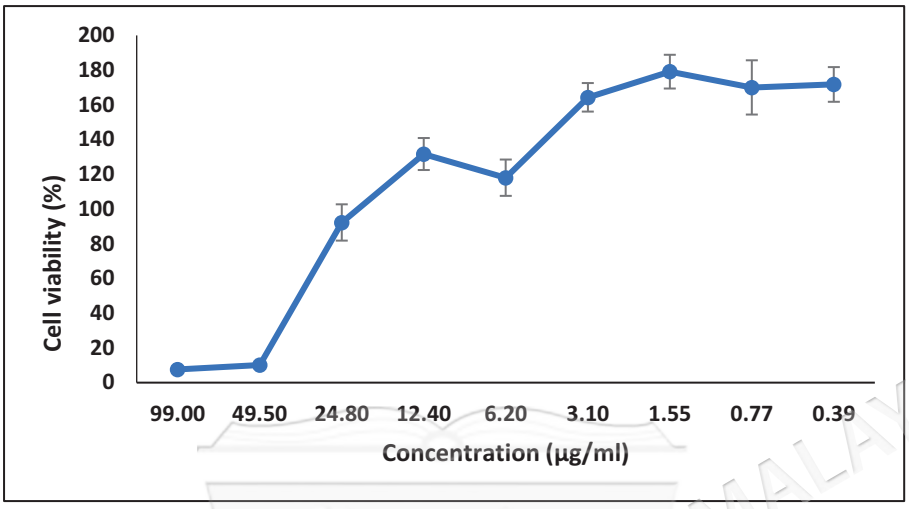

APPENDIX C3

CURVE GRAPH DEPICTING CYTOTOXICITY VALU OF PYRANO[2,3-C]PYRAZOLE-4-AMINOQUINOLINE 24C

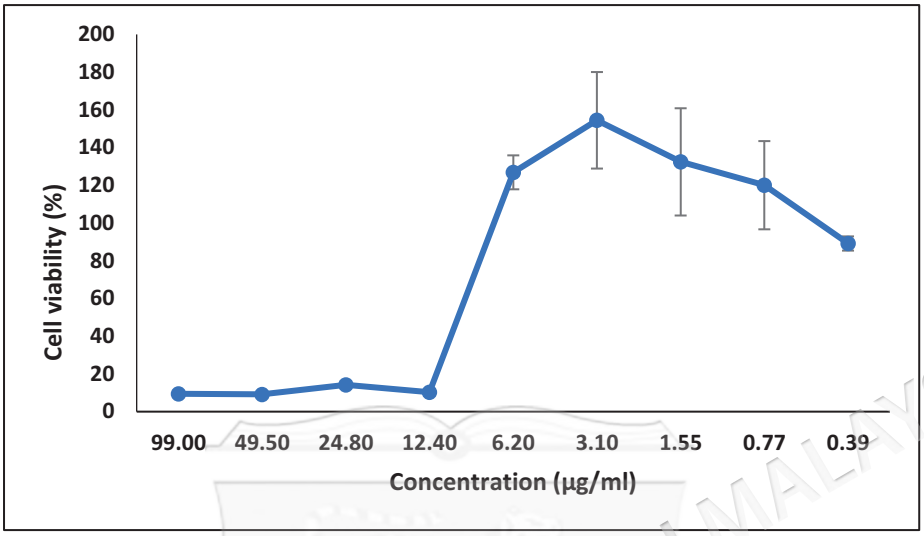

APPENDIX C4

CURVE GRAPH DEPICTING CYTOTOXICITY VALU OF PYRANO[2,3-C]PYRAZOLE-4-AMINOQUINOLINE 24D

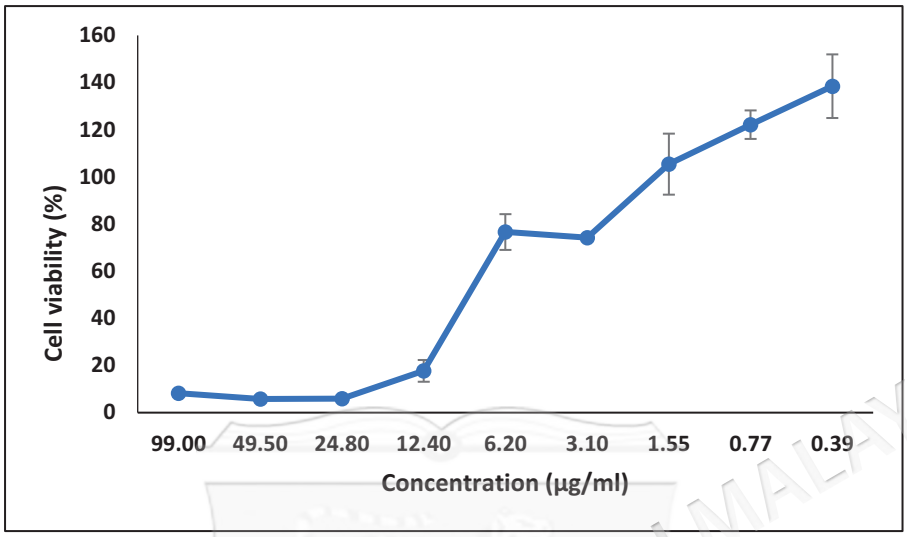

APPENDIX C5

CURVE GRAPH DEPICTING CYTOTOXICITY VALU OF PYRANO[2,3-*C*]PYRAZOLE-4-AMINOQUINOLINE 24E

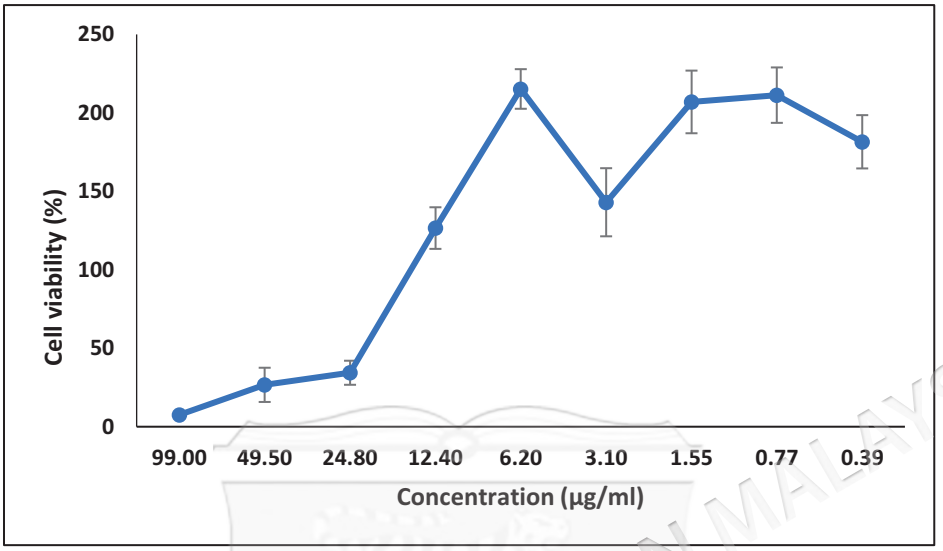

APPENDIX C6

CURVE GRAPH DEPICTING CYTOTOXICITY VALU OF PYRANO[2,3-*C*]PYRAZOLE-4-AMINOQUINOLINE 24F

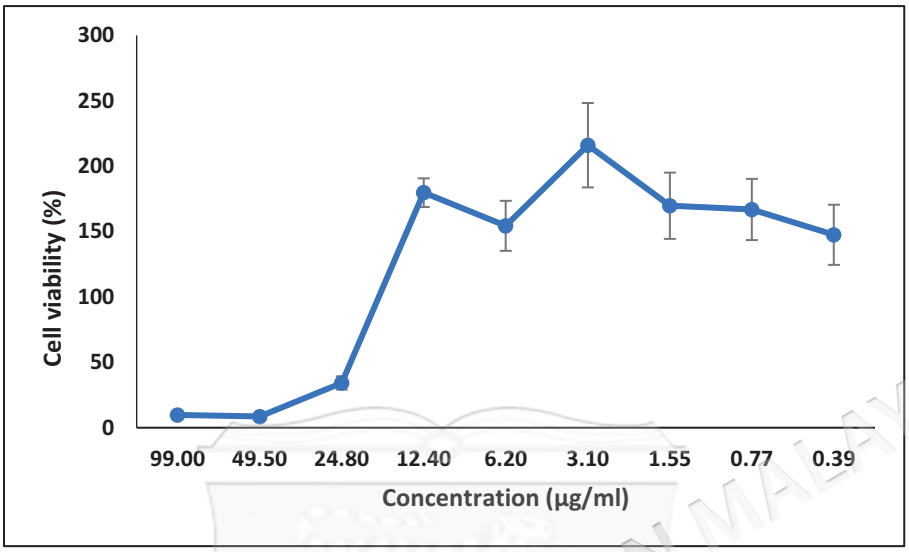

APPENDIX C7

CURVE GRAPH DEPICTING CYTOTOXICITY VALU OF PYRANO[2,3-*C*]PYRAZOLE-4-AMINOQUINOLINE 24G

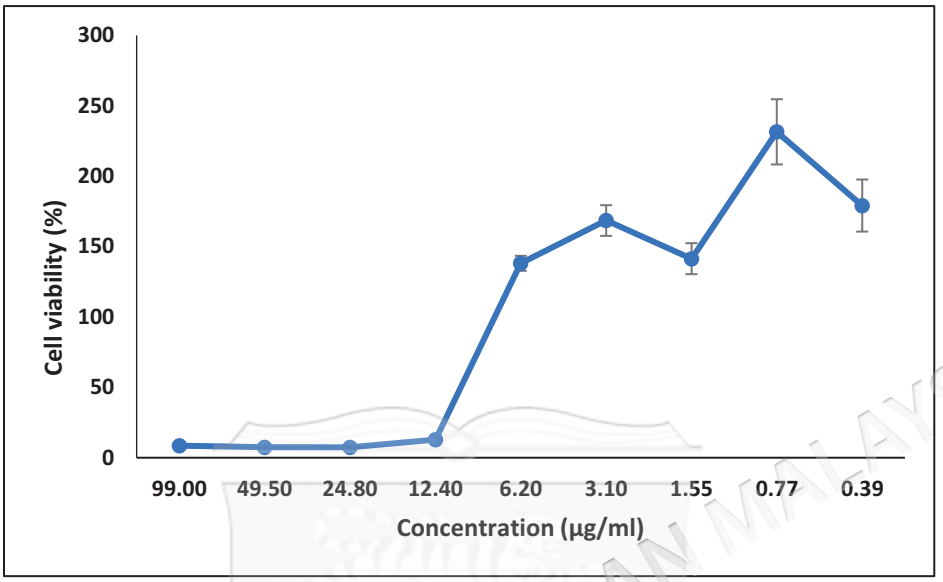

APPENDIX C8

CURVE GRAPH DEPICTING CYTOTOXICITY VALU OF PYRANO[2,3-*C*]PYRAZOLE-4-AMINOQUINOLINE 24H

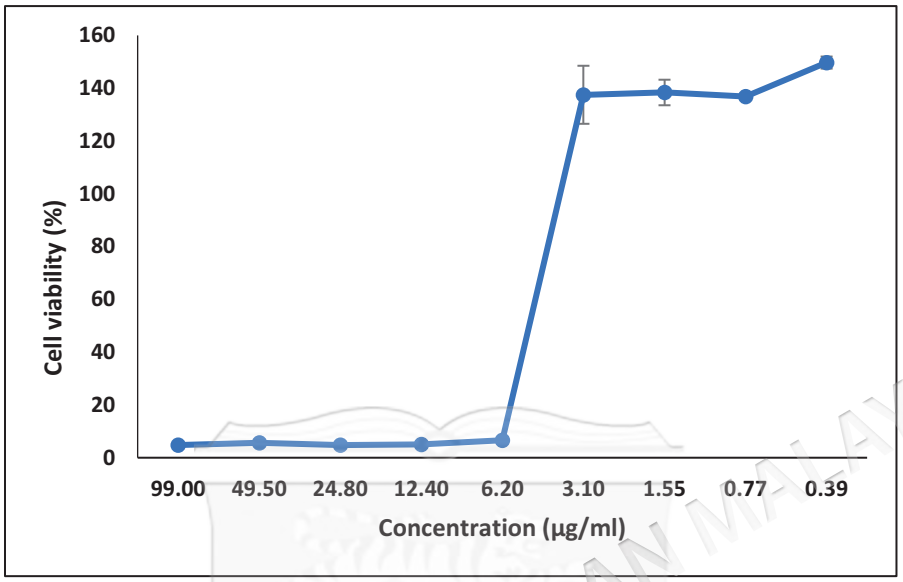

APPENDIX C9

CURVE GRAPH DEPICTING CYTOTOXICITY VALU OF PYRANO[2,3-C]PYRAZOLE-4-AMINOQUINOLINE 24I

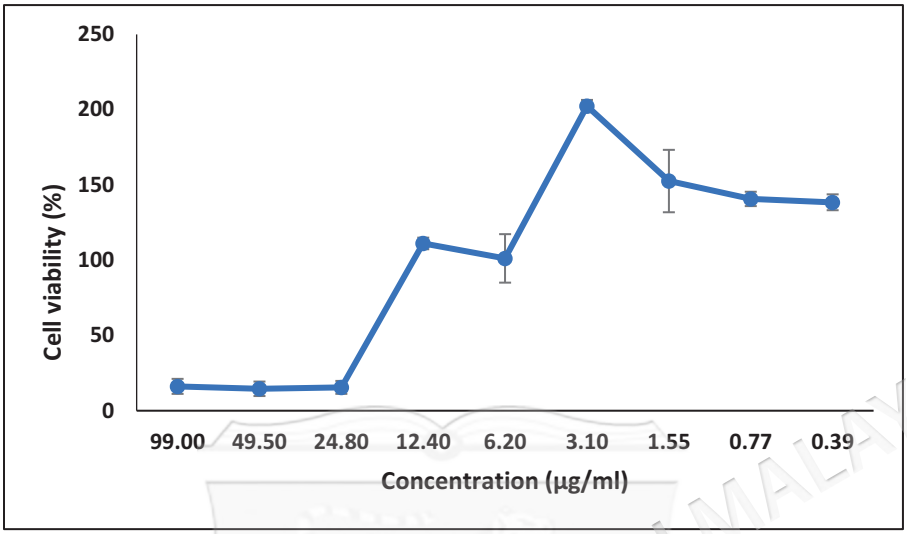

APPENDIX C10

CURVE GRAPH DEPICTING CYTOTOXICITY VALU OF PYRANO[2,3-*C*]PYRAZOLE-4-AMINOQUINOLINE 24J

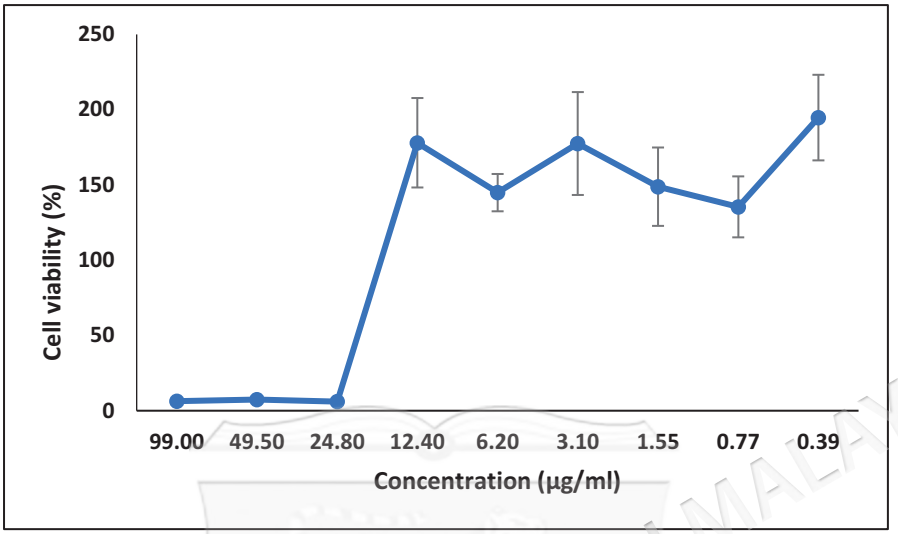

APPENDIX C11

CURVE GRAPH DEPICTING CYTOTOXICITY VALU OF PYRANO[2,3-*C*]PYRAZOLE-4-AMINOQUINOLINE 24K

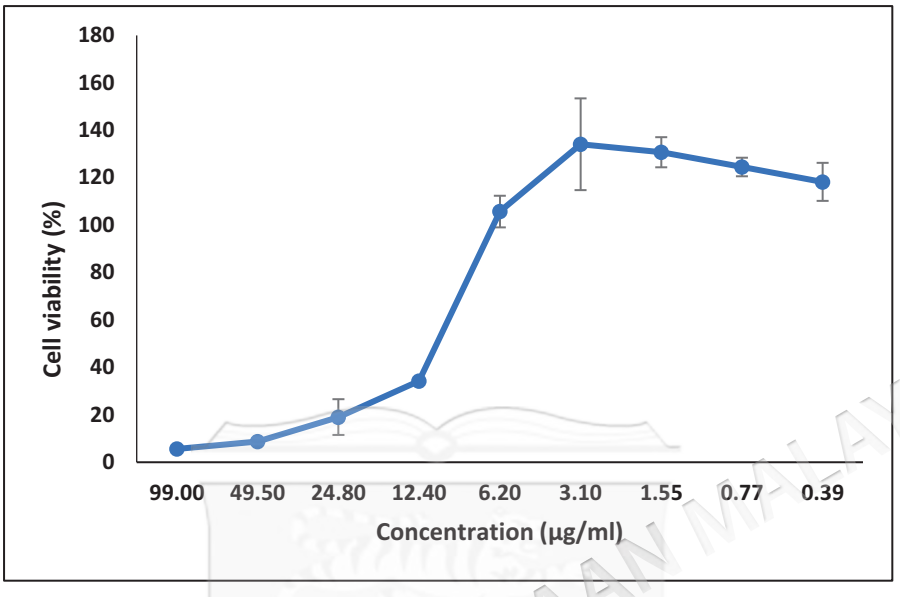

APPENDIX C12

CURVE GRAPH DEPICTING CYTOTOXICITY VALU OF PYRANO[2,3-*C*]PYRAZOLE-4-AMINOQUINOLINE 24L

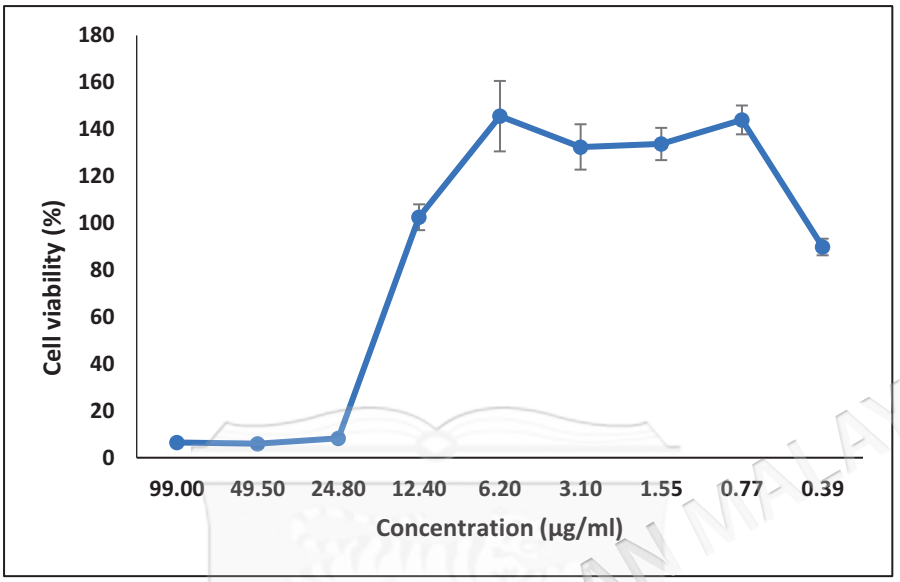

APPENDIX C13

CURVE GRAPH DEPICTING CYTOTOXICITY VALU OF PYRANO[2,3-*C*]PYRAZOLE-4-AMINOQUINOLINE 24M

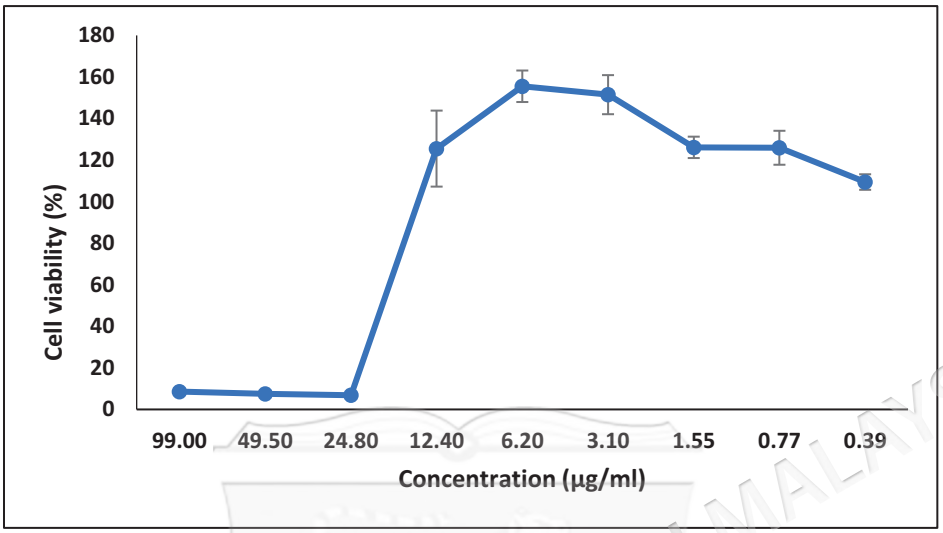

APPENDIX C14

CURVE GRAPH DEPICTING CYTOTOXICITY VALU OF PYRANO[2,3-*C*]PYRAZOLE-4-AMINOQUINOLINE 24N

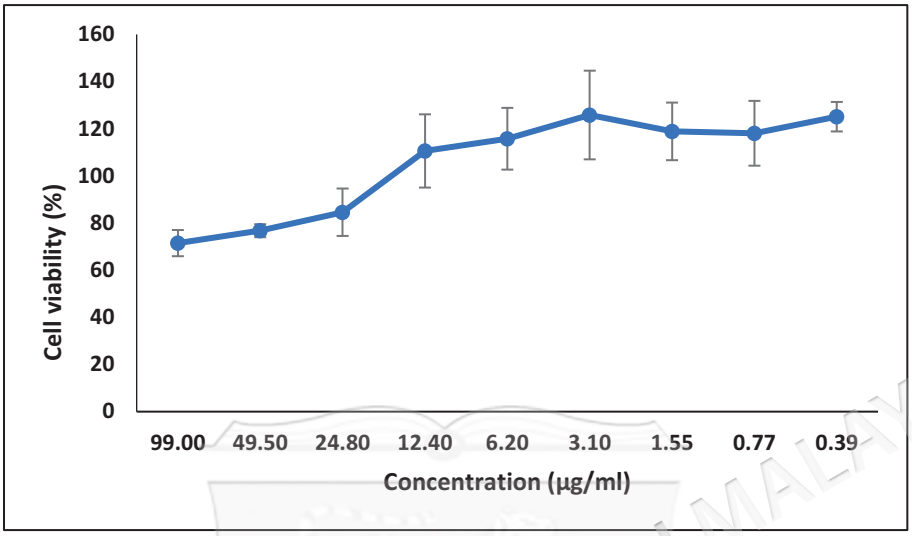

APPENDIX C15

CURVE GRAPH DEPICTING CYTOTOXICITY VALU OF PYRANO[2,3-*C*]PYRAZOLE-4-AMINOQUINOLINE 24O

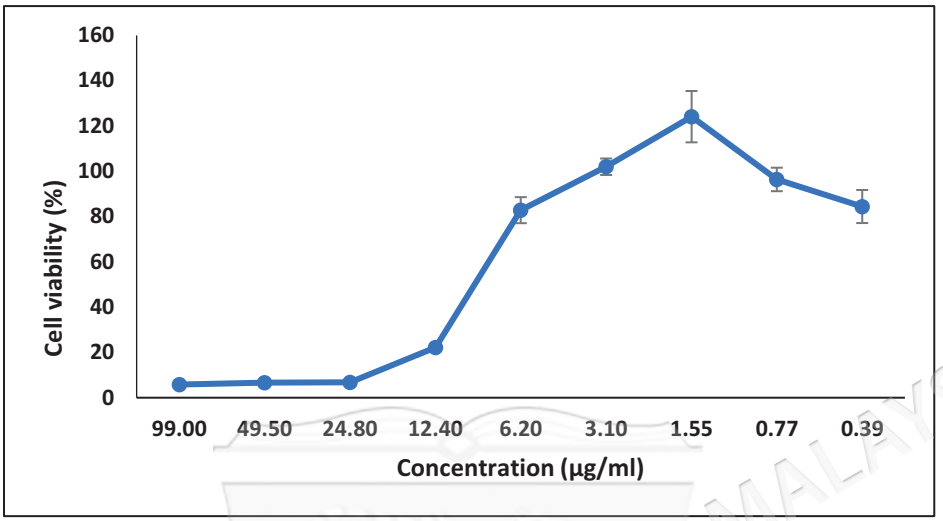

APPENDIX C16

CURVE GRAPH DEPICTING CYTOTOXICITY VALU OF PYRANO[2,3-*C*]PYRAZOLE-4-AMINOQUINOLINE 24P

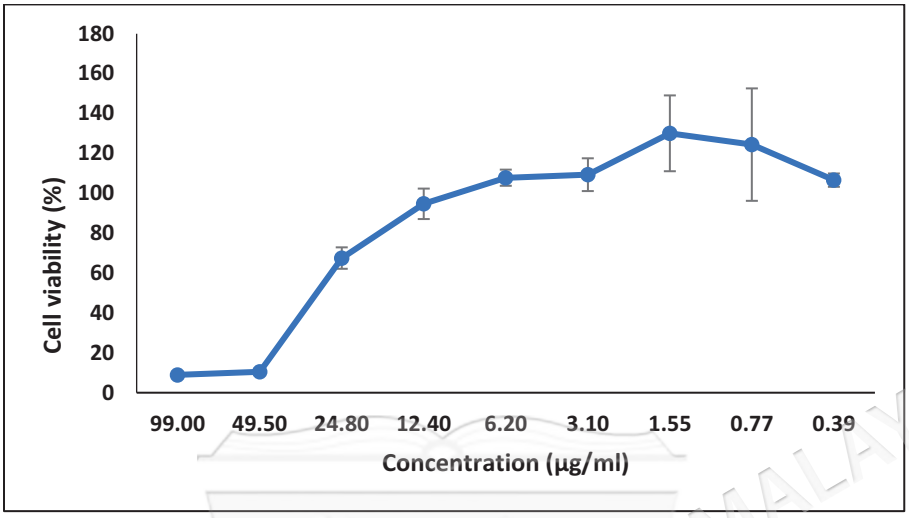

APPENDIX C17

CURVE GRAPH DEPICTING CYTOTOXICITY VALU OF PYRANO[2,3-*C*]PYRAZOLE-4-AMINOQUINOLINE 24Q

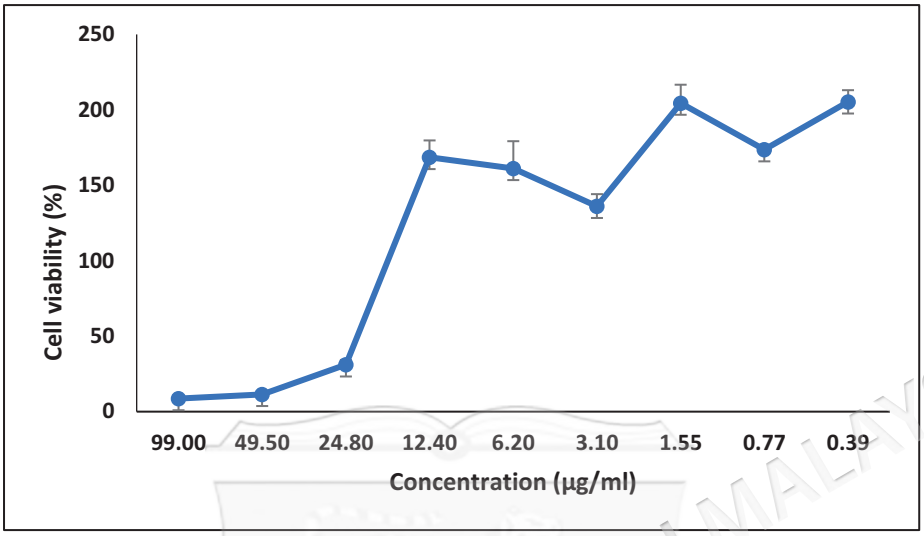

APPENDIX C18

CURVE GRAPH DEPICTING CYTOTOXICITY VALU OF PYRANO[2,3-C]PYRAZOLE-4-AMINOQUINOLINE 24R

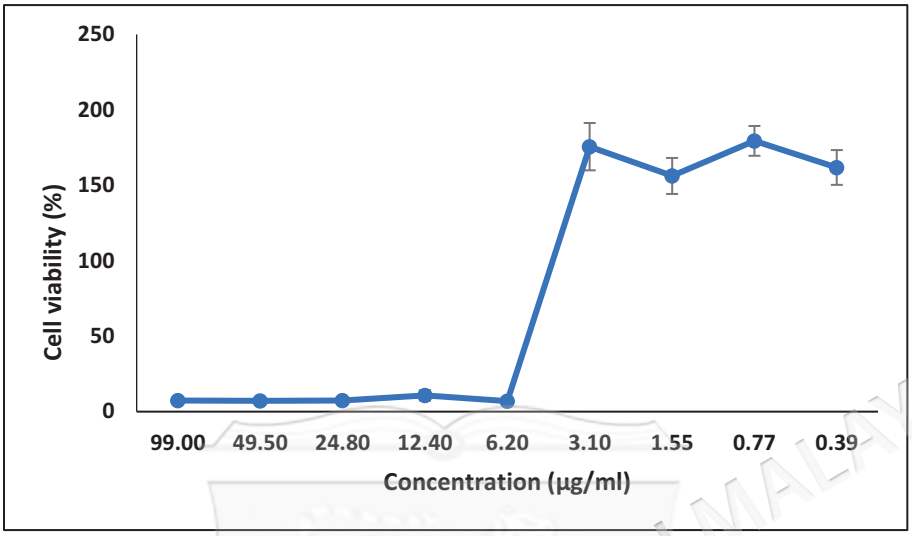

APPENDIX C19

CURVE GRAPH DEPICTING CYTOTOXICITY VALU OF PYRANO[2,3-*C*]PYRAZOLE-4-AMINOQUINOLINE 24S

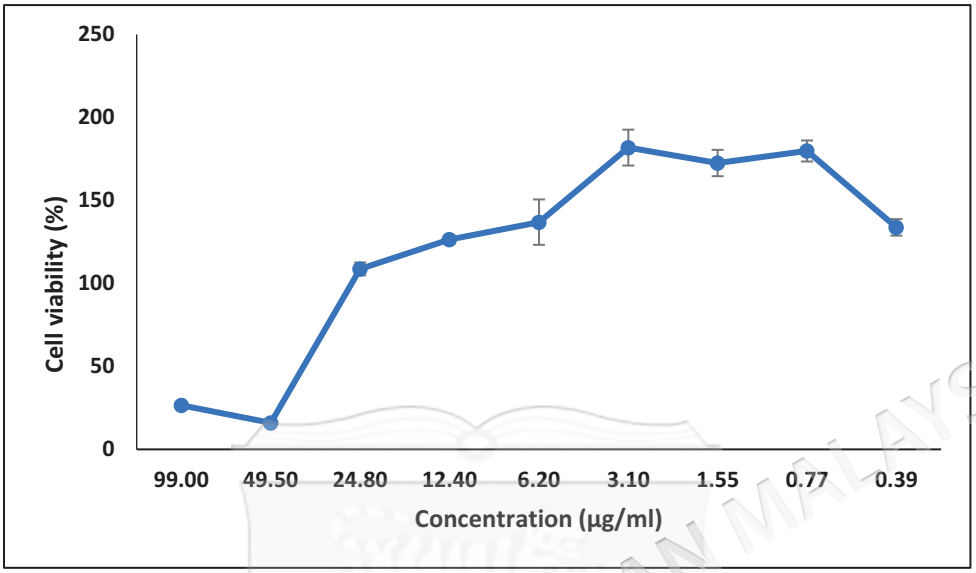

APPENDIX C20

CURVE GRAPH DEPICTING CYTOTOXICITY VALU OF CHLOROQUINE DIPASPATE

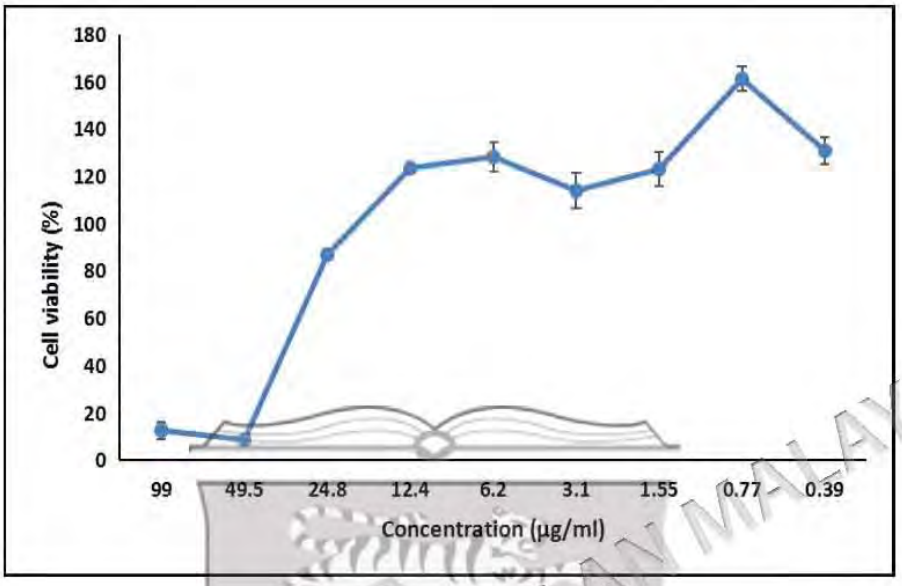

APPENDIX D1

CURVE GRAPHS DEPICTING THE ANTIMALARIAL ACTIVITY OF PYRANO[2,3-*C*]PYRAZOLE-4-AMINOQUINOLINE 24A

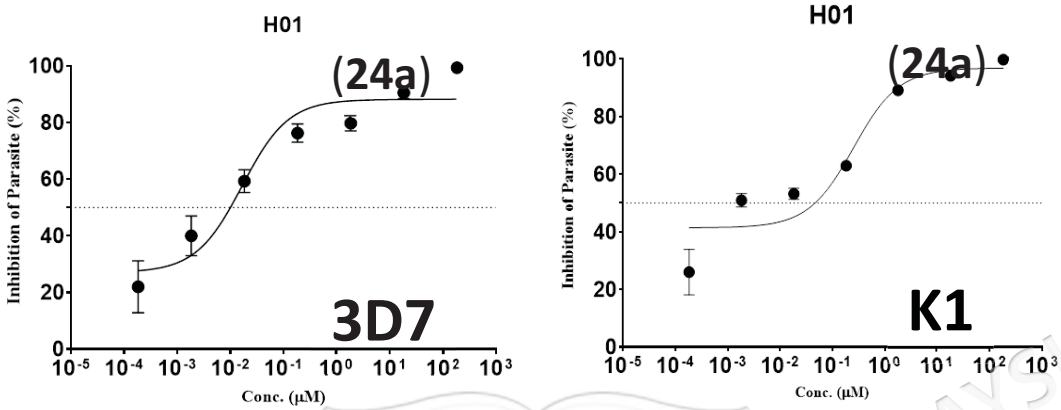

APPENDIX D2

CURVE GRAPHS DEPICTING THE ANTIMALARIAL ACTIVITY OF PYRANO[2,3-*C*]PYRAZOLE-4-AMINOQUINOLINE 24B

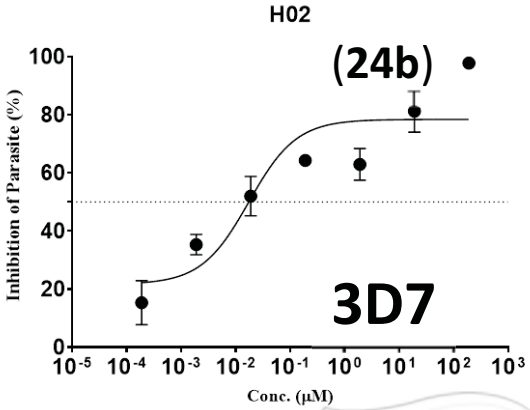

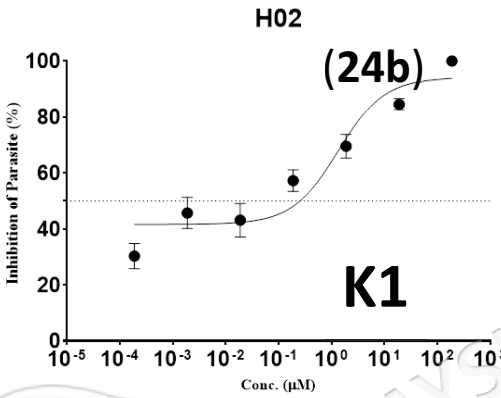

APPENDIX D3

CURVE GRAPHS DEPICTING THE ANTIMALARIAL ACTIVITY OF PYRANO[2,3-*C*]PYRAZOLE-4-AMINOQUINOLINE 24C

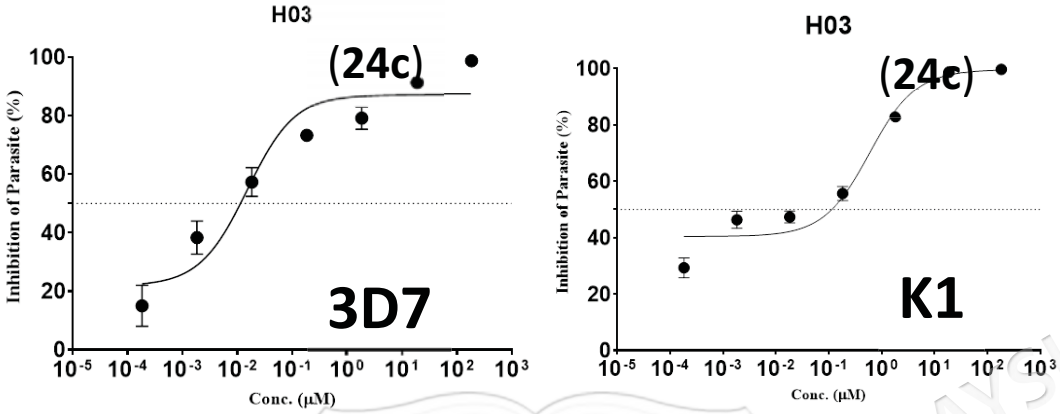

APPENDIX D4

CURVE GRAPHS DEPICTING THE ANTIMALARIAL ACTIVITY OF PYRANO[2,3-*C*]PYRAZOLE-4-AMINOQUINOLINE 24D

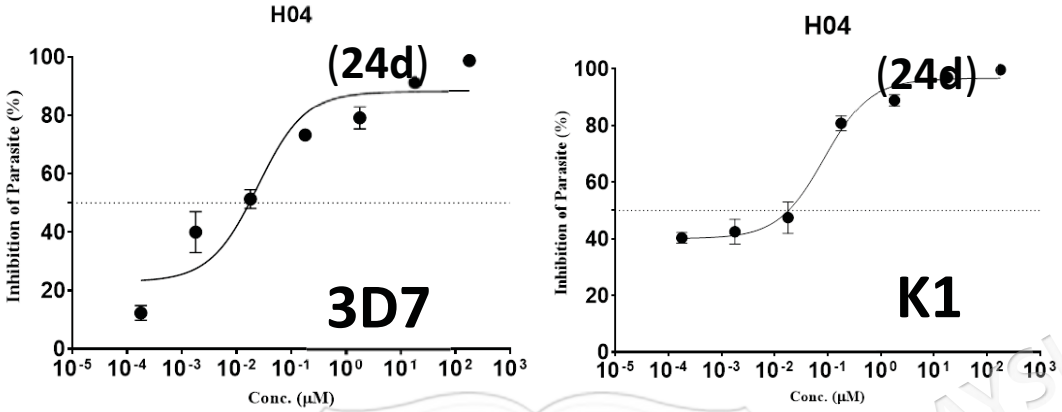

APPENDIX D5

CURVE GRAPHS DEPICTING THE ANTIMALARIAL ACTIVITY OF PYRANO[2,3-*C*]PYRAZOLE-4-AMINOQUINOLINE 24E

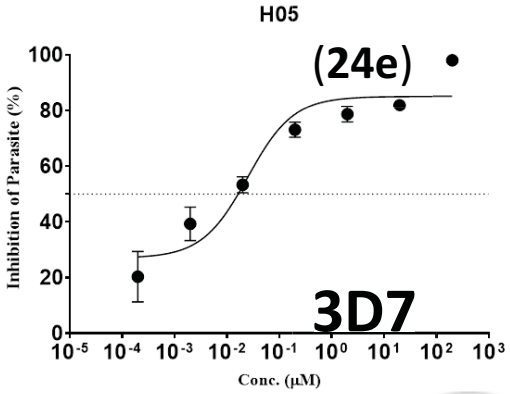

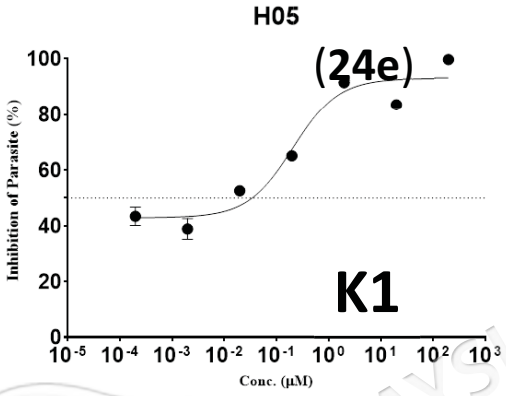

APPENDIX D6

CURVE GRAPHS DEPICTING THE ANTIMALARIAL ACTIVITY OF PYRANO[2,3-*C*]PYRAZOLE-4-AMINOQUINOLINE 24F

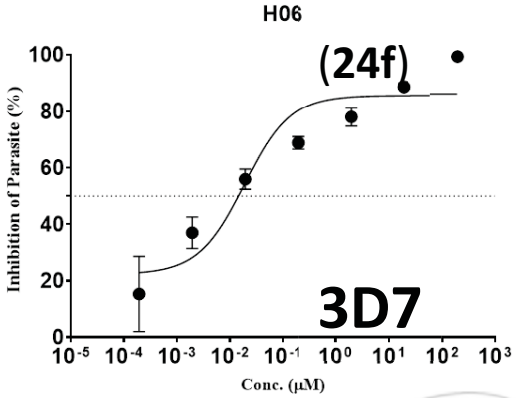

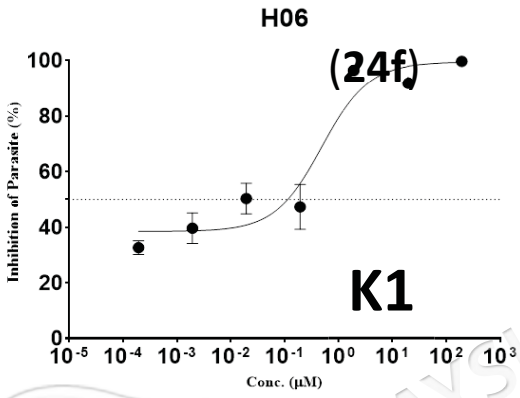

APPENDIX D7

CURVE GRAPHS DEPICTING THE ANTIMALARIAL ACTIVITY OF PYRANO[2,3-*C*]PYRAZOLE-4-AMINOQUINOLINE 24G

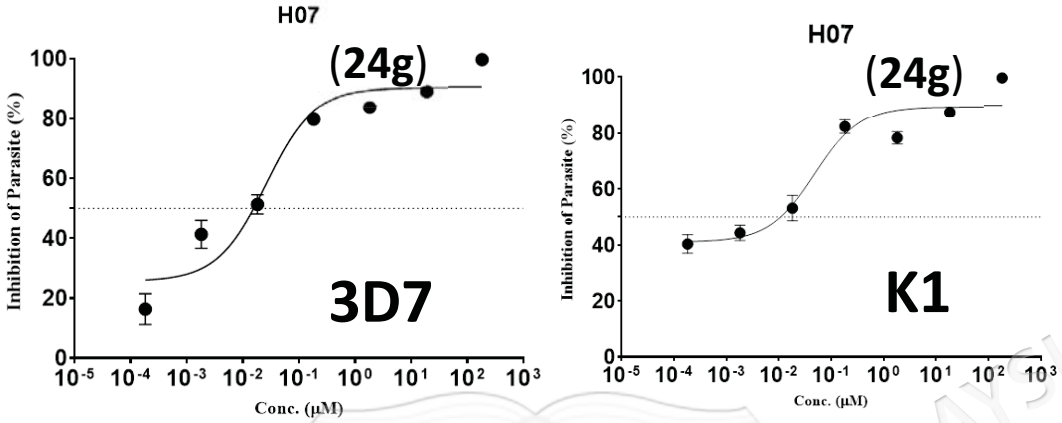

APPENDIX D8

CURVE GRAPHS DEPICTING THE ANTIMALARIAL ACTIVITY OF PYRANO[2,3-*C*]PYRAZOLE-4-AMINOQUINOLINE 24H

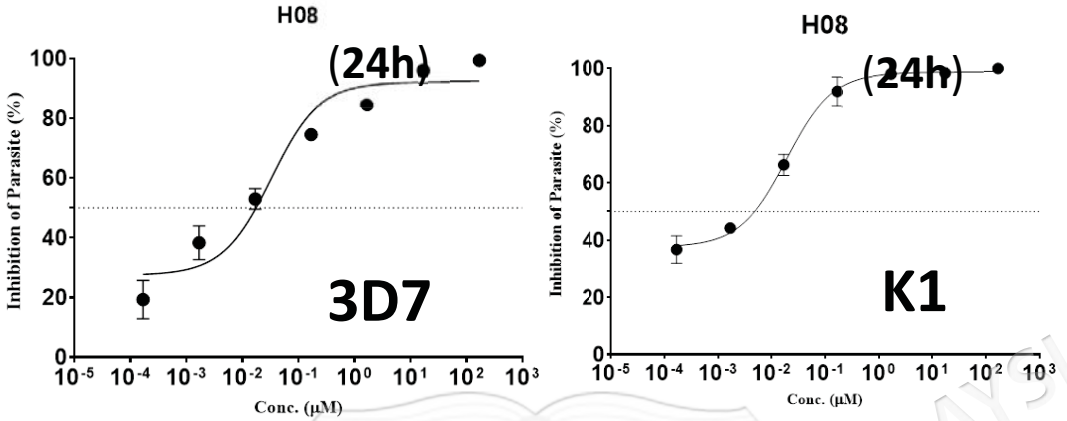

APPENDIX D9

CURVE GRAPHS DEPICTING THE ANTIMALARIAL ACTIVITY OF PYRANO[2,3-*C*]PYRAZOLE-4-AMINOQUINOLINE 24I

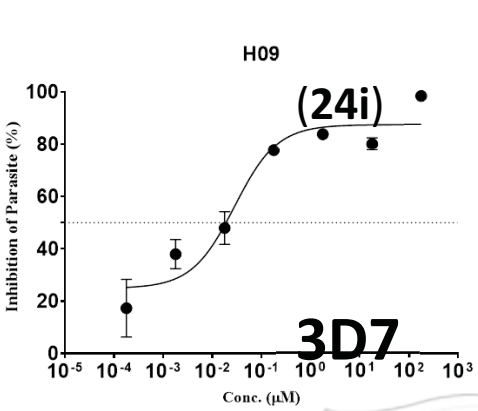

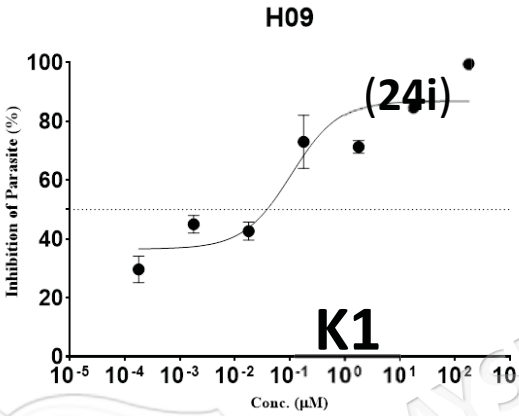

APPENDIX D10

CURVE GRAPHS DEPICTING THE ANTIMALARIAL ACTIVITY OF PYRANO[2,3-*C*]PYRAZOLE-4-AMINOQUINOLINE 24J

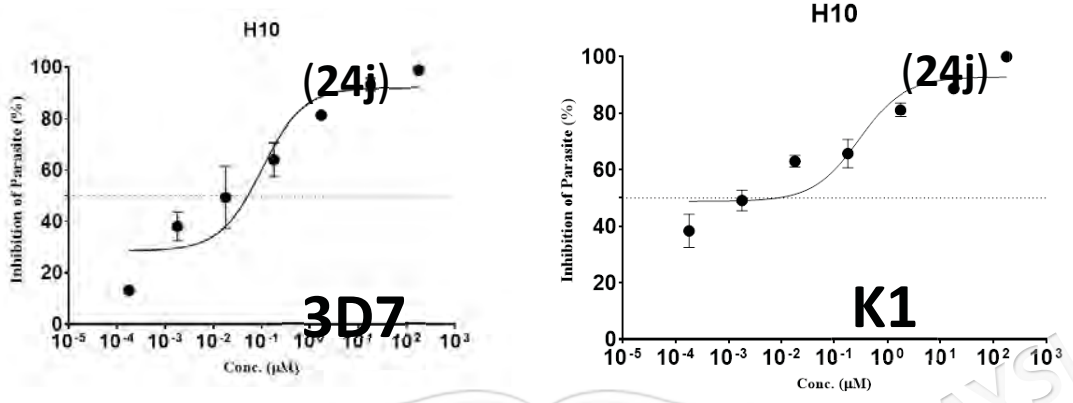

APPENDIX D11

CURVE GRAPHS DEPICTING THE ANTIMALARIAL ACTIVITY OF PYRANO[2,3-*C*]PYRAZOLE-4-AMINOQUINOLINE 24K

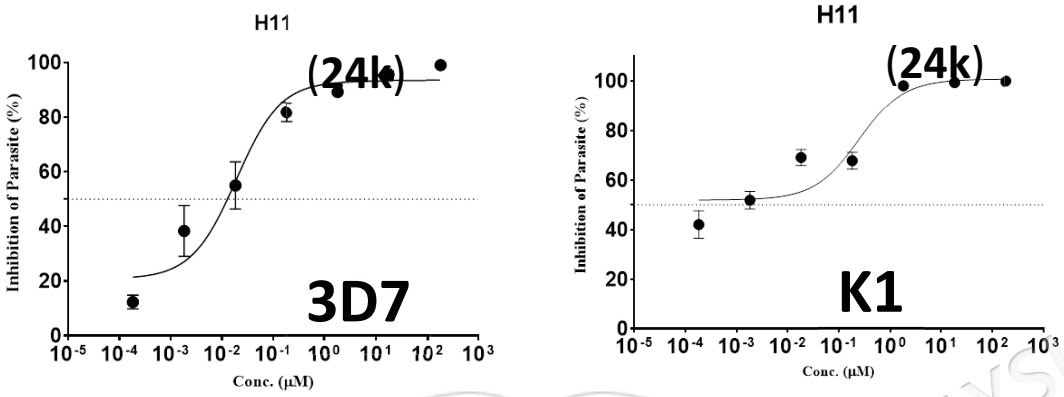

APPENDIX D12

CURVE GRAPHS DEPICTING THE ANTIMALARIAL ACTIVITY OF PYRANO[2,3-*C*]PYRAZOLE-4-AMINOQUINOLINE 24L

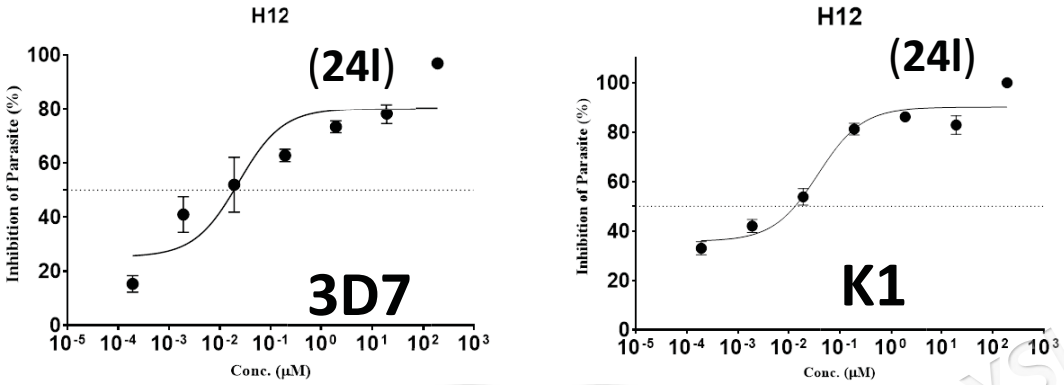

APPENDIX D13

CURVE GRAPHS DEPICTING THE ANTIMALARIAL ACTIVITY OF PYRANO[2,3-*C*]PYRAZOLE-4-AMINOQUINOLINE 24M

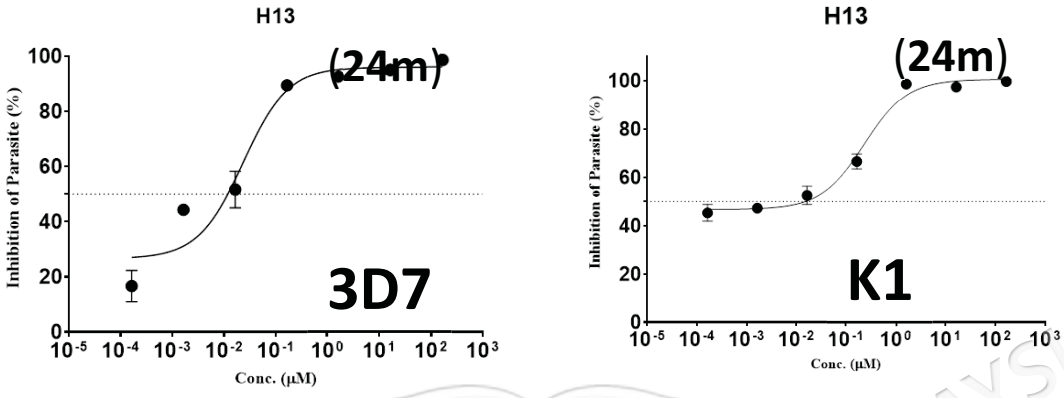

APPENDIX D14

CURVE GRAPHS DEPICTING THE ANTIMALARIAL ACTIVITY OF PYRANO[2,3-*C*]PYRAZOLE-4-AMINOQUINOLINE 24N

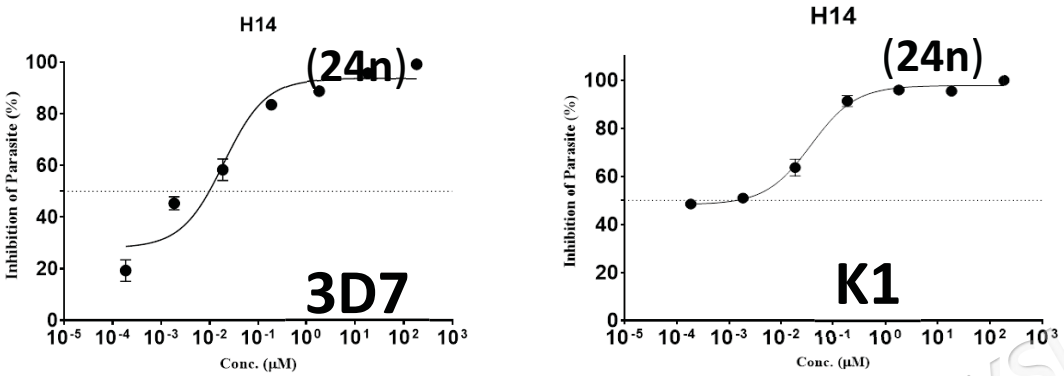

APPENDIX D15

CURVE GRAPHS DEPICTING THE ANTIMALARIAL ACTIVITY OF PYRANO[2,3-*C*]PYRAZOLE-4-AMINOQUINOLINE 24O

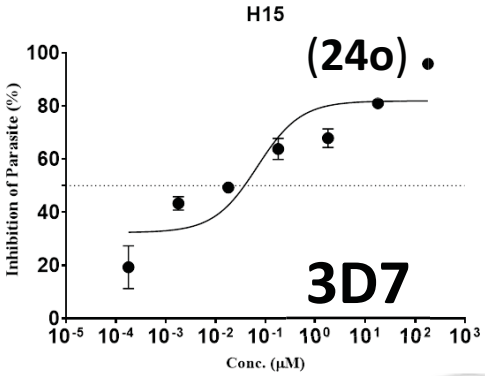

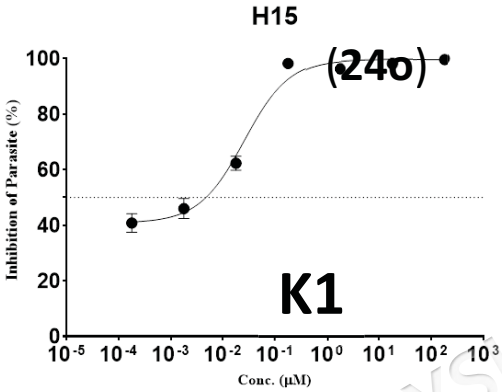

APPENDIX D16

CURVE GRAPHS DEPICTING THE ANTIMALARIAL ACTIVITY OF PYRANO[2,3-*C*]PYRAZOLE-4-AMINOQUINOLINE 24P

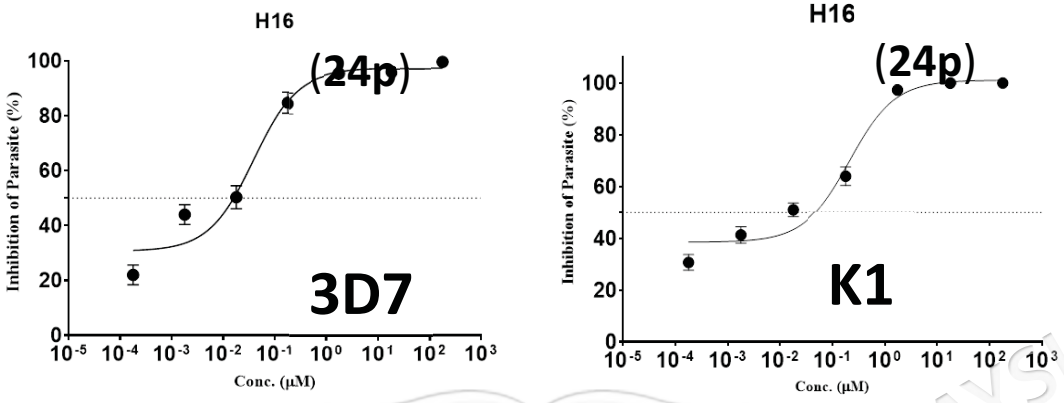

APPENDIX D17

CURVE GRAPHS DEPICTING THE ANTIMALARIAL ACTIVITY OF PYRANO[2,3-*C*]PYRAZOLE-4-AMINOQUINOLINE 24Q

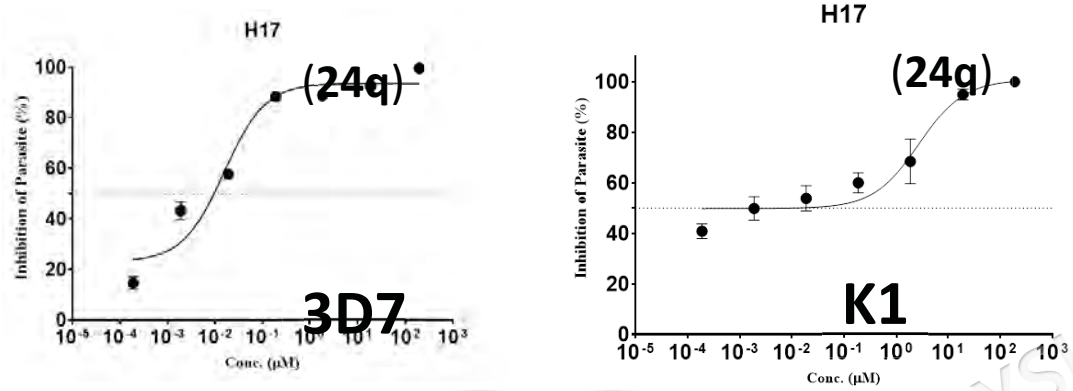

APPENDIX D18

CURVE GRAPHS DEPICTING THE ANTIMALARIAL ACTIVITY OF PYRANO[2,3-*C*]PYRAZOLE-4-AMINOQUINOLINE 24R

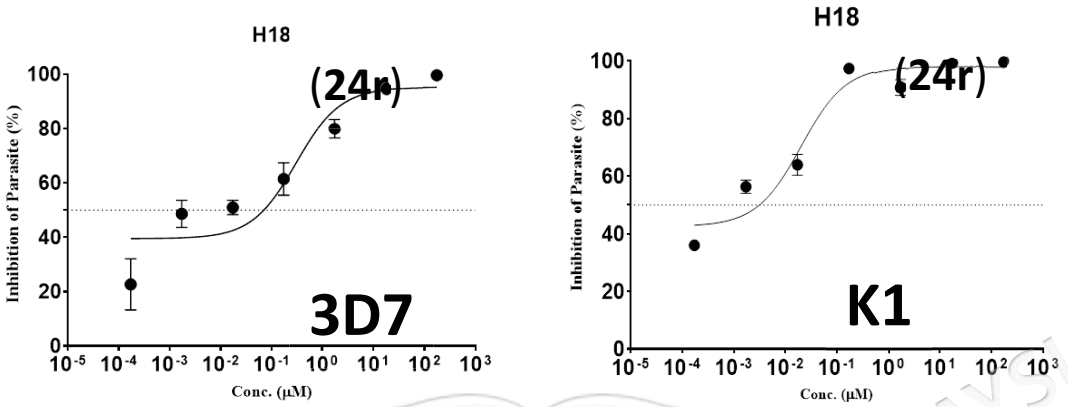

APPENDIX D19

CURVE GRAPHS DEPICTING THE ANTIMALARIAL ACTIVITY OF PYRANO[2,3-*C*]PYRAZOLE-4-AMINOQUINOLINE 24S

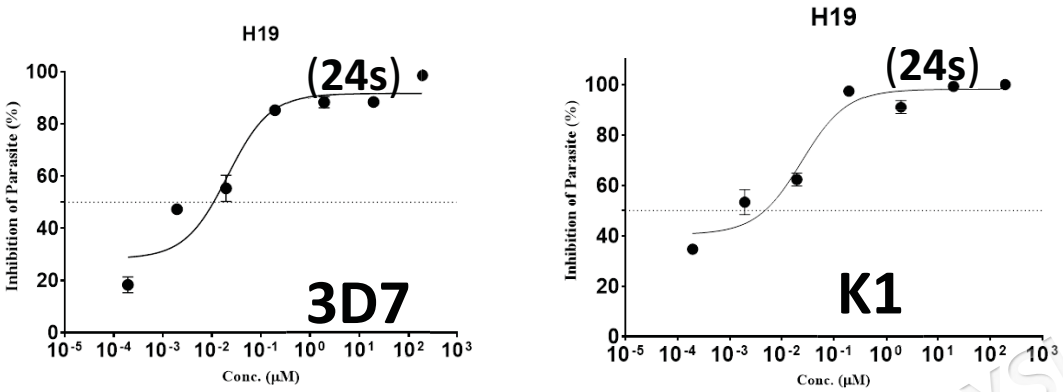

APPENDIX D20

CURVE GRAPHS DEPICTING THE ANTIMALARIAL ACTIVITY OF CHLOROQUINE DIPASPATE

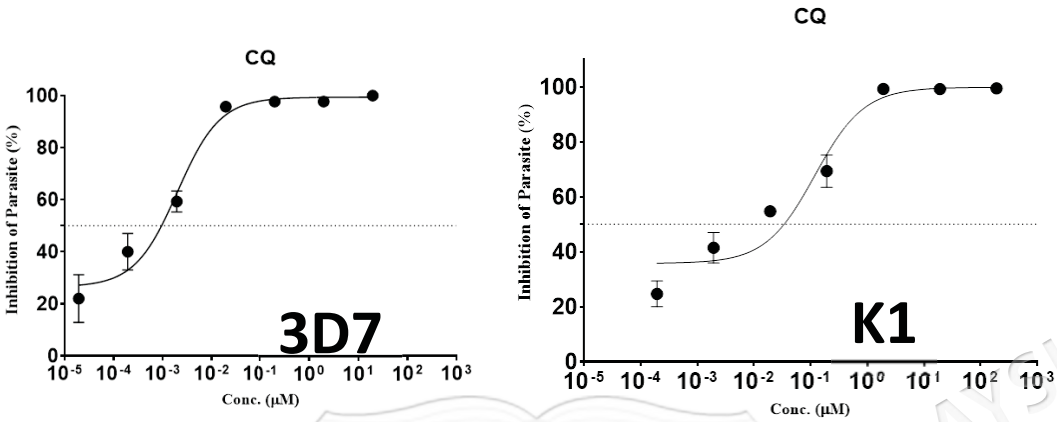

APPENDIX E

LIST OF PUBLICATION AND CONFERENCES

Journal Publications:

1. **Ravindar, L.,** Hasbullah, S.A., Hassan, N.I. & Qin, H-L. (2022). Cross-Coupling of C−H and N−H Bonds: A Hydrogen Evolution Strategy for the Construction of C−N Bonds. *European Journal of Organic Chemistry,* 31, e202200596. (Published-Q2).

2. **Ravindar, L.,** Hasbullah, S.A., Rakesh, K.P. & Hassan, N.I. (2023). Pyrazole and pyrazoline derivatives as antimalarial agents: A key review. *European Journal of Pharmaceutical Sciences* 183: 106365. (Published-Q2).

3. **Ravindar, L**., Hasbullah, S.A., Rakesh, K.P. & Hassan, N.I. (2023). Recent developments in antimalarial activities of 4-aminoquinoline derivatives. *European Journal of Medicinal Chemistry* 256: 115458. (Published-Q1).

4. **Ravindar, L.,** Hasbullah, S.A., Rakesh, K.P. & Hassan, N.I. (2023). Triazole hybrid compounds: A new frontier in malaria treatment. *European Journal of Medicinal Chemistry* 259: 115694. (Published-Q1).

5. **Ravindar, L.,** Hasbullah, S.A., Rakesh, K.P., Raheem, S., Agustar, H.K., Ismail, N., Ling, L.Y. & Hassan, N.I. (2023). Exploring diverse frontiers: Advancements of bioactive 4-aminoquinoline-based molecular hybrids in targeted therapeutics and beyond, *European Journal of Medicinal Chemistry* 264: 116043. (Published-Q1).

6. **Ravindar, L**., Hasbullah, S.A., Rakesh, K.P., Raheem, S., Ismail, N., Ling, L.Y. & Hassan, N.I. (2024). Pyridine and Pyrimidine hybrids as privileged scaffolds in antimalarial drug discovery: A recent development, *Bioorganic & Medicinal Chemistry Letters* 114: 129992. (Published -Q2).

7. **Ravindar, L.,** Hong, N.Y., Bakar, K.A., Hidayat, A.F.A., Feroz, S.R., Raheem, S., Hasbullah, S.A. & Hassan, N.I. (2024). Synthesis, molecular docking and heme detoxification of pyrano[2,3-c]pyrazole-aminoquinoline hybrids as antimalarial agents. *Sains Malaysiana* 53: 1953. (Published -Q4).

8. Norazmi, N.A.Z., Mukhtar, N.H., **Ravindar, L.**, Saaidin, A.S., Karim, N.H.A., Ali, A.H., Agustar, H.K., Ismail, N., Ling, L.Y., Ebihara, M. & Hassan, N.I. (2024). Exploring antimalarial potential: Conjugating organometallic moieties with organic fragments for enhanced efficacy. *Bioorganic Chemistry* 149: 107510. (Published-Q1).

9. **Ravindar, L**., Hong, N.Y., Feroz, S.R., Norazmi, N.A.Z., Ali1, A.H., Hasbullah, S.A., Ismail, N., Agustar, H.K., Ling L.Y. & Hassan, N.I. (2024). Design and synthesis of pyrano[2,3-c]pyrazole-4-aminoquinoline hybrids as

effective antimalarial compounds. *European Journal of Medicinal Chemistry* 279: 116828 (Published -Q1).

10. **Ravindar, L**.; Hasbullah, S.A. & Hassan, N.I. Recent developments in antimalarial and anticancer activities of chalcone hybrids: A key review. (2024). *Bioorganic & Medicinal Chemistry* (Under Review-Q2).

Conferences:

1. 3rd Virtual Symposisum on Advances in Malaria Research (MALARIA-2023) (Jul 27, 2023. Online).

2. 4th Commonwealth Chemistry Poster (Sep 4 and 5, 2023. Online). Presenter (poster).